

GEOPHYSICAL SURVEY REPORT

103783-ENN-MMT-SUR-REP-SURVWPA
REVISION C | FOR USE
SEPTEMBER 2022

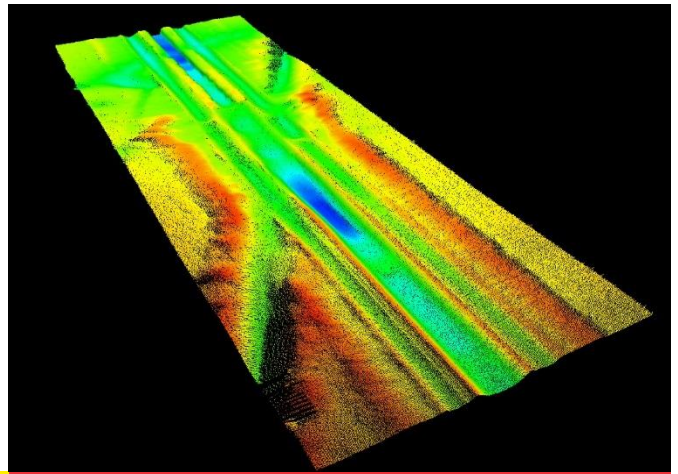


ENERGINET

ENERGY ISLANDS - NORTH SEA EAST

GEOPHYSICAL SURVEY FOR OFFSHORE
WIND FARMS AND ENERGY ISLAND

NORTH SEA
MAY-AUGUST 2021



REVISION HISTORY

REVISION	DATE	STATUS	CHECK	APPROVAL	CLIENT APPROVAL
C	2022-09-07	Issue for Use	DO	KG	
B	2022-08-10	Issue for Use	DP	KG	
A	2022-04-29	Issue for Use	DO	KG	
02	2021-12-13	Issue for Client Review	DP	KG	
01	2021-12-11	Issue for Internal Review	SC/DP	KG	

REVISION LOG

DATE	SECTION	CHANGE
2022-09-07	8.6.7	Figure 156 updated.
2022-04-29	Various	As per client comments received on 2022-02-17.
2022-08-10	Various	As per client comments received on 2022-06-28.

DOCUMENT CONTROL

RESPONSIBILITY	POSITION	NAME
Content	MMT Senior Data Processor	Andrew Stanley / Clayton Summers / Chris Bulford
Content	MMT Geologist	Jack Turner / Jeshua Guzman Castro
Content	MMT Senior Geologist	Sophie Clark
Content	MMT Project Geophysicist	Gerald Bishop / Hanna Åkerblom
Content	GeoSurveys Interpreter Reviewer / Principal Interpreter	Ana Maia
Content	GeoSurveys Onshore Team Coordinator	Bruno Simao
Content	GeoSurveys Deputy Project Manager	Miguel Oliveira
Content	Geosurveys Project Manager / Deputy Project Manager	Henrique Duarte / Jhonny Miranda
Content / Check	MMT Project Report Coordinator	David Oakley / Darryl Pickworth
Check	MMT Document Controller	Pontus Frost / Rebecca Österberg
Approval	MMT Project Manager	Karin Gunnesson

TABLE OF CONTENTS

1 	INTRODUCTION.....	17
1.1	PROJECT INFORMATION	17
1.2	SURVEY INFORMATION – MMT OWF AREA.....	20
1.3	SURVEY OBJECTIVES	20
1.4	SCOPE OF WORK – OWF SURVEY AREA	20
1.4.1	DEVIATIONS TO SCOPE OF WORK	20
1.5	PURPOSE OF DOCUMENT	21
1.6	REPORT STRUCTURE	21
1.6.1	GEOPHYSICAL SURVEY REPORT	22
1.6.2	CHARTS	22
1.7	REFERENCE DOCUMENTS.....	24
1.8	AREA LINE PLAN	25
1.8.1	2D UHRS REFERENCE LINES.....	25
1.8.2	2D UHRS MAIN AND CROSS LINES	27
1.8.3	GEOPHYSICAL MAIN AND CROSS LINES	28
1.8.4	SURVEY BLOCKS.....	29
2 	SURVEY PARAMETERS	31
2.1	GEODETIC DATUM AND GRID COORDINATE SYSTEM.....	31
2.1.1	ACQUISITION.....	31
2.1.2	PROCESSING	31
2.1.3	TRANSFORMATION PARAMETERS	31
2.1.4	PROJECTION PARAMETERS.....	32
2.1.5	VERTICAL REFERENCE	32
2.2	VERTICAL DATUM.....	33
2.3	TIME DATUM.....	34
3 	SURVEY VESSELS.....	35
3.1	M/V NORTHERN FRANKLIN.....	35
3.2	M/V RELUME	36
4 	DATA PROCESSING AND INTERPRETATION METHODS	38
4.1	BATHYMETRY.....	38
4.2	BACKSCATTER.....	42
4.3	SIDE SCAN SONAR	42
4.4	MAGNETOMETER	44
4.5	SEISMIC - 2D UHRS	47
4.6	SUB-BOTTOM PROFILER - INNOMAR.....	47
5 	PROCESSED DATA QUALITY.....	50
5.1	BATHYMETRY DATA	50
5.2	BACKSCATTER DATA	61
5.3	SIDE SCAN SONAR DATA	67
5.4	MAGNETOMETER DATA.....	71
5.5	SEISMIC 2D UHRS DATA QUALITY ANALYSIS.....	72

5.5.1	FEATHERING	74
5.5.2	SIGNAL & NOISE ANALYSIS.....	74
5.5.3	SOURCE RECEIVER OFFSETS.....	77
5.5.4	STREAMER GROUP BALANCING	78
5.5.5	INTERACTIVE VELOCITY ANALYSIS.....	79
5.5.6	CDP FOLD.....	80
5.5.7	BRUTESTACK.....	81
5.5.8	GEOM OUTPUT	82
5.6	SEISMIC 2D UHRS DATA PROCESSING OFFICE	83
5.7	SUB-BOTTOM PROFILER DATA – INNOMAR	83
6 	BACKGROUND DATA AND CLASSIFICATIONS	86
6.1	SEABED GRADIENT CLASSIFICATION	86
6.2	SEABED SEDIMENT CLASSIFICATION	86
6.3	SEABED FEATURE / BEDFORM CLASSIFICATION.....	88
6.4	SUB-SEABED GEOLOGY CLASSIFICATION	90
6.5	GRAB SAMPLE CLASSIFICATION.....	96
7 	GEOLOGICAL FRAMEWORK.....	97
8 	RESULTS.....	102
8.1	GENERAL	102
8.2	BATHYMETRY.....	104
8.2.1	PROFILE 1.....	107
8.2.2	PROFILE 2.....	108
8.2.3	PROFILE 3.....	109
8.2.4	PROFILE 4.....	111
8.2.5	SLOPE ANALYSIS	114
8.3	SURFICIAL GEOLOGY AND SEABED FEATURES.....	126
8.3.1	SEABED SEDIMENTS	126
8.3.2	MOBILE SEDIMENTS	128
8.3.3	BOULDERS	132
8.3.4	TRAWL MARKS.....	134
8.3.5	OTHER - SEDIMENT MOUND.....	135
8.3.6	OTHER - AREAS OF INTEREST	137
8.4	CONTACTS AND ANOMALIES.....	138
8.4.1	WRECKS	140
8.5	EXISTING INFRASTRUCTURE (CABLES AND PIPELINES)	147
8.6	SEISMOSTRATIGRAPHIC INTERPRETATION	149
8.6.1	SUB-SEABED GEOLOGY – GEOMODEL.....	151
8.6.1	SEISMIC UNIT U05	159
8.6.2	SEISMIC UNIT U10	161
8.6.3	SEISMIC UNIT U20	171
8.6.4	SEISMIC UNIT U25	179
8.6.5	SEISMIC UNIT U30	188
8.6.6	SEISMIC UNIT U35	194

8.6.7	SEISMIC UNIT U40	201
8.6.8	SEISMIC UNIT U50	213
8.6.9	SEISMIC UNIT U60	220
8.6.10	SEISMIC UNIT U70	227
8.6.11	SEISMIC UNIT U85	236
8.6.12	SEISMIC UNIT U90	242
8.6.13	SEISMIC UNIT UKS	248
8.6.14	BASE SEISMIC UNIT BSU.....	257
8.6.15	SUMMARY AND DISCUSSION.....	259
8.7	SEABED HAZARDS	261
8.7.1	GRADIENTS	261
8.7.2	MOBILE SEDIMENT AND BEDFORMS.....	261
8.7.3	BOULDERS	261
8.7.4	EXISTING INFRASTRUCTURE AND WRECKS	261
8.8	SUB-SEABED HAZARDS.....	262
8.8.1	SEDIMENT DEFORMATION.....	263
8.8.2	BURIED CHANNELS AND TUNNEL VALLEYS.....	286
8.8.3	SOFT SEDIMENTS AND ORGANIC-RICH DEPOSITS.....	294
8.8.4	COARSE SEDIMENTS / GRAVEL BEDS / BOULDERS	314
8.8.5	TILL DEPOSITS.....	318
8.8.6	FLUID FLOW AND GAS FEATURES.....	320
8.8.7	LACUSTRINE SEDIMENTS	324
8.9	ARCHAEOLOGY CONSIDERATIONS.....	327
8.10	GRAB SAMPLE SUMMARY	327
9 	CONCLUSIONS.....	330
10 	RESERVATIONS AND RECOMMENDATIONS	332
11 	REFERENCES.....	333
12 	DATA INDEX	336

APPENDICES

APPENDIX A	LIST OF PRODUCED CHARTS.....	338
APPENDIX B	CONTACT AND ANOMALY LIST	338
APPENDIX C	GRAB SAMPLE LAB REPORT	338
APPENDIX D	2D UHRS PROCESSING REPORT	338

LIST OF FIGURES

Figure 1	Overview of survey scopes performed.....	19
Figure 2	Line plan – 2D UHRS reference lines (including geophysical data).....	26
Figure 3	Line plan – 2D UHRS main and cross lines (including geophysical data).....	27
Figure 4	Line plan - geophysical main and cross lines.	28
Figure 5	Overview of survey block divisions.	29
Figure 6	Overview of the reporting tiles.....	30
Figure 7	Overview of the relation between different vertical references.	33
Figure 8	M/V Northern Franklin.....	35
Figure 9	M/V Relume.....	36
Figure 10	Workflow MBES processing.....	39
Figure 11	Example of division of MBES data acquisition in BM6.....	40
Figure 12	BM1 contour export parameters.....	41
Figure 13	Example of exported contours with 50 cm interval.	41
Figure 14	Workflow side scan sonar processing (1 of 2).	43
Figure 15	Workflow side scan sonar processing (2 of 2).	44
Figure 16	Data example for Northern Franklin from B3.	45
Figure 17	Data example for Relume from B3.....	45
Figure 18	Workflow MAG processing (1 of 2).	46
Figure 19	Workflow MAG processing (2 of 2).	46
Figure 20	Workflow SBP processing (1 of 2).	48
Figure 21	Workflow SBP processing (2 of 2).	49
Figure 22	Caris HIPS Standard deviation surface in an overlapping section of data.	52
Figure 23	Area of overlapping bathymetry which displays a wavy pattern.	52
Figure 24	Cross section through Block 2.	53
Figure 25	Standard deviation at 95% confidence interval for the MMT OWF survey area.	54
Figure 26	Example of MBES data acquired in good weather with a relatively stable sound velocity... ..	55
Figure 27	Example of MBES data acquired in area with variable sound velocity.....	56
Figure 28	QC surfaces (red and blue cells) highlighting boulders in Block 4.....	57
Figure 29	Total Vertical Uncertainty surface for the MMT OWF survey area.	58
Figure 30	Total Horizontal Uncertainty surface for the MMT OWF survey area.	59
Figure 31	Example of anomaly in MBES caused by pycnocline.....	60
Figure 32	Overview of backscatter normalised values for the MMT OWF survey area.....	62
Figure 33	Backscatter mosaic with artefacts.....	63
Figure 34	Outer beam busts visible in the M/V Relume section of the dataset.	64
Figure 35	700m stretch of M/V Relume outer-beam noise visible in the backscatter dataset.	65
Figure 36	Beam busts caused by excessive vessel motion and/or bubble entrainment.	66
Figure 37	Example of good high frequency SSS data from block BM06.....	67
Figure 38	Example 1 of high frequency SSS image from block BM01, Northern Franklin.	68
Figure 39	Example 2 of high frequency SSS image from block BM01, Northern Franklin.	68
Figure 40	Example 1 of high frequency SSS image from block BM01, Relume.....	69
Figure 41	Example 2 of high frequency SSS image from block BM01, Relume.....	69
Figure 42	Example of low frequency SSS image from block BM01, Relume.	70
Figure 43	SSS coverage plots for each of the survey blocks.....	70
Figure 44	Pie chart illustration of Average Altitudes, Percentages and Distances	71

Figure 45 Magnetometer profile showing low background noise level for Northern Franklin.	72
Figure 46 Magnetometer profile showing low background noise level for Relume.	72
Figure 47 Processing workflow applied to the seismic lines.	73
Figure 48 Feathering plot calculated for the line BM3_OWF_E_2D_07560.	74
Figure 49 Main noise sources identified in the working limit noise test.	75
Figure 50 Main noise sources identified while in production.	75
Figure 51 Fugro Pioneer shooting while in SIMOPS.	76
Figure 52 Frequency spectrum comparison.	76
Figure 53 Channel domain showing the calculated offsets.	77
Figure 54 Profile BM4_OWF_E_2D_08820 in channel domain.	78
Figure 55 Profile BM5_OWF_E_2D_15540 in channel domain.	78
Figure 56 Channel domain with flattened seabed.	79
Figure 57 Velocity Analysis display for line BM3_OWF_E_2D_07770.	80
Figure 58 Trace fold values plotted on the top of stacked sections.	81
Figure 59 Brutestack for line BM4_OWF_E_2D_10080_01.	82
Figure 60 Innomar data showing achieved penetration of 10 m.	84
Figure 61 Raw Innomar data showing vertical striping Sparker interference.	84
Figure 62 Processed Innomar data showing improved signal to noise ratio.	85
Figure 63 Major Danish structural elements.	97
Figure 64 Regional geological map (After Nielsen et al., 2008); MMT OWF survey area in red.	98
Figure 65 The Quaternary glaciations and an overview of Quaternary valleys in northwest Europe. ...	99
Figure 66 General stratigraphy model of the geology in the eastern Danish North Sea.	100
Figure 67 The MMT OWF survey area with the tile schema used for the description of results.	103
Figure 68 Overview of the bathymetry data.	105
Figure 69 Profiles across the MMT OWF survey area showing depth relative to DTU21 MSL.	106
Figure 70 MBES data with profile, in reporting areas T01-T02.	107
Figure 71 MBES data with profile in reporting areas T07 and T08.	108
Figure 72 MBES data with profile in reporting Tile T13- slope.	109
Figure 73 MBES data with profile in reporting Tile T13- deepest depth.	110
Figure 74 MBES data with profile in reporting Tile T15.	111
Figure 75 MBES image depicting undulating seabed in reporting tile T19.	112
Figure 76 MBES image depicting gentle slope.	113
Figure 77 Overview of slope angles across the MMT OWF survey area.	115
Figure 78 Overview highlighting the regions with Very Steep slope angles.	116
Figure 79 Very steep slopes on the western edge of the southern sand wave/sandbar field.	117
Figure 80 Wreck 86 with 56° slope angle.	118
Figure 81 Accepted soundings over wreck in Figure 80.	119
Figure 82 Large boulder with 47° slope angle.	120
Figure 83 Accepted soundings over boulder contact in Figure 82.	121
Figure 84 Location of large boulders with 38 - 42° slope angle.	122
Figure 85 Large boulder with 38° slope angle.	123
Figure 86 Accepted soundings over suspected boulder contact in Figure 85.	124
Figure 87 Bedform feature (Other-Area of Interest) with slope angles up to 44°.	125
Figure 88 Overview of seabed sediments in the MMT OWF survey area.	127
Figure 89 High frequency SSS example of boulder fields of variable density.	128
Figure 90 Distribution of bedforms.	129
Figure 91 High frequency SSS example.	130
Figure 92 MBES DTM image showing ripples.	130
Figure 93 High frequency SSS mosaic showing sand waves in reporting tile T08.	131
Figure 94 Distribution of boulder fields in the MMT OWF survey area.	133
Figure 95 Distribution of trawl marks in the MMT OWF survey area.	134
Figure 96 High frequency SSS example of trawl marks in silty SAND.	135
Figure 97 MBES data of a sediment mound in reporting tile T12.	136
Figure 98 SBP Innomar data of a sediment mound in reporting tile T12.	137
Figure 99 SSS data example of an area of interest in reporting tile T19.	137
Figure 100 High frequency SSS and MBES images of debris item not seen before 28/07/2021.	139

Figure 101 Overview of wreck locations within the MMT OWF survey area.....	141
Figure 102 MBES image of HMS Tarpon Submarine Wreck_86 (S_FR_B03_0006).....	142
Figure 103 SSS image of HMS Tarpon Submarine Wreck_86 (S_FR_B03_0006).....	143
Figure 104 MBES image of Wreck_85 (S_FR_B03_0069).....	144
Figure 105 MBES image of Wreck_94 (S_RE_B01_0324).....	145
Figure 106 MBES image of a possible unknown wreck (S_RE_B05_0547).....	146
Figure 107 High frequency SSS image of possible unknown wreck with associated debris.	146
Figure 108 SSS image of possible exposed TAT-14 cable.....	147
Figure 109 Map overview of possible cable exposure	148
Figure 110 Seabed of the MMT OWF survey area – UHRS grid. Units in metres MSL.	152
Figure 111 General sub-surface architecture of the survey area.....	155
Figure 112 General sub-surface architecture of the North sector.....	156
Figure 113 General sub-surface architecture of the Central sector.....	157
Figure 114 General sub-surface architecture of the South sector	158
Figure 115 Map showing the lateral extent of U05.....	159
Figure 116 Depth below seabed of H05.....	160
Figure 117 Thickness of unit U05.....	161
Figure 118 Map showing the lateral extent of U10 from UHRS data.	162
Figure 119 Map showing the lateral extent of U10 from SBP data.	163
Figure 120 Depth below seabed of H10.....	164
Figure 121 Depth below seabed of H10i.....	165
Figure 122 Thickness of unit U10.....	166
Figure 123 General facies of Seismic Unit U10, and the character of horizon H10 (light green).	167
Figure 124 Area in which horizon H10 has a stippled character (light green).	168
Figure 125 Internal facies of Seismic Unit U10, and horizon H10 (light green).	169
Figure 126 Grid overlay from interpretation of H10 as interpreted on the Innomar SBP.	170
Figure 127 Map showing the lateral extent of H20.....	172
Figure 128 Depth below seabed of H20.....	173
Figure 129 Thickness of unit U20.....	174
Figure 130 Infilled channel of Seismic Unit U20, and the character of horizon H20 (dark green).	175
Figure 131 Infill facies of a wide shallow basin of Seismic Unit U20, and character of horizon H20..	176
Figure 132 Two distinct facies of Seismic Unit U20.....	177
Figure 133 Grid overlay from interpretation of H20 as interpreted on the Innomar SBP.....	178
Figure 134 Map showing the lateral extent of U25.....	180
Figure 135 Depth below seabed of H25.....	181
Figure 136 Thickness of unit U25.....	182
Figure 137 General facies of Seismic Unit U25, and character of horizon H25.....	183
Figure 138 Facies of Seismic Unit U25 present in areas where U25 is thinner.....	184
Figure 139 U25 facies within the central basin, where the unit is thicker.	185
Figure 140 Homogeneous transparent facies of an internal channel of Unit U25.	186
Figure 141 Grid overlay from interpretation of H25 as interpreted on the Innomar SBP.....	187
Figure 142 Map showing the lateral extent of U30.....	189
Figure 143 Depth below seabed of H30.....	190
Figure 144 Thickness of unit U30.....	191
Figure 145 General facies of Seismic Unit U30, and the character of horizon H30 (orange).....	192
Figure 146 H30 truncating the underlying deposits, and the thicker facies of U30.....	193
Figure 147 Map showing the lateral extent of U35.....	195
Figure 148 Depth below seabed of H35.....	196
Figure 149 Thickness of unit U35.....	197
Figure 150 General facies of Seismic Unit U35, and the character of horizon H35.....	198
Figure 151 General facies of Unit U35, and the pronounced relief of H35 truncating the BSU.....	199
Figure 152 Facies of seismic Unit U35 in an area where the unit is thinner.	200
Figure 153 Map showing the lateral extent of U40.....	203
Figure 154 Depth below seabed of H40.....	204
Figure 155 Thickness of unit U40.....	205
Figure 156 Spatial distribution of the different types of channels identified for Seismic Unit U40.	206

Figure 157. U40 channels subdivision into 4 distinct types.....	207
Figure 158 General facies of Type A channels of Seismic Unit U40.	208
Figure 159 General facies of Type B channels of Seismic Unit U40.	209
Figure 160 General facies of Type C channels of Seismic Unit U40.	210
Figure 161 General facies of Type D channels of Seismic Unit U40.	211
Figure 162 Interpreted glaciolacustrine deposits on the upper levels of Seismic Unit U40.	212
Figure 163 Map showing the lateral extent of U50.....	214
Figure 164 Depth below seabed of H50.....	215
Figure 165 Thickness of unit U50.....	216
Figure 166 Transparent facies of Seismic Unit U50 in the NE region of the site.	217
Figure 167 Layering at the base of Seismic Unit U50, and the character of horizon H50.....	218
Figure 168 Facies of Seismic Unit U50 towards NW of the site, and the character of horizon H50...	219
Figure 169 Map showing the lateral extent of U60.....	221
Figure 170 Depth below seabed of H60.....	222
Figure 171 Thickness of unit U60.....	223
Figure 172 Spatial distribution of the major incisions identified for Seismic Unit U60.	224
Figure 173 General facies of Seismic Unit U60, and the character of horizon H60.....	225
Figure 174 General facies of Seismic Unit U60, and the character of horizon H60.....	226
Figure 175 Map showing the lateral extent of U70.....	228
Figure 176 Depth below seabed of H70.....	229
Figure 177 Thickness of unit U70.....	230
Figure 178 Spatial distribution of the major incisions identified for Seismic Unit U70.	231
Figure 179 General facies of a V-shaped channel of Seismic Unit U70.	232
Figure 180 General facies of a U-shaped channel of Seismic Unit U70.	233
Figure 181 Composite facies in a U70 channel.....	234
Figure 182 Composite facies in a U70 channel and the extensional features below H70.....	235
Figure 183 Map showing the lateral extent of U85.....	237
Figure 184 Depth below seabed of H85.....	238
Figure 185 Thickness of unit U85.....	239
Figure 186 General facies of Seismic Unit U85, and the character of horizon H85.....	240
Figure 187 General facies of Seismic Unit U85, and the character of horizon H85.....	241
Figure 188 Map showing the lateral extent of U90.....	243
Figure 189 Depth below seabed of H90.....	244
Figure 190 Thickness of unit U90.....	245
Figure 191 General facies of Seismic Unit U90, and the character of horizon H90.....	246
Figure 192 Thrust deformation affecting Seismic Unit U90.....	247
Figure 193 Map showing the lateral extent of horizon KSA.	249
Figure 194 Depth below seabed of horizon KSA.	250
Figure 195 Thickness of unit UKSA.	251
Figure 196 Map showing the lateral extent of horizon KSB.	252
Figure 197 Depth below seabed of horizon KSB.	253
Figure 198 Thickness of unit UKSB.	254
Figure 199 Thrust complex of Seismic Unit UKSA.....	255
Figure 200 Thrust complex of Seismic Unit UKSB.....	256
Figure 201 Thickness of Base Seismic Unit BSU.	257
Figure 202 General facies of the Base Seismic Unit.....	258
Figure 203 Different levels of deformation observed within the site.....	264
Figure 204 Minor folding and faulting affecting the BSU sequence.	265
Figure 205 Small scale faults within a thrust complex.	266
Figure 206 Large scale faults within a thrust complex.	267
Figure 207 Intense deformation within a thrust complex.....	268
Figure 208 Map displaying all the interpreted faults in the site.	269
Figure 209 Thrust complex of Seismic Unit UKSA.....	270
Figure 210 Thrust complex of Seismic Unit UKSA.....	271
Figure 211 Internal deformation of Seismic Unit U25.	272
Figure 212 Deformation domains within the Seismic Unit UKS (composite of UKSA and UKSB)	274

Figure 213 Seismic Unit UKSA truncating the deposits of the Base Seismic Unit BSU.	275
Figure 214 Seismic Units U85 and U90 not being affected by UKSB deformation,.....	276
Figure 215 Fault pattern analysis of the faults present in the north sector.	277
Figure 216 Fault pattern analysis of the faults present in the south sector.....	278
Figure 217 Subsidence area bounded by large normal faults at the centre of the survey area.	280
Figure 218 Older strata dipping opposite directions; likely related to salt tectonics deformation.	281
Figure 219 Structural map of the base of the Chalk deposits (GEUS).	282
Figure 220 Extensional features below a U70 valley.	284
Figure 221 Internal deformation of U25, increasing in intensity from E to W.....	285
Figure 222 Composite surface from the addition of all base horizons of units U10 to U70.	287
Figure 223 Composite surface.	288
Figure 224 Interpreted major channels not delineated by any unit's basal horizon.	289
Figure 225 Interpreted major channels not delineated by any unit's basal horizon.	290
Figure 226 Major infilled valley H70_CH_08 and its internal facies associations.....	291
Figure 227 U40 channel exploiting an older U70 incision.	292
Figure 228 Different channel infills of U40 and U70.....	293
Figure 229 Lateral extent of the negative impedance contrasts deposits within U10.	295
Figure 230 Depth below seabed of GHz_SK_U10.....	296
Figure 231 Lateral extent of the negative impedance contrasts deposits within U20.	297
Figure 232 Depth below seabed of GHz_SK_U20.....	298
Figure 233 Lateral extent of the negative impedance contrasts deposits within U25.	299
Figure 234 Depth below seabed of GHz_SK_U25.....	300
Figure 235 Lateral extent of the negative impedance contrasts deposits within U30.	301
Figure 236 Depth below seabed of GHz_SK_U30.....	302
Figure 237 Lateral extent of the negative impedance contrasts deposits within U35.	303
Figure 238 Depth below seabed of GHz_SK_U35.....	304
Figure 239 Lateral extent of the negative impedance contrasts deposits within U40.	305
Figure 240 Depth below seabed of GHz_SK_U40.....	306
Figure 241 Lateral extent of the negative impedance contrasts deposits within U40.	307
Figure 242 Depth below seabed of GHz_SK_U50.....	308
Figure 243 Lateral extent of the negative impedance contrasts deposits within U60.	309
Figure 244 Depth below seabed of GHz_SK_U60.....	310
Figure 245 Lateral extent of the negative impedance contrasts deposits within U85.	311
Figure 246 Depth below seabed of GHz_SK_U85.....	312
Figure 247 Negative impedance contrasts at the base of U85.	313
Figure 248 Lateral extent of GHz_Gravel.....	315
Figure 249 Depth below seabed of GHz_Gravel.....	316
Figure 250 Possible coarse layer within U35.	317
Figure 251 possible till deposits below H70.	319
Figure 252 Lateral extent of horizon GHz_Gas.....	320
Figure 253 Depth below seabed of horizon GHz_Gas.....	321
Figure 254 Structure within U25.....	322
Figure 255 Structure within U20.....	323
Figure 256 Lateral extent of the interpreted lacustrine deposits.....	324
Figure 257 Depth below seabed of horizon GHz_Lacustrine.....	325
Figure 258 Interpreted glaciolacustrine deposits on the upper levels of Seismic Unit U40.	326
Figure 259 Location plot of grab sample with material types in MMT OWF survey area.	328

LIST OF TABLES

Table 1 Survey area details.....	17
Table 2 Work Package descriptions.....	17
Table 3 Project details.....	17
Table 4 Deviations from the SOW during survey (M/V Northern Franklin).	21
Table 5 Reference documents.	24
Table 6 Survey line parameters.	25

Table 7 Survey line breakdown.....	25
Table 8 Geodetic parameters used during acquisition.....	31
Table 9 Geodetic parameters used during processing.....	31
Table 10 Transformation parameters.....	31
Table 11 Official test coordinates.....	32
Table 12 Projection parameters.....	32
Table 13 Vertical reference parameters.....	32
Table 14 Average Height comparison between DTU21 and DVR90.....	33
Table 15 M/V Northern Franklin equipment.....	35
Table 16 M/V Relume equipment.....	36
Table 17 Gridding parameters.....	47
Table 18 Summary of Average Altitudes, Percentages and Distances.....	71
Table 19 Seabed gradient classification.....	86
Table 20 Sediment classification.....	87
Table 21 Seabed features classification.....	88
Table 22 Summary of the seismic units.....	91
Table 23 Summary of SSS and MBES contacts.....	138
Table 24 Contact confidence classification.....	138
Table 25 Summary of magnetic anomalies.....	139
Table 26 Summary of SBP Contacts.....	139
Table 27 Summary of wrecks observed inside the MMT OWF survey area.....	140
Table 28 List of horizons, grids and associated polygons present in the Kingdom Suite Project.....	150
Table 29 List of geohazards present in the Kingdom Suite Project.....	151
Table 30 Distribution of interpreted seismic units.....	153
Table 31 General characteristics of the large incisions within seismic unit U70.....	227
Table 32 Distribution of soft kick features within the survey area.....	294
Table 33 Grab sample summary.....	327
Table 34 Deliverables.....	336

ABBREVIATIONS AND DEFINITIONS

BSB	Below Seabed
CM	Central Meridian
DTU21	Denmark Technical University 2021
DPR	Daily Progress Report
DTM	Digital Terrain Model
DVR90	Dansk Vertikal Reference 1990
EEZ	Exclusive Economic Zone
EI	Energy Island
EPSG	European Petroleum Survey Group
ESRI	Environmental Systems Research Institute, Inc.
ETRS	European Terrestrial Reference System
FME	Feature Manipulation Engine
FMGT	Fledermaus GeoCoder Toolbox
GIS	Geographic Information System
GMSS	Geo Marine Survey Systems
GNSS	Global Navigation Satellite System
GRS80	Geodetic Reference System 1980
GS	Grab Sample / GeoSurveys
HF	High Frequency
HiPAP	High Precision Acoustic Positioning
INS	Inertial Navigation System
IHO	International Hydrographic Organisation
IMU	Inertial Measurement Unit
ITRF	International Terrestrial Reference Frame
LF	Low Frequency
LGM	Last Glacial Maximum
WP-A	Work Pack – Defines survey area and requirement
MAG	Magnetometer
MBBS	Multibeam Backscatter
MBES	Multibeam Echo Sounder
MIG	Migrated
MMO	Man Made Object
MSL	Mean Sea Level
MUL	Multiple Attenuated Stack
M/V	Motor Vessel
OWF	Offshore Wind Farm
POS MV	Position and Orientation System for Marine Vessels
POSPac	Position and Orientation System Package
PPS	Pulse Per Second
QC	Quality Control
ROTV	Remotely Operated Towed Vehicle
S-CAN	Scalgo Combinatorial Anti Noise
SBET	Smoothed Best Estimated Trajectory

SBP	Sub-Bottom Profiler
SOW	Scope of Work
SSS	Side Scan Sonar
STW	Speed Through Water
SVP	Sound Velocity Profile
THU	Total Horizontal Uncertainty
TPU	Total Propagated Uncertainty
TVU	Total Vertical Uncertainty
TWT	Two Way Time
UHRS	Ultra High Resolution Seismic
USBL	Ultra Short Baseline
UTC	Coordinated Universal Time
UTM	Universal Transverse Mercator
UXO	Unexploded Ordnance

EXECUTIVE SUMMARY

AREA OF INVESTIGATION, MMT OWF SURVEY AREA	
INTRODUCTION	
Survey Dates	M/V Relume: 01 May to 12 June 2021 M/V Northern Franklin: 11 June to 18 August 2021
Equipment	Multibeam Echo Sounder (MBES), Side Scan Sonar (SSS), Magnetometer (MAG), Innomar Sub-bottom Profiler (SBP), 2 Dimensional-Ultra High Resolution Seismic (2D-UHRS), Sediment Grab Samples (GS).
Coordinate System	Datum: European Terrestrial Reference System 1989 (ETRS89) Projection: Universal Transverse Mercator (UTM) Zone 32N, Central Meridian (CM) 9°E
BATHYMETRY AND SEAFLOOR MORPHOLOGY	
<p>The bathymetric survey recorded water depths across the MMT OWF survey area ranged between 25.75 m and 48.17 m (DTU21 MSL) with depth generally increasing from the west to the east across the site.</p> <p>The seabed has a range of natural topographic variability occurring throughout the site with extensive areas of mobile sediments present across much of the MMT OWF survey area. The mobile sediments range from smaller wavelength bedforms such as ripples, large ripples and megaripples to larger scale sediment bedforms such as sand waves and sandbars.</p>	
SURFICIAL GEOLOGY	
<p>The surficial geology in the MMT OWF survey area is dominated by Muddy SAND, GRAVEL and coarse SAND, and SAND.</p> <p>The GRAVEL and coarse SAND, and the SAND are more prominent in the eastern and western extents of the area. The muddy SAND is concentrated more in a central north-south running band within the survey area. Infrequent and isolated patches of MUD and SANDY mud are occasionally present in the eastern and western extents of the area.</p> <p>In areas of muddy SAND and MUD and SANDY mud, the seabed is usually featureless, whilst mobile bedforms occur mostly in areas of SAND or GRAVEL and coarse SAND.</p>	
SEAFLOOR FEATURES AND CONTACTS	
<p>A total of 64595 individual seabed contacts (61309 MBES contacts and 3286 SSS contacts) were detected within the MMT OWF survey area. They were classified as boulders (64130) and man-made objects such as debris (437), fishing equipment (11) and wire (4). 9 contacts were classified as other which includes possible sediment mounds. Three known wrecks were identified and one possible unknown wreck was observed. There are extensive boulder fields ranging from intermediate to high density throughout the survey area – only boulders over >1 m were select within boulder fields.</p> <p>A total of 773 magnetic anomalies were detected within the MMT OWF survey area. 513 of these were individual discrete anomalies, whilst 260 anomalies were interpreted to form 33 linear anomaly features. One of these linear anomalies corresponded to the database position of the buried TAT-14 cable.</p> <p>Extensive areas of mobile sediment are observed, ranging from smaller wavelength ripples, large ripples and megaripples to larger scale bedforms such as sand waves and sandbars. One large (160 m x 120 m x 9.5 m), isolated sediment mound was also observed.</p> <p>Evidence of trawling is found across much of the survey area.</p> <p>Occasional areas of interest have been identified as possible biogenic features. These areas have been assessed by a senior biologist who determined these areas of interest are unlikely to be biogenic in nature. The areas have maintained their feature in case further investigation to these areas is deemed necessary. These areas are more likely to be erosional features.</p>	

AREA OF INVESTIGATION, MMT OWF SURVEY AREA	
GEOLOGY	
The MMT OWF survey area is located within a complex geologic setting. The interpreted Ground Model is based on twelve horizons that correspond to erosive surfaces and make up the base of the seismostratigraphic units.	
U05 (Holocene)	The uppermost unit (U05) is occasionally present on top of U10 and consists of fine-grained mobile sediments.
U10 (Holocene)	Unit (U10) is present at the seabed for the majority of the survey area and consists of marine Holocene sand deposits. A localised internal reflector was interpreted within U10 defined as H10i (internal). H10i is a discontinuous reflector which usually highlights the boundary between transparent and non-transparent facies within U10.
U20	Infills of small basins and channels, likely in a restricted marine-tidal setting, partially associated to a subaerial fluvial system.
U25	Fine sediments: fine sands-silts (?) deposited in a relatively low-energetic setting, possibly a transgressive estuary.
U30	Fining-upward sequence, likely fluvial in nature.
U35	High energy fluvial bedforms (flash floods?), interpreted to consist of gravel and sands with enclaves of coarser-grained clasts, fining-upward (?)
U40	Drainage system of glacial melt back from the north, and outwash plains, with variable sediment content. Glacial period (Weichselian?)
U50	Fine sediment deposits with boulders, possibly related to glacial drift deposit (aqua till?) or glaciolacustrine deposition (?). Glacial period (Weichselian?)
U60	High energy fluvial bedforms (flash floods?) comprising mainly sands with gravel and silt (?).
U70	Glaci-fluvial deposition, in a proglacial, sub-aerial environment (reoccupation of tunnel valley depressions by fluvial systems?), with variable sediment content. Glacial period (Weichselian?)
UKS (A)	Deformed deposits of variable sediment content. Glaciotectonism (Weichselian?):
U85	High energy fluvial (possibly outwash plain?), composed of mainly sands with gravel and silt (?). Organic-rich muds at the base.
U90	Fan delta deposits comprising mainly sands and fine sediments.
UKS (B)	Deformed deposits of variable sediment content. Glaciotectonism (Saalian?):
Base Seismic Unit	Pre-quaternary sequence – marine clays, silts to sands.
SEABED AND SUB-SEABED HAZARDS	
Seabed gradients	Slope angles across the site are typically very gentle (<1°) and gentle (1° to 5°). Despite the fact that large bedforms such as sand waves and sandbars constitute a large portion of the survey area; the seafloor topography is typically gently undulating. Areas of moderate to very steep slopes are largely restricted to the edges of bedforms and the lee slopes of the most defined sand waves. Very steep slope angles (15° to a maximum of 42°) are associated with boulders, the edges of depressions and steep banks on the western side of the Artificial Island area of investigation. Slope angles up to 56° were observed, but were associated with known wrecks in the MMT OWF survey area.
Mobile seabed sediments	Mobile sediments are present frequently throughout the surveyed area. The mobile sediments comprise of ripples, megaripples, large ripples, sand waves as well as larger scale sediment accumulations forming sandbars.

AREA OF INVESTIGATION, MMT OWF SURVEY AREA	
Wreck	<p>Three known wrecks were detected during the survey, correlating with the background information; Wreck_94 (S_RE_B01_0324) was found at 347322.99 m E, 6253311.32 m N; Submarine HMS Tarpon Wreck_86 (S_FR_B03_0006) was found at 348875.51 m E, 6284050.96 m N; Wreck_85 (S_FR_B03_0069) was found at 349881.86 m E, 6284268.86 m N.</p> <p>One possible unknown wreck (S_RE_B05_0547) was observed at 358715.58 m E, 6272109.03 m N.</p>
Cable	There is one buried cable (TAT-14) crossing the southern end of the survey area shown in the background data and detected in the MAG and SBP data.
Pipeline	According to available background data, there are no known pipelines in the area. No pipelines were observed in the survey area.
Sediment deformation	<p>Areas of tectonization/deformation have been observed predominately within UKS. The origin of these deformed deposits is interpreted to be mainly glacial tectonics, but locally may be related to salt tectonics (see section 5.c) and gravitational deformation.</p> <p>Deformed deposits have geotechnical significance given their complex stress/load histories. Faults are present ubiquitous within the subsurface, and do not greatly affect sediments younger than U20.</p>
Buried channels and tunnel valleys	<p>Buried channels occur throughout the site. The more relevant erosive events that carved these channels correspond to the unit bases of U40, U60, and U70.</p> <p>A potential geo-hazard related with the channels is the sharp contrasts in physical properties between the channel infill and surrounding units.</p>
Soft sediments and organic-rich deposits	High-amplitude, negative impedance features occur within seismic units U10 to U50, and U85. These features are interpreted to be fine sediments, most likely organic-rich muds due to their strong negative acoustic impedance.
Coarse sediments/gravel beds/boulders/tills	Coarser material, such as boulder accumulations, cobbles, and gravel lags are present in glacial deposits in the site, as well as in unit U35. These are potential hazards and may constitute a constraint on drilling and other operations.
Fluid flow and gas features	No unambiguous seismic anomalies suggesting the presence of detectable gas in the subsurface were identified in the UHRS and SBP data. However rare, localised features were identified that may be related to upward fluid migration within the sub-surface.
Lacustrine sediments	Lacustrine deposits were identified in the area, typically associated to unit U40.

1 | INTRODUCTION

1.1 | PROJECT INFORMATION

Energinet are developing the proposed Offshore Wind Farm (OWF) and Artificial Island in the Danish sector of the North Sea (Figure 1). MMT have been contracted to provide geophysical survey (including 2D UHRS) and grab sampling in the east part of the 3 GW OWF project site (the MMT OWF survey area).

The project includes various survey areas which are detailed in Table 1 and shown in Figure 1.

The scope of work was divided into separate Work Packages (WP), detailed in Table 2.

This report covers Work Package A – Offshore Windfarm, MMT OWF survey area (the east part of the 3 GW OWF project site).

Table 1 Survey area details.

Description	Comment
3 GW OWF Project Site	Complete project site area, including both the western and eastern zones.
3 GW OWF Area of Investigation	MMT OWF survey area (eastern part of the 3 GW OWF project site)
Artificial Island Area of Investigation	10 km x 10 km area around the Artificial Island Project Site
Artificial Island Project Site	2.5 km x 2.5 km focused area for detailed development of the Artificial Island.

Table 2 Work Package descriptions.

	Description	Survey Area
Work Package A – Offshore Windfarm	Geophysical site survey	MMT OWF survey area (zone east).
Work Package A – Energy Island	Geophysical site survey	Artificial Island Area of Investigation.
Work Package B	Magnetometry box survey	Box surveys within the MMT OWF survey area.
Work Package C	UHR seismic survey	Artificial Island Project Site.
Work Package D	UXO survey and inspection	Artificial Island Project Site.

A summary of the project details is presented in Table 3.

Table 3 Project details.

CLIENT:	Energinet
PROJECT:	Energy Islands - North Sea
MMT SWEDEN AB (MMT) PROJECT NUMBER:	103783
SURVEY TYPE:	Geophysical and Grab Sample offshore windfarm site survey
AREA:	Danish North Sea

SURVEY PERIOD:	May – August 2021 (covers the MMT OWF survey area and Artificial Island survey area)
SURVEY VESSELS:	M/V Northern Franklin, M/V Relume
MMT PROJECT MANAGER:	Karin Gunnesson
CLIENT PROJECT MANAGER:	Jens Colberg-Larsen / Martin Bak Hansen

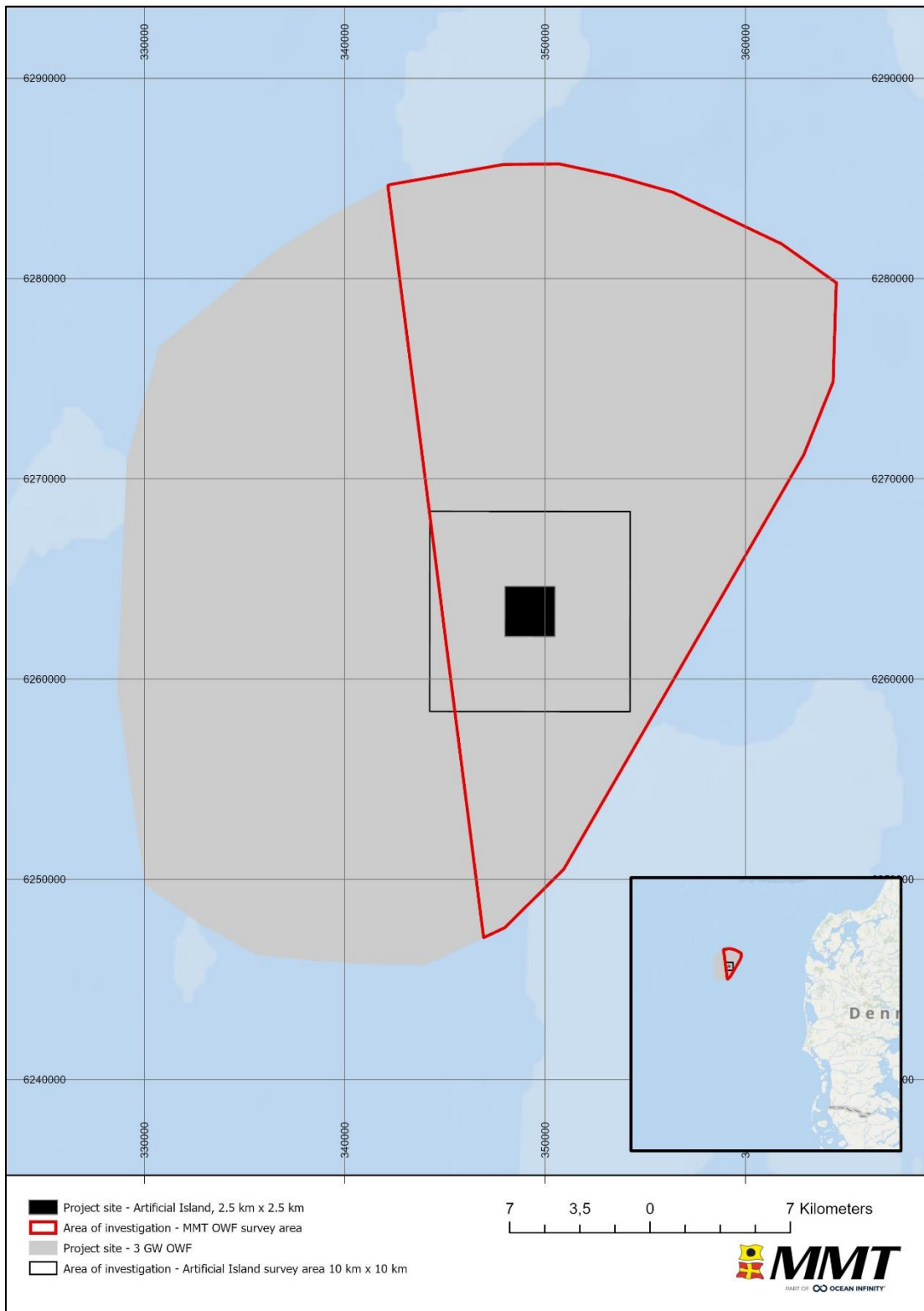


Figure 1 Overview of survey scopes performed

1.2 | SURVEY INFORMATION - MMT OWF AREA

The MMT OWF survey area work scope comprises several tasks including:

- Project Management and Administration
- Geophysical surveys (MBES, SSS, SBP, MAG)
- 2D UHRS Survey
- Grab Sampling

The MMT OWF (zone East) Wind Farm site investigation covers an approximately 526 km² area acquired by MMT and is located roughly 90 km offshore the coast of Jutland (Figure 1).

This report covers the geophysical survey of the MMT OWF survey area (the east part of the 3 GW OWF project site) with integrated grab sample data results (Appendix C). This report also integrates the 2D UHRS survey dataset acquired by GeoSurveys Ltd (Appendix D).

1.3 | SURVEY OBJECTIVES

The survey objectives for this project were to acquire bathymetric soundings, magnetometer, side scan sonar and sub-seabed geological information within the MMT OWF survey area. The acquisition of these datasets was to provide comprehensive bathymetric soundings, seabed features maps including contact listings and shallow geological information to inform a ground model and mapping of magnetic anomalies. The interpretation of the datasets was charted and reported to inform cable route micro-routing and subsequent engineering.

The main objectives with the surveys were:

- Acquire and interpret high quality seabed and sub-seabed data for project planning and execution. As a minimum, this includes local bathymetry, seabed sediment distribution, seabed features, seabed obstructions, wrecks and archaeological sites, crossing cables and pipelines and evaluation of possible mobile sediments
- Sub-bottom profiling and 2D UHRS survey along the survey lines to map shallow geological units.
- Mapping of magnetic targets and to identify infrastructure crossings and large metallic debris.
- Ground truthing grab samples were acquired in order to aid the surficial interpretation of seabed sediments.

1.4 | SCOPE OF WORK - OWF SURVEY AREA

GEOPHYSICAL SITE SURVEY

A geophysical site survey including 2D UHR seismic survey shall be performed with commencement in 2021 and completion as soon as possible. The survey shall have full coverage in the area of investigation. The survey must map the bathymetry, the static and dynamic elements of the seabed surface and the sub-surface geological soil layers to at least 100 m below seabed.

1.4.1 | DEVIATIONS TO SCOPE OF WORK

2D UHRS AND GEOPHYSICAL SURVEY (M/V NORTHERN FRANKLIN AND M/V RELUME)

During the geophysical survey there were no deviations from the original SOW.

GEOPHYSICAL SURVEY AND GRAB SAMPLING (M/V NORTHERN FRANKLIN)

During the geophysical survey there were 2 deviations from the original SOW (Table 4).

Table 4 Deviations from the SOW during survey (M/V Northern Franklin).

Date	Description	Decision/Result/Conclusion
2021-08-10	Reduced Scope of work	Due to forecasted poor weather, Energinet decided to only infill 100% coverage in pycnocline areas and reduce sample amount.
2021-08-11	Reduced Scope of work	Due to forecasted poor weather, Energinet agreed to reduce the remaining GS number from 80 to approximately half in order to maximise the weather window.

1.5 | PURPOSE OF DOCUMENT

This report details the interpretation of the geophysical survey and grab sample results from the MMT OWF survey area.

The report summarises the conditions within the survey area with regards to; bathymetry, surficial geology and seabed features, contacts and anomalies, existing infrastructure, and subsurface geology. Geo-hazard identification and interpretation has also been considered.

All data obtained from the geophysical survey and grab sample results have been correlated with each other and compared against the existing background information, in order to ground-truth the survey results.

Separate reports include the Artificial Island Area of Investigation Geophysical Survey Report and Operations reports. A full list of reports is given in Table 5 (Reference Documents).

1.6 | REPORT STRUCTURE

The results from the MMT OWF and Artificial Island survey campaign are presented in two separate reports.

- Geophysical Survey Report (this report) – Includes a chart series of results. A full chart list is provided within Appendix A|.
- Operations Report – Covering the field operations conducted.

The Geophysical Survey Report (this report) chart series includes:

- Overview Chart
- Trackline Charts
- Bathymetry Charts
- Backscatter Mosaic Charts
- Seabed Geology Classification Charts
- Seabed Substrate Type Classification Charts
- Seabed Morphology Classification Charts
- Seabed Objects Charts

- Seabed Features Charts
- Sub-Seabed Geology Charts (Isopach)
- Sub-Seabed Geology Profile Charts (34 across the site)

1.6.1 | GEOPHYSICAL SURVEY REPORT

Attached to the report are the following appendices:

- Appendix A| List of Produced Charts
- Appendix B| Contact and Anomaly List
- Appendix C| Grab Sample Lab Report
- Appendix D| 2D UHRS Processing Report

1.6.2 | CHARTS

The MMT Charts describe and illustrate the results from the survey. The charts include an overview chart with a scale of 1:65 000, north up charts at a scale of 1:10 000 and longitudinal profile charts with a horizontal scale of 1:10 000 and a vertical scale of 1:500.

The overview and north up charts contain background data (existing infrastructure, Exclusive Economic Zones (EEZ), 12 nautical mile zone and wreck database) alongside survey results.

A list of all produced charts is presented in Appendix A|.

OVERVIEW CHART

Shows coastlines, EEZ, large scale bathymetric features and area of investigations.

TRACKLINE CHARTS

The actual performed survey lines are presented along with seabed grab sampling positions.

BATHYMETRY CHARTS

The bathymetry is presented as a shaded relief colour image with 1 m colour interval, overlain with contour lines (1 m (minor) and 5 m (major)) with depth labels.

BACKSCATTER MOSAIC CHARTS

The backscatter mosaic imagery is presented.

SEABED SURFACE GEOLOGY CLASSIFICATION CHARTS

The surface geology is divided into 4 different classes; MUD and sandy MUD, Muddy SAND, SAND, GRAVEL and coarse SAND and are presented as solid hatches.

SURFICIAL MORPHOLOGY CHARTS

The surface morphology is divided into 10 different classes; Ripples, Large Ripples, Megaripples, Sand Waves, Sandbars, Sediment Mound, Area of Interest, Trawl Mark Area and Boulder Fields (intermediate and high density) and are presented as hatches with patterns.

SURFICIAL SUBSTRATE CHARTS

The substrate charts are divided in to six classes as per the Danish Råstof-bekendtgørelsen (BEK no. 1680 of 17/12/2018, Phase IB).

- Substrate type 1a - Sand, soft silty bottom
- Substrate type 1b – Sand, solid sandy bottom
- Substrate type 2a - Sand, gravel and pebbles, few larger stones
- Substrate type 2b - Sand, gravel and pebbles, seabed cover of larger stones 1% to 10%
- Substrate type 3 - Sand, gravel and pebbles, seabed cover of larger stones 10% to 25%
- Substrate type 4 – Stony areas and stone reefs, seabed cover of larger stones 25% to 100%

SEABED OBJECTS CHARTS

The SSS, MBES and magnetic contacts and linear features are presented.

SEABED FEATURES CHARTS

The seabed features are divided into 11 different classes; Ripples, Large Ripples, Megaripples, Sand Waves, Sandbars, Sediment Mound, Area of Interest, Trawl Mark Area and Boulder Fields (intermediate and high density) and are presented as hatches with patterns

The SSS, MBES and magnetic contacts are also presented.

SUB-SEABED GEOLOGY CHARTS

Depth below seabed (BSB) for each interpreted horizon is presented as a gridded surface with contour lines and depth labels at 1 m interval.

SUB-SEABED GEOLOGY PROFILE CHARTS

A total of 35 profile charts shows the interpretation of the horizons and structures across the site.

1.7 | REFERENCE DOCUMENTS

The documents used as references to this report are presented in Table 5.

Table 5 Reference documents.

Document Number	Title	Author
1100046209	Proposed Artificial Island Danish North Sea Geoarchaeology and geological desk study	From Client
103783-ENN-MMT-QAC-PRO-PROJMANU-06	Project Manual	MMT
103783-ENN-MMT-QAC-PRO-CADGIS	CAD and GIS Specification	MMT
103783-ENN-MMT-MAC-REP-FRANKLIN-A	Mobilisation and Calibration Report – Northern Franklin	MMT
103783-ENN-MMT-MAC-REP-RELUME-A	Mobilisation and Calibration Report – Relume	MMT
103783-ENN-MMT-SUR-REP-OPREPWPA-REVA	Operations Report WP-A (OWF survey area)	MMT
103783-ENN-MMT-SUR-REP-SURWP AEI	Artificial Island Area of Investigation Geophysical Survey Report	MMT

1.8 | AREA LINE PLAN

The survey line spacing and minimum parameters in the MMT OWF survey area are detailed in Table 6.

A breakdown of the survey lines is provided in Table 7, and described in Sections 1.8.1|, 1.8.2| and 1.8.3|.

Table 6 Survey line parameters.

GEOPHYSICAL SURVEY SETTINGS	SCOPE
Investigation area	Ca. 526 km ²
Line spacing Geophysical Main Lines	70 m
Line spacing Geophysical and 2D UHRS Main Lines	210 m
Line spacing Geophysical and 2D UHRS Cross Lines	1000 m

Table 7 Survey line breakdown.

SURVEY LINE BREAKDOWN	SCOPE	ACTUAL SURVEYED
Geophysical Main Lines (Northern Franklin)	5018.3 km/206 Lines	5018.3 km/206 Lines
Geophysical Infill Lines (Northern Franklin)	N/A	224.9 km/157 Lines
2D UHRS Main Lines (incl. in geophysical main lines) (Relume)	2427.3 km/100 Lines	2427.3 km/100 Lines
2D UHRS Reference Main Lines (Relume)	101.1 km/4 Lines	101.1 km/4 Lines
2D UHRS Reference Cross Lines (Relume)	126.5 km/5 Lines	126.5 km/5 Lines
Geophysical and 2D UHRS Cross Lines (Relume)	444.3 km/33 Lines	444.3 km/33 Lines
Geophysical and 2D UHRS Infill Lines (Relume)	N/A	98.3 km/14 Lines
Geophysical Totals	8117.5 km/348 Lines	8440.7 km/519 Lines
2D UHRS Totals	3099.2 km/142 Lines	3197.5 km/156 Lines

Note: All 2D UHRS lines also had MBES, SSS, SBP Innomar and MAG acquired simultaneously.

1.8.1 | 2D UHRS REFERENCE LINES

Reference lines were surveyed to acquire a representative 2D UHRS seismic dataset of the MMT OWF survey area. All 2D UHRS lines also had geophysical MBES, SSS, SBP Innomar and MAG acquired simultaneously. The reference lines were selected from the seismic mainline dataset (4 mainlines and 5 intersecting crosslines). The dataset formed the bases of the first 2D UHRS stratigraphic model used as an interpretation guide for the entire project.

The reference lines were acquired following mobilisation and survey verification, to enable maximum time for review. A framework and strategy were then agreed with the Client prior to further interpretation

Reference lines are illustrated in Figure 2.

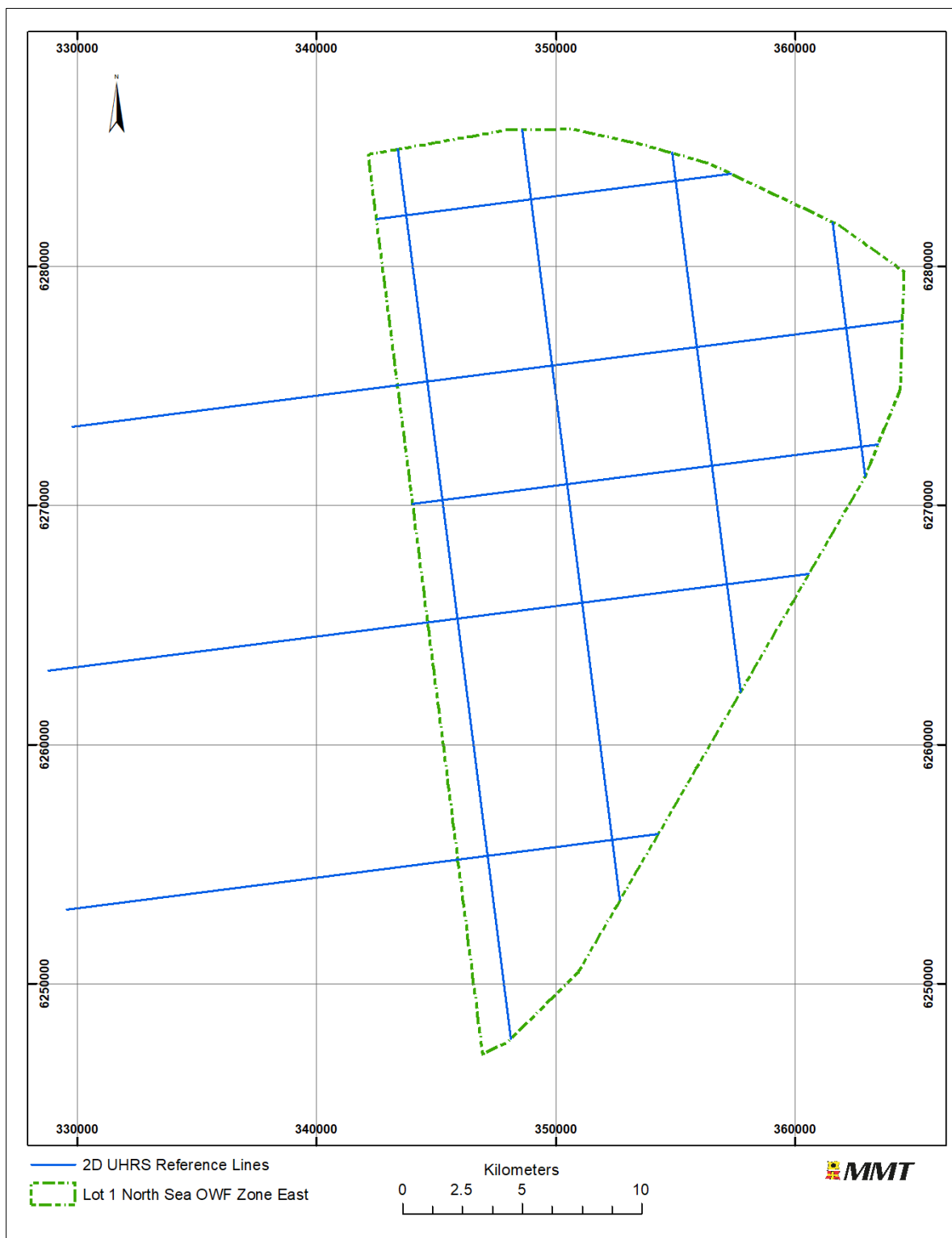


Figure 2 Line plan – 2D UHRS reference lines (including geophysical data).

1.8.2 | 2D UHRS MAIN AND CROSS LINES

The OWF survey area included 2D UHRS main lines (orientated north to south) and cross lines (orientated west to east). All 2D UHRS lines also had geophysical MBES, SSS, SBP Innomar and MAG acquired simultaneously.

2D UHRS main lines and cross lines are illustrated in Figure 3.

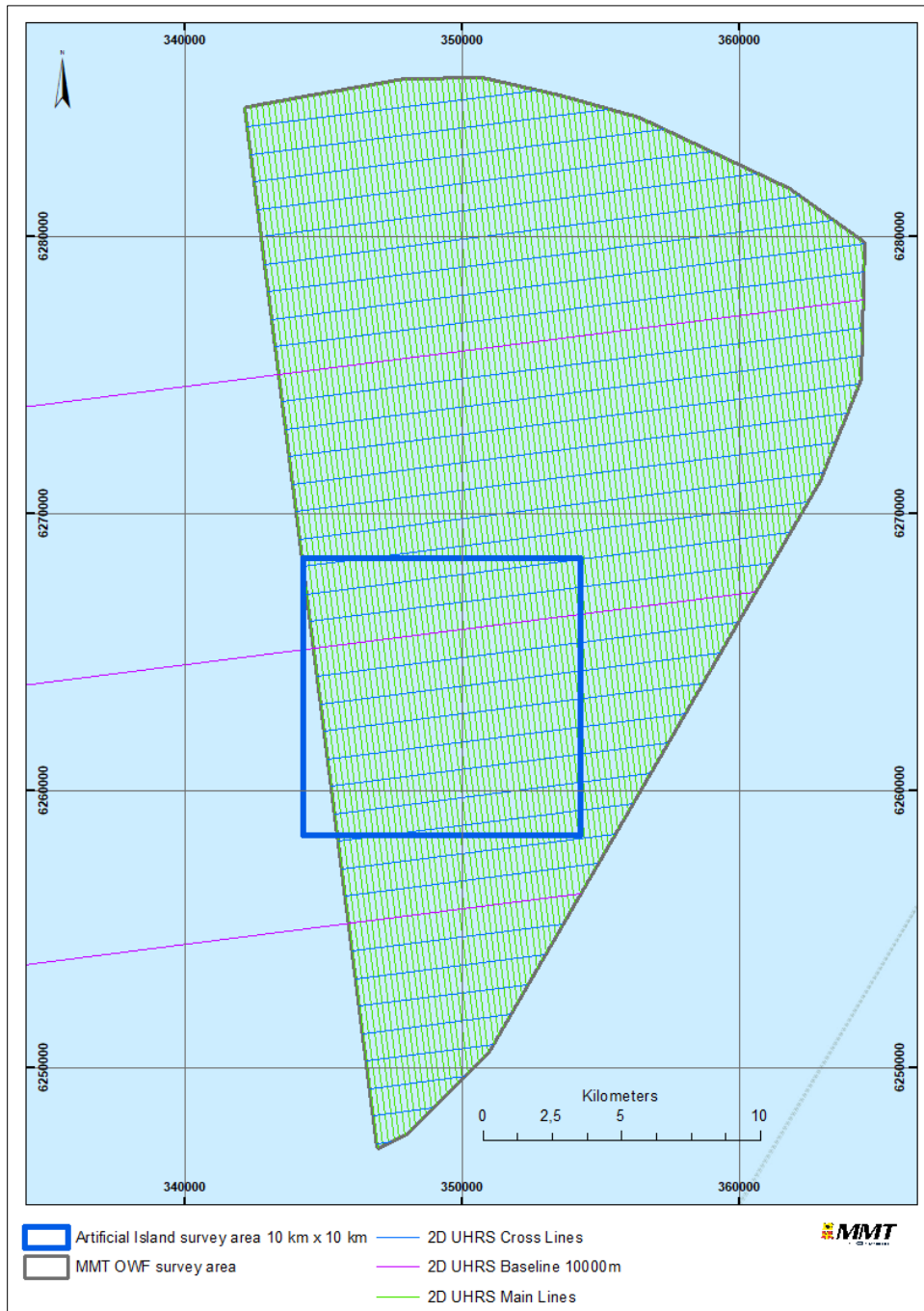


Figure 3 Line plan – 2D UHRS main and cross lines (including geophysical data).

1.8.3 | GEOPHYSICAL MAIN AND CROSS LINES

The MMT OWF survey area included geophysical main lines (orientated north to south) and cross lines (orientated west to east).

Geophysical main lines and cross lines are illustrated in Figure 4.

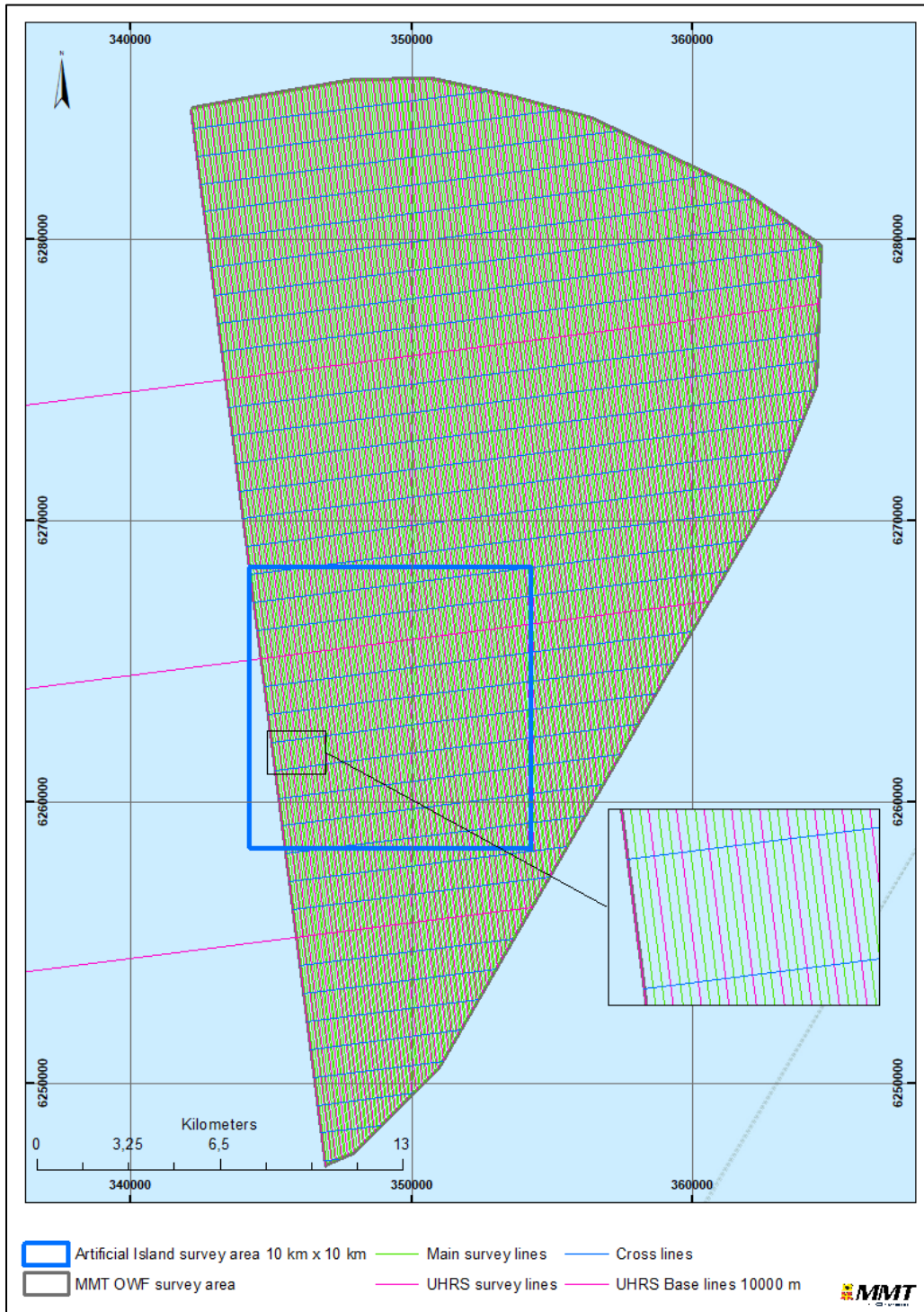


Figure 4 Line plan - geophysical main and cross lines.
All UHRS lines also had geophysical sensors recorded concurrently.

1.8.4 | SURVEY BLOCKS

To facilitate survey data management and survey planning, and to allow the fishing community to plan around the survey work, MMT OWF survey area was divided into 22 blocks. These included six blocks for the main lines (BM1 to BM6) and four blocks for the cross lines (BX1 to BX4) and are shown in Figure 5. Reporting tiles were also used to aid when describing specific areas (Figure 6).

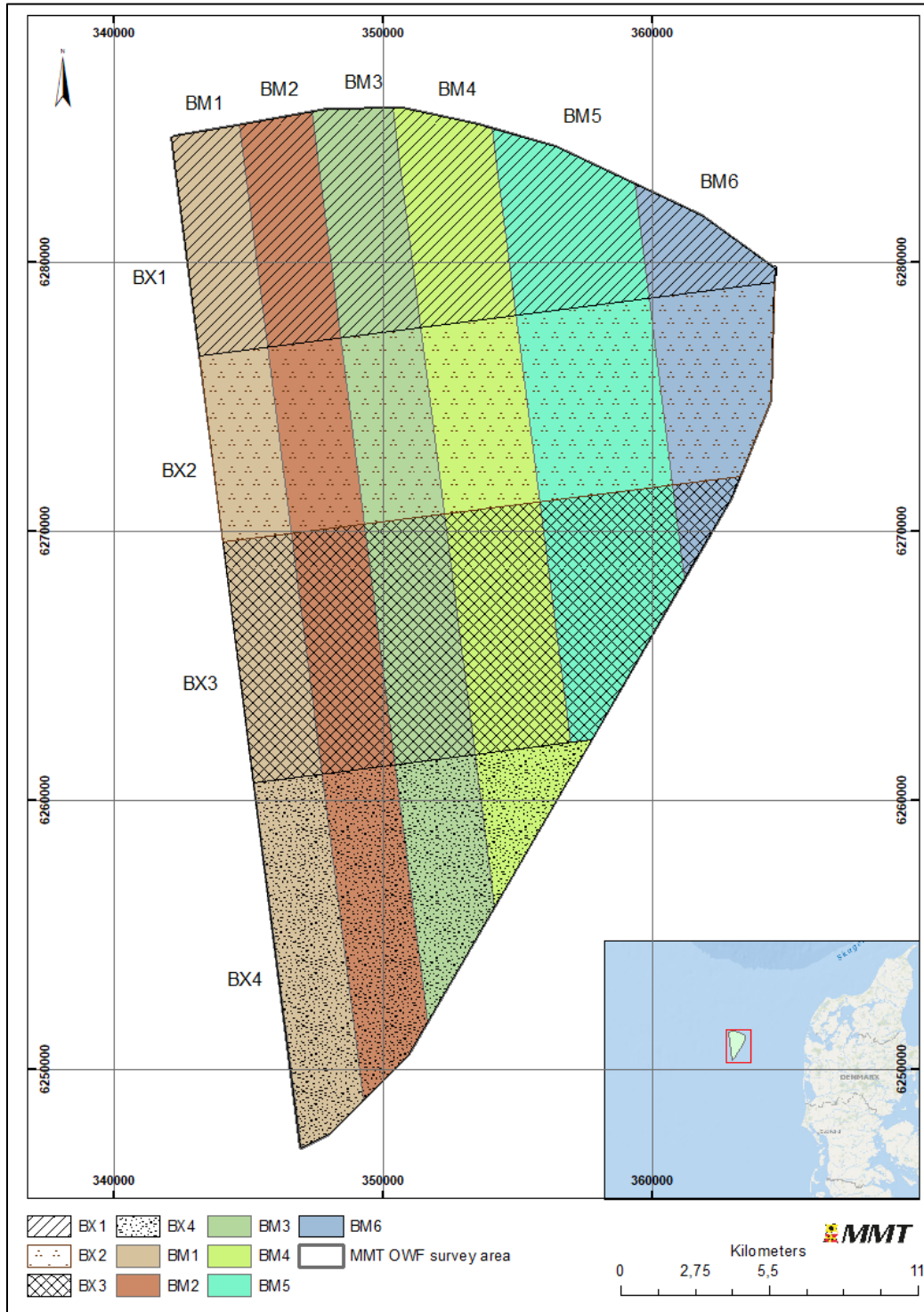


Figure 5 Overview of survey block divisions.

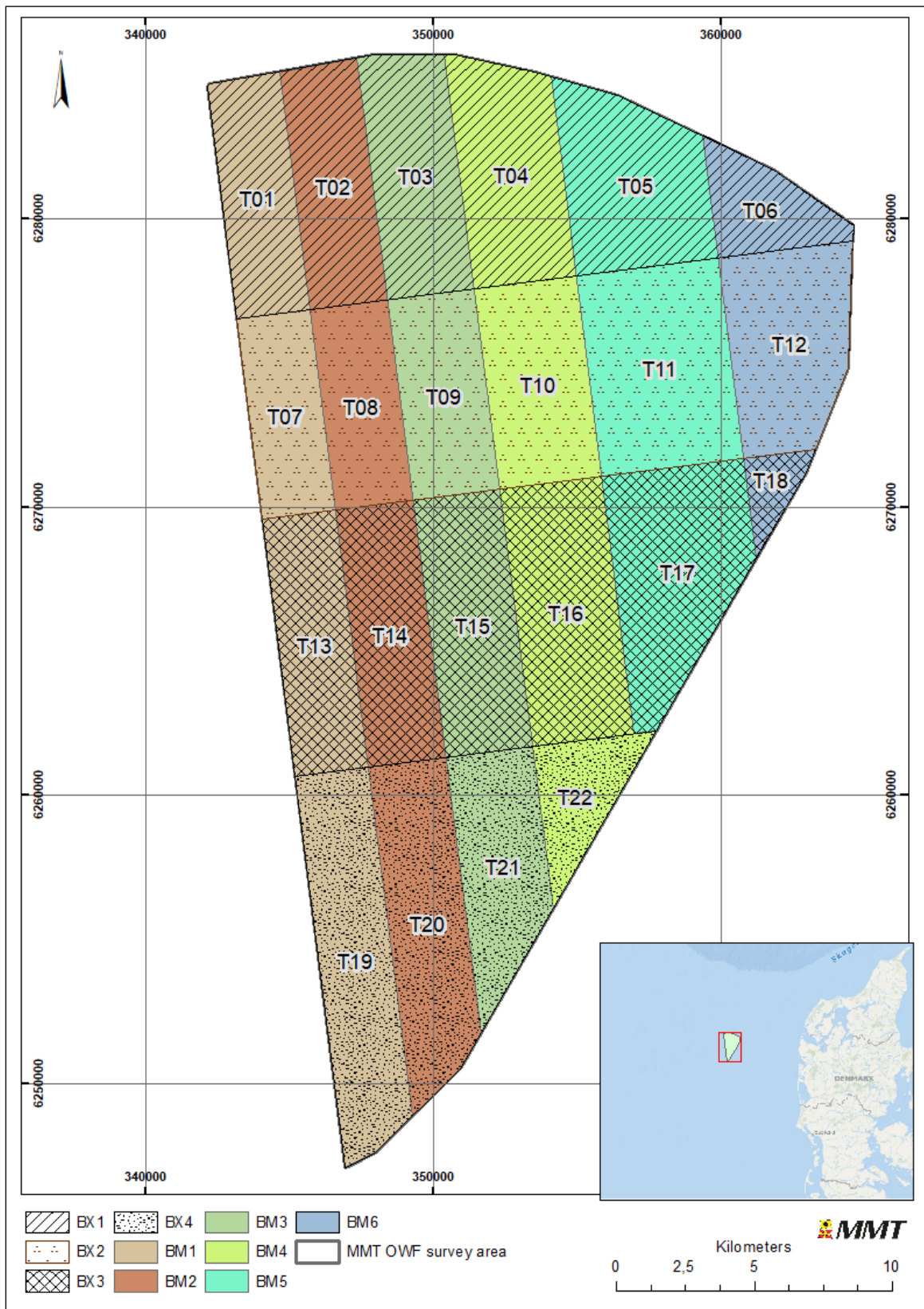


Figure 6 Overview of the reporting tiles.

2 | SURVEY PARAMETERS

2.1 | GEODETIC DATUM AND GRID COORDINATE SYSTEM

2.1.1 | ACQUISITION

The geodetic datum used for survey equipment during acquisition are presented in Table 8.

Table 8 Geodetic parameters used during acquisition.

Horizontal datum: WGS 84	
Datum	World Geodetic System 1984
ESPG Datum code	6326
Spheroid	World Geodetic System 1984 (7030)
Semi-major axis	6 378 137.000m
Semi-minor axis	6 356 752.3142m
Inverse Flattening (1/f)	298.257223563

2.1.2 | PROCESSING

The geodetic datum used during processing and reporting are presented in Table 9.

Table 9 Geodetic parameters used during processing.

Horizontal datum: European Terrestrial Reference System 1989 (ETRS89)	
Datum	ETRS89
European Petroleum Survey group (EPSG) Datum Code	25832
Spheroid	GRS80
Semi-major axis	6 378 137.000m
Semi-minor axis	6 356 752.314m
Inverse Flattening (1/f)	298.257222101

2.1.3 | TRANSFORMATION PARAMETERS

The transformation parameters used to convert from acquisition datum (WGS 84) to processing/reporting datum (ETRS89) are presented in Table 10.

Table 10 Transformation parameters.

DATUM SHIFT FROM WGS 84 TO ETRS89 (RIGHT-HANDED CONVENTION FOR ROTATION - COORDINATE FRAME ROTATION)	
PARAMETERS	EPOCH 2021.5
Shift dX (m)	0.10665
Shift dY (m)	0.06613
Shift dZ (m)	-0.12873
Rotation rX (")	-0.003409

DATUM SHIFT FROM WGS 84 TO ETRS89 (RIGHT-HANDED CONVENTION FOR ROTATION - COORDINATE FRAME ROTATION)	
Rotation rY (")	-0.014065
Rotation rZ (")	0.025207
Scale Factor (ppm)	0.0032

In order to verify that the transformation parameters have been correctly entered into the navigation system the following test coordinates were used (Table 11).

Table 11 Official test coordinates

UTM Zone	Datum	Easting (m)	Northing (m)	Latitude	Longitude
32	WGS84	-	-	56° 33' 00.000" N	6° 33' 00.000" E
	ETRS 89	349393.437	6269982.594	56° 32' 59.981" N	6° 32' 59.970" E

2.1.4 | PROJECTION PARAMETERS

The projection parameters used for processing and reporting are presented in Table 12.

Table 12 Projection parameters.

Projection Parameters	
Projection	UTM
Zone	32 N
Central Meridian	09° 00' 00" E
Latitude origin	0
False Northing	0 m
False Easting	500 000 m
Central Scale Factor	0.9996
Units	metres

2.1.5 | VERTICAL REFERENCE

The vertical reference parameters used for processing and reporting are presented in Table 13.

Table 13 Vertical reference parameters.

Vertical Reference Parameters	
Vertical reference	MSL
Height model	DTU21

The difference between the vertical height models (DTU21 and DVR90) are given below in Table 14. The average for each 5km MBES grid was compared.

Table 14 Average Height comparison between DTU21 and DVR90.

AVE HEIGHT DTU21 MSL (METRES)	AVE HEIGHT DVR90 MSL (METRES)	DIFFERENCE (METRES)
40.64	40.92	0.28

2.2 | VERTICAL DATUM

Global navigation satellite system (GNSS) tide was used to reduce the bathymetry data to Mean Sea Level (MSL) the defined vertical reference level (Figure 7). The vertical datum for all depth measurements was MSL via DTU21 MSL Reduction from WGS84-based ellipsoid heights.

This tidal reduction methodology encompasses all vertical movement of the vessel, including tidal effect and vessel movement due to waves and currents. The short variations in height are identified as heave and the long variations as tide.

This methodology is very robust since it is not limited by the filter settings defined online and provides very good results in complicated mixed wave and swell patterns. The vessel navigation is exported into a post-processed format, Smoothed Best Estimated Trajectory (SBET) that is then applied onto the multibeam echo sounder (MBES) data.

The methodology has proven to be very accurate as it accounts for any changes in height caused by changes in atmospheric pressure, storm surge, squat, loading or any other effect not accounted for in a tidal prediction.

Within the OWF survey area, all positions below the sea surface are referred to as **depths** in the results section of this report.

The bathymetric processing software packages EIVA NaviModel and Caris HIPS inherently stores MBES DTMs and sounding data with a positive down depth convention. Report imagery obtained from these packages show the data in this convention.

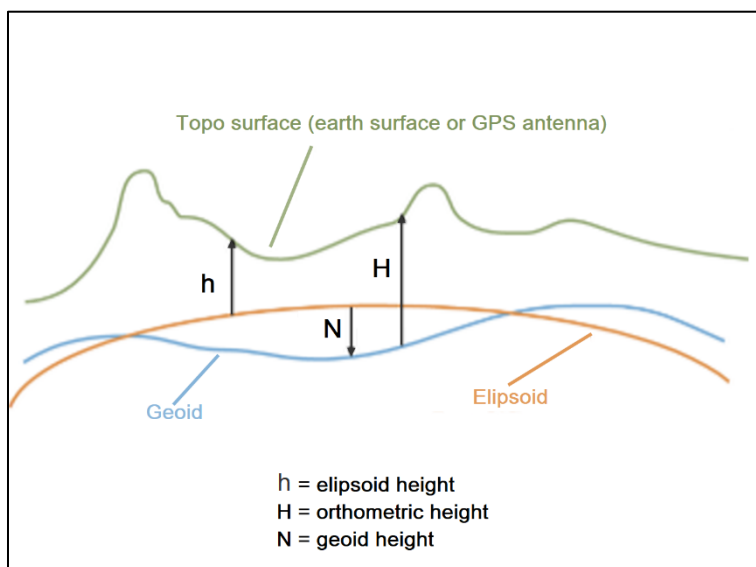


Figure 7 Overview of the relation between different vertical references.

2.3 | TIME DATUM

Coordinated universal time (UTC) is used on all survey systems on board the vessel. The synchronisation of the vessels on board system is governed by the pulse per second (PPS) issued by the primary positioning system. All displays, overlays and logbooks are annotated in UTC as well as the daily progress report (DPR) that is referred to UTC.

3 | SURVEY VESSELS

3.1 | M/V NORTHERN FRANKLIN

GEOPHYSICAL & ENVIRONMENTAL SURVEY OFFSHORE

Part of the offshore geophysical survey operation was conducted by the survey vessel M/V Northern Franklin (Figure 8). The vessel equipment is shown in Table 15.



Figure 8 M/V Northern Franklin.

Table 15 M/V Northern Franklin equipment.

INSTRUMENT	NAME
Navigational System	
Primary Positioning	Applanix POS MV 320 with C-NAV 3050 and C2 (SF2) corrections
Secondary Positioning	C-NAV 3050 and C2 (SF1) corrections
Primary Gyro and INS	Applanix POS MV 320
Underwater Positioning	iXSEA GAPS III
Surface Pressure Sensor	Vaisala Pressure Sensor
Survey Navigation Software	QPS QINSy 9.3.1
Sound Velocity	
Hull-mounted SV at MBES transducer	Valeport MiniSVS
Sound Velocity Profiler	Valeport SVX2
Geophysical Hull Mounted Equipment	
MBES	Kongsberg EM2040 Dual Head (EM2040D)
SBP	INNOMAR SES-2000 Medium 100
ROTV (towed)	
Primary Gyro and INS	iXsea Octans Nan / iXblue ROVINS
Sound Velocity Sensor	Valeport MiniSVS
Altimeter	Kongsberg MS1007
USBL transponders	iXsea MT8

INSTRUMENT	NAME
SSS	Edgetech 2200 300/600 kHz
Magnetometer	Geometrics G882
Geotechnical	
Grab sampler	Day Grab

3.2 | M/V RELUME

GEOPHYSICAL & ENVIRONMENTAL SURVEY OFFSHORE

Part of the offshore geophysical survey operation was conducted by the survey vessel M/V Relume (Figure 9). The vessel equipment is shown in Table 16.



Figure 9 M/V Relume.

Table 16 M/V Relume equipment.

INSTRUMENT	NAME
Navigational System	
Primary Positioning	Applanix POS MV 320 with C-NAV 3050 and C2 (SF2) corrections
Secondary Positioning	C-NAV 3050 and C2 (SF1) corrections
Tertiary Positioning	Veripos LD6 with Ultra corrections
Primary Gyro and INS	Applanix POS MV 320
Underwater Positioning	Kongsberg HiPAP 501 USBL
Surface Pressure Sensor	Vaisala Pressure Sensor
Survey Navigation Software	QPS QINSy v8.18.5
Sound Velocity	
Hull-mounted SV at MBES transducer	Valeport miniSVS
Sound Velocity Profiler	Valeport MIDAS SVX2, deployed over the side as MVP

INSTRUMENT	NAME
Geophysical Hull Mounted Equipment	
MBES	Kongsberg EM2040D (200-400 kHz)
SBP	Innomar Medium 100
ROTV (towed)	
Primary Gyro and INS	iXblue ROVINS
Sound Velocity Sensor	Valeport miniSVS
Altimeter	Kongsberg MS1007
DVL	LinkQuest NavQuest microDVL (600 kHz)
USBL transponders	Kongsberg MST 319
SSS	EdgeTech 2200 300/600 kHz
Magnetometer	Geometrics G882
2D UHRS System	
Sparker	Geo marine surveys systems B.V., 3 x Geo-Source stacked 200 LW
Streamer	Geo marine surveys systems B.V., Geo-Sense Ultra Hi-Res 96 channels

4 | DATA PROCESSING AND INTERPRETATION METHODS

4.1 | BATHYMETRY

The objective of the processing workflow is to create a Digital Terrain Model (DTM) that provides the most realistic representation of the seabed with the highest possible detail. The processing scheme for MBES data comprised two main scopes: horizontal and vertical levelling in order to homogenise the dataset and data cleaning in order to remove outliers.

The MBES data is initially brought into Caris HIPS to check that it has met the coverage and density requirements. It then has a post-processed navigation solution applied in the form of an SBET. The SBET was created by using post-processed navigation and attitude derived primarily from the POS M/V Inertial Measurement Unit (IMU) data records. This data is processed in POSpac MMS and then applied to the project in Caris HIPS.

In addition to the updated position data, a file containing the positional error data for each SBET is also applied to the associated MBES data. The positional error data exported from POSpac MMS contributes to the Total Horizontal Uncertainty (THU) and Total Vertical Uncertainty (TVU) which is computed for each sounding within the dataset. These surfaces are generated in Caris HIPS and are checked for deviations from the THU and TVU averages.

After the post-processed position and error data is applied, a Global Navigation Satellite System (GNSS) tide is calculated from the SBET altitude data which vertically corrects the bathymetry using the DTU21 MSL to GRS80 Ellipsoidal Separation model within Caris HIPS. The bathymetry data for each processed MBES data file is then merged together to create a homogenised surface which can be reviewed for both standard deviation and sounding density. Once the data has passed these checks it is ready to start the process of removing outlying soundings which can be undertaken within Caris HIPS or in EIVA NaviModel.

In the Caris HIPS workflow an average surface is derived from the sounding data and from this it is possible to remove outliers that lie at a specified numerical distance from the surface, or by setting a standard deviation threshold. Manual cleaning can also be performed using the Subset Editor tool to clean areas around features that would be liable to being removed by the automatic cleaning processes.

In the EIVA NaviModel workflow, the data is turned into a 3D model which undergoes further checks and data cleaning processes. Typically, a Scalgo Combinatorial Anti-Noise (S-CAN) filter is applied to the data to remove any outliers although some manual cleaning may also take place. This data cleaning is then written back to the data in the Caris HIPS project ready for Quality Check (QC).

In Caris HIPS the QC surfaces are recalculated to integrate any sounding flag editing that has occurred in NaviModel or within HIPS and examined to check that the dataset complies with the project specification. If the dataset passes this QC check, then products (DTMs, contours and shaded images) can be exported from either Caris HIPS or NaviModel for delivery or for further internal use.

The work flow diagram for MBES processing is shown in Figure 10.

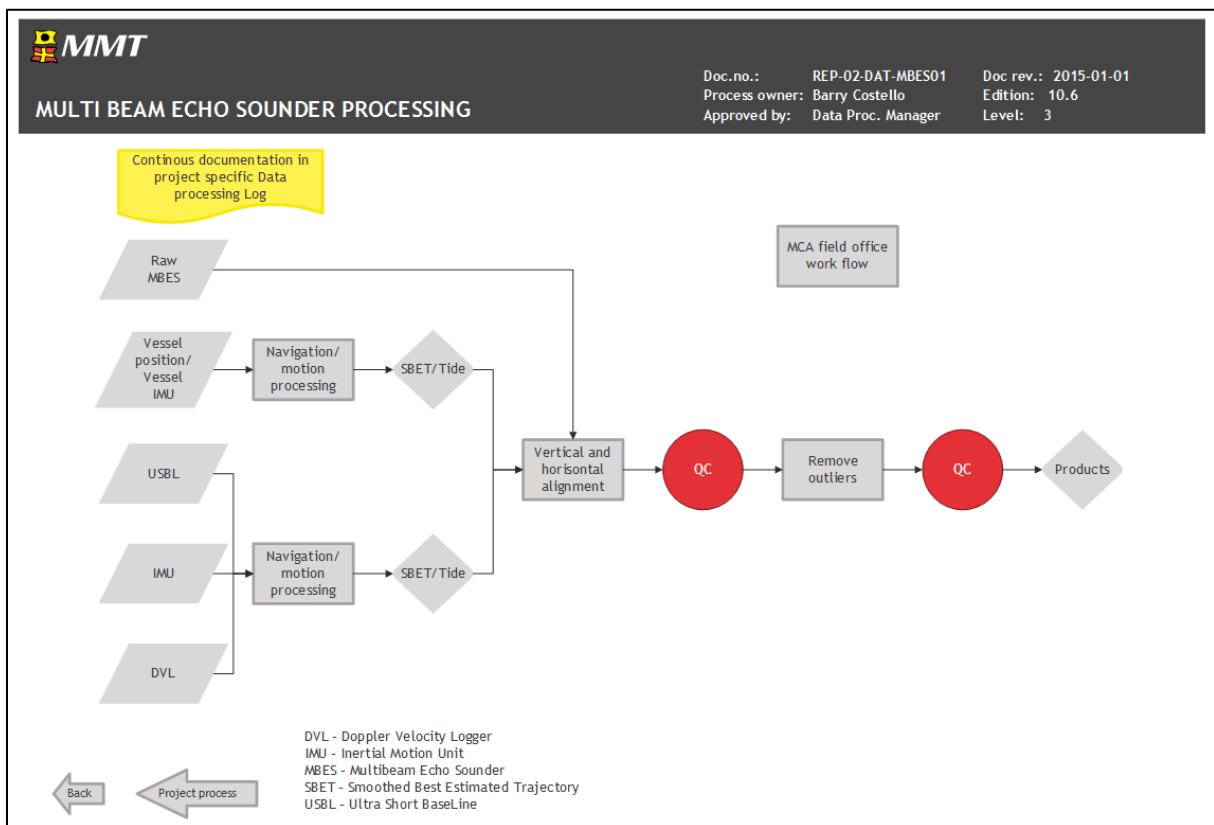


Figure 10 Workflow MBES processing.

The workflow outlines the processing that occurred on both M/V Relume and M/V Northern Franklin. Due to data acquisition requirements the M/V Northern Franklin acquired MBES data for the 2D UHRS component of the survey with M/V Relume completing the remaining Geophysical survey lines. In some instances, the vessels were processing survey lines that had no overlapping data from adjacent lines, so vertical alignment checks across the entire survey area during acquisition were not possible. During survey operations, once M/V Northern Franklin had completed the 2D UHRS scope, she became available to assist M/V Relume acquire the Geophysical Survey lines. An example of the pattern of survey line running can be seen in Figure 11. Here M/V Northern Franklin was able to complete overlapping survey lines in the far southwest corner with the alternating pattern of vessels covering the majority of the survey area shown.

Both datasets were combined in the office and QC steps followed to check for vertical alignment between each vessel's MBES data.

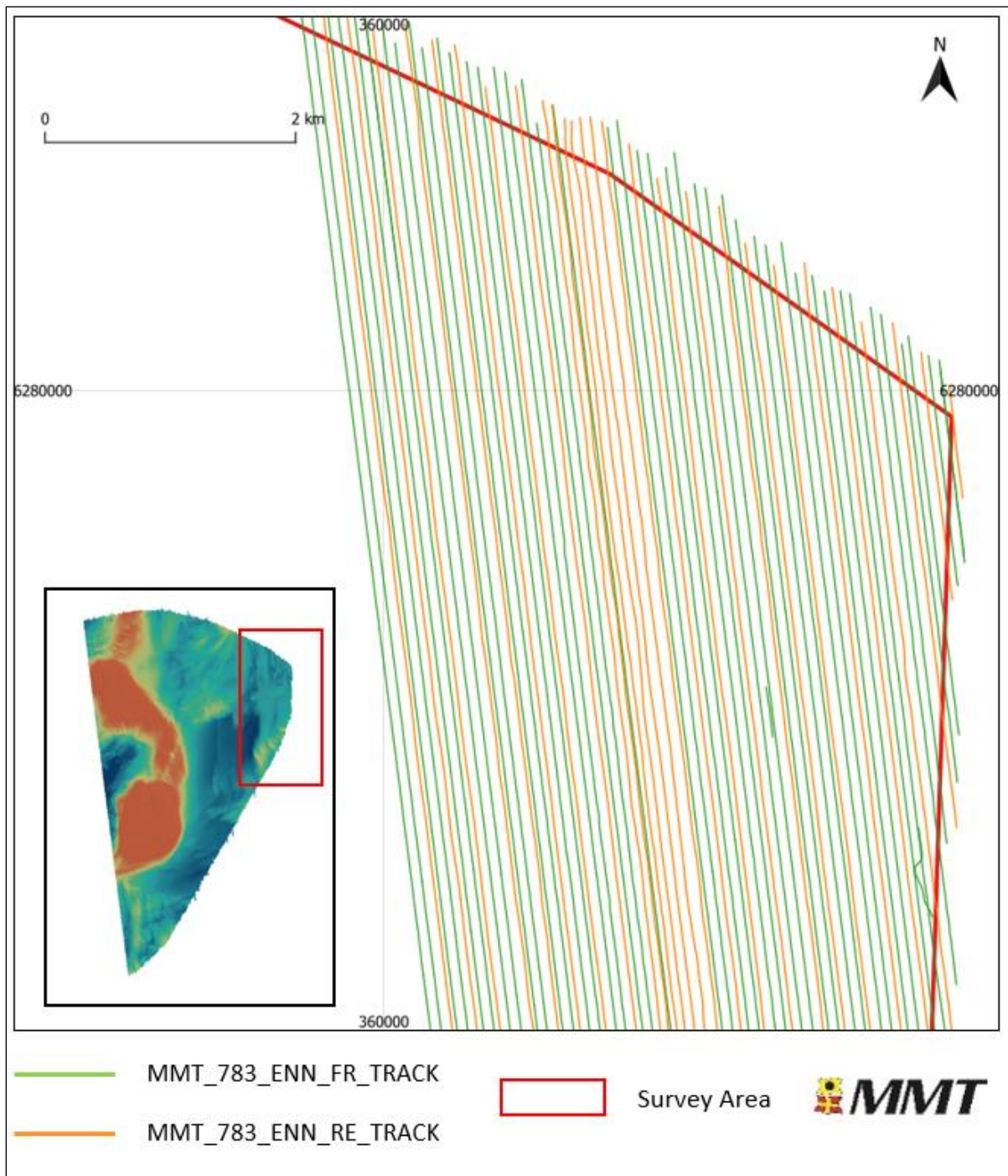


Figure 11 Example of division of MBES data acquisition in BM6.
M/V Relume (orange) and M/V Northern Franklin (green).

Bathymetric contours were generated from the 1 m DTM in combination with scaling factors applied to generalise the contours to ensure the charting legibility. The contour parameters used are shown in Figure 12 and an example of the exported contours presented over the DTM is shown in Figure 13.

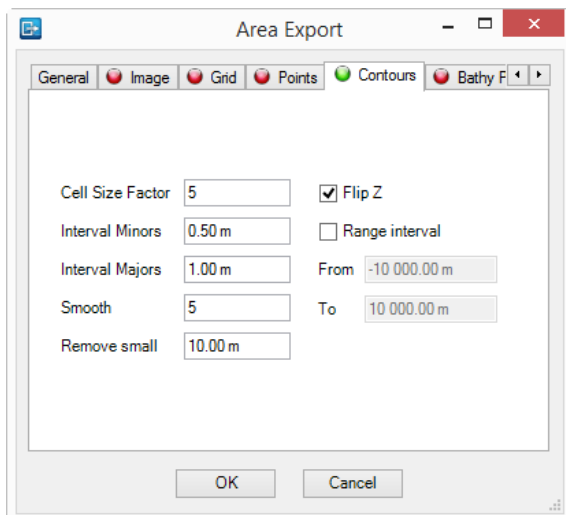


Figure 12 BM1 contour export parameters.

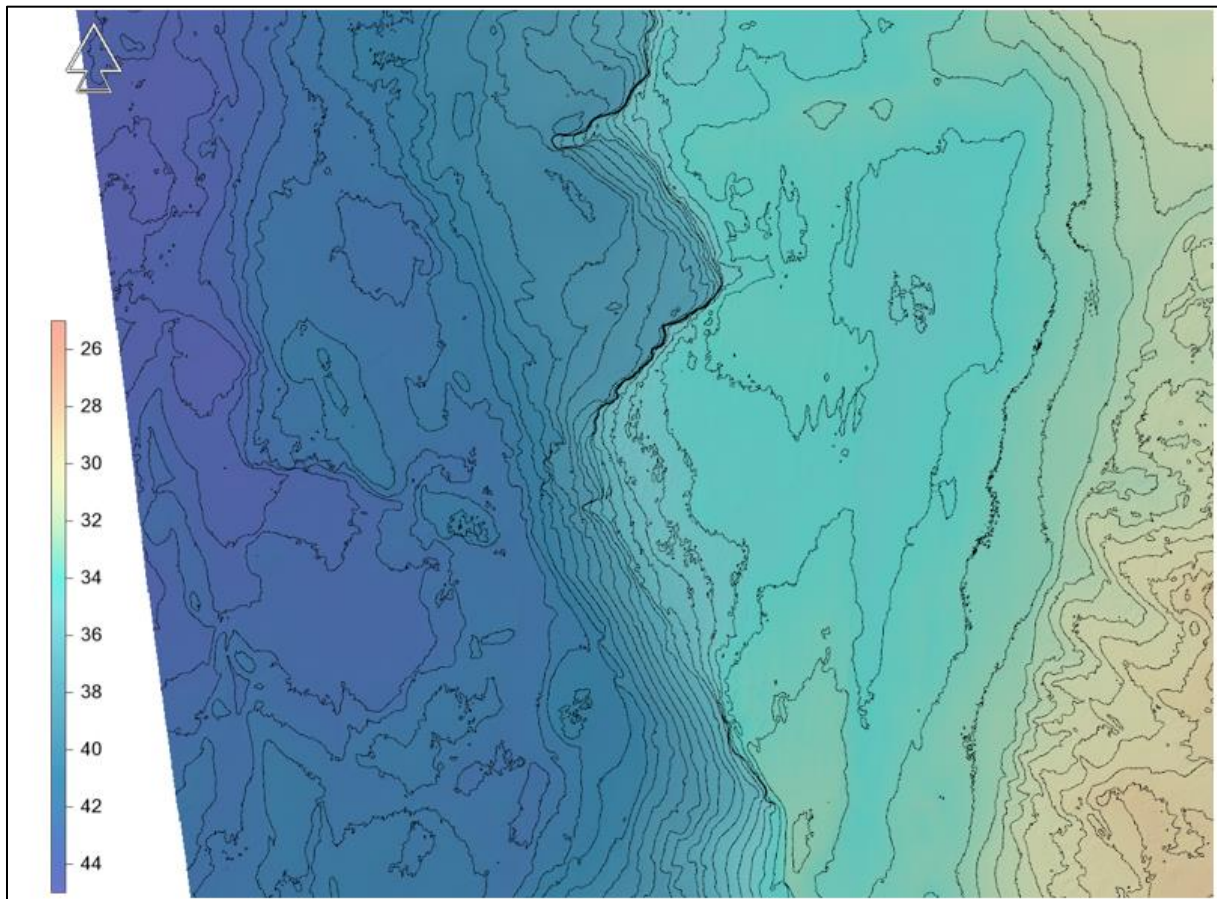


Figure 13 Example of exported contours with 50 cm interval.
The image shows contours over the western side of the Artificial Island area of investigation in BM1.
Navimodel depth convention is positive down.

4.2 | BACKSCATTER

MBES backscatter data was processed on both M/V Relume and M/V Northern Franklin using QPS Fledermaus GeoCoder Toolbox (FMGT). The aim of this process was to provide information of sediment boundary positions to the geologists on-board. Since the two vessels were not obtaining 100% sea floor coverage individually the data from each vessel needed to be combined in the office after acquisition was completed. Products generated on the vessel could then be used as an interim dataset for the surficial geology interpretation and contact picking whilst final backscatter processing was taking place.

The final processing was performed for the WP-A survey area which was split into 6 blocks. Data from both M/V Northern Franklin and M/V Relume were processed in the same FMGT project to optimise the blending of overlapping data from the two vessels. Survey lines that run obliquely to the main survey line direction are excluded to reduce the presence of artefacts in areas that already have 100% coverage.

FMGT reads the intensity of each returned ping and applies a sequence of normalising algorithms to account for the variations in intensity generated by vessel motion, beam angle and high frequency, along track variability. In addition, FMGT effectively back-calculates other intensity changes generated by any automatic changes to the EM2040D (MBES) operating settings and results in a homogenous grayscale backscatter mosaic that accurately represents the spatial variations in seafloor sediments.

ASCII files containing XY and backscatter intensity (XY+i) were exported from FMGT at 0.5 m resolution and these were re-projected using Feature Manipulation Engine (FME) to the project coordinate system. The 6 individual block ASCII files were merged before being clipped to 5 km x 5 km grid tiles using the Tile Schema (783_Energinet_TileSchema_ETRS89_32N_5KM). These XY+i ASCII files were used to create tiled 32bit FLT GeoTiffs for delivery and import to ArcGIS. The XY+i files were also used to create RGB GeoTiff image.

4.3 | SIDE SCAN SONAR

SSS processing and interpretation was conducted within SonarWiz. Prior to importing raw SSS JSF files the water sound velocity at towing depth was confirmed and updated within the SonarWiz import settings. The raw SSS data was then imported into SonarWiz without the application of any gains, and the following QC/processes were conducted:

1. Navigation data QC'd and any occasional spikes removed
2. Seabed auto tracked, QC'd and manually adjusted if necessary
3. User controlled gains applied to the data and manually adjusted to enhance seabed sediment contrasts and seabed features
4. SSS data QC'd against MBES data by locating features/contacts clearly distinguishable in both data sets and comparing appearance and position
5. Coverage QC'd and any gaps flagged and infilled in order to meet client coverage requirements

The SSS processing workflow is outlined in Figure 14 and Figure 15.

The processing was conducted with the following objectives:

- To classify seabed surface sediments
- To classify mobile bedforms and other potential hazards
- To identify natural and anthropogenic seabed features
- To detect contacts
- To detect cables and pipelines

The interpretation of SSS geo-boundaries was conducted within SonarWiz and AutoCAD software. Within SonarWiz geo-boundaries were digitised as features and exported as DXF files. For digitisation in AutoCAD, SSS mosaics were exported from SonarWiz loaded into AutoCAD and line and polygon features mapped. Before the mosaic were exported as a GeoTiffs, the files were arranged so the best available data is uppermost. The nadir was made transparent in order for data in overlapping files that cover the nadir gap to be seen. This process is conducted for both high frequency (HF) and low frequency (LF) data sets.

The geo-boundaries (interpreted changes in surface geology) were reviewed against backscatter, MBES and magnetometer (MAG) grid data so an integrated interpretation was obtained based upon all available data. Seabed sediment classifications were also reconciled against the geotechnical grab sample (GS) results. Interpretations were QC'd and finalised by a Senior Geologist.

The interpretation of SSS contacts was initially conducted within SonarWiz. The SSS data was viewed in digitising mode and man-made objects were digitised. Wrecks/cables were correlated to existing databases. Contacts were initially picked using an auto-picking algorithm in NaviModel. Based on the results, boulder fields were delineated in AutoCAD according to the boulder field classification provided. Once boulder field polygons were generated, the boulders within them were filtered to remove boulders less than 1m in either dimension. Remaining contacts were then QC'd against the mosaics and MBES, and any missing contacts were added using SonarWiz. The contact list was then correlated to MAG.

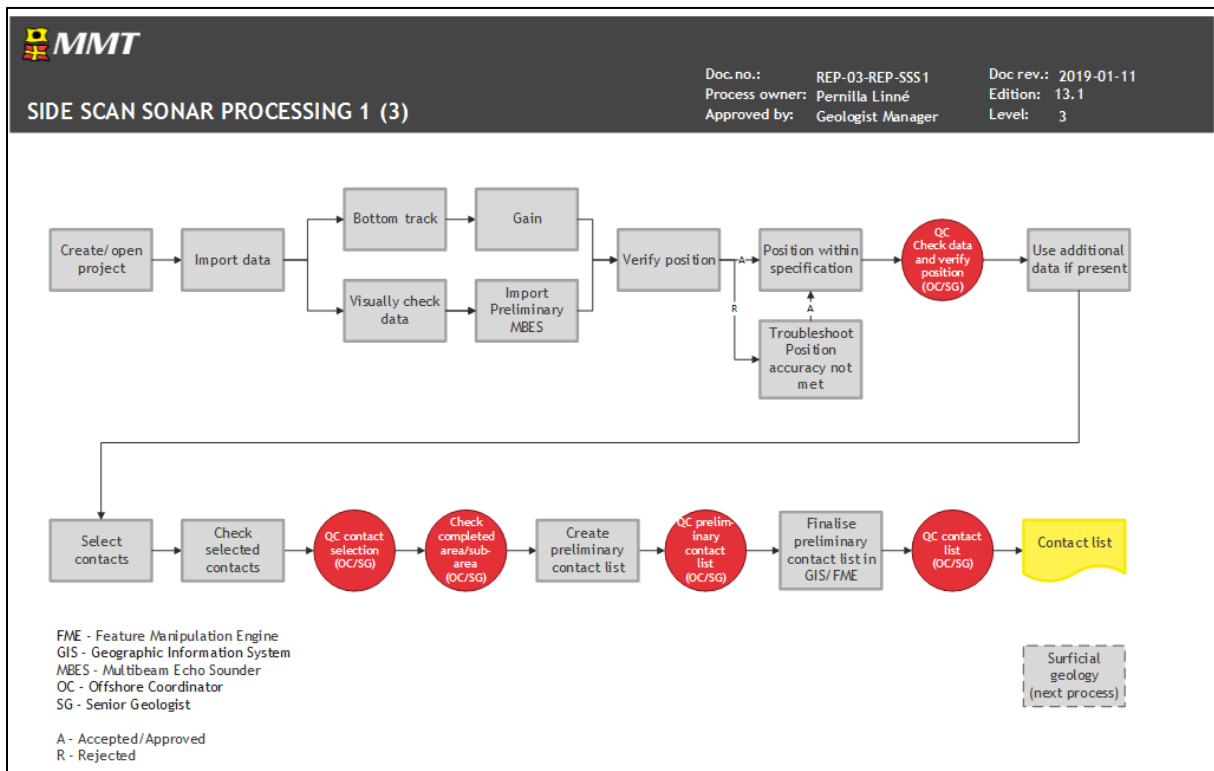


Figure 14 Workflow side scan sonar processing (1 of 2).

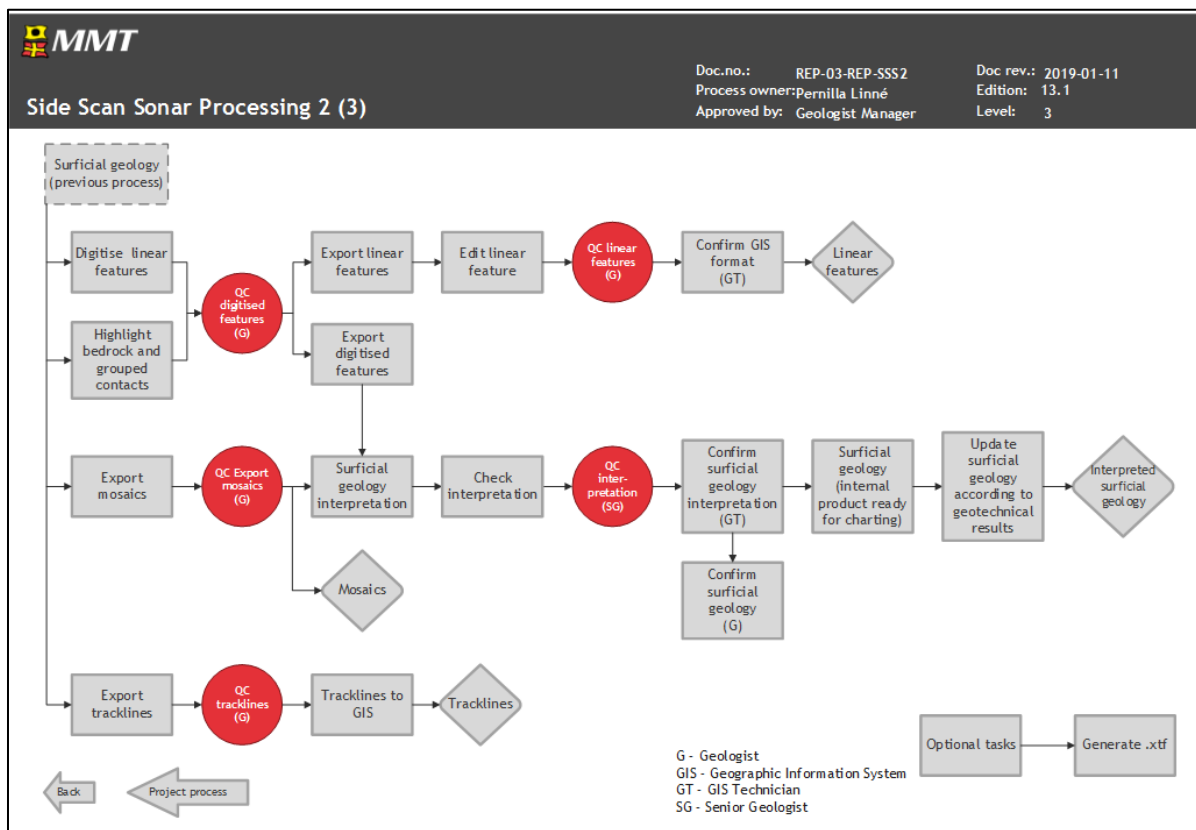


Figure 15 Workflow side scan sonar processing (2 of 2).

4.4 | MAGNETOMETER

MAG data was processed and interpreted within Oasis Montaj software.

Navigation is despiked removing outliers through a set distance from the navigational trend, after a manual check is performed and additional spikes are removed as needed. Small gaps are interpolated and bigger navigational gaps are flagged for infill. 100 samples are interpolated: at 4 knots survey speed with a sample rate of 10 Hz, approximately 20m is the maximum interpolation distance. Once the navigation has been despiked a small rolling statistic smoothing filter is applied.

Altitude, depth and motion is despiked removing outliers through a set value that incorporates real data for each sensor but excludes spikes as these vastly differ from the real data, after a manual check is performed and additional spikes removed as needed. Once despiked a small rolling statistic smoothing filter is applied for each sensor.

The raw MAG data was de-spiked using a pre-set cut off value of 45000 nT and 56000 nT to remove occasional spikes. To generate the regional background field, a series of four filters were used. The regional background field was then subtracted from the total field to generate the residual field.

Applied filters to generate background:

- Non-linear filter 1; Width = 60, Tolerance = 1.2
- Non-linear filter 2; Width = 30, Tolerance = 0.5
- Non-linear filter 3; Width = 15, Tolerance = 0.25
- Non-linear filter 4; Width = 7, Tolerance = 0.125

Example of the filter result can be seen in Figure 16 for Northern Franklin and Figure 17 for Relume.

The same set of filters were used over the whole dataset to remove the regional background field.

No altitude correction has been performed on the magnetic data set.

Each file was individually studied for anomalies. The criteria for magnetic anomalies are 10 nT (peak to peak). However, clear anomalies below the threshold have also been picked.

Once an anomaly was identified a comparison was carried out between the different sensor information available (altitude, depth, motion and quality) to determine if the anomaly is real or induced by low quality or rapid changes in MAG movement. Once an anomaly was confirmed to be real the location was added to a database and the anomaly's amplitude and wavelength was manually measured. Once completed, each picked anomaly was individually Quality Checked to confirm stored values.

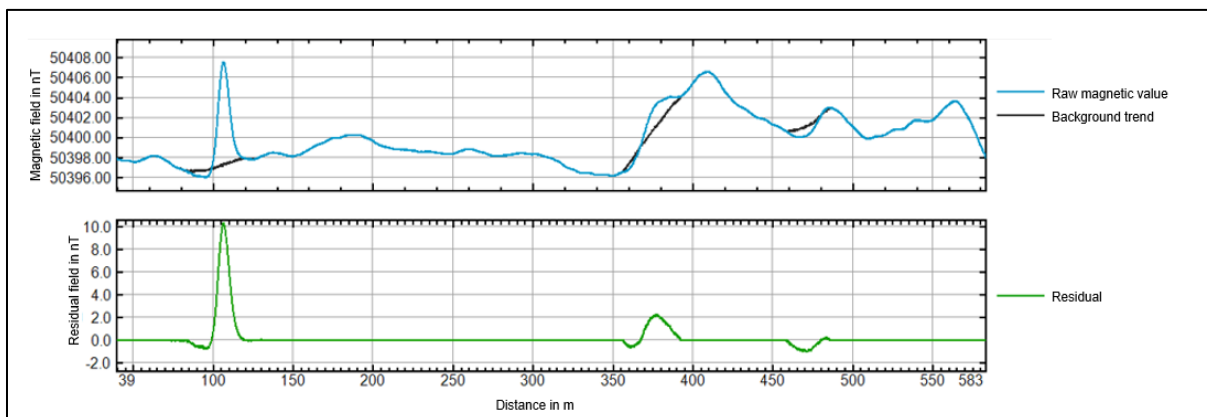


Figure 16 Data example for Northern Franklin from B3.
Raw, processed background trend and the resulting residual signal of the magnetometer data.

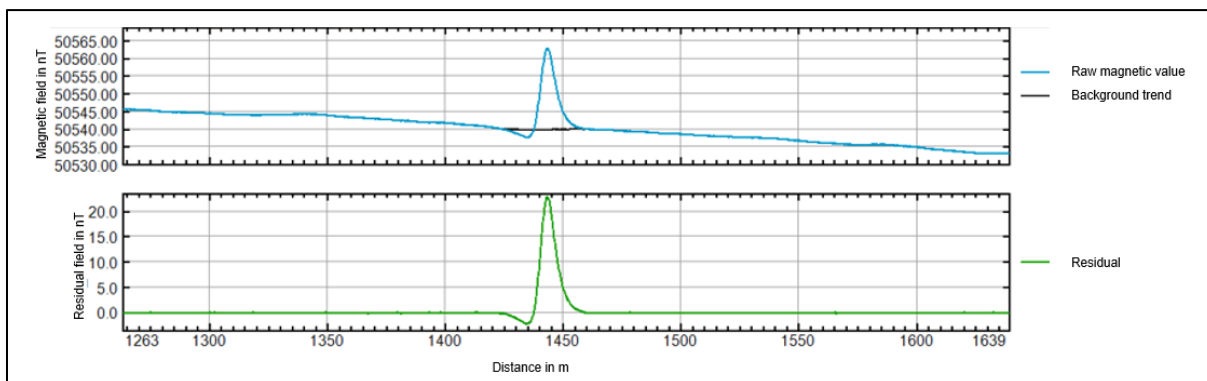


Figure 17 Data example for Relume from B3.
Raw, processed background trend and the resulting residual signal of the magnetometer data.

The general workflow of the MAG processing is outlined in Figure 18 and Figure 19.

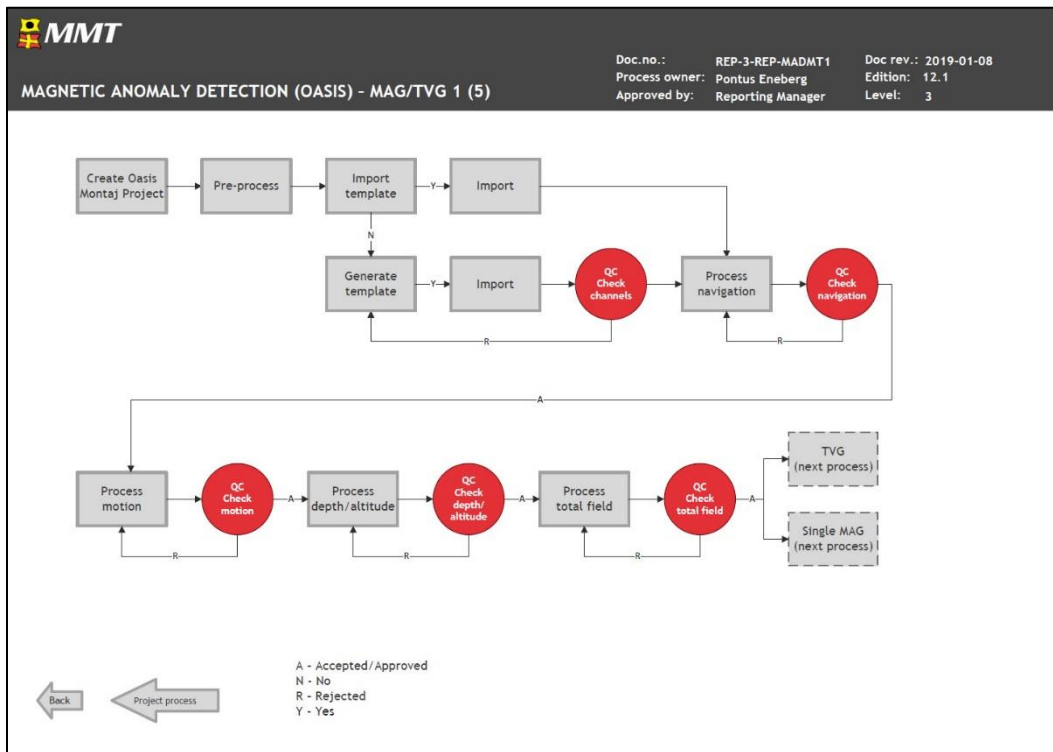


Figure 18 Workflow MAG processing (1 of 2).

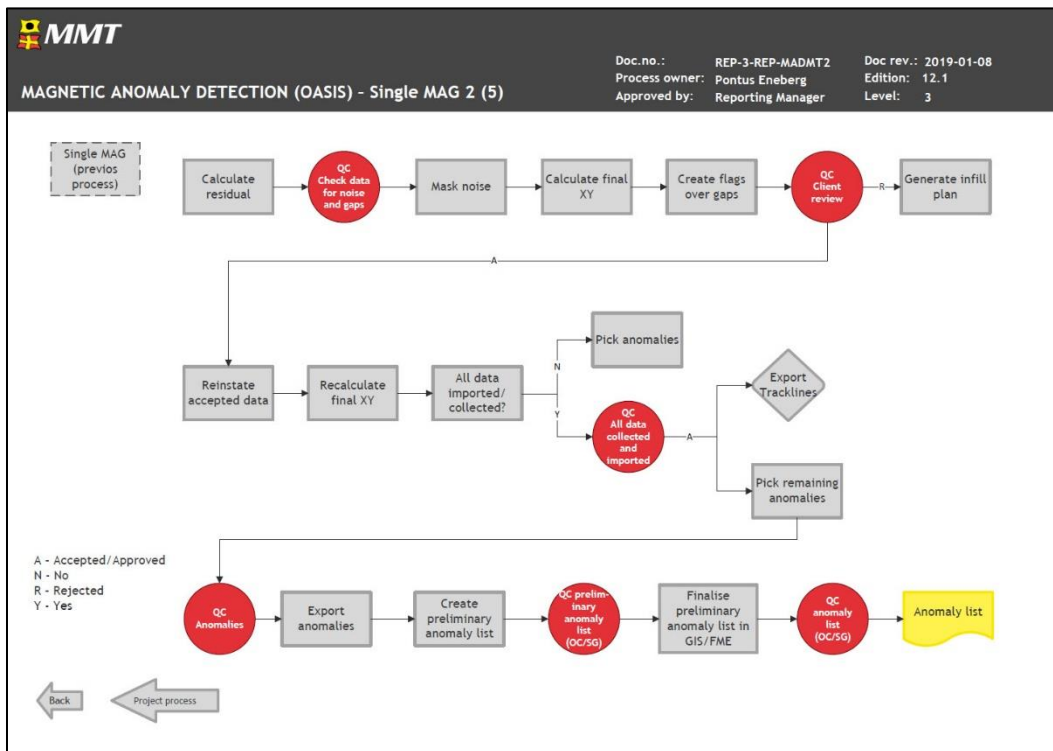


Figure 19 Workflow MAG processing (2 of 2).

4.5 | SEISMIC - 2D UHRS

The flow was divided into two main processing tracks: pre-stack TRIM track and FULL track.

- The main purposes of the TRIM track were to perform source signature deconvolution and to estimate a proper residual motion correction.
- The aim of the FULL track processing was to achieve the final seismic sections (MUL and MIG datasets) used for the final (refined) seismic interpretation.

Table 17 summarises the gridding parameters (used for all grids in the Kingdom Suite project). The selected settings were based on their ability to deliver optimal results (coverage between lines and minimising artefacts and edge effects).

Table 17 Gridding parameters.

Cell Size	5 m
Algorithm	Flex Gridding
Smoothness	6 (scale is 0 to 11)
Search radius	120 m

For full description of and details on the 2D UHRS processing see Appendix D].

4.6 | SUB-BOTTOM PROFILER - INNOMAR

Prior to import, the SBP data files were converted from SES3 format to SGY format using an in-house software; MMT GeoTools. The conversion software corrects the navigation and applies vertical corrections to the data with the application of an SBET (Smoothed Best Estimate Trajectory) exported from PosPAC. The SGY files were then imported into RadExPro for signal processing. The seabed was auto tracked and then quality checked and manually adjusted, if required. Positional accuracy was verified during the MAC by using MBES data to locate features clearly distinguishable in both data sets and comparing the positions. Within RadExPro the processing flows were designed to improve the quality and resolution of the data by removing noise and enhancing the primary signal. In general, the signal processing flow applied to the data was:

- Burst noise removal
- TFD noise attenuation
- Source signature deconvolution
- Butterworth filtering
- Amplitude correction
- Amplitude recovery
- 2D spatial filter
- Export in standard SGY

Visual QC was performed before and after each processing step to check:

- The natural continuity of geological units was preserved
- Creations of artefacts which could mislead the interpretation process
- Suppression and/or removal of all kind of noise without compromising the true signal

Another in-house software, MMT PostProc GeoTools, was then used to write the final processed ASCII textual header to all SGYs. This program was also used to export corrected instrument tracklines, high

resolution images of each SGY and conduct the depth conversion. The depth conversion is executed using water sound velocities acquired on the vessel. SVP data is loaded into the software to calculate the average sound speed in the water, and then a layer-cake velocity is used for the sediment. The velocity value for the sediment was 1600 m/s.

MMT PostProc GeoTools exports 3 final SGYs; time domain with corrected ASCII header, depth domain and an interval velocity SGY. All three of these SGYs are loaded into Kingdom Suite using Seismic Direct. Geological interpretation is then carried out on the data in the time domain, and later converted to the depth domain using the interval velocity SGY as a reference.

The general workflow of the SBP processing is outlined in Figure 20 and Figure 21.

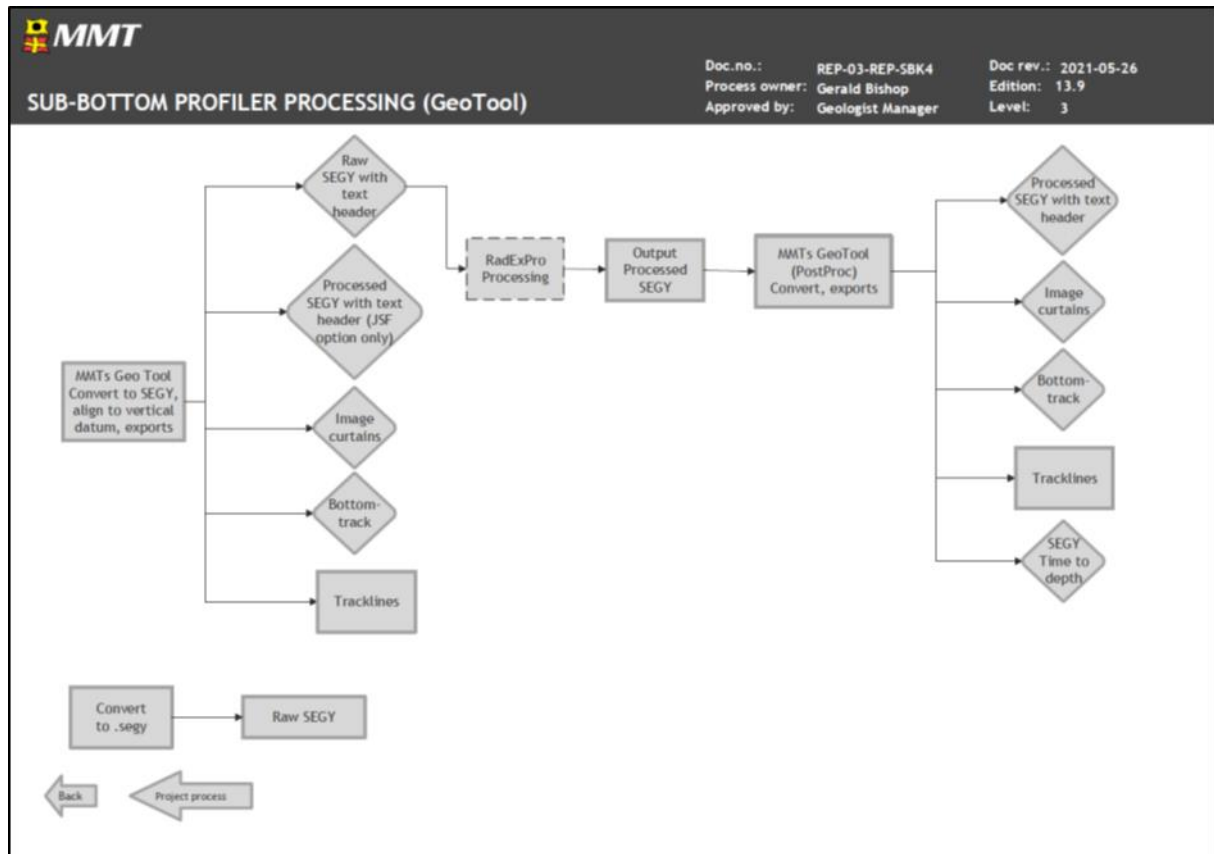


Figure 20 Workflow SBP processing (1 of 2).

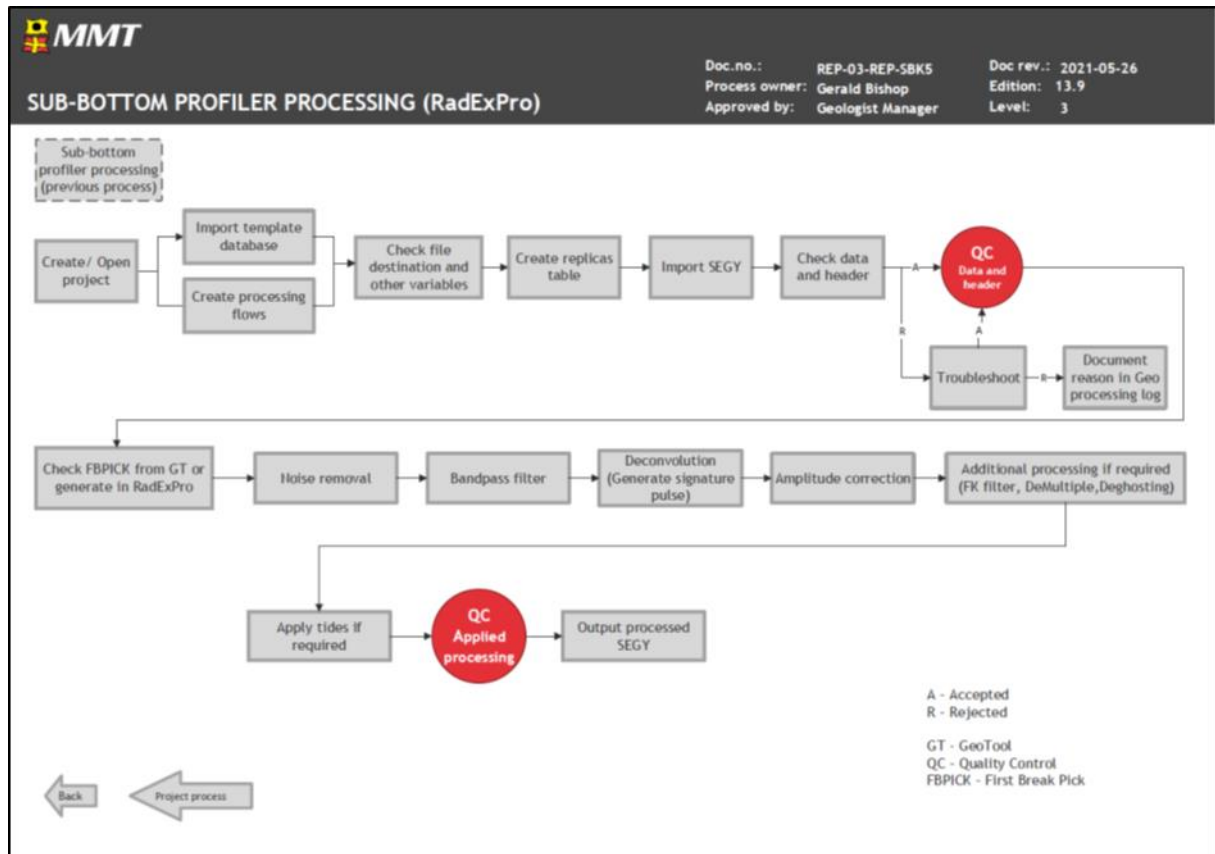


Figure 21 Workflow SBP processing (2 of 2).

5 | PROCESSED DATA QUALITY

5.1 | BATHYMETRY DATA

The processed MBES bathymetry data meets the required specifications. The horizontal and vertical uncertainty of the soundings data were, for the vast majority of the survey area, within acceptable tolerance. Checks were made during acquisition to ensure that sounding density conformed to the 16 soundings per 1 m cell criteria. Some low-density cells exist in the final dataset. In some instances, the low-density cells were evident during the survey, however they were discussed with the Client Representative and deemed acceptable. In other instances, the low-density cells correspond to areas that were flagged as rejected during office data cleaning after both vessels had left the survey area.

The MBES data from M/V Relume and M/V Northern Franklin was combined in the office after survey operations were completed (Figure 24). The principal QC check that was required was to ensure that data from both vessels was vertically aligned. To do this the same methodology for checking vertical alignment within a single dataset was followed.

This is done by generating Caris HIPS QC surfaces from all MBES data within a survey block. A range of properties are computed for each surface and these are checked systematically to ensure the data falls within specification. The Standard Deviation at 95% confidence interval is checked in order to highlight areas where the vertical spread of soundings within a DTM grid node is high and checks can be made to determine the cause. If necessary, action can be taken to bring the soundings into closer alignment. Regions that have high standard deviations can occur where there are sound velocity errors, errors in the post-processed navigation, acquiring data in heavy weather and where there are steep slopes such as boulder fields. Due to the scale of the survey, where data is within the specified range of vertical uncertainty no further steps are taken to improve the alignment.

To expand further on this, it should be understood that within-specification vertical misalignments exist in all areas of the dataset where there is overlapping data. This is the same where data from one survey vessel overlaps another and where a single survey vessel overlaps its own data. If the data is from the same survey vessel you remove the error sources that result from differences in vessel setup (physical arrangement of the MBES on the vessel and the model of MBES itself), the accuracy of the dimensional control and how that is input to the acquisition software. MMT has stringent procedures to ensure that vessels are setup to produce reliable depth measurements and alignment checks are performed during multi-vessel operations to test the configuration. An example where there is a within-specification misalignment between data acquired from a single vessel is shown in Figure 22.

During normal processing procedures all MBES files are gridded into a single surface with the final depth for any particular cell being the average of all contributing soundings. This means that where data is overlapping (or in fact where more than one sounding is present within a cell) the DTM depth will lie at the average position between all the soundings. The degree of vertical spread of soundings from the mean surface is presented by the standard deviation QC layer in Caris HIPS. When data for individual soundings files are gridded independently before being compared it can lead to an incorrect understanding of the degree of misalignment within the dataset as a whole. The QC process measures the difference between the soundings and the depth of the gridded surface, since each individual sounding is not more-or-less accurate than the next one, a degree of aggregation is required for confidence.

One of the main sources of depth error between survey lines is the sound velocity profile. As the sound pulse travels through the water it encounters water masses of varying densities. At each density boundary the path of the sound pulse is altered due to refraction and the degree of deviation is dictated by the difference in density and the angle of incidence; increasing angles of incidence create greater degrees of refraction. Furthermore, with increasing water depth, the ray has more time to travel along it's refracted path. Ultimately, the deviation in position between the detected seabed from the natural seabed is controlled by depth, beam angle and the density profile of the water column.

During acquisition the density structure of the water column is sampled by taking profiles of the sound velocity. These need to be taken with sufficient frequency to ensure that the vertical spread of data across the swath remains within the specified vertical uncertainty. However, no frequency or spatial arrangement of profiles will model the water column during the full period of the survey with absolute accuracy and as a result, small misalignments will exist within the dataset.

The accuracy of the post-processed position also plays its role. Small misalignments in the vessel position in X, Y or Z planes can be superimposed and create separations between survey lines. For example, if the vessel Z position on line 1 is 10cm above the true vessel position but on line 2 it is 10cm below the true vessel position the survey data will be vertically separated by 20cm. Positional misalignments can also combine with vertical errors induced by sound velocity to increase the vertical spread of data between MBES files.

Whether or not this misalignment is problematic depends on the permitted vertical uncertainty, which is usually dependent on water depth (i.e. permitted vertical uncertainty increases proportionally with depth). Where the vertical uncertainty is not specified by the client MMT will follow the guidance from the International Hydrographic Organisation and adhere to the Order 1A limits for vertical uncertainty which is appropriate for hull mounted survey operations. Applying this guidance for an example depth of 40 m gives a permitted vertical uncertainty of +/- 0.76 m from the mean. Should the vertical separation between two survey lines be 0.2 m this results in a vertical uncertainty from the mean of +/-0.1 m which is well inside the permitted spread of data. This alignment would also meet the most stringent specification, IHO Exclusive Order, which, for the same 40 m depth, would permit a spread of data of +/- 0.37 m from the mean.

In some areas of overlapping data a wavy-imbrication artefact is visible within the 0.25 m DTM (Figure 23). The data in the affected areas are within specification for vertical uncertainty and sounding density. This pattern arises mostly due to a relationship between DTM cell size and required sounding density.

The wave-like pattern is a result of the operating system making minor, automatic, changes in frequency across the swath to avoid interference between the two separate receiver elements of the MBES system. This is inherent within a Kongsberg EM2040D system. The wave-like pattern may be further emphasized by vessel motion.

For this survey MMT were required to achieve a density of 16 soundings per 1 m cell. When gridded at 0.25 m (and with perfect, even distribution of soundings) this results in 1 sounding per cell. This means that, even in areas where data overlaps, there are relatively few soundings from which an average depth can be calculated. This limits the degree that the within-specification vertical misalignments and systematic noise can be ameliorated by the averaging process. It appears that within affected areas the gridding algorithm alternately favours the underlapping and overlapping line (instead of picking an average of the two) and makes the pattern visible.

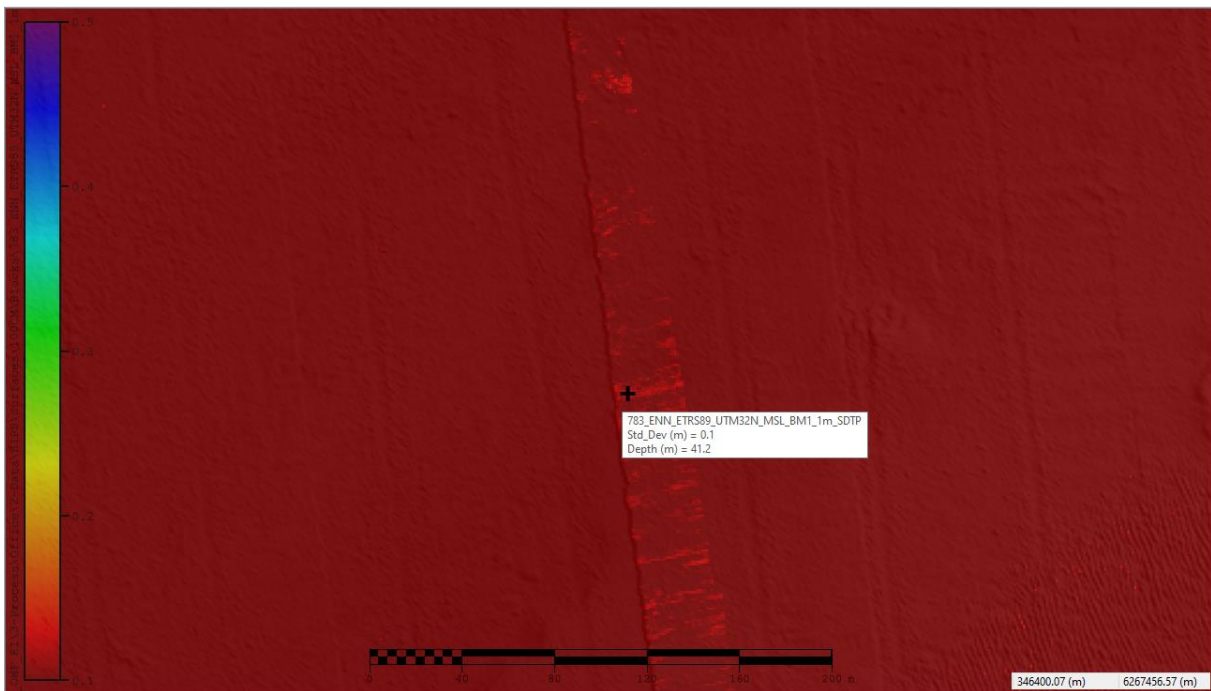


Figure 22 Caris HIPS Standard deviation surface in an overlapping section of data. Acquired by the MV Relume. The Std Dev surface is overlain by the shaded bathymetry relief for context.

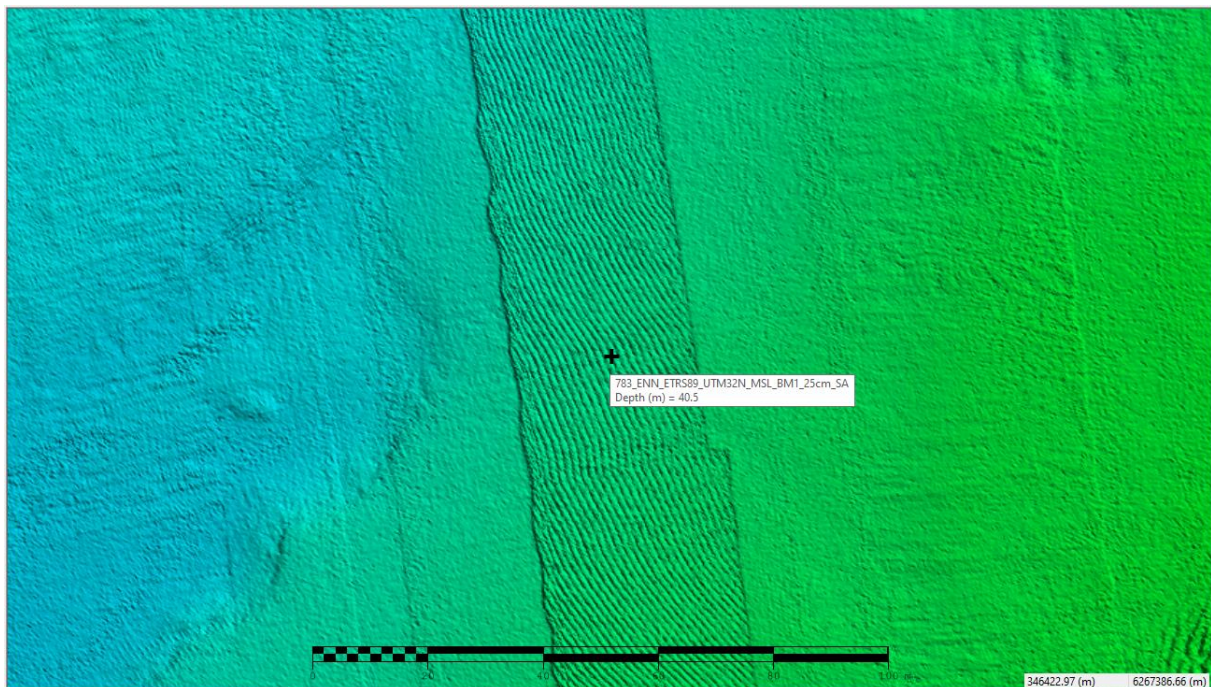


Figure 23 Area of overlapping bathymetry which displays a wavy pattern. This pattern is emphasized with a strong vertical exaggeration.

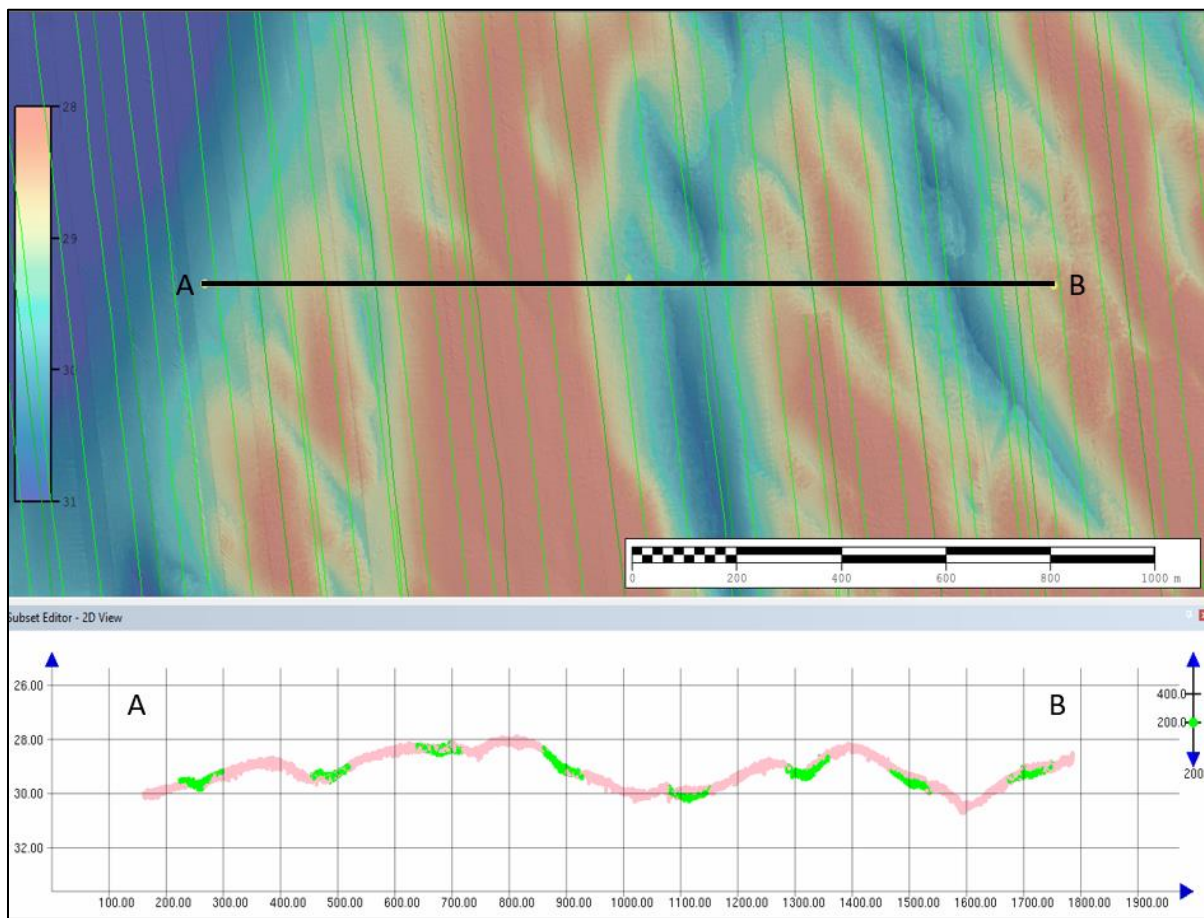


Figure 24 Cross section through Block 2.
Image shows vertical alignment of M/V Relume (green) and M/V Northern Franklin (pink). View centred on 348598 E, 6266092 N. Caris HIPS depth convention is positive down. Vertical exaggeration of cross section is x200.

Figure 25 shows an overview of the Standard Deviation surface for the survey area, which presents regions as having low, medium and high standard deviations in green, orange and red, respectively. Regions where there are numerous boulders can be seen in the north western and the north eastern parts of the survey area as clusters of red points. Since boulders naturally have a high vertical spread of soundings within a node, they are not areas of poor data. Towards the western half of the survey area, and particularly in Block 2, there are long north-south trending strips of orange colour. These correspond to survey lines that were acquired during times with a high variability in the sound velocity through the water column causing the vertical spread of soundings to be higher than elsewhere.

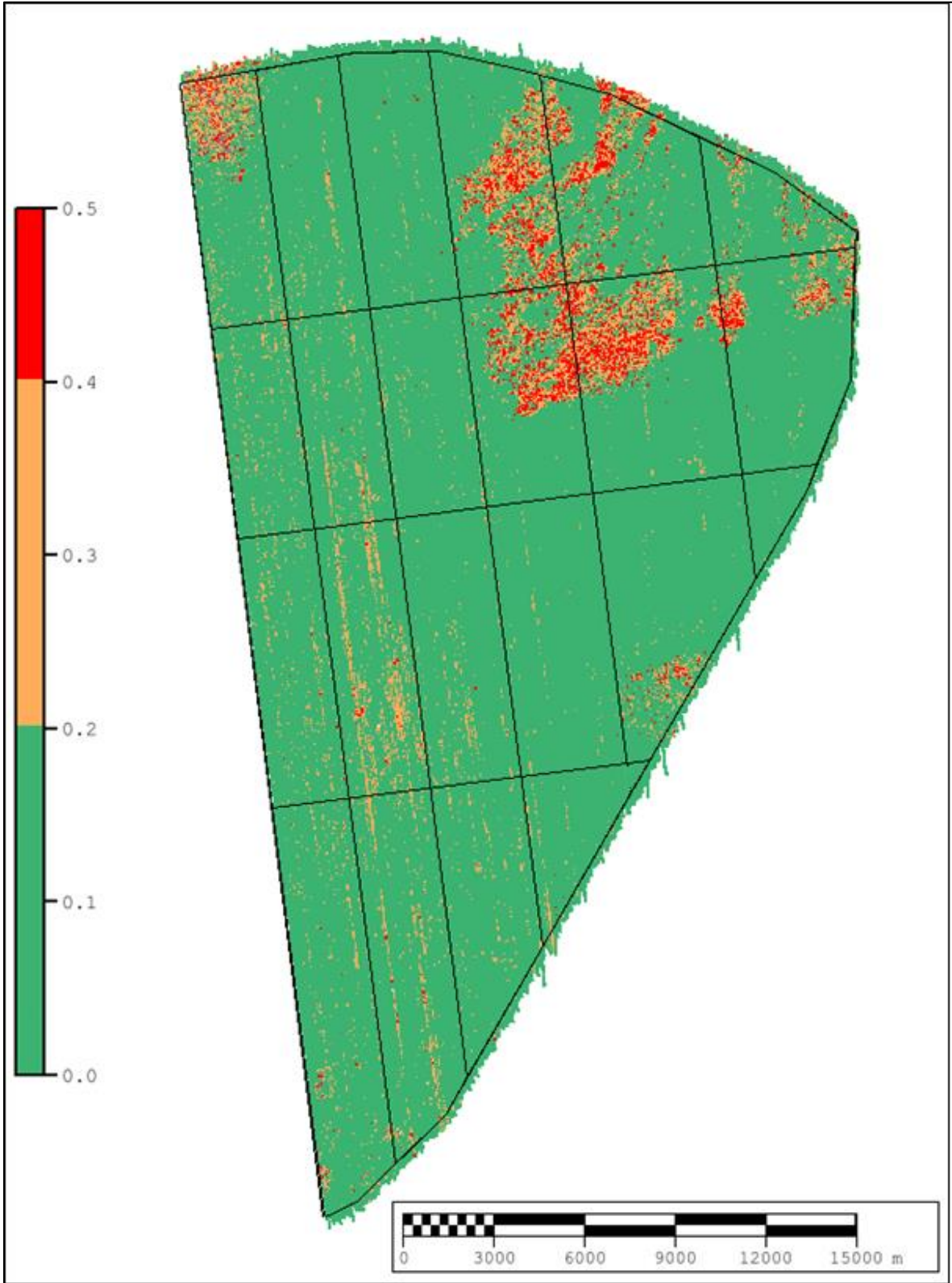


Figure 25 Standard deviation at 95% confidence interval for the MMT OWF survey area. Values are in metres.

Figure 26 and Figure 27 provide examples of the standard deviation surface and cross sections through the soundings data for areas where the sound velocity was stable and variable. Figure 26 shows a region with low standard deviation in the southern part of Block 4. This highly exaggerated cross section shows that M/V Northern Franklin and M/V Relume produced data that was well aligned and displays a similar vertical spread of soundings with no sound velocity induced artefacts.

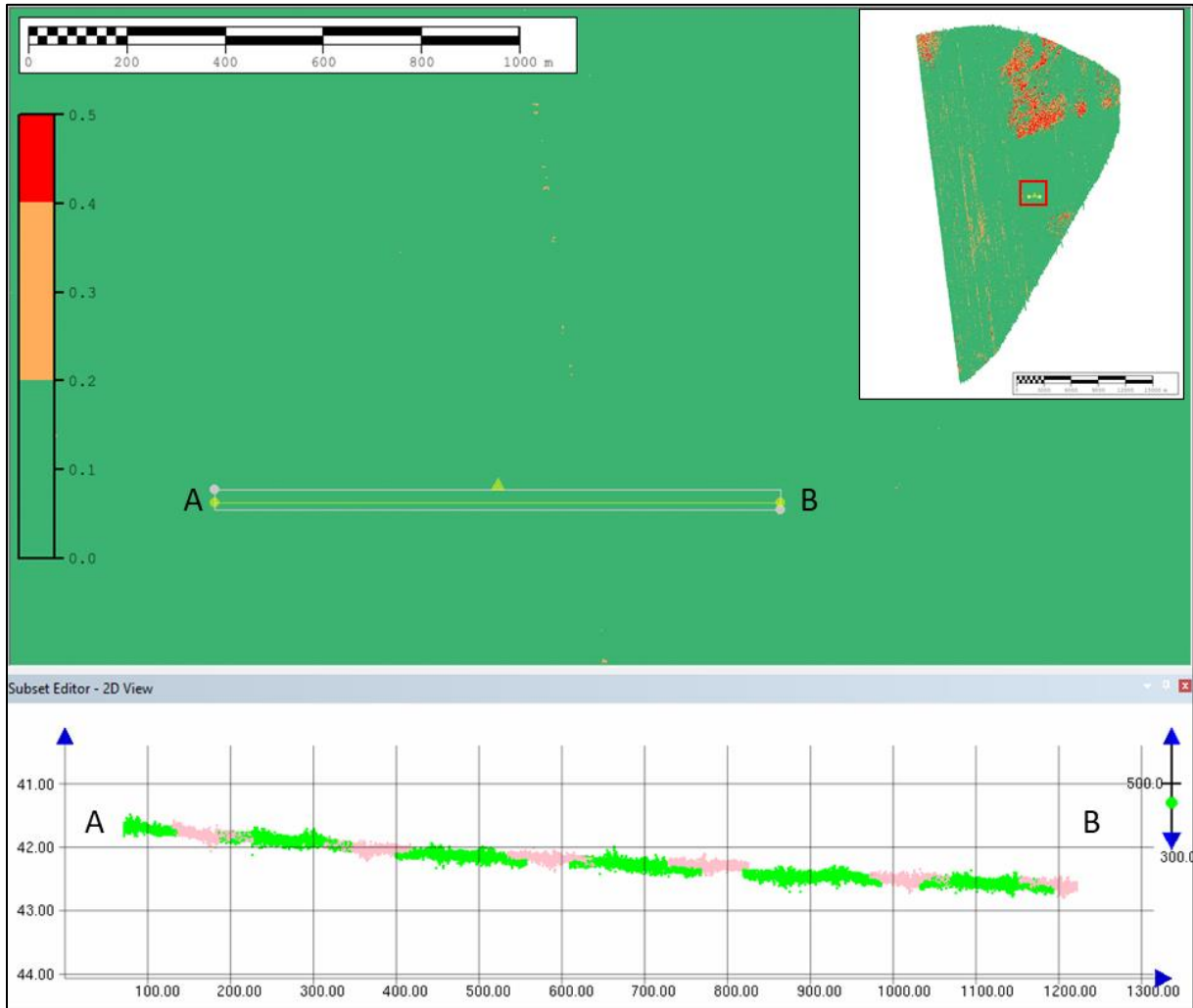


Figure 26 Example of MBES data acquired in good weather with a relatively stable sound velocity with a similar vertical spread of soundings for M/V Northern Franklin and M/V Relume. Soundings from M/V Northern Franklin shown in pink and M/V Relume in green. The yellow bar marks the location of the cross section in lower half of image. Caris HIPS depth convention is positive down, vertical exaggeration of cross section is x200.

Figure 27 shows a region in the centre of Block 2 which had variable sound velocity during the period of M/V Relume's acquisition. In the cross section the M/V Northern Franklin data shows a tighter vertical agreement of data than the contribution from M/V Relume. In general, the sound velocity had higher degrees of variability to the west of the survey area. In order to minimise the impact of sound velocity variations on the acquired data the profile of the water column is sampled frequently during survey operations. These profiles sample a single point in time and space and in combination build up a spatial and temporal model of the sound velocity variability within the survey area. These profiles and their application during acquisition and during processing are sufficient to bring the dataset into an acceptable alignment. However, it is not feasible to eradicate highly localised variations using accepted data processing practices.

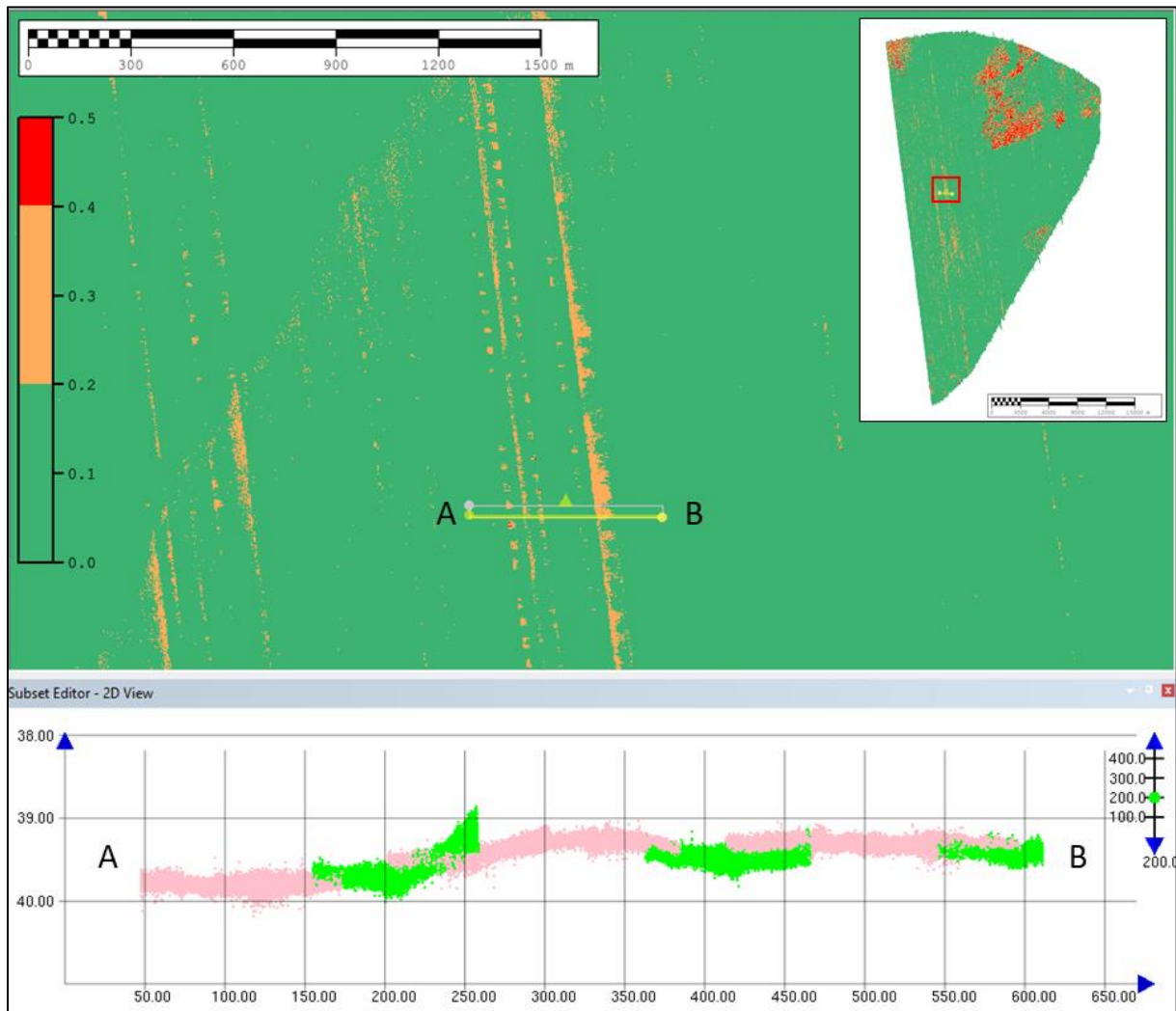


Figure 27 Example of MBES data acquired in area with variable sound velocity with sound velocity artefacts seen in the M/V Relume data. Soundings from M/V Northern Franklin shown in pink and M/V Relume in green. The yellow bar marks the location of the cross section in lower half of image. Caris HIPS depth convention is positive down, vertical exaggeration of cross section is x200.

QC surfaces were computed to show the vertical separation between the mean seabed position and the positions of the shallowest and deepest soundings within a cell. The QC surfaces are used to target both systematic error correction and data cleaning. However, seabed features, such as boulders, as well as outlying soundings are highlighted by these surfaces so careful assessment is made of all areas flagged as requiring data cleaning to ensure that real features are not removed from the dataset.

An example of these QC surfaces is shown in Figure 28. Contacts within the boulder field are highlighted in red and blue since the sounding data deviates from the mean surface by an amount greater than the threshold value for that depth. The surfaces are coloured to indicate the direction of the deviation. Cells where soundings are shallower than the mean surface are highlighted in red and cells where soundings are deeper than the mean surface are highlighted in blue.

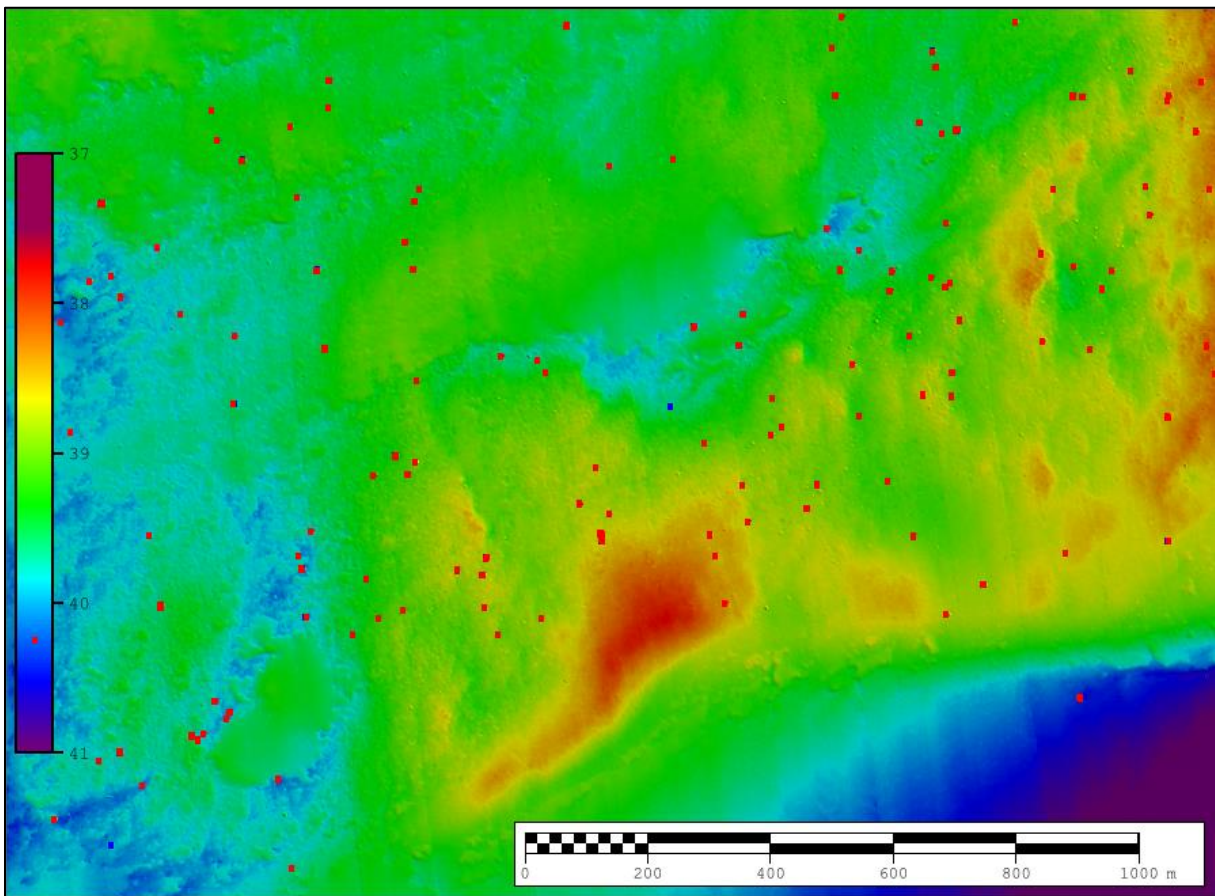


Figure 28 QC surfaces (red and blue cells) highlighting boulders in Block 4.

Also, within Caris HIPS, surfaces were generated to show the Total Horizontal Uncertainty (THU) and Total Vertical Uncertainty (TVU) at 1 m resolution.

Figure 29 shows the combined TVU surface for the survey area. The colour scale represents areas where the TVU is low as green, medium as orange, and above 0.5 m as red. The results show that the survey area has TVU values within acceptable tolerance. The TVU values are calculated from all of the combined error sources associated with a sounding.

An overview of the THU results is shown in Figure 30. The range of values has been restricted to show areas with low THU as blue-green, medium THU as orange and higher THU as red. Spread across the western region of the survey area are survey lines that have THU values between 0.25 m and 0.5 m. These moderately high THU values relate to survey lines that have higher than usual error associated with the post-processed navigation data, however cross sections through the soundings (not shown) indicate that the data is well aligned.

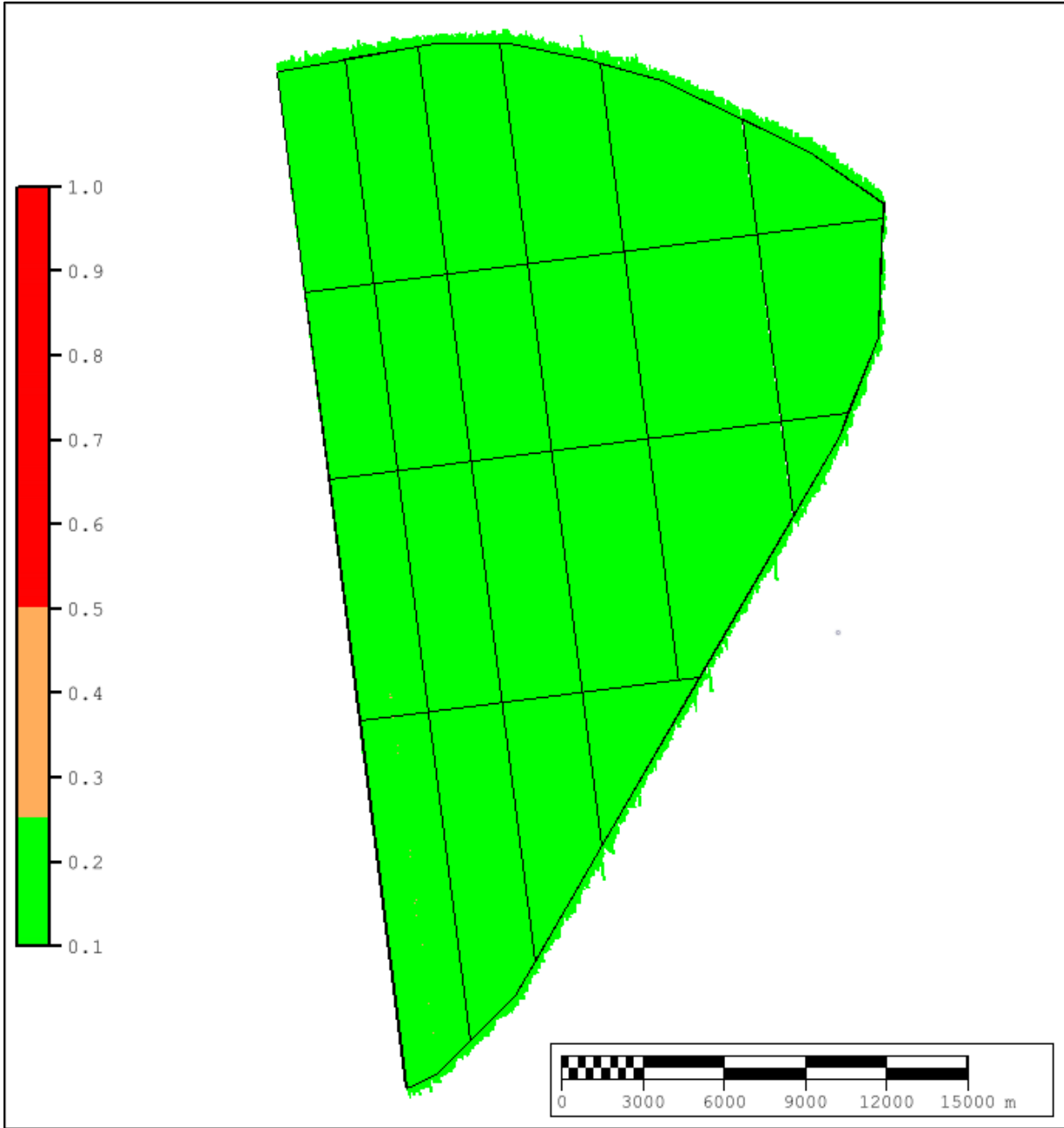


Figure 29 Total Vertical Uncertainty surface for the MMT OWF survey area.

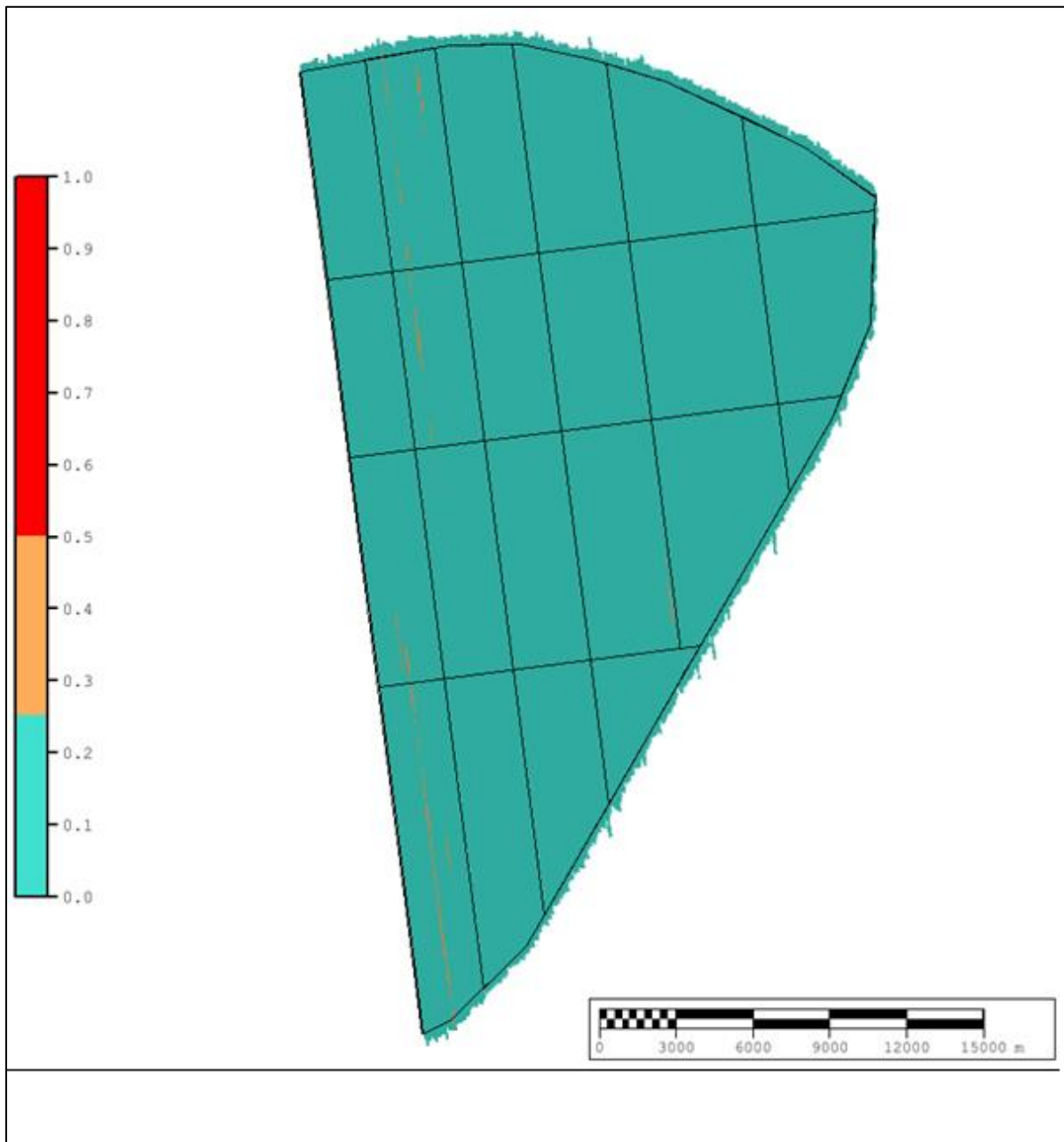


Figure 30 Total Horizontal Uncertainty surface for the MMT OWF survey area.

An artefact was seen in the data both on board the survey vessels and later in the office. The artefact appears as a ripple in the shoal surface when viewed from a 2D perspective and as a ripple on the outer beams of the swath when viewed as a point cloud from the side. This artefact is mainly seen in Blocks 1 and 2, towards the western side of the survey area.

It is believed that the artefact is caused by a pycnocline in the area which affects the sound velocity. This in turn affects the position of the soundings as they are incorrectly calculated as being in a ripple formation. Unfortunately, standard refraction techniques aimed at minimising sound velocity-based errors are not effective in resolving the issue. Additional infill lines were run to replace lines that were affected, and soundings that were outside of the IHO Order 1a specifications were deleted, to minimise the effect of the anomaly on the final surface.

An image showing the typical appearance of these anomalies is shown in Figure 31.

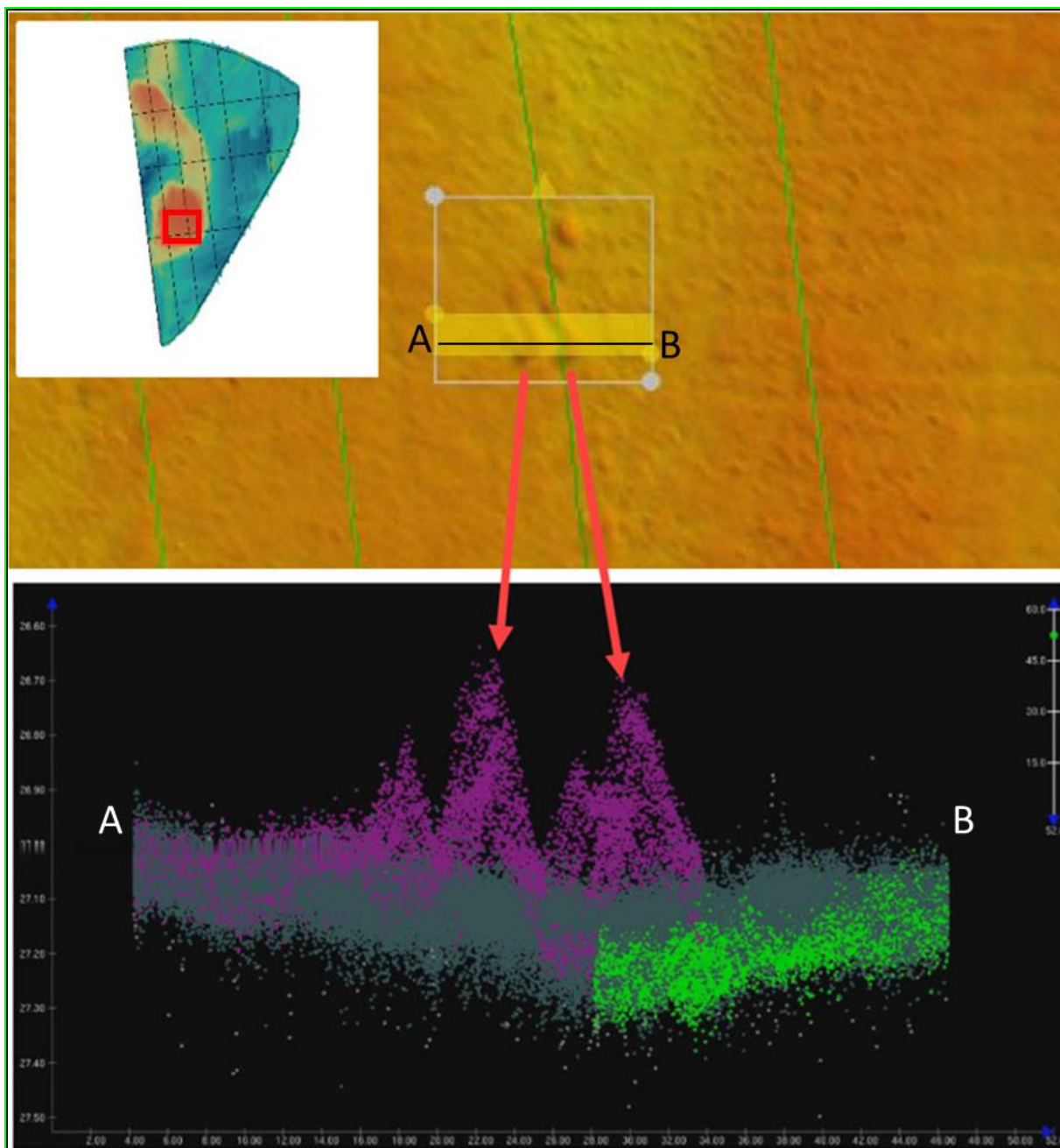


Figure 31 Example of anomaly in MBES caused by pycnocline.
Effect of anomaly seen in shoal surface on top and in soundings on the bottom.

5.2 | BACKSCATTER DATA

To assess the quality of the final processed backscatter data the XY+Intensity data for each block was imported to ArcGIS where they could be viewed as a single dataset (Figure 32). The colour scales for each block were adjusted so that they showed matching backscatter values in the same grey tone.

Assessment of the combined mosaic indicates that the boundaries between different sediment types were well delineated with good agreement between the relative intensities of the data acquired by M/V Relume and M/V Northern Franklin.

Since M/V Relume and M/V Northern Franklin were acquiring data on alternate survey lines there are some residual artefacts that arise from small differences in backscatter values detected by the two systems. As a result, some stripes that are aligned with the survey line direction are visible in the dataset (Figure 33).

Some outer beam noise that occurred with the M/V Relume dataset has carried through to the final mosaics (Figure 34). However, these are also aligned with the survey line direction and can be accounted for during interpretation. The largest example is located at 364236.0 mE, 6278917.0 mN and stretches for approximately 700 m (Figure 35).

Beam-busts caused by excessive motion and bubble-entrainment (air-bubbles from white-water pass directly across the transducer face) are visible as dark lines that run perpendicular to the survey line direction and are restricted to a single MBES swath. An example of this is shown in Figure 36.

Despite the presence of these artefacts, the backscatter data is of sufficient quality to derive sediment boundaries and assist in the identification of contacts.

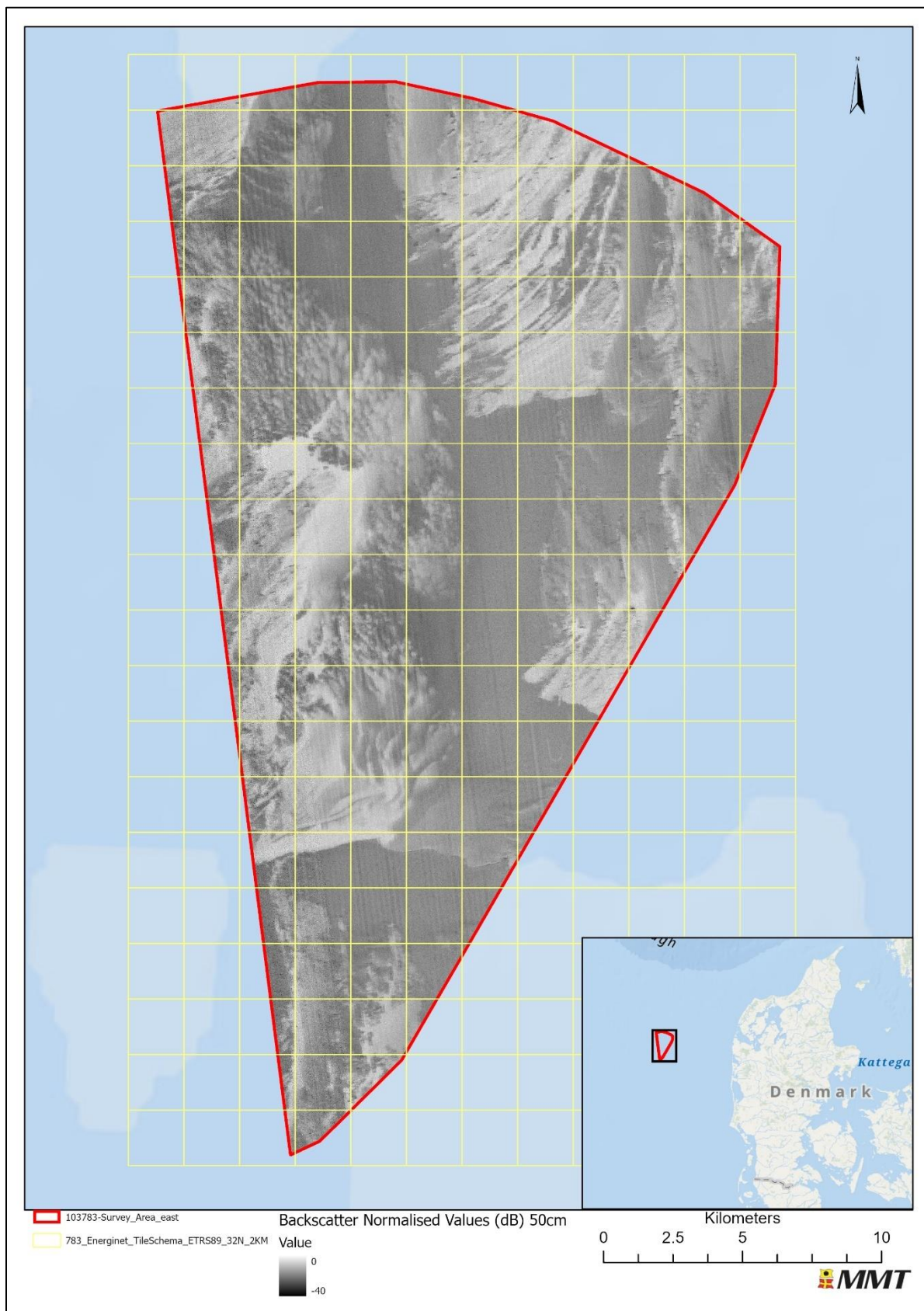


Figure 32 Overview of backscatter normalised values for the MMT OWF survey area.

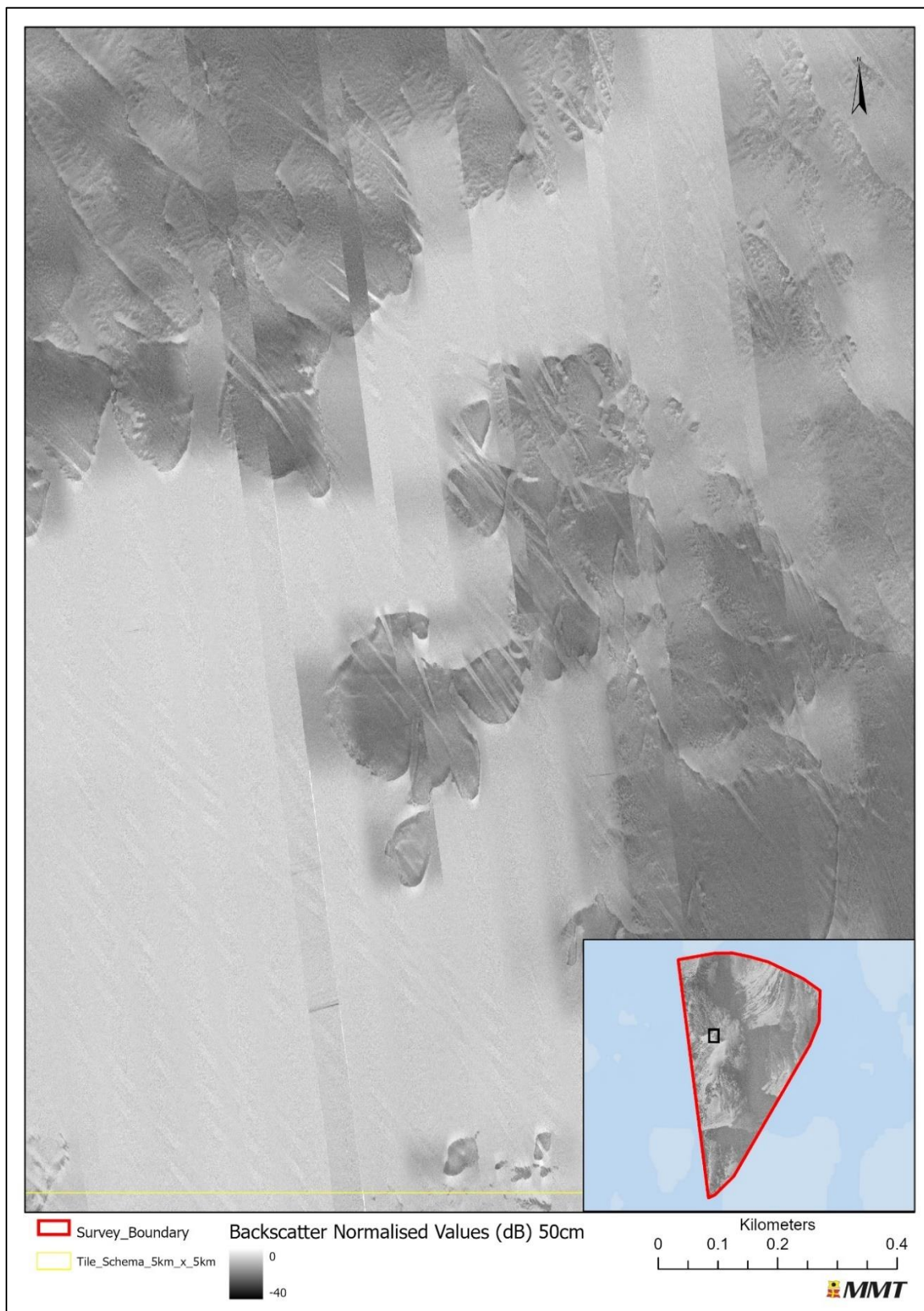


Figure 33 Backscatter mosaic with artefacts.
The artefacts are caused by smearing of data across sediment boundaries with large differences in backscatter intensity.

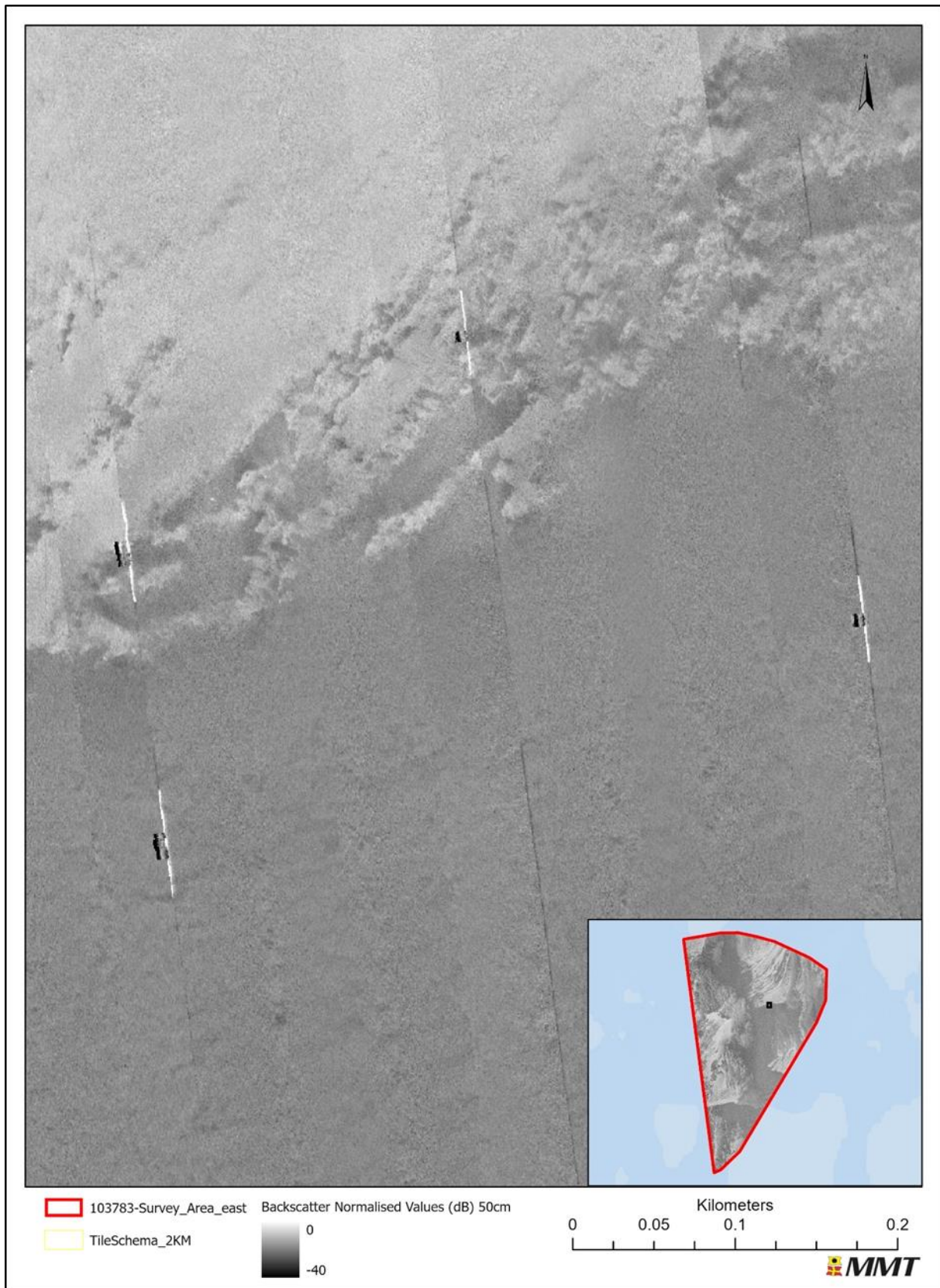


Figure 34 Outer beam busts visible in the M/V Relume section of the dataset.



Figure 35 700m stretch of M/V Relume outer-beam noise visible in the backscatter dataset.

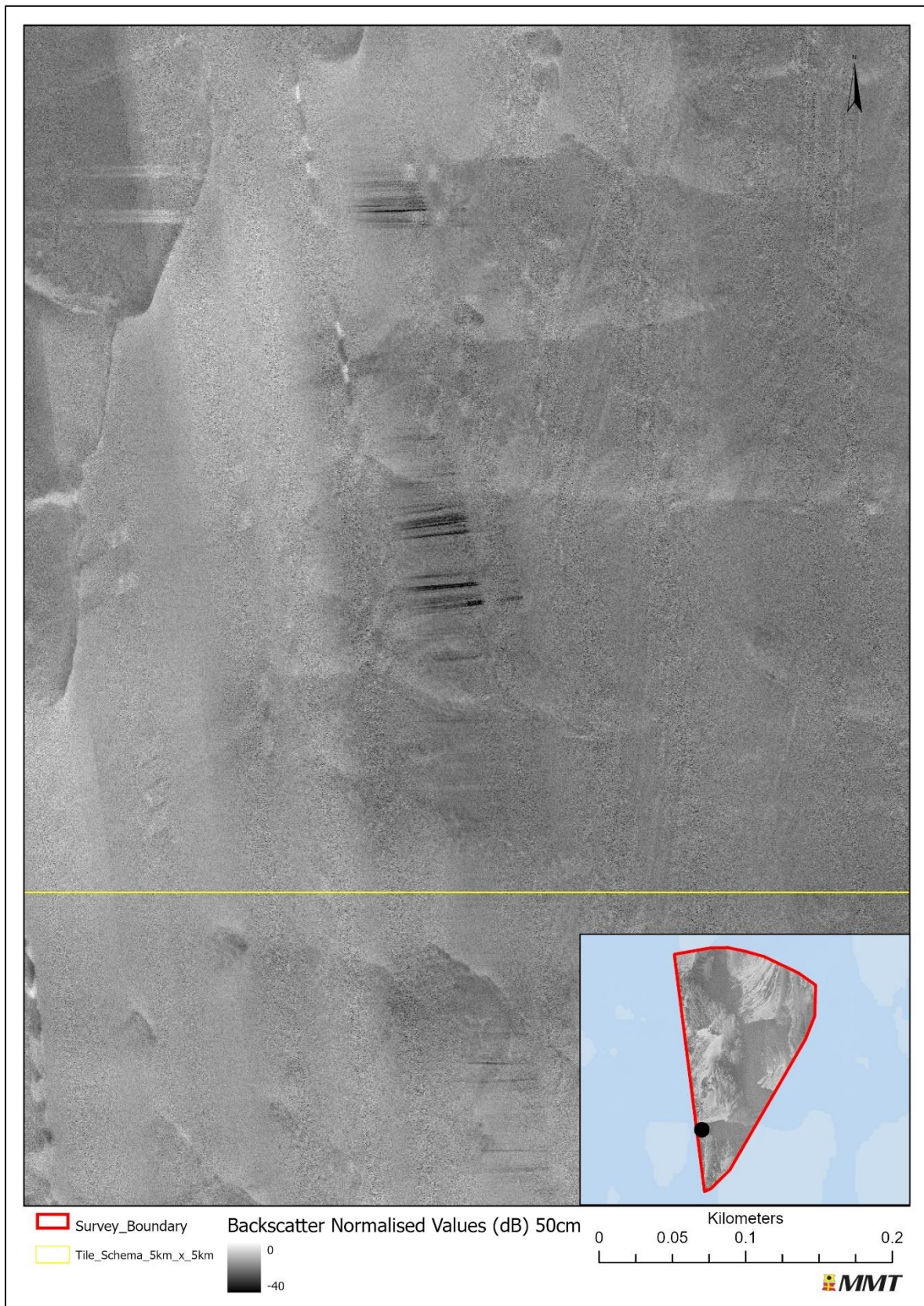


Figure 36 Beam busts caused by excessive vessel motion and/or bubble entrainment.

5.3 | SIDE SCAN SONAR DATA

The SSS data acquired at 80 m range with at 300/600kHz frequency. The altitude of the SSS was kept at 10-12% of the range. 200% coverage was to be achieved, however in areas of pycnocline the specification was reduced to account for trimming out bad quality data caused by the pycnocline (see Section 1.4.1)). Coverage plots can be seen in Figure 43.

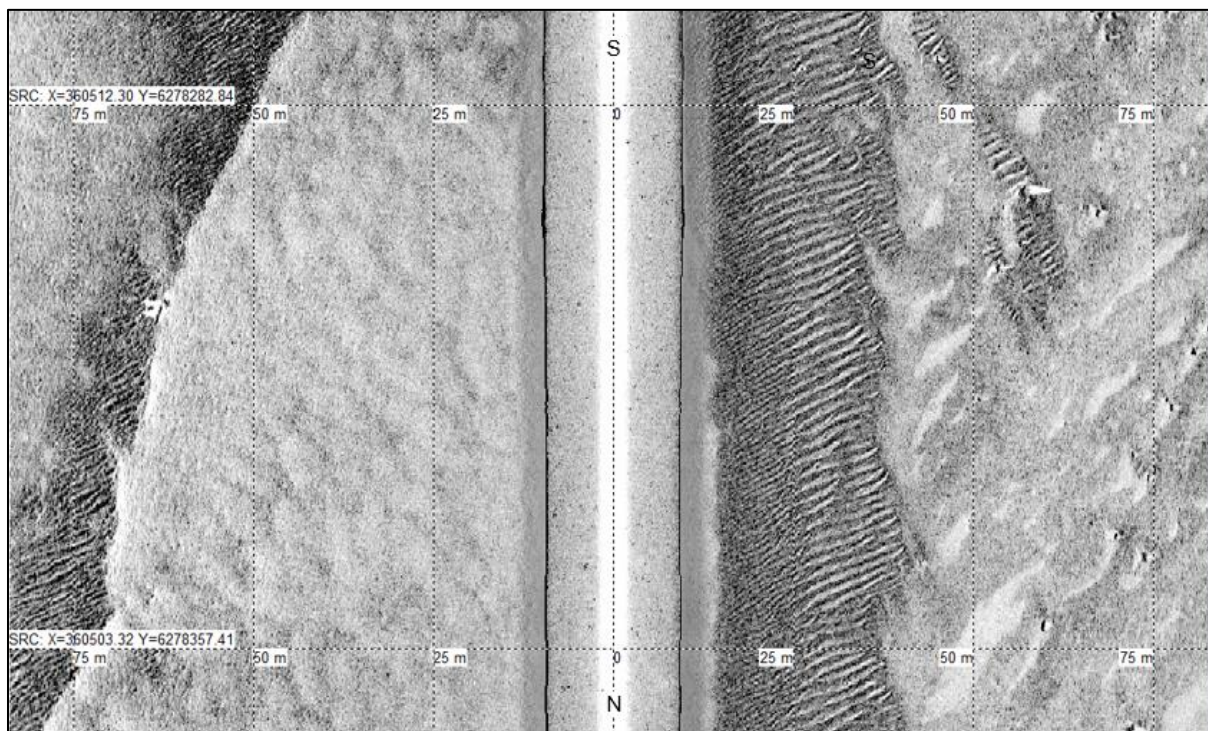


Figure 37 Example of good high frequency SSS data from block BM06. Horizontal scale lines at 75 m intervals.

The SSS data quality was generally good but there were areas of marginal data, due to environmental factors (detailed below). The multibeam and acquired backscatter were used in conjunction with the side scan data to ensure a comprehensive understanding of surficial sediments and interpretation of seabed contacts. This approach also mitigated any observed environmental factors on the sonar data.

A strong pycnocline was observed across the area particularly in shallower areas, such as the Artificial Island area of investigation, mostly affecting the data in the outer ranges. The pycnocline effects obscure up to 35% of the data in some sections. An example from Relume is shown in Figure 40 and Figure 42. The noise varies along the lines and in most cases, it is possible to cover it with adjacent lines, achieving 100% coverage. The pycnocline artefacts are also visible in the SSS mosaics. Backscatter mosaics were delivered as per the scope of work.

Artefacts due to marginal weather were observed on some SSS records. These are due to roll and pitch motion on the towfish causing a 'striping' effect on the data, shown in Figure 38. The data had various amounts of gain applied to improve the overall appearance of the data and reduce the appearance of weather-related artefacts.

The high frequency data was generally more affected by environmental factors, such as weather and pycnocline, than the low frequency. An example showing the two frequency data sets from the same location is provided in Figure 40 and Figure 42. Despite all of the environmental factors described, 200% coverage was achieved for the majority of the survey area; in the areas where pycnocline interference

were observed, re-runs were tasked with gathering a minimum of 100% coverage, Figure 43. For more details on the reduced coverage please refer to section 1.4.1].

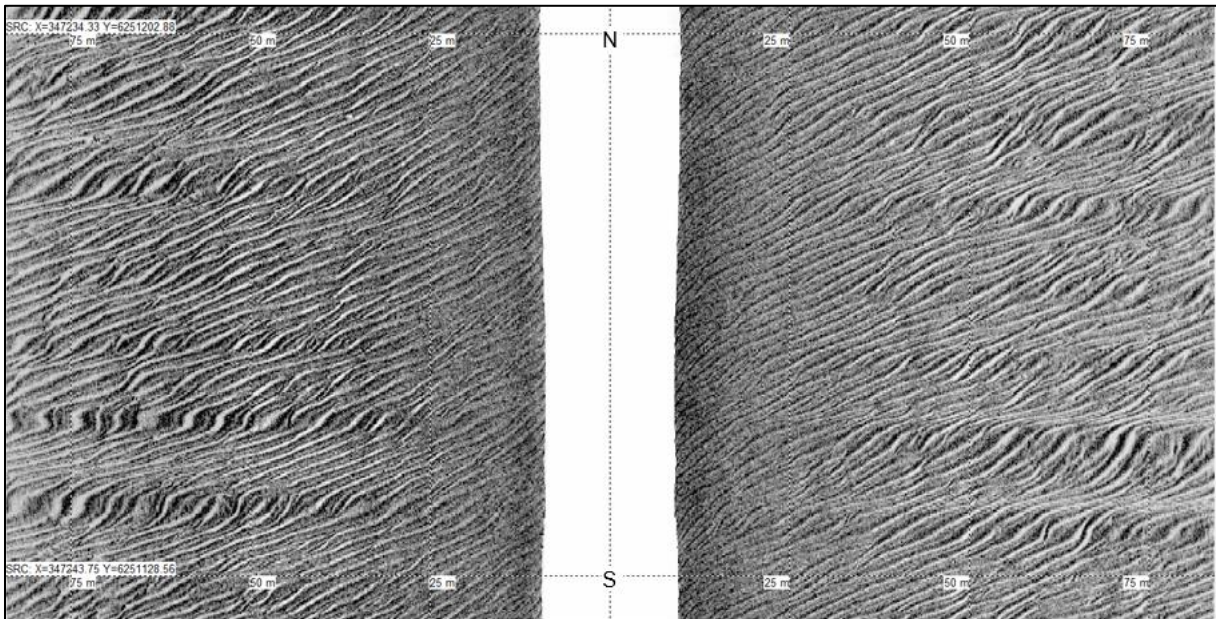


Figure 38 Example 1 of high frequency SSS image from block BM01, Northern Franklin. The example is displaying a 'striping' effect. Horizontal scale lines at 75 m intervals.

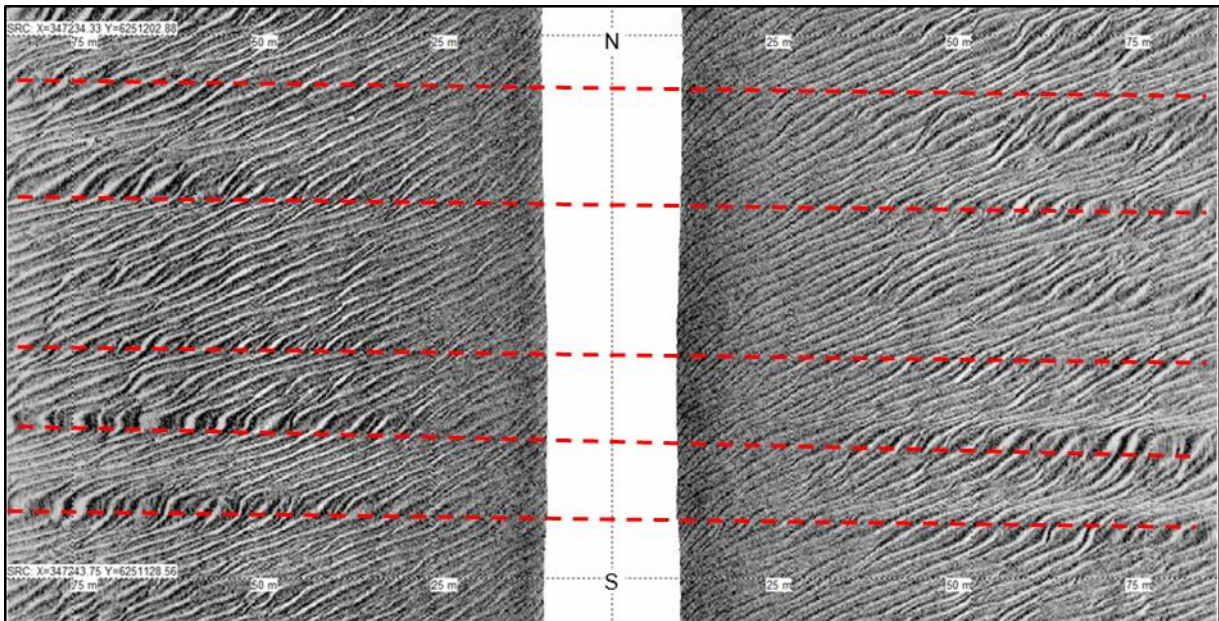


Figure 39 Example 2 of high frequency SSS image from block BM01, Northern Franklin. The 'striping' effect is highlighted with red dotted lines. Horizontal scale lines at 75 m intervals.

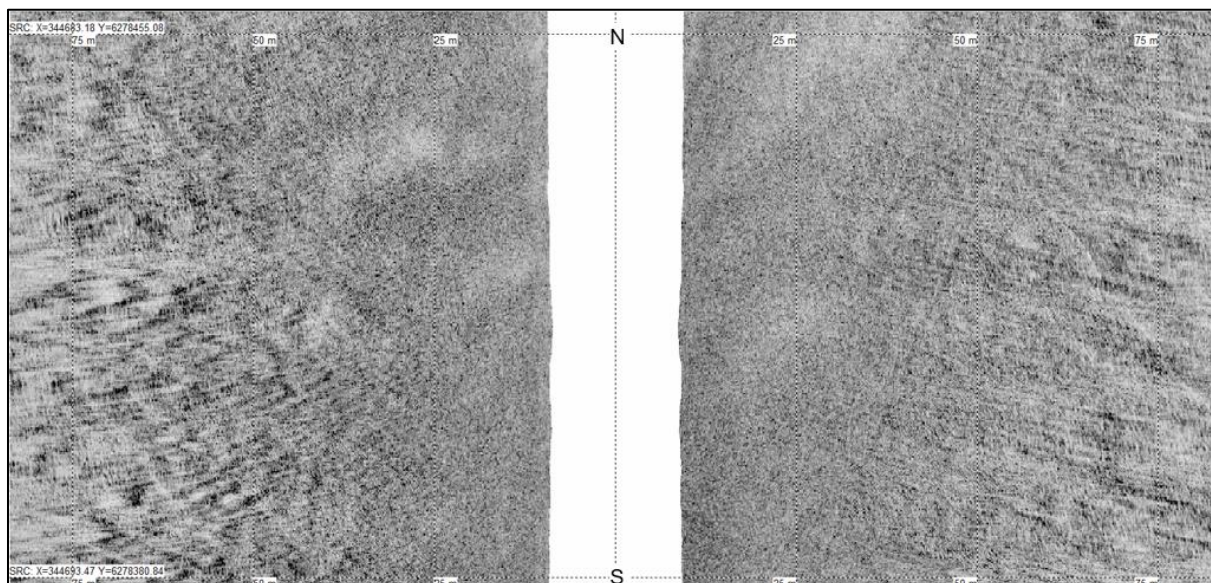


Figure 40 Example 1 of high frequency SSS image from block BM01, Relume. The example is displaying pycnocline. Horizontal scale lines at 75 m intervals.

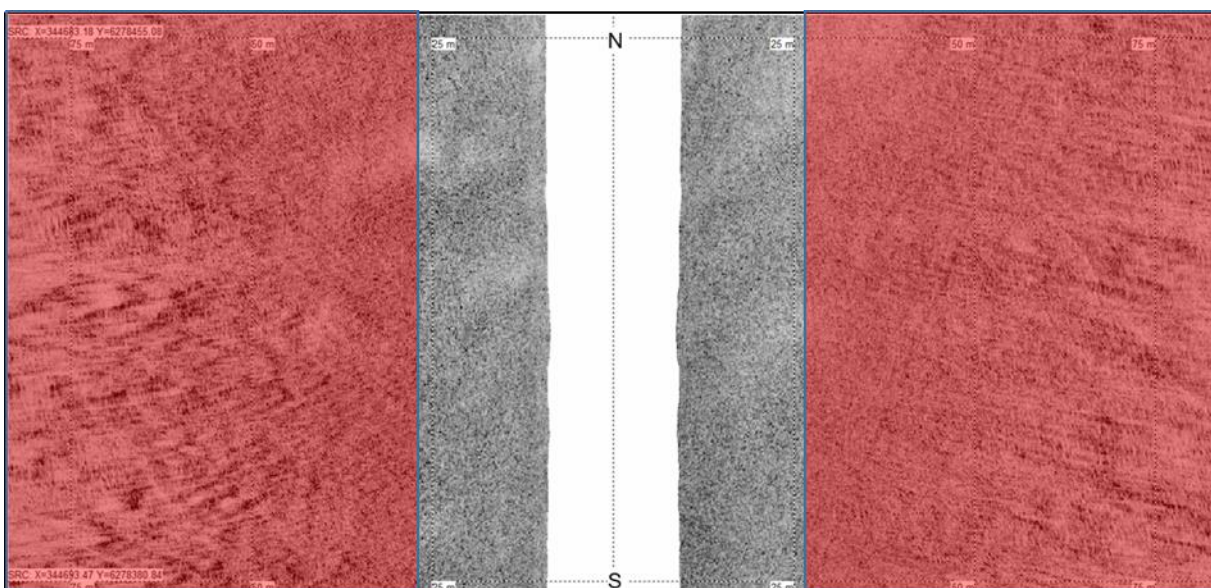


Figure 41 Example 2 of high frequency SSS image from block BM01, Relume. The areas affected by pycnocline are highlighted red. Horizontal scale lines at 75 m intervals.

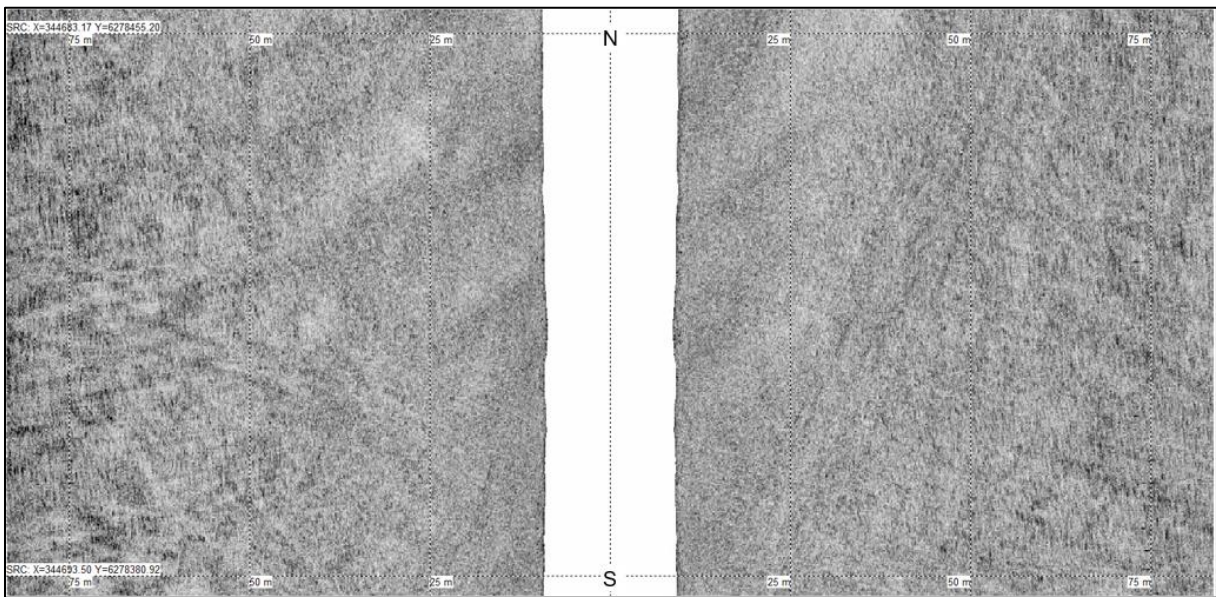


Figure 42 Example of low frequency SSS image from block BM01, Relume. The example is displaying pycnocline. Horizontal scale lines at 75 m intervals.

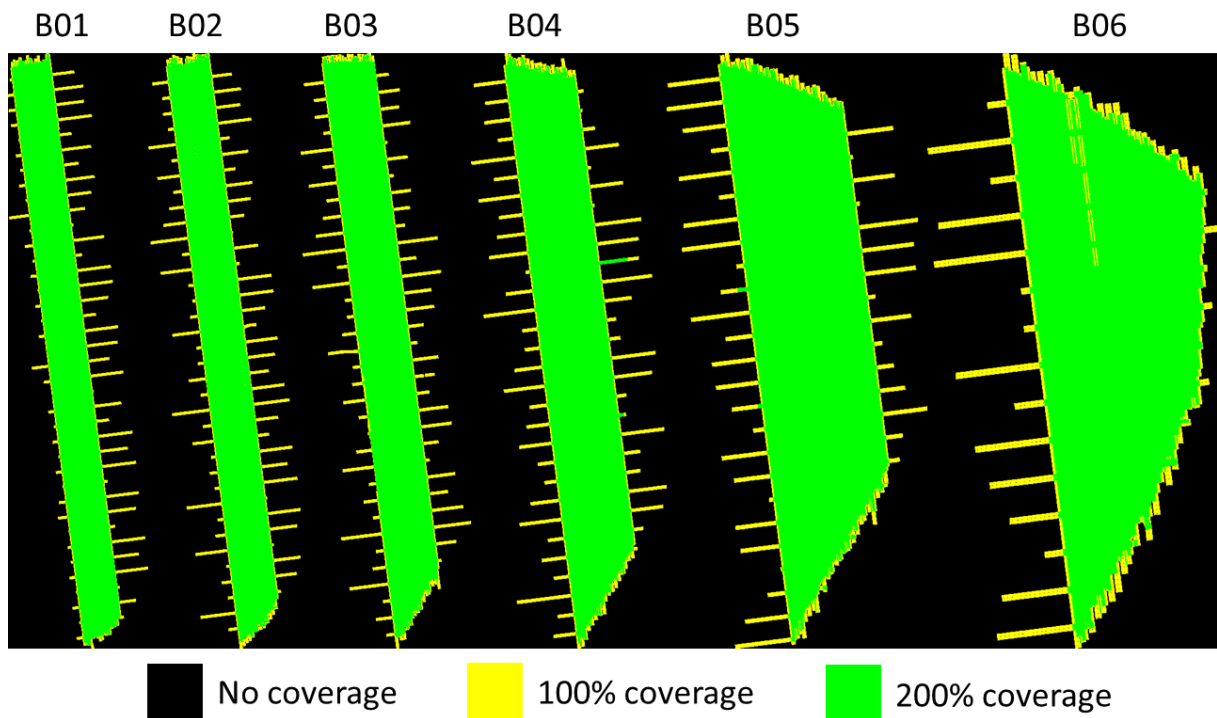


Figure 43 SSS coverage plots for each of the survey blocks. Accounted for adjusted range and 5 m nadir.

5.4 | MAGNETOMETER DATA

The MAG data was piggy backed behind the SSS tow fish. The intention was to keep the MAG altitude at less than 5 m. The aim was to be able to pick large anomalies as well as linear features such as cables and pipelines.

A statistical analysis for MAG altitude was conducted. In total, 2619 sections of lines were assessed, representing a total distance of 8530.42 km surveyed in the MMT OWF survey area. While 95.29% of this distance was surveyed with an altitude of below 5.5 m. A total of 4807 km was surveyed at the target altitude below 5 m, representing 56.35% of the data. The Total Weighted Average Altitude for the whole survey was 4.91 m. Table 18 and Figure 44 outlines final figures for the MMT OWF survey area.

Table 18 Summary of Average Altitudes, Percentages and Distances

Average Altitude (m)	Number of files / Line sections	Percentage (%)	Distance (km)
Alt ≤ 5m	1373	56.351	4807.00
Alt 5 – 5.5m	1113	38.942	3321.90
Alt 5.5 – 6m	130	4.647	396.37
Alt 6 – 6.5m	2	0.057	4.89
Alt 6.5 – 7m	1	0.003	0.26
Alt ≥ 7m	0	0.00	0.00
Totals	2619	100	8530.42

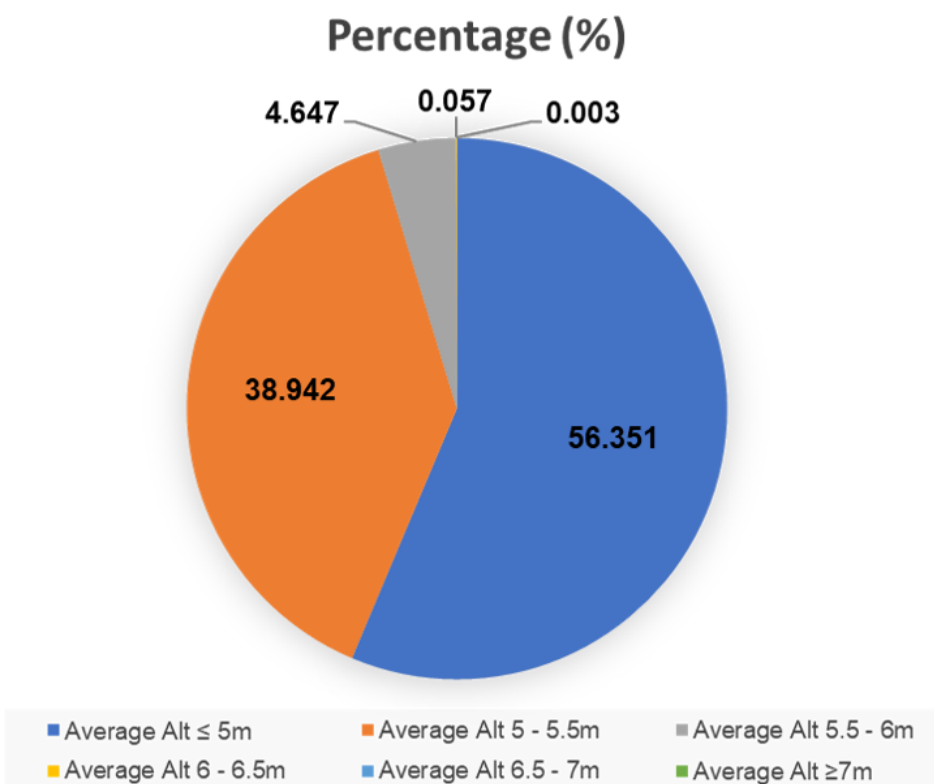


Figure 44 Pie chart illustration of Average Altitudes, Percentages and Distances

MAG data quality was generally good. Background noise levels were below +/- 5 nT (Figure 45 and Figure 46). No data had to be rerun due to noise.

A number of reruns were required where the altitude was out of specifications or where the line was off track due to fishing gear. In general, navigation was good and minimal dropouts from the USBL system were observed. Where navigation was lost the total time of dropout had negligible impact on the overall positioning of the magnetometer.

The altitude averaged 5 m across the area and the signal strength was very good with a mean of approximately 1200.

The data was deemed fit to identify large hazards and cables as per the requirements of the work scope.

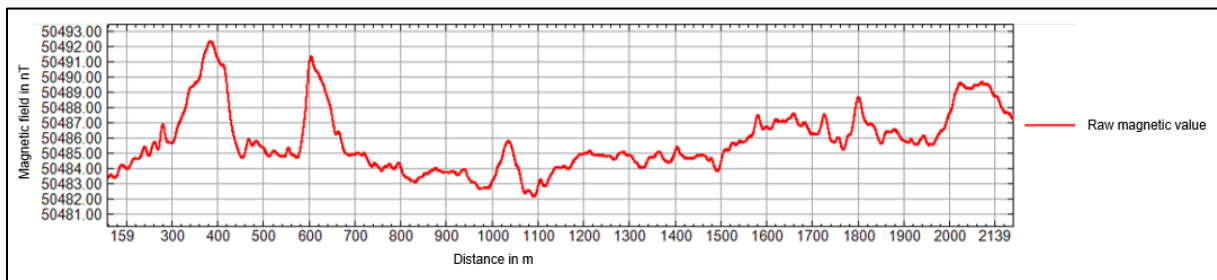


Figure 45 Magnetometer profile showing low background noise level for Northern Franklin.

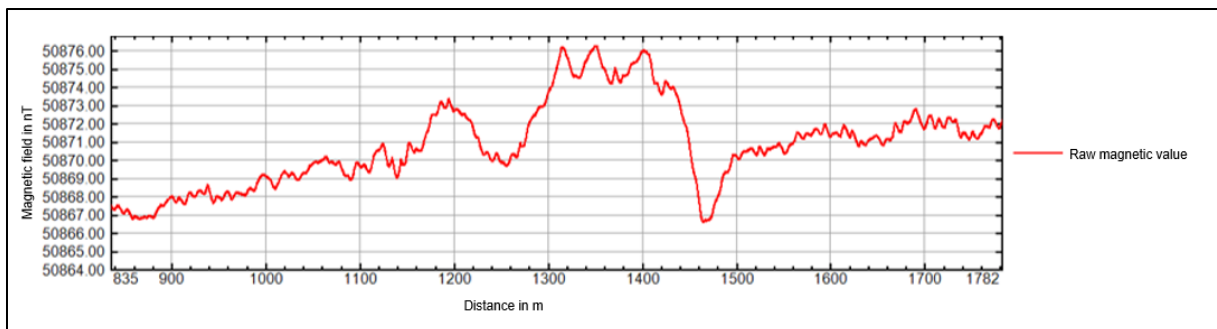


Figure 46 Magnetometer profile showing low background noise level for Relume.

5.5 | SEISMIC 2D UHRS DATA QUALITY ANALYSIS

In order to assess the data quality of every acquired line, the following Offline QC processing flow was applied to all lines, along with all external steps (Figure 47).

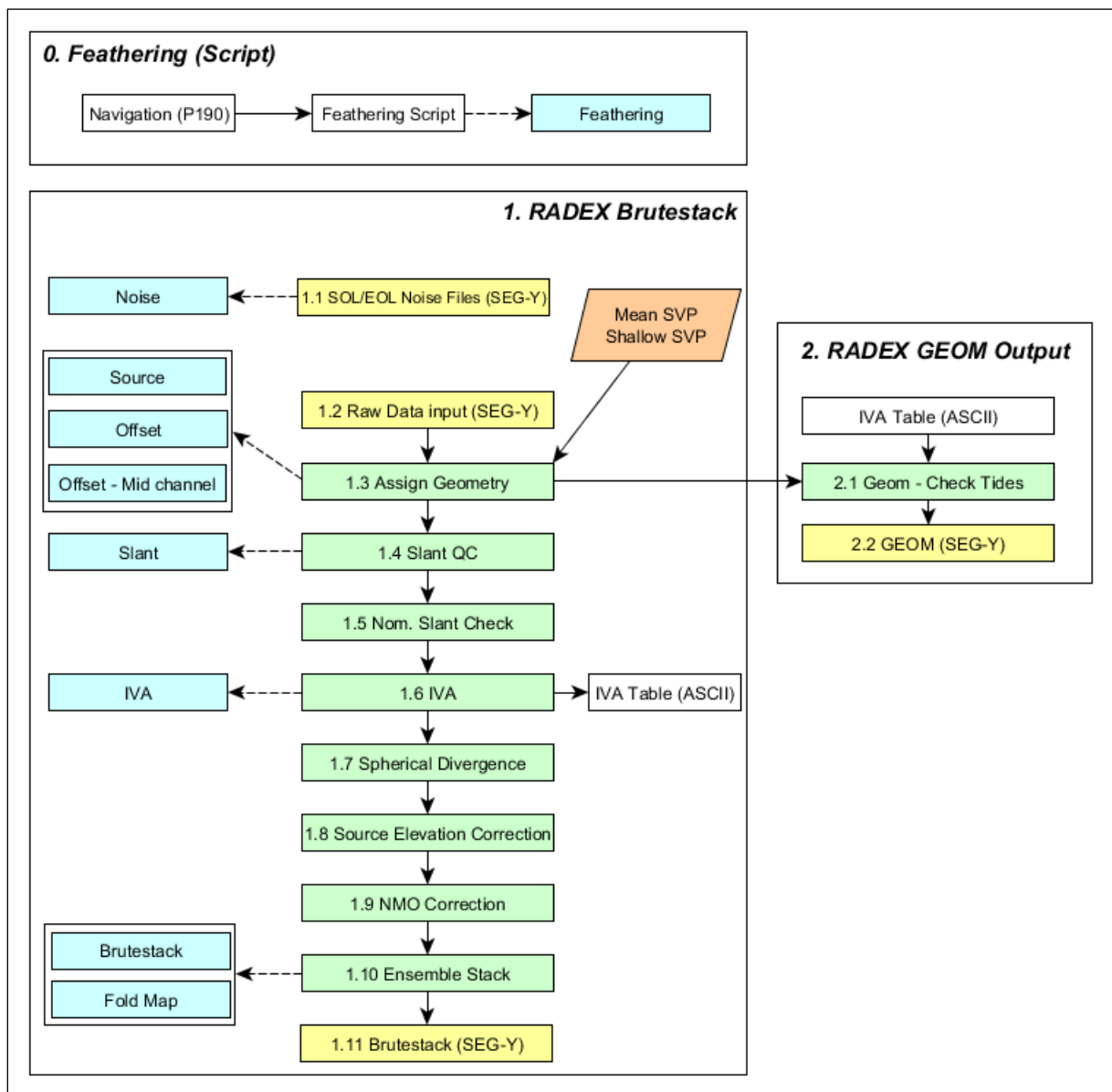


Figure 47 Processing workflow applied to the seismic lines. Green boxes represent the processing steps, blue boxes represent the QC plots, yellow boxes represent the imported and exported SEG-Y data, white boxes represent the intermediate data and the orange box the Sound Velocity Profile (SVP) data.

The UHRS QC & QA is a seismic processing service that ensures that the acquired UHRS data meets the contracted technical requirements:

- Throughout the survey the data was QC'd and made available for review within 24 hours of completion of survey operations;
- The agreed quality criteria were ensured during the QC/QA of the 2D seismic data in regards to:
 - Coverage;
 - Line keeping;

- Data resolution;
- Signal penetration;
- Signal quality;
- Feathering;
- Data fold.

The offline QC was performed with key software and in house developed processing flows necessary to carry out the job to completion. The software used was RadEx Pro from Deco Geophysical.

5.5.1 | FEATHERING

The feathering angle was calculated along all the seismic profiles (see example in Figure 48). A maximum feathering angle of 8° was initially established for vessel steering and 15° for strong water currents. For the duration of the survey only the steering limit was surpassed on a few lines. On the other hand, the feathering values resulting from currents was always substantially below the established limit.

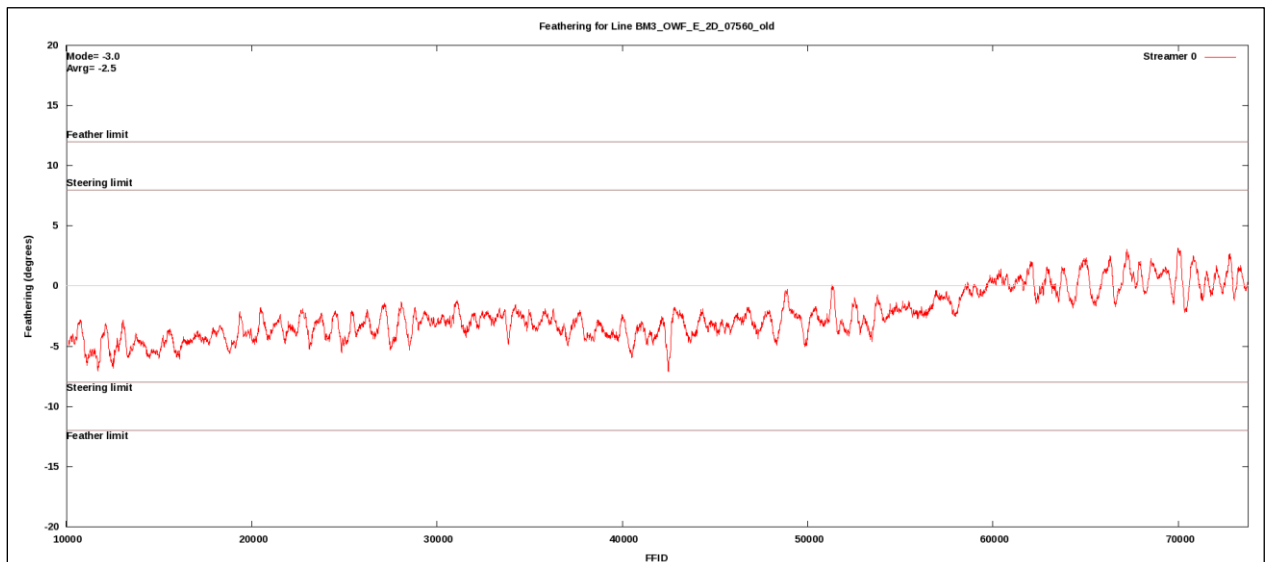


Figure 48 Feathering plot calculated for the line BM3_OWF_E_2D_07560.

5.5.2 | SIGNAL & NOISE ANALYSIS

The main sources of noise identified during the survey were (see Figure 49):

- Vessel noise – in red in Figure 49. This is a directional noise, that can be filtered using extended processing techniques without major negative impact on the signal.
- Front and tail cable tugging noise represented in blue and red, respectively, in Figure 49. The front/tail tugging occurs when the front/tail frame is pulled by waves and currents and that creates a low frequency vibration along the streamer. This is a directional noise that can be removed using an F-K filter.
- SIMOPS noise interference (Figure 50 and Figure 51) – Sporadic events when other vessels (Fugro Pioneer) came close to the Relume. In some cases, it was even possible to record a seismic pulse from their equipment (Figure 51).

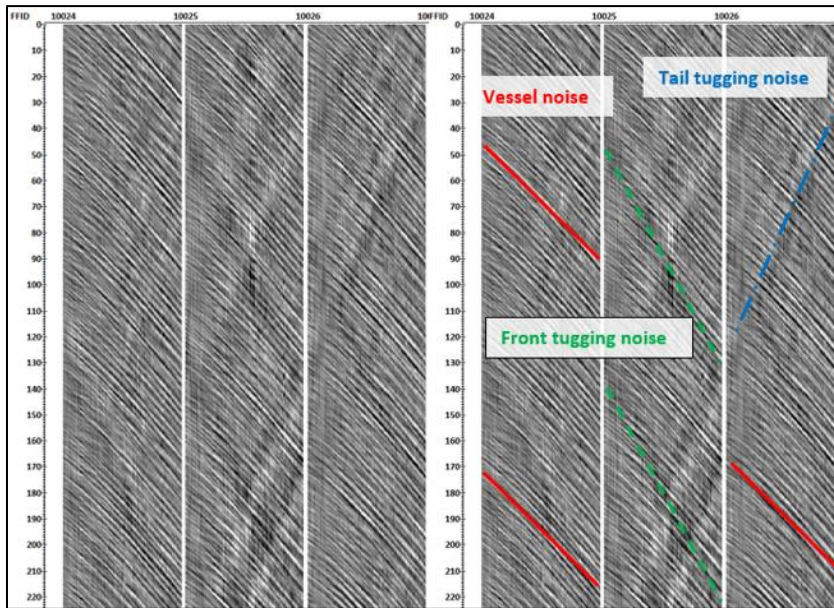


Figure 49 Main noise sources identified in the working limit noise test. Vessel acoustic noise and cable tugging at the front and tail recorded by the M-UHRS streamer.

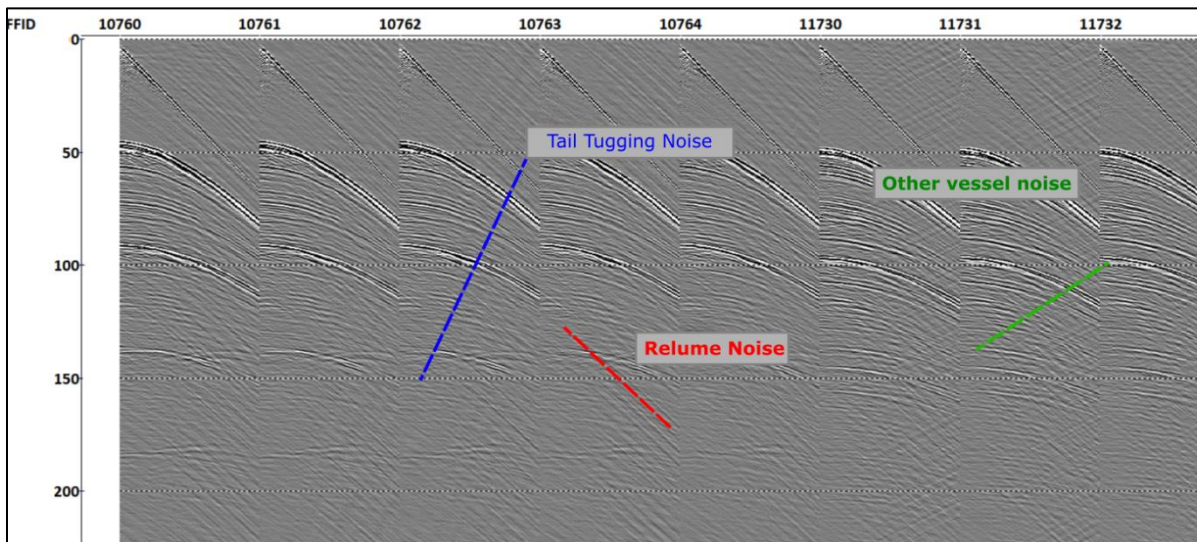


Figure 50 Main noise sources identified while in production. Relume acoustic noise (Red), cable tail tugging (Blue) and another vessel passing nearby (Green) recorded by the M-UHRS streamer.

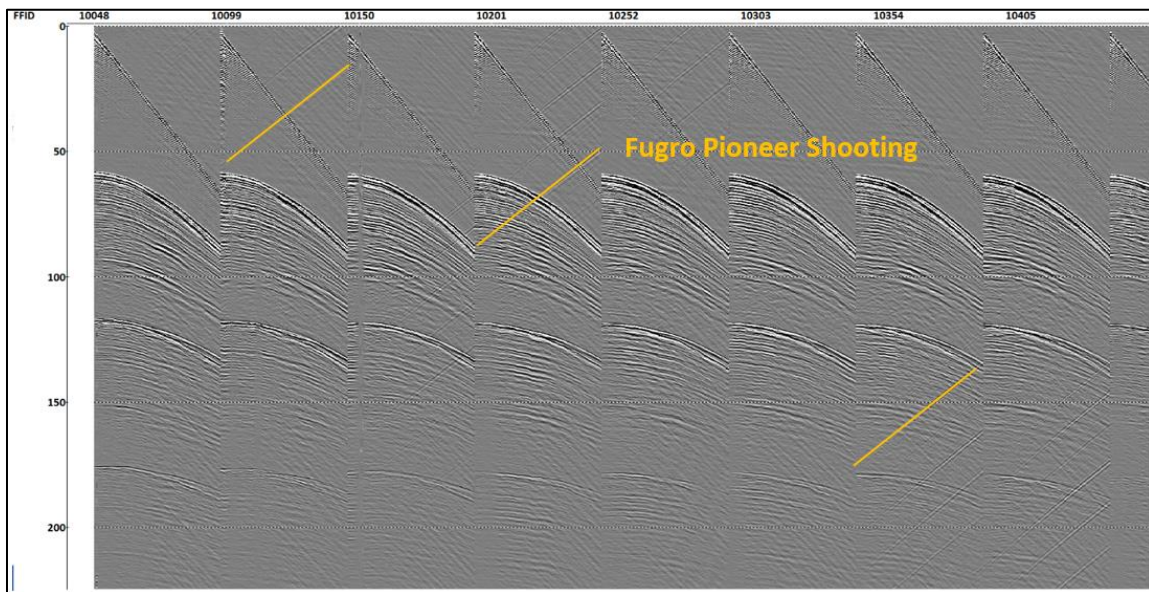


Figure 51 Fugro Pioneer shooting while in SIMOPS.

All the above-mentioned types of noise were thoroughly analysed. On a line-by-line basis, a noise check was performed before and after line acquisition, in order to assess the noise level variations. Generally, a difference of +/- 20 dBs between sparker and the noise was achieved (Figure 52). The noise levels did not represent a major risk for the M-UHRS survey.

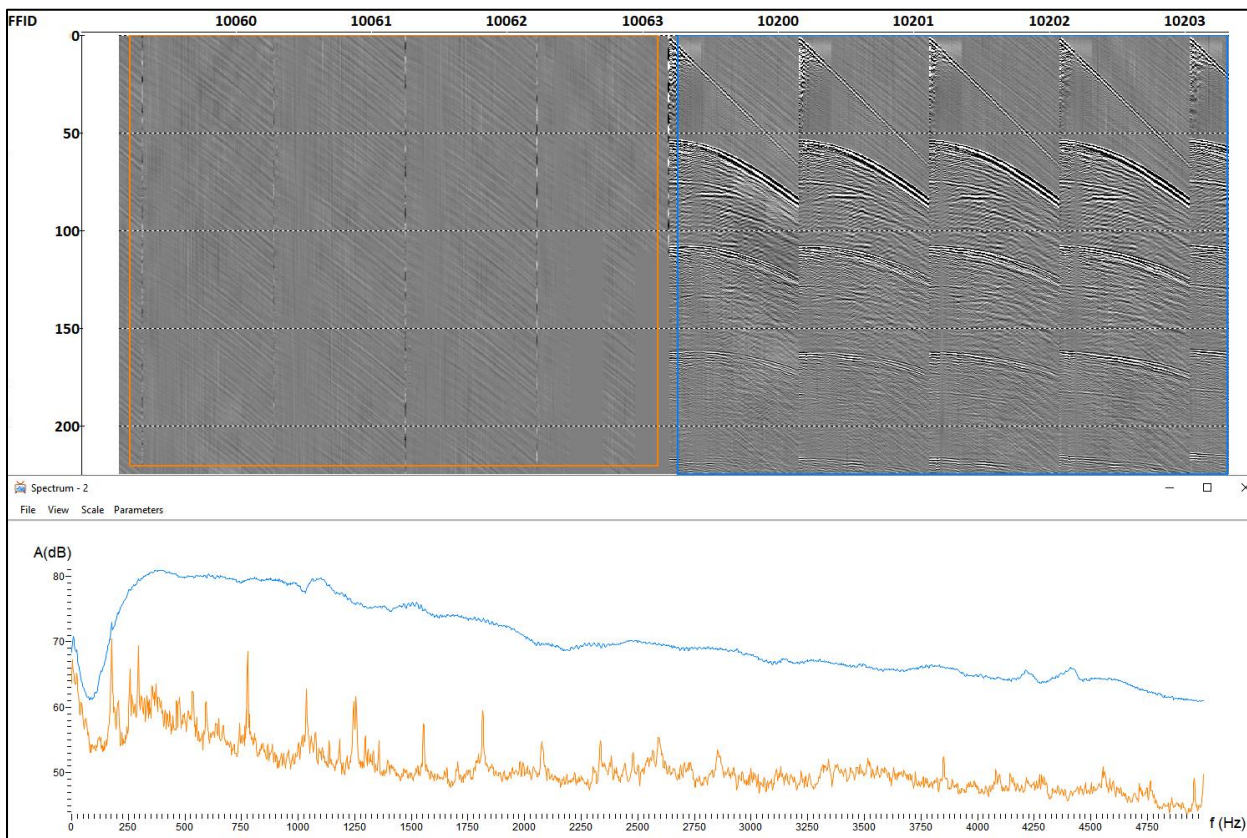


Figure 52 Frequency spectrum comparison.
Background noise (orange) and sparker signal (blue).

5.5.3 | SOURCE RECEIVER OFFSETS

Source and receiver positions and the relative offsets were initially calculated using the DGPS antennas located on top of the sources and on the streamer front and tail buoys. The accuracy of the source and receiver positioning was checked by comparing the offsets calculated from the source and receiver positions with direct arrival times (Equation 1). The offsets were estimated using the calculated distance between two points explained in Equation 1 and converted to time by dividing the obtained offset in metres by the measured water sound velocity (the sound velocity in the water was obtained from measured SVPs during the survey).

$$offset = \sqrt{(Sou_X - Rec_X)^2 + (Sou_Y - Rec_Y)^2}$$

Equation 1 – Equation used for calculating the offsets based on the positioning.

On average, the inline offset between the near channel of the streamer and the source was 1 m, and the crossline offset was 3 m. The source-receiver relative position did not change during the survey, although some variations could occur mainly due to surface currents.

In general, the offsets based on antenna position have a good match with the direct arrival (Figure 53 and Figure 54). Occasional mismatch was observed, mainly due to the loss of differential correction on the DGPS antenna (Figure 55), nevertheless the difference between the direct arrival and calculated offsets was reasonable and most of the time below 1 ms.

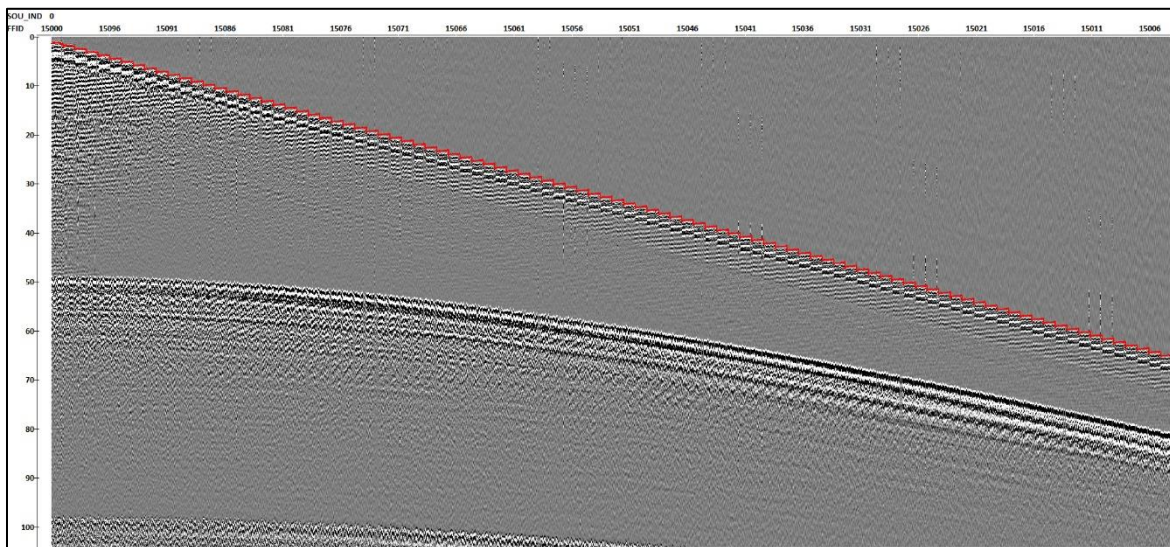


Figure 53 Channel domain showing the calculated offsets. The offsets are based on the DGPS positioning (red line) on top of the direct arrival, for all 96 channels, for line BM2_OWF_E_2D_02730. Vertical scale in TWT (ms).

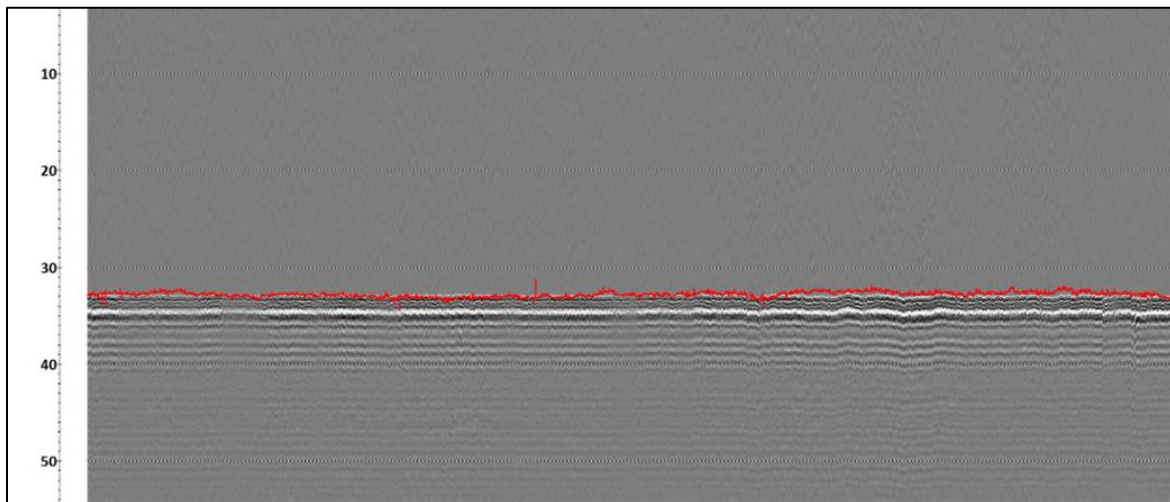


Figure 54 Profile BM4_OWF_E_2D_08820 in channel domain.
The image is showing the calculated offsets based on the DGPS positioning (red line) on top of the direct arrival for channel 48. Vertical scale in TWT (ms).

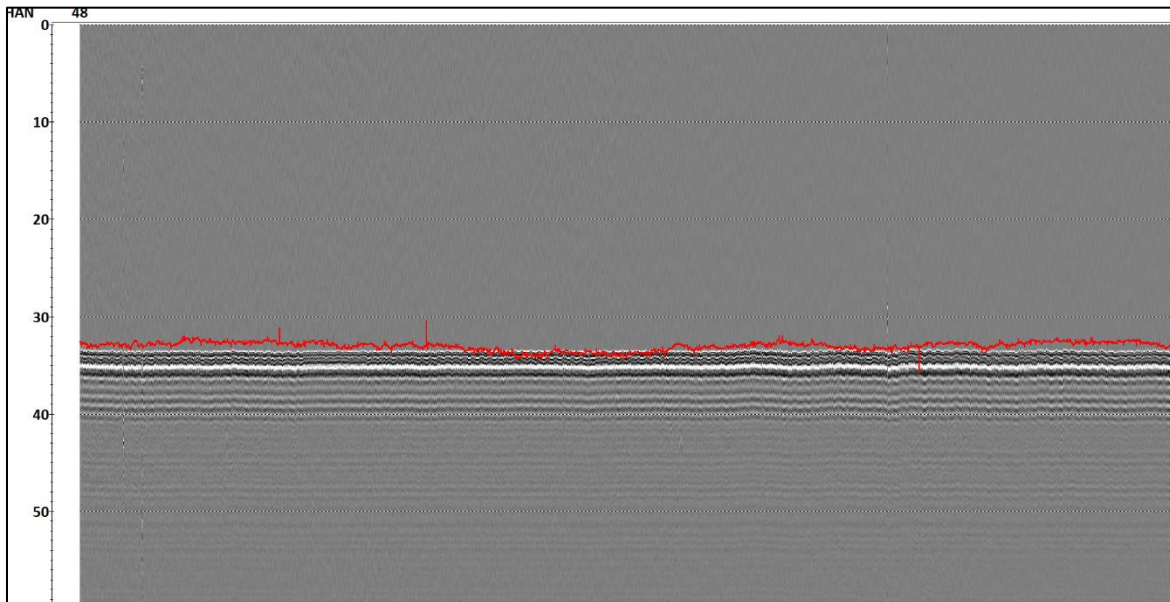


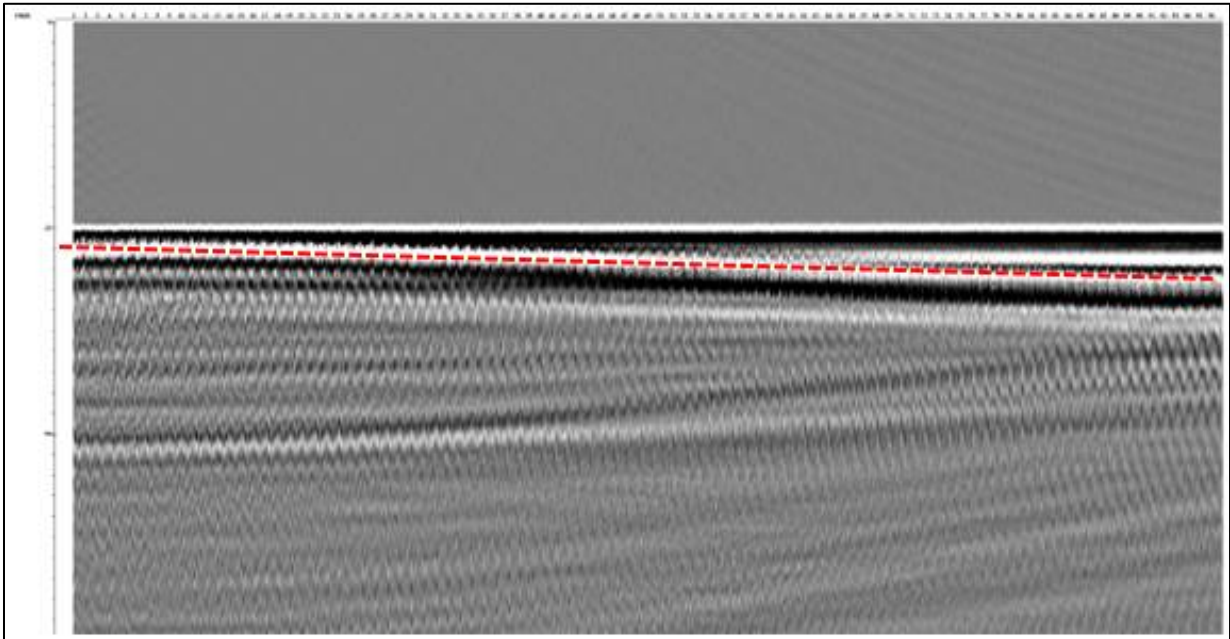
Figure 55 Profile BM5_OWF_E_2D_15540 in channel domain.
The image is showing the calculated offsets based on the DGPS positioning (red line) on top of the direct arrival for channel 48. Vertical scale in TWT (ms).

5.5.4 | STREAMER GROUP BALANCING

The streamer was balanced for the survey speed range of 3.5 - 3.8 knots Speed Through Water (STW). Along the streamer, several lead weights were placed in order to achieve the slant shape. To evaluate if the cable was properly slanted, a direct observation of the receiver ghost along all channels was done on a line-by-line basis (Figure 56).

Streamer balance integrity can vary depending on sea conditions, wave motion, vessel steering, surface currents, acquisition velocity, positioning precision and minor modifications of the system geometry during equipment recovery and deployment operations. All these factors may have negative impact on the final UHRS data.

All the seismic profiles underwent to QC/QA in order to assess the streamer balancing and to ensure that the data could be successfully processed.



*Figure 56 Channel domain with flattened seabed.
The image is showing the increasing ghost reflection depth along the channels (see the ghost reflection – red dashed line) for line BM3_OWF_E_2D_05880, vertical scale in TWT (ms).*

5.5.5 | INTERACTIVE VELOCITY ANALYSIS

Supergathers were generated every 1000 CDP comprising 3 CDP to build the dynamic stack. RMS velocity curves were generated through the interactive velocity analysis for all lines and were used for NMO corrections and stacking (Figure 57). Interactive velocity analysis was also used as a tool for data QC, mainly regarding penetration.

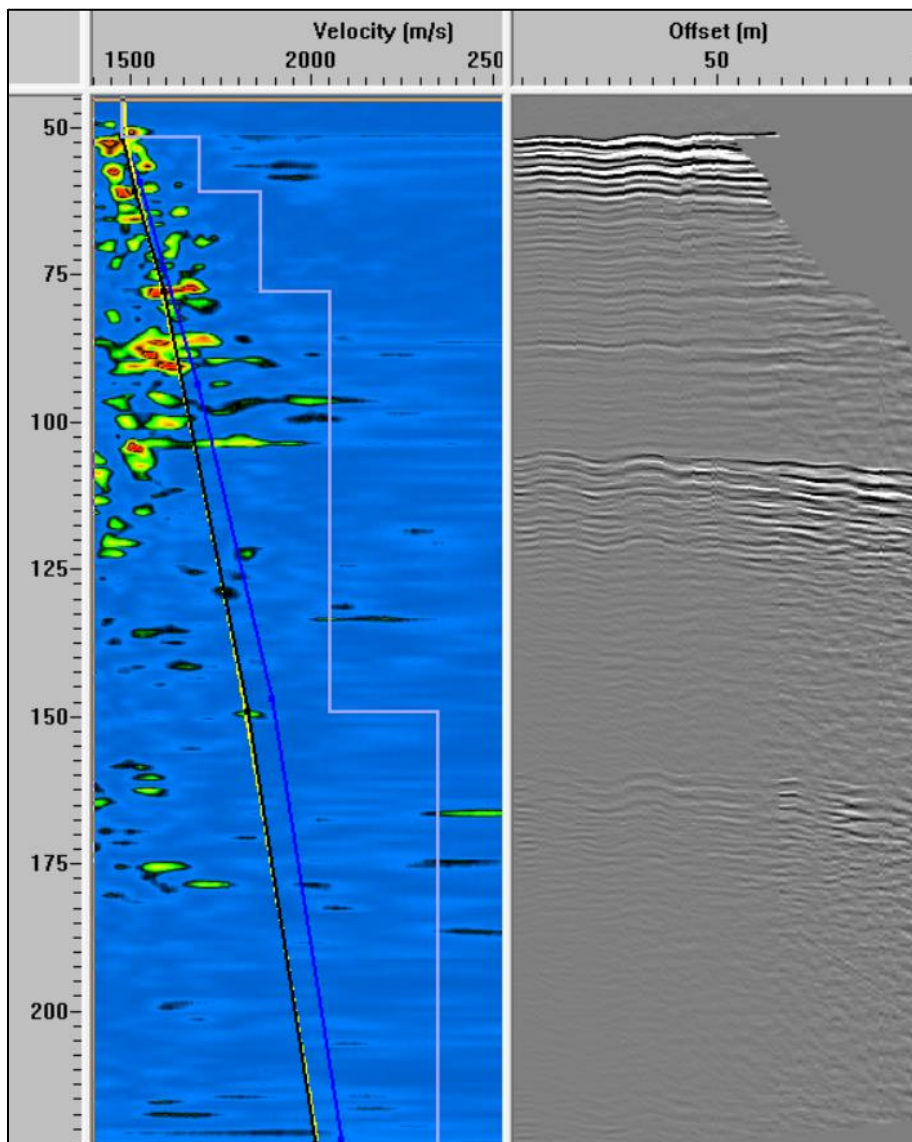


Figure 57 Velocity Analysis display for line *BM3_OWF_E_2D_07770*.
The grey line represents the interval velocities and the black line shows the RMS velocity in the actual CDP gather; vertical scale in TWT (ms).

5.5.6 | CDP FOLD

The impact of the positioning solution, triggering, steering, feathering, navigation and the number of bad shots on the CDP bin fold regularity was assessed with CDP fold track plots (Figure 58). With minor deviations, all processed lines show a mean CDP fold around 192. Trace fold header recorded values were used to assess the cumulative impact of steering & feathering and bad shots on the seismic data.

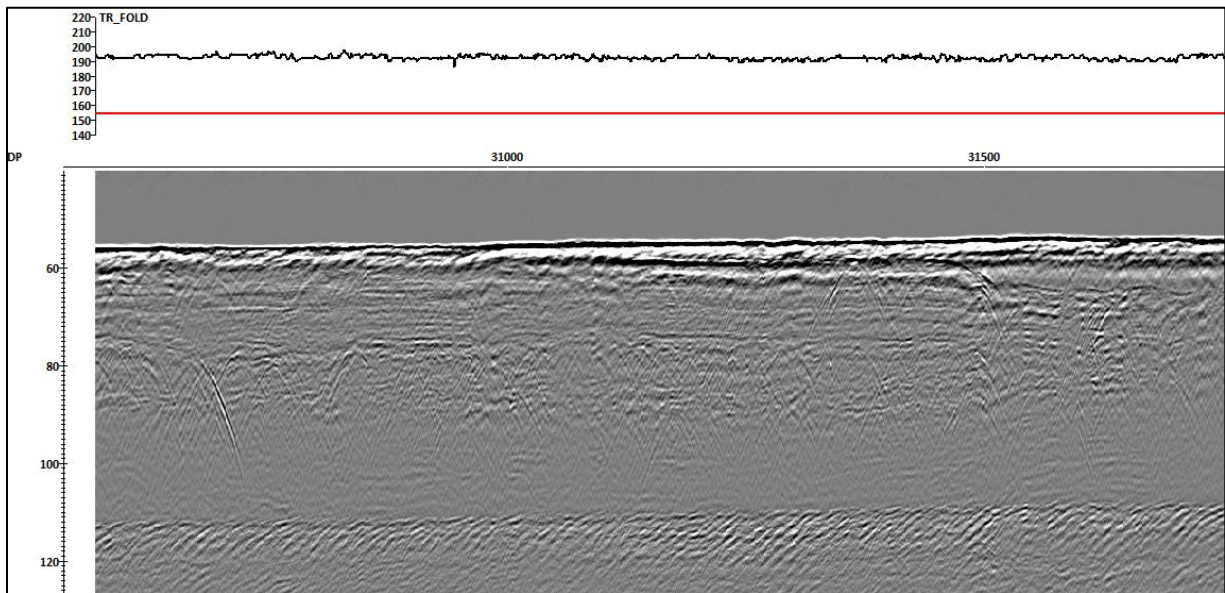


Figure 58 Trace fold values plotted on the top of stacked sections.
The image shows line BM2_OWF_E_2D_05040 (black curve). Vertical scale in TWT (ms).

5.5.7 | BRUTESTACK

The offshore brutestack of every seismic profile provided a quick image of expected data quality and signal penetration (Figure 59). Several parameters were considered:

- Coverage – confirm by MMT if there were any gaps in the seismic data. Verified by MMT in QGIS project with the CDP Track Plots supplied by Geosurveys;
- Line keeping and coverage – verify if the steering of the vessel were along the line plan with a maximum error of 25 m – verified by MMT in QGIS project with the CDP Track Plots supplied by Geosurveys;
- Signal penetration – Identification of correlative reflections in the brutestack up to 225 ms below seabed, fulfilling the 100 m penetration requirement;
- Signal quality – verification of the existence of any artefacts in the seismic data.

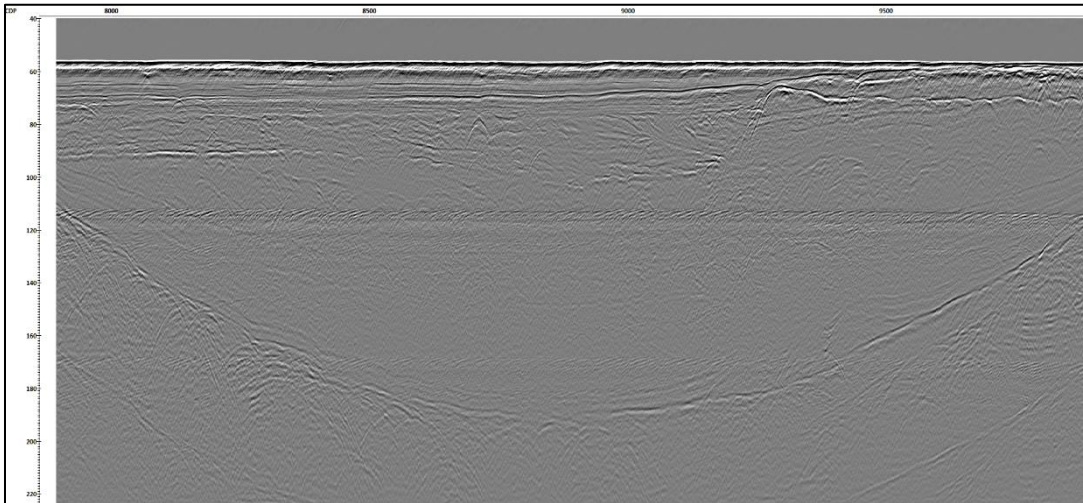


Figure 59 Brutestack for line *BM4_OWF_E_2D_10080_01*.
The image is showing penetration until the end of the record and good signal to noise ratio. Vertical scale in TWT (s).

5.5.8 | GEOM OUTPUT

The raw SEG-Y data acquired by Geo Marine Survey Systems (GMSS) had the following information on the headers:

- FFID number (Byte location 9);
- Channel number (Byte location 13);
- Source positions (SOU_X - Byte location 73, SOU_Y - Byte location 77);
- Receiver positions (REC_X - Byte location 81, REC_Y - Byte location 85).

The raw SEG-Y data was then imported into RadEx Pro (by GS personnel offshore) for data QC/QA, geometry assignment and tidal values import. Due to the more limited computational power on the offshore laptops, the geometry was assigned with a bin size of 1 m. This bin size was used for QC/QA purposes, with no impact on data quality assessment. Once the data arrived to GS office, the bin size was then recalculated to the agreed 0.5 m bin. Crooked-line geometry assignment gives a truer picture of the subsurface when compared with other geometry assignment methods because it considers the angular relationships between the shots and their receivers.

The GEOM SEG-Y dataset (raw data with filled headers - Linename_GEOM.sgy) was then exported with the additional headers filled:

- CDP number (CDP – Byte location 21);
- Source Receivers Offset (OFFSET – Byte location 37);
- CDP position (CDP_X – Byte location 181, CDP_Y – Byte location 185);
- Tide Height (TIDE_HGHT – Byte location 233).

5.6 | SEISMIC 2D UHRS DATA PROCESSING OFFICE

Quality control procedures were carried out throughout the processing scheme, as detailed within the present report and data control was registered along specifically designed logs. All processing steps were checked for the proper application of the seismic imaging enhancement. Several of these quality control plots were delivered to the client as part of this project submission, such as trace and offset QC; streamer slant check; source and receiver heave; image of the TRIM_STK (including trace fold) and image of final MIG (FULL).

Furthermore, at some stages, quality control supervision was carried out by the project's Principal Interpreter to ensure that the seismic processing was being properly applied and for troubleshooting purposes. Finally, and after all intermediate quality controls, lines were inspected by both geophysicists and geologists for acceptance.

Several challenges were encountered during the processing stage of the 2D UHRS seismic dataset received, mainly related to the following:

- Data processing on some profiles was negatively affected by sea conditions;
- Seismic amplitude balancing was corrected to all seismic profiles in order to achieve similar imaging of the subsurface;
- Fine tuning of the post-stack demultiple and post-stack migration in order to attain real geological features but also to attenuate the multiple energy and undesired diffraction effects, respectively;
- Seismic resolution improvement, both horizontal and vertical, was always the priority in all processing steps.

A full processing report detailing all quality control steps, is available in Appendix D].

5.7 | SUB-BOTTOM PROFILER DATA - INNOMAR

The Innomar data was collected in order to acquire good resolution data in the upper 10 m of the seabed. The settings of the Innomar were adjusted to achieve this.

SBP data quality was generally good (Figure 60). Some interference was introduced by the 2D UHRS Sparker (Figure 61) but was mostly removed by noise removal techniques using RadExPro (Figure 62). Penetration achieved up to 10 m (target depth), this was variable across the site due to changing ground conditions; achieved penetration was dependent on the distribution of channelling beneath an initial coarse unit and dependent on the presence of observable units below H10 (Figure 60). Average penetration was 5-8 m.

Data from Relume and Northern Franklin were signal processed to ensure consistent gains across datasets.

The Innomar SBP data was reviewed and compared to the 2D UHRS data specifically for shallow geology information. Interpretation was compared for consistency between SBP and UHRS datasets. SSS and MBES data was also used to confirm sediment boundaries on the surface.

In areas where horizons could not be tracked in the SBP data due to geological factors, the UHRS interpretation was used to interpolate the SBP interpretation for the purpose of producing more complete grids and isopachs. On some SBP lines, additional interpretation was added for the purpose of aligning with UHRS data. Some of these horizons appear below the area of interest on the SBP data.

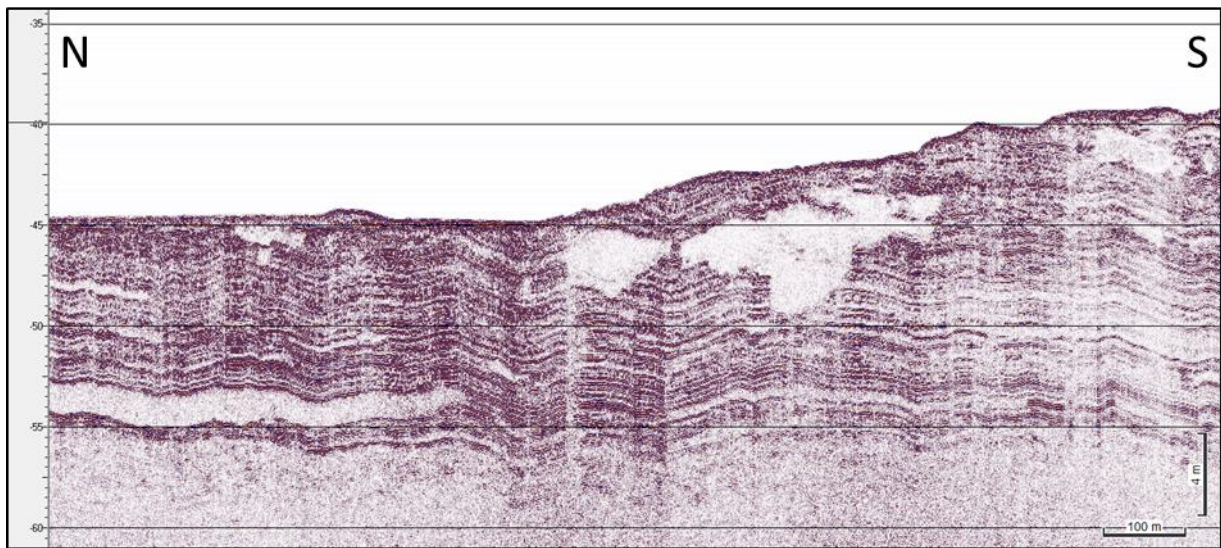


Figure 60 Innomar data showing achieved penetration of 10 m.



Figure 61 Raw Innomar data showing vertical striping Sparker interference.

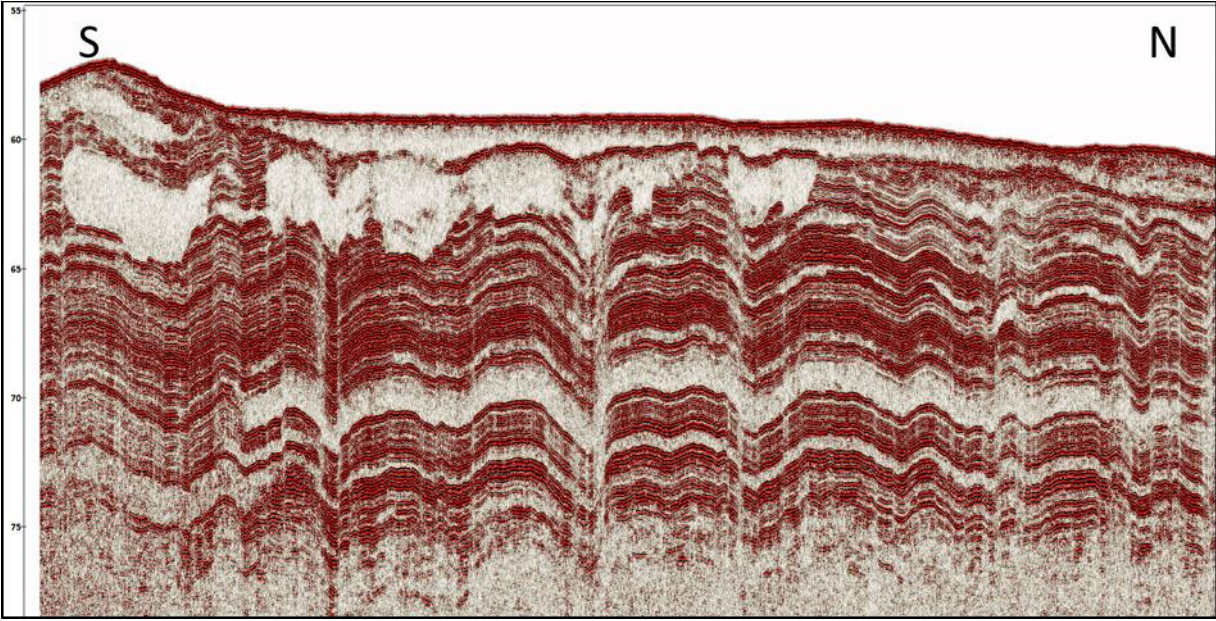


Figure 62 Processed Innomar data showing improved signal to noise ratio.



6 | BACKGROUND DATA AND CLASSIFICATIONS

Client provided background information and the GIS database were the main resources used during data interpretation. Additionally, academic literature resources were used to support interpretations and are listed within the references in Section 11|.

6.1 | SEABED GRADIENT CLASSIFICATION

The seabed gradient is classified according to Table 19.

Table 19 Seabed gradient classification.

CLASSIFICATION	GRADIENT
Very Gentle	< 1°
Gentle	1° - 4.9°
Moderate	5° - 9.9°
Steep	10° - 14.9°
Very Steep	> 15°

6.2 | SEABED SEDIMENT CLASSIFICATION


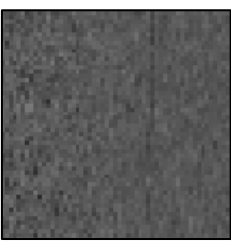
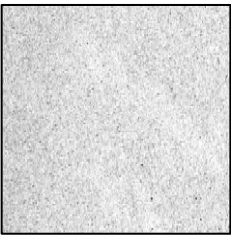
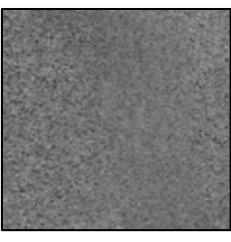

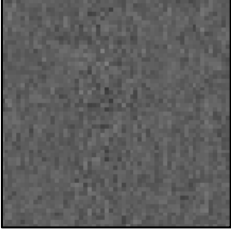

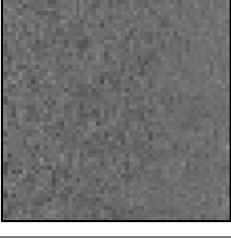
The interpretation of surficial sediment types was derived from the acoustic character of the high frequency side scan sonar (SSS) data, and the interpretations aided by multibeam echo sounder (MBES) bathymetric 3D surfaces, multibeam backscatter (MBBS) and sub-bottom profiler (SBP) data, along with the results from the grab sampling. During the review of the SSS survey data, higher intensity sonar returns (darker grey to black colours) were interpreted as relatively coarser grained sediments, and lower intensity sonar returns (lighter grey colours) were interpreted as relatively finer grained sediments. Bathymetric data was used to assist in boulder field interpretation and to correct for the effects of seabed slope on sonar returns.

The MBBS data shows the intensity of the reflected MBES signal and is used to assist interpretation of surficial sediment types (in conjunction with geotechnical data). In MBBS data high intensity sonar returns (lighter grey colours) were interpreted as relatively coarser grained sediments and low intensity sonar returns (darker grey colours) were interpreted as relatively finer grained sediments. Despite this representation being opposite to how SSS data is presented, MBES processing convention dictates this tonal relationship with MBBS data intensity.

The MBBS data is processed within QPS FMGT on a block-by-block basis and a single raster created using Safe Software FME. The resolution of the final MBBS raster is 0.5 m. The MBBS data was used to assist the surficial sediment interpretation.

The ID column in Table 20 defines the colour in the charts for the specific sediment type. All particle sizes refer to the soil classification in ISO 14688-1 (2002).

Table 20 Sediment classification.

ID	SSS Image	BS Image	Acoustic Description	Lithological Interpretation	Class*
			Low acoustic reflectivity. No texture. Texture indicates wave and stream working of the sediment.	MUD and SANDY mud Predominantly mud (silt & clay), may contain sand.	1a
			Low to medium acoustic reflectivity. No texture.	Muddy SAND Predominantly sand with variable fractions of mud (silt & clay).	1a
			Medium acoustic reflectivity, slightly grainy texture.	SAND Predominantly sand, may have minor fractions of clay, silt and/or gravel.	1b
			Medium to high acoustic reflectivity. Slightly grainy to grainy texture, coarse texture in places.	GRAVEL and coarse SAND Predominantly gravelly sand, may contain silt. The ratio between sand and gravel can vary within this sediment type.	2a

* Danish Råstof-bekendtgørelsen

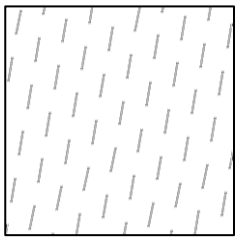
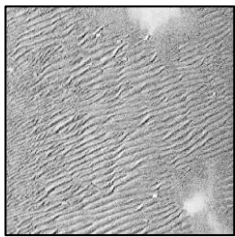
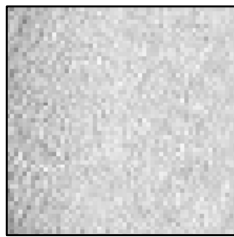
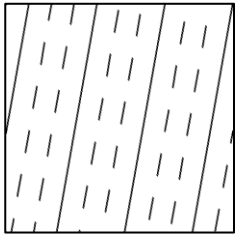
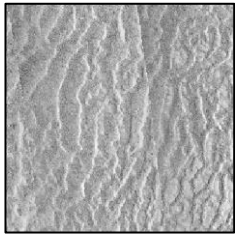
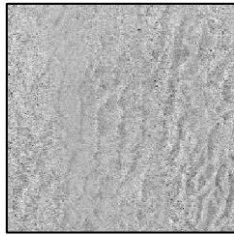
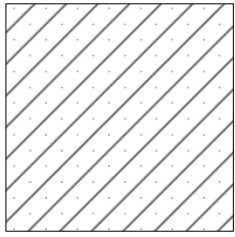
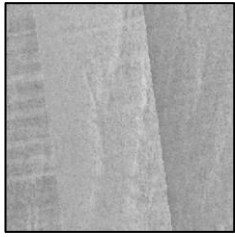
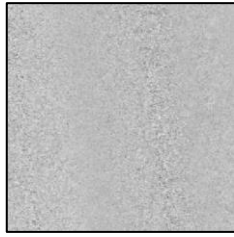
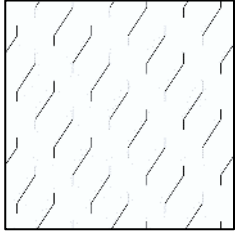
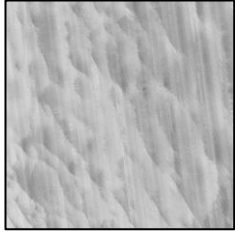
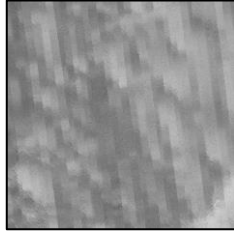
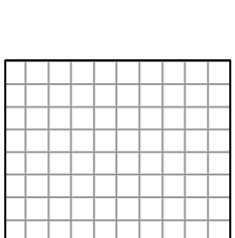
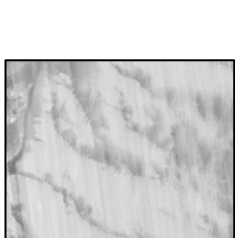
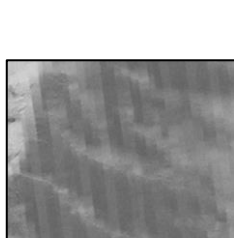
Note: the definition MUD has been used to keep in line with the TSG standards. MUD is comprised of SILT and/or CLAY.

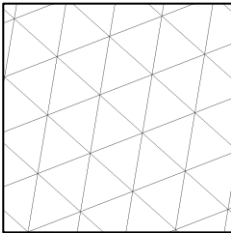
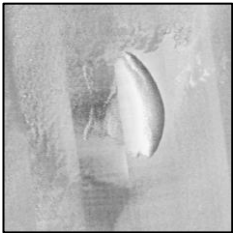
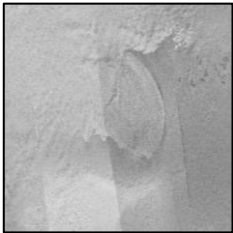
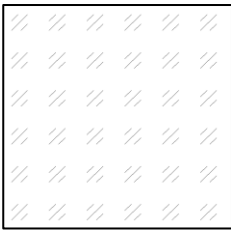
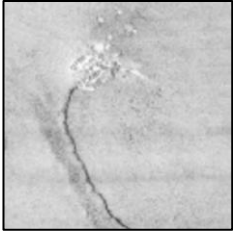
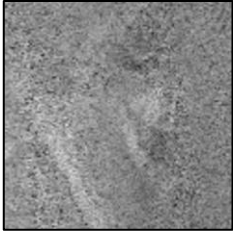
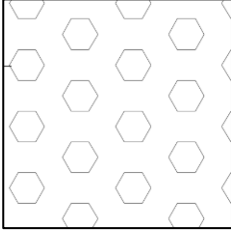
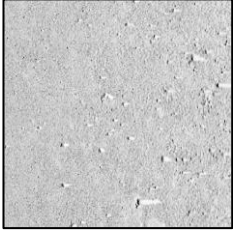
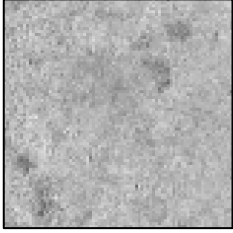
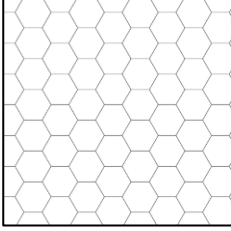
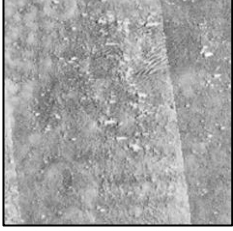
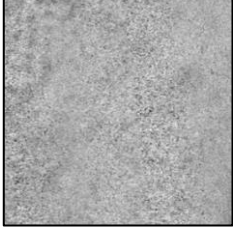
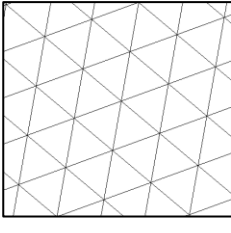

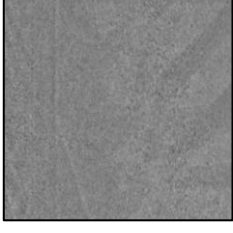
6.3 | SEABED FEATURE / BEDFORM CLASSIFICATION

The ID column in Table 21 defines the pattern in the charts for the specific feature type. Apart from the ones presented here, trawl marks were also digitized.

SSS, MBES and MBBS data have been used for interpretation of the seabed feature boundaries.

Table 21 Seabed features classification.

ID	SSS Image	BS Image	Seabed Feature	Criteria
			Ripples	Wavelength <5 m Height < 0.1 m Wavelength is the primary classifier.
			Large Ripples	Wavelength 5 – 15 m Height 0.1- 1 m Wavelength is the primary classifier.
			Megaripples	Wavelength 15 - 50 m Height 1 - 3 m Wavelength is the primary classifier.
			Sand Waves	Wavelength 50 - 200 m Height 3 - 5 m Wavelength is the primary classifier.
			Sandbars	Wavelength > 200 m Area of large-scale sediment transport/migration forming massive bedforms such as sandbars, sand ridges and sand dunes. This feature was added post scriptum to account for sediment formations which are larger than 200 m WL.

ID	SSS Image	BS Image	Seabed Feature	Criteria
			Other-Sediment Mound	Isolated sediment mass topographically higher than surrounding area.
			Other-Area of Interest	Unknown features – assessed for biogenic origins.
			Boulder zone type 1: Intermediate boulder density	40 - 80 boulders per 100x100 m.
			Boulder zone type 2: High boulder density	> 80 boulders per 100x100 m.
			Trawl Mark Area	Area with multiple trawl marks/seabed scars.

The SSS and MBES contacts were classified according to the following criteria:

- Boulder
- Man-made object (MMO) (Debris, fishing gear, man-made structures etc.)
- Wreck
- Other

Boulders were grouped into boulder fields based on their spatial density:

- < 40 boulders per 100x100 m – not a boulder zone
- 40 - 80 boulders per 100x100 m – boulder zone type 1: Intermediate boulder density
- > 80 boulders per 100x100 m – boulder zone type 2: High boulder density

Boulders ≥ 1.0 m were interpreted inside and outside of boulder fields.

Boulders were primarily interpreted in the MBES data. Subsequently, remaining boulders and all other contacts were interpreted in the SSS data.

In the GIS database all MAG anomalies are categorized as MMO, due to the inherent uncertainties of magnetic anomaly interpretation. Best efforts were made to avoid selecting anomalies that are likely to be geological in nature, but in the cases where differentiation between man-made or geologically derived anomalies were not possible, the anomaly was selected but with a comment of “Likely Geology”.

All MAG anomalies were compared to all MBES and SSS contacts. If a MAG anomaly was within 5 m of any contact detected in either MBES or SSS, it was automatically deemed a correlation and commented on in the contact listing, as well as in the GIS database.

MAG anomalies forming a linear pattern were commented as such as these could indicate the presence of fishing gear, cables, wire/chain or anything of a ferrous linear nature. Some linear anomalies were inferred to be of a geological nature and these were also commented as such.

6.4 | SUB-SEABED GEOLOGY CLASSIFICATION

The subsurface geological interpretation and description is based on the assessment of the 2D UHRS and Innomar SBP data acquired within the survey area.

The original contract regarding the geomodel for this project was based on mapping eight horizons, however twelve horizons were mapped in order to properly capture the subsurface complexity of the geological framework in this site.

The descriptions of the seismic units are provided according to the seismic facies, stratigraphic boundaries, and internal reflector terminations. The units used are presented in Table 22. Further details on the seismostratigraphic interpretation and the proposed Geological Ground Model can be found in section 8.6| Seismostratigraphic Interpretation.

SBP contacts are selected when diffraction hyperbolas are present and can be clearly related to a single object.

For further information on the processing steps and classification methods, see sections 4.5| and 4.6|.

Table 22 Summary of the seismic units.

SEISMIC UNITS	ACOUSTIC FACIES AND INTERNAL CONFIGURATION	LOWER BOUNDING SURFACE		EXPECTED COMPOSITION	KINGDOM REFLECTOR COLOUR	STRATIGRAPHY (TENTATIVE CORRESPONDENCE)	
		MORPHOLOGY	NATURE				
U05	The seismic facies is exclusively transparent and always forms on top of U10.	Irregular and discontinuous	Depository	Clay to fine Sand	Gold	Consists of marine sand deposits	Holocene
U10	Generally low amplitude. At the base may be homogenously transparent or with small mound-channel patterns to chaotic; overlaid by oblique downlap reflectors and small lenses. Above, sub-horizontal parallel reflectors. Common discontinuous soft kicks. An internal reflector (H10i) was identified within U10, defined by a Dark Blue horizon.	Mostly flat, tabular	Wave cut ravinement surface; Erosive	Silty sands; gravels; gravelly sand lags	Light Green	Marine sand deposits	Holocene
U20	Two distinct facies: Channels: Micro-meso scale channels, chaotic to parallel infill, commonly mounded-chaotic at the base; Wide shallow basins: low amplitude to transparent homogeneous, faint micro-parallel reflectors and common negative high amplitude anomalies.	V-shape channels and tabular	Erosive	Basins: clays-silts-fine sands; channel infills: fine sands-sands (even gravelly lags/layers?). possible organic-rich.	Dark Green	Infills of small basins and channels, likely in a restricted marine-tidal setting, partially associated to a subaerial fluvial system	
U25	Low amplitude micro-parallel reflectors, undulating; small-scale, scattered box-shaped channels with transparent infill negative amplitude at	Tabular	Erosive	Fine sediments: fine sands-silts (?)	Rosy Brown	Relatively low-energetic setting, possibly a	

SEISMIC UNITS	ACOUSTIC FACIES AND INTERNAL CONFIGURATION	LOWER BOUNDING SURFACE		EXPECTED COMPOSITION	KINGDOM REFLECTOR COLOUR	STRATIGRAPHY (TENTATIVE CORRESPONDENCE)	
		MORPHOLOGY	NATURE				
	the base; channels frequency increase towards the top.					transgressive estuary	
U30	Composite facies; medium to high amplitude; upper section: sub-horizontal, parallel-wavy; centre: meso-micro channels-mounds-oblique; base: mounds, lenses, channel lateral migration, hummocky reflectors, and chaotic in parts.	Tabular	Erosive	Fining-upward, sandier at the base (?)	Orange	Higher energy than U25, fluvial	
U35	Base of three major basins. A composite facies, low to high amplitude; complex meso mounds-channels-lenses; internal erosion surfaces; base: large oblique lenses; the thickness of the internal packages decreases towards the top, becoming more sub-horizontal and sub-parallel, grading up.	Tabular	Erosive	Gravel and sands with enclaves of coarser-grained clasts, fining-upward (?)	Yellow	High energy fluvial bedforms (flash floods?)	
U40	Four types of channels and their lateral deposits: Type A: Base: mound-chaotic-composite, grading up meso-micro scale, chaotic in places; Top: channels, micro parallel wavy oblique reflectors; variable amplitudes from high to low.	V and U-shaped channels	Erosive	Variable: sands, silts, clays	Dark Magenta	Drainage of glacier melt back from the north, and outwash plains	Glacial period (Weichselian?)

SEISMIC UNITS	ACOUSTIC FACIES AND INTERNAL CONFIGURATION	LOWER BOUNDING SURFACE		EXPECTED COMPOSITION	KINGDOM REFLECTOR COLOUR	STRATIGRAPHY (TENTATIVE CORRESPONDENCE)	
		MORPHOLOGY	NATURE				
	<p>Type B: Generally chaotic-oblique-mound-channel to oblique above, common internal mounds-channels; variable amplitude.</p> <p>Type C; Base: chaotic-mound-channel, medium-high amplitude; Top: oblique-channel-mounds to meso-micro parallel wavy, chaotic, and homogenous.</p> <p>Type D: Composite with three facies associations; chaotic base with medium-high amplitude to composite mounds; middle facies sub-tabular with medium amplitude, meso-micro parallel obliques, wavy in places; top facies truncating the deposits below, mounds-channels.</p> <p>Channel lateral deposits/fringes: composite mound-channel facies.</p>						
U50	Two distinct characters: NE region: uniform low to transparent amplitude; faint layering; scattered anomalies of positive amplitude. Elsewhere: low amplitude, parallel at base, chaotic above, common oblique, local channels and transparent deposits.	Tabular	Erosive	Fine sediments, boulders (?)	Medium Orchid	Uncertain: glacial drift deposit (aqua till?) or glaciolacustrine deposition (?)	Glacial period (Weichselian?)
U60	Composite facies, low to high amplitude, complex internal features, meso mounds, channels, and lenses.	V-shape asymmetric	Erosive	Mainly sands with gravel and silt (?)	Red	High energy fluvial bedforms (flash floods?)	Glacial period (Weichselian?)

SEISMIC UNITS	ACOUSTIC FACIES AND INTERNAL CONFIGURATION	LOWER BOUNDING SURFACE		EXPECTED COMPOSITION	KINGDOM REFLECTOR COLOUR	STRATIGRAPHY (TENTATIVE CORRESPONDENCE)	
		MORPHOLOGY	NATURE				
	Numerous oblique internal erosion surfaces. Large clinofold layers fill-in the larger incisions.	channels and tabular					
U70	Infilled channels/valleys. V-shaped: composite infill, two facies associations. U-shaped: Base:medium-high amplitude, meso mounds-channels-parallel, occasionally chaotic; Top: truncating base, lower amplitudes, meso-micro composite mounds-channels, parallel-obliques; common chaotic-homogeneous transparent.	V and U-shape channels	Erosive	Variable: sands, silts, clays	Blue	Glaci-fluvial deposition, in a proglacial, sub-aerial environment (reoccupation of tunnel valley depressions by fluvial systems?)	Glacial period (Weichselian?)
U85	Composite facies, low-high amplitude, complex meso mounds, channels, and lenses, oblique reflectors, internal erosion surfaces. Strong negative amplitude near or at the base.	V-shape channels and tabular	Erosive	Mainly sands with gravel and silt (?).Organic-rich muds (?) at the base	Medium Magenta	High energy fluvial (possibly outwash plain?)	
U90	Parallel-homogeneous facies at the base, association of parallel-mound-channel-shingled facies above, all prograding towards NW or W. Scattered small mounds.	Tabular	Erosive	Mainly sands-fine sediments	Cyan	Fan delta	
KSA	Complex, wide range of internal structures affected by variable degrees of deformation, from better-preserved faulted blocks to completely	Variable	Deformation front	Variable: sands, silts, clays	Dark Red	Deformed deposits	Glacial period (Weichselian?)

SEISMIC UNITS	ACOUSTIC FACIES AND INTERNAL CONFIGURATION	LOWER BOUNDING SURFACE		EXPECTED COMPOSITION	KINGDOM REFLECTOR COLOUR	STRATIGRAPHY (TENTATIVE CORRESPONDENCE)	
		MORPHOLOGY	NATURE				
	disturbed/chaotic regions, to transparent and incoherent.						
KSB	Complex, wide range of internal structures affected by variable degrees of deformation, from better-preserved faulted blocks to completely disturbed/chaotic regions, to transparent and incoherent.	Variable	Deformation front	Variable: sands, silts, clays	Dark Red	Deformed deposits	Glacial period (Saalian?)
BSU	Layered sequence of parallel facies of variable amplitude, locally deformed.	-	-	Marine clays, silts to sands	Black	Subparallel deposits, locally deformed	Pre-Quaternary

6.5 | GRAB SAMPLE CLASSIFICATION

For details on the grab sample classification, see section 8.10| and Appendix C|.

7 | GEOLOGICAL FRAMEWORK

The Danish sector of the North Sea basin is connected to the east by the Scandinavian Shield and by the WNW-ESE striking Sorgenfrei-Tornquist fault zone (Figure 63). The Ringkøbing-Fyn High, located further south, emerged during the Late Permian (Pre-Zechstein) as a result of tectonic subsidence (Vejbæk, 1997; Vejbæk et al., 2007). This structural feature divides the Danish sector of the North Sea basin into the North German Basin, located south of the Ringkøbing-Fyn High, and the Danish-Norwegian Basin, north of Ringkøbing-Fyn High. During the Zechstein (Late Permian), four to five cycles of evaporites were deposited, infilling the structural lows (Sorgenfrei and Buch, 1964; Vejbæk et al., 2007). Further deepening of the North Sea basin resulted in thousands of metres of Mesozoic sediment deposition over the evaporites. The thick Mesozoic deposits activated diapirism of the underlying evaporites. Subsequently, several cycles of glaciations resulted in further loading, inducing reactivation and upward migration of the salt diapirs (Nielsen et al., 2008). This halokinesis is likely to be ongoing in modern times, also indicated by a high level of earthquakes in the Danish Basin, measured in the period 1920 to 1995 (Gregersen et al. 1998)

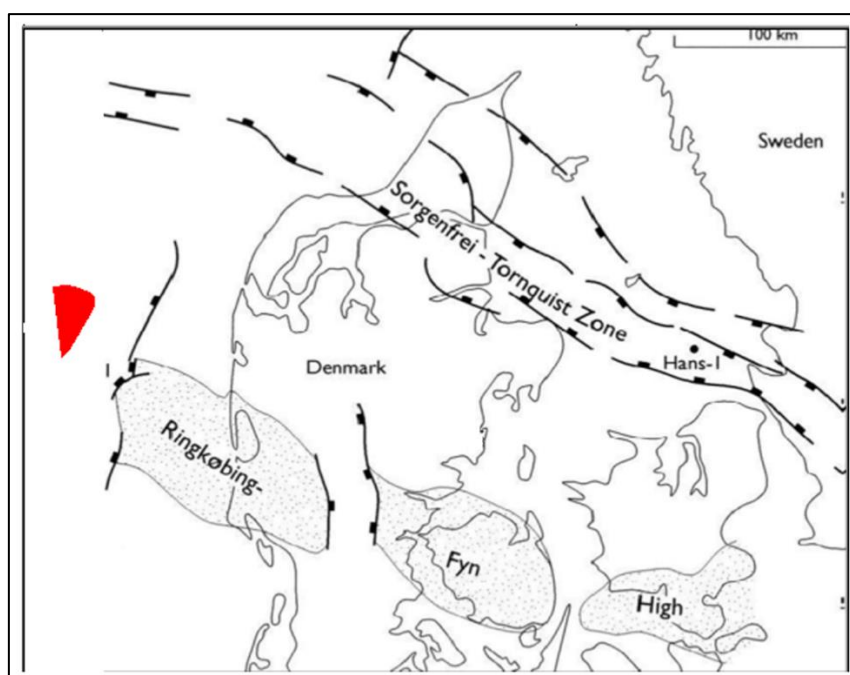


Figure 63 Major Danish structural elements
(After Stemmerik et al., 2000); MMT OWF survey area in red.

During the Late Cretaceous, a major tectonic inversion episode affected the North Sea region, associated with initiation of the Alpine Orogeny, (Clausen and Huuse, 1999; Japsen, 2000). Cretaceous tectonism was followed by sequential episodes of uplift and major sea level fluctuations during the Paleogene to Neogene (Japsen et al. 2008). These events resulted in variable rates and types of sediment deposition. A major regional unconformity occurs between the Upper Eocene and lower Upper Oligocene, Brejning Fm. (Mica Clay) (Rasmussen et al., 2010). The Neogene deltaic deposits show a general shift moving from east to west. The Miocene succession is hundreds of metres thick in the Danish sector of the North Sea. From the rim of the North Sea basin at the Sorgenfrei-Tornquist Zone towards the central basin, the Pre-Quaternary deposits are successively younger below the base of the Quaternary. The Quaternary base represents an unconformity east of the so-called the transition zone in the North Sea (Nielsen et al. 2008, Japsen 2003) (Figure 64). West of the transition, the Quaternary sequences rest conformably on Pliocene deltaic sediments (Nielsen et al. 2008). Often, the unconformity shows a significant relief due to Quaternary glacial processes, and occurs at depths of a few hundred

metres within valley structures to just below the seabed along the Danish west coast (Andersen, 2004; Huuse and Lykke-Andersen, 2000b; Leth et al., 2004, Novak and Duarte 2018). Across the wider region (e.g. central North Sea) this surface is characterized by strong undulation controlled by variable-scale structures in the Pre-Quaternary basement.

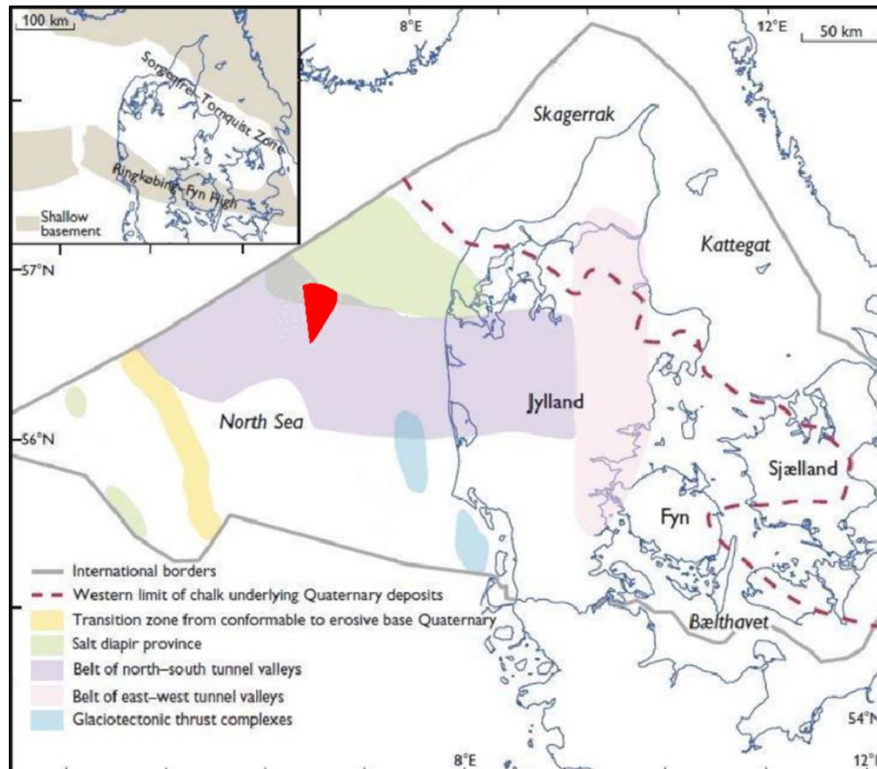


Figure 64 Regional geological map (After Nielsen et al., 2008); MMT OWF survey area in red.

Only a few studies have been performed on the Quaternary deposits in the Danish North Sea. However, onshore studies provide a decent foundation for outlining the regional geology in the eastern North Sea (e.g. Sjørring and Frederiksen, 1980; Ehlers, 1990; Sandersen and Jørgensen, 2003; Pedersen, 2005; Jørgensen and Sandersen, 2006; Jacobsen, 2003; Høyer A-S et al., 2013; Houmark-Nielsen, 2007).

In general, the Quaternary sequence thins from the central North Sea towards the Danish mainland. The Elster and Saale ice sheets extended across the entire North Sea (Figure 65). Glaciation came from the northwest over northeast and from the Baltic region (Sjørring and Frederiksen, 1980; Ehlers, 1990). The Weichselian ice sheet extended north and east of the main stationary line at the Late Glacial Maximum (LGM), which was located from inland Jutland towards the northwest into the North Sea (Figure 65). Morphological elements such as moraine ridges and elongated boulder reefs, occurring perpendicular to the main stationary line, indicate the location of the ice boundary on the seabed west of the Thyborøn at the Danish west coast (Nicolaisen, 2010). Onshore, southwest of the LGM, the so called "hill islands" (Dalgas, 1867), which outline the Saalian landscape, are found to extend into the North Sea (Larsen, 2003; Larsen & Andersen, 2006, Leth et al., 2001; Anthony, 2001; Leth, 2003). Morphological remnants are absent on the seabed due to marine erosion. However, seismic profiles reveal horizons that have been interpreted to represent this same landscape. The northern part of the actual survey area is expected to cross over the LGM stationary line; however, central and southern survey area has only been overridden by Saaleian or older glaciations.

Large-scale glaciotectonic thrust complexes have been identified in the Danish North Sea, as well as onshore the Danish main land (e.g. Huuse and Andersen 2000a, 2000b, Larsen and Andersen 2005, Vaughan-Hirsch and Phillips 2017, Novak and Duarte 2018, Høyner et al. 2013, Shack Pedersen 2005, Jacobsen 2003). In the eastern North Sea, the décollement surfaces are located in the Miocene or in the Quaternary level, and the thrust blocks comprise these sediments. The formation of glacial tectonic complexes found to the west and south of the Weichselian LGM boundary are attributable to the Saalian or older ice cover (Andersen, 2004; Huuse and Lykke-Andersen, 2000b; Vaughan-Hirsch and Phillips, 2017).

Systems of buried shelf valleys, 100-300m deep and several tens of kilometres long, are present (Figure 65) (Andersen, 2004; Huuse and Lykke-Andersen, 2000b; Novak and Duarte 2018). The submarine valleys can be correlated to onshore valleys and are considered to be of the Elster and Saale ages. Younger, reactivated Saale valleys have been found north and east of the Weichselian main stationary line (Smed 1979, 1981a; Jørgensen et al., 2005).

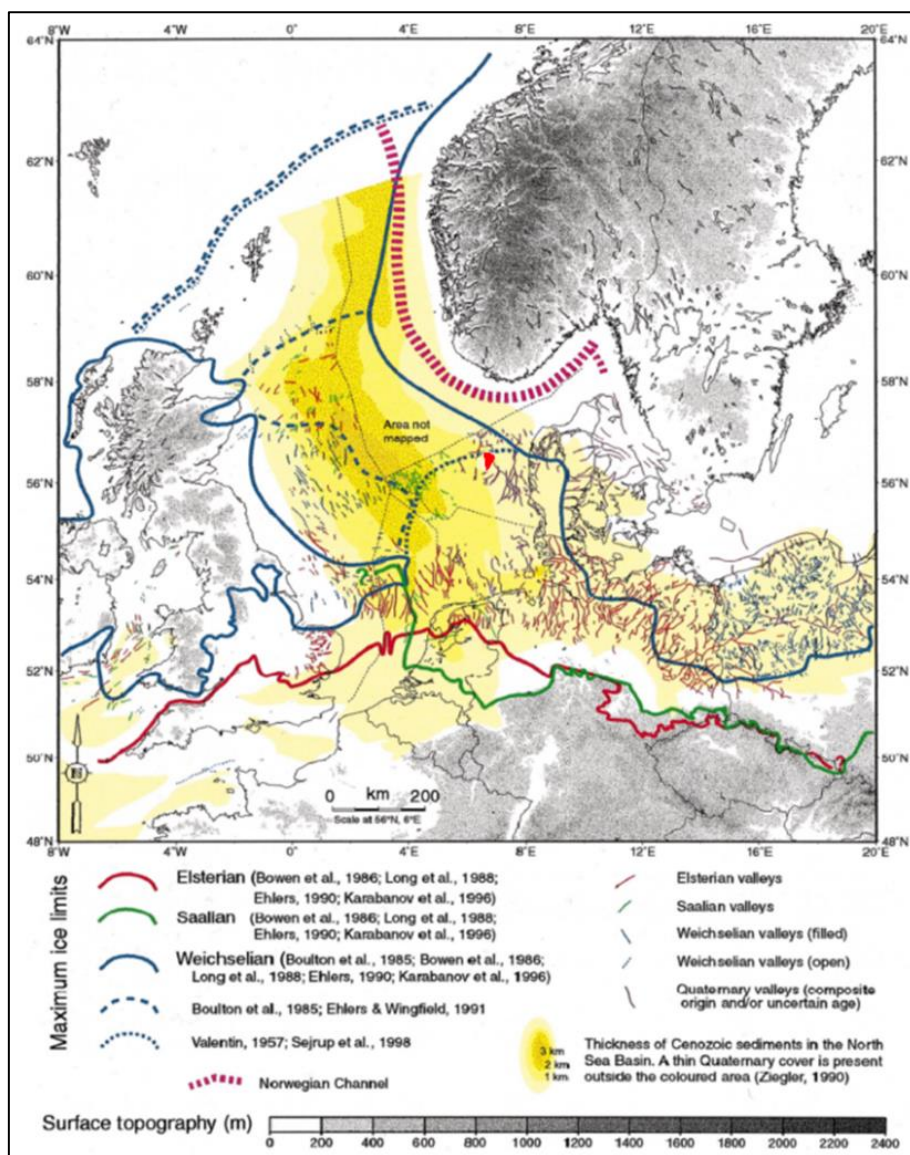


Figure 65 The Quaternary glaciations and an overview of Quaternary valleys in northwest Europe. (Huuse, M., and Lykke-Andersen, H. 2000); site location in red.

The Paleo-North Sea extended across the region during the Eemian period. Eemian deposits are described both on and offshore in the south-westerly North Sea (Konradi et al., 2005), and Eem deposits representing valley infill were found in a borehole in the Vesterhav South OWF survey area (Fugro 2014).

Deposits from the Weichselian glaciations (Figure 66) comprise tills alternating with glacioluvial sand and gravel, glaciolacustrine clay, silt, and sand, toward the north and east of the main stationary line. Towards the west and south of the LGM, glacioluvial sand and gravel were deposited in morphological lows above the older Saale landscape (Houmark-Nielsen, 2007). The LGM occurred in the region around 22ka BP. The glaciers' subsequent retreat generated accommodation space close to the ice front, where deposition of glaciolacustrine clay filled in, e.g Younger Yoldia Clay around 16-15ka BP. As Weichselian ice melted back, the subglacial-generated valleys emerged and laminated clay, silt, and fine sand deposited in the valleys (Figure 66).

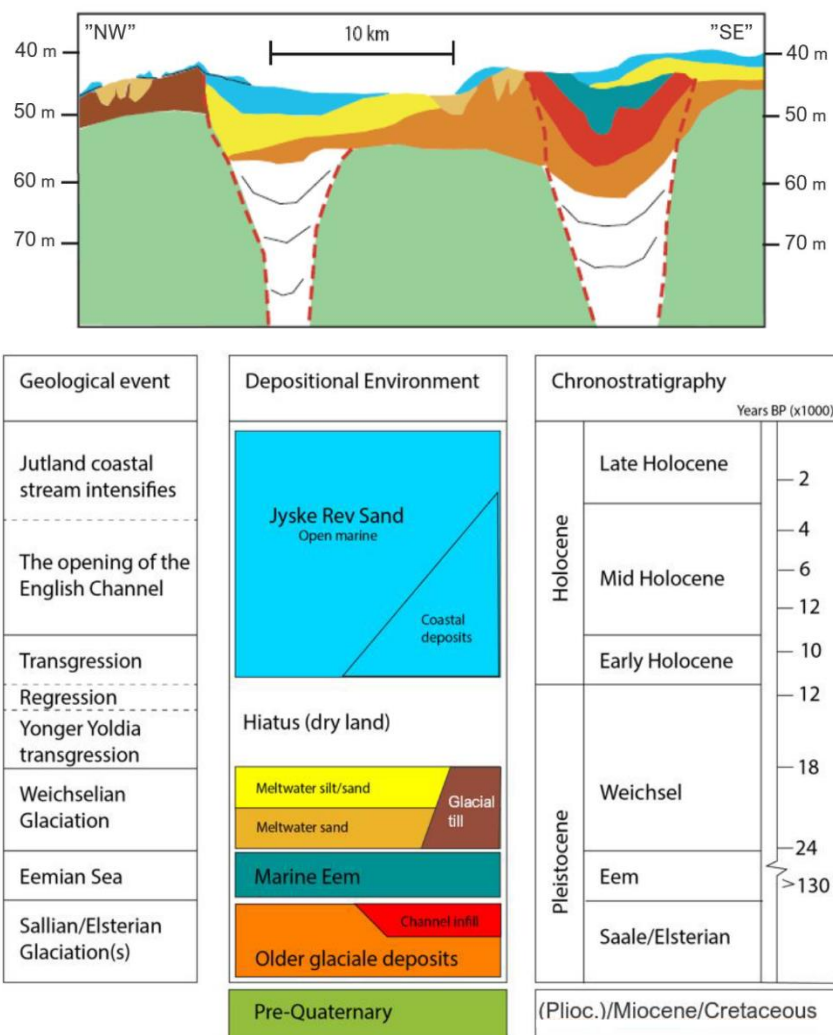


Figure 66 General stratigraphy model of the geology in the eastern Danish North Sea. A composite profile from NW towards SE representing approximately 50 km from Jyske Rev and towards the shore. Below: Stratigraphic unit names and their relative age. Same colour code used above and below. (After Nicolaisen, 2010).

The removal of the glacial load triggered isostatic rebound and a regression that took place until 11ka BP. During this timeframe, relative sea level was, at a minimum, 55 to 45 metres lower than present, thus maintaining the eastern Danish shelf above sea level. Terrestrial conditions and rising temperatures increased organic material production, resulting in peat accumulations. This marker horizon has been found in many survey areas across Danish waters (Leth, 1996; Bennike et al., 1998, 2000; Novak and Björck, 2002; Novak and Pedersen, 2000). In the eastern Danish North Sea, fine-grained material was deposited in sheltered areas between till "islands", e.g. the Agger Clay unit (Leth, 1996). During the Holocene transgression, from 11ka BP to 6 ka BP, the Agger Clay depocenter shifted coastward and offshore low-lying islands were submerged. At the same time, coastal processes overtook the glaciogenic landscape where it was exposed to waves and currents. The result was the formation of spit/platform/lagoon deposits throughout the region (Nielsen and Johannesen, 2004; Johannesen et al., 2008; Novak and Pedersen, 2000).

In the eastern North Sea, metre-thick fossil sand waves were present at Jyske Rev (Leth 1996). These current- and wave-generated structures have often been formed around sandy-gravelly fossil beach ridges. Seismic data depict multiple generations of these events. After 6 ka BP, sea level was at its highest and the North Sea tidal system and coast-parallel Jylland current developed.

A recent mobile sediment unit is the latest deposit and is found to cover major areas of the eastern North Sea seabed. Coast-parallel strong currents and waves generate the active bedforms, i.e., mobile sandwaves and dunes. The Danish Coast Agency has documented bedform migrations of up to 20-50m per year; the dunes and waves are organized in kilometre-wide areas migrating across an apron of relict gravelly sand (Anthony and Møller, 2003; Anthony and Leth, 2001; Leth et al., 2004).

8 | RESULTS

8.1 | GENERAL

The results from the Area of investigation, MMT OWF geophysical survey area are presented in this report together with associated north-up charts. The charts are presented in Appendix A|. The results of the grab sample campaign are presented in Appendix C|.

To facilitate survey data management and survey planning, and to allow the fishing community to plan around the survey work, the MMT OWF survey area was divided into 22 smaller areas. These included six blocks for the main lines (BM1 to BM6) and four areas for the cross lines (BX1 to BX4) and are shown in Figure 5.

To assist with organisation in reporting, the survey area was separated into a reporting tile schema. The layout of the tiles and the survey area are shown in Figure 67.

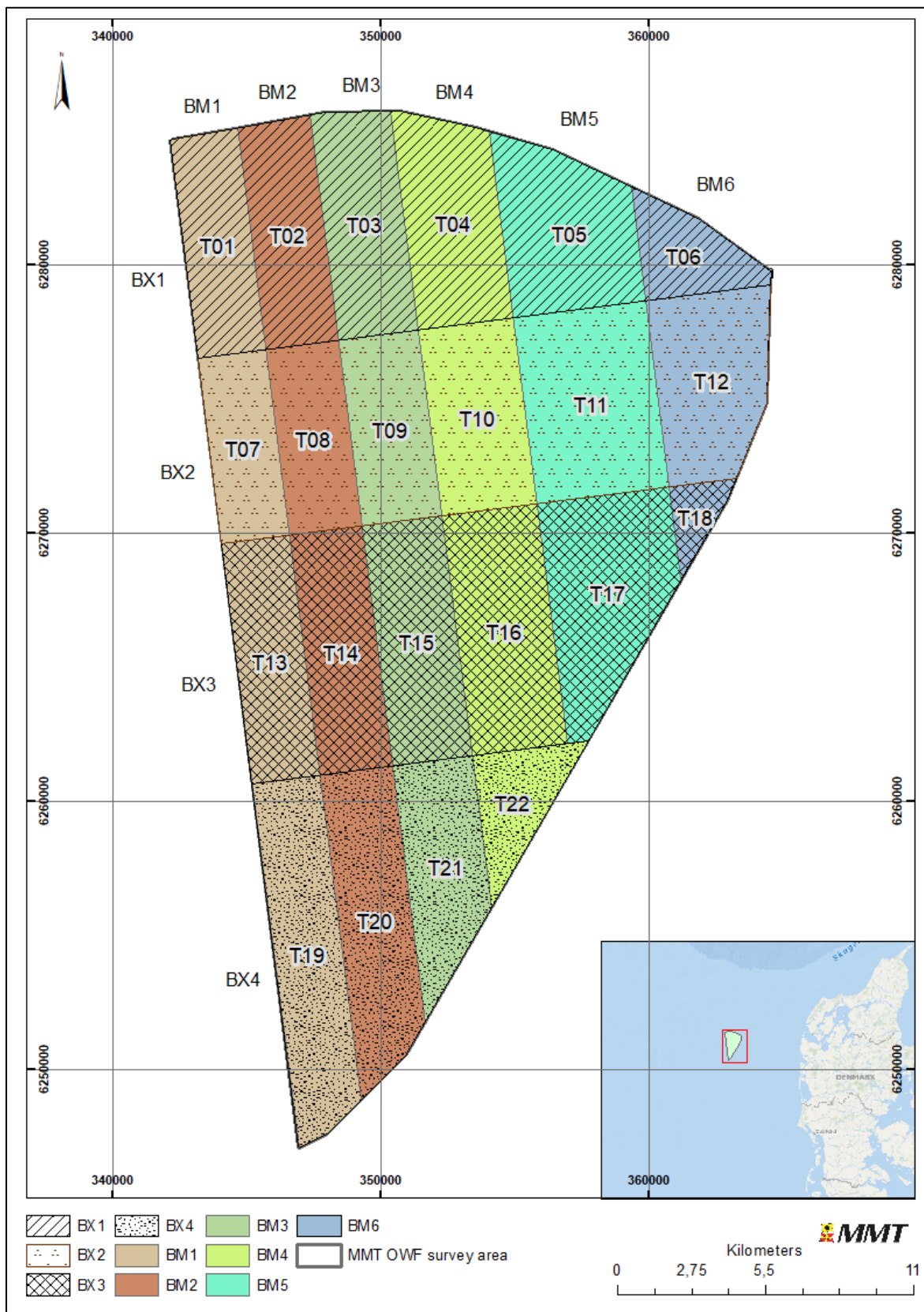


Figure 67 The MMT OWF survey area with the tile schema used for the description of results.

8.2 | BATHYMETRY

Overall, the bathymetric depth changes moderately across the MMT OWF survey area. The minimum surveyed depth is 25.75 m at 350741.55 m E, 6264515.14 m N on the project site, Artificial Island (Tile 15). The maximum surveyed depth is 48.17 m at 344390.62 m E, 6267808.20 m N in the western area (Tile 13). The depth range across the site is 22.4 m. Figure 68 shows an overview of the bathymetry within the MMT OWF survey area. Four profile lines are shown running from west to east across the site.

Profile data derived from these lines is shown in Figure 69. The horizontal positions of the profiles have been shifted to match the KP values of the northern most line, Line 1. This has been done so the relative positions of the profiles are normalised and permits any features that may extend between the profiles to be visually aligned. The profiles have a strong vertical exaggeration so that features can be identified along the profiles.

The profiles show that the water depth generally increases from west to east across the MMT OWF survey area.

The profiles are used to manage the presentation of the bathymetry results over the extensive MMT OWF survey area, with a sub-section of the report for each profile and regionally related features of interest.

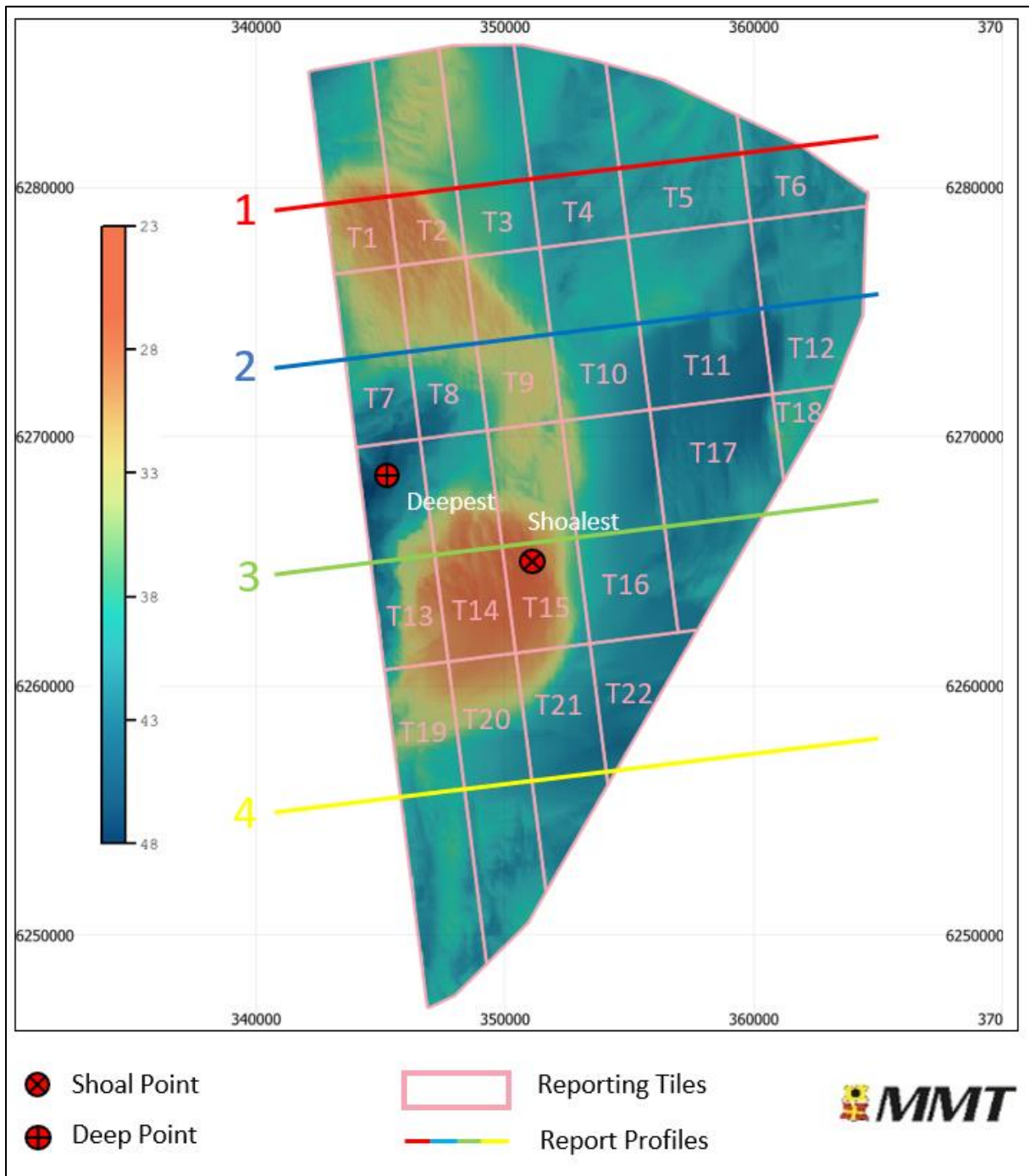


Figure 68 Overview of the bathymetry data.
 Bathymetry and positions of profile lines in Figure 69.

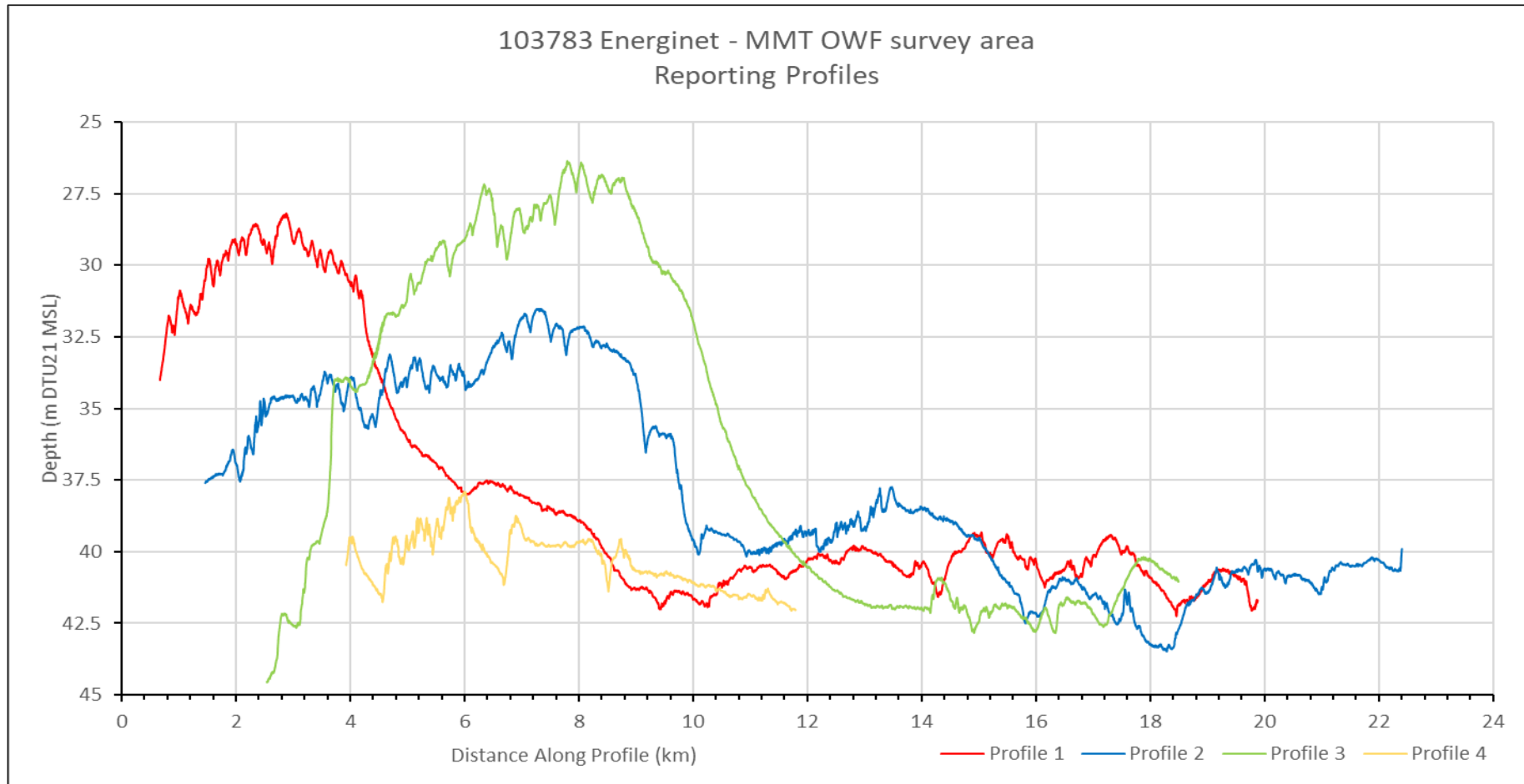


Figure 69 Profiles across the MMT OWF survey area showing depth relative to DTU21 MSL. Profiles have been shifted so that all KP values correspond to the westernmost extent of the Zone East survey area. Profiles exported from NaviModel with depth convention positive down.

8.2.1 | PROFILE 1

Profile 1 (Figure 69) crosses the northern section of the survey area and spans 21 km of the site. The profile shows the overall trend within this northern region is one of a flat seabed to the east with a gentle rise to the west. This trend is superimposed with variations in topography relating to the presence of sand waves composed of SAND alternating with GRAVEL and coarse SAND to the west, whilst larger scale bedforms/sandbars are to the east. The depth variation along the profile is 14.05 m from a minimum depth of 28.18 m at 345011.0 m E, 6279681.0 m N to a maximum depth of 42.24 m at 360486.0 m E, 6281496.0 m N.

Reporting Tiles T01 to T06 cover the northern parts of the MMT OWF survey area. The seabed in T04 to T06 is generally flat but interspersed with sand wave formations that are 1 – 2 m high. Reporting Tiles T01 and T02 are shallower than the tiles to the east due to the presence of a sand wave and sandbar field that is up to 10 m shallower than the adjacent seabed (shown in Figure 70).

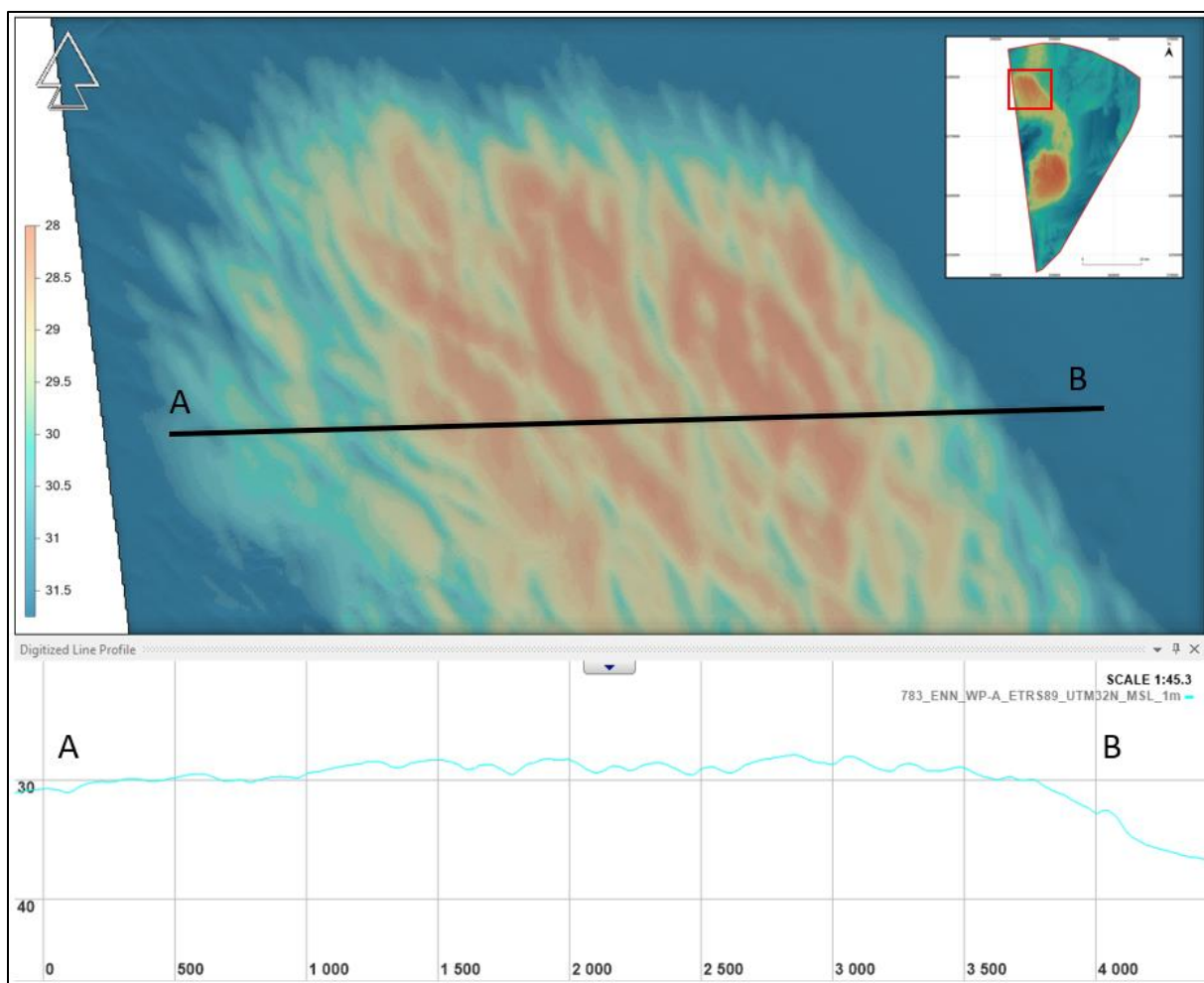


Figure 70 MBES data with profile, in reporting areas T01-T02. The image shows bedforms in the shoal, northern sand wave area. Profile shows depth variation. NaviModel depth convention is positive down, vertical exaggeration of profile x45. Red box in inset map highlights figure location.

8.2.2 | PROFILE 2

Profile 2 (Figure 69) crosses the centre of the site and spans 19 km of the survey area. This profile shows an overall trend of shallower depths to the west and a gradual slope down to the deeper depths in the east. On the western side of the site the depth profile is variable relating to the presence of sand waves, composed of SAND alternating with GRAVEL and coarse SAND. On the eastern side the profile crosses two sandbar ridges formed by mass sediment transport comprised of alternating SAND and GRAVEL and coarse SAND. Each of these spans approximately 1.5 km of the profile and stand 3.5 m to 4.0 m higher than the seabed either side. The depth variation along this profile is 11.9 m from a minimum depth of 31.49 m at 349397.0 m E, 6273934.0 m N to a maximum depth of 43.48 m at 360317.0 m E, 6275229.0 m N.

Reporting Tiles T07 to T12 cover Profile 2. In general Tiles T07 to T09 are dominated by the shallower depths relating to the southern edge of the northern sand wave and sandbar field. The bedforms present include sand waves and sandbars, with crestlines orientated in a NW-SE direction, with wavelengths of 100 to 300 m and heights between 1.0 to 2.0 m (Figure 71).

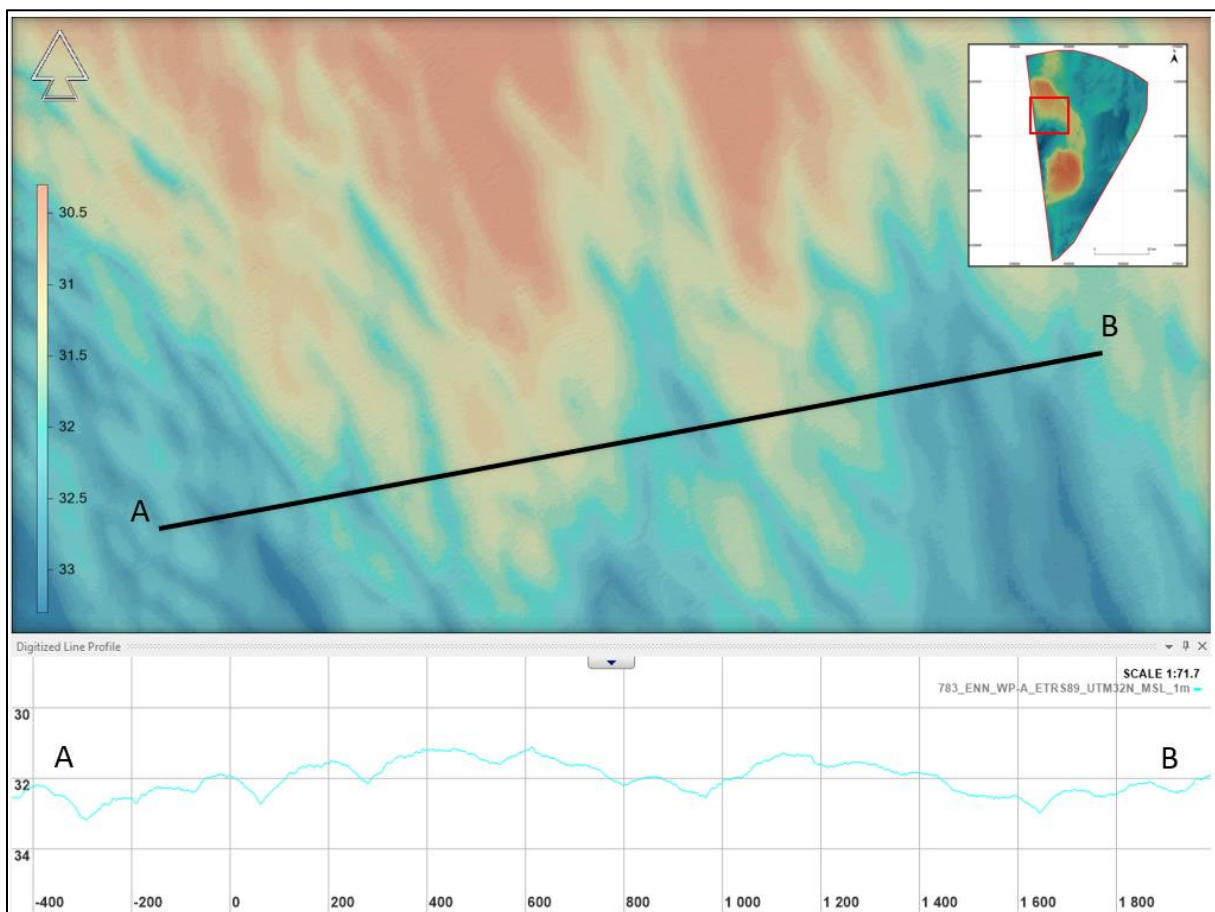


Figure 71 MBES data with profile in reporting areas T07 and T08. Image shows area of sand waves typical over the shallower areas of the MMT OWF survey area. NaviModel depth convention is positive down, vertical exaggeration of profile x71. Red box in inset map highlights figure location.

8.2.3 | PROFILE 3

Profile 3 (Figure 69) crosses the south of the site and spans 13 km of the survey area. This profile shows the most dramatic change in depth with steep sides on either side of the Artificial Island area of investigation (10 km x 10 km) area. The profile shows that the water depth generally increases in depth from east to west but crosses a broad expanse of muddy SAND in the central part of the survey area. This manifests in the profile as a series of broad undulations. To the west of this the profile shows higher frequency variations in depth which relate to ripples and sand waves composed of GRAVEL and coarse SAND and to the east the profile crosses a local topographic high formed of sandbars and mass sediment deposits.

The depth variation along this profile is 18.2 m from a minimum depth of 26.35 m at 349878.0 m E, 6265573.0 m N to a maximum depth of 44.55 m at 344670.0 m E, 6264871.0 m N. Reporting Tiles T13 to T18 cover Profile 3.

The steepest bedform slopes observed in the MMT OWF survey area are on the western side of the Artificial Island area of investigation in Tile T13, with the steepest slope observed at the north west of the Artificial Island area of investigation (Figure 72). The deepest part of the MMT OWF survey area is found within Tile T13 with a depth of 48.17 m at 344390.6 m E, 6267808.2 m N (Figure 73).

The shallowest part of the MMT OWF survey area is found within Tile T15 with a depth of 25.75 m at 350741.6 m E, 6264515.1 m N on the Artificial Island project site (Figure 74). This area is characterised by large sand wave formations with a wavelength of 100 to 300 m and heights between 1.0 to 2.0 m.

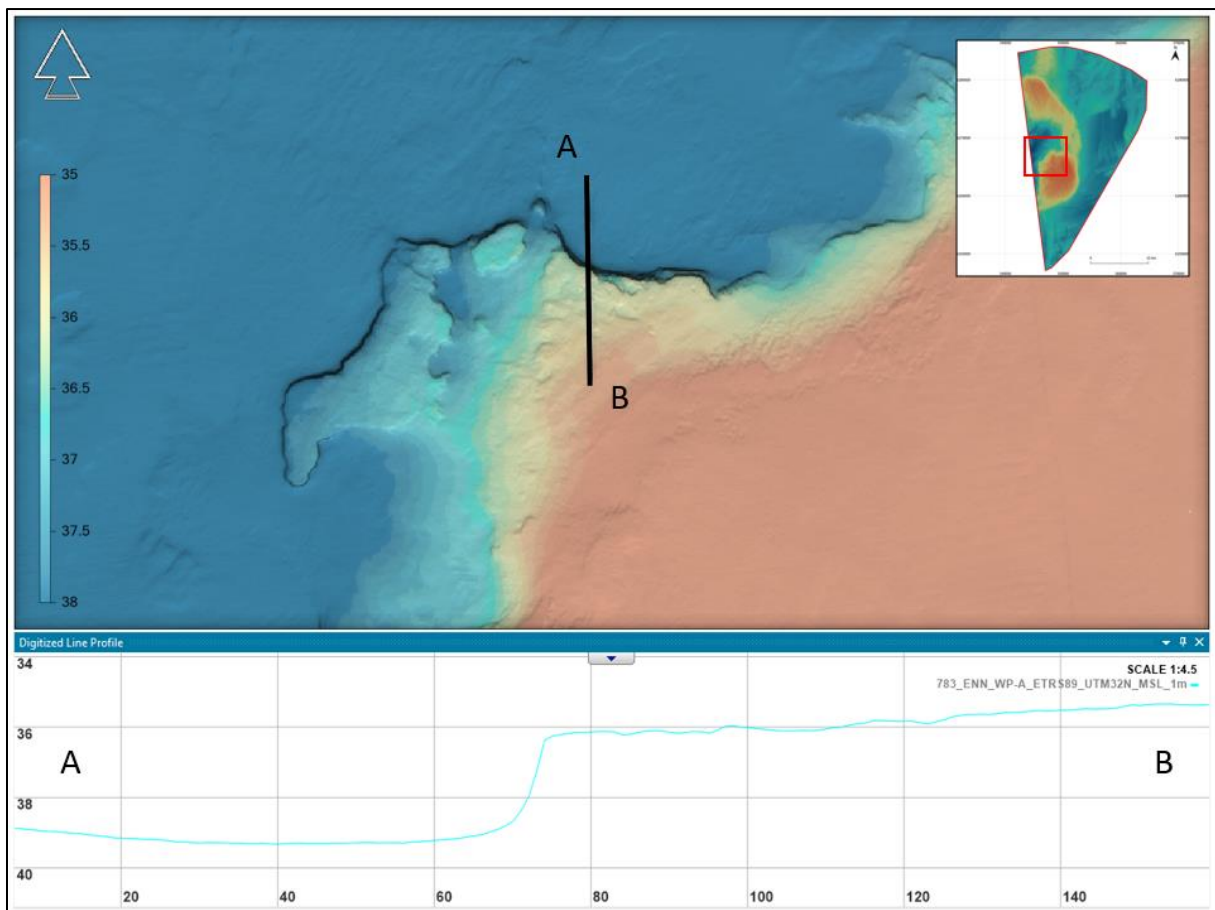


Figure 72 MBES data with profile in reporting Tile T13- slope.

Image showing steepest bedform slope of the MMT OWF survey area and surrounding seabed, Tile 13. NaviModel depth convention is positive down, vertical exaggeration of profile x4.5. Red box in inset map highlights figure location.

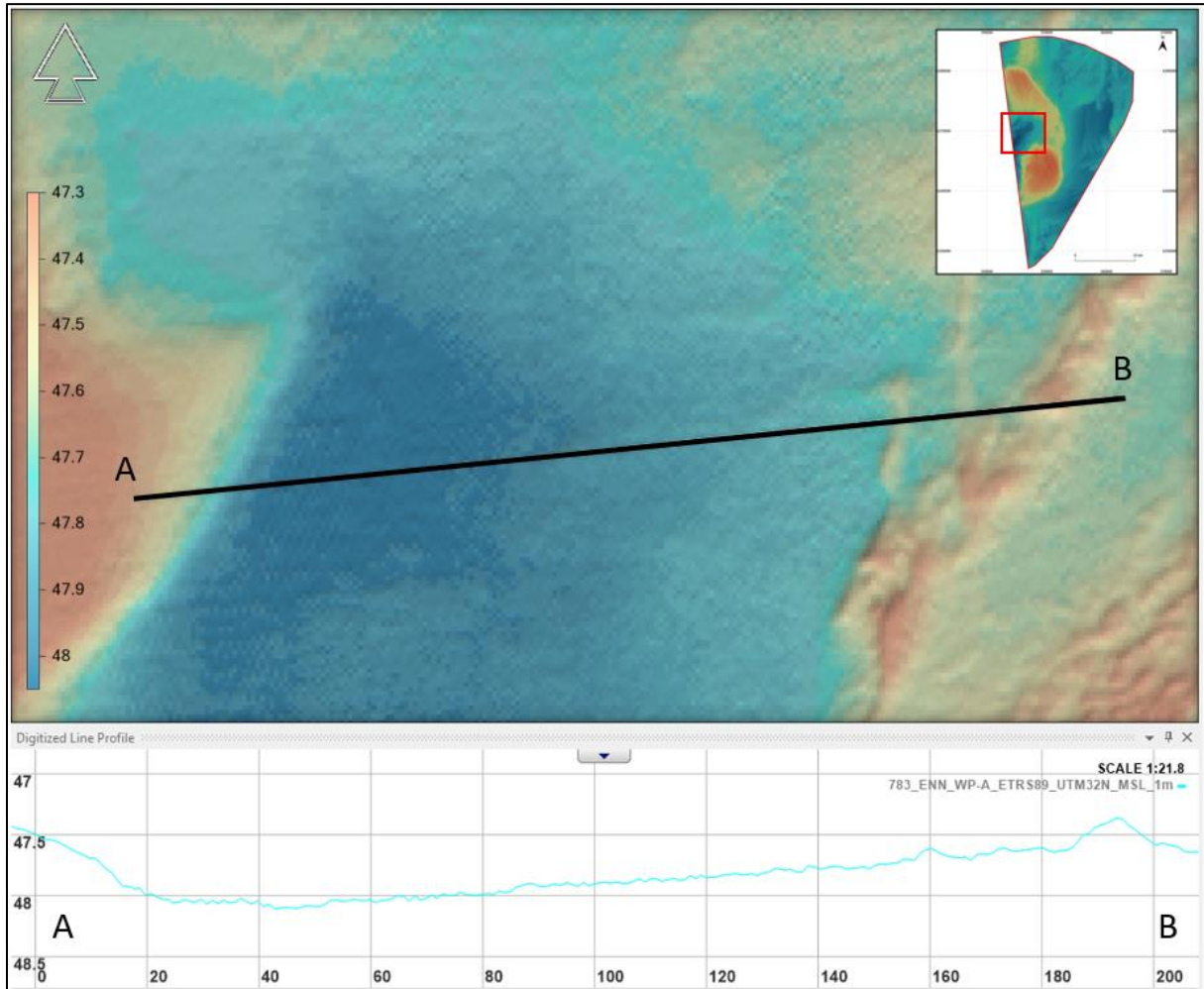


Figure 73 MBES data with profile in reporting Tile T13- deepest depth.
Image showing deepest depth of the MMT OWF survey area and surrounding seabed, Tile 13.
NaviModel depth convention is positive down, vertical exaggeration of profile x21. Red box in inset map highlights figure location.

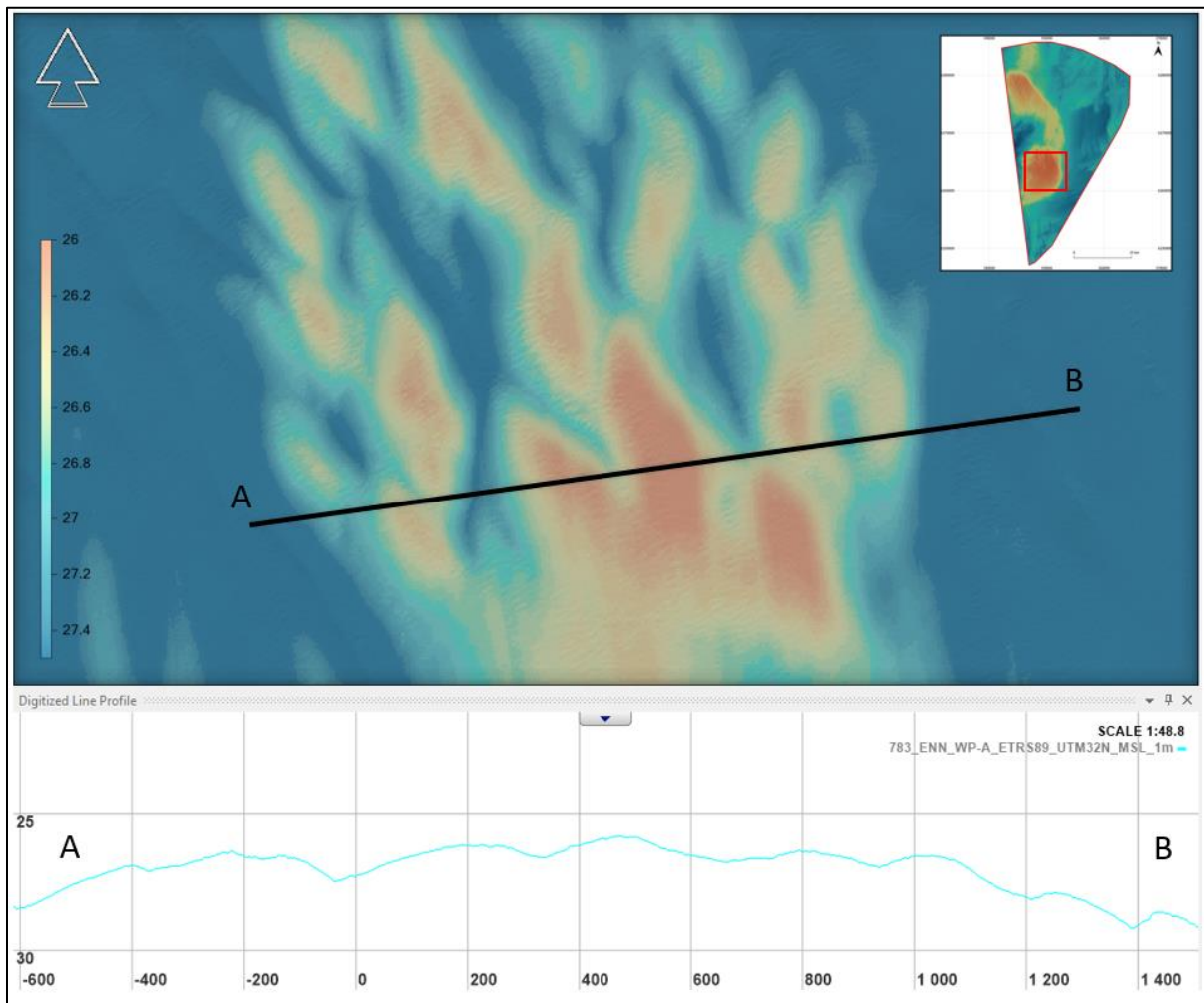


Figure 74 MBES data with profile in reporting Tile T15. Image showing shallowest depth of the MMT OWF survey area and surrounding seabed, Tile 15. NaviModel depth convention is positive down, vertical exaggeration of profile x48. Red box in inset map highlights figure location.

8.2.4 | PROFILE 4

Profile 4 (Figure 69) crosses the south of the site and spans 8 km of the survey area. The profile shows that the water depth is consistent in this area which indicates a relatively flat seabed, especially towards the eastern side. The west of the profile shows higher frequency variations in depth which relate to sandbars composed of GRAVEL and coarse SAND, whilst to the east the profile crosses a broad expanse of muddy SAND.

The depth variation along this profile is only 4.17 m from a minimum depth of 37.90 m at 348080.0 m E, 6254524.0 m N to a maximum depth of 42.07 m at 353724.0 m E, 6255434.0 m N.

Reporting Tiles T19 to T22 cover Profile 4. The shallower depths seen in the west in the previous blocks continue in Tile T19 with similar undulating sand wave features (Figure 75) as seen on the Artificial Island area of investigation area (10 km x 10 km).

To the east, in Tiles 20 – 22 the seabed is generally flat and featureless.

The northern part of Tiles 19 – 21 contain the southern part of the Artificial Island area of investigation. This side of the area has a gentle slope (Figure 76) that gradually drops in a south easterly direction to the flat and featureless seabed extending further to the east.

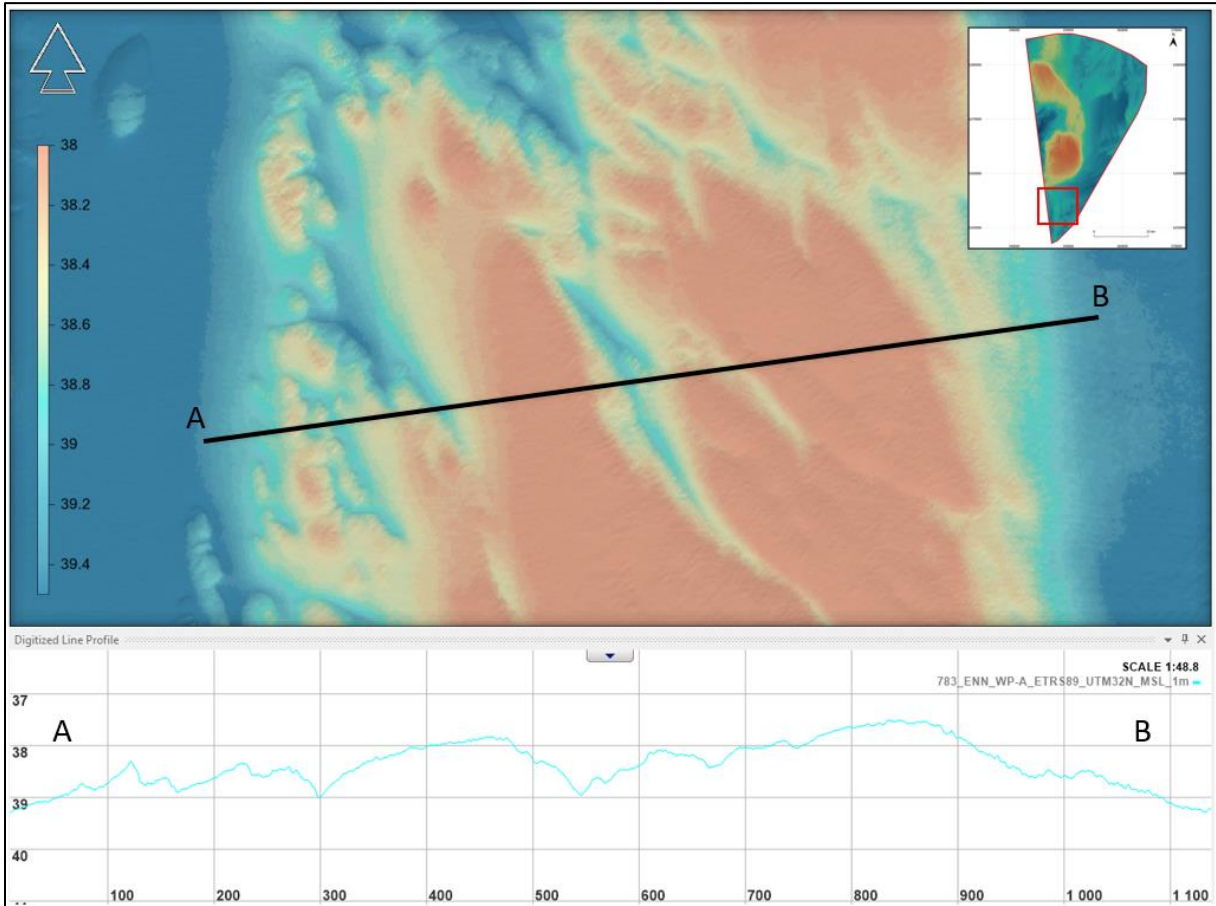


Figure 75 MBES image depicting undulating seabed in reporting tile T19. NaviModel depth convention is positive down, vertical exaggeration of profile x48. Red box in inset map highlights figure location.

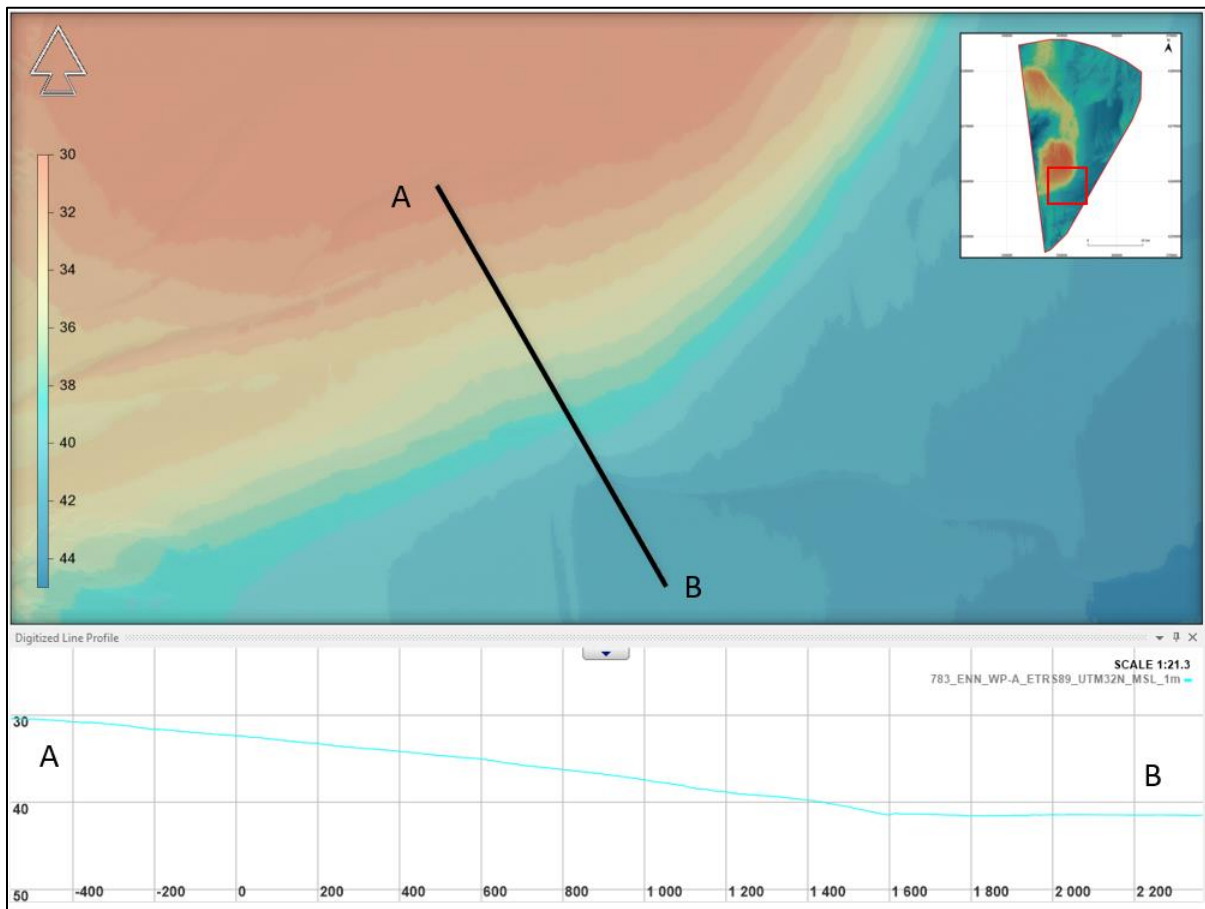


Figure 76 MBES image depicting gentle slope
From the Artificial Island area of investigation in reporting tile T20.
NaviModel depth convention is positive down, vertical exaggeration of profile x21. Red box in inset map highlights figure location.

8.2.5 | SLOPE ANALYSIS

Slope angles were derived from the 1 m resolution bathymetry data in Caris HIPS. This data has been used as the basis for examining gradients across the site as it is less susceptible to picking up system noise as areas with high angles of slope.

Figure 77 shows the slope raster for the MMT OWF survey area. This shows that slope angles are typically very gentle ($<1^\circ$) and gentle (1° to 5°). At this scale the overview image obscures the presence of the regions with very steep gradients. To emphasize these, the slope raster was contoured and filtered with the resulting contours divided into groups of 15° - 20° , 20° - 30° , 30° - 45° and $>45^\circ$. This overview map is shown in Figure 78.

The image also shows the locations of the larger contacts as the orange, red and pink dots which are mostly present in the northeastern quarter, the far northwestern corner and at lower densities along the eastern boundary and southern corner. These contacts typically feature slope angles between 15° and 20° but also exceed of 30° .

Along the western boundary this map shows convoluted linear features within the Artificial Island area of investigation (Figure 79). The map shows that the high slope areas define the western edge of the sandwave/sandbar field. Along these scarps maximum values regularly exceed 30° towards the northern half of their extent. Towards the south the maximum gradients are between 20° and 30° .

The highest slope angle associated with natural seabed feature is 44° and this is located on the side of a steep bank at 345825.0 m E, 6265890.0 m N (Figure 87). This steep bank is classified as Other-Area of Interest and is located on the north western edge of the area.

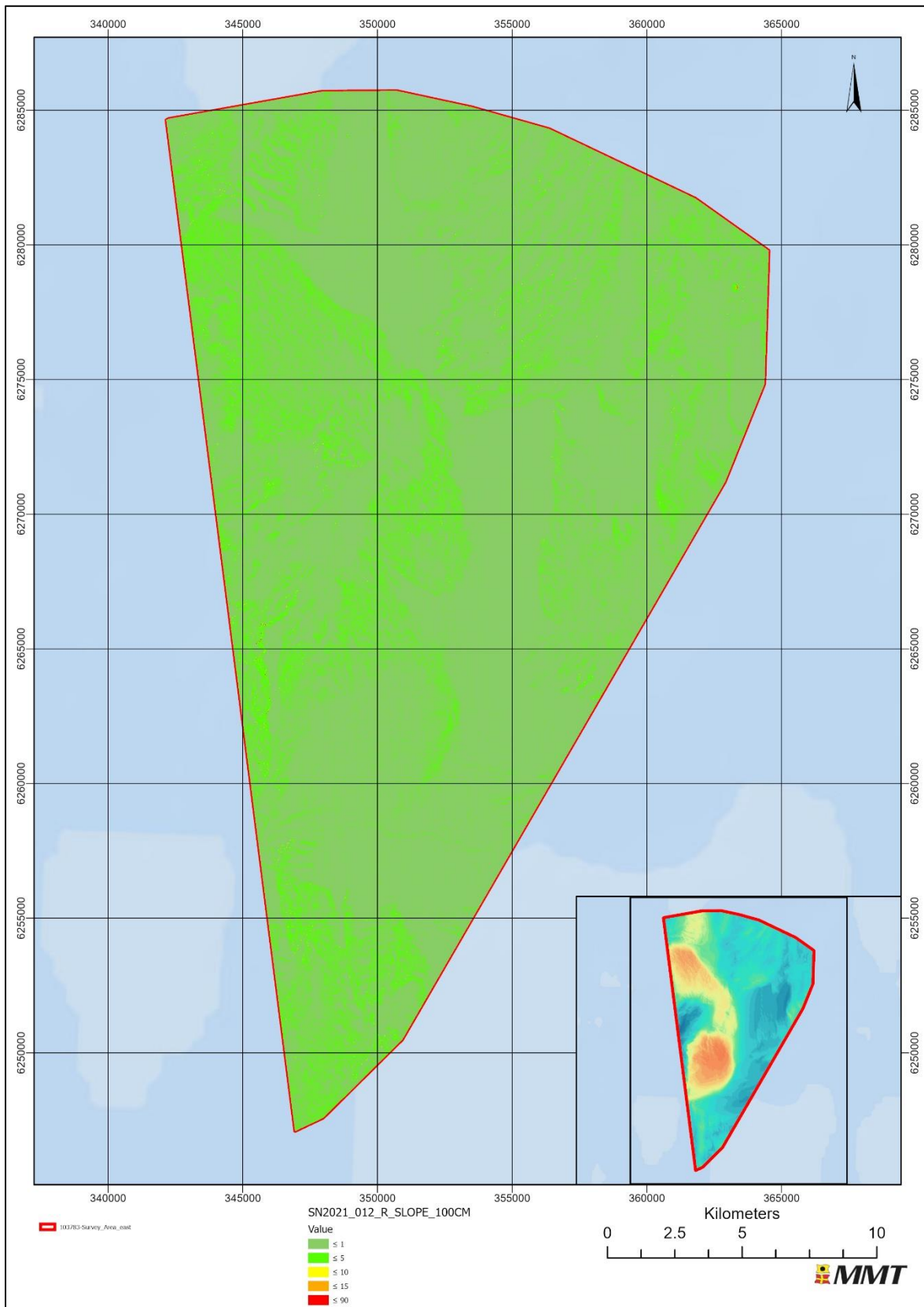


Figure 77 Overview of slope angles across the MMT OWF survey area.

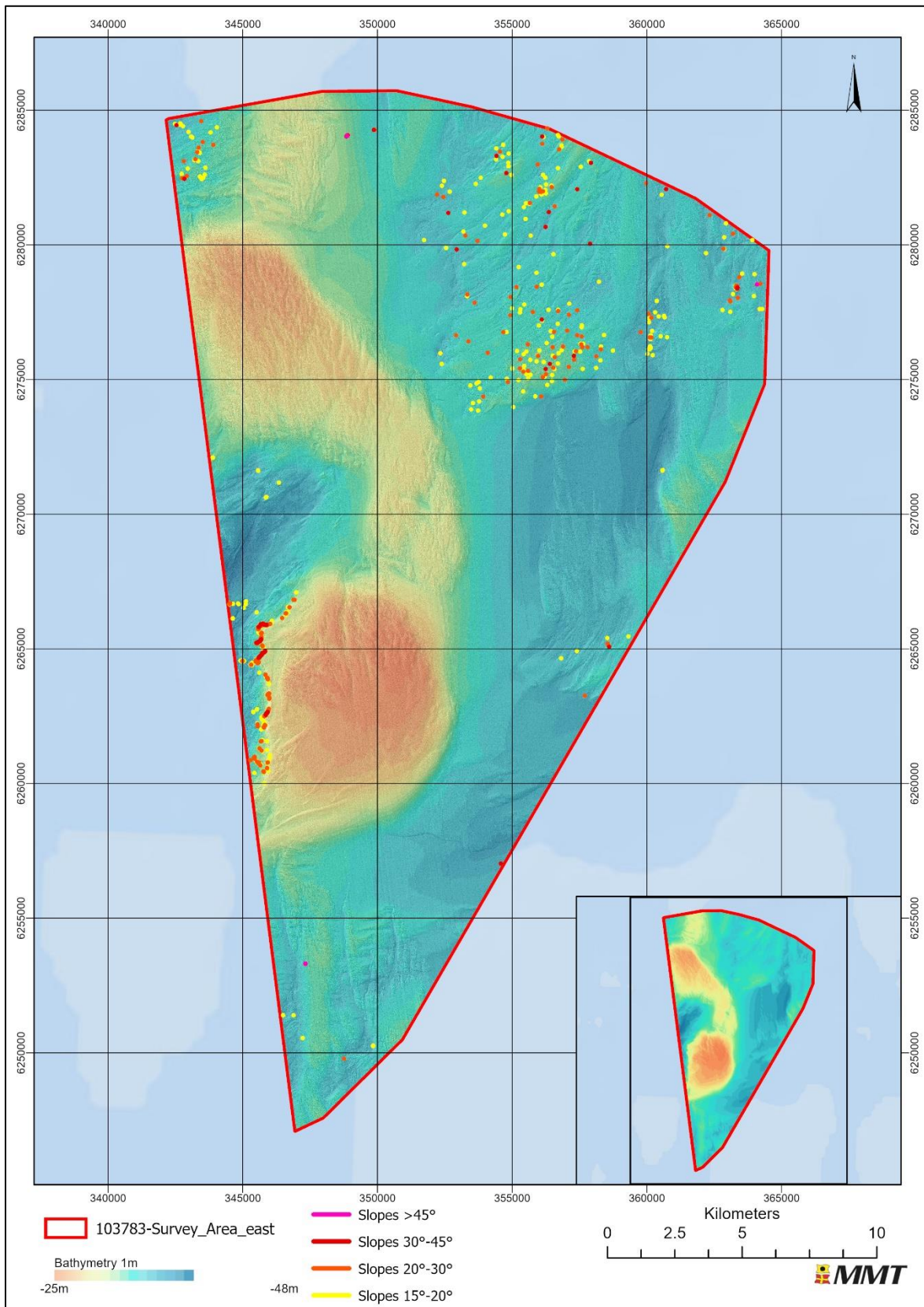


Figure 78 Overview highlighting the regions with Very Steep slope angles across the MMT OWF survey area.

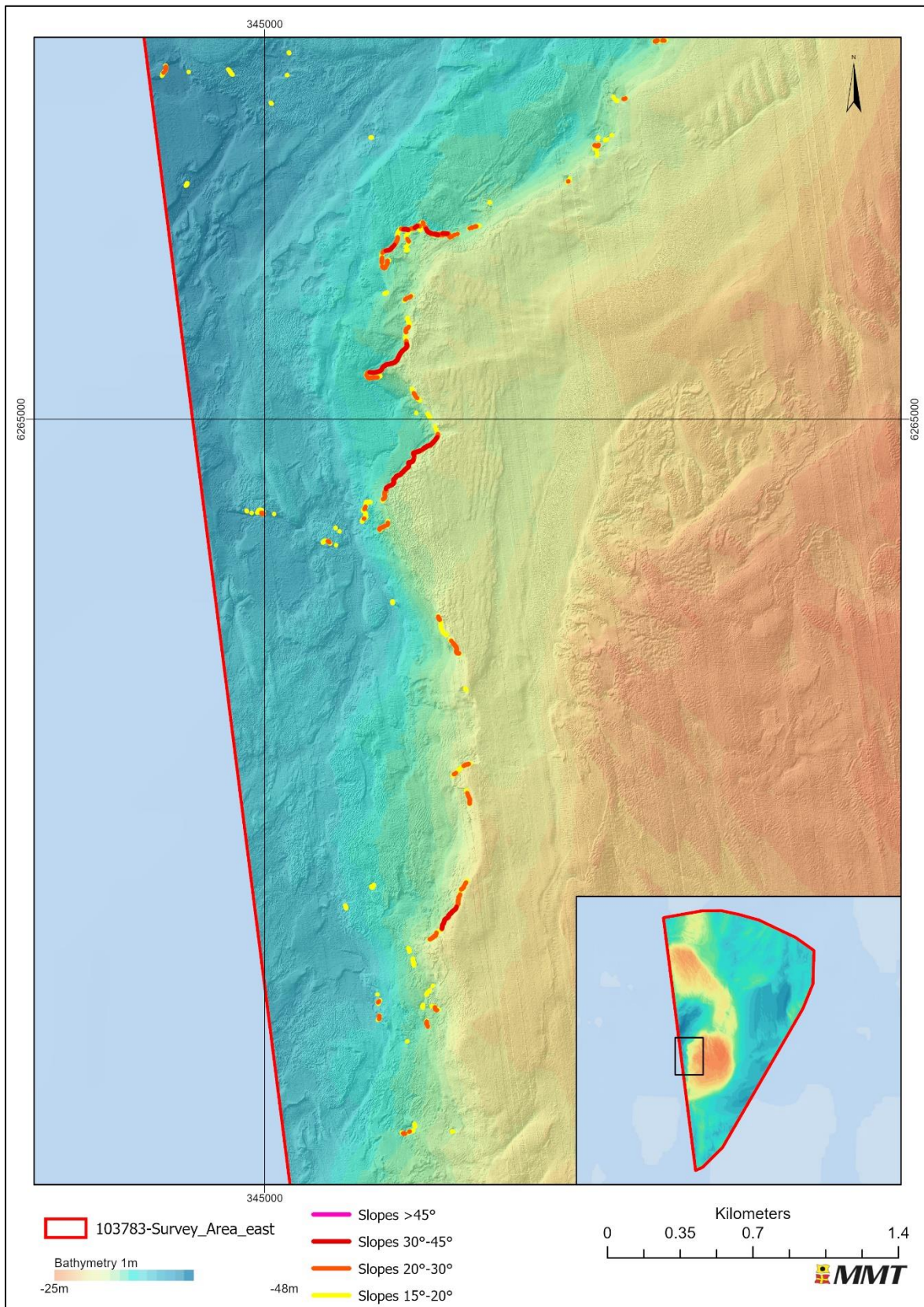


Figure 79 Very steep slopes on the western edge of the southern sand wave/sandbar field.

Very steep gradients exist on anthropogenic features within the MMT OWF survey area. Slope angles between 47° and 56° on the sides of the wrecks, with the maximum slope angle of 56° located on wreck 86, the HMS Tarpon, at 348871.0 m E, 6284049.0 m N. The maximum slope is presented in Figure 80.

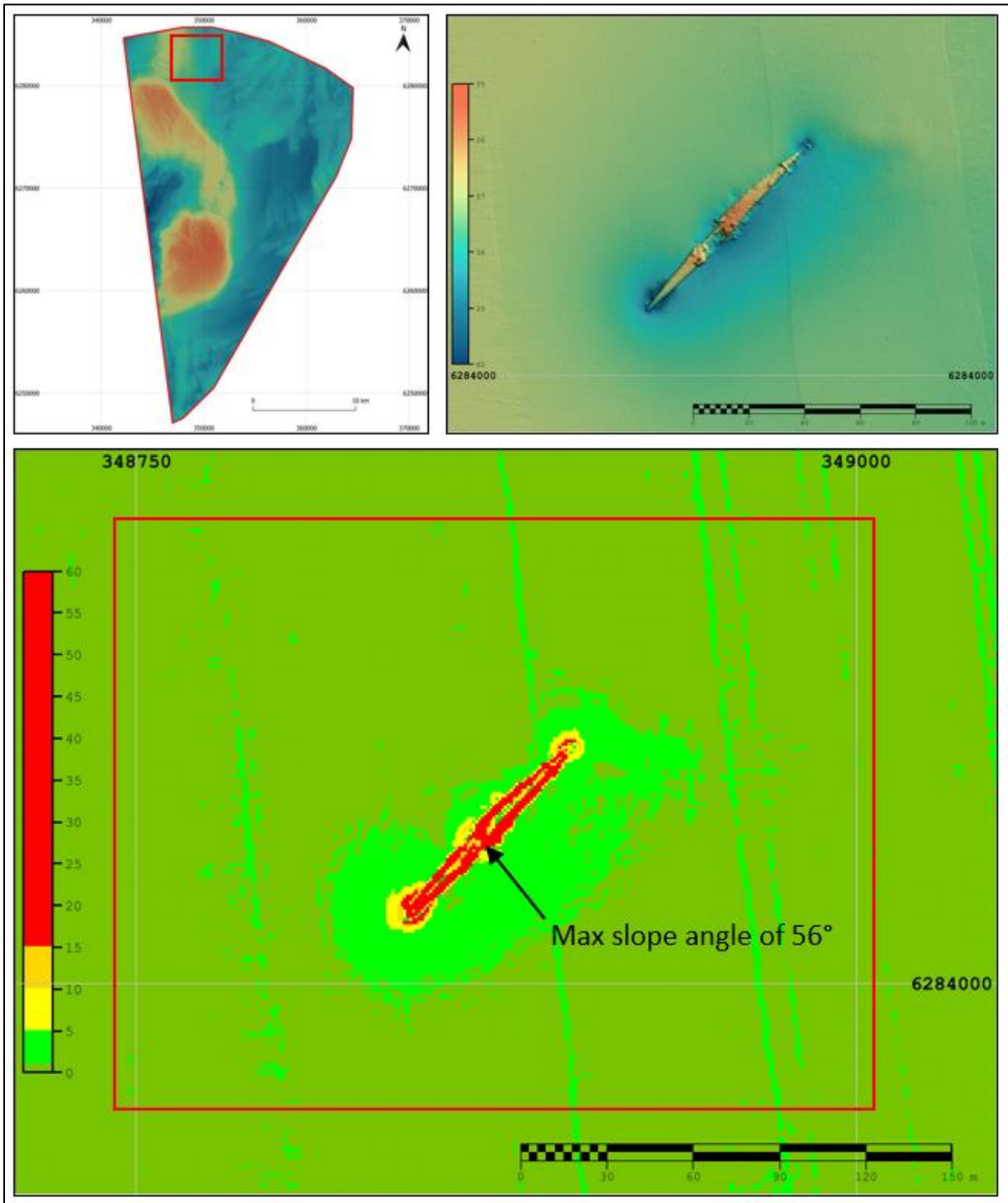


Figure 80 Wreck 86 with 56° slope angle.
Red box in lower frame corresponds to area of soundings shown in Figure 81.

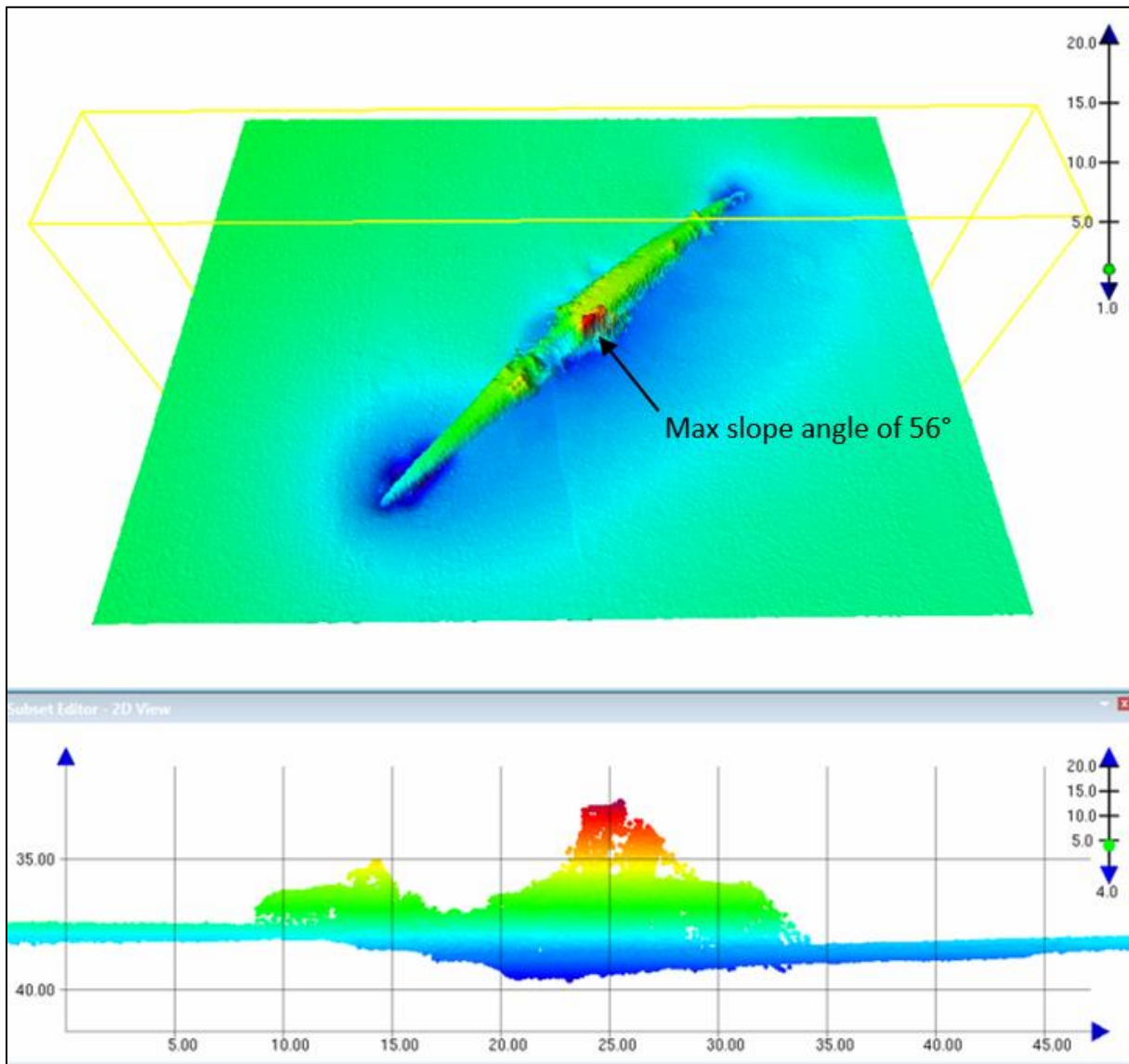


Figure 81 Accepted soundings over wreck in Figure 80.
Caris HIPS depth convention is positive down, vertical exaggeration of cross section is x4.

There is a large boulder (S_FR_B06_0727) with dimensions 6.2 m (l) 5.4 m (w) 2.4 m (h) with a slope angle of up to 47° in the eastern part of the survey area at 364087.7 m E, 6278530.6 m N as shown in Figure 82. The contact sits at a general depth of 41.0 m.

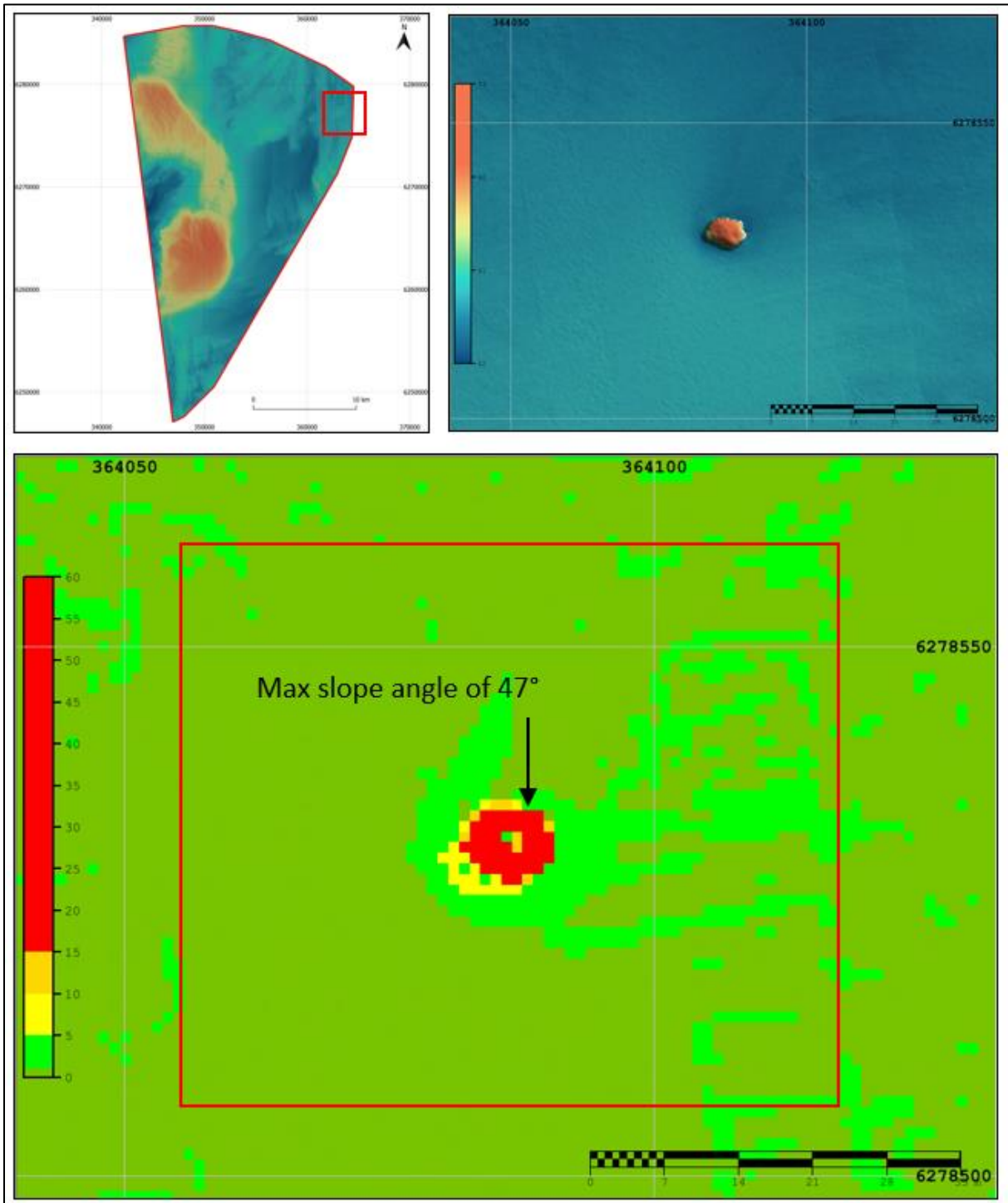


Figure 82 Large boulder with 47° slope angle.
Red box in lower frame corresponds to area of soundings shown in the following image.

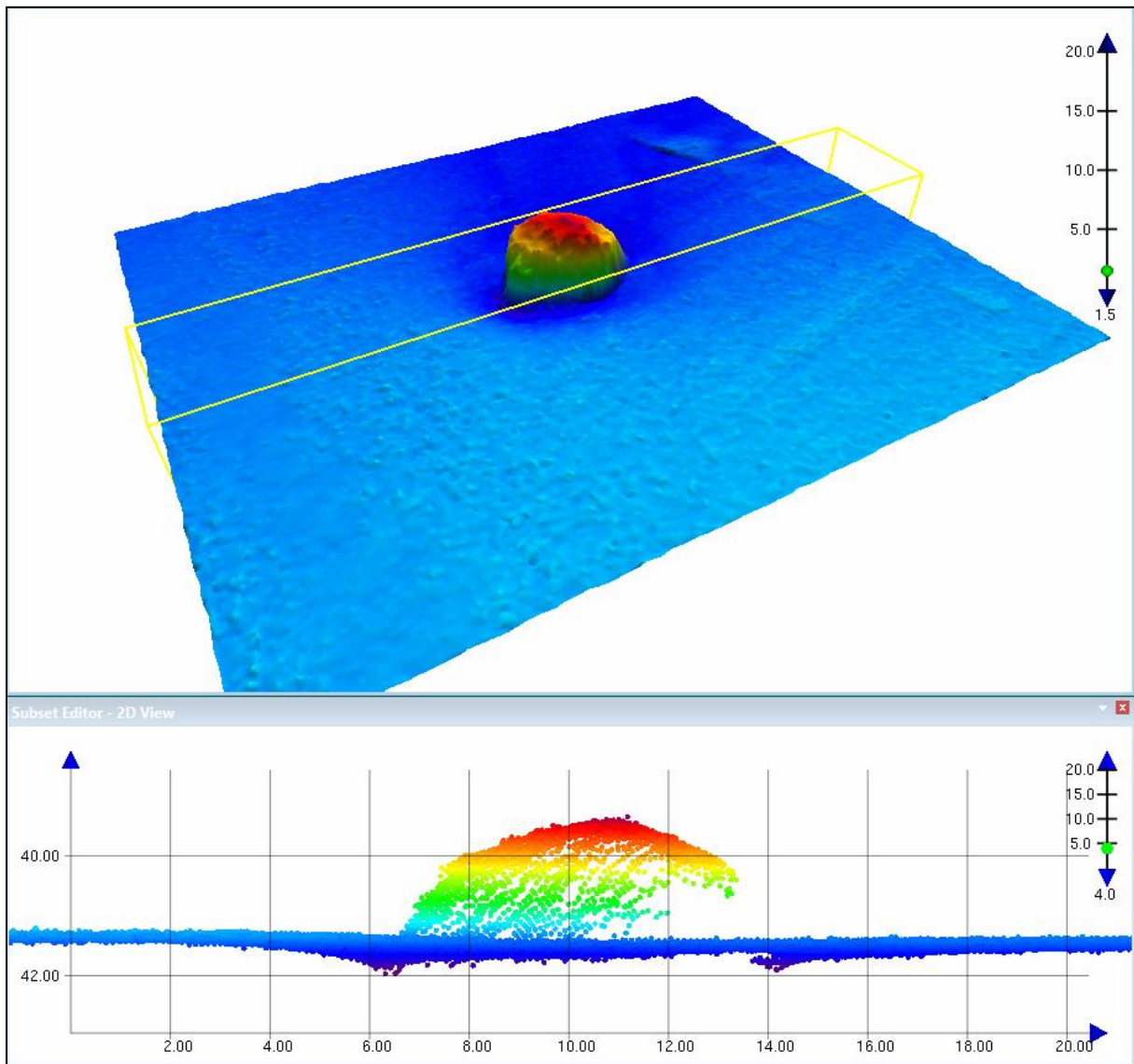


Figure 83 Accepted soundings over boulder contact in Figure 82.
Caris HIPS depth convention is positive down, vertical exaggeration of cross section is x4.

There are slope angles between 35° and 42° that are associated with large boulders in the northern part of the survey area as shown in Figure 84. An example boulder is shown in Figure 85 where a slope angle of 38° was observed on the side of a boulder at 356361.0 m E, 6281217.0 m N.

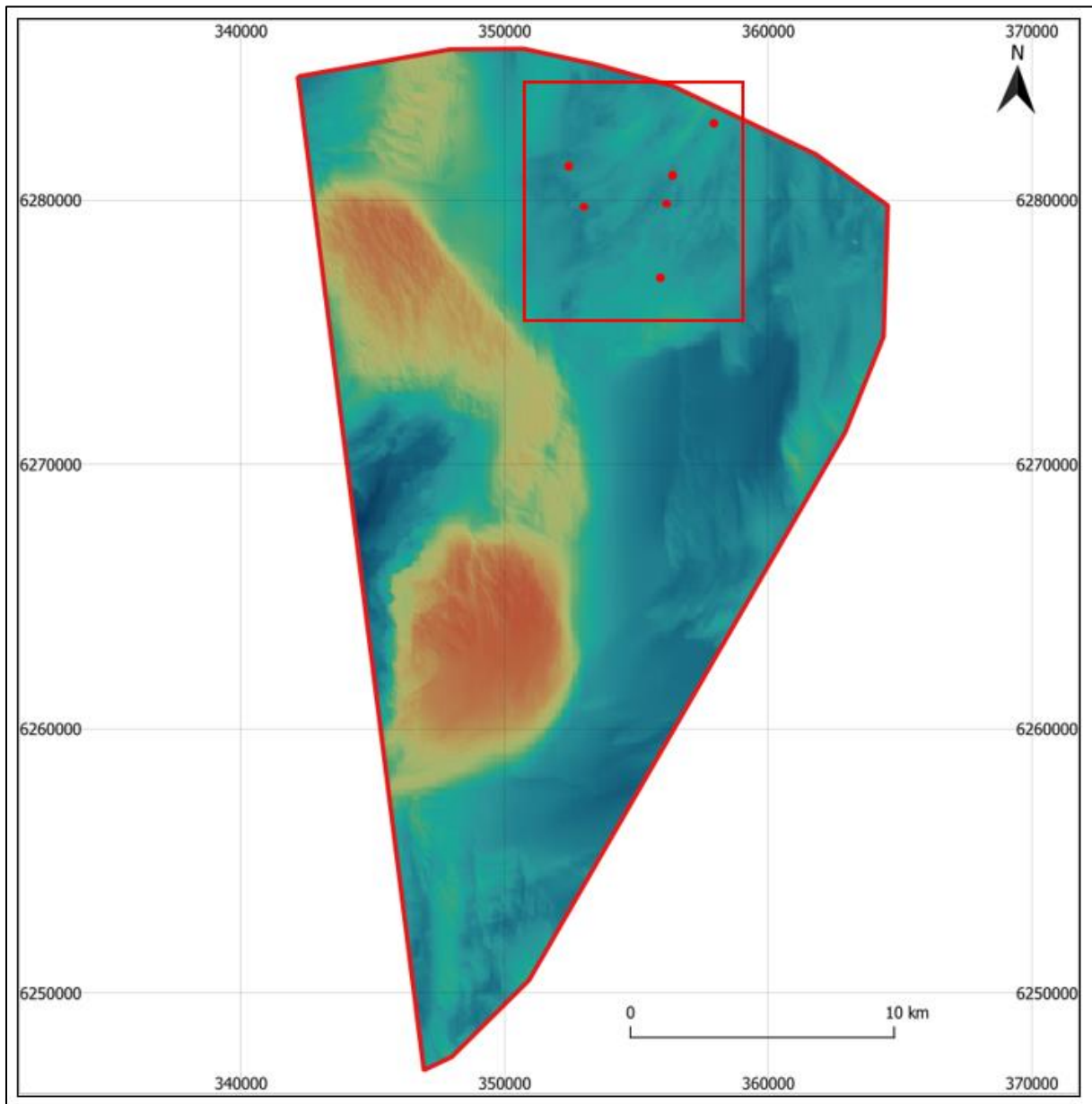


Figure 84 Location of large boulders with $38 - 42^\circ$ slope angle.
Red box shows area where large boulders are located.

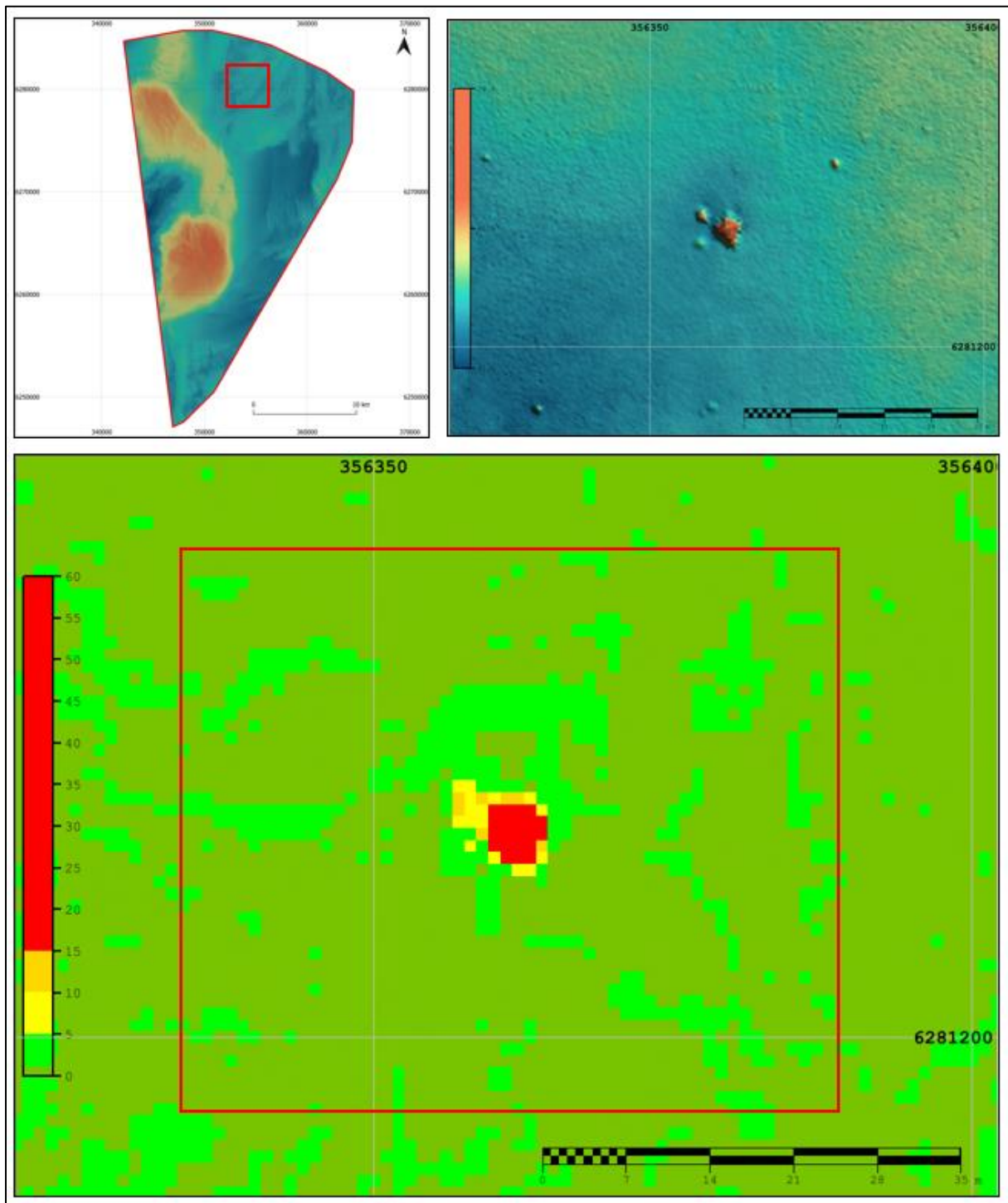


Figure 85 Large boulder with 38° slope angle.
Red box in lower frame corresponds to area of soundings shown in the following image.

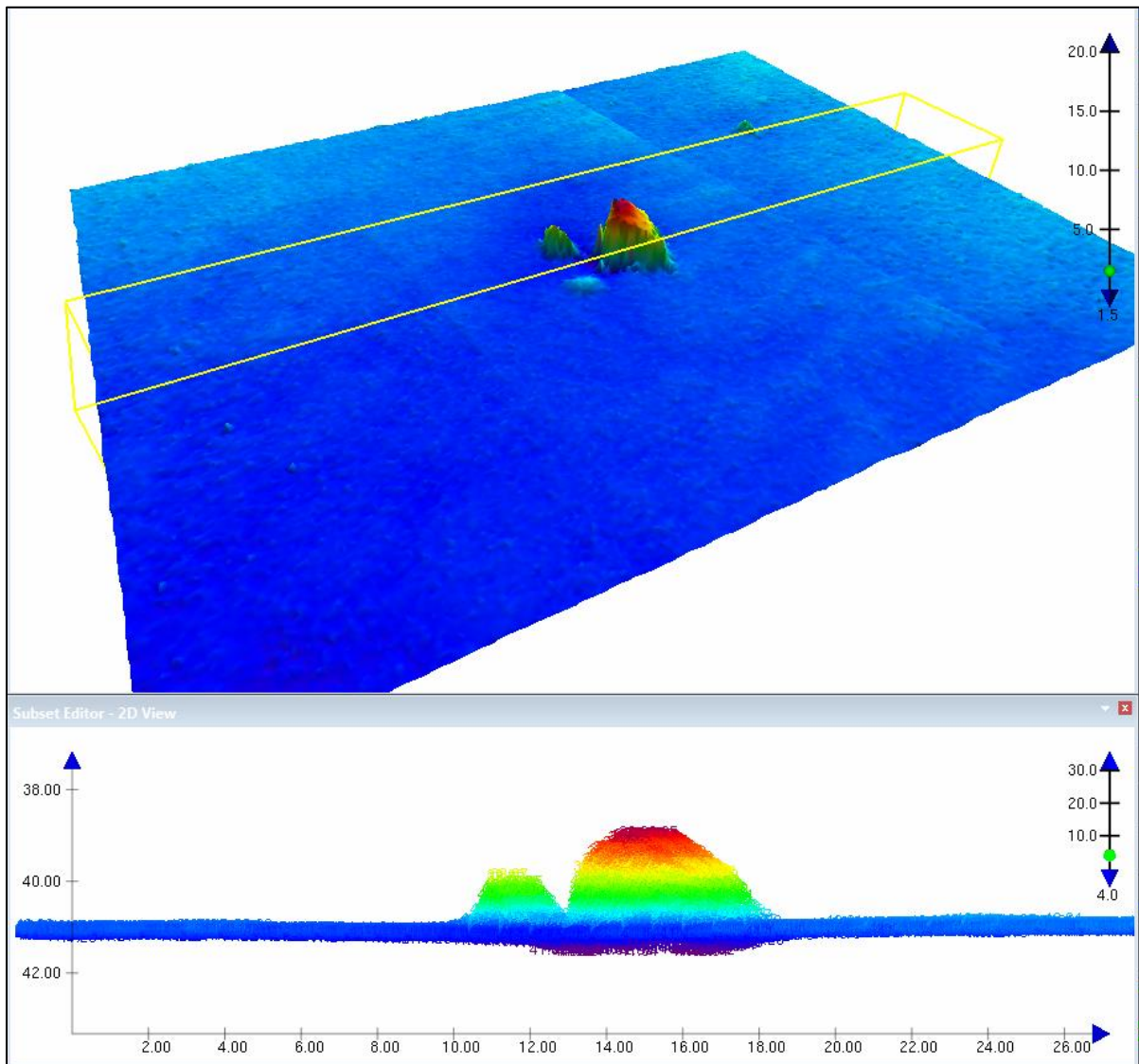


Figure 86 Accepted soundings over suspected boulder contact in Figure 85.
Caris HIPS depth convention is positive down, vertical exaggeration of cross section is x4.

The highest slope angle associated with a bedform feature is 44° and this is located on the side of a steep bank at 345825.0 m E, 6265890.0 m N (Figure 87). This steep bank is classified as an Other-Area of Interest and is located on the north western edge of the Artificial Island area of investigation.

To the south of this location there are further very steep slope angles between 30° and 44° which coincide with other steep banks (Other-Area of Interest features) on the western edge of the Artificial Island area of investigation.

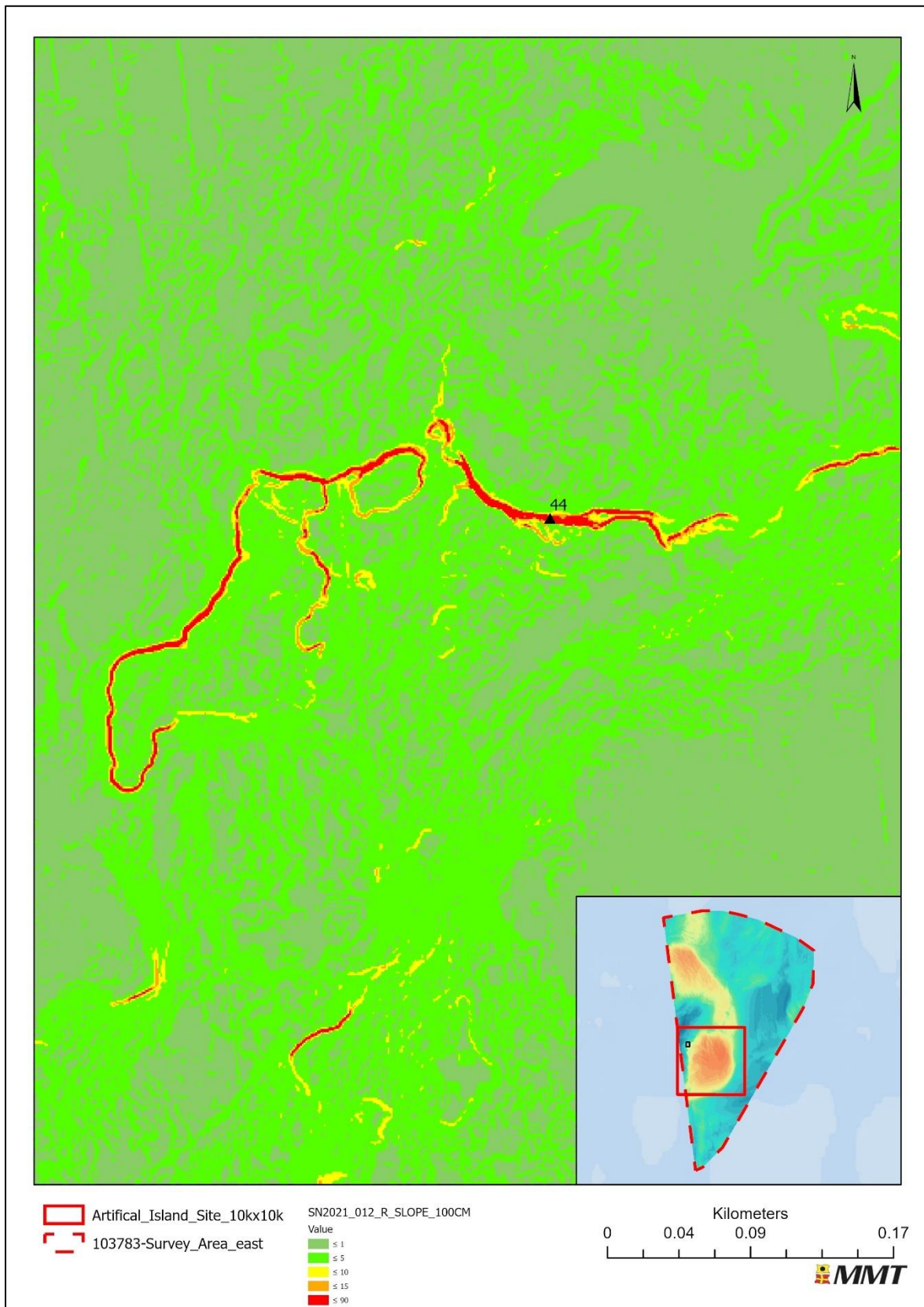


Figure 87 Bedform feature (Other-Area of Interest) with slope angles up to 44°. The feature is located in the southwest of the survey area.

8.3 | SURFICIAL GEOLOGY AND SEABED FEATURES

8.3.1 | SEABED SEDIMENTS

The surficial geology is interpreted from the SSS imagery based on the relative SSS reflectivity, where lighter reflectivity is interpreted as relatively finer grained sediments and darker reflectivity is interpreted as relatively coarser grained sediments. The SSS imagery has low to medium acoustic reflectivity overall. Backscatter data was used to confirm sediment boundaries. MBES bathymetric data was used to correct the interpretation for the effects of seabed slope on sonar returns. MBBS data was also used to confirm the interpretation of SSS data and to assist with boulder picking. Please refer to Section 6.3| for classification of seabed sediments and features.

A total of 125 Grab Sample locations were sampled in the MMT OWF survey area and were used to aid interpretation (section 8.10| and Appendix C|).

The seabed sediments in the MMT OWF survey area are dominated by GRAVEL and coarse SAND (medium to high acoustic reflectivity), muddy SAND (low to medium acoustic reflectivity) and SAND (medium acoustic reflectivity). The GRAVEL and coarse SAND is more prominent in the eastern central parts of the area (Reporting Tiles T04, T05, T06, T10, T11, T12, T17 T18) and western central parts of the area (Reporting Tiles T01, T02, T07, T08, T09, T13, T14, T15, T19, T20. The muddy SAND is more prominent in the central areas trending north to south (Reporting Tiles T02, T03, T10, T11, T16, T20, T21, T22). Areas of SAND are found predominantly in the eastern and western parts of the area (Reporting Tiles T01, T02, T05, T06, T07, T08, T09, T11, T13, T14, T15, T19, T20, T21, T22). Small, isolated patches of MUD and SANDY mud are also present in the east and west (Reporting Tiles T04, T05, T07, T08, T13, T14, T19, T20).

In the muddy SAND and MUD and SANDY mud areas, the seabed is usually featureless with ripples occurring mostly in areas of GRAVEL and coarse SAND or SAND, see section 8.3.2| and Figure 91 for details.

Extensive boulder fields ranging from intermediate to high density are particularly common in the northeast of the survey area, but also found as more isolated features in the northwest, central eastern, central western and southern part of the area, see section 8.3.3| and Figure 94 for details.

An SSS data example showing different sediment and boulder field types is presented in Figure 89.

Figure 88 shows an overview of the seabed sediments observed in the MMT OWF survey area.

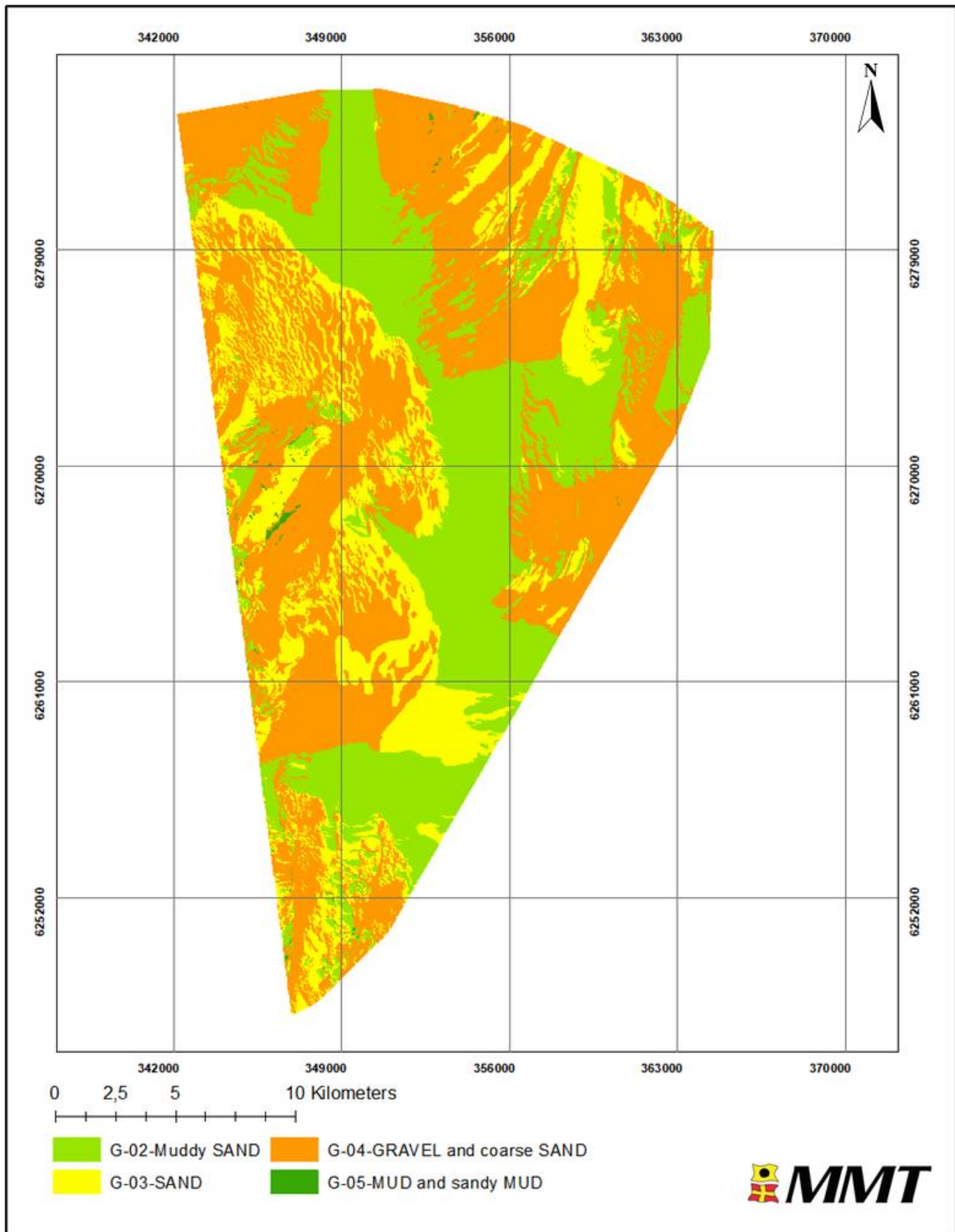


Figure 88 Overview of seabed sediments in the MMT OWF survey area.

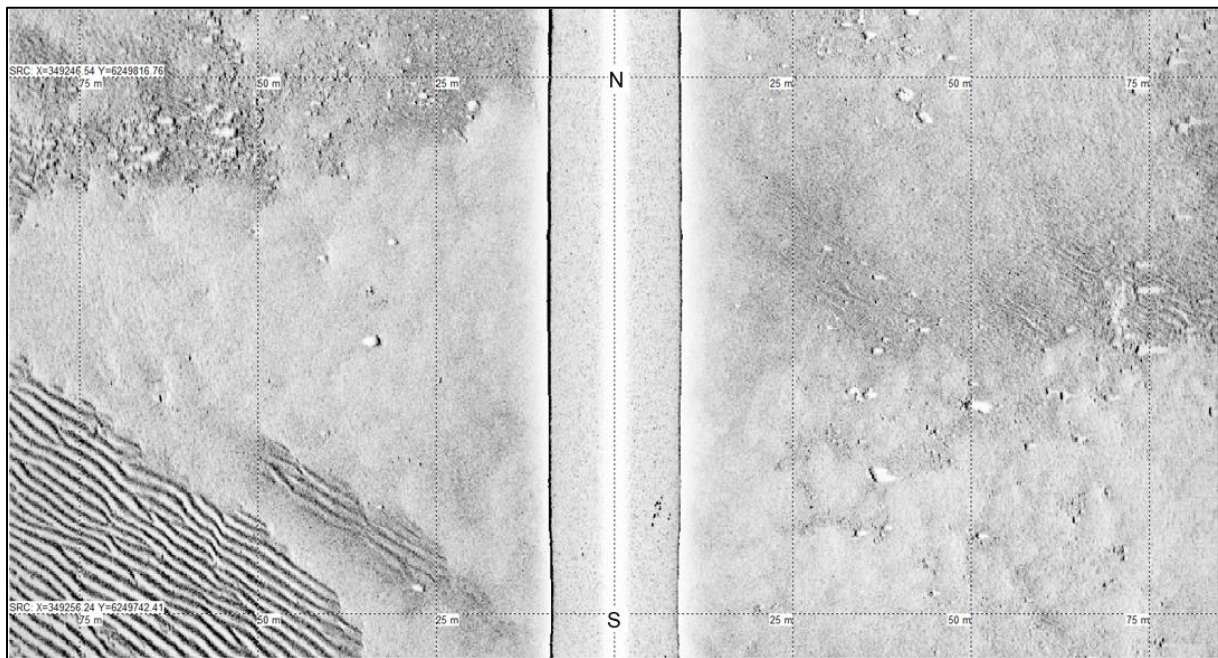


Figure 89 High frequency SSS example of boulder fields of variable density. The boulder fields are located in sediments of GRAVEL and coarse SAND (medium to high acoustic return) and sediments of SAND (medium acoustic return). Horizontal scale lines at 75 m intervals.

8.3.2 | MOBILE SEDIMENTS

Extensive areas of ripples, large ripples and megaripples, indicative of mobile sediments, are present across a large part of the MMT OWF survey area. Figure 90 shows an overview of mobile sediments observed in the MMT OWF survey area.

The extensive areas of ripples are seen in the east and west of the survey area (Reporting Tiles T01, T02, T04, T05, T06, T07, T08, T10, T11, T12, T13, T14, T17, T18, T19, T20). The ripples typically exhibit wavelengths of less than 2 m, are approximately 0.1 to 0.2 m in height and appear in elongated bands of variable width. Occasional areas of large ripples are seen in the west of the survey area (Reporting Tiles T07, T08 and T13) and typically exhibit wave lengths of 5-7 m. One area of megaripples is visible in the west of the survey area (Reporting Tile T13), with wavelength of ~30 m.

The ripples, large ripples and mega ripples are all in areas of GRAVEL and coarse SAND (Figure 91) and exhibit a northeast-southwest orientation (Figure 92), with the dominating current regime (and hence direction of sediment transport) from northwest to southeast.

Sand waves areas are visible frequently, particularly in the northwest of the survey area (Reporting Tiles T01, T02, T03, T07, T08, T09, T12, T14, T15, T16, T18), with wavelengths ranging between 50 m - 200 m and orientated north-south. The sand waves typically comprise of SAND or GRAVEL and coarse SAND (Figure 93).

Across much of the survey area, large scale massive mobile sediment bedforms are observed, upon which the smaller scale, more mobile and more recent bedforms, mentioned above are often superimposed. These areas of mass sediment migration form sediment accumulations such as sandbars, sand ridges and sand dunes; they have all been defined under the same seabed feature category of sandbars but have various wavelengths (>200 m) and various orientations.

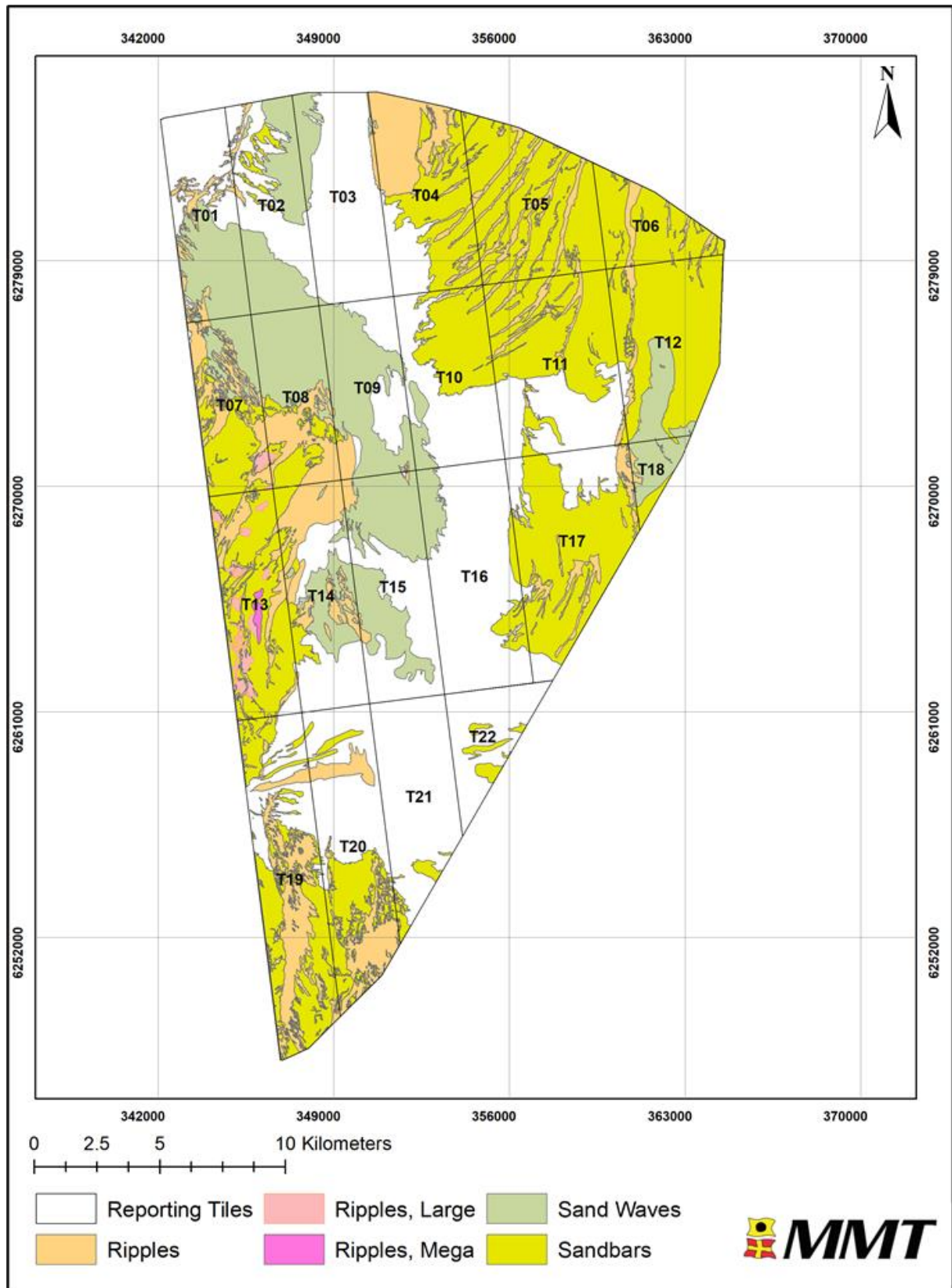


Figure 90 Distribution of bedforms.
 Ripples, Large Ripples, Megaripples, Sand Waves and Sandbars in the MMT OWF survey area.

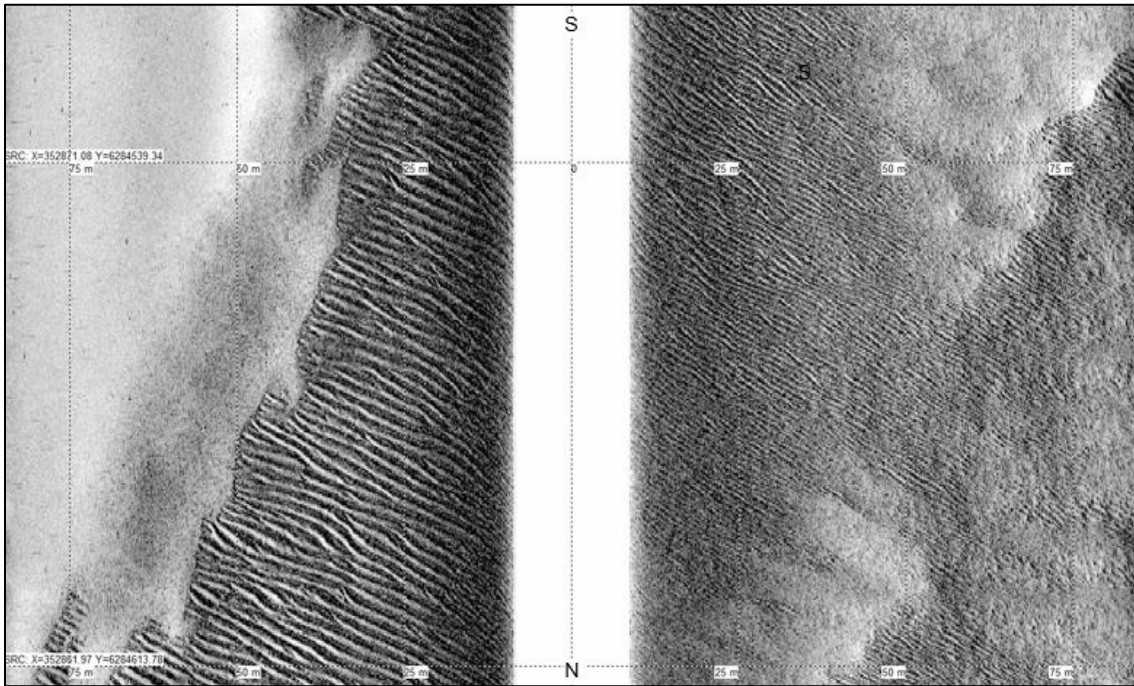


Figure 91 High frequency SSS example.
The example shows GRAVEL and coarse SAND with ripples (medium to high acoustic return) and SAND (medium acoustic return). Horizontal scale lines at 75 m intervals.

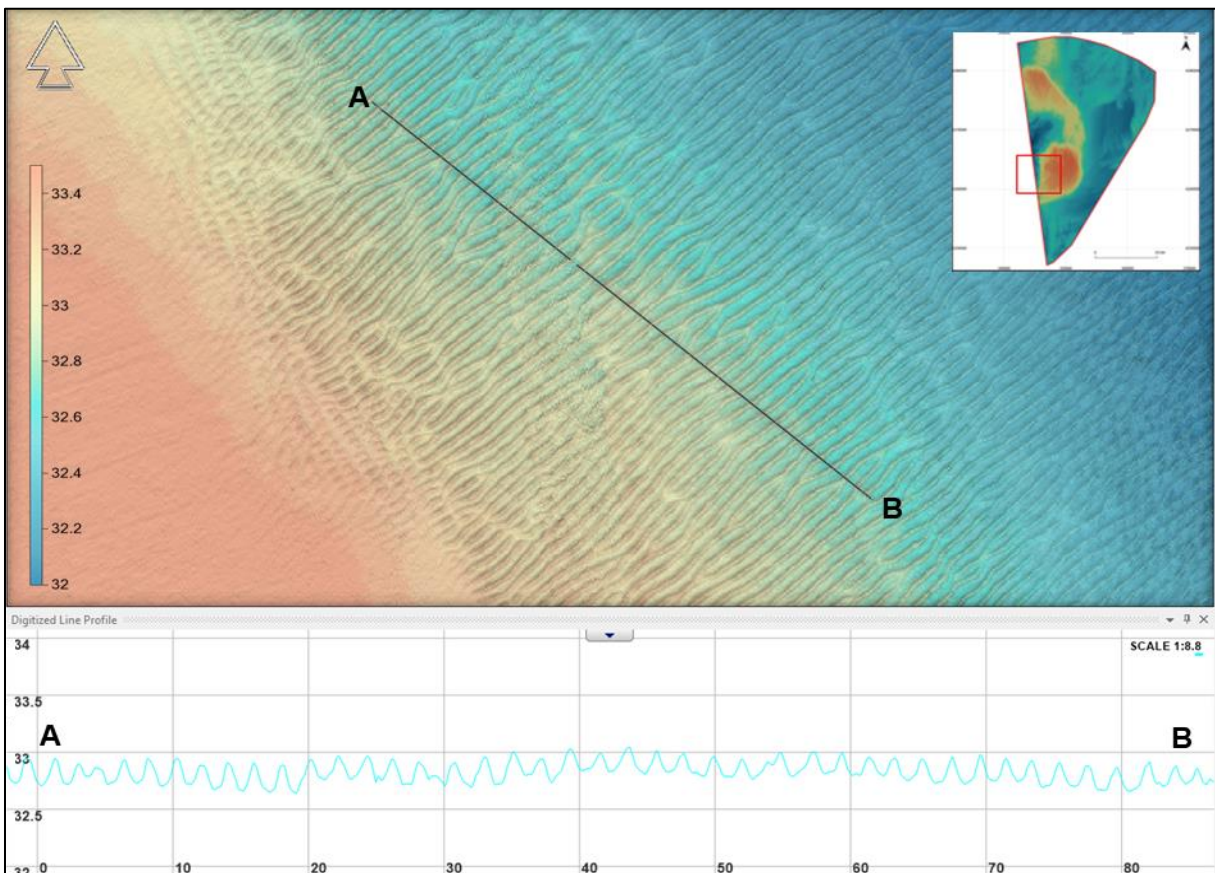


Figure 92 MBES DTM image showing ripples.

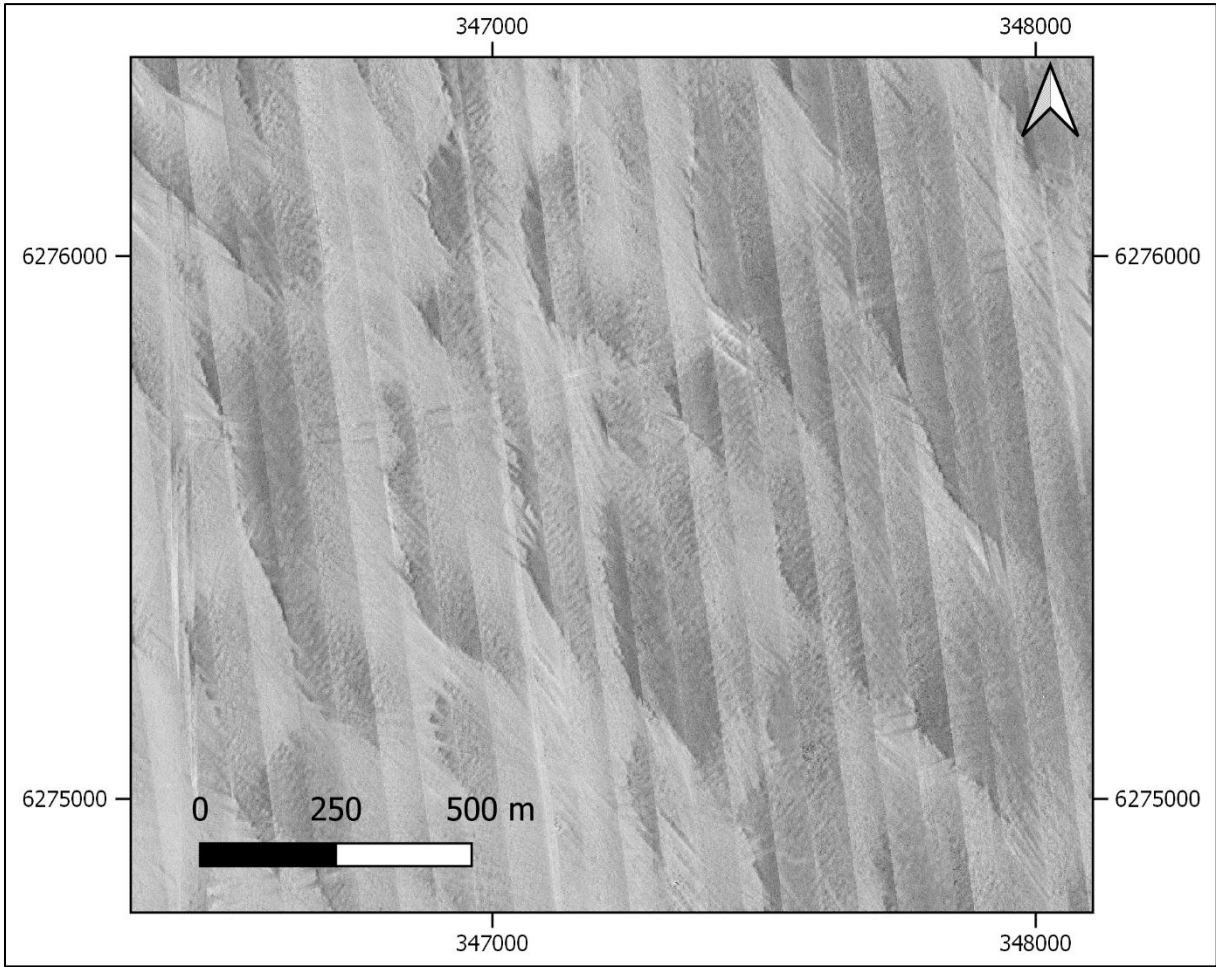


Figure 93 High frequency SSS mosaic showing sand waves in reporting tile T08. The example is from an area of SAND alternating with GRAVEL and coarse SAND.

8.3.3 | BOULDERS

Extensive boulder fields (likely glacial deposits) ranging from intermediate to high density are particularly common in the northeast (Reporting Tiles T04, T05, T06, T10, T11, T12) of the survey area. They are found as more isolated features in the northwest (Reporting Tile T01), central eastern (Reporting Block T17), central western (Reporting Block T07) and southern (Reporting Tiles T19, T20) part of the area. Fields with intermediate density are more common than high density boulder fields. Boulder fields are generally associated with areas of GRAVEL and coarse SAND. Individual boulders more frequently occur in the vicinity of boulder fields, but scattered boulders are also present throughout the area.

Within the boulder field areas, boulders >1 m have been identified and are part of the GIS TGS data set. For charting only boulders >2.5 m within boulder fields are included for visual purposes.

Throughout the survey area a total of 64130 boulders have been picked both inside and outside boulder field areas.

Figure 94 shows an overview of the boulder fields observed in the MMT OWF survey area.

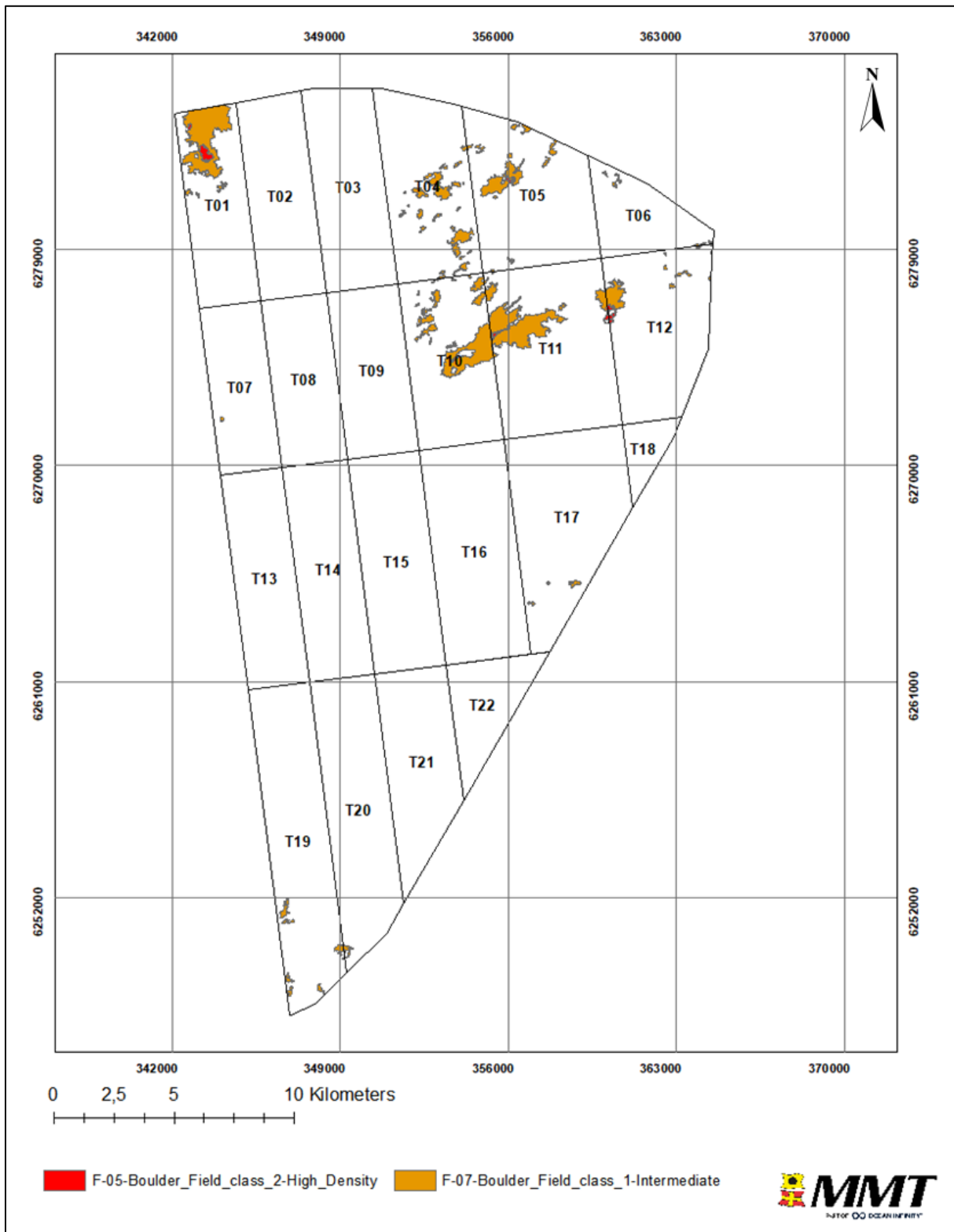


Figure 94 Distribution of boulder fields in the MMT OWF survey area.

8.3.4 | TRAWL MARKS

Evidence of trawling is found across the majority of the survey area (Reporting Tiles T01, T02, T03, T04, T07, T08, T09, T10, T11, T12, T14, T15, T16, T17, T18, T19, T20, T21, T22), see Figure 95 and Figure 96. Evidence of both older and more recent activity can be observed through areas of fainter scars overlaid by more prominent scars displaying greater seabed interference and suggesting a highly active area. The observed trawl scars show no predominant orientation and mostly consist of two parallel scars, each ~10-15 m wide, spaced approximately 30 m apart.

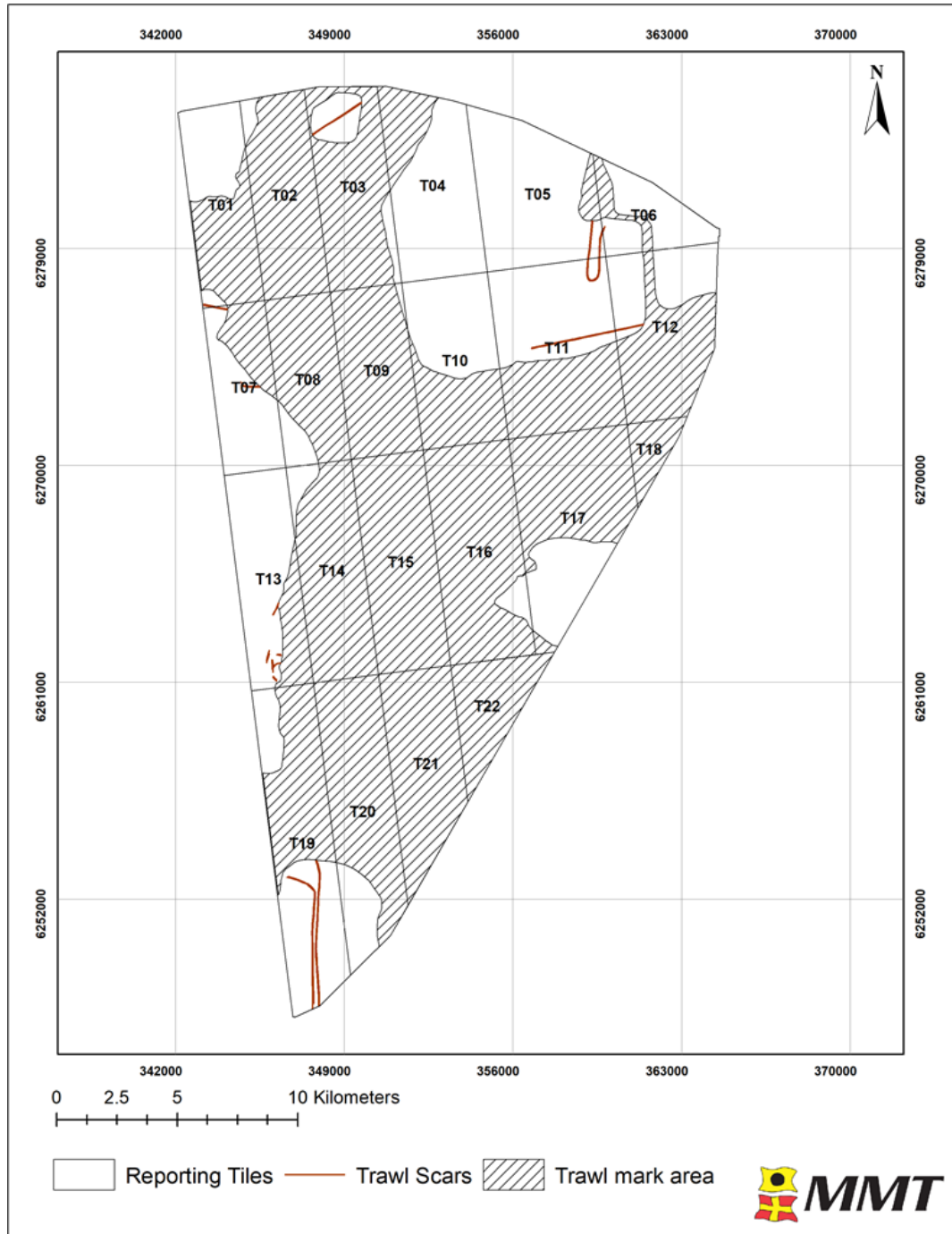


Figure 95 Distribution of trawl marks in the MMT OWF survey area.

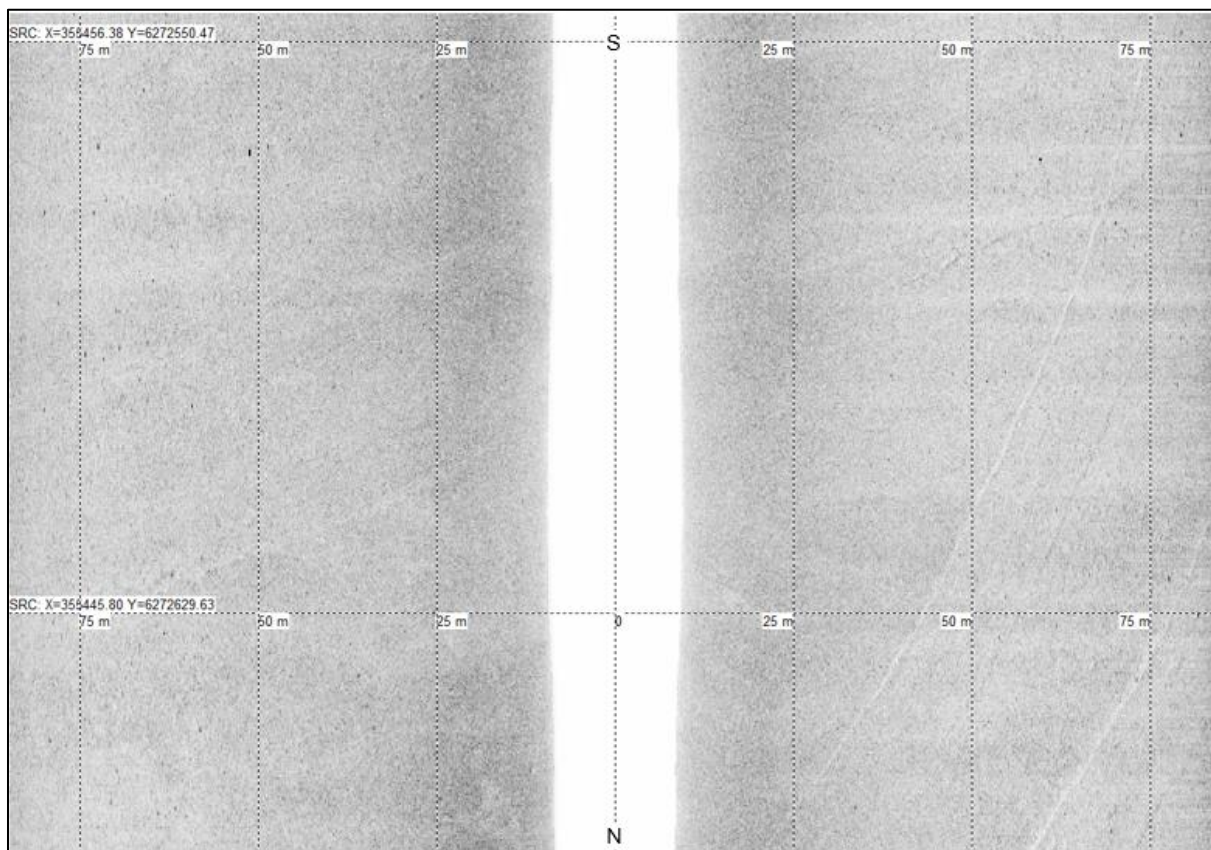


Figure 96 High frequency SSS example of trawl marks in silty SAND.
Horizontal scale lines at 80 m intervals.

8.3.5 | OTHER - SEDIMENT MOUND

One Isolated sediment mound was observed in the north-east of the survey area (Reporting Tile T12) at 363325.8 m E, 6278412.9 m N, that is significantly higher than surrounding area, with dimensions approximately 160 m (l) x 120 m (w) x 9.5 m (h), see Figure 97.

The feature is formed of tightly compact clays-silts-fine sands which appears to show an outcropping of an older seismic unit U20, see Figure 98.

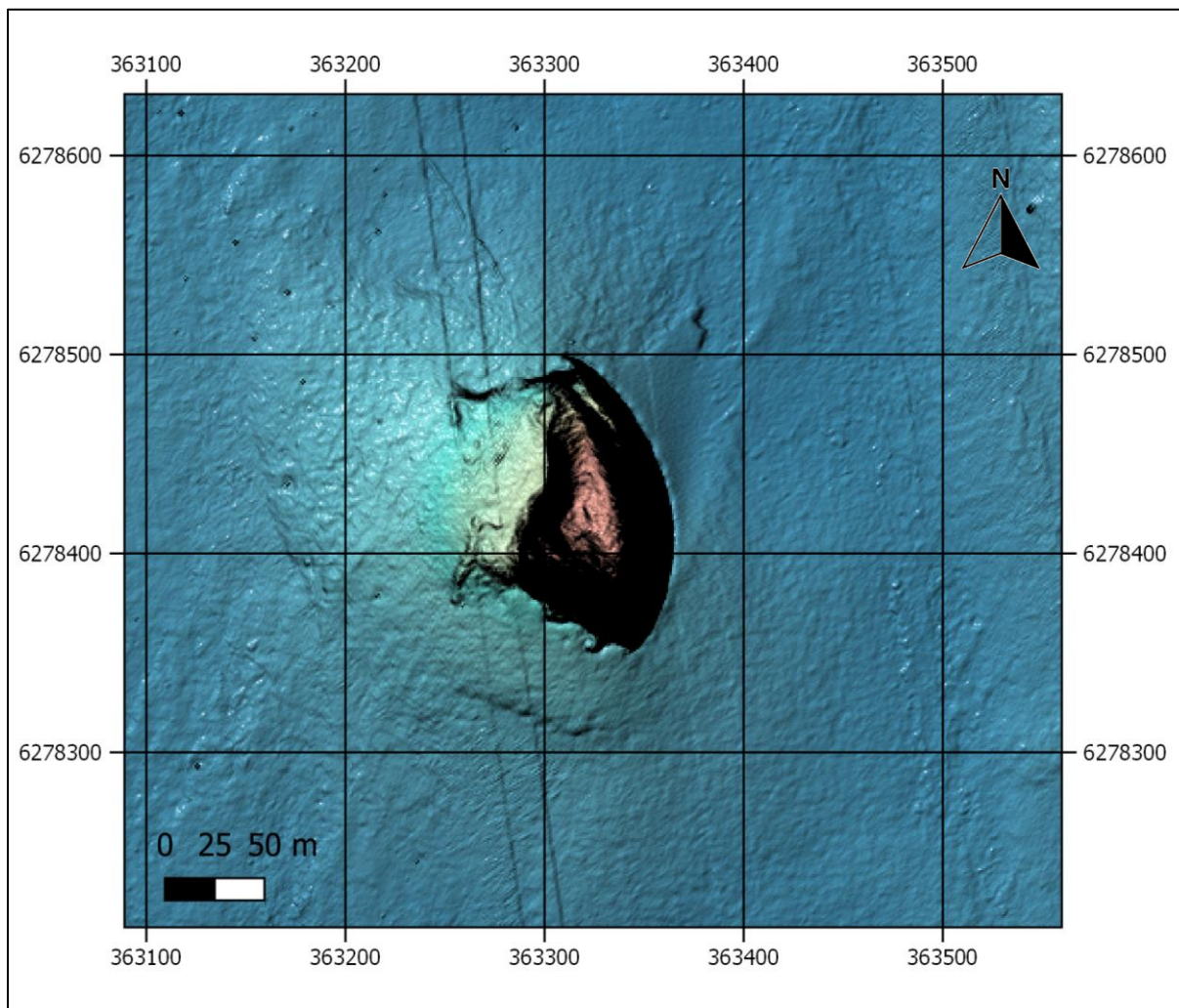


Figure 97 MBES data of a sediment mound in reporting tile T12.

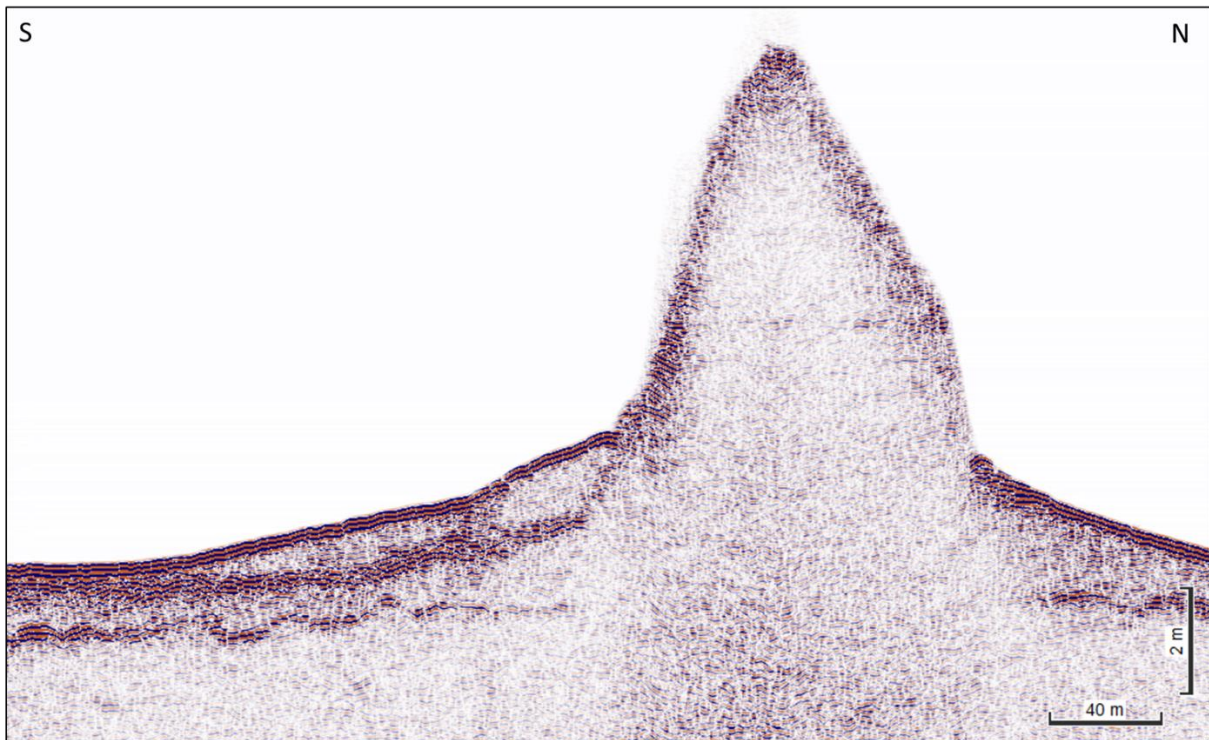


Figure 98 SBP Innomar data of a sediment mound in reporting tile T12

8.3.6 | OTHER - AREAS OF INTEREST

Some occasional areas have been defined as features of interest across the survey area (see Figure 99), in particular in the south and west (Reporting Tiles T03, T12, T13, T19, T21, T22). These areas comprise of mounds that were assessed to determine whether they could be biogenic in origin. Assessment by a senior biologist determined they are unlikely to be of a biogenic nature. They have been retained as a feature for future consideration.

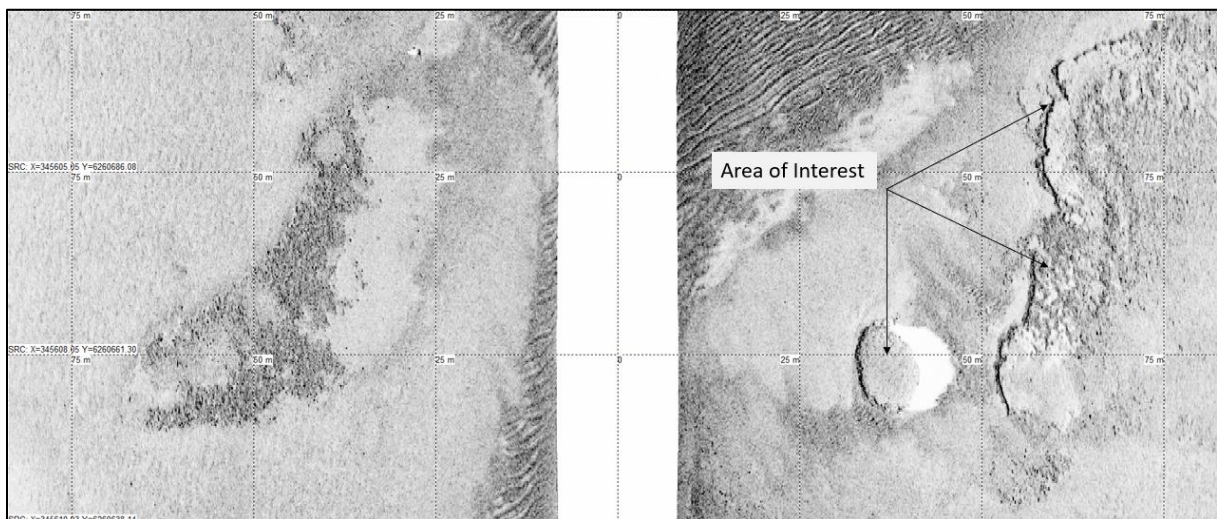


Figure 99 SSS data example of an area of interest in reporting tile T19.
Horizontal scale lines at 25 m intervals.

8.4 | CONTACTS AND ANOMALIES

In total, 65368 individual seabed contacts and magnetic anomalies were detected in the MMT OWF survey area. These were detected with SSS, MBES and/or MAG. All seabed objects are detected with either SSS or MBES. Boulders were primarily interpreted in the MBES data. Subsequently, remaining boulders and all other contacts were interpreted in the SSS data. All duplicates have been removed. Positional accuracy between contacts visible in the MBES and SSS data is good, less than 2 m.

A total of 64595 contacts - 61309 MBES and 3286 SSS contacts - were detected within the MMT OWF survey area. They were classified as: wrecks (3), possible unknown wreck (1), wire (4), debris (437), fishing equipment (11), other (9) and boulders (64130). All MBES contacts have been classified as boulders.

One large item of debris measuring 7.4 x 4.1 x 1.1 m (Figure 100) was found on an SSS line acquired 28/07/2021 but had not been seen on adjacent line acquired before this date. It is thought to be associated with fishing activity, as it is found next to a trawl scar that also appeared on 28/07/2021. It is found at 360909 m E, 6273946 m N and is associated with one magnetic anomaly.

SSS and MBES contacts are summarised in Table 23.

A total of 773 magnetic anomalies were detected within the MMT OWF survey area. 513 of these were individual discrete anomalies, whilst 260 anomalies were interpreted to form 33 linear anomalies. One of these linear anomalies corresponded to the database position of the buried TAT-14 cable and was associated with 97 discrete anomalies (see Section 8.5).

If a SSS or MBES contact were located within 5 m of a MAG anomaly, correlation information was added in the contact listings. A total of 50 discrete anomalies correlates with SSS or MBES contacts, including one of the known wrecks. Clusters of magnetic anomalies were also identified at the other wreck locations at a distance greater than the 5 m correlation distance used, see section 8.4.1.

Magnetic anomalies are summarised in Table 25.

Full details of all contacts and anomalies are presented in Appendix B.

Table 23 Summary of SSS and MBES contacts.

CLASSIFICATION	NUMBER OF CONTACTS
Boulder	64130
Wreck	3
Possible unknown wreck	1
Wire	4
Debris	437
Fishing equipment	11
Other	9
Total	64595

Table 24 Contact confidence classification

CONFIDENCE	CLASSIFICATION
HIGH	Observed on multiple sensors and/or adjacent lines. Target is well resolved and there is high confidence in the measurements made.

CONFIDENCE	CLASSIFICATION
MEDIUM	Observed on multiple lines of the same sensor. Target can be resolved to satisfactory resolution and there is medium confidence in the measurements made.
LOW	Target is not well resolved and there is low confidence in the measurements made.

Table 25 Summary of magnetic anomalies.

CLASSIFICATION	NUMBER OF ANOMALIES
Discrete	513
Discrete forming linear	260 (33 magnetic linear features)
Total	773

Sub-seabed contacts were identified in the SBP data, with contacts selected when diffraction hyperbolas were visible, summarised in Table 26.

Table 26 Summary of SBP Contacts.

CLASSIFICATION	NUMBER OF CONTACTS
SBP Point Contacts (hyperbola)	69
Total	69

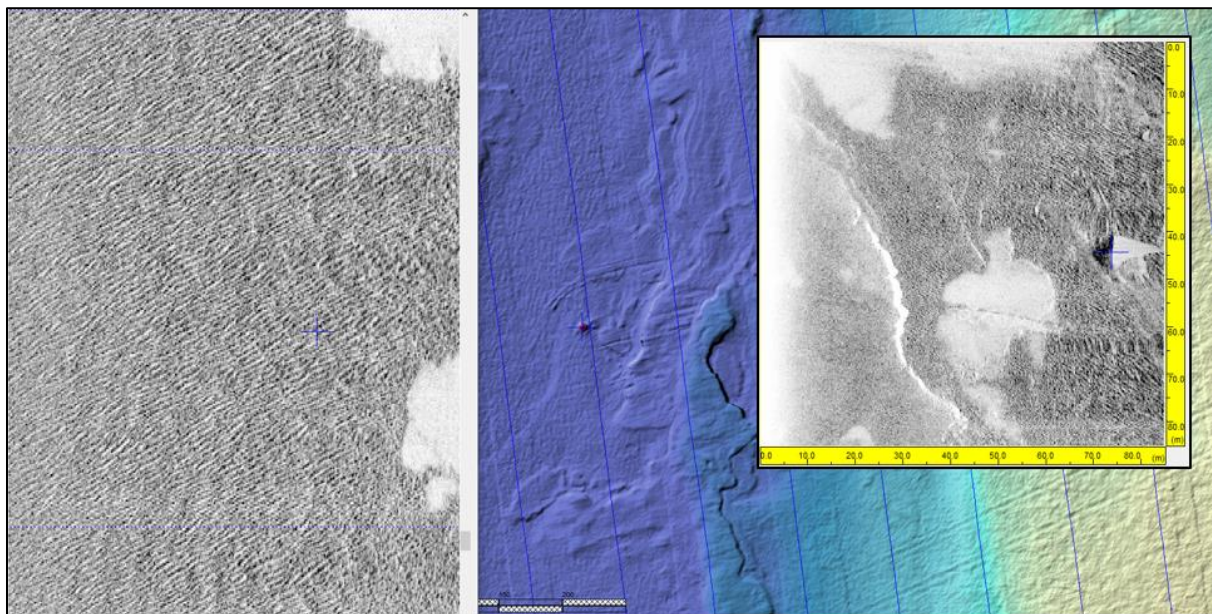


Figure 100 High frequency SSS and MBES images of debris item not seen before 28/07/2021. Left: SSS line acquired before 28/07/2021; centre: MBES image; inset on right: SSS line acquired on 28/07/2021.

8.4.1 | WRECKS

Three charted wrecks and one possible unknown wreck were observed within the MMT OWF survey area. The charted wrecks were present in the background data provided by the client.

A wreck (Contact ID: S_RE_B01_0324) was found at 347323.0 m E, 6253311.3 m N (Figure 105), 60.41 m offset from client supplied position (Client ID: Wreck_94). Five magnetic anomalies were observed in the vicinity. The as-found dimensions were 19.77 x 15.80 x 1.66 m.

A wreck (Contact ID: S_FR_B03_0006) was found at 348875.5 m E, 6284051.0 m N (Figure 102), 3.2 m offset from client supplied position (Client ID: Wreck_86). Two magnetic anomalies were observed in the vicinity. On background information, the wreck is identified as the HMS Tarpon submarine. The as-found dimensions were 82.78 x 8.46 x 5.11 m.

A wreck (Contact ID: S_FR_B03_0069) was found at 349881.9 m E, 6284268.9 m N (Figure 104), 17.9 m from the client supplied position (Client ID: Wreck_85). Eight magnetic anomalies were observed in the vicinity. The as-found dimensions were 56.22 x 20.43 x 1.37 m.

A possible unknown wreck (Contact ID: S_RE_B05_0547) was found at 358715.6 m E, 6272109.0 m N (Figure 106 and Figure 107). Three magnetic anomalies were observed in the vicinity. The as found dimensions were 12.15 x 5.09 x 0.46 m.

Table 27 Summary of wrecks observed inside the MMT OWF survey area.

MMT SSS ID	Client ID	EASTING (m)	NORTHING (m)	TYPE	COMMENT
S_RE_B01_0324	94	347323.0	6253311.3	Shipwreck	
S_FR_B03_0006	86	348875.5	6284051.0	Shipwreck	HMS Tarpon Submarine
S_FR_B03_0069	85	349881.9	6284268.9	Shipwreck	
S_RE_B05_0547	-	358715.6	6272109.0	Possible unknown shipwreck	

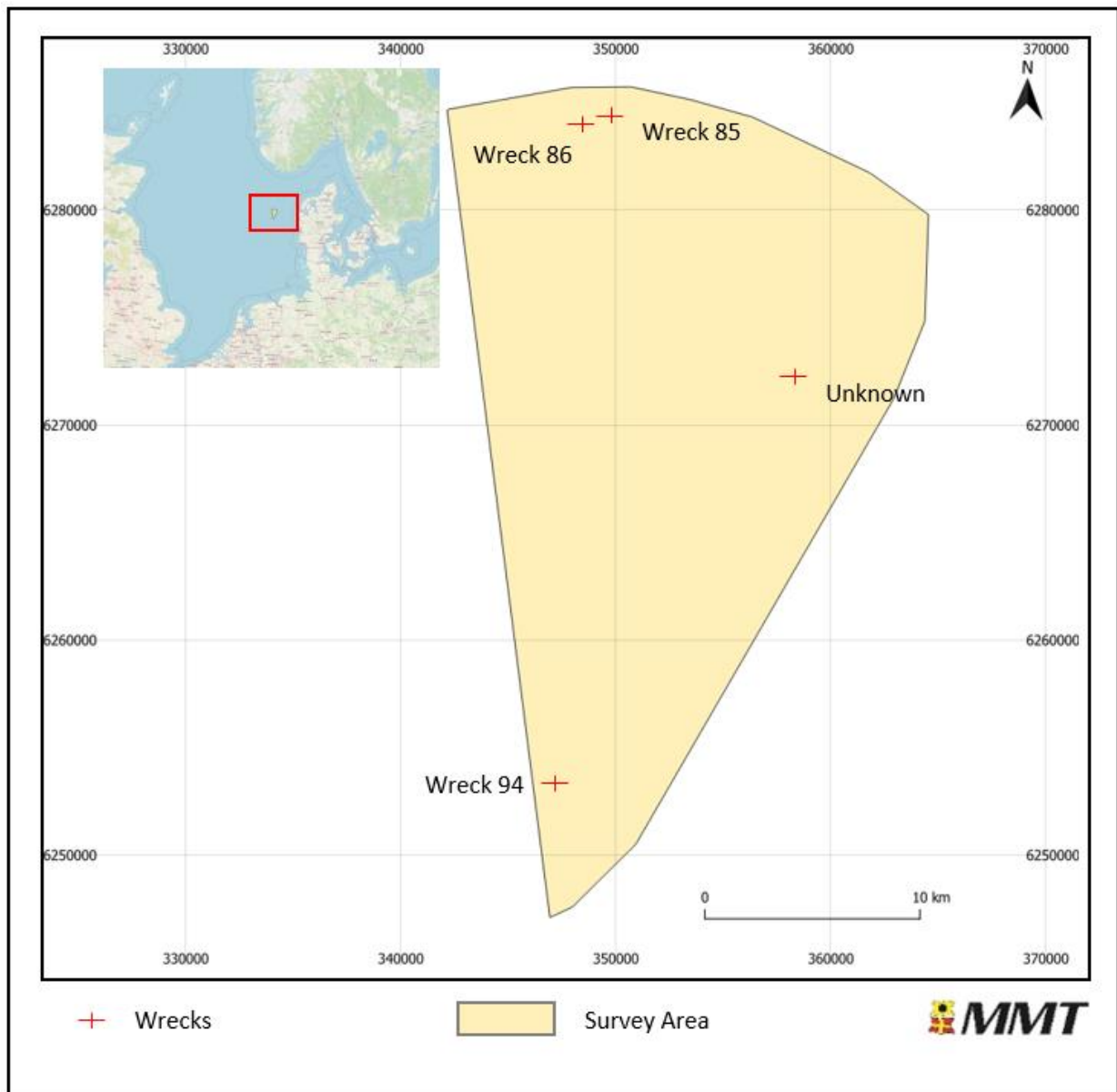


Figure 101 Overview of wreck locations within the MMT OWF survey area.

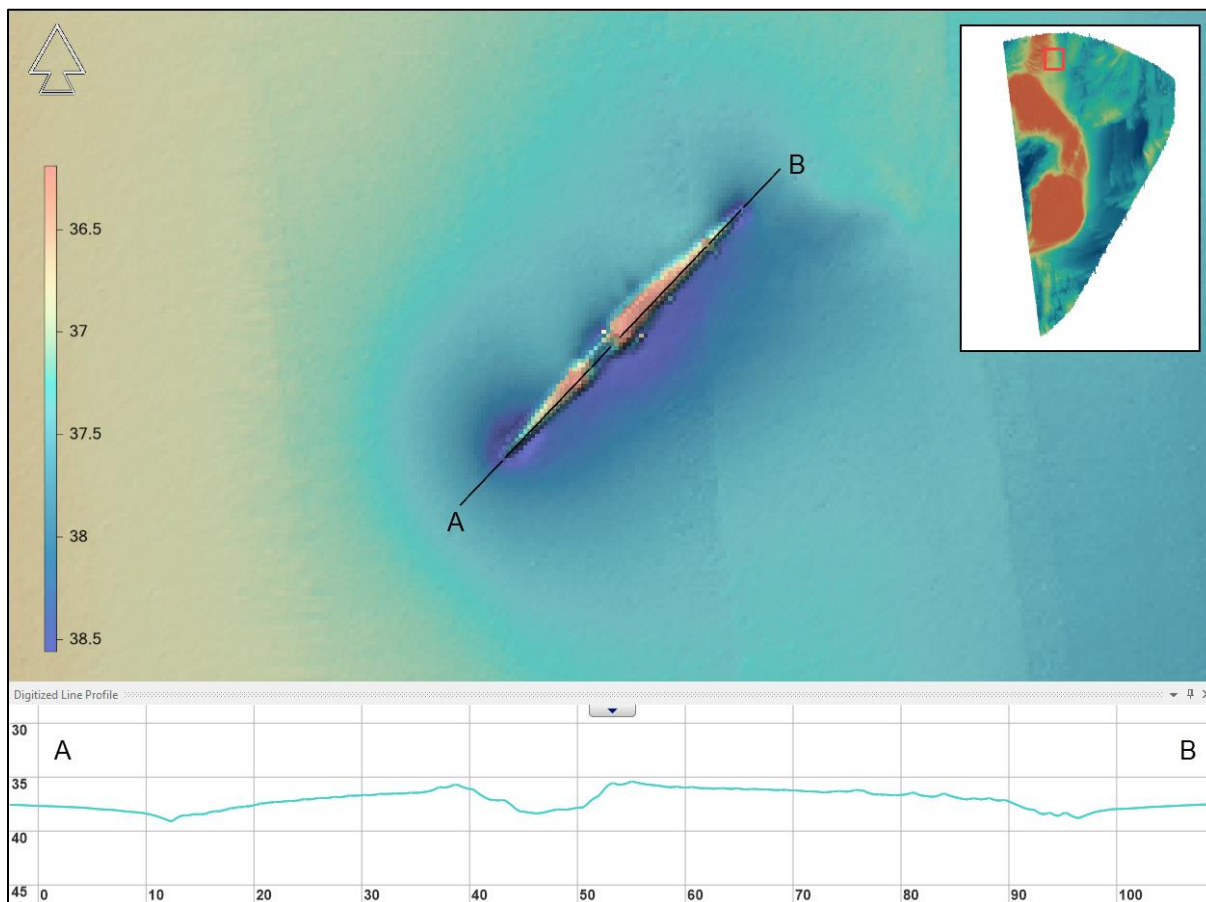


Figure 102 MBES image of HMS Tarpon Submarine Wreck_86 (S_FR_B03_0006). NaviModel depth convention is positive down, vertical exaggeration of profile is x1. Red box in inset map highlights figure location.

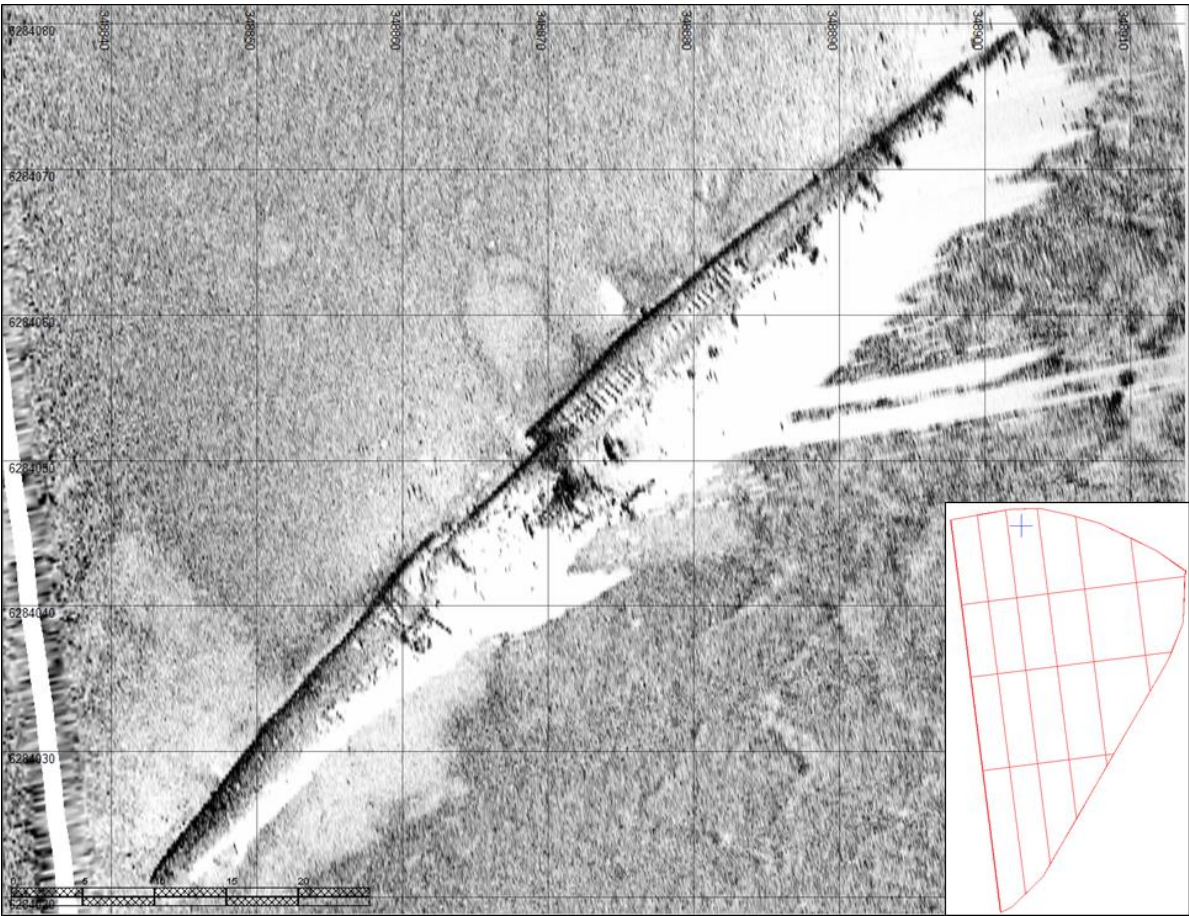


Figure 103 SSS image of HMS Tarpon Submarine Wreck_86 (S_FR_B03_0006).

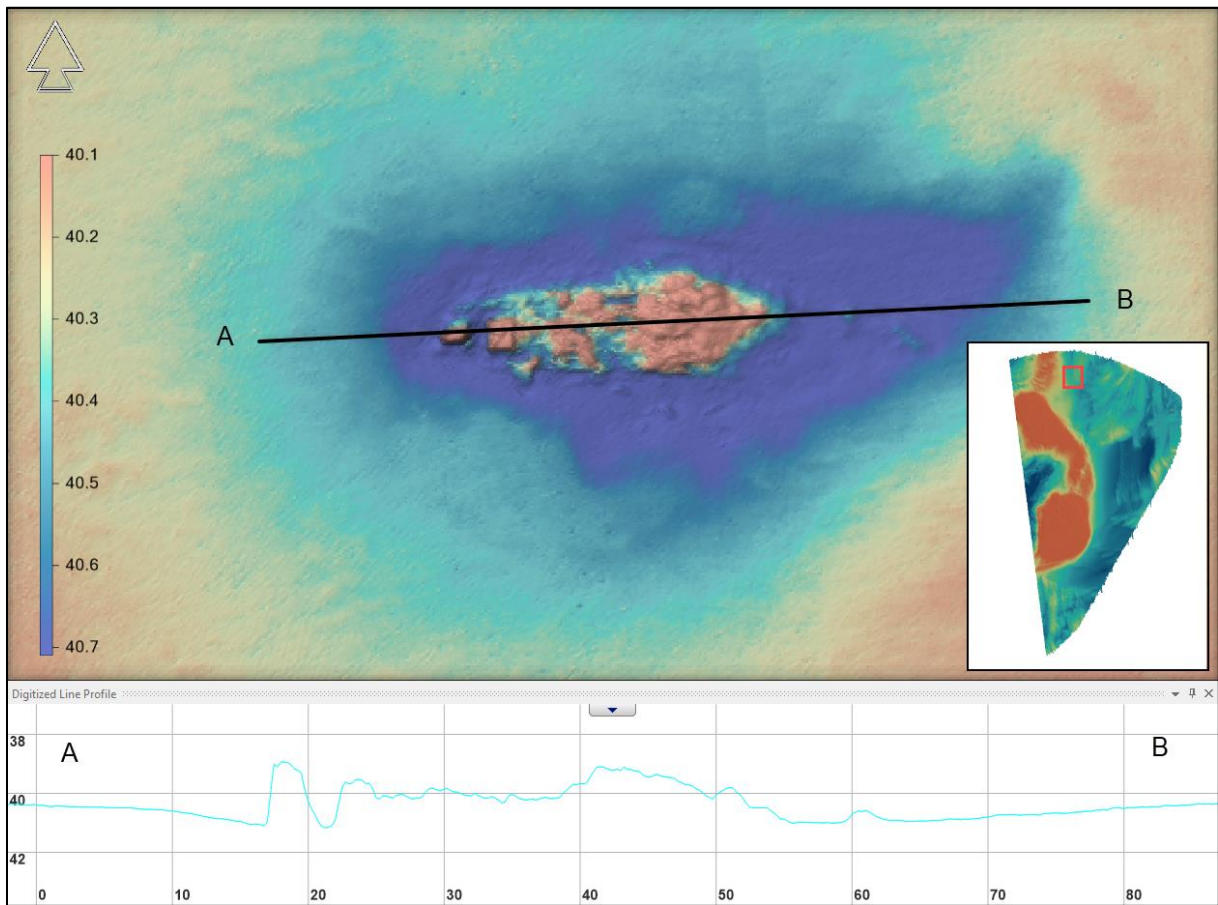


Figure 104 MBES image of Wreck_85 (S_FR_B03_0069).
NaviModel depth convention is positive down, vertical exaggeration of profile is x2. Red box in inset map highlights figure location.

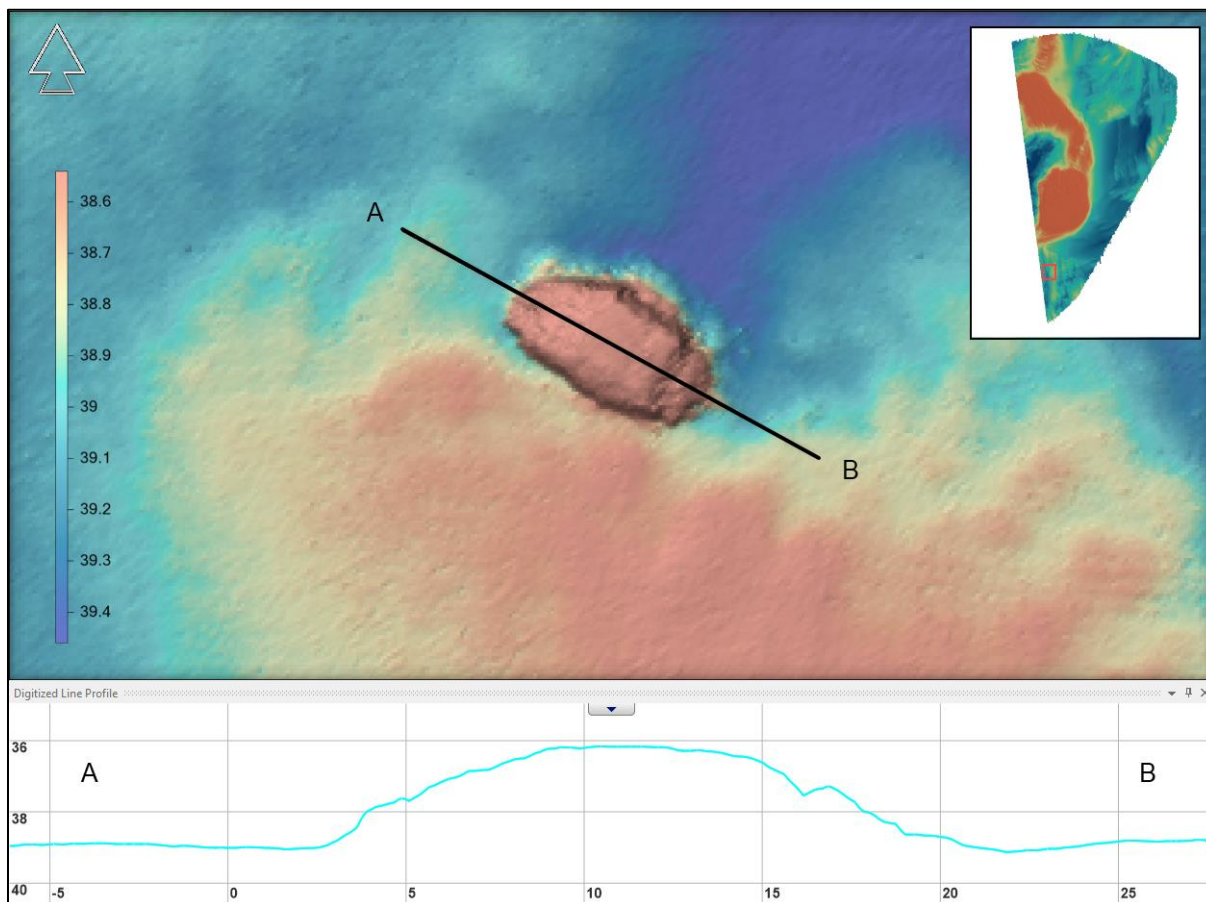


Figure 105 MBES image of Wreck_94 (S_RE_B01_0324).
NaviModel depth convention is positive down, vertical exaggeration of profile is x1. Red box in inset map highlights figure location.

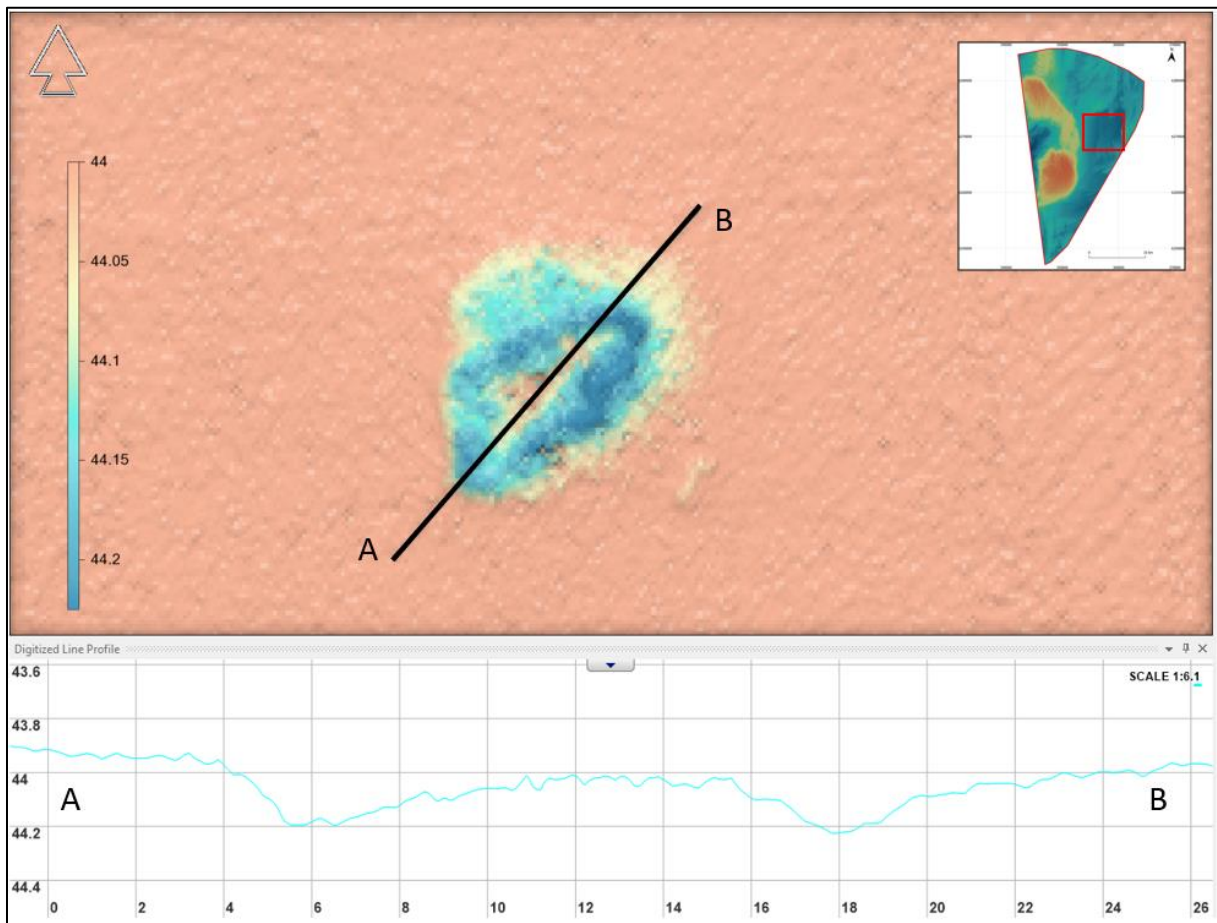


Figure 106 MBES image of a possible unknown wreck (S_RE_B05_0547). NaviModel depth convention is positive down, vertical exaggeration of profile is x6. Red box in inset map highlights figure location.

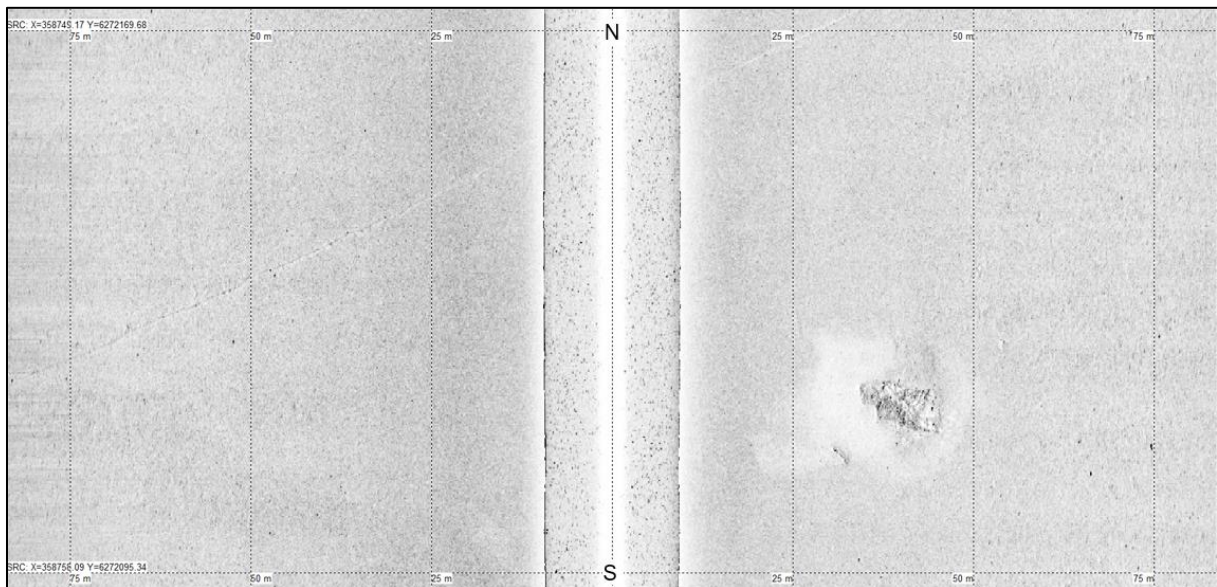


Figure 107 High frequency SSS image of possible unknown wreck with associated debris. Horizontal scale lines at 75 m intervals.

8.5 | EXISTING INFRASTRUCTURE (CABLES AND PIPELINES)

A cable presented in the background data (TAT-14) and confirmed with Mag anomalies and SBP hyperbola contacts, crosses the southern extent of the MMT OWF survey area, trending northwest to southeast. The cable is buried across most of the site and observed on almost all magnetometer lines as well as on some SBP lines. One possible exposure is found in the far west of the site where it might be exposed for 39.2 m, see Figure 108. This exposure is between 345275.33 N, 6259616.20 E, and 345310.08 N, 6259594.56 E. This exposure is approximately 57 m outside of the MMT OWF East area.

A total of 97 discrete Magnetic anomalies correlates with the client-supplied database position of the cable.

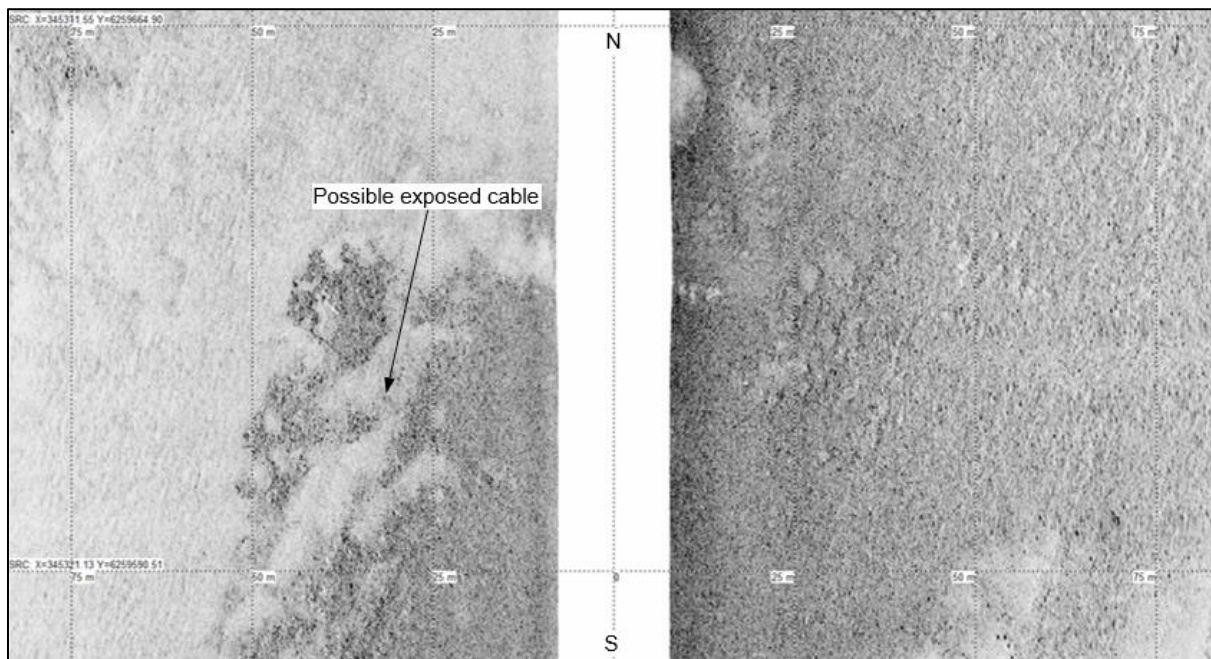


Figure 108 SSS image of possible exposed TAT-14 cable.
Horizontal scale lines at 75m intervals.

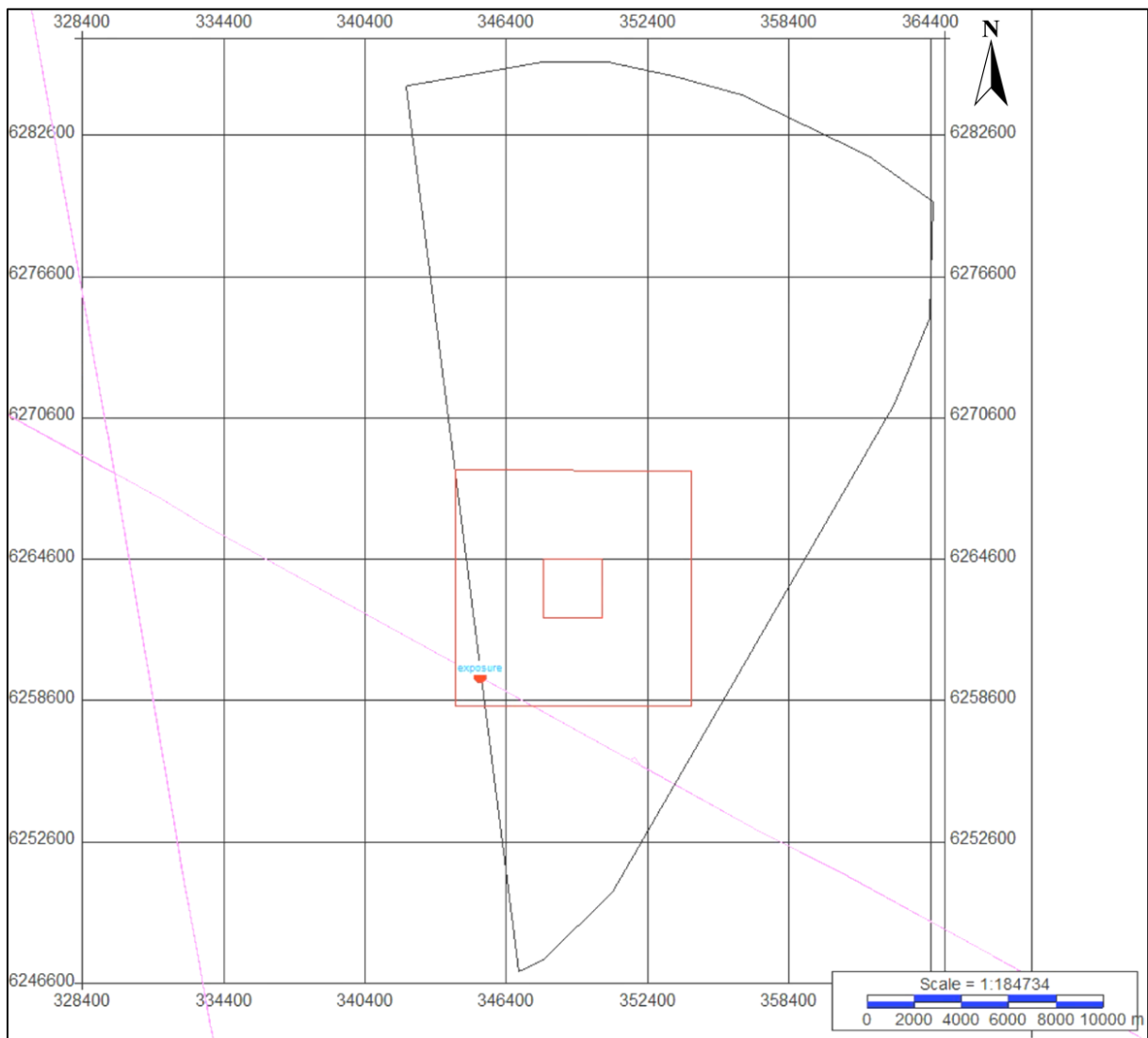


Figure 109 Map overview of possible cable exposure

8.6 | SEISMOSTRATIGRAPHIC INTERPRETATION

The subsurface geological interpretation and description is based on the assessment of the 2D UHRS and SBP data acquired within the survey area.

The original contract regarding the geomodel for this project was based on mapping eight horizons, however sixteen horizons were mapped in order to properly capture the subsurface complexity of the geological framework in this site.

The full seismic interpretation is available in the accompanying Kingdom Suite project. Its contents are presented below:

Kingdom Suite Project v2020 (SQL 2014) – **MMT_783_SBP_UHRS_WPA**:

- UHRS Seismic datasets: DPT, MIG, MUL, Vint, and Vrms; (179 X 5 = 895 SEG-Ys);
- SBP Seismic datasets: DPT_MSL, TWT_MSL and VelRMS (1987 X 3 = 5961 SEG-Ys);
- Culture:
 - **12 Shapefiles;**
 1. Surficial_Geology,
 2. Surficial_Morphology
 3. MAG_ANOMALY_LIN,
 4. MAG_ANOMALY_PTS,
 5. GEOTECHNIC_PTS,
 6. MBES_ANOMALY_PTS,
 7. SSS_ANOMALY_PTS,
 8. 103783-Survey_Area_and_Exclusion_Zone_ERTS89-UTM32N,
 9. 103783-Survey_Area_east,
 10. Artificial_Island_Site_10kx10k,
 11. Artificial_Island_Site_rev1
 - **6 Group Background;**
 1. All_cables_ETRS89-UTM32,
 2. SurveyAreaCable_200m_buffer,
 3. EnergyIslandWrecks20200305_500m_buffer,
 4. Paleochannels_georeferenced,
 5. Base_Chalk,
 - **10 Group Block Outlines;**
 - **164 SSS Mosaic TIFFs;**
 - **22 MBES TIFFs;**
 - **33 MBES Backscatter TIFFs;**
 - **19 Residual MAG TIFFs (WPA & WPD);**
- Interpretation Deliverables:
 - 16 Horizons in TWT, Depth & BSB;
 - 119 Horizons in total;
 - 136 Grids in meters;
 - 14 Hazards in TWT, depth, and meters BSB;
 - Unassigned Faults (TWT and depth).
- 155 Wells;
- 40 Polygons
 1. 10x10 km Artificial Island
 2. Basins
 3. H40_CH_01_C
 4. H40_CH_02_D
 5. H40_CH_03_B
 6. H40_CH_04_C
 7. H40_CH_05_A
 8. H40_CH_06_B
 9. H40_CH_07_A
 10. H40_CH_08_B
 11. H40_CH_09_D
 12. H40_CH_10_D
 13. H40_CH_11_D
 14. H40_CH_12_A
 15. H40_CH_13_A
 16. H40_CH_14_A
 17. H40_CH_15_D
 18. H40_ComplexArea

- | | |
|---------------|---------------------------|
| 19. H60_CH_01 | 30. H70_CH_08 |
| 20. H60_CH_02 | 31. H70_CH_09 |
| 21. H60_CH_03 | 32. KSA_Extension |
| 22. H60_CH_04 | 33. KSA_Subsidence |
| 23. H70_CH_01 | 34. KSA_Thrusting |
| 24. H70_CH_02 | 35. KSA_TunnelValley |
| 25. H70_CH_03 | 36. KSB_Thrusting |
| 26. H70_CH_04 | 37. Sector_centre |
| 27. H70_CH_05 | 38. Sector_N |
| 28. H70_CH_06 | 39. Sector_S |
| 29. H70_CH_07 | 40. U50_TransparentFacies |

Nomenclature:

- HXXX – horizons;
- UXXX_THK – thickness of unit UXXX;
- HXXX_BSB – unit base (HXXX) depth below seabed;
- UXXX_TOP_BSB – depth below seabed of the top of unit UXXX.

Table 28 List of horizons, grids and associated polygons present in the Kingdom Suite Project.

Kingdom Suite Colour Code	HORIZONS			Associated Polygons	GRIDS (m)			
	Horizon Name	TWT and DPT	BSB		HORIZON	THICK	BSB	BSB TOP UNIT
Dodger Blue	H00	X	X		X			
Gold	H05	X	X		X	X	X	
Dark Blue	H10i	X	X		X		X	
Light Green	H10	X	X		X	X	X	
Dark Green	H20	X	X		X	X	X	X
Rosy Brown	H25	X	X		X	X	X	X
Orange	H30	X	X		X	X	X	X
Yellow	H35	X	X		X	X	X	X
Dark Magenta	H40	X	X	H40 CH 01 to 15	X	X	X	X
Medium Orchid	H50	X	X	U50 Transparent Facies	X	X	X	X
Red	H60	X	X	H60 CH 01 to 04	X	X	X	X
Blue	H70	X	X	H70 CH 01 to 09	X	X	X	X
Medium Magenta	H85	X	X		X	X	X	X
Cyan	H90	X	X		X	X	X	X
Dark Red	KSA	X	X	KSA Extension, KSA_Subsidence, KSA_Thrusting & KSA_TunnelValley	X	X	X	X
Dark Red	KSB	X	X	KSB Thrusting	X	X	X	X
Black	BSU					X		X

Table 29 List of geohazards present in the Kingdom Suite Project.

Kingdom Suite Colour Code	HAZARDS		
	Horizon Name	TWT and DPT	BSB
Slate Blue	GHz Channels	X	X
Orange Red	GHz Gas	X	X
Cadet Blue	GHz Gravel	X	X
Orchid	GHz Lacustrine	X	X
Green	GHz SK U10	X	X
Dark Cyan	GHz SK U20	X	X
Light Pink	GHz SK U25	X	X
Dark Rosy Brown	GHz SK U30	X	X
Light Yellow	GHz SK U35	X	X
Violet	GHz SK U40	X	X
Light Plum	GHz SK U50	X	X
Wheat	GHz SK U60	X	X
Light Orchid	GHz SK U85	X	X
Tomato	SBP_targets	X	X
Salmon	UHRS_Faults	X	X

8.6.1 | SUB-SEABED GEOLOGY - GEOMODEL

The Geological Ground Model was defined from the integration of geophysical survey and grab sample results acquired within the MMT OWF survey area. Geotechnical information, provided by Energinet in the form of borehole data, was scarce. The data comprise six vibrocores from the Jupiter Well Database (GEUS), limited to the upper 5.8 m of sediments below the seabed and away from any 2D UHRS line. Given the paucity of geotechnical sampling (vintage 5m vibrocore data) across the site, extrapolations of sediment type and characteristics away from the coring locations was reliant on seismic facies analysis. A thorough revision of the available scientific literature was carried out to steer the seismic interpretation and ensure the formulation of a Geological Ground Model that is consistent with the known geologic evolution of the region.

Seismostratigraphic interpretation of the 2D UHRS and the single-channel SBP data was the basis for the geological ground model presented here. The interpretation approach employed included aspects of sequence stratigraphy, kinetostratigraphy, lithostratigraphy, and seismic facies analysis.

The geological ground model comprises 12 horizons that correspond to seismic reflectors and/or boundaries deemed significant to build the main sub-surface geological framework, distinct depositional and erosion events, marking relevant environmental changes, and shifts in sediment types. The criteria for horizon selection were structure significance in the site's stratigraphic framework, spatial reflector continuity, and delimitation of seismic facies interfaces. The mapped horizons represent the bounding surfaces of the 12 seismic units described here. An additional seismic unit, referred to as the Base Unit, is also included in the model, the details of which are discussed later in this section. The lateral assemblage and vertical stacking of these units represent the structural aspect of the geological ground model. The associations and relationships amongst the structural elements represent the geologic evolution of the depositional environments at the site. Alongside the model, a careful and detailed analysis of direct seismic indicators (e.g., diffractions, amplitude anomalies, acoustic blanking, etc.) was carried out as part of the assessment of potential geohazards within the sub-surface.

An analytical interpretation of the Geological Ground Model is provided in the Discussion section 8.6.15]. However, a short introduction to the site's seismostratigraphic character is provided here to assist the descriptions of the individual seismic units comprising the model.

Due to the complex geological architecture of the area and to facilitate the description of the model, the site was divided in three sectors, believed to represent distinct domains of sediment deposition and deformation: North sector; Central sector; and South sector (Figure 107). The spatial distribution of the interpreted seismic units across these sectors is shown in Table 30. These sectors are described in detail in the Discussion section 8.6.15].

The interpretation of the SBP data was done with the guidance of preliminary 2D UHRS grids to facilitate the interpretation, especially of deeper horizons. Interpretation of the Holocene sediments (U05 & U10) was done mutually exclusive and then interpretation was compared between the sensors to ensure cohesion. Surficial data and interpretation were used to ensure sediment boundaries at the surface were properly mapped to develop a full understanding of the geomodel.

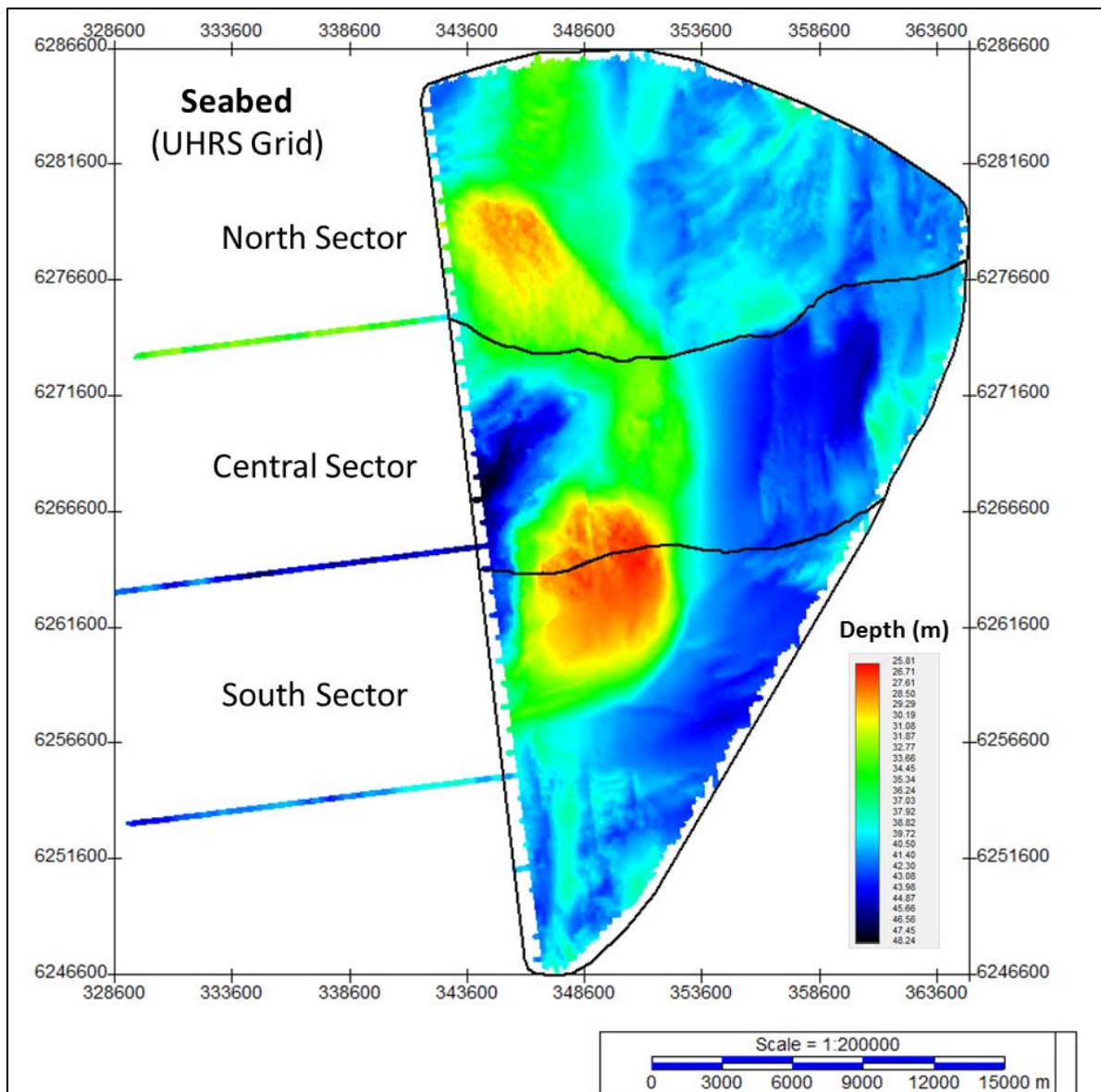


Figure 110 Seabed of the MMT OWF survey area – UHRS grid. Units in metres MSL.
 Note that the three tie lines project in to the Fugro OWF survey area.

Table 30 Distribution of interpreted seismic units.
 The table presents the distribution within the North, central, and South sectors of the survey area.

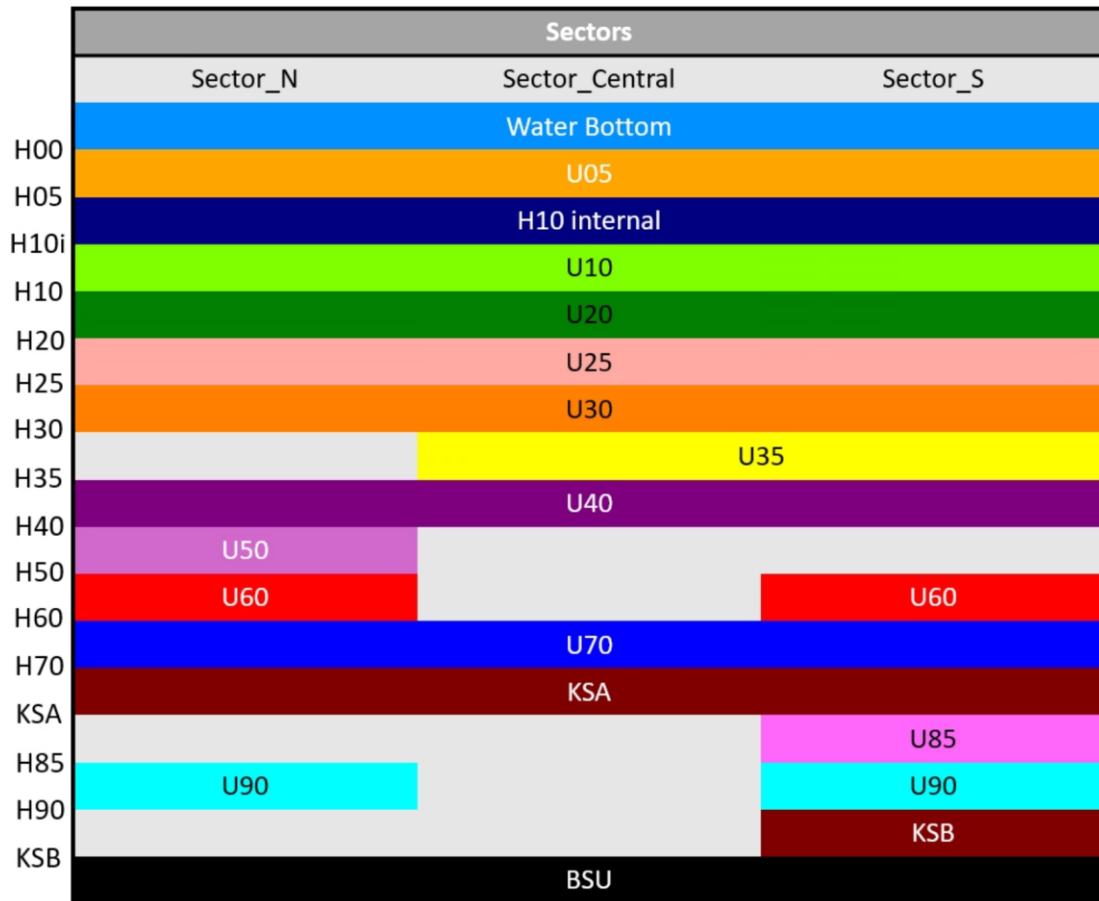


Figure 111 below shows a north-south profile with seismostratigraphic interpretation, displaying the mapped horizons and the interpreted seismic units. The horizons that bound the seismic units represent seismostratigraphic boundaries and mark the base of the deposits they define. As such, these boundaries have chronostratigraphic and kinetostratigraphic meaning, and should not be interpreted in lithostratigraphic terms. The bases and units are numbered sequentially based on their stratigraphic position, and have an alphanumeric naming convention (e.g., H10 corresponds to the base of seismic unit U10 (Figure 111)). The deepest and oldest seismic unit is referred to Base Seismic Unit (BSU). The top of the Base Seismic Unit is defined by a composite surface produced from the amalgamation of the deepest mapped horizons. The bottom of the Base Seismic Unit corresponds to the processing “last knee” that is an artificial, linear boundary near the terminus of the seismic record. The labelling scheme in Figure 111 was applied to all seismic examples in this report.

The fundamental stratigraphic controls on the site’s geology, as inferred from the seismic data, are eustacy, isostasy, autogenic processes, and glaciogenic deposition and deformation. The deeper deposits exhibit a strong glacial signal, and the upper deposits carry a eustatic-isostatic and autogenic signal. The separation of the two structural regimes is approximated by H70 and H35. Most of the seismic units beneath this boundary are characterized by glaciogenic deposition and deformation.

The deepest seismic units BSU, U90, and U85 have origins ascribed to non-glacial processes. However, their physical contact with the grounded shelf ice has rendered them tectonized and possibly otherwise modified by glacial processes. These strongly-deformed strata were individualised from the better-preserved sequences with horizon KS. Horizon KS represents a deformation front boundary and,

although part of the geological model, should not be interpreted with a chronostratigraphic meaning. Horizon KS defines the base of Unit UKS, which encompasses sediments belonging to seismic units BSU, U90, and U85 that were deformed to a degree in which their physical properties may be significantly different than their stratigraphically-equivalent strata.

The upper assemblage of seismic units, those occurring above UKS and H70, demonstrate characteristics of high frequency sedimentary sequences. These deposits are interpreted to represent cycles of deposition and erosion associated with sea-level fluctuations (transgressions and regressions). Superimposed on the eustatic-isostatic signal is the complex sedimentological arrangement produced by autogenic processes, including channel migration and avulsion, shallow basin, and coastal sediment dynamics.

Both systems of eustacy-isostacy and glacial dynamics taken in isolation are complex. The combination of the two, in conjunction with a strong overprinting of autogenic signal, has produced a highly fragmented and heterogeneous geologic structure. Furthermore, despite not being directly imaged in the UHRS record, some deeper structures indicate the occurrence of salt tectonics, which may have partially influenced the overall distribution of all the sedimentary sequences observed. Thus, the preservation of the geological sequences is limited due to the complex geological evolution of the area; variable sedimentary cycles; distinct erosional events; various stages of glaciers emplacement, erosion, and deformation. Attribution of seismic units to time specific regions of the quaternary sea-level curve was not possible with the available data.

In summary, despite the complex nature of the of site's stratal architecture, a reasonable approximation of the prevailing geologic conditions was captured in the 12 seismic units that were mapped. These units represent the structural elements of the Geological Ground Model and relate to two general different processes. The upper process is represented by the high frequency shelf sequences, and the lower represents the deposits directly impacted by shelf glaciation. The principal characteristics of the model's individual seismic units are detailed below.

All figures and seismic interpretation work that are included in this report are part of the Kingdom Suite project associated to this report. All seismic profiles are FULL-processed, migrated and in depth (metres). Numbers on the horizontal and vertical axis refer to distance in metres. The colour bar for the seismic display is identical for all profiles ('Black to White 200' in Kingdom Suite). The colour bar used to show the lateral extension for each basemap is the 3D Effects: warm colours (red) indicate shallower depths, and cool colours (blue) indicate greater depths (unless stated otherwise). For every seismic unit, three basemaps are presented: (1) spatial extent of the mapped horizon, (2) grid of the depth below seabed of the base of the unit, (3) grid of the thickness of the unit. Vertical exaggeration on seismic section figures is variable: horizontal and vertical scales were adjusted to best illustrate the features of interest

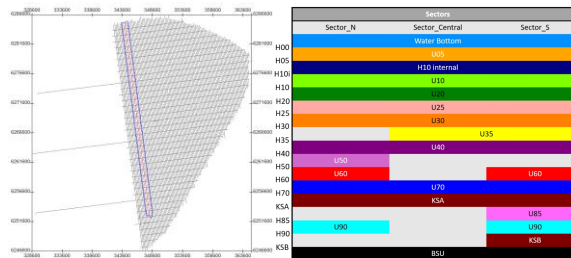
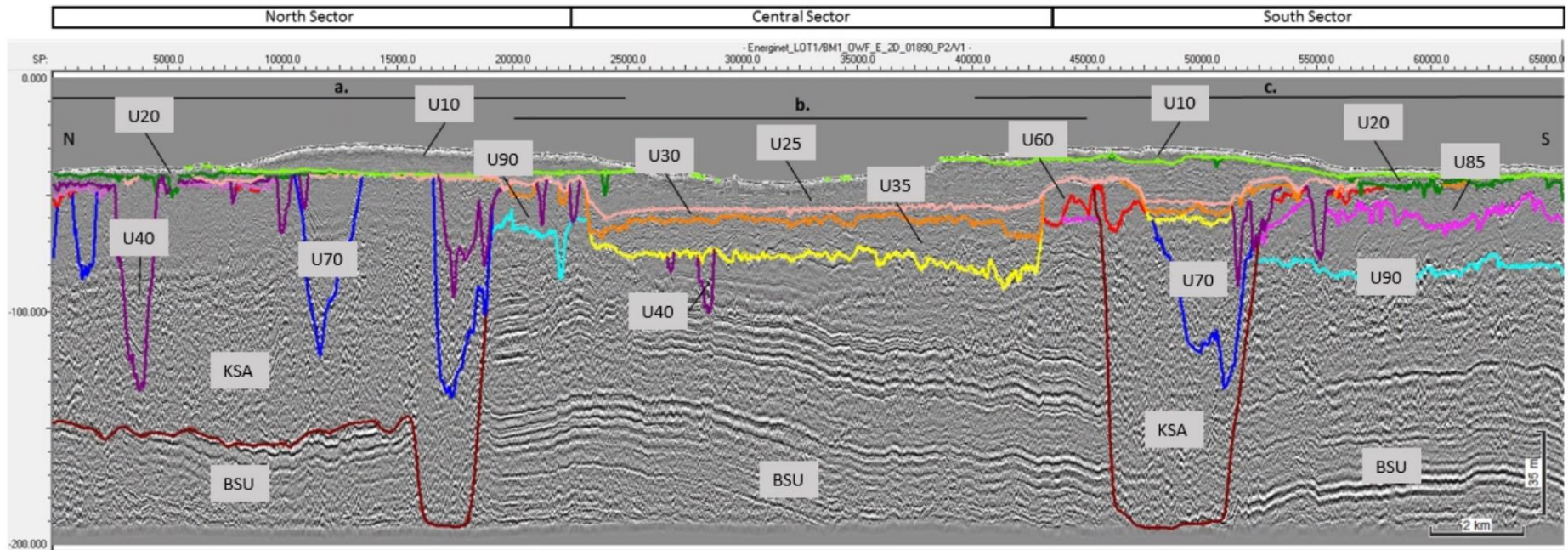


Figure 111 General sub-surface architecture of the survey area. The image shows interpreted seismic units and nomenclature used for the Geological Ground Model, and site sub-division into sectors North, Central, and South. Subsequent figures a, b, and c show in more detail the different sectors. Seismic Profile BM1_01890_P2.

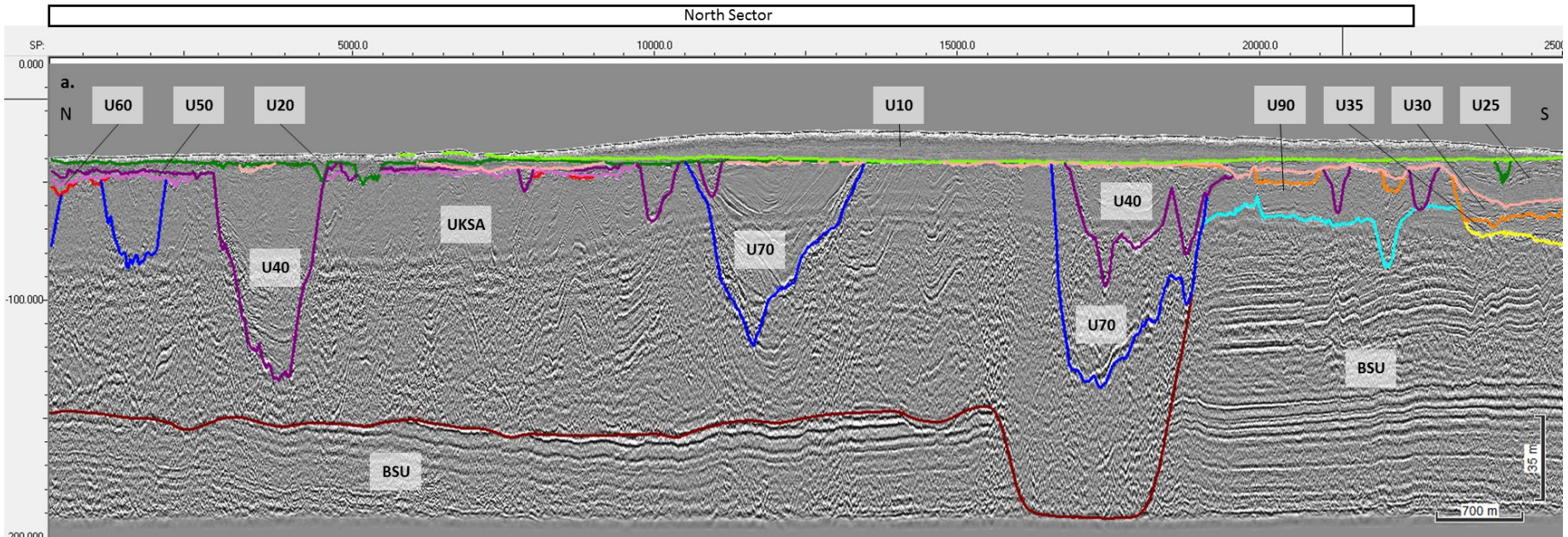
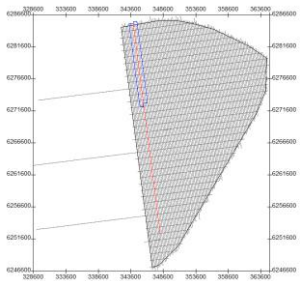


Figure 112 General sub-surface architecture of the North sector.
The image shows interpreted seismic units and nomenclature used. Seismic Profile BM1_01890_P2

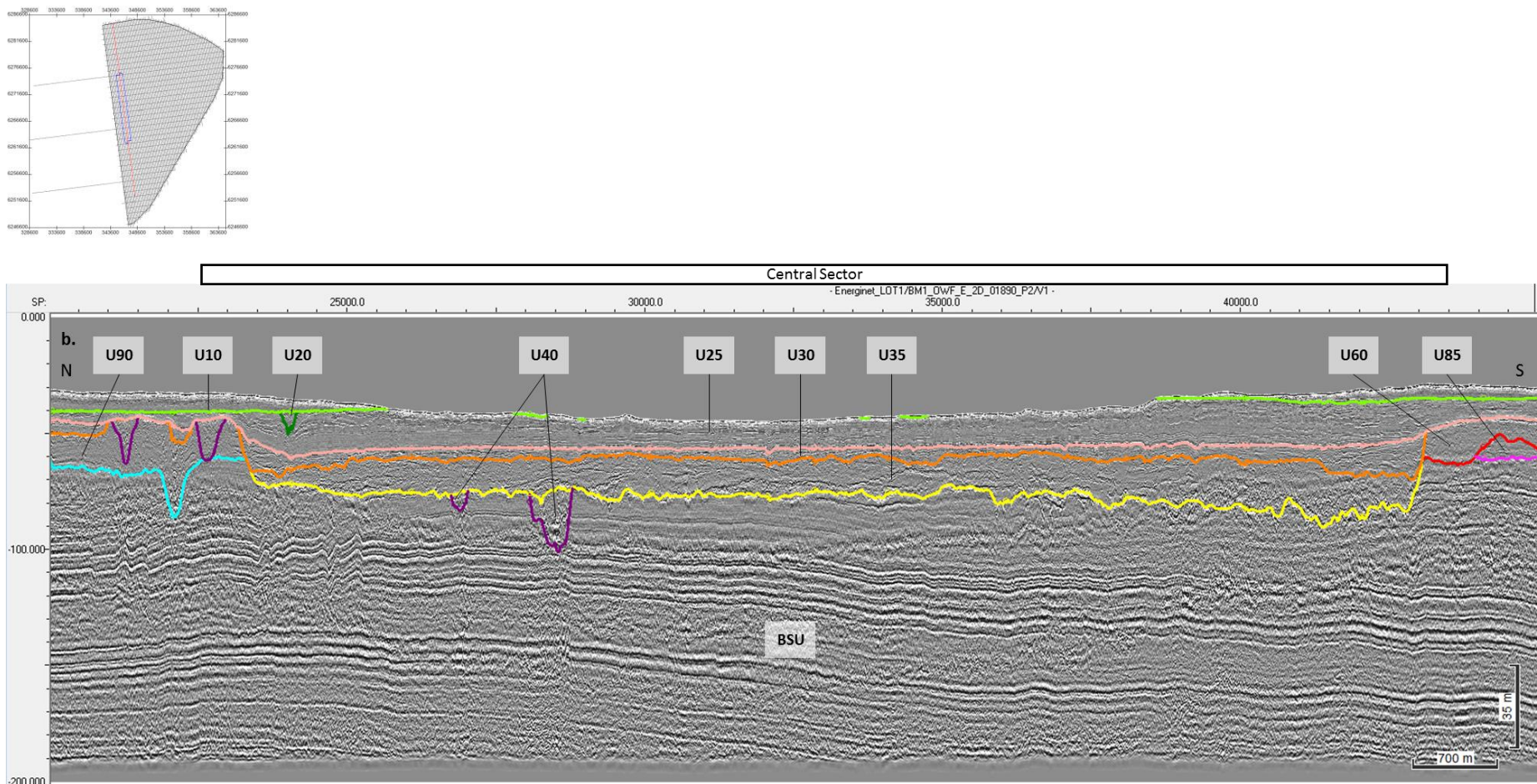


Figure 113 General sub-surface architecture of the Central sector.
The image shows interpreted seismic units and nomenclature used. Seismic Profile BM1_01890_P2.

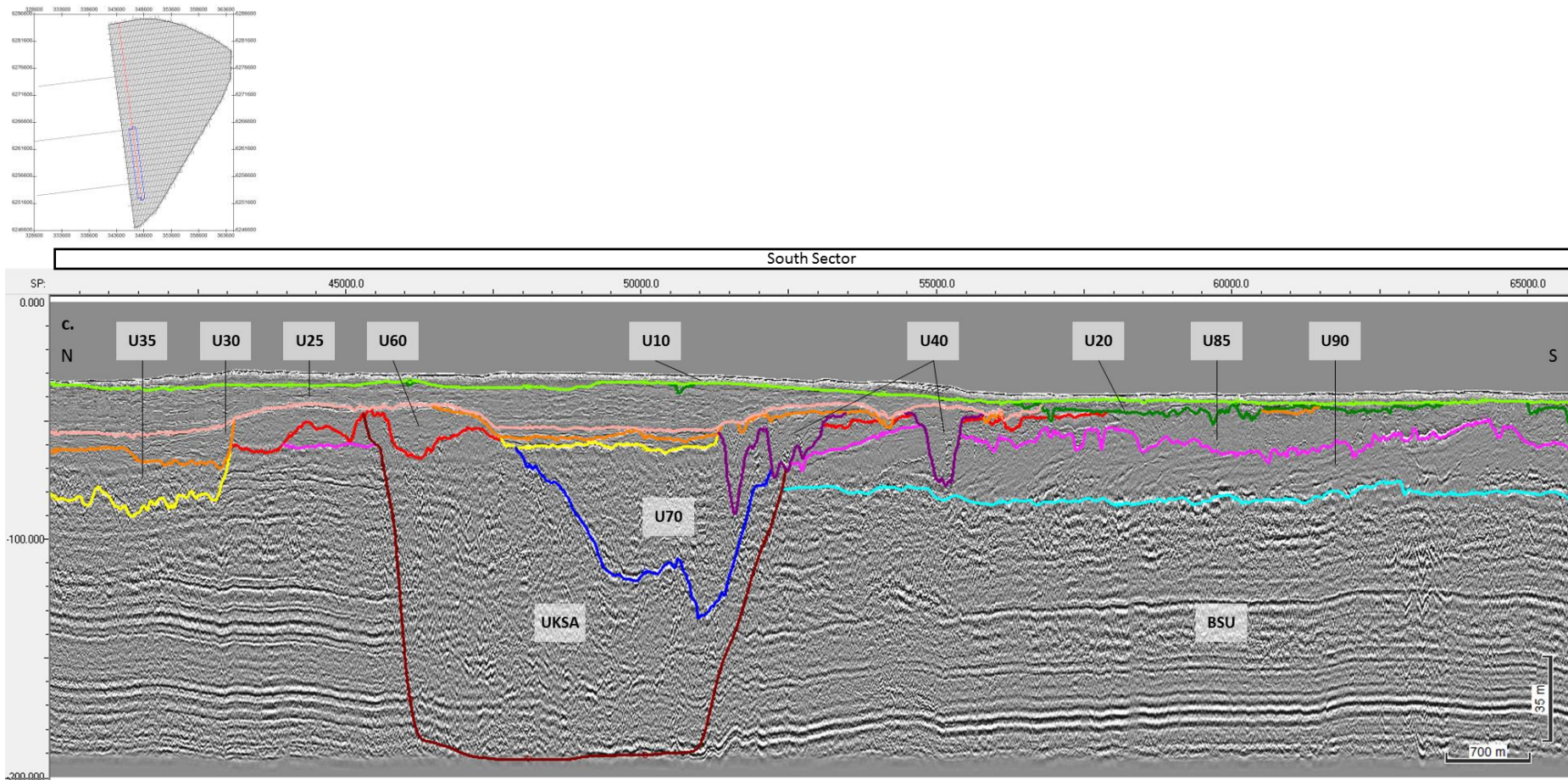


Figure 114 General sub-surface architecture of the South sector
The image shows interpreted seismic units and nomenclature used. Seismic Profile BM4_01890_P2.

8.6.1 | SEISMIC UNIT U05

Seismic unit U05 is mostly presented in the northern half and central region of the survey area, where unit U10 is relatively thick. The base of unit U05 is defined by horizon H05. Seismic unit U05 comprises of recent marine sediments and are likely mobile in nature. The spatial distribution, vertically referenced to MSL, depth below seabed and thickness, are presented in Figure 115, Figure 116 & Figure 117 respectively.

Horizon H05 ranges in depths between 26.4 m and 43.7 m below MSL (Figure 115) and between 0.0 m and 3.9 m depth below seabed (Figure 116). It follows a flat, low to medium amplitude reflector. Unit U05 only exists on top of U10, especially where thicker, such as mounded structures and sand waves, and is likely made up of silty-sands. U05 is interpreted to be of Holocene in age.

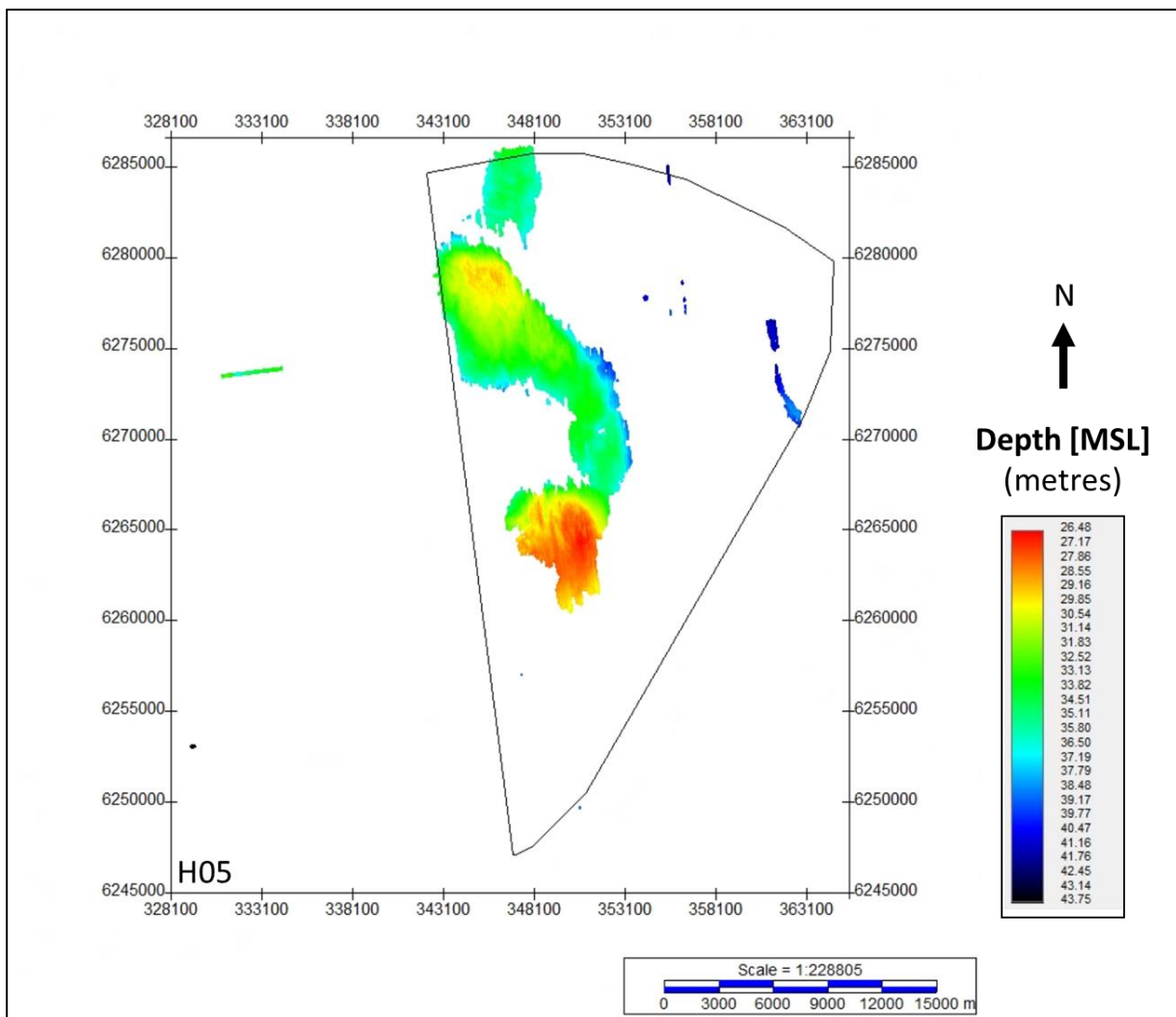


Figure 115 Map showing the lateral extent of U05.
Units in metres below MSL.

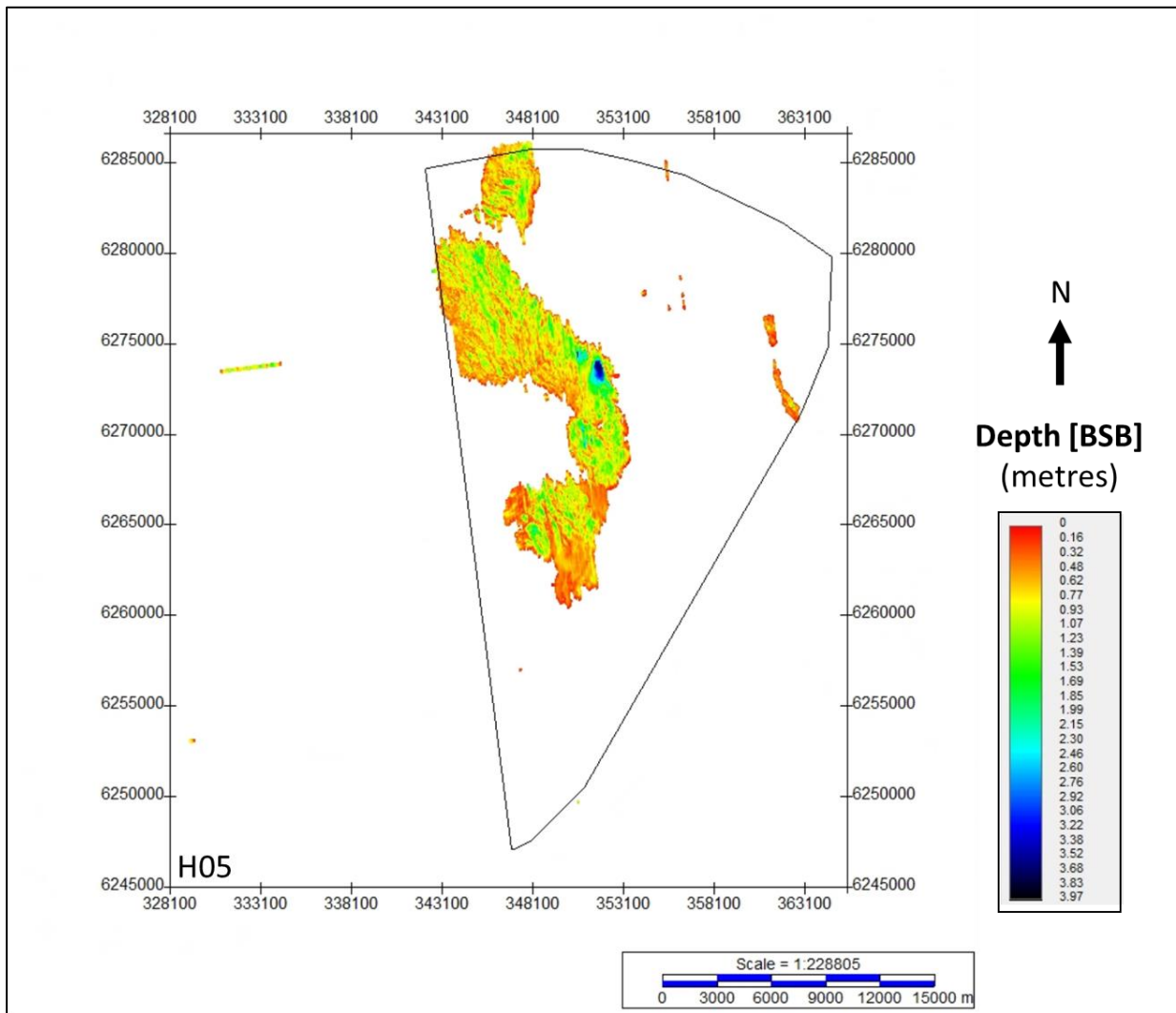


Figure 116 Depth below seabed of H05.
Units in metres below seabed.

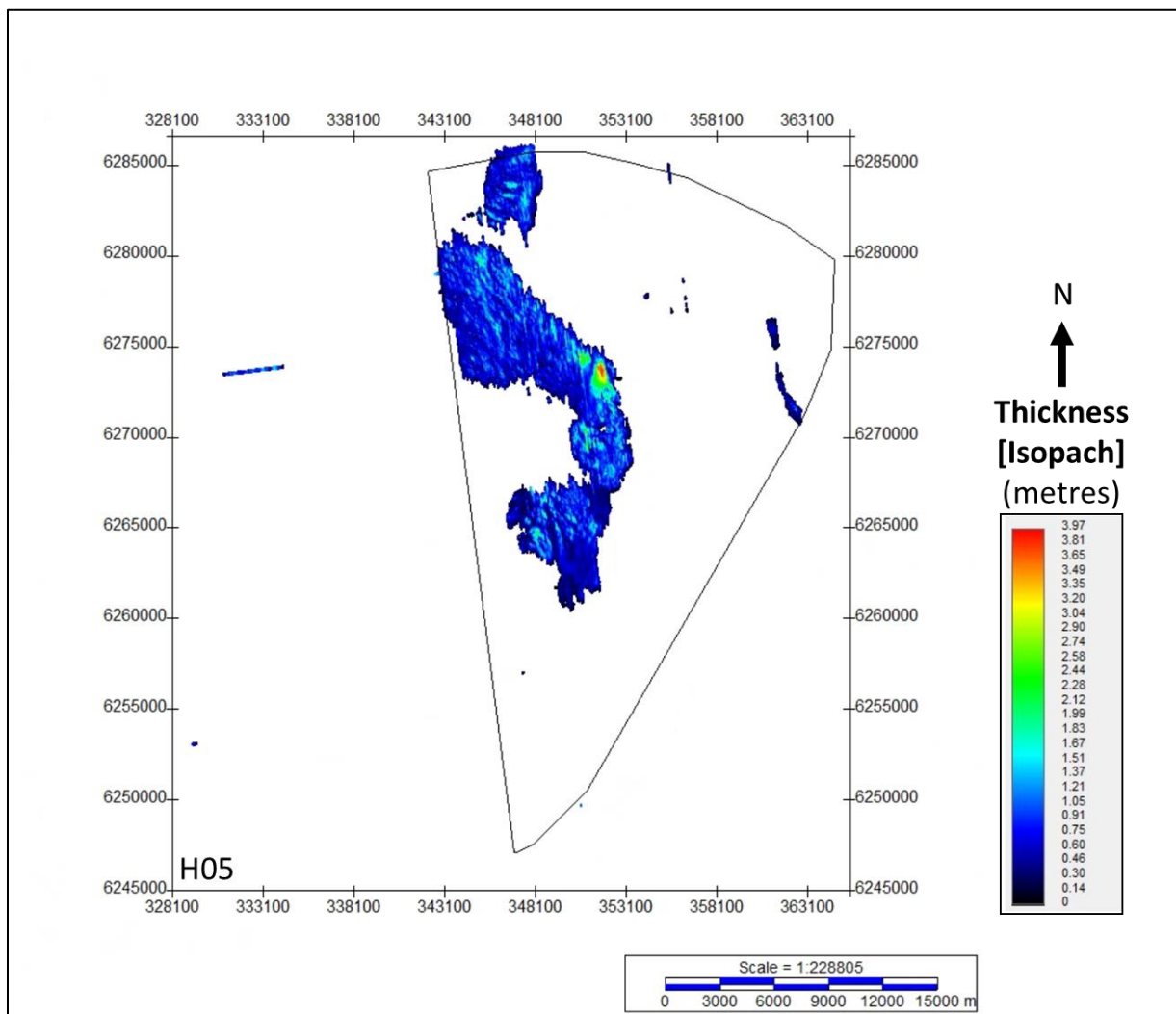


Figure 117 Thickness of unit U05.
 Units in metres.

8.6.2 | SEISMIC UNIT U10

Seismic unit U10 is a major element of the ground model, and extends spatially across the three sectors of the site. The base of Seismic Unit U10 is defined by horizon H10 and is present discontinuously within the survey area. Seismic unit U10 comprises the recent marine sediments that make up the seabed bedforms where present. The spatial distribution, vertical reference to MSL and the seabed, and thickness of the unit are presented in Figure 118, Figure 120, and Figure 122.

Horizon H10 ranges in depth between 31.7 m and 51.8 m below MSL (Figure 118), and between 0.0 m and 18.1 m depth below the seabed (Figure 120). It follows a flat, planar, and even reflector of medium to high amplitude (Figure 123); or it is observed as a micro-undulating (hyperbolic) reflector with stippled high amplitudes (Figure 124). On localised facies shift, H10 follows a faint low amplitude reflector, and rarely displays reversed polarity. A localised internal reflector was interpreted within H10 defined as H10i (internal). H10i (Figure 121) is a discontinuous reflector which usually highlights the boundary between transparent and non-transparent facies within U10.

Seismic unit U10 has a tabular external morphology in regions where it is thinner (from 0 m to 4 m thick); or it forms wide mounds of thicker sediment accumulation (up to 18.1 m thick).

The seismic facies of U10 have a generally low to medium amplitude response. Where thicker, within the mounded structures, its internal facies varies both vertically and laterally: at the base it may be homogeneously transparent or with small mound-channel patterns to chaotic; overlaid by oblique downlap reflectors and small lenses (Figure 125). Above these, sits a thinner deposit of sub-horizontal and parallel reflectors. The latter is also observed in areas where U10 is thinner. Stippled high amplitude facies are locally observed at the base. Common discontinuous high amplitude reflectors and negative high impedance contrasts occur across the unit's extent.

Horizon H10 is interpreted as a transgressive ravinement surface. The deposits of U10 are interpreted to be related to a marine transgressive setting (possibly high stand). Seismic unit U10 is likely made up of silty-sands and a gravelly sand lag that rest above the H10 ravinement surface. U10 is interpreted to be of Holocene in age. Stippled high amplitude facies may indicate coarser-grained material, such as gravel.

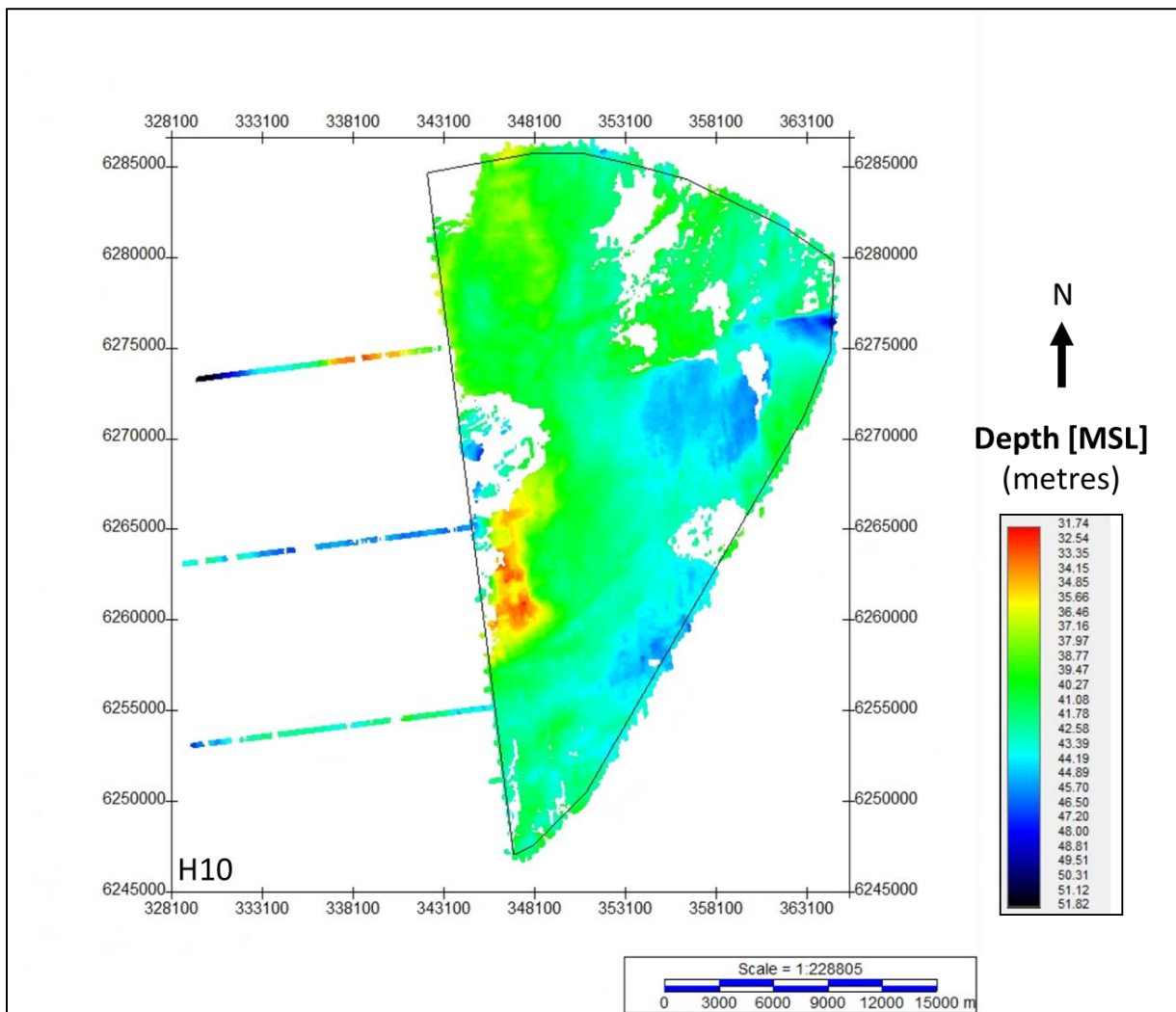


Figure 118 Map showing the lateral extent of U10 from UHRS data.
 Units in metres below MSL.

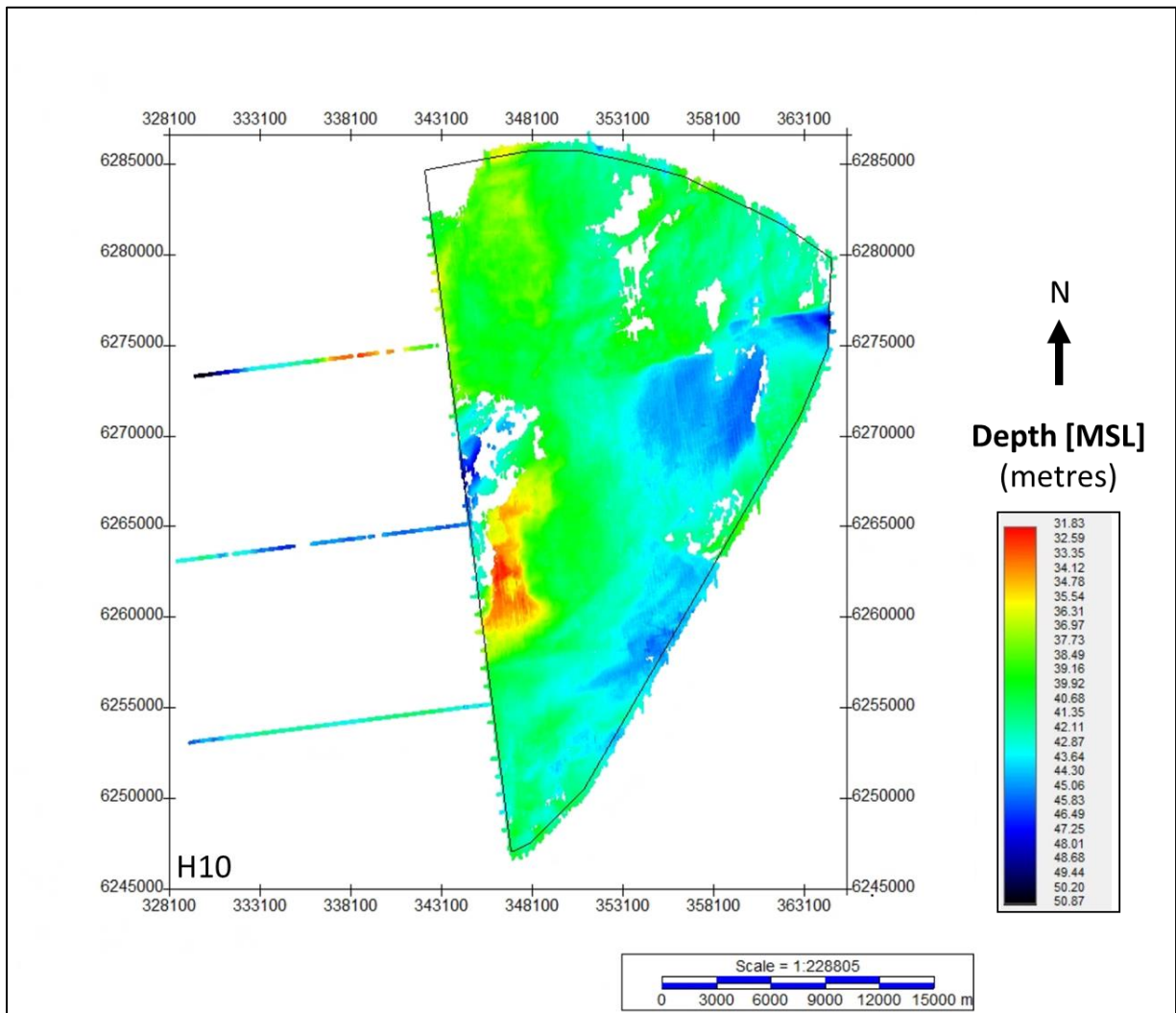


Figure 119 Map showing the lateral extent of U10 from SBP data.
 Units in metres below MSL.

The lateral extents as interpreted from the SBP data shows a wider distribution of U10 at the surface. This is due to the higher resolution of the SBP data, allowing for more accurate interpretation where H10 is near the seabed.

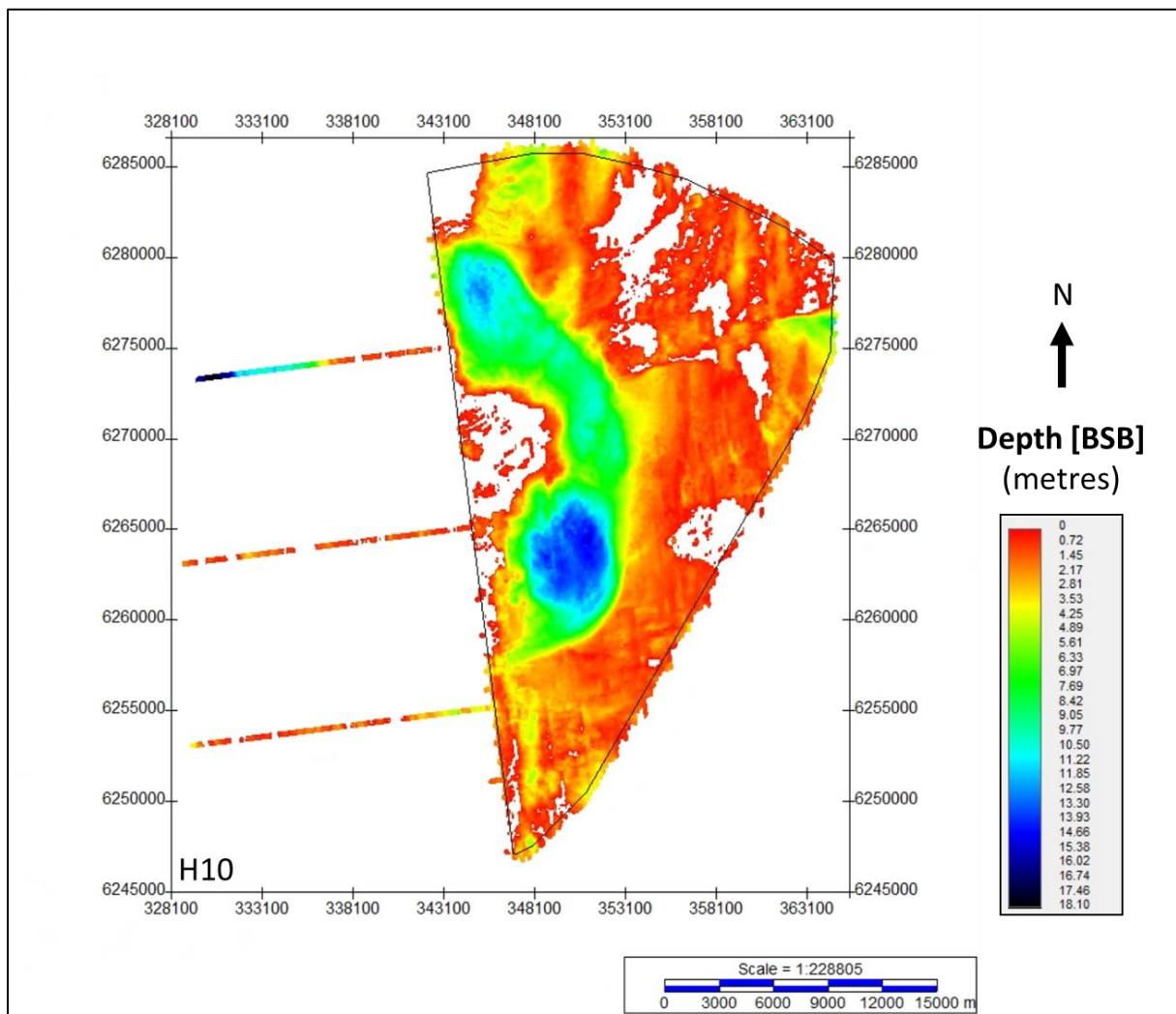


Figure 120 Depth below seabed of H10.
Units in metres below seabed.

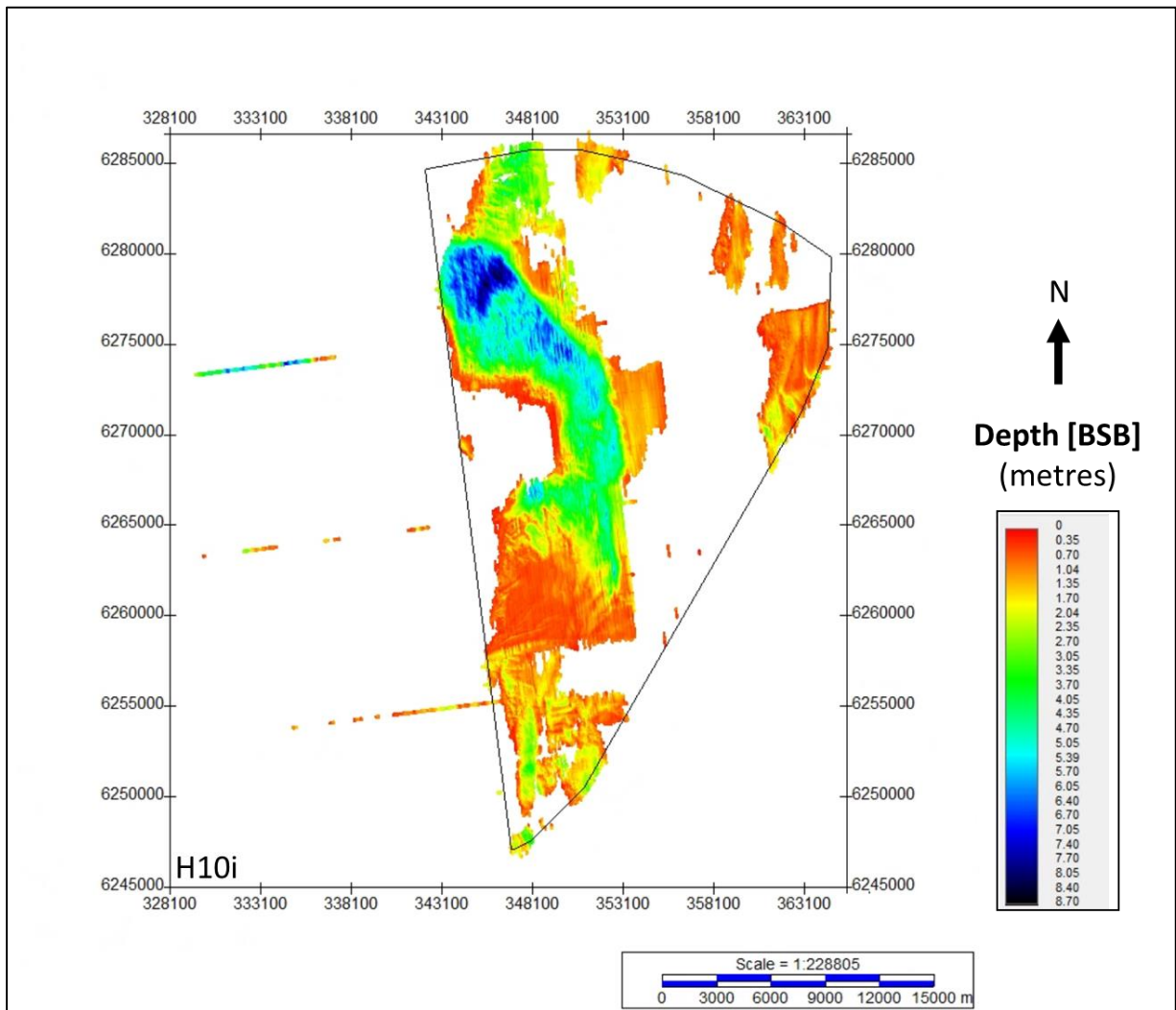


Figure 121 Depth below seabed of H10i.
Units in metres below seabed.

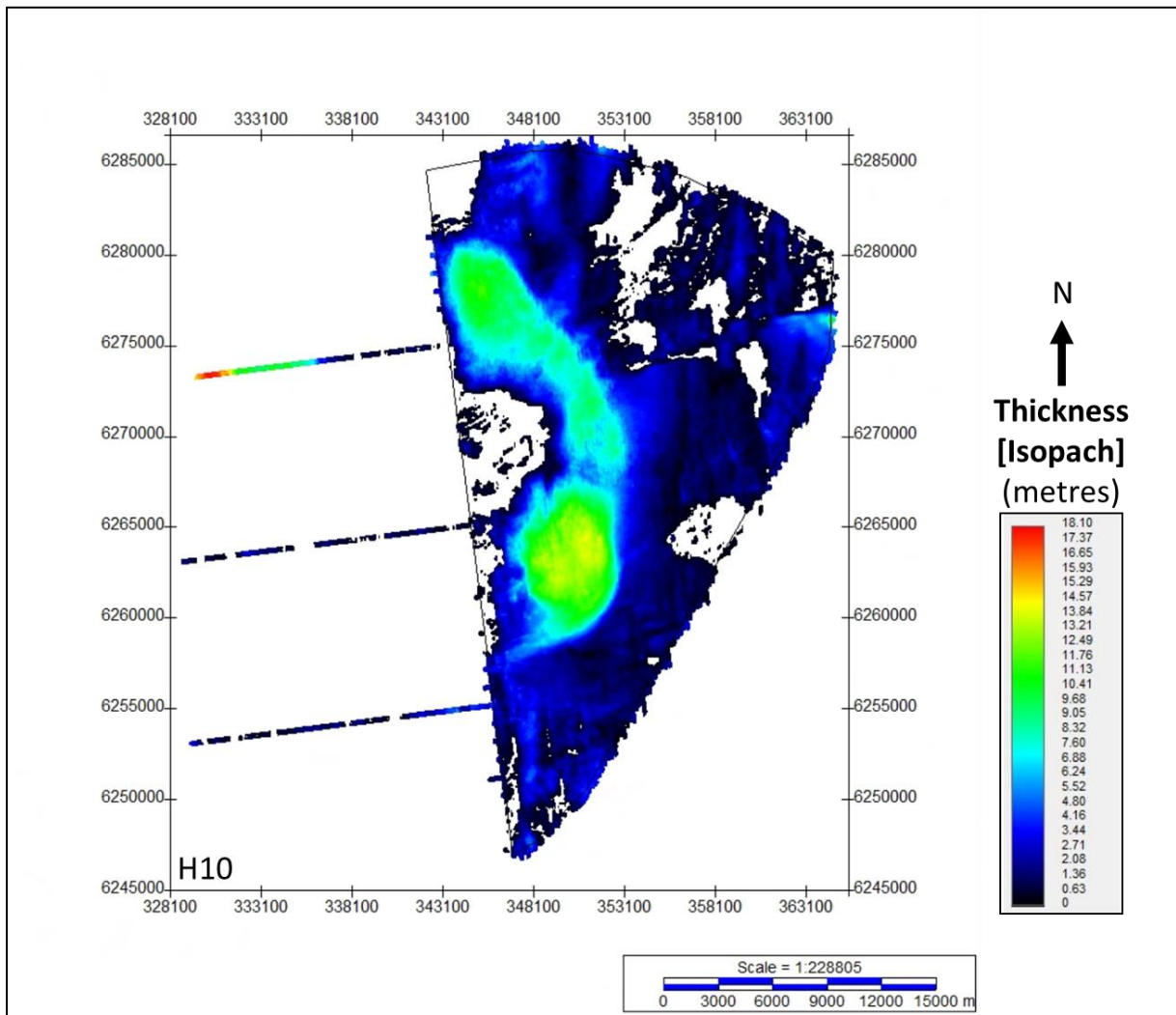


Figure 122 Thickness of unit U10.
Units in metres.

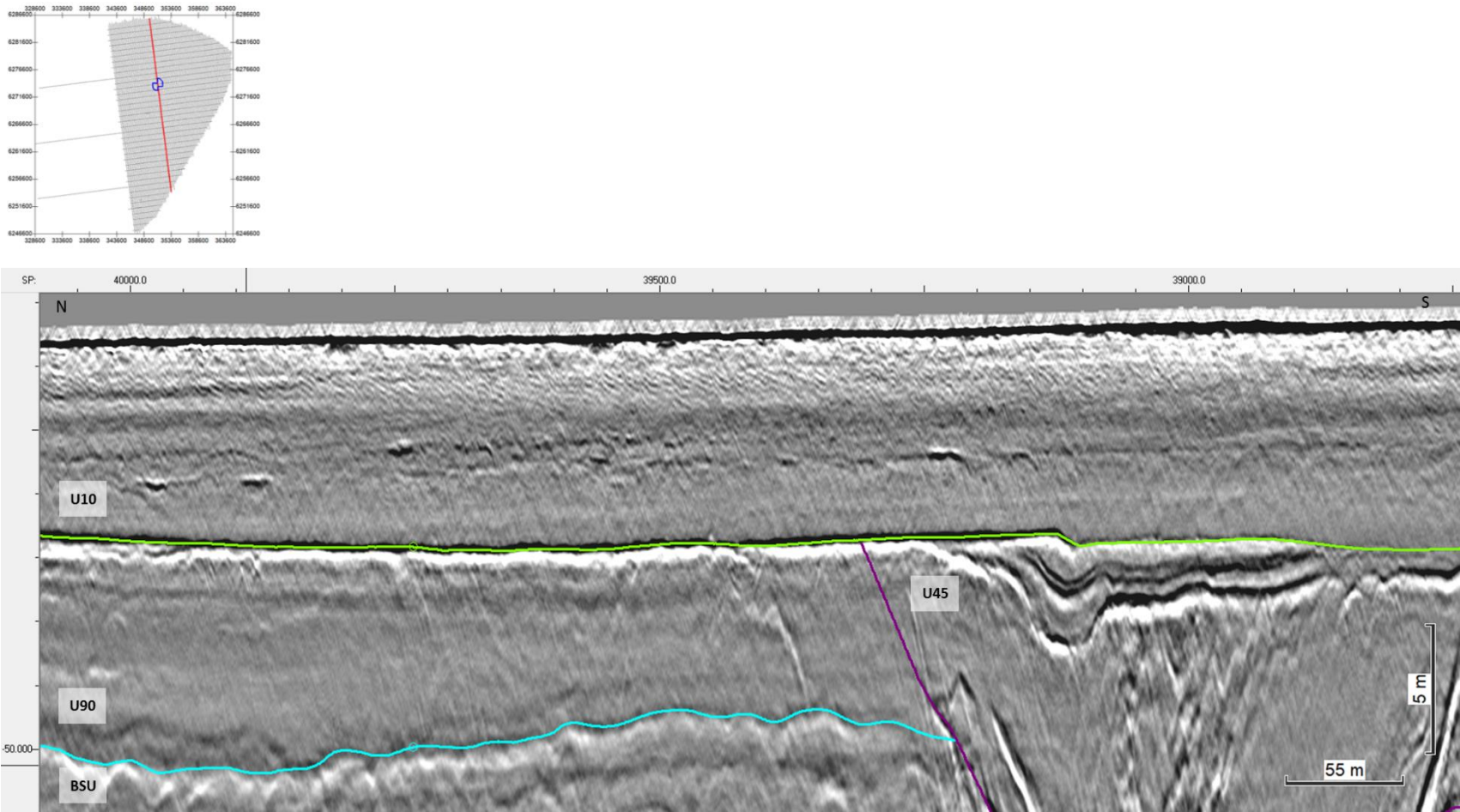


Figure 123 General facies of Seismic Unit U10, and the character of horizon H10 (light green).
Seismic profile BM3_OWF_E_2D_07560.

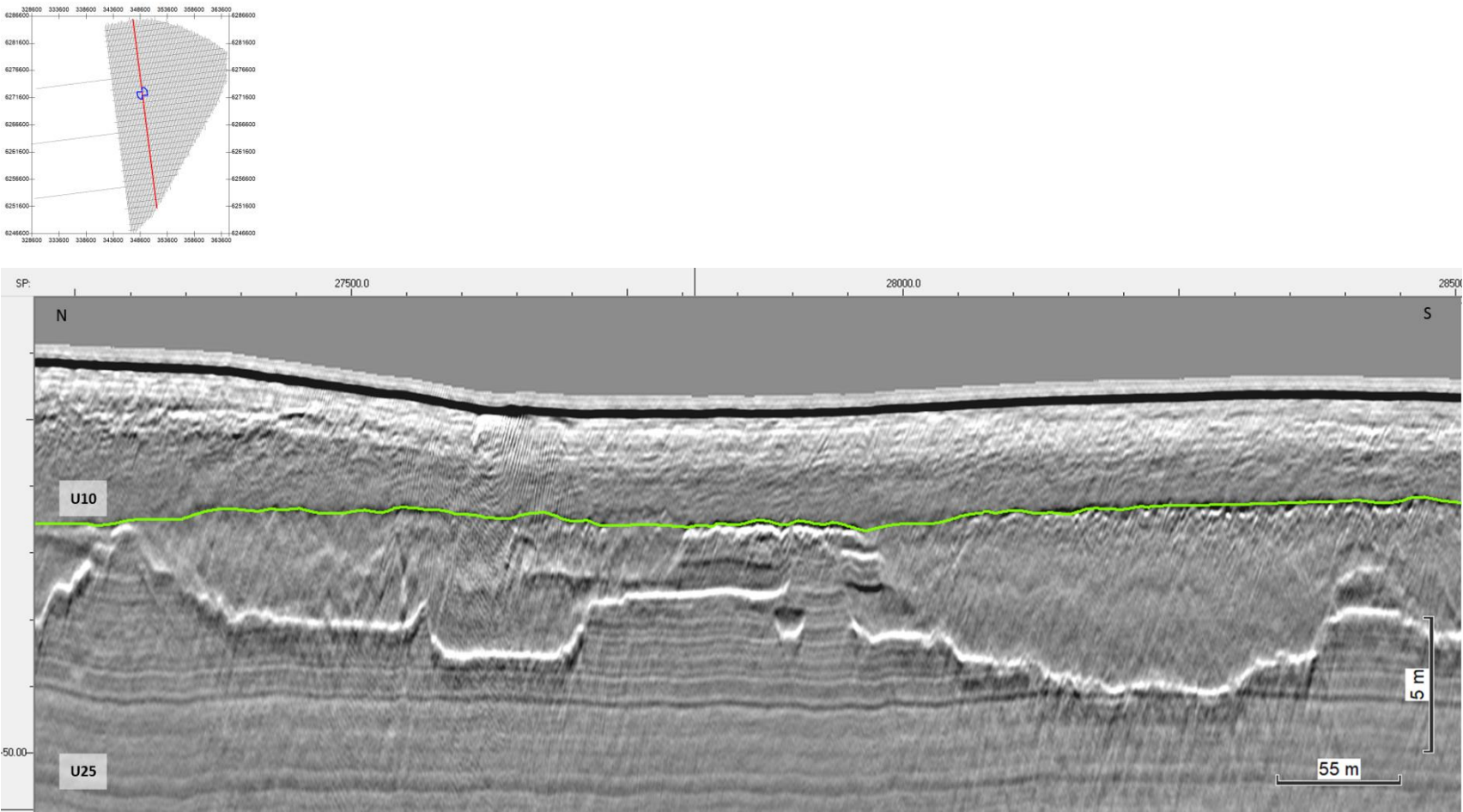


Figure 124 Area in which horizon H10 has a stippled character (light green).
Seismic profile BM2_OWF_E_2D_05250

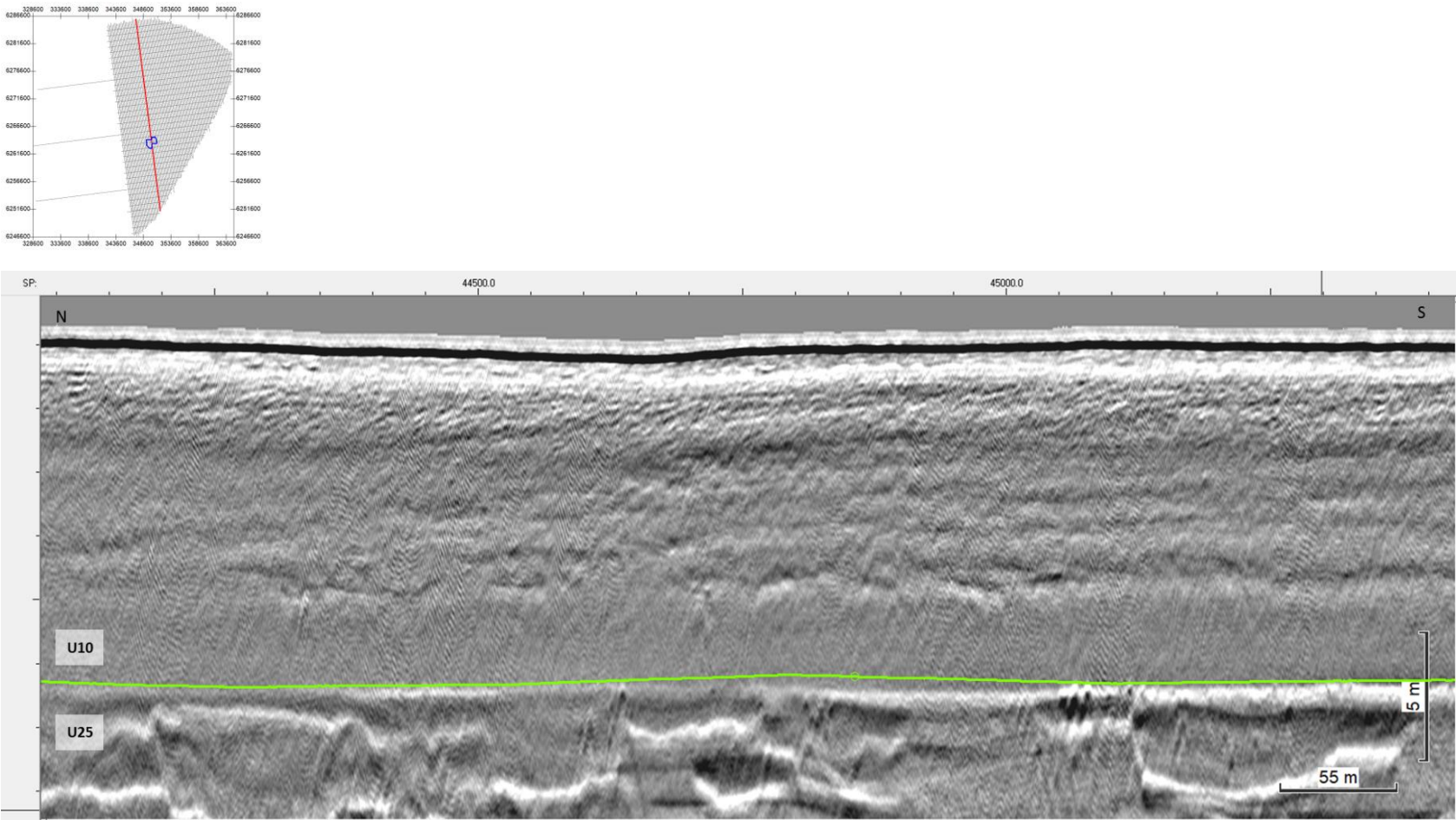


Figure 125 Internal facies of Seismic Unit U10, and horizon H10 (light green).
Seismic profile BM2_OWF_E_2D_05250.

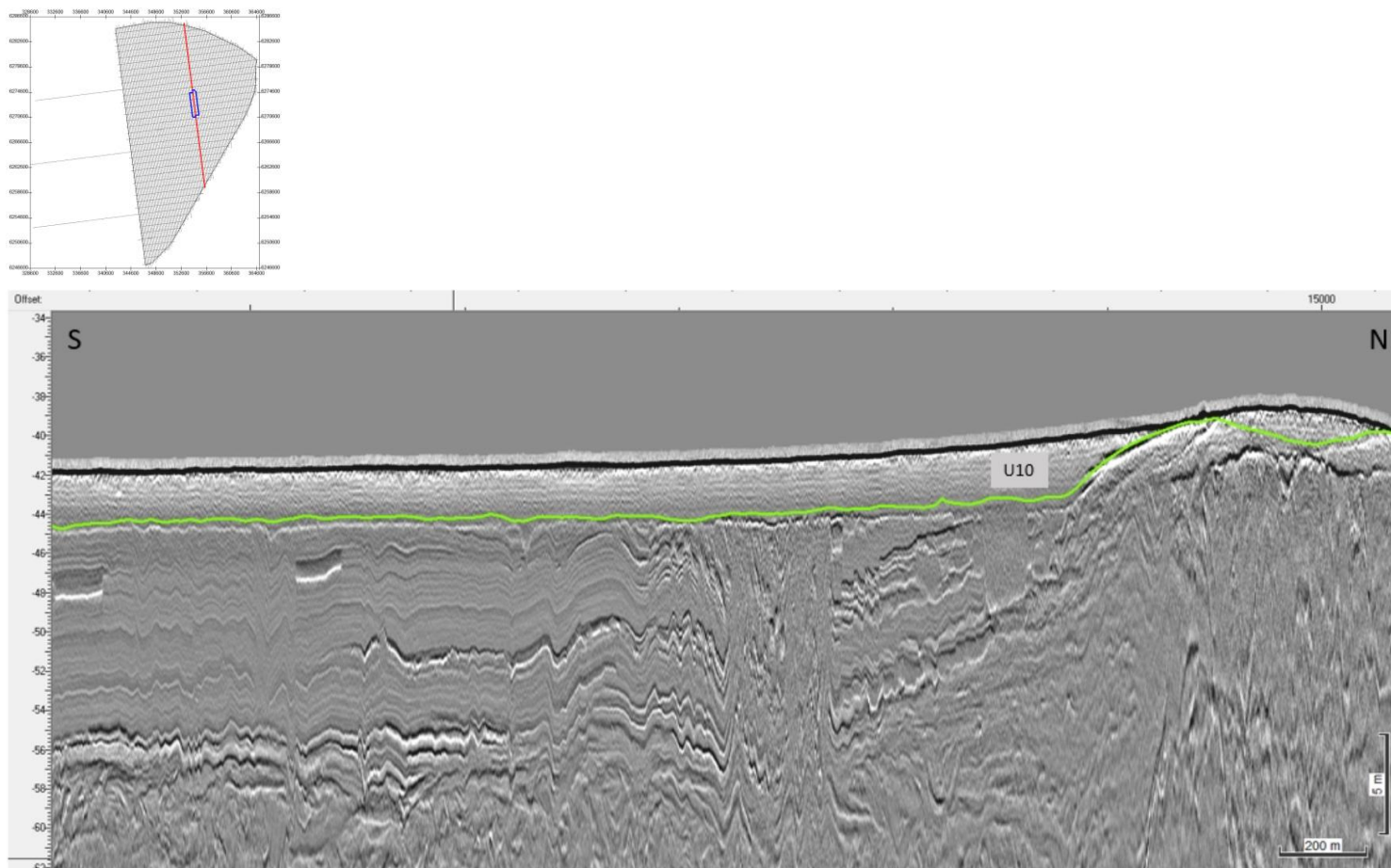


Figure 126 Grid overlay from interpretation of H10 as interpreted on the Innomar SBP.
Seismic profile BM4_OWF_E_2D_10920

8.6.3 | SEISMIC UNIT U20

The base of Seismic Unit U20 is delineated by H20 and is found discontinuously across the site, although extending spatially across the three sectors of the site. The spatial distribution, vertical reference to MSL and the seabed, and thickness of the unit are presented in Figure 127, Figure 128, and Figure 129.

Horizon H20 ranges in depth between 32.9 m and 92.4 m below MSL (Figure 127), and between 0.0 m and 48.8 m depth below the seabed (Figure 128). It delineates the base of channelised incisions (Figure 130) and wide shallow basins (Figure 131), following a reflector of varying amplitude (from medium-high to low-medium), and often marking a significant facies shift. Below the basins, it is usually flat to slightly undulating. Where present in channel incisions, H20 marks an erosion surface, with reliefs of 3 to 15 m.

Seismic unit U20 has tabular morphology in basin areas, where the unit thickness range between 0 m to 10 m. V-shaped channels are incised up to 70-75 m depth MSL (30-35 m BSB), corresponding to the areas where U20 is thicker, especially towards the south (maximum 46.8 m).

Seismic unit U20 comprises two distinct facies:

- 1) **Channels:** Micro to meso-scale channels with chaotic to parallel infill, commonly mounded-chaotic at the base (Figure 130);
- 2) **Wide shallow basins:** Low amplitude to transparent homogeneous, with faint micro-parallel reflectors and common negative high amplitude anomalies at the base and internally (Figure 132).

Where these two facies are associated, the channel facies association occurs at the base of U20, with the wide basin facies above it (Figure 132). Separating these facies is usually a strong reflector of negative high amplitude.

Horizon H20 is interpreted as a truncating erosional surface, and the general spatial arrangement of U20 is indicative of a drainage network. U20 is interpreted to have been deposited in restricted marine-tidal setting, partially associated to a subaerial fluvial system.

Within the wide basins, the deposits of U20 are expected to comprise fine sediments, from clays-silts-fine sands; whereas channel infills are likely to contain slightly coarser sediments such as fine sands-sands (even gravelly lags/layers?). The large amount of observed negative high amplitude reflectors may be related to the occurrence of organic matter within this unit.

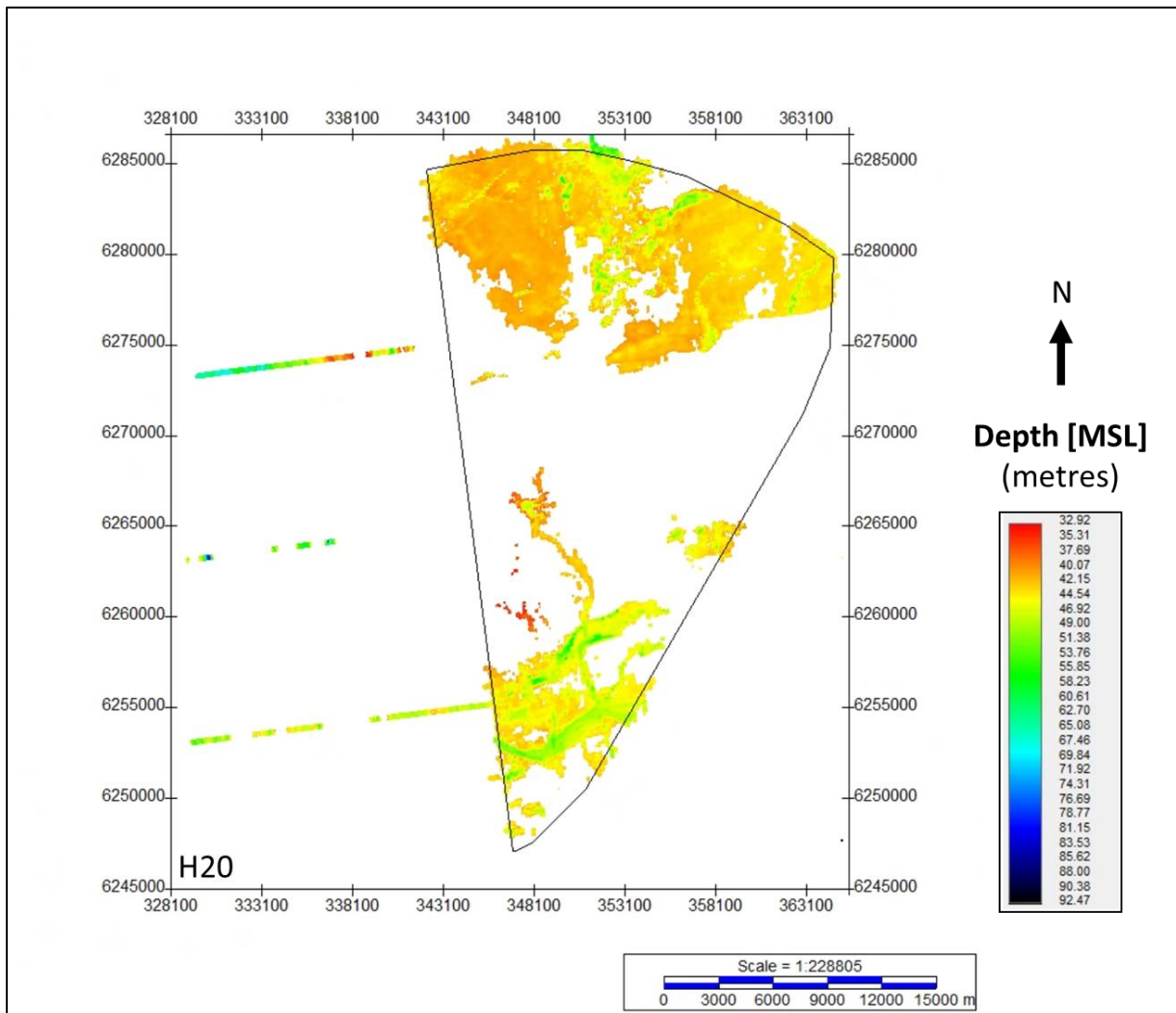


Figure 127 Map showing the lateral extent of H2O.
Depth below MSL. Units in metres.

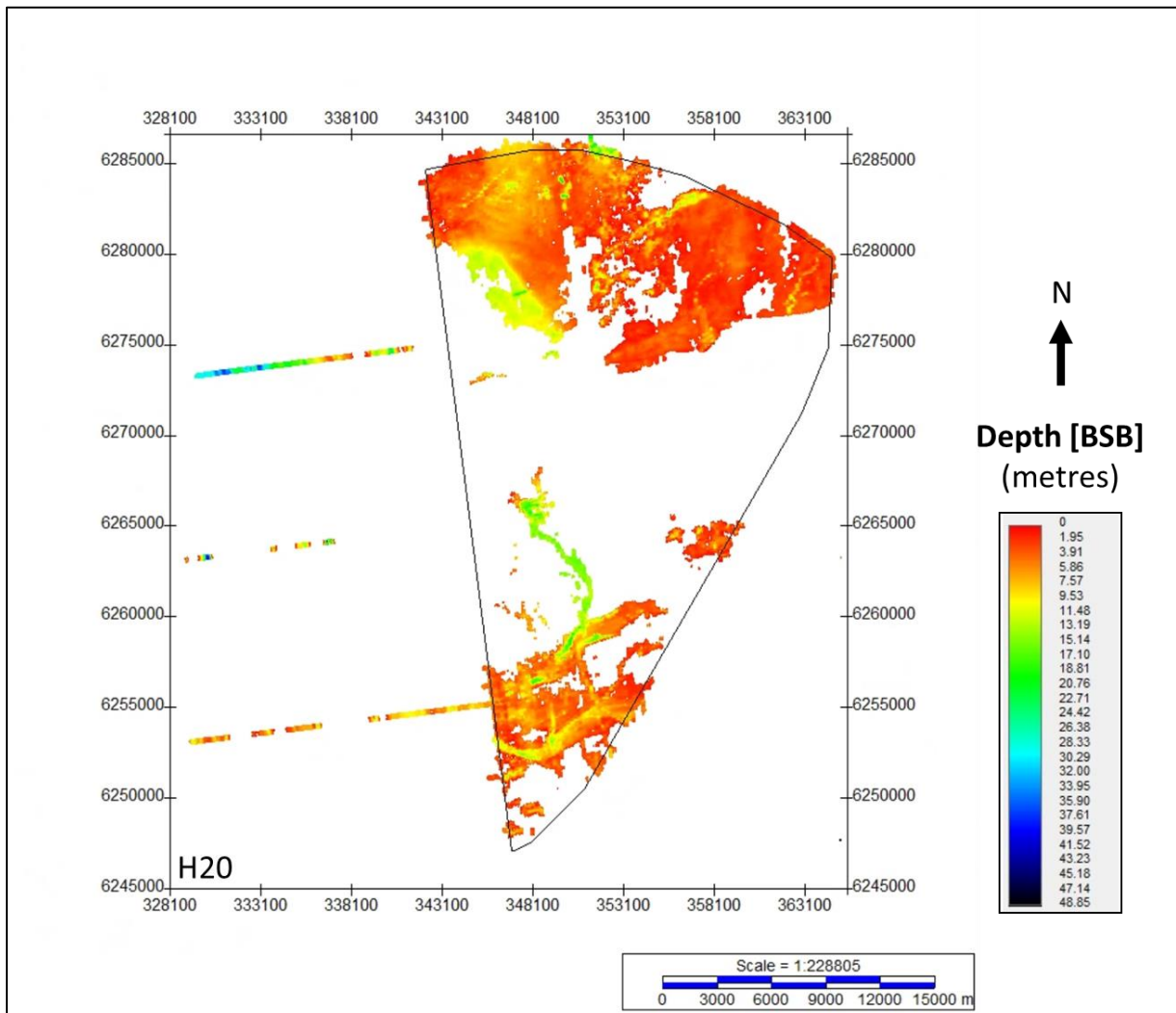


Figure 128 Depth below seabed of H20.
Units in metres below seabed.

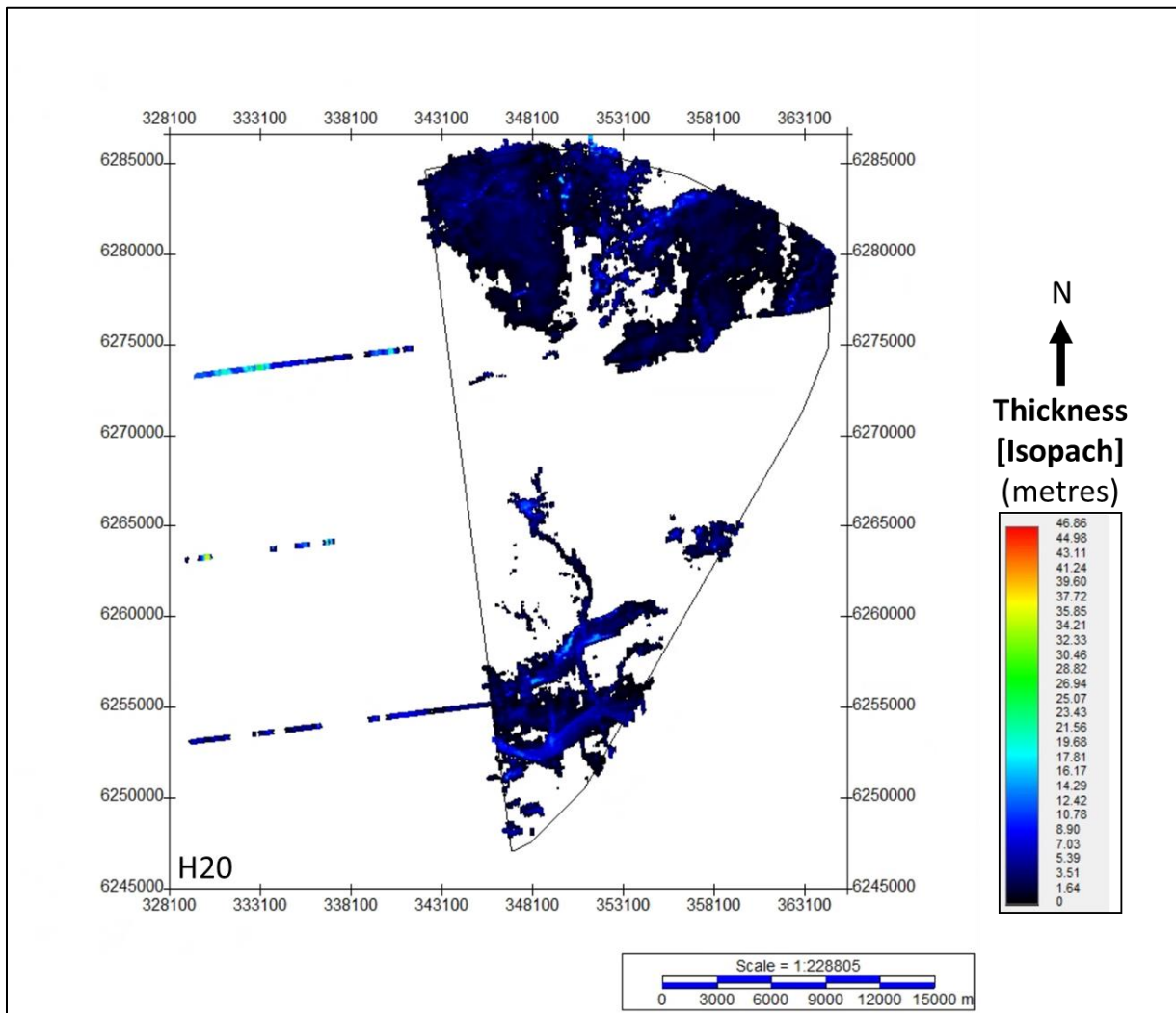


Figure 129 Thickness of unit U20.
Units in metres.

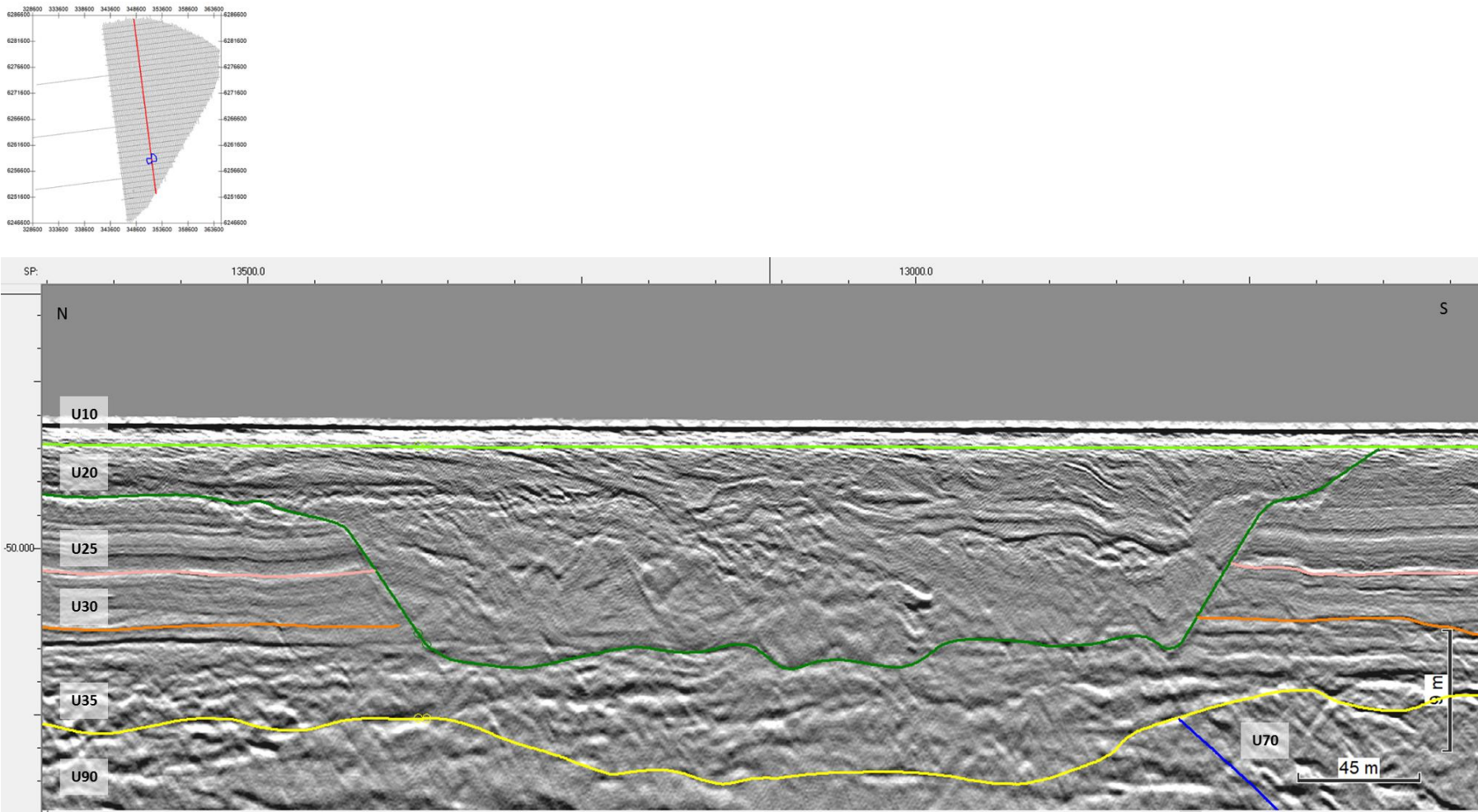


Figure 130 Infilled channel of Seismic Unit U20, and the character of horizon H20 (dark green).
Seismic profile BM3_OWF_E_2D

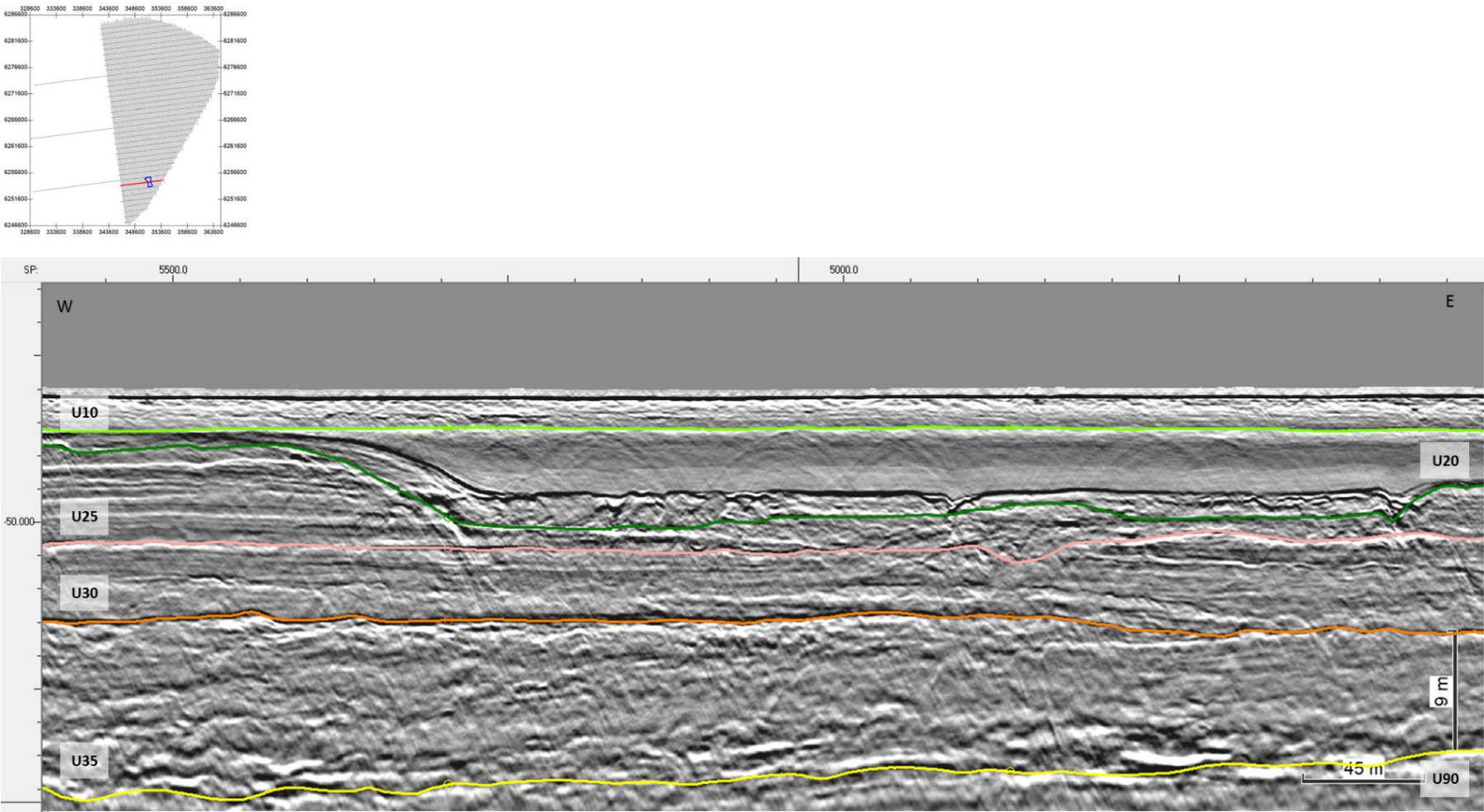


Figure 131 Infill facies of a wide shallow basin of Seismic Unit U20, and character of horizon H20. H20 is shown in light green. Seismic profile BX4_OWF_E_XL_31000

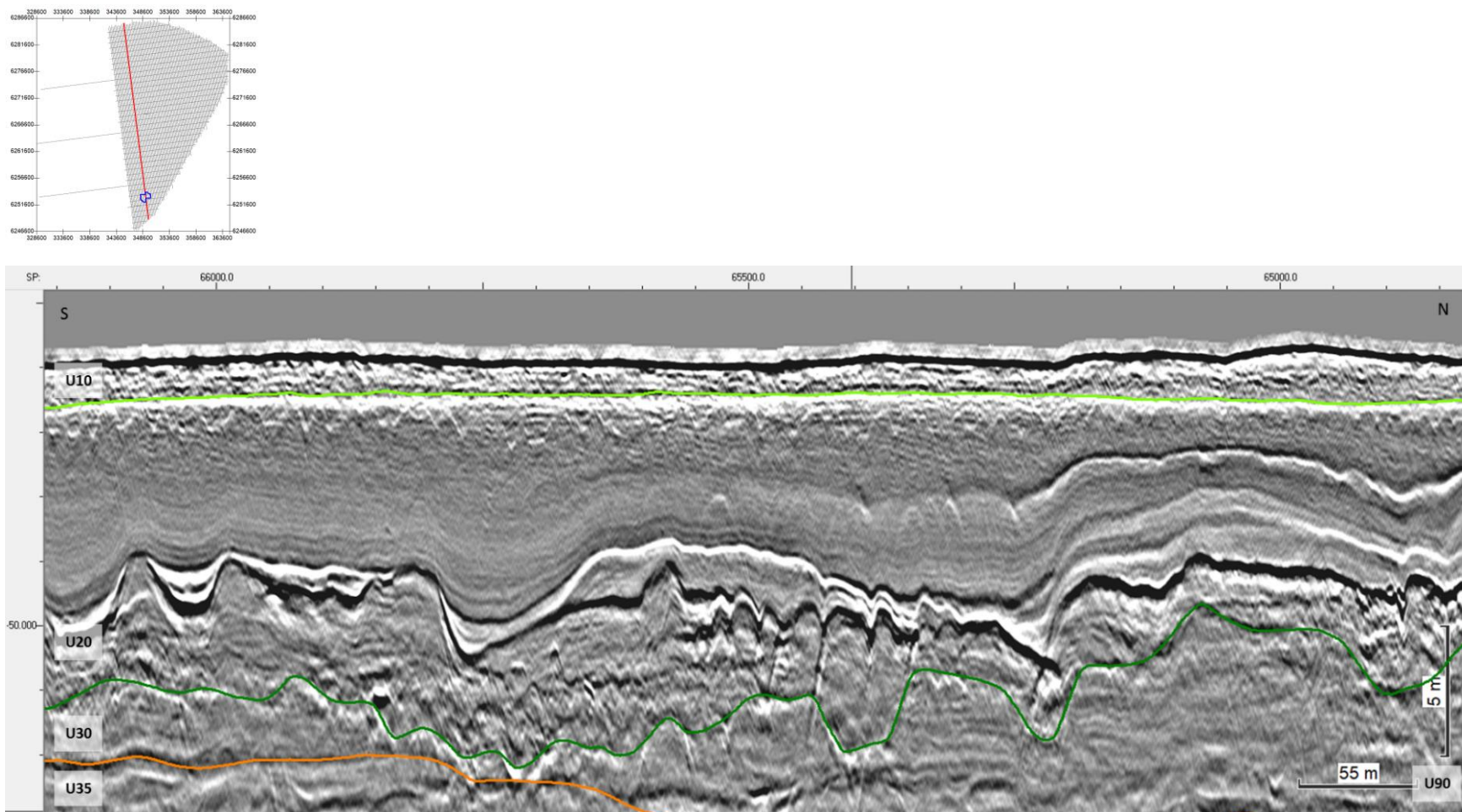


Figure 132 Two distinct facies of Seismic Unit U20.
The two distinct facies are: channel facies at the base; basin facies at the top.
Seismic profile BM2_OWF_E_2D_02940.

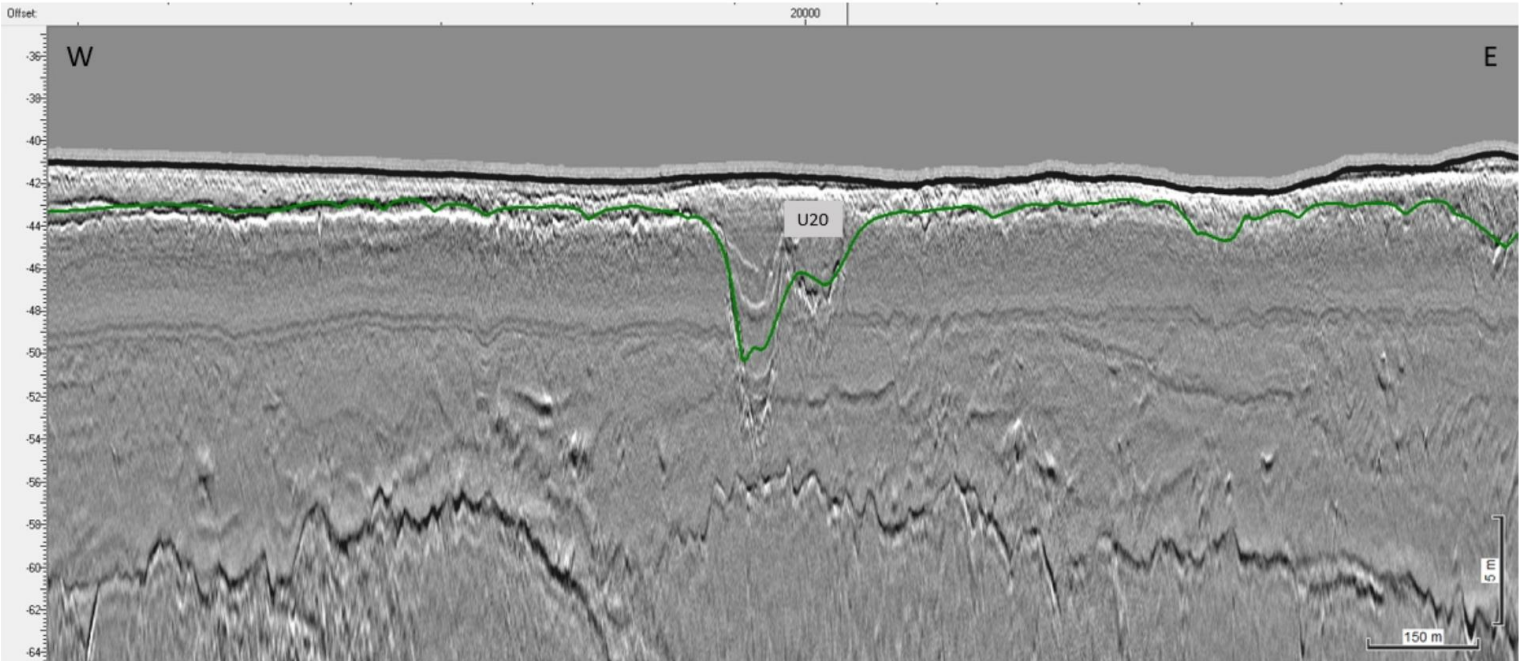
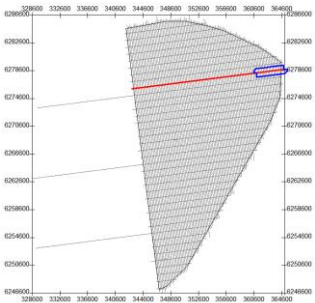


Figure 133 Grid overlay from interpretation of H20 as interpreted on the Innomar SBP.
Seismic profile BM2_OWF_E_XL_09000

8.6.4 | SEISMIC UNIT U25

Seismic unit U25 is a major component of the ground model, and extends spatially across the three sectors of the site, although being more prominent in the central sector. The spatial distribution, vertical reference to MSL and the seabed, and thickness of the unit are presented in Figure 134, Figure 135, and Figure 136.

The base of U25 is defined by horizon H25, between 38.8 m and 73.1 m depth below MSL (Figure 134), and between 0.0 m and 30.6 m depth below the seabed (Figure 135). H25 is a continuous and slightly undulating reflector of variable amplitude (low-high). Locally this horizon defines a vertical facies shift from U30 below and the deposits of U25, commonly marking variations of acoustic impedance.

Seismic unit U25 has different expressions across the survey sectors. In areas of the north and south sectors, where it is thinner (1-5 m thick), U25 has a tabular morphology. In the central sector and parts of the south sector, U25 infills wide basins, reaching its maximum thickness of up to 25.7 m (Figure 136). It is often truncated by H20.

In general, the seismic facies of U25 are characterized by low amplitude micro-parallel reflectors, gently undulating in places (Figure 137). In the north sector, where the unit is thinner, its facies is usually transparent and homogeneous at the base (Figure 138), and above may exhibit faint small channels and mounds.

The central sector delineates the margins of a wide basin, with 9-10 km width (N-S direction) and at least 21.5 km long (E-W direction) inside the survey area (Figure 134). It is expected that this elongated basin extends further towards the West, as it can be mapped along the profiles BX2_OWF_2D_Baseline_1 and BX3_OWF_2D_Baseline 2. Connected to this central basin at its southern limit are two other elongated depressions (south sector), that may also extend further towards the SE. The largest of the two (towards W), with a general orientation N-S, is at least 14.7 km long and 6 km at its widest part. The smaller basin (towards E) is oriented NW-SE and is 5.8 km x 3.8 km in size.

Within these basins, seismic unit U25 is thicker, comprising mostly low amplitude parallel facies, gently undulating in places (Figure 139). The thickness and acoustic amplitude decrease towards the top. Small-scale, box-shaped channels with transparent infill are scattered at several levels within U25, truncating the thinly-layered sequence (Figure 140). The base of these channels is generally marked by a negative amplitude reflector. The occurrence and size of these channels increase towards the top of the unit, with common vertical stacking.

In the south sector, between the two basins, U25 facies exhibits the same characteristics as in the north.

The sediments constituting seismic unit U25 are interpreted to have been deposited in a relatively low-energetic setting, possibly related to a flood plain/transgressive estuary. However, the increase of small channel-incisions within the upper deposits of U25 suggests the onset of a regressive event/fluctuation. From the seismic character of U25 and its interpreted depositional system, it is estimated that the thinly-layered deposits comprise fine sediments, such as fine sands-silts (?), and that the transparent channel infill may correspond to unstructured fine sediments (?).

Local areas of seismic unit U25 exhibit variable degrees of internal deformation. This deformation is discussed in section (8.8.1|5.d).

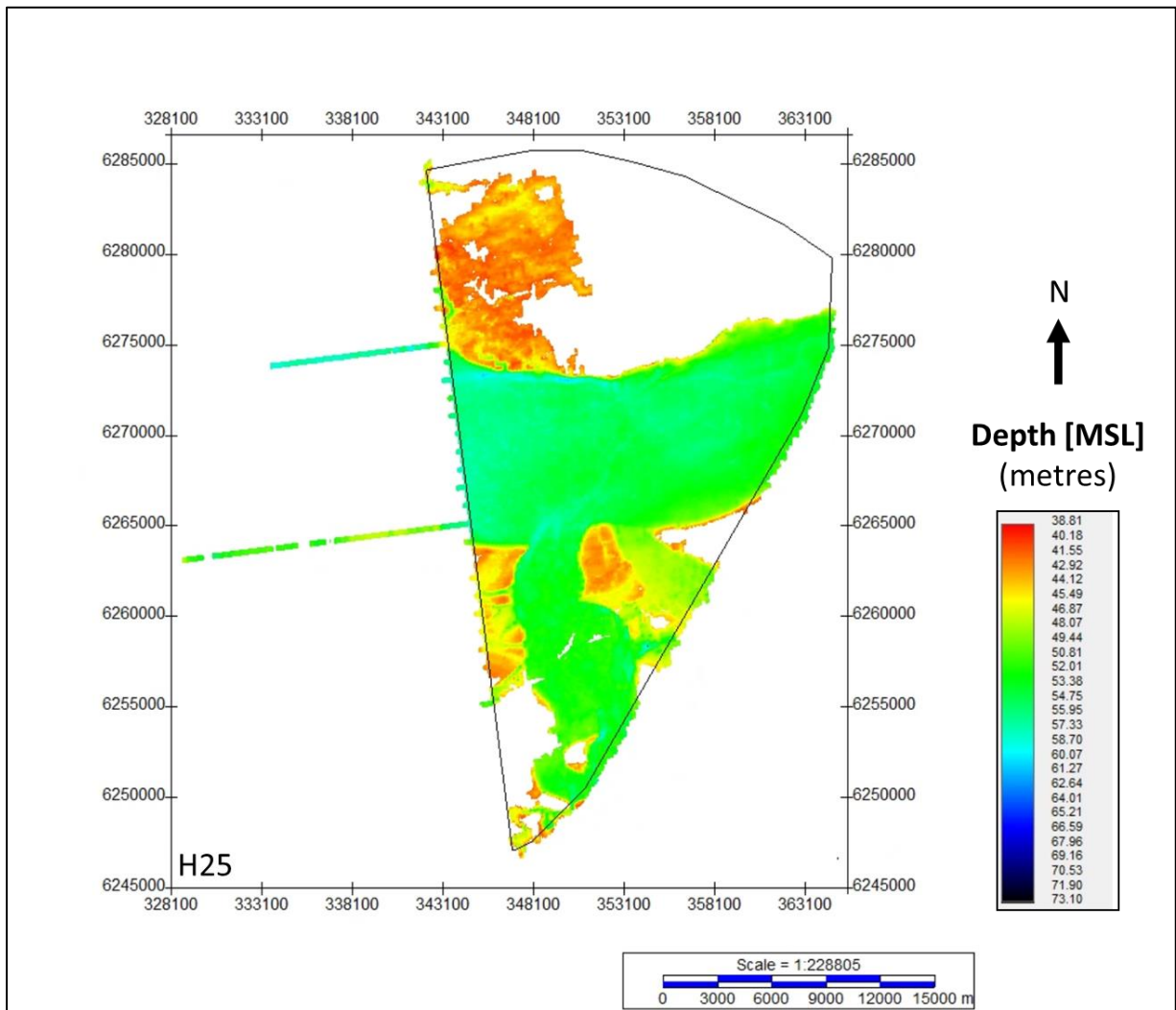


Figure 134 Map showing the lateral extent of U25.
Units in metres below MSL.

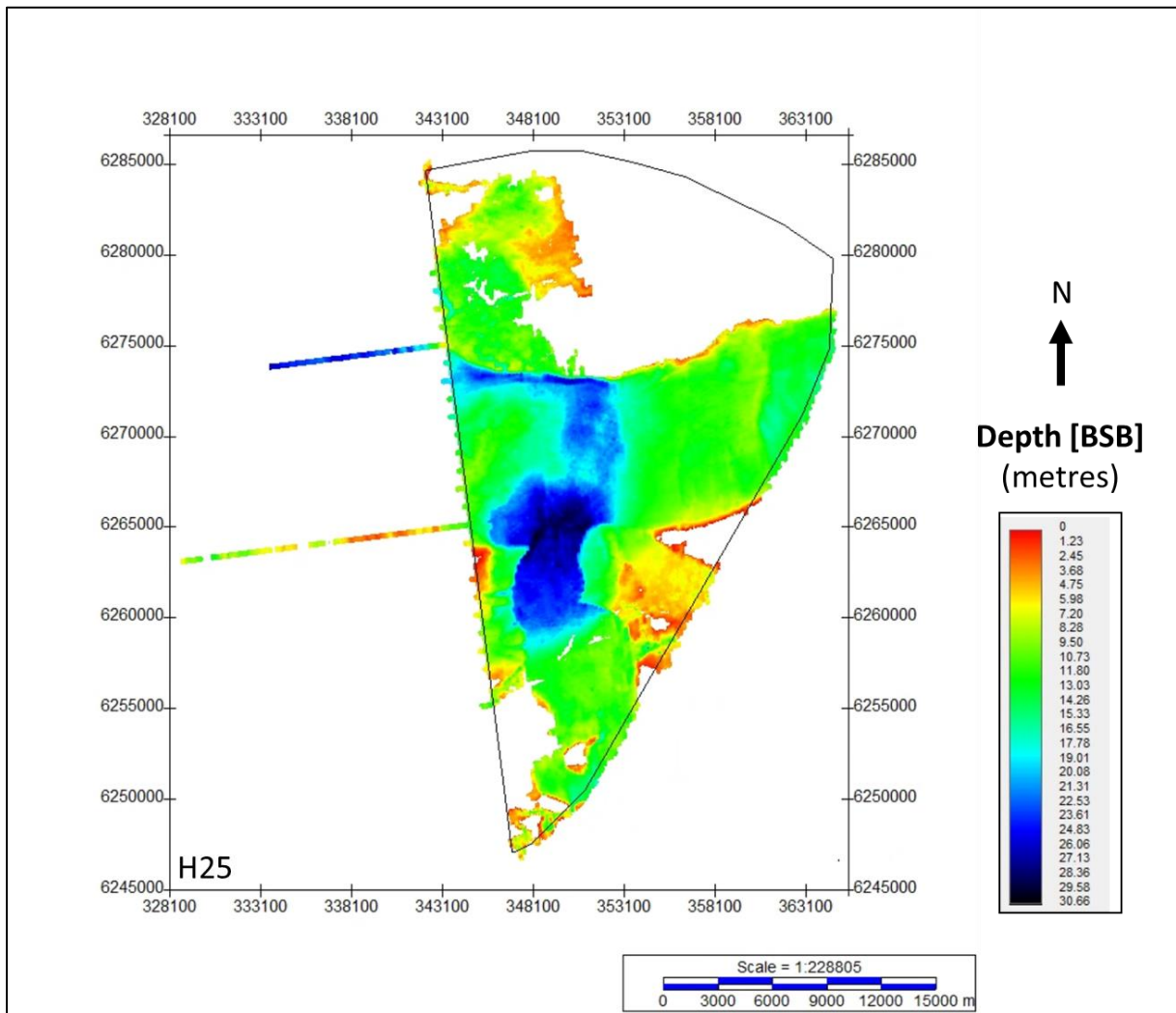


Figure 135 Depth below seabed of H25.
Units in metres below seabed.

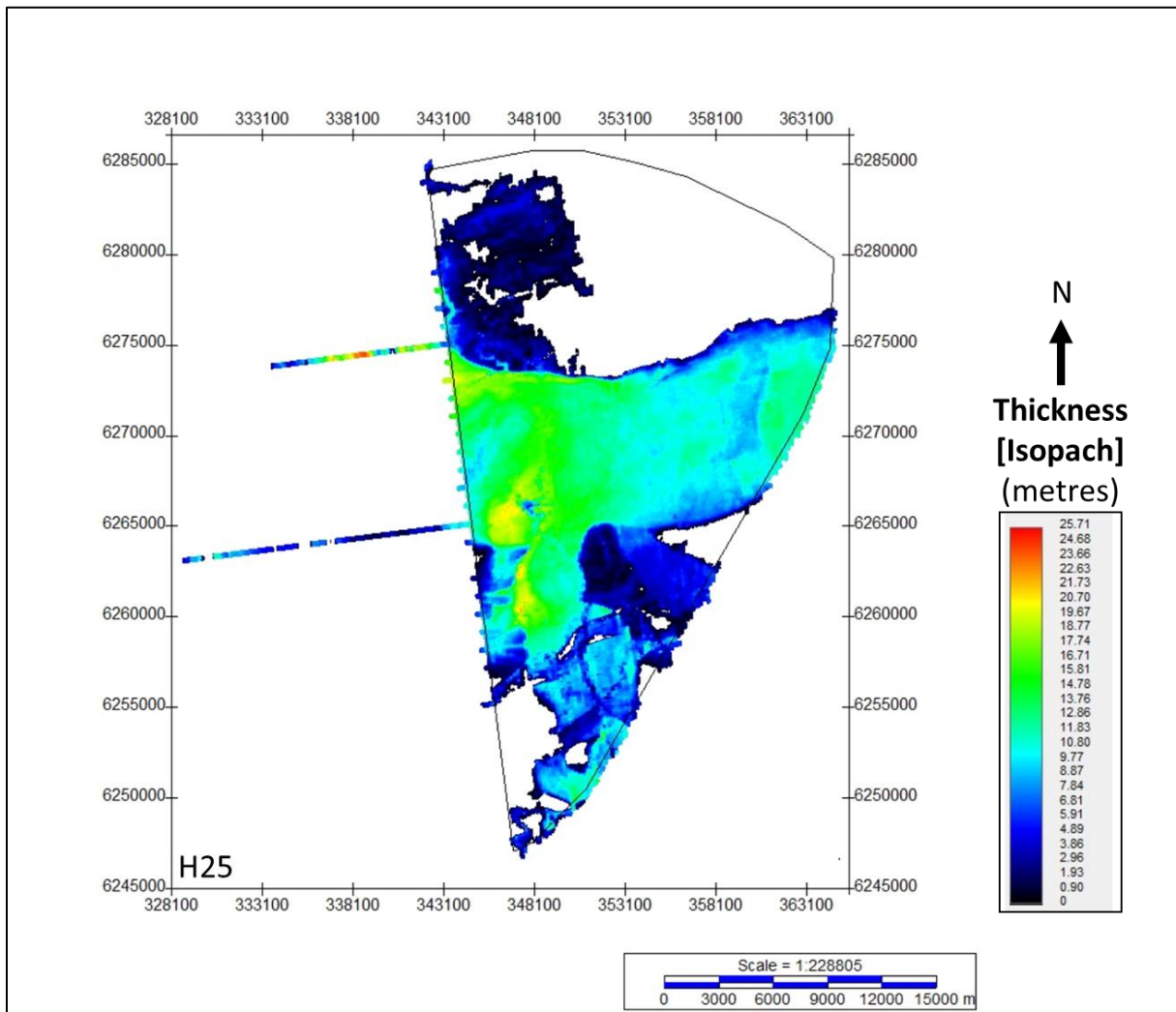


Figure 136 Thickness of unit U25.
Units in metres.

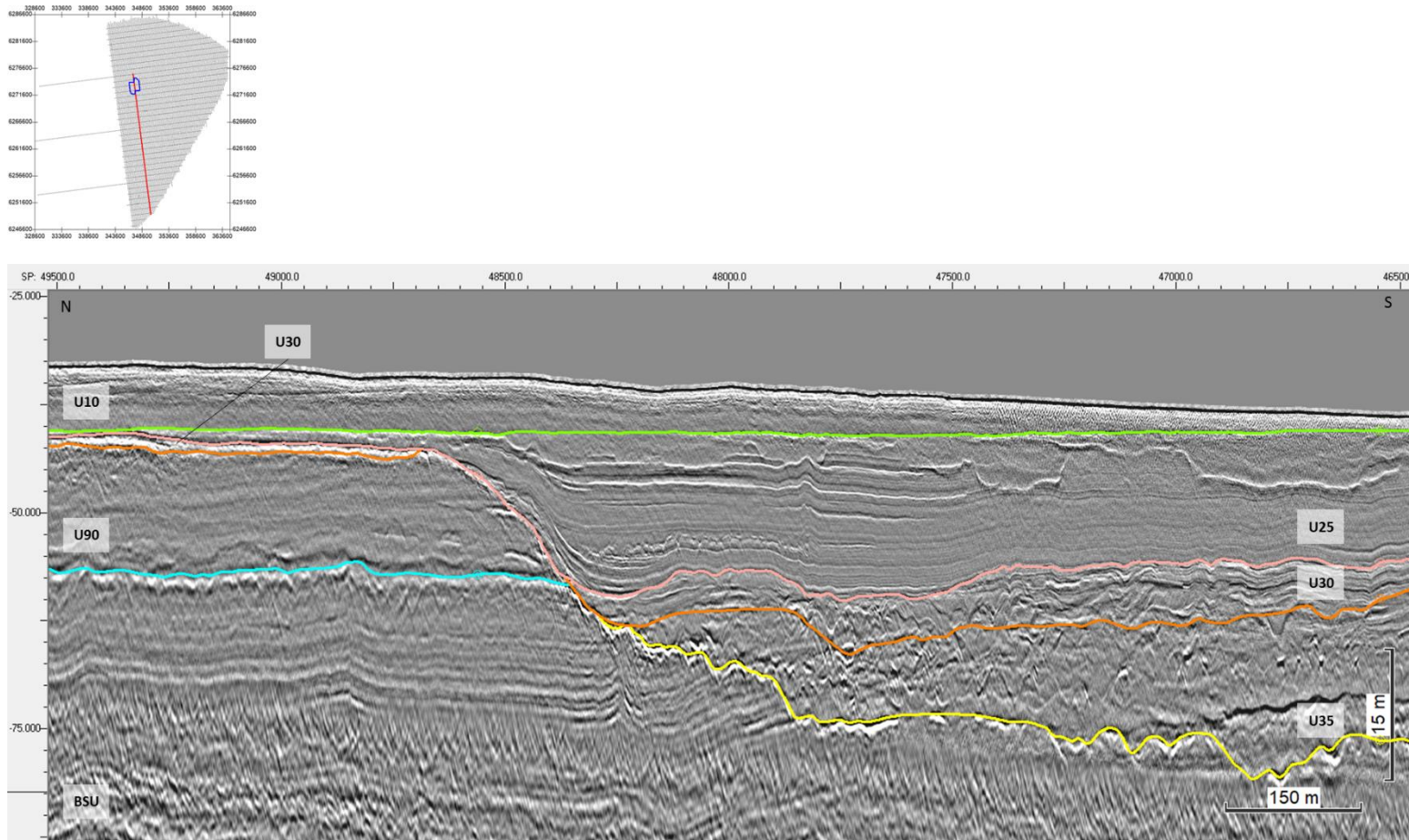


Figure 137 General facies of Seismic Unit U25, and character of horizon H25
H25 is shown in rosy brown.
Seismic profile BM2_OWF_E_2D_03570

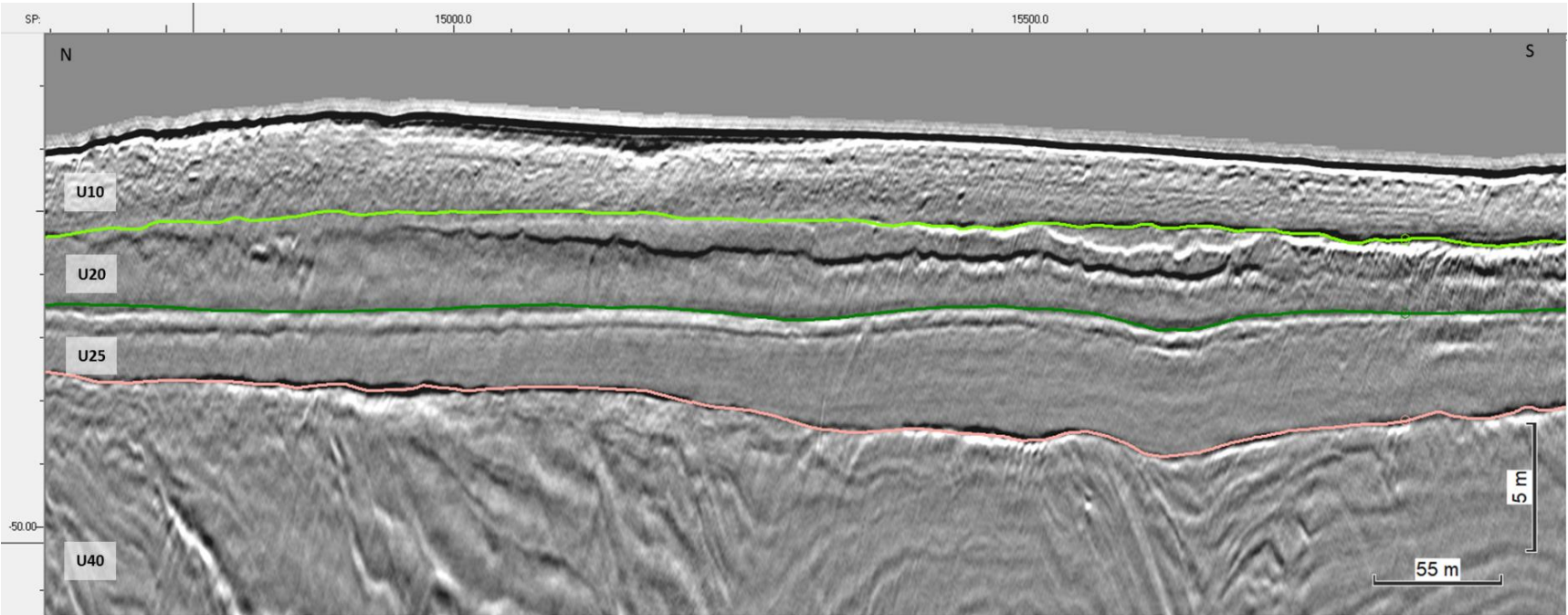
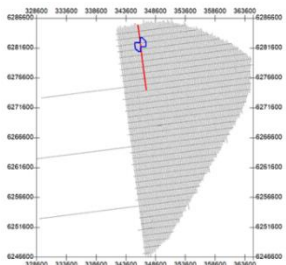


Figure 138 Facies of Seismic Unit U25 present in areas where U25 is thinner.
Seismic profile Inf_RE_BM2_2D_017_01

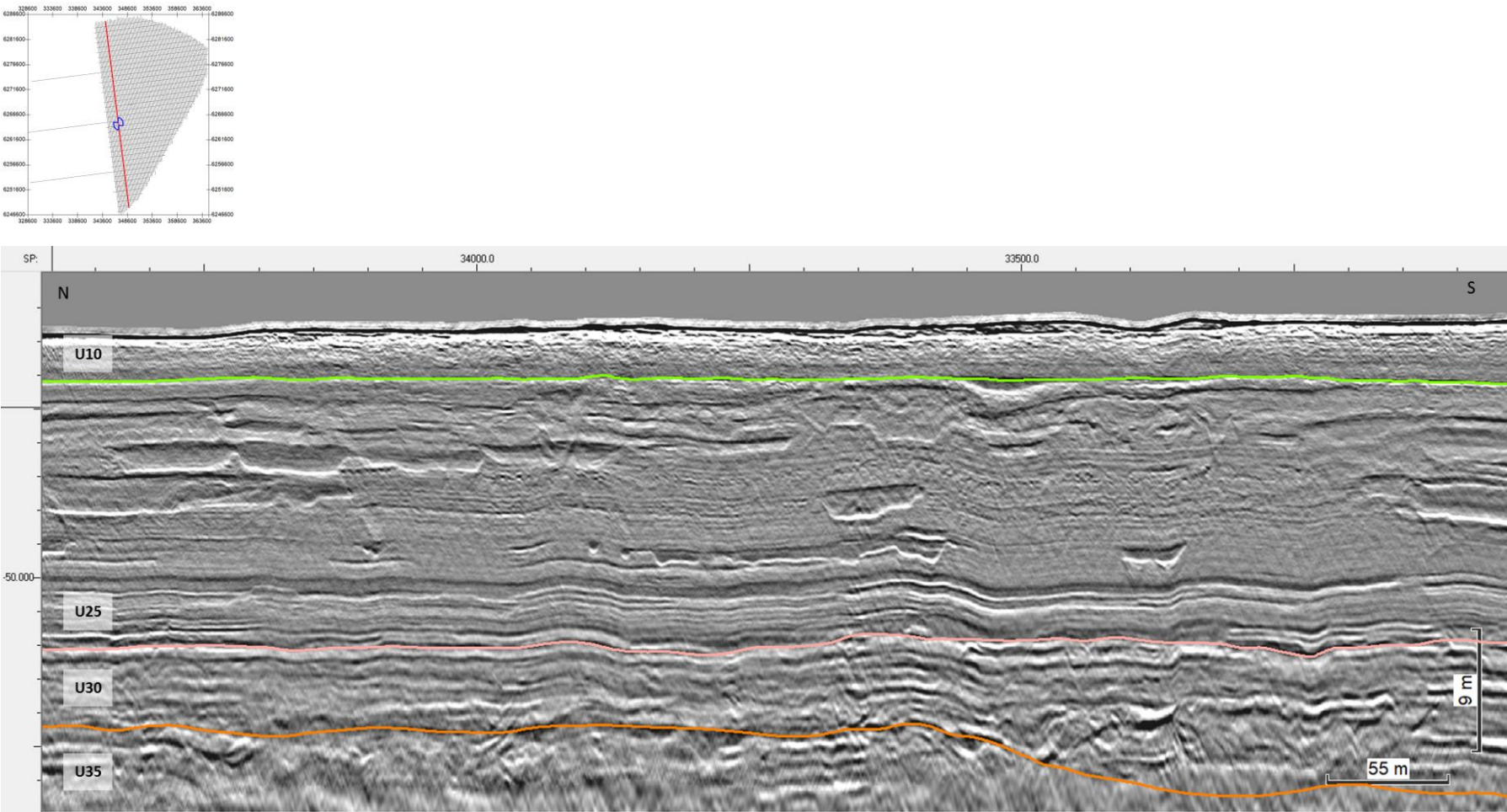


Figure 139 U25 facies within the central basin, where the unit is thicker. Channel frequency is increasing towards the top. Seismic profile BM1_OWF_E_2D_02100.

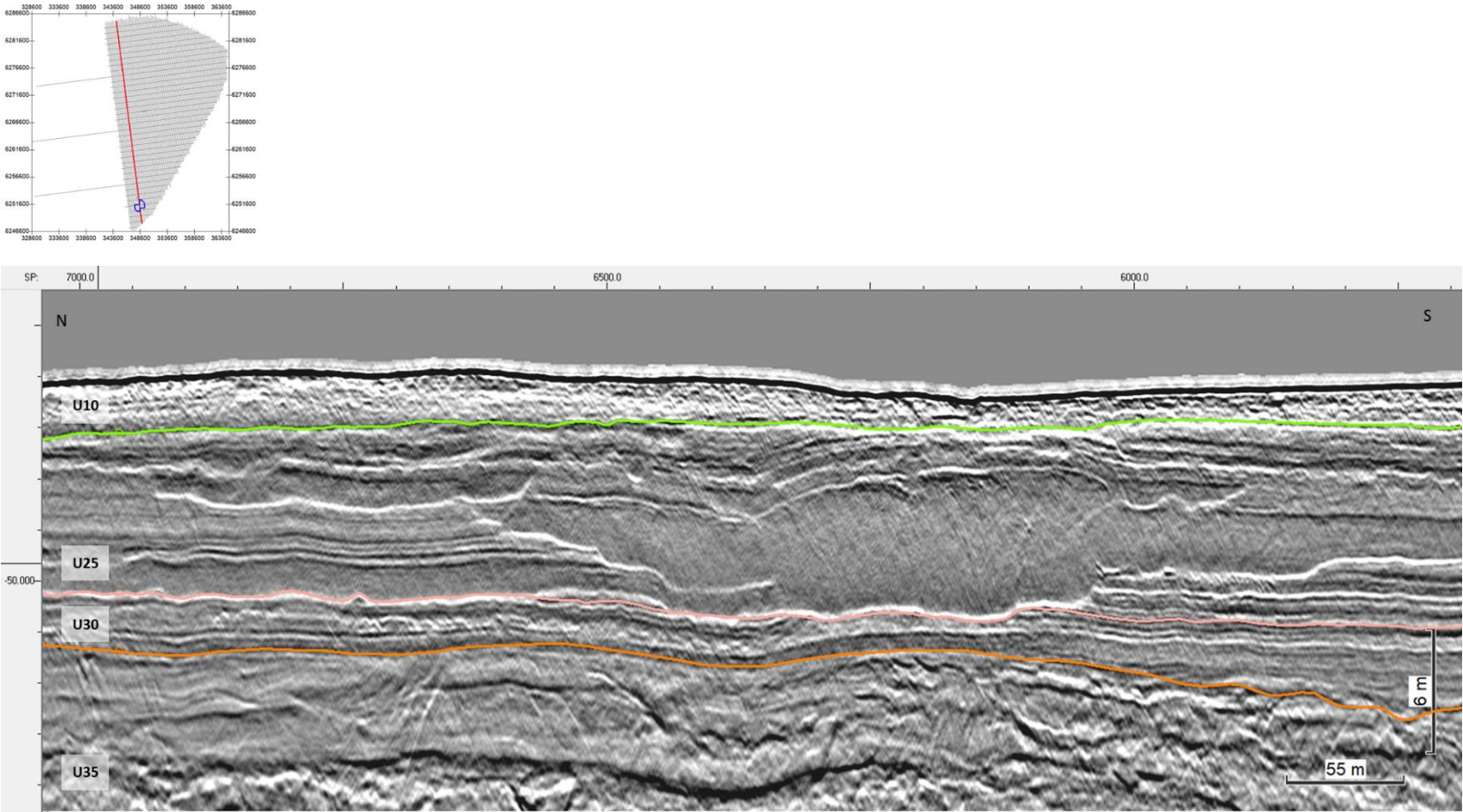


Figure 140 Homogeneous transparent facies of an internal channel of Unit U25.
Seismic profile BM1_OWF_E_2D_02100

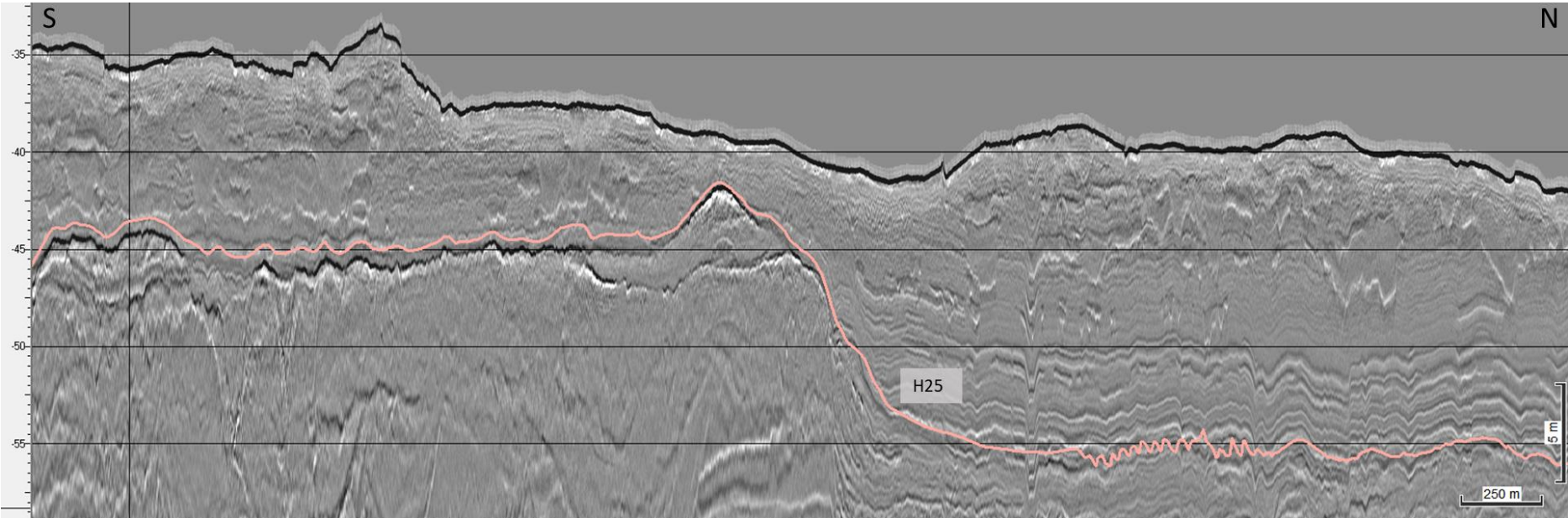
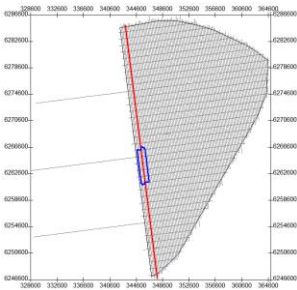


Figure 141 Grid overlay from interpretation of H25 as interpreted on the Innomar SBP.
Seismic profile BM1_OWF_E_2D_00840.

8.6.5 | SEISMIC UNIT U30

Seismic unit U30 is a major element of the ground model, and has the same spatial distribution of U25 across the three sectors. The base of Seismic Unit U30 is defined by horizon H30 and is present discontinuously within the survey area. The spatial distribution, vertical reference to MSL and the seabed, and thickness of the unit are presented in Figure 142, Figure 143, and Figure 144.

Horizon H30 ranges in depth between 39.7 m and 80.3 m below MSL (Figure 142), and between 0 m and 42.1 m depth below the seabed (Figure 143). Horizon H30 represents an uneven, undulating surface, occasionally defined by a significant vertical facies shift (Figure 145). When present and continuous, H30 was mapped along a reflector of variable amplitude (low to high). This uneven base marks an erosional surface that truncates the deposits below it (Figure 146).

Seismic unit U30 has a tabular or tabular wavy morphology, usually 2 m to 10 m thick. The thickest deposits of U30 are located along the margins of the central basin (Figure 144) with a maximum thickness of 31.5 m. U30 is locally truncated by H20 incisions.

Within the central basin and the two minor ones, unit U30 is characterized by composite facies of medium to high amplitude configurations (Figure 146). Towards the top, reflectors are sub-horizontal, parallel and wavy. Below the latter, meso- to micro-scale channels and mounds are observed, with internal oblique, parallel, downlapping reflectors. Towards the base, the complexity of the seismic facies increases, with common mounds, lenses, patterns of channel lateral migration, hummocky reflectors, and chaotic in parts.

The sediments constituting seismic unit U30 are interpreted to have been deposited in setting of slightly higher energy than the overlying U25, as evidenced by the occurrence of channel and chaotic deposits at the base. The sequence of seismic facies within U30 is indicative of decrease of energy from the base towards the top, possibly associated to a transgressive event. From the seismic character of U30 and its interpreted depositional system, it is estimated that, in general, there is a decrease in grain size towards the top, with probable sandier sediments at the base, getting progressively finer upwards (?).

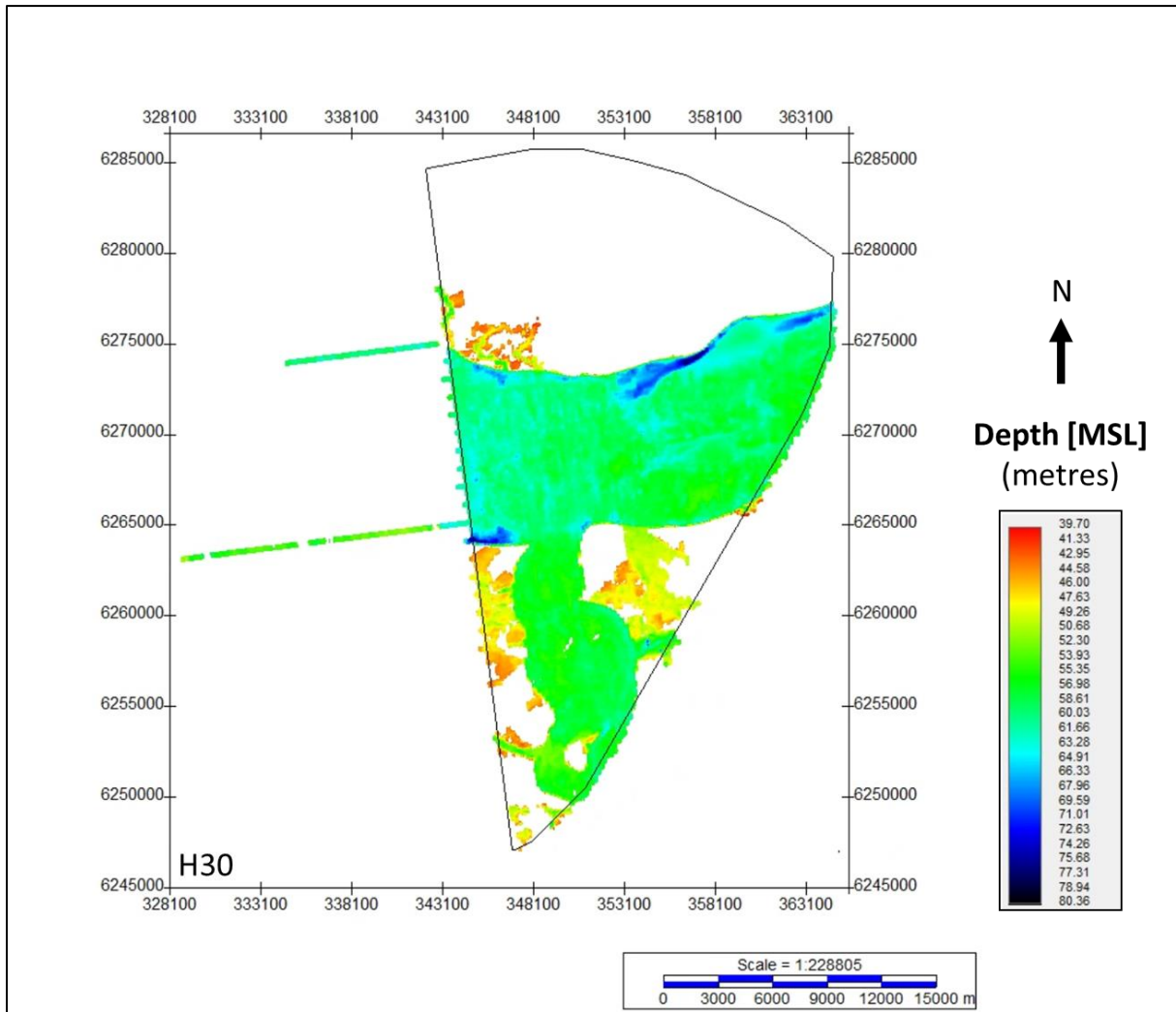


Figure 142 Map showing the lateral extent of U30.
Units in metres below MSL.

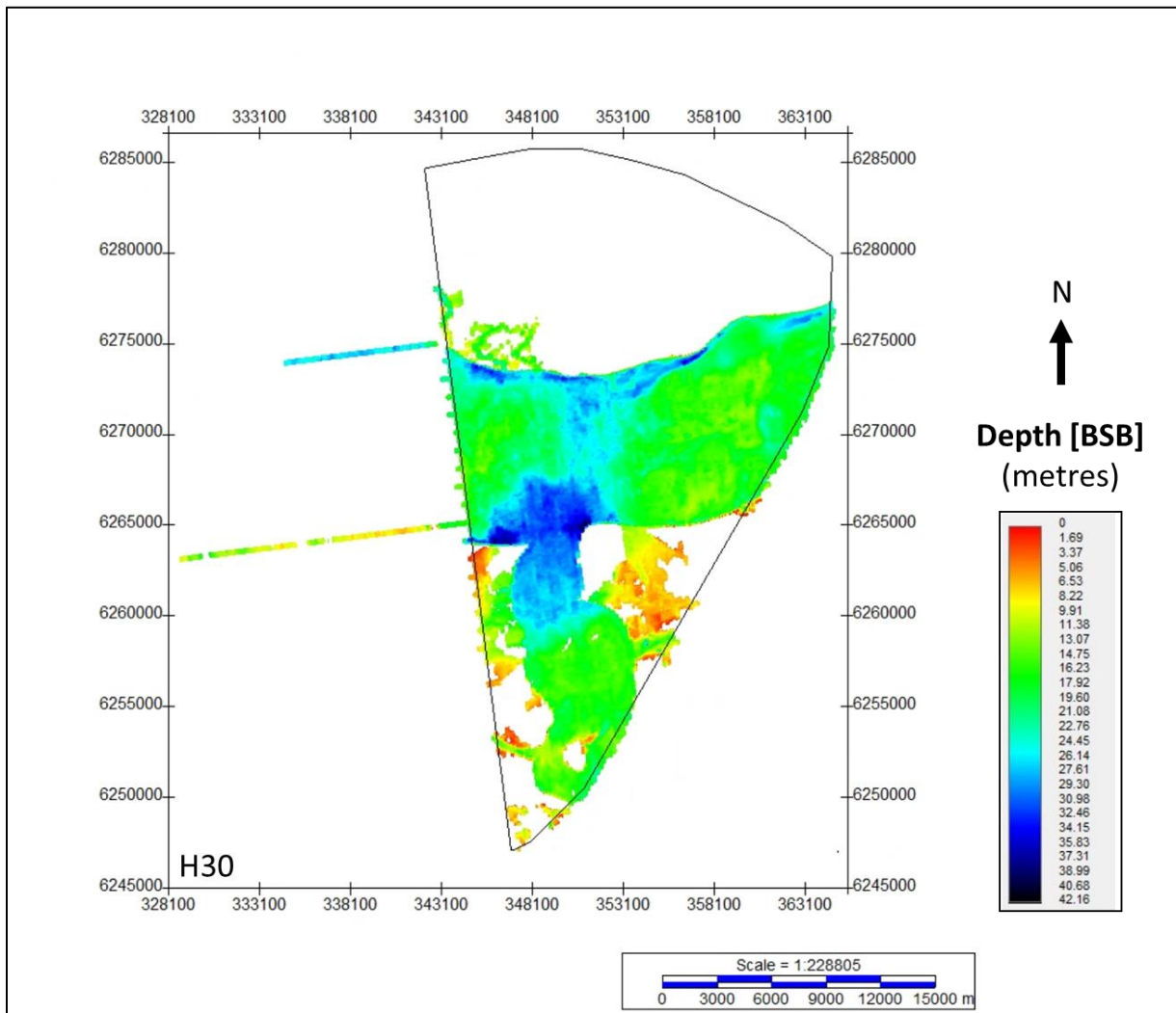


Figure 143 Depth below seabed of H30.
Units in metres below seabed.

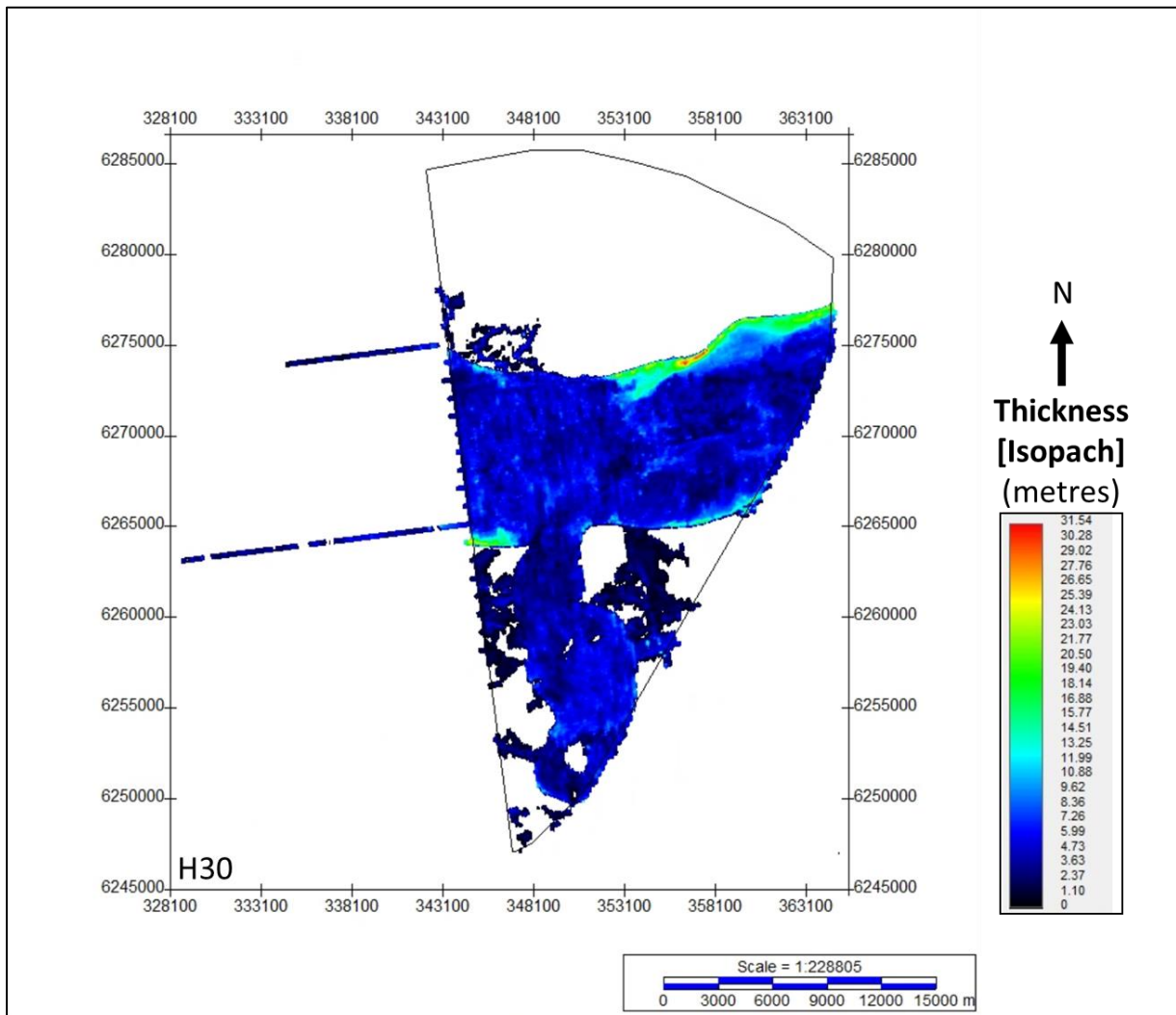


Figure 144 Thickness of unit U30.
Units in metres.

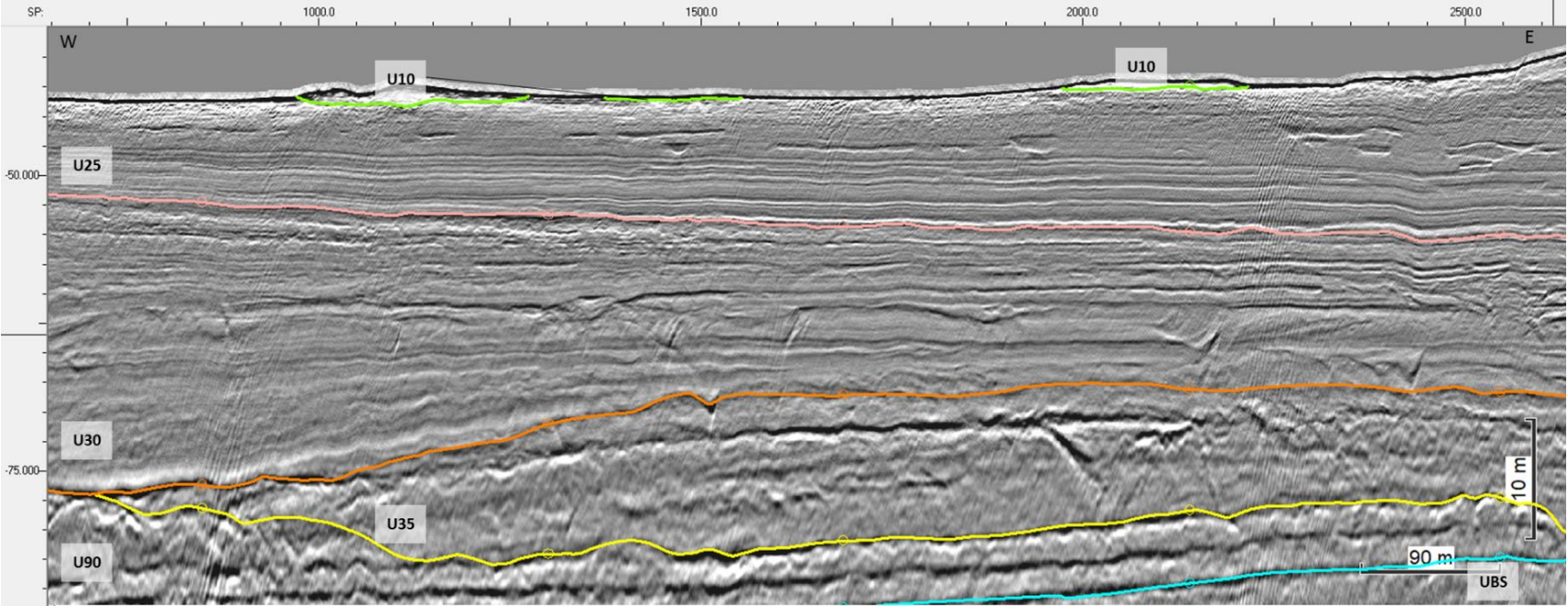
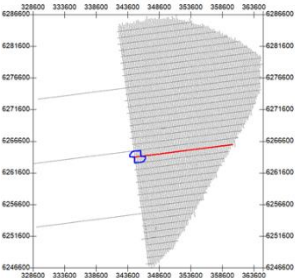


Figure 145 General facies of Seismic Unit U30, and the character of horizon H30 (orange).
Seismic profile BX3_OWF_E_XL_21000

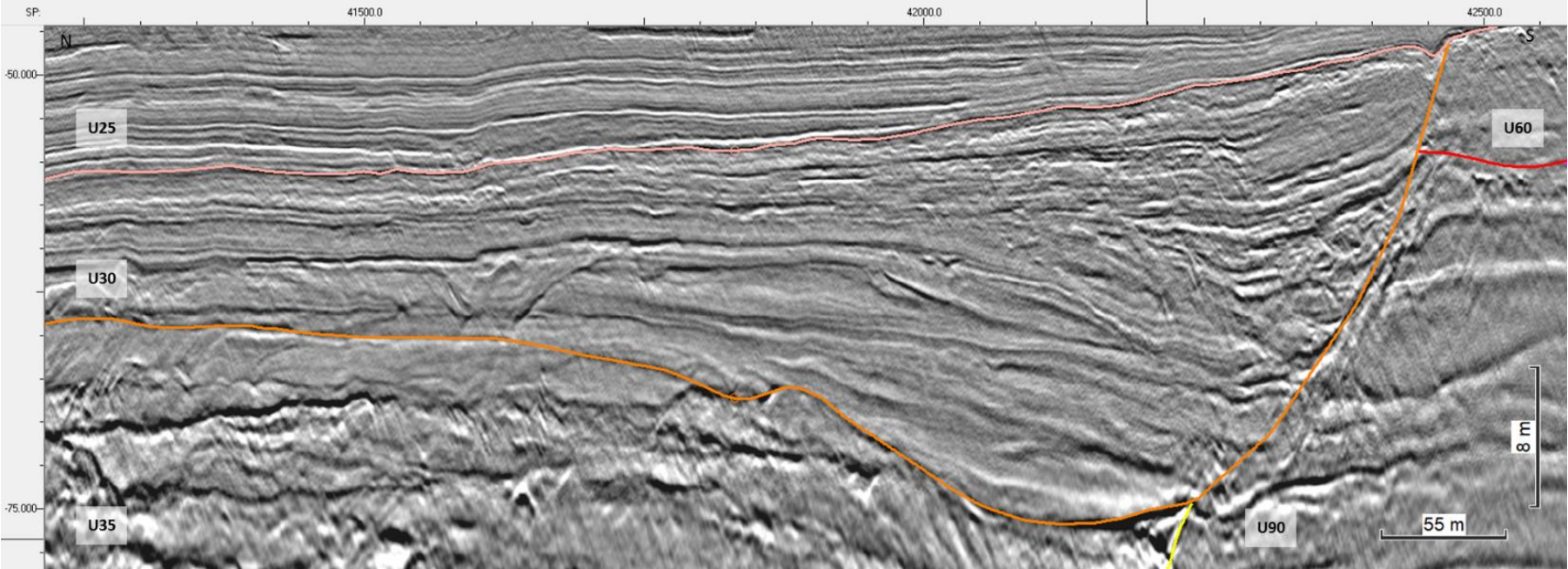
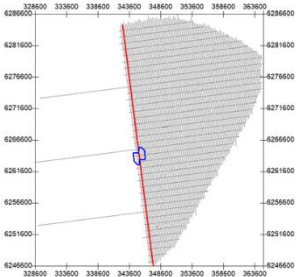


Figure 146 H30 truncating the underlying deposits, and the thicker facies of U30.
The image shows an area near the SE margin of the central basin. Seismic profile BM1_OWF_E_2D_00420

8.6.6 | SEISMIC UNIT U35

Seismic unit U35 is found exclusively within the three major basins of the site, only occurring in the central and south sectors. The base of Seismic Unit U35 is defined by horizon H35. The spatial distribution, vertical reference to MLS and the seabed, and thickness of the unit are presented in Figure 147, Figure 148, and Figure 149.

Horizon H35 ranges in depth between 42.4 m and 113.2 m below MSL (Figure 147), and between <0.5 m and 72.3 m depth below the seabed (Figure 148). Horizon H35 represents an uneven, rugose, undulating surface (<5 m relief) marking an additional vertical facies shift within the basins' deposits (Figure 150). This uneven base marks an erosional surface (Figure 151). When present and continuous, H35 was mapped along a reflector of variable amplitude (low to high). The basemap of H35 reveals ENE_WSW striking ridges of 1 km in length and hundreds of metres wide, occurring in the central basin. The trenches between the ridges are asymmetric, deepening north (Figure 149).

Seismic unit U35 has a tabular to a mega lens-shaped morphology, usually 2 m to 20-25 m thick. The thickest deposits of U35 are located within a deeper area in the NE corner of the central basin, reaching up to 54.9 m thick (Figure 149). The thinner packages occur within the two basins in the south sector of the site.

U35 comprises the basal deposits of the three major basins. This unit is characterized by composite facies of low to high amplitude reflectors (Figure 150 and Figure 152). Compared to U30 above, U35 comprises larger proportioned and more complex seismic facies associations, such as meso-scale mounds, channels, and lenses. There are numerous internal erosional surfaces separating these features. Large oblique lenses with internal downlaps forming clinofold structures occur at the base. In general, the thickness of the internal packages decreases towards the top, becoming more sub-horizontal and sub-parallel, grading up.

Seismic unit U35 sediments are interpreted to have been deposited in a high energy setting, as evidenced by the meso-scale facies association, the numerous internal erosional surfaces, and more complex geometries. Horizon H35 is an unconformity surface that shaped the base of all three major basins. The ridges and trenches observed at the base are associated to a major erosional event. The trench infill constitutes mega-bedforms (500-800 m wide, and 10 m thick), comprising high energy fluvial bedforms (flash floods?). The combined sequence of seismic facies U35-U30-U25 present within these is indicative of an overall decrease of energy from the base towards the top. From the seismic character of U35 and its interpreted depositional system, it is estimated that the sediments are likely gravel and sands with enclaves of coarser-grained clasts, possibly decreasing in grain size towards the top of the unit (fining-upward sequence?).

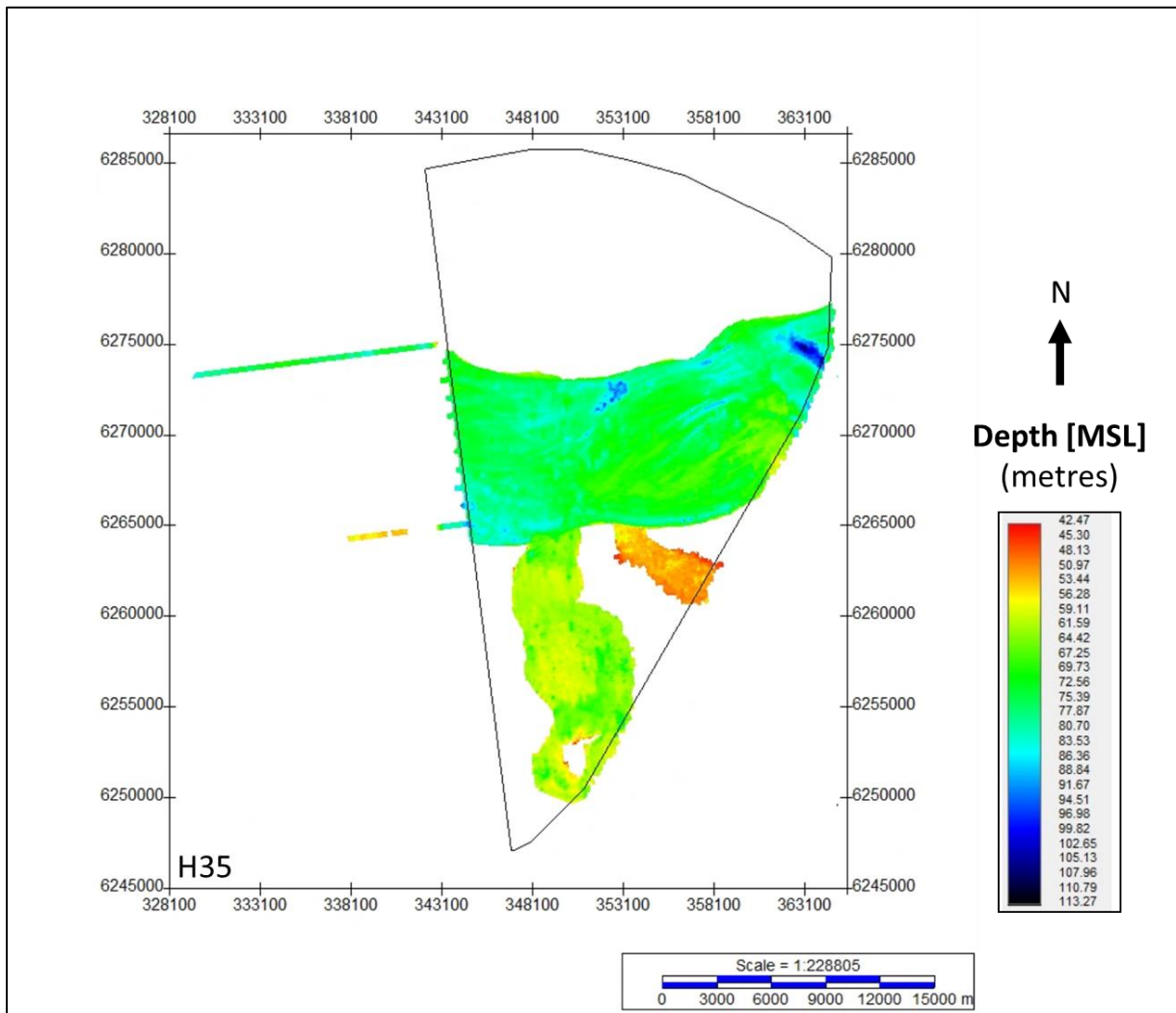


Figure 147 Map showing the lateral extent of U35.
Units in metres below MSL.

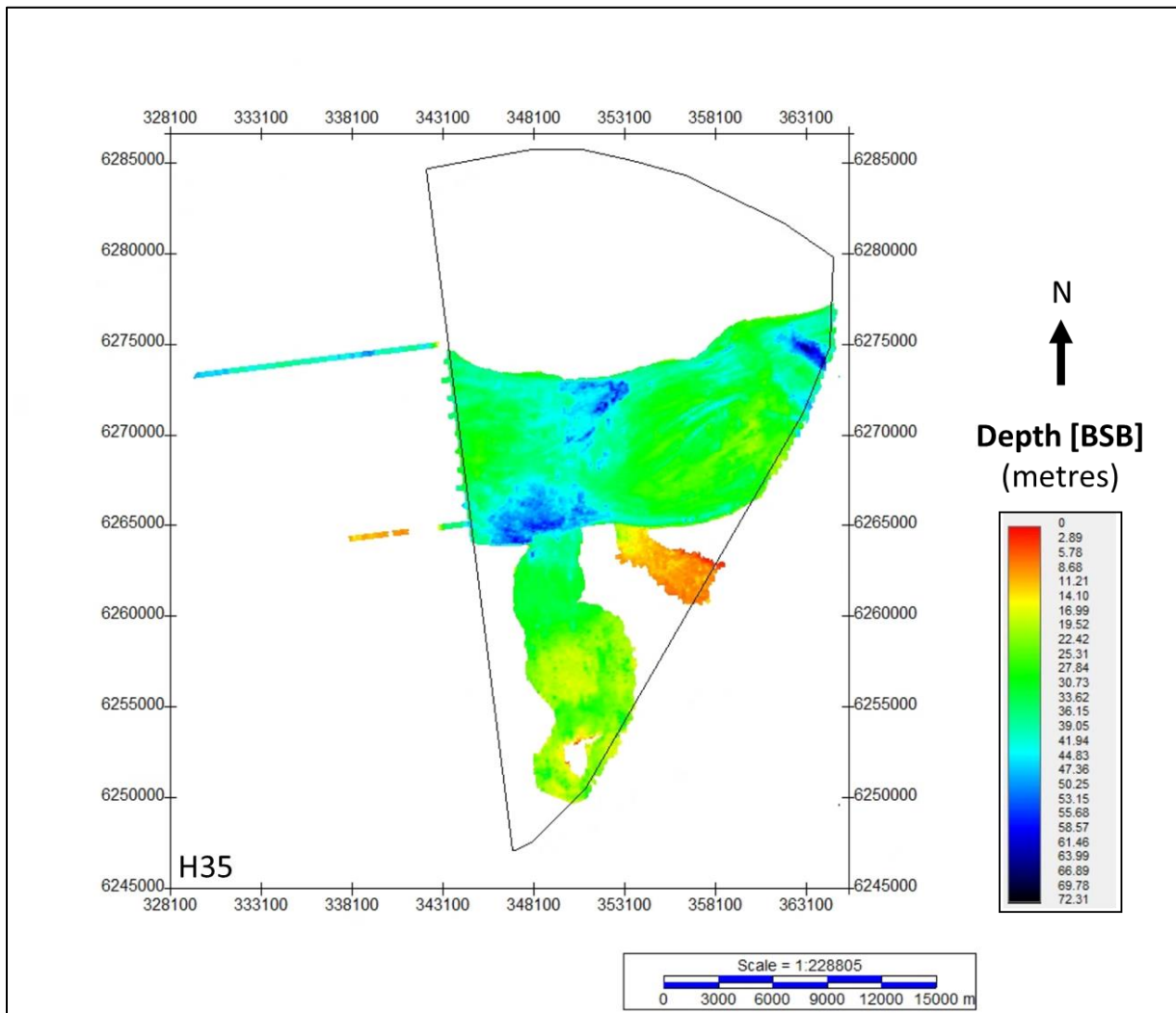


Figure 148 Depth below seabed of H35.
Units in metres below seabed.

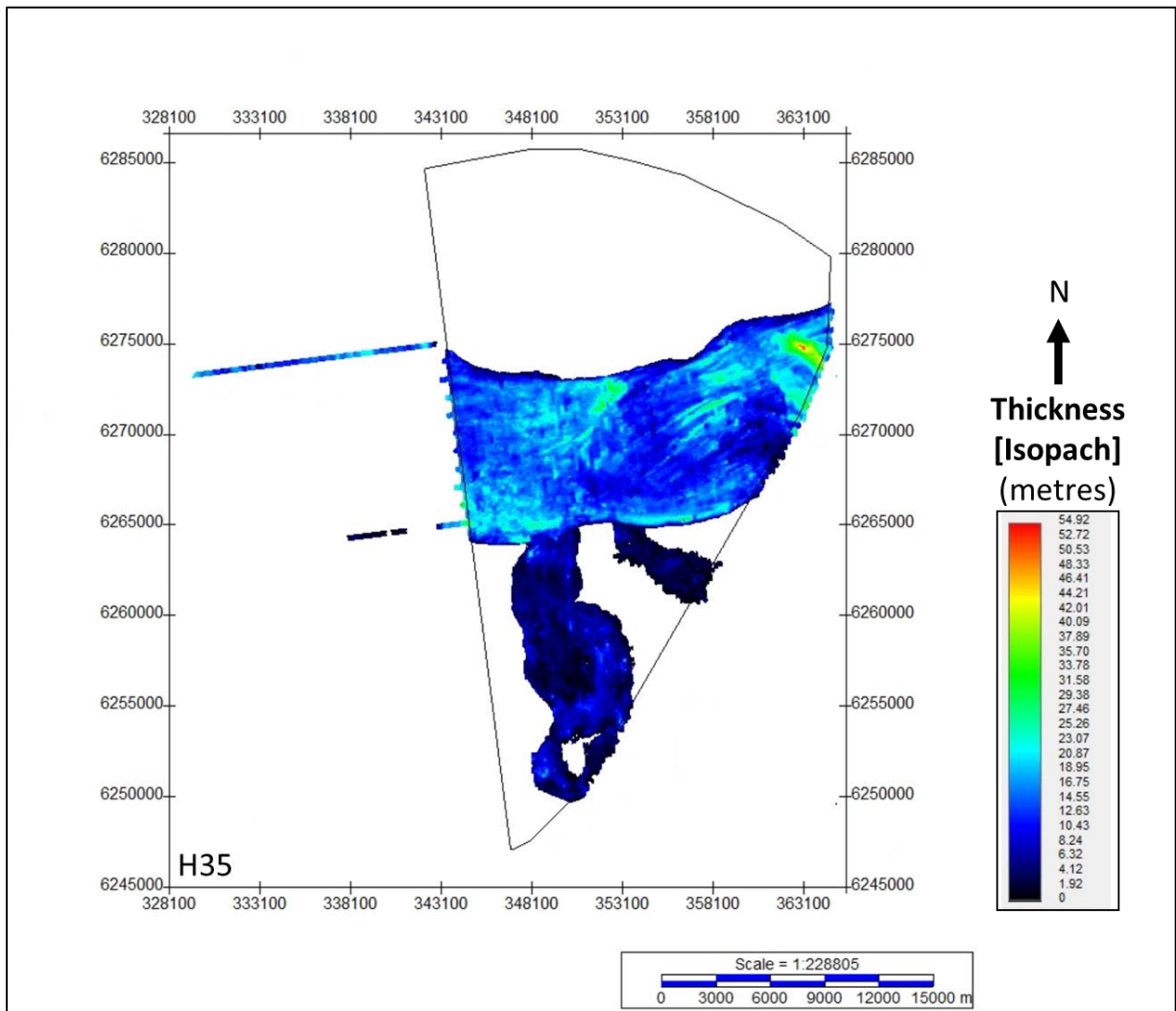


Figure 149 Thickness of unit U35.
Units in metres.

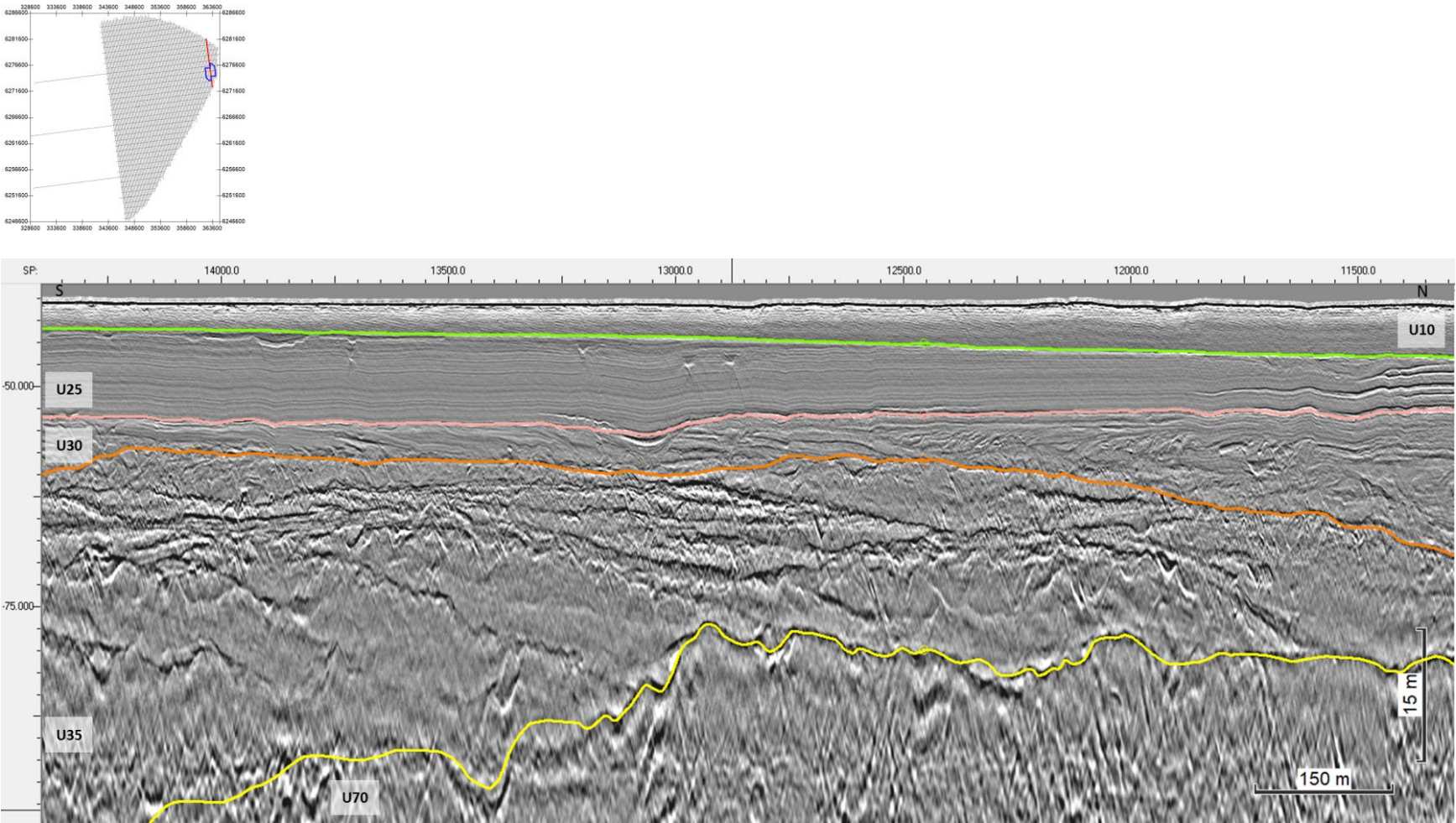


Figure 150 General facies of Seismic Unit U35, and the character of horizon H35
H35 is shown in yellow. Seismic profile BM6_OWF_E_2D_19740

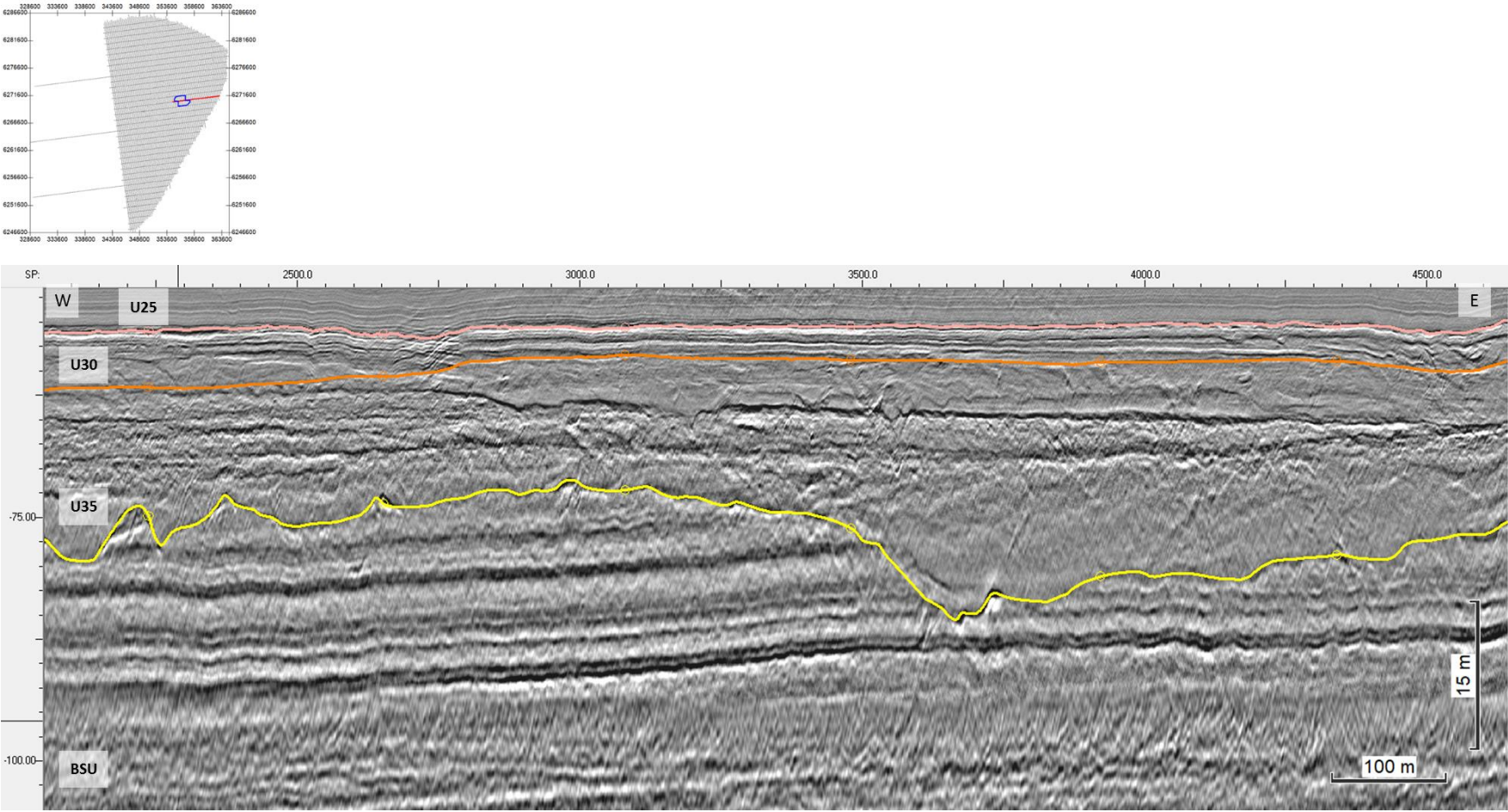


Figure 151 General facies of Unit U35, and the pronounced relief of H35 truncating the BSU.
Seismic profile BX3_OWF_E_XL_16000_01

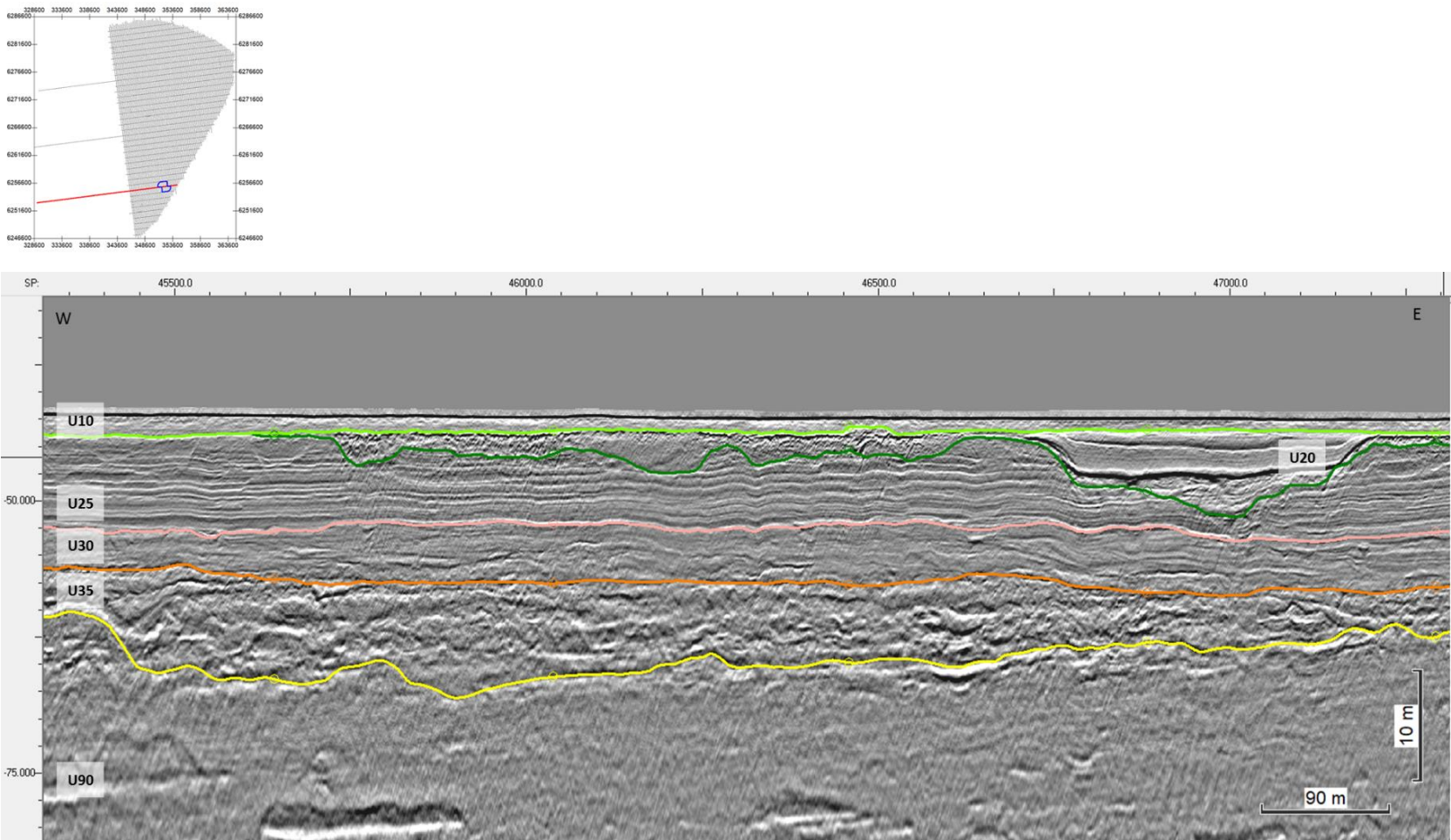


Figure 152 Facies of seismic Unit U35 in an area where the unit is thinner.
Seismic profile BX4_OWF_2D_Baseline_3

8.6.7 | SEISMIC UNIT U40

Seismic unit U40 is a key element of the ground model, and extends spatially across the three sectors of the site. The base of Seismic Unit U40 is defined by horizon H40 and is present discontinuously within the survey area. The spatial distribution, vertical reference to MLS and the seabed, and thickness of the unit are presented in Figure 153, Figure 154, and Figure 155.

The main features of seismic unit U40 are large channel incisions delineated at the base by horizon H40, often defined by a vertical facies shift and truncation of the underlying unit. H40 also traces the undulating base of the channel lateral deposits, following a discontinuous reflector of low to medium amplitude. Horizon H40 ranges in depth between 38.4 m and 173.9 m below MSL (Figure 153), and between <0.5 m and 136.0 m depth below the seabed (Figure 154).

The channel incisions of U40 exhibit a wide range of sizes and depositional characteristics, but typically display a V-shape morphology, or U-shape. The larger incisions (total = 15 channels) have been classified into four types of channels – A, B, C, and D –, in order to best describe their wide variability in size, orientation, and seismic facies (described below; Figure 156). Smaller incisions have not been included in this assessment, although they may have been mapped by H40.

Type A channels (polygons H40 CH_05, CH_07, CH_12, CH_13, CH_14)

Shape: V or U; Orientation: E-W; Max Depth BSL: 60-80 m; Relief: 25-30 m; Width: 800-2200 m; Length: 3000-4000 m.

Example: H40_CH_13 (Figure 158)

Seismic facies: Base deposits characterised by mound-chaotic facies with composite mounds above, grading up from meso to micro scale, chaotic in places; upper sections usually with channel facies, with micro parallel wavy and oblique reflectors; variable amplitudes from high to low.

Type B channels (polygons H40 CH_03, CH_06, CH_08)

Shape: V or U; Orientation: variable, NW-SE, NE-SW; Max Depth BSL: 100-120 m; Relief: <45 m; Width: ~1000 m; Length: 3000-8000 m.

Example: H40_CH_08 (Figure 159)

Seismic facies: Generally chaotic-oblique-mound-channel facies to oblique above, with common internal mounds-channels; variable amplitude.

Type C channels (polygons H40 CH_01, CH_04)

Shape: V or U; Orientation: NW-SE; Max Depth BSL: 150 m; Relief: 25-30 m; Width: 1400-1800 m; Length: 8000-11000 m.

Example: H40_CH_01 (Figure 160)

Seismic facies: Base exhibiting chaotic-mound-channel-parallel channel facies of medium to high amplitudes; upper deposits varying from oblique-channel-mounds to meso-micro parallel wavy, chaotic, and homogenous.

Type D channels (polygons H40 CH_2, CH_09, CH_10, CH_11, CH_15)

Shape: U; Orientation: ENE-WSW; Max Depth BSL: 110-140 m; Relief: 60-90 m; Width: 1000-2000 m; Length: 6000-13000.

Example: H40_CH_02 (Figure 161)

Seismic facies: Composite facies usually comprising three associations; chaotic base with medium-high amplitude to composite mounds; middle facies characterised by sub-tabular deposits with medium amplitude, meso-micro parallel obliques, wavy in places; top facies truncating the deposits below, comprising mounds-channels.

The channel lateral deposits/fringes make up a tabular package 3-5 m thick (Figure 155), comprising composite mound-channel facies.

Some U40 channels are positioned (at least partially) directly above older incisions (commonly of U70), exploiting pre-existing incisions. In the north, some of the channel seem to have been affected by deformation (ex., type D channels, and smaller segments not classified within the polygon H40_ComplexArea), whereas other are positioned above deformed units (ex., CH_13_A). Further south, U40 appears to be not affected by any deformation. The U40 channel system is therefore interpreted to be associated with drainage of glacier melt back from the north, and outwash plains. The seismic facies pattern in U40 is interpreted to represent channel deposition with variable infill history – i.e., periods with high energy and coarser material deposition, and periods of lower energy with deposits of (clay) silt and sand, which may be related to glaciolacustrine deposition (Figure 162).

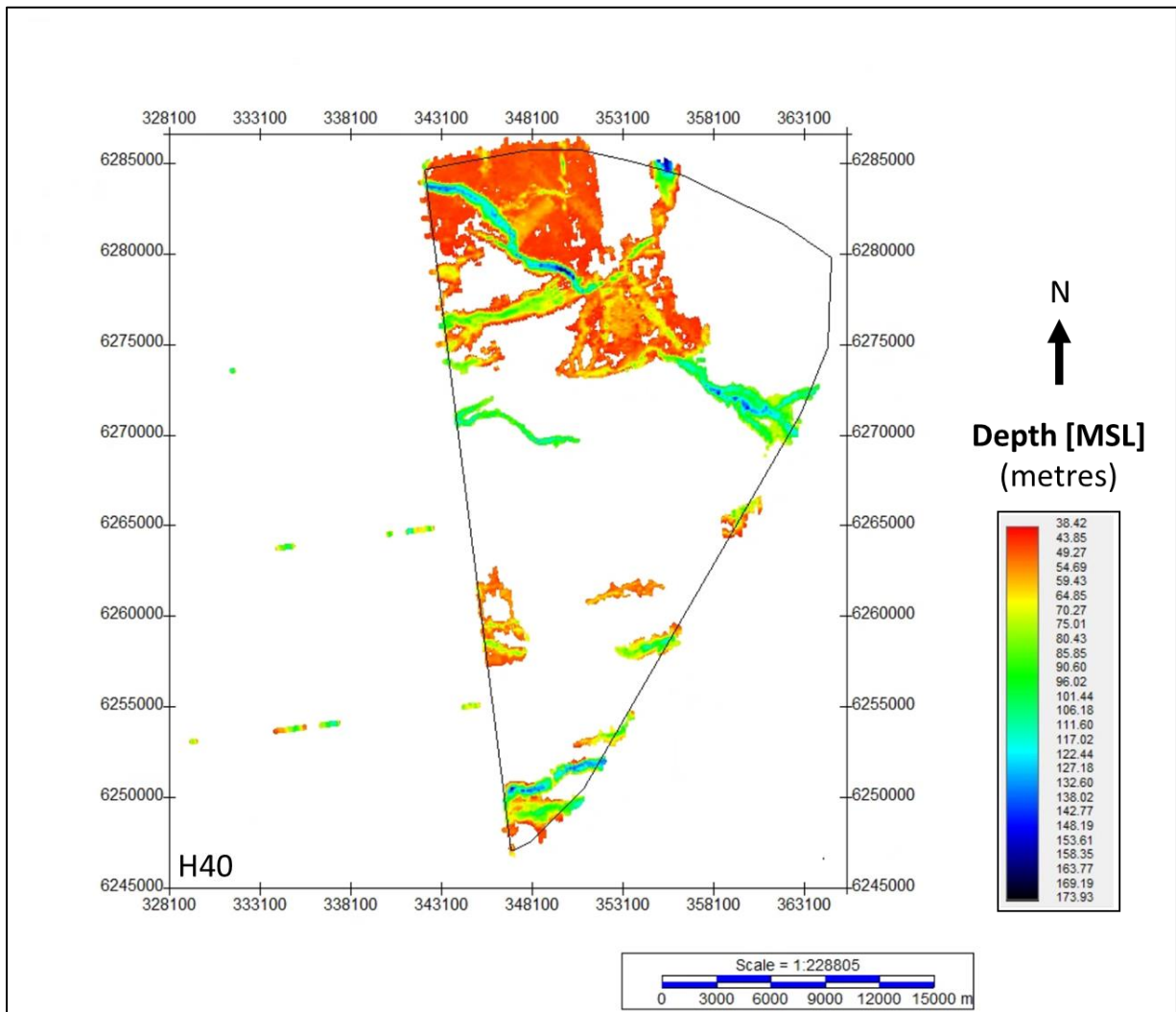


Figure 153 Map showing the lateral extent of U40.
Units in metres below MSL.

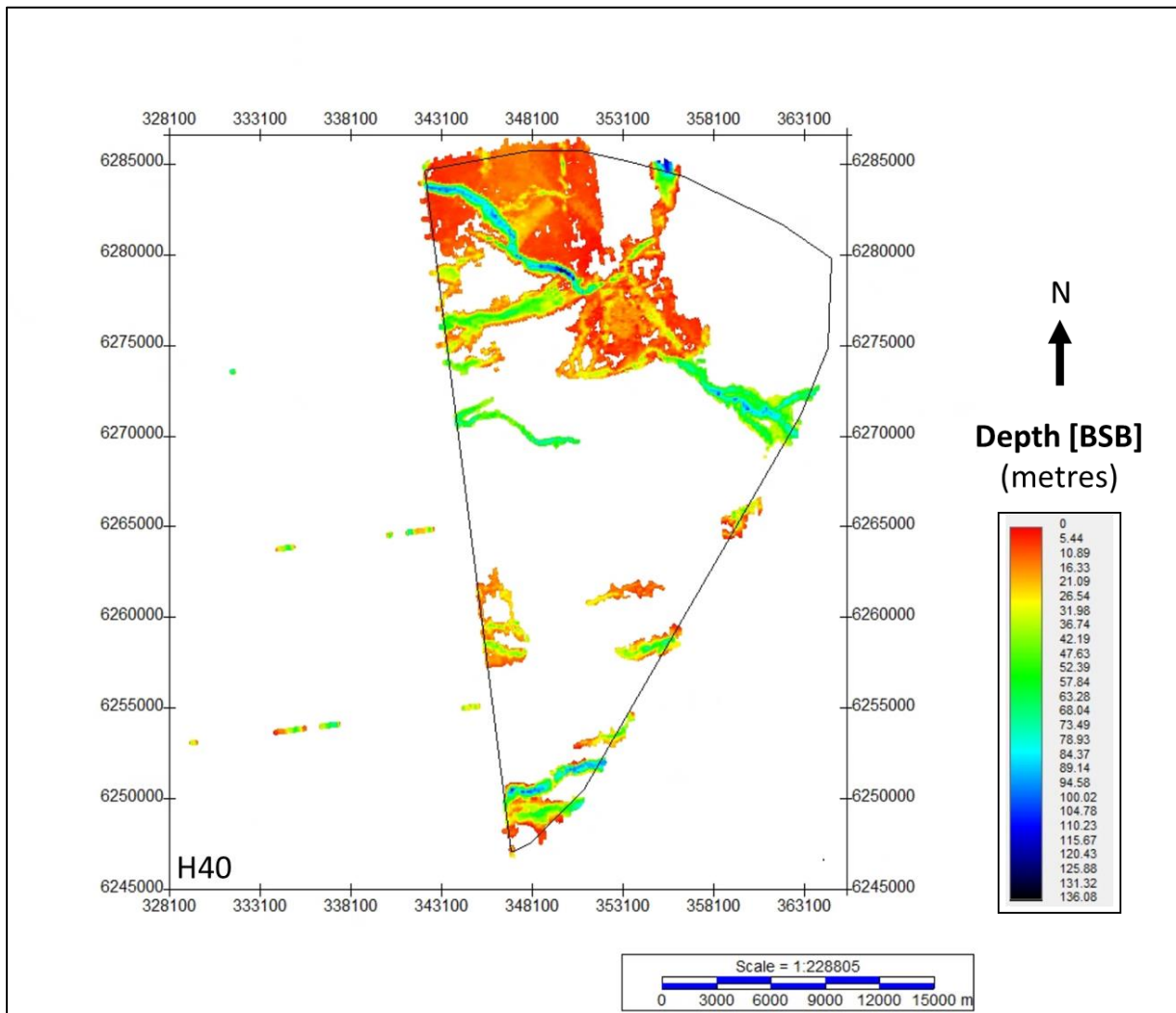


Figure 154 Depth below seabed of H40.
Units in metres below seabed.

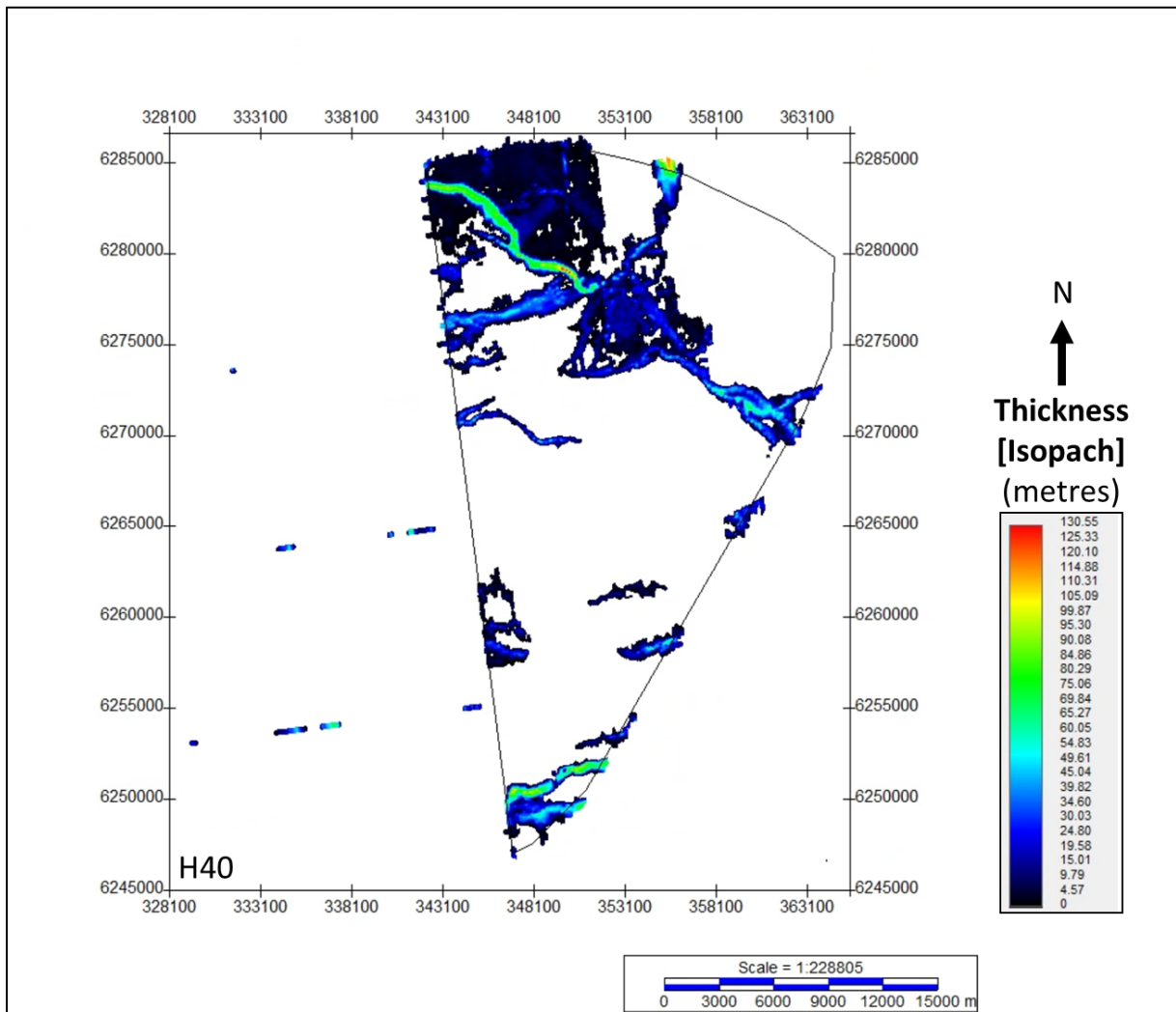


Figure 155 Thickness of unit U40.
Units in metres.

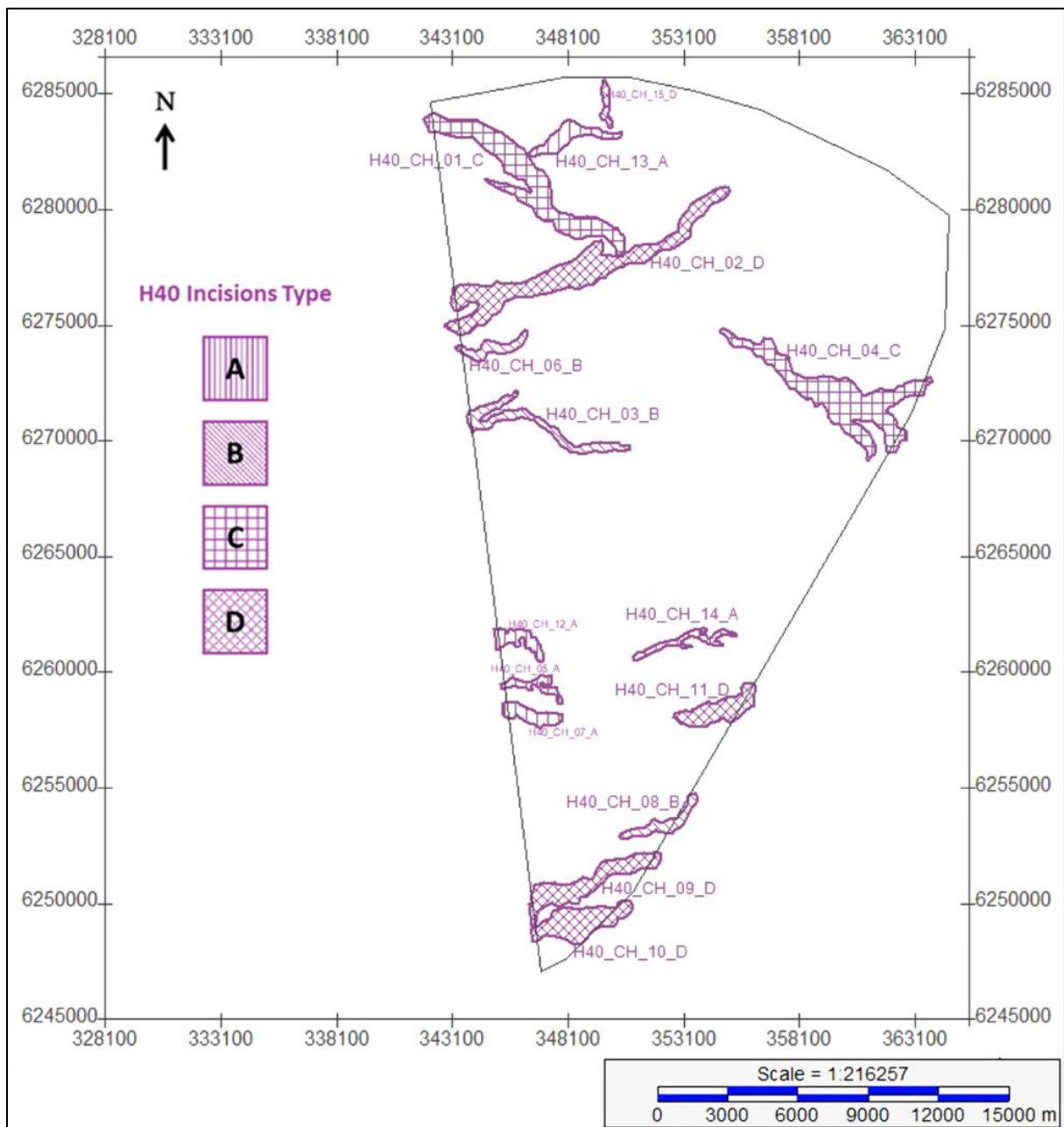


Figure 156 Spatial distribution of the different types of channels identified for Seismic Unit U40.

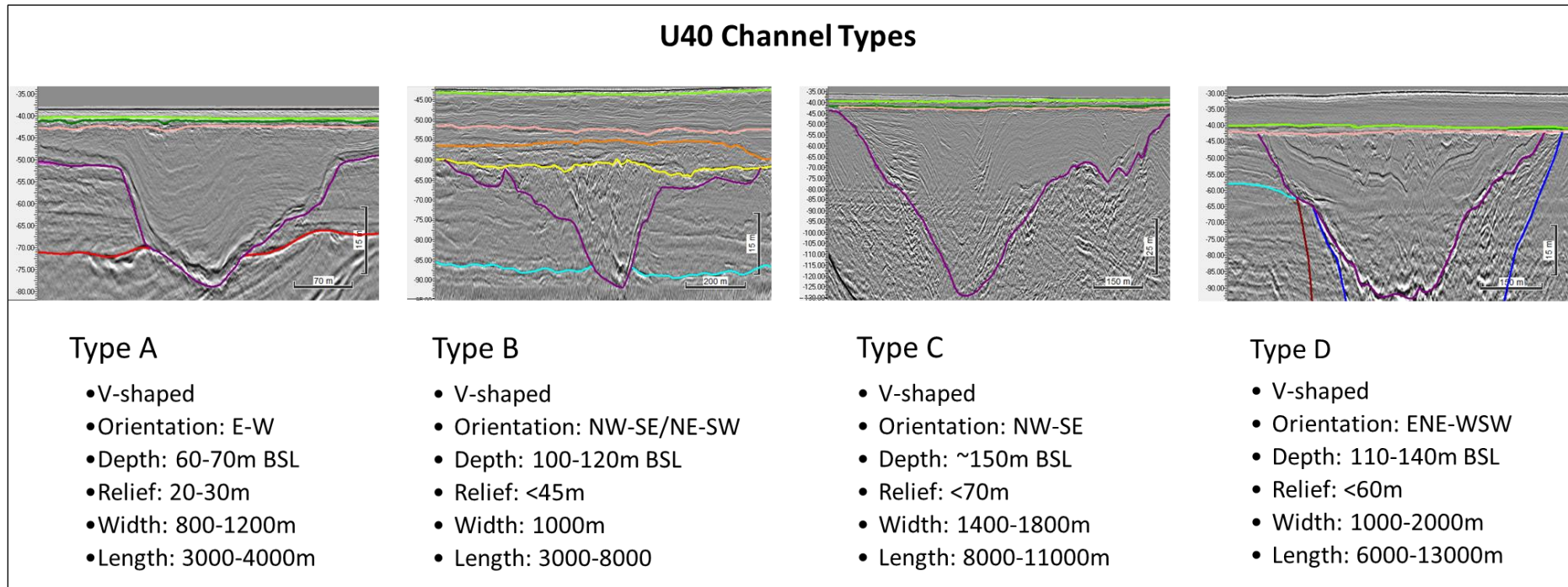


Figure 157. U40 channels subdivision into 4 distinct types.
 The image also shows the main morphological characteristics of the 4 types.
 Seismic profiles shown in detail in Figure 158 to Figure 161.

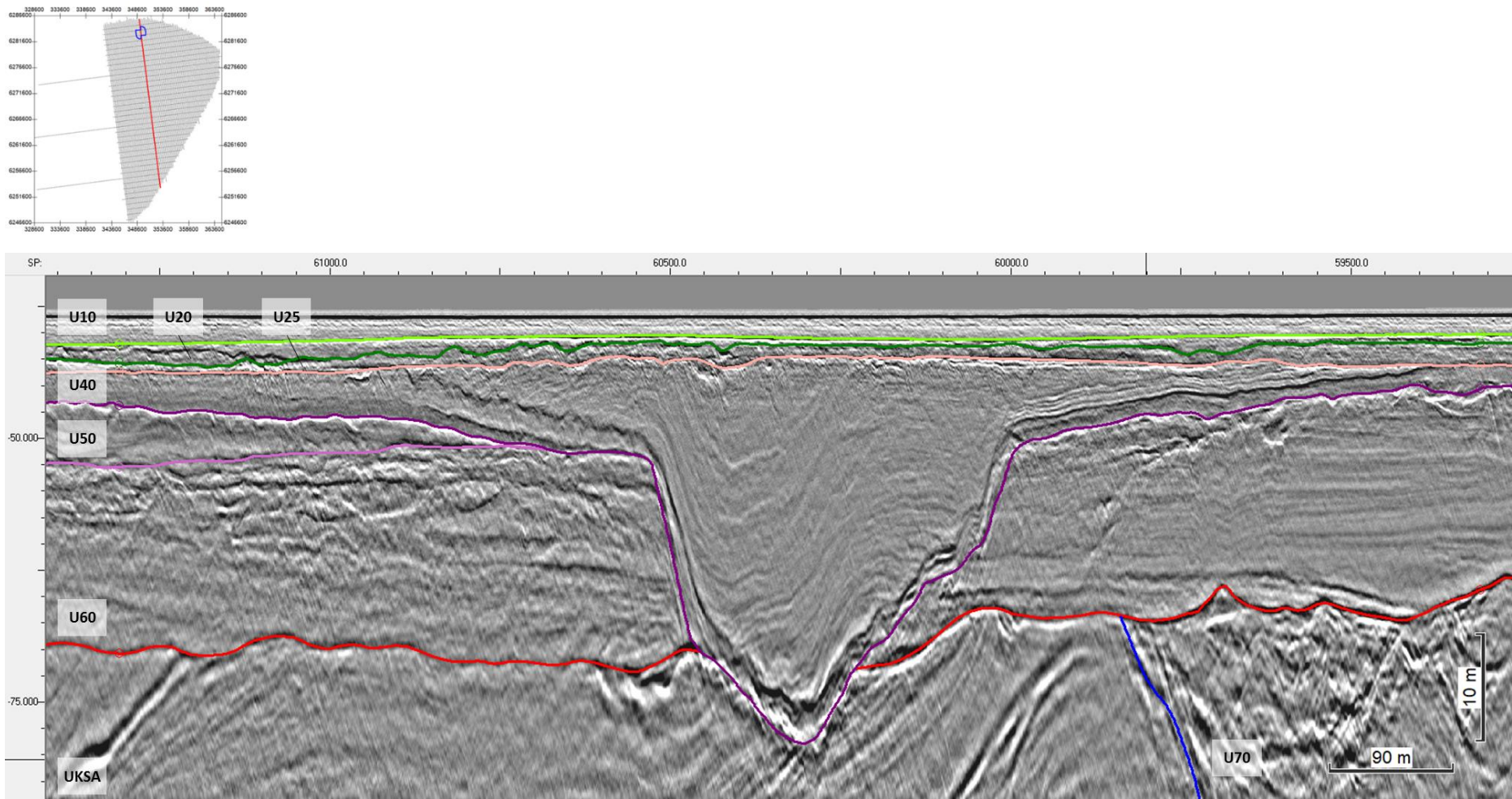


Figure 158 General facies of Type A channels of Seismic Unit U40.
The image also shows the character of horizon H40 (deep magenta). Seismic profile BM3_OWF_E_2D_06930. Example shown: H40_CH_13.

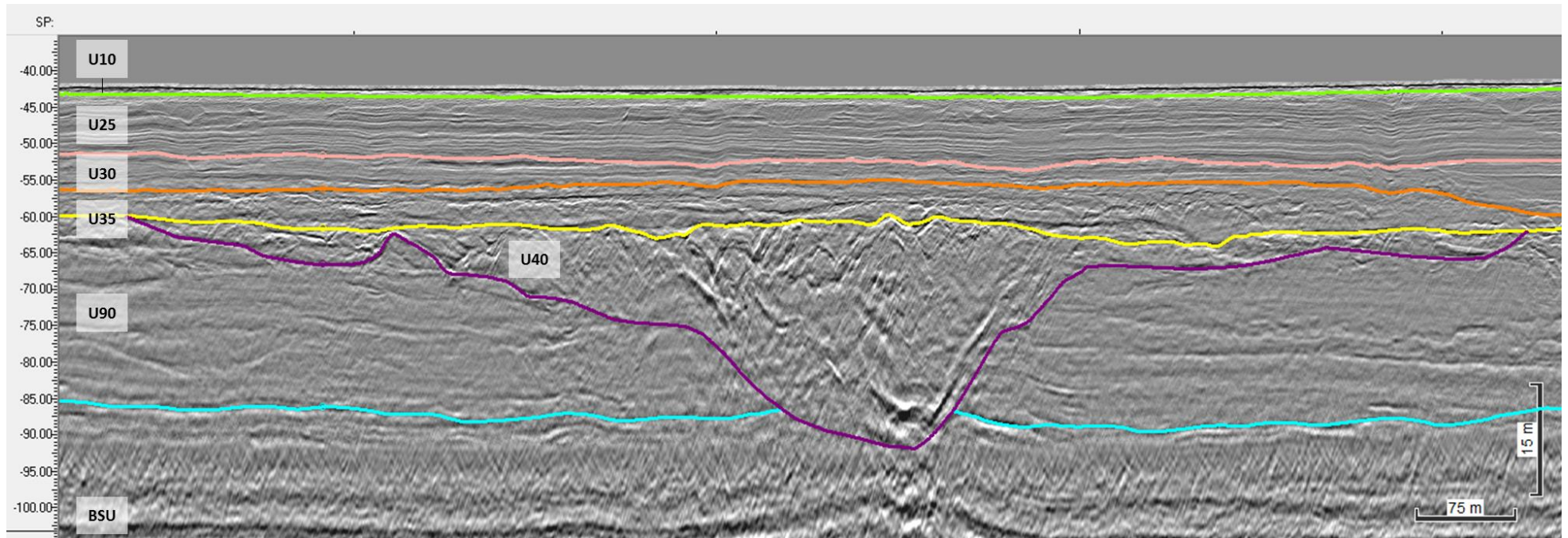
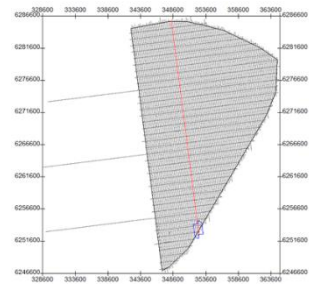


Figure 159 General facies of Type B channels of Seismic Unit U40.
The image also shows the character of horizon H40 (deep magenta). Seismic profile BM3_OWF_2D_06300. Example shown: H40_CH_08.

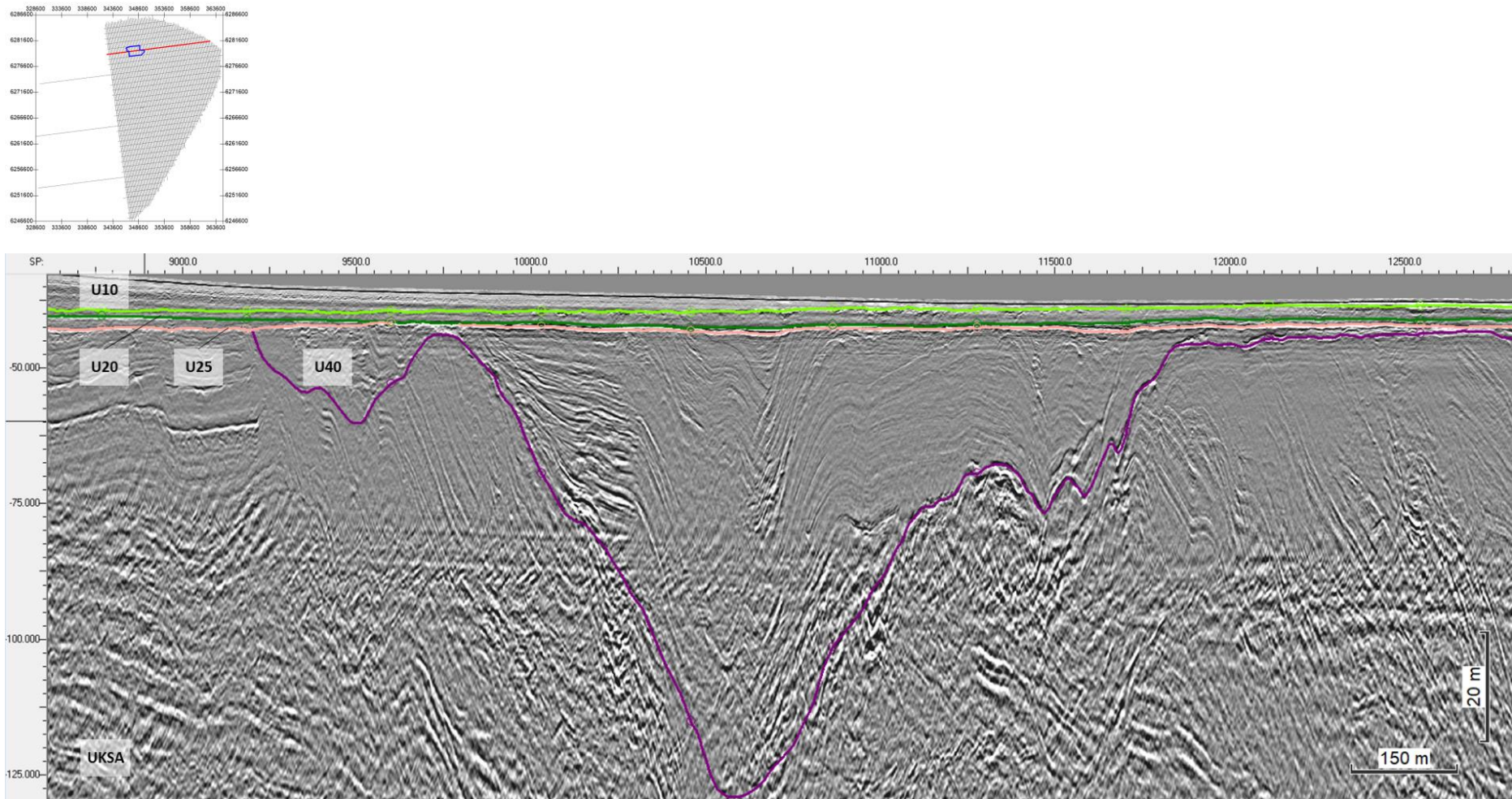


Figure 160 General facies of Type C channels of Seismic Unit U40.
The image also shows the character of horizon H40 (deep magenta). Seismic profile BX1_OWF_E_XL_06000. Example shown: H40_CH_01.

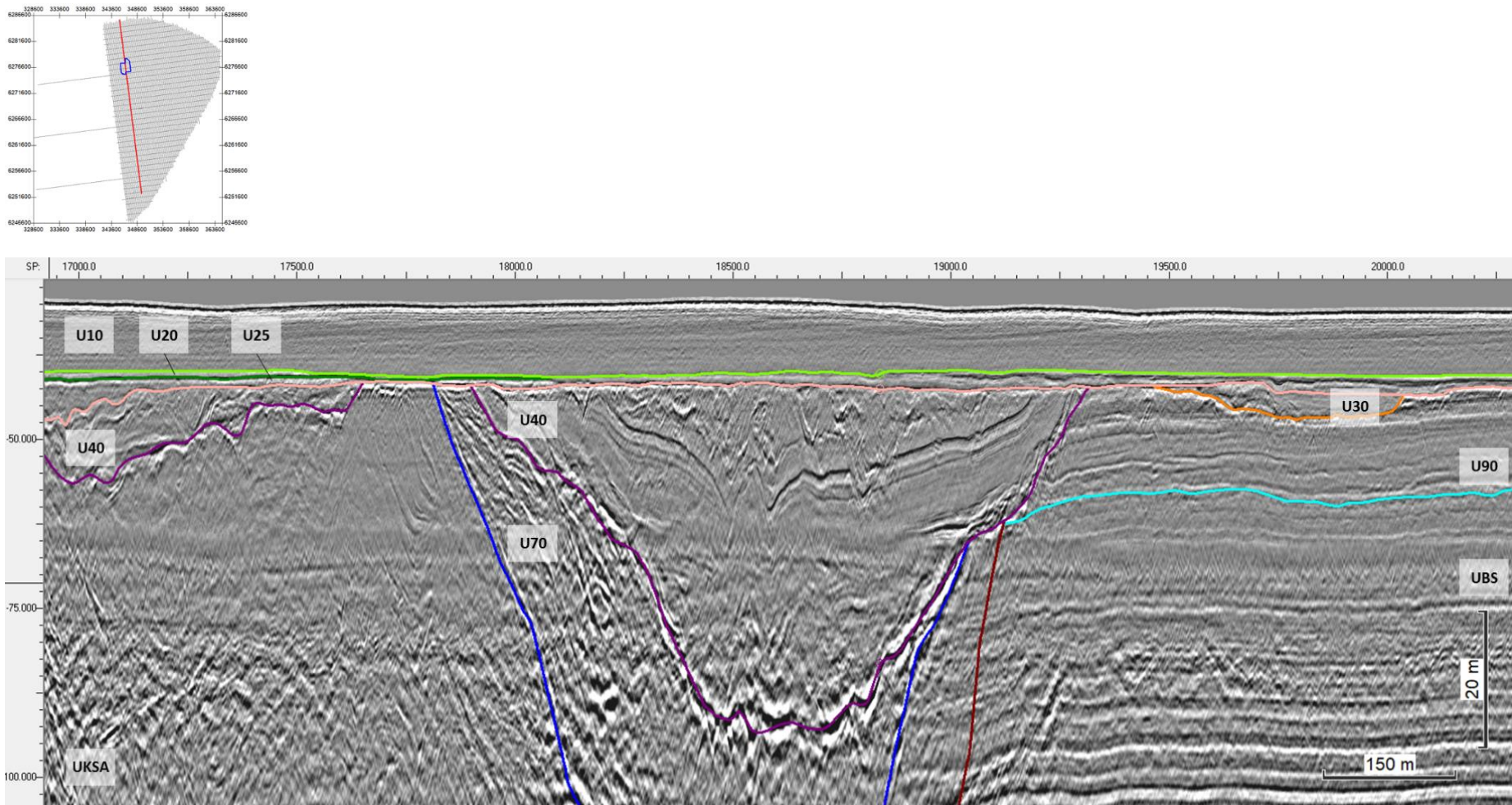


Figure 161 General facies of Type D channels of Seismic Unit U40.
The image also shows the character of horizon H40 (deep magenta). Seismic profile BM2_OWF_E_2D_03150. Example shown: H40_CH_02.

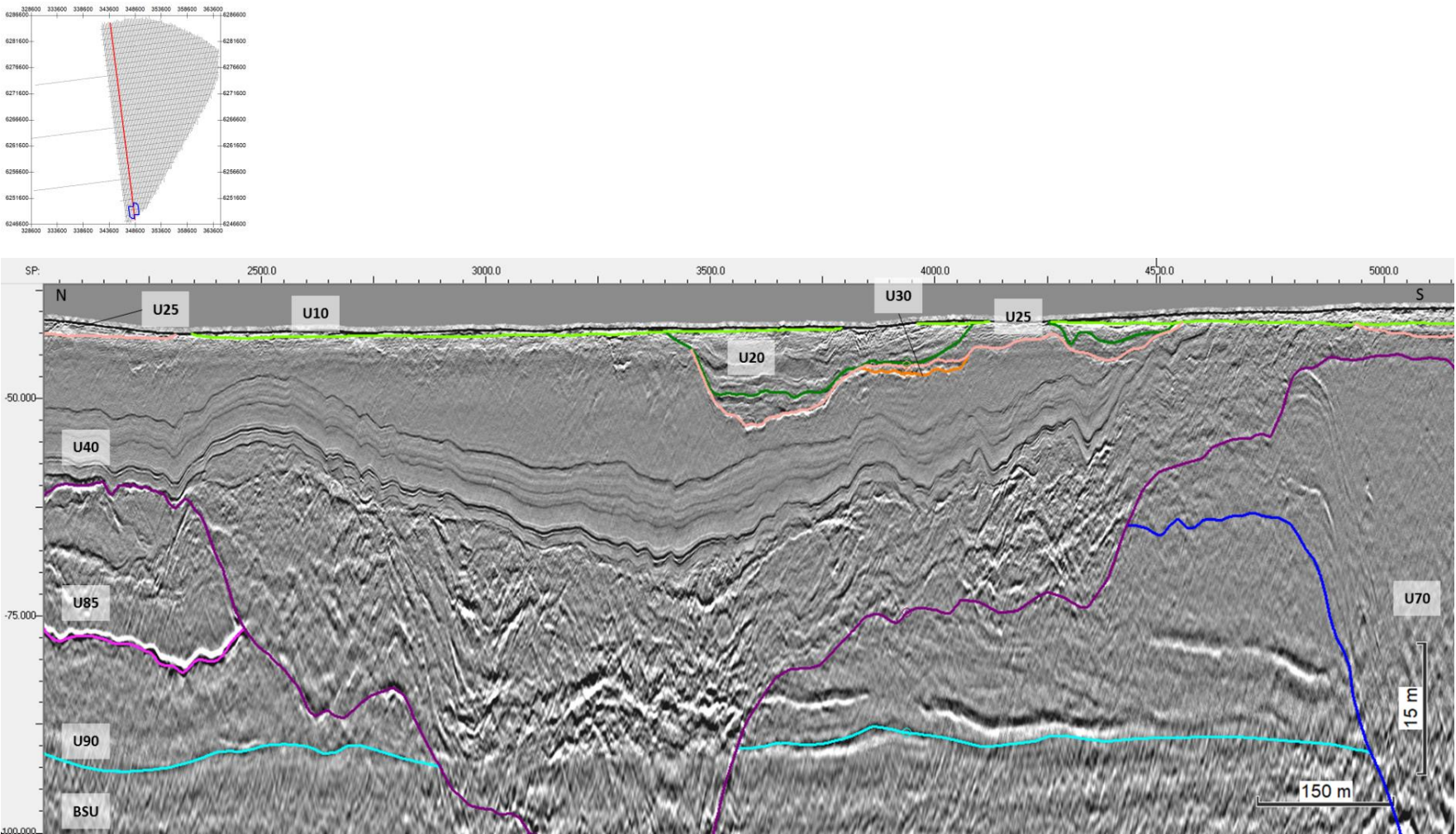


Figure 162 Interpreted glaciolacustrine deposits on the upper levels of Seismic Unit U40.
Seismic profile BM1_OWF_E_2D_01680.

8.6.8 | SEISMIC UNIT U50

Seismic unit U50 only occurs within the north sector of the site. The base of Seismic Unit U50 is defined by horizon H50 and is present discontinuously within the survey area. The spatial distribution, vertical reference to MSL and the seabed, and thickness of the unit are presented in Figure 163, Figure 164, and Figure 165.

Horizon H50 ranges in depth between 38.0 m and 65.6 m below MSL (Figure 163), and between 0 m and 25.8 m depth below the seabed (Figure 164). Horizon H50 traces an uneven, undulating surface that truncates the deposits below it (Figure 166). H50 was mapped along a reflector of medium to high positive amplitude.

Seismic unit U50 has a tabular morphology, usually 4 m to 6 m thick. The thickest deposits of U50 are located within a deeper depression near the NNE limit of survey, reaching up to 17.8 m thick (Figure 165). The thinner packages occur in areas where U50 is truncated by U40 and U20.

The seismic facies of U50 have two distinct characters. In the NE region of the north sector, delineated by the polygon U50_TransparentFacies, U50 has very uniform facies of low to transparent amplitude (Figure 167). Internal layering is faint, but is slightly more pronounced at the base, where a thin set of parallel reflectors have a slightly higher amplitude. These internal reflectors follow the same geometry as the base H50. Scattered anomalies of positive amplitude (hyperbolae) are frequently observed, becoming more common towards the top (Figure 167).

The remaining deposits of U50 (towards W) also have a generally low amplitude facies, but are internally more complex (Figure 168). At the base often sits a set of parallel reflectors, followed by more chaotic facies above, with common oblique, opposite-dipping geometries. Locally channels and transparent deposits are observed.

U50 deposits are interpreted to comprise fine sediments. Scattered point diffractors within U50 may be related to the presence of boulders. The origin of seismic unit U50 is uncertain, as it may correspond to a glacial drift deposit (aqua till?) or be associated to glaciolacustrine deposition (?).

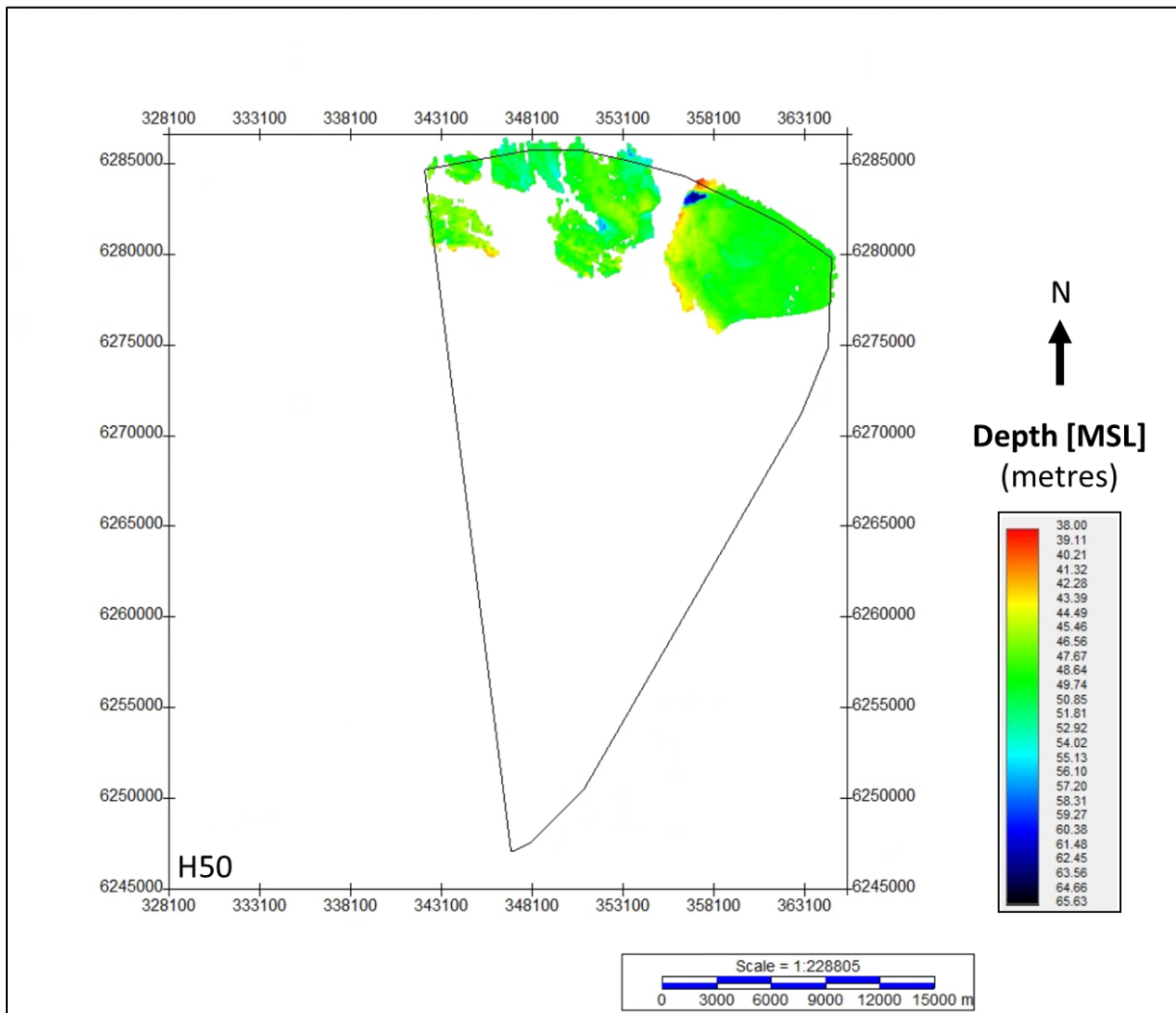


Figure 163 Map showing the lateral extent of U50.
Units in metres below MSL.

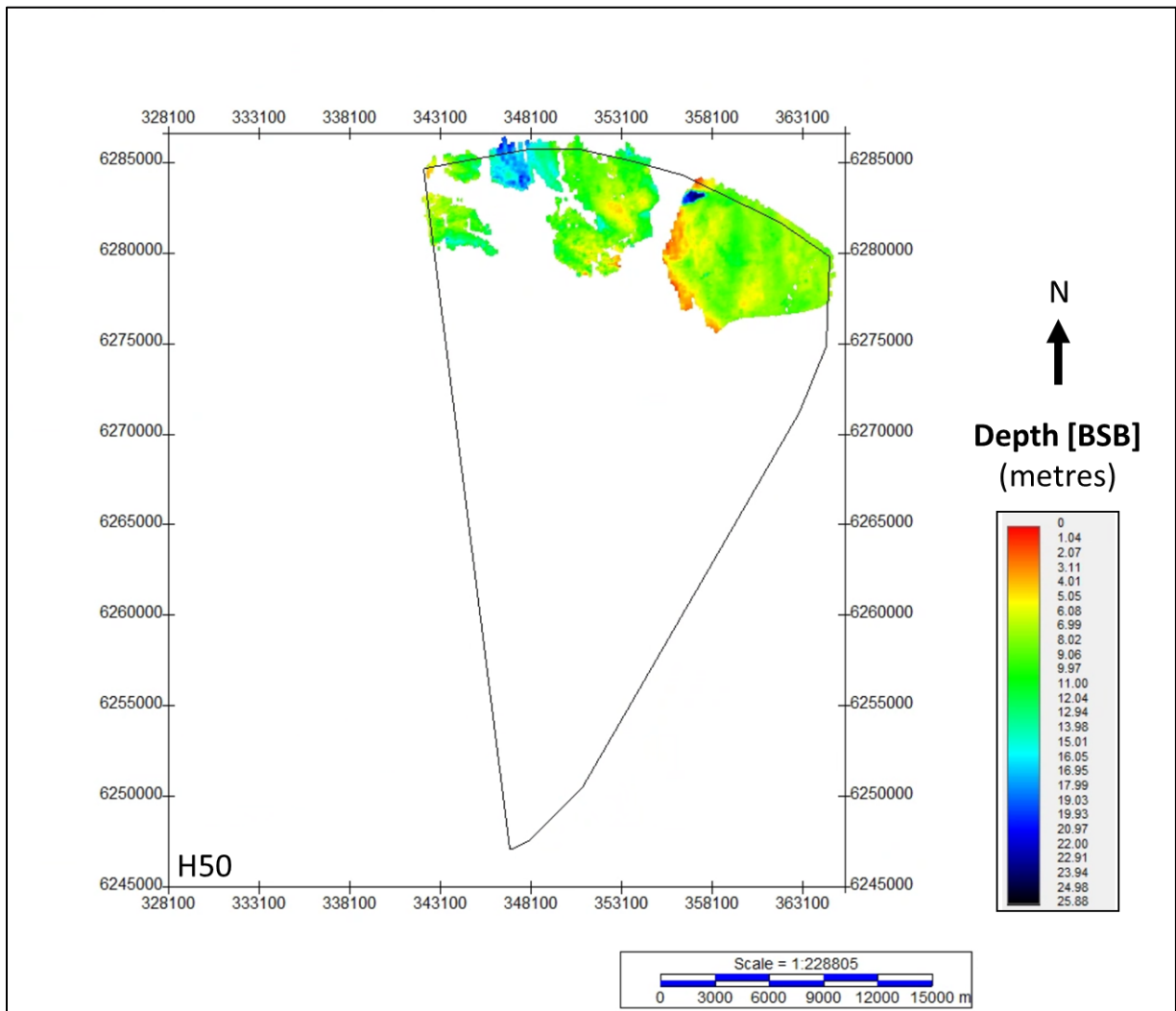


Figure 164 Depth below seabed of H50.
Units in metres below seabed.

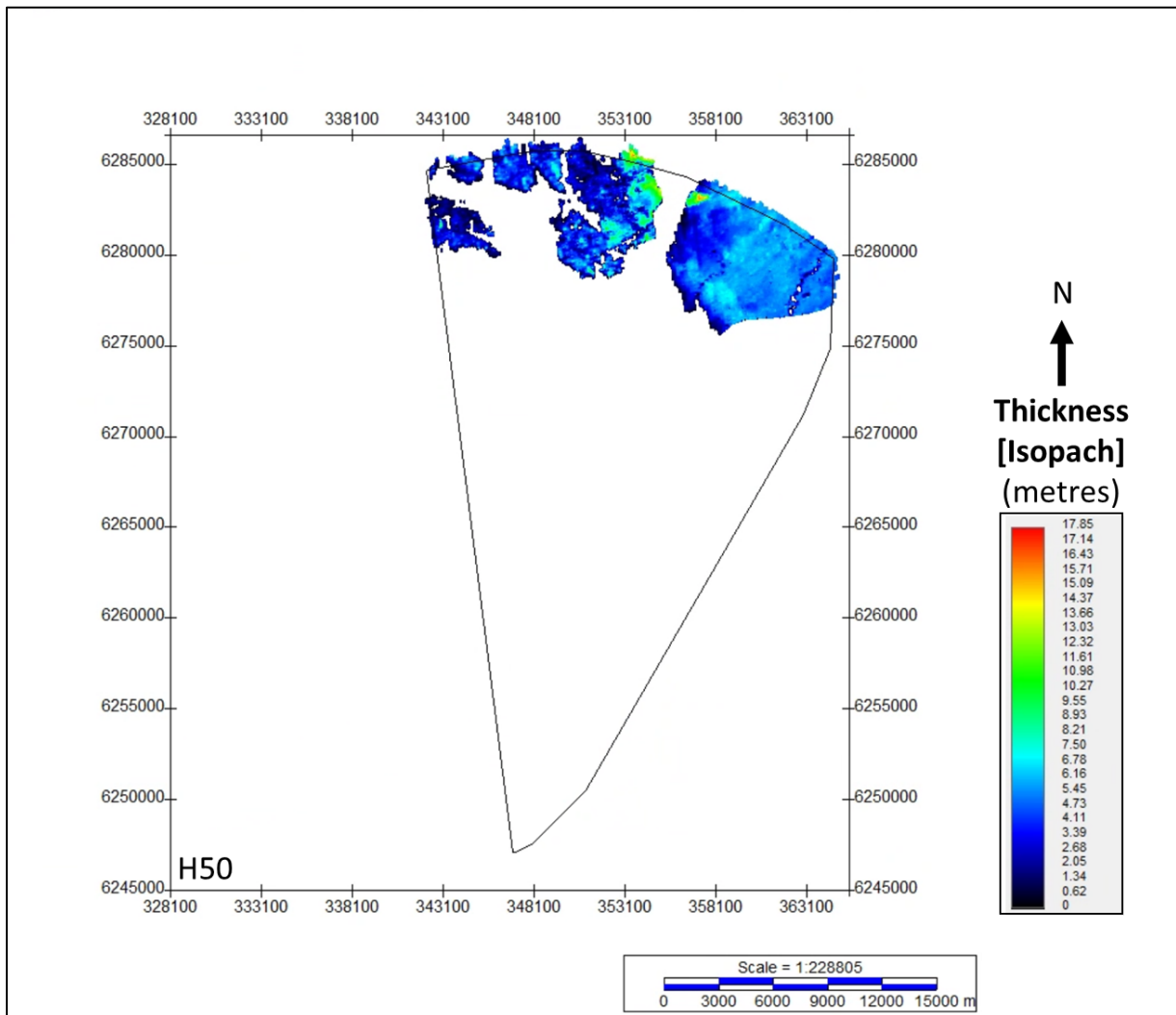


Figure 165 Thickness of unit U50.
Units in metres.

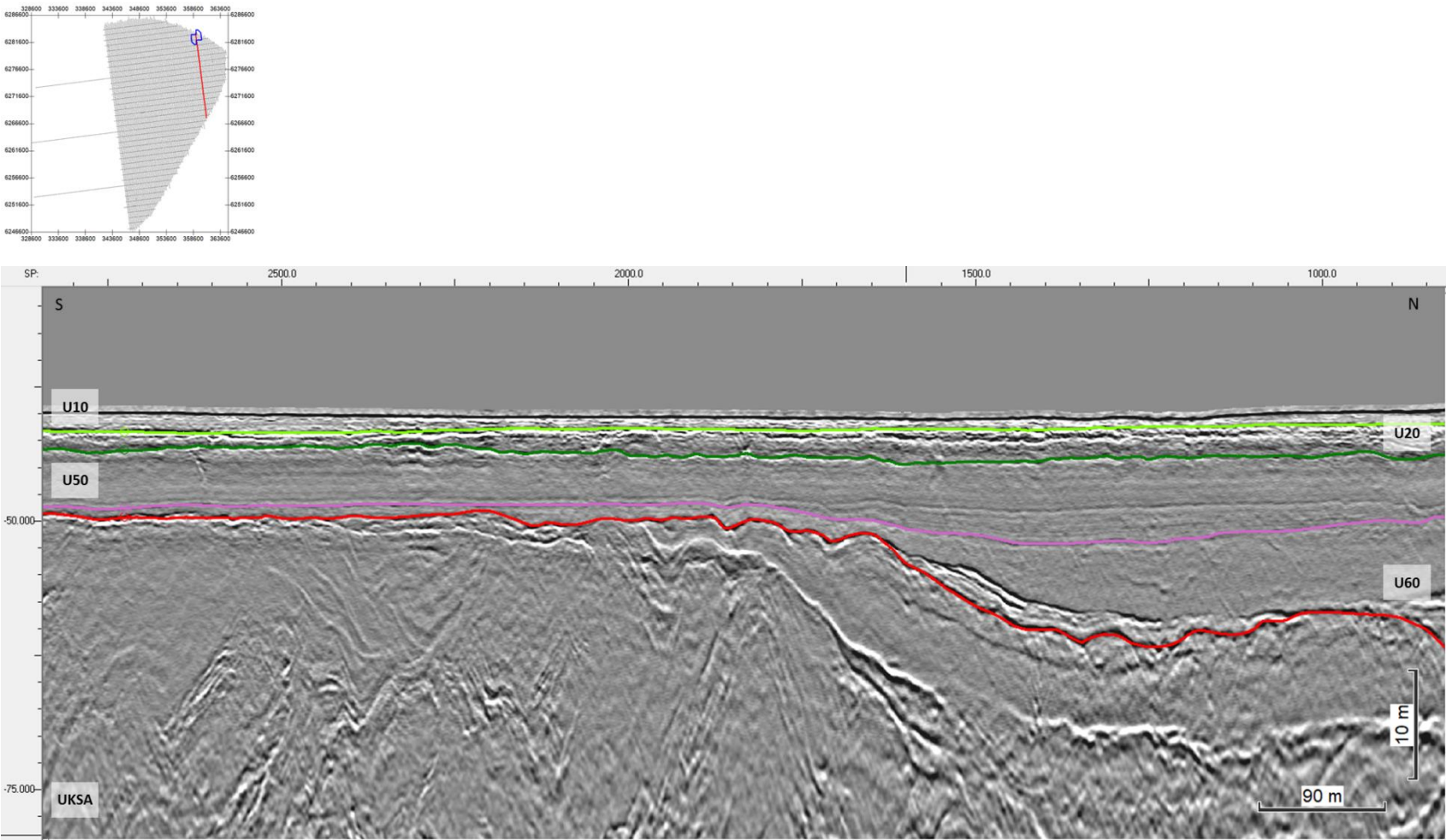


Figure 166 Transparent facies of Seismic Unit U50 in the NE region of the site.
The image also shows the character of horizon H50 (medium orchid). Seismic profile BM5_OWF_E_2D_16590

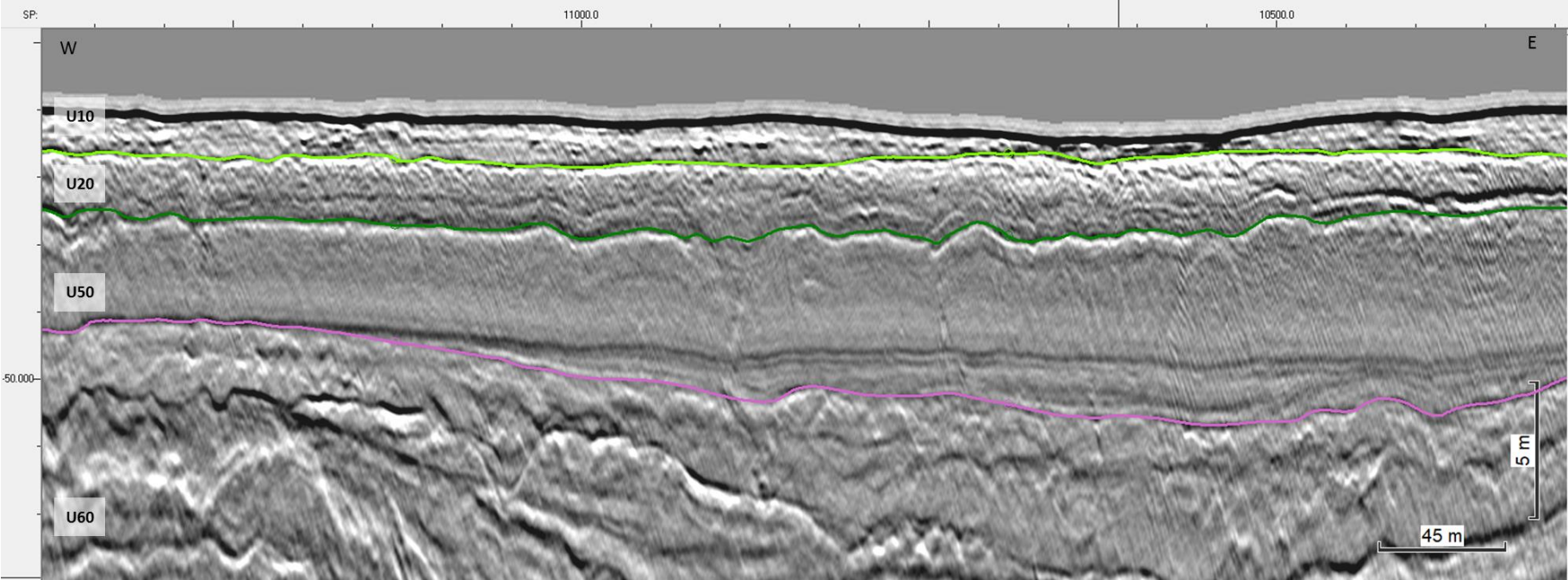
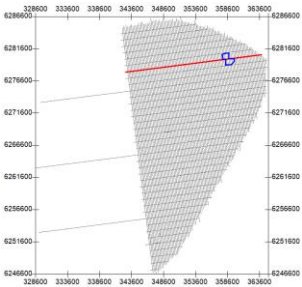


Figure 167 Layering at the base of Seismic Unit U50, and the character of horizon H50
H50 is shown in medium orchid. Seismic profile BX1_OWF_E_XL_07000

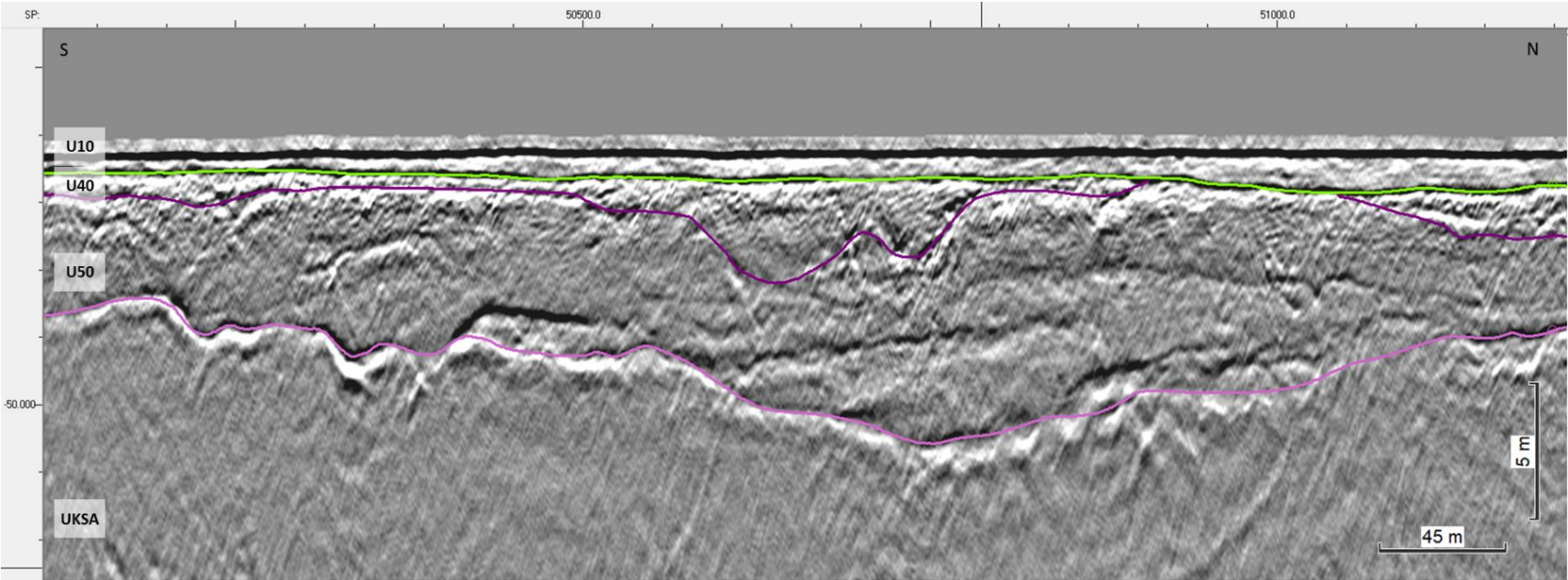
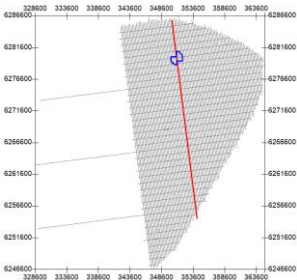


Figure 168 Facies of Seismic Unit U50 towards NW of the site, and the character of horizon H50. H50 is shown in medium orchid. Seismic profile BM3_OWF_E_2D_08190

8.6.9 | SEISMIC UNIT U60

Seismic unit U60 occurs within the north and south sectors of the survey area. The base of Seismic Unit U60 is defined by horizon H60 and is present discontinuously within the survey area. The spatial distribution, vertical reference to MSL and the seabed, and thickness of the unit are presented in Figure 169, Figure 170, and Figure 171.

Horizon H60 ranges in depth between 37.7 m and 114.2 m below MSL (Figure 169), and between <0.5 m and 76.0 m depth below the seabed (Figure 170). Horizon H60 traces an uneven, rugose, undulating surface of pronounced relief (up to 56 m vertical range), truncating the units below it (Figure 173). H60 follows a positive reflector of high amplitude.

Seismic unit U60 is generally a thick (10-20 m) unit of sub-horizontal tabular to mega-lens shape, thickening at localized incisions of variable size (up to 55.5 m thick) (Figure 171). These incisions form channelized areas with a symmetrical to asymmetrical V-shape, with heights ranging from <5 m to ~35 m depth (Figure 173). The larger incisions are delimited by polygons H60_CH_01 to 04 (Figure 172).

Seismic unit U60 is recognizable in the UHRS dataset by its composite facies of low to high amplitude reflectors (Figure 174). U60 comprises complex internal features of meso-scale proportions, such as mounds, channels, and lenses. There are numerous oblique internal erosional surfaces separating these features, marked by high amplitude reflectors. Large clinoform layers fill-in the larger incisions. In general, the thickness of the internal packages decreases towards the top, becoming more sub-horizontal and sub-parallel.

Seismic unit U60 sediments are interpreted to have been deposited in a high energy setting. The infill within the wide valleys are mega-bedforms (lenses measuring 3-600 m wide and 8 m thick), interpreted to be high energy fluvial bedforms (related to flash floods?), evidenced by the meso-scale seismic facies association, the numerous internal erosional surfaces, and more complex geometries. Horizon H60 is an unconformity that shaped a pronounced paleo-relief. From the seismic character of U60 and its interpreted depositional system, it is estimated that the sediments are mainly sands with gravel and silt (?).

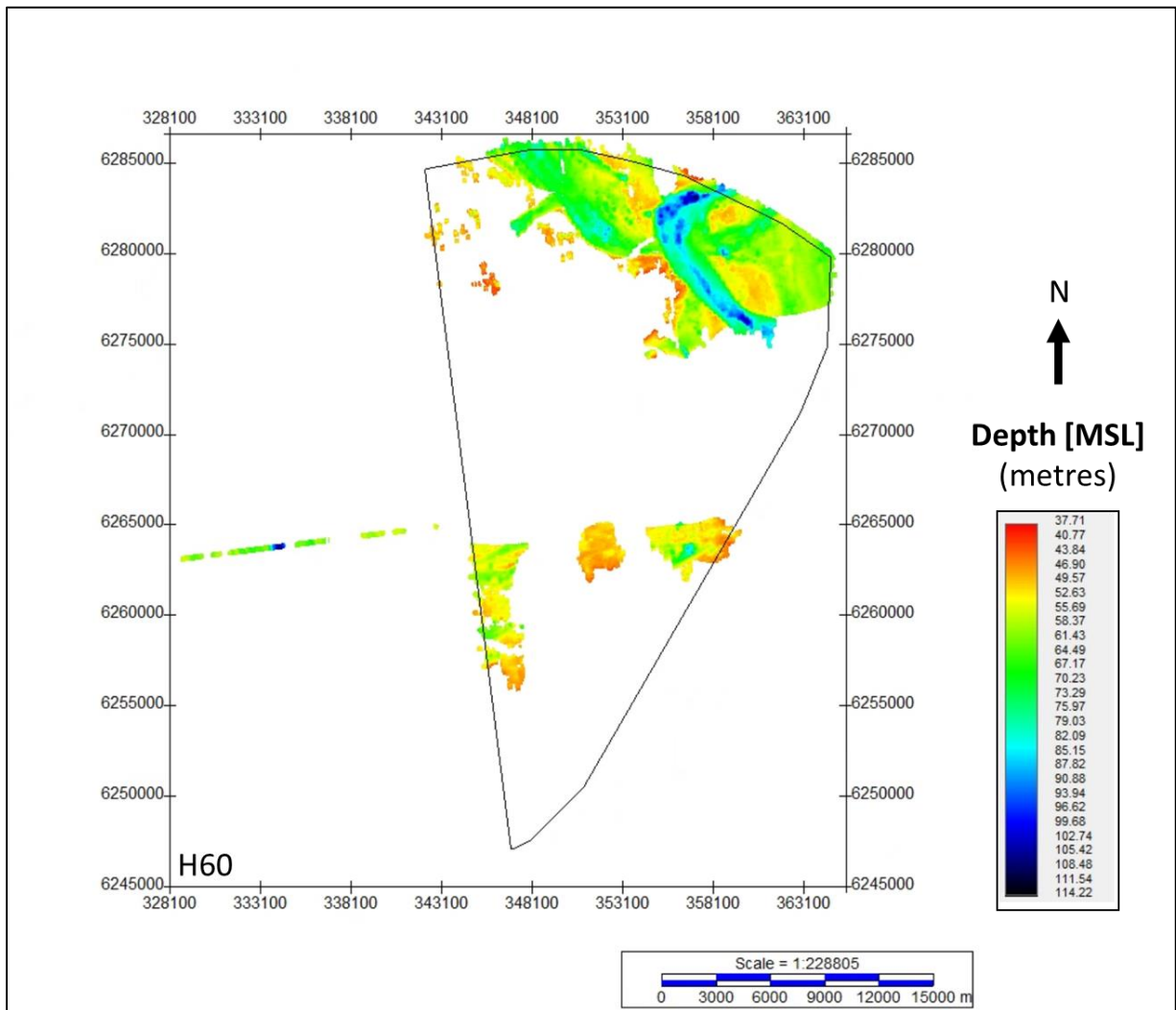


Figure 169 Map showing the lateral extent of U60.
Units in metres below MSL.

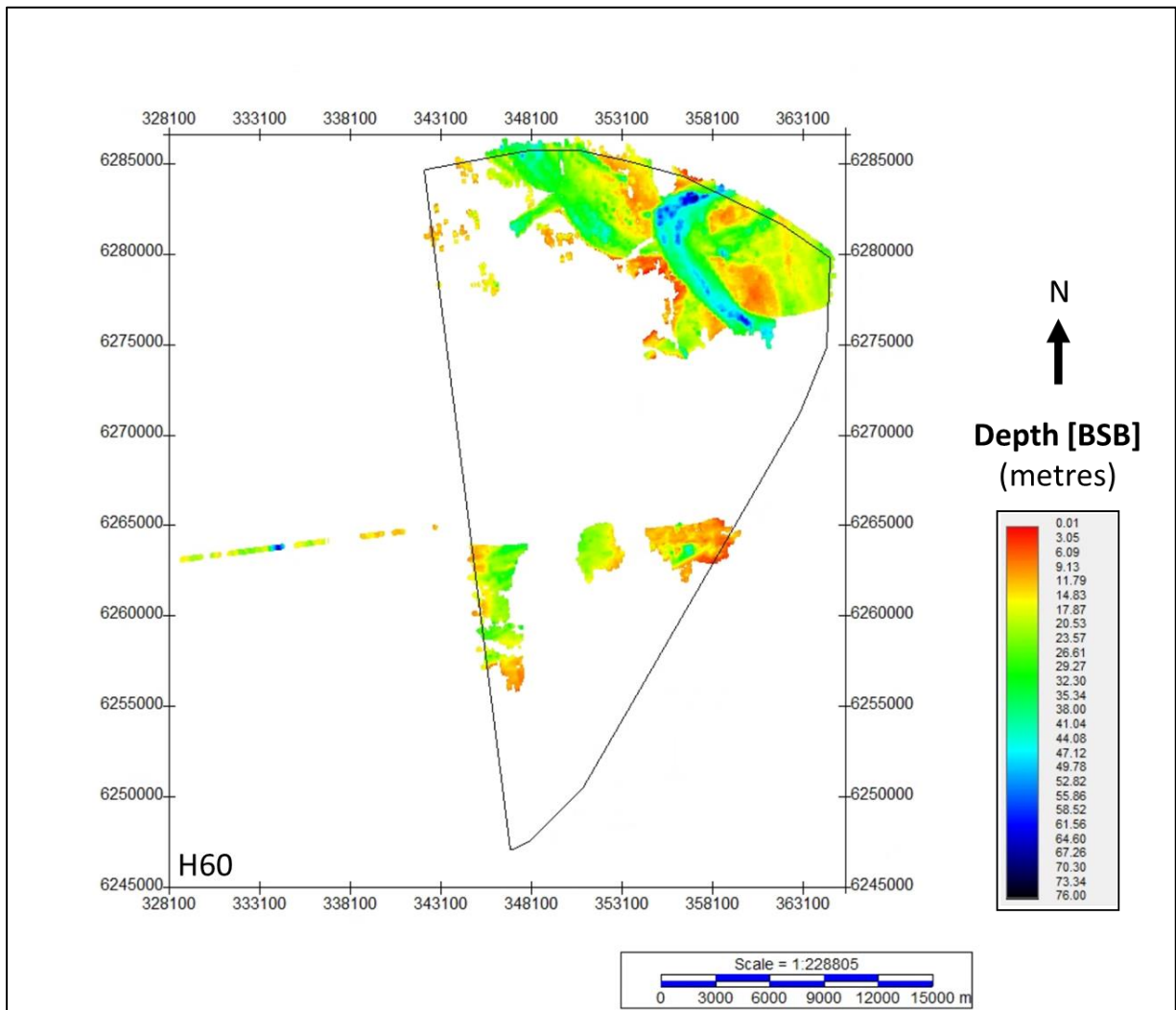


Figure 170 Depth below seabed of H60.
Units in metres below seabed.

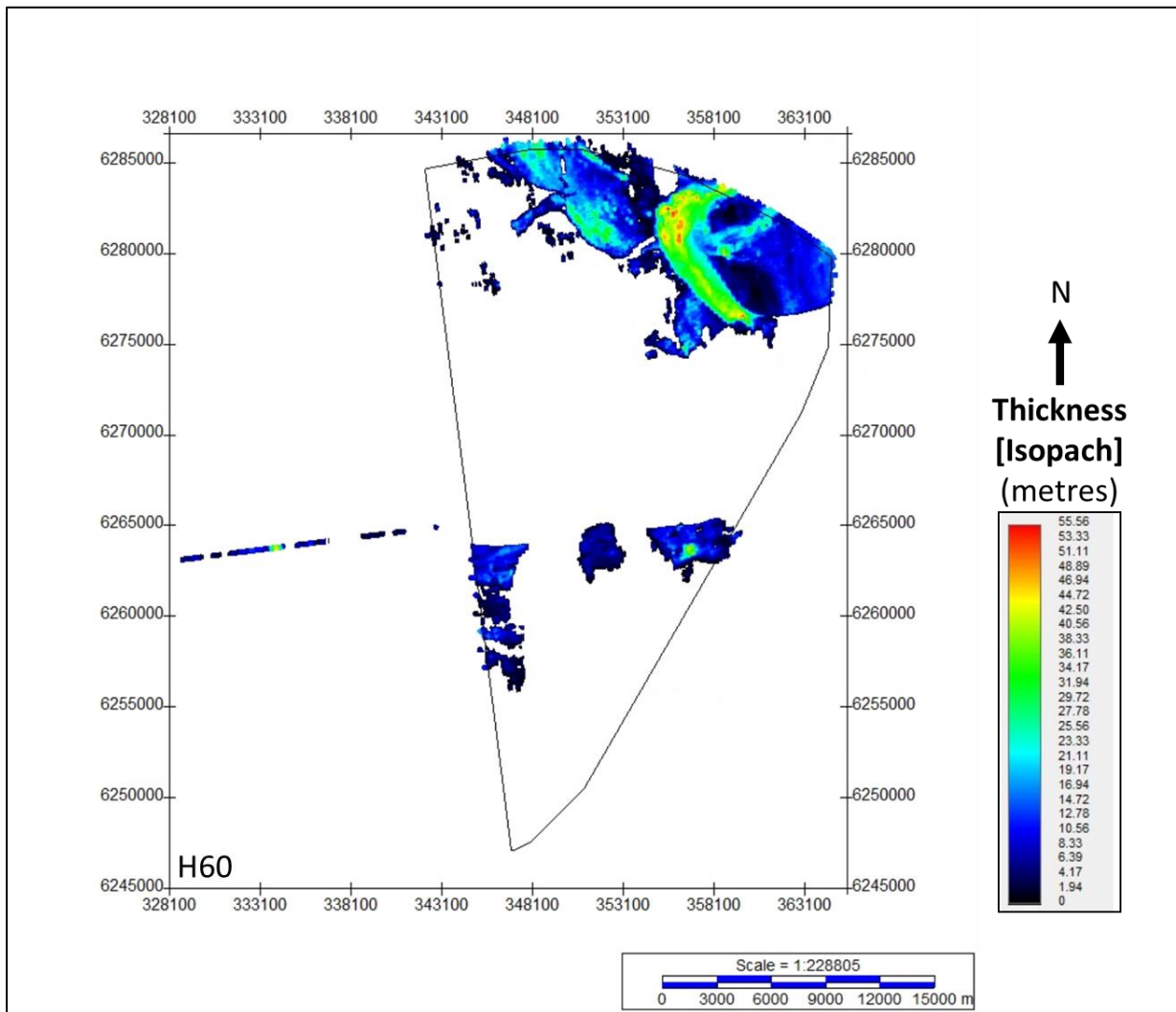


Figure 171 Thickness of unit U60.
 Units in metres.

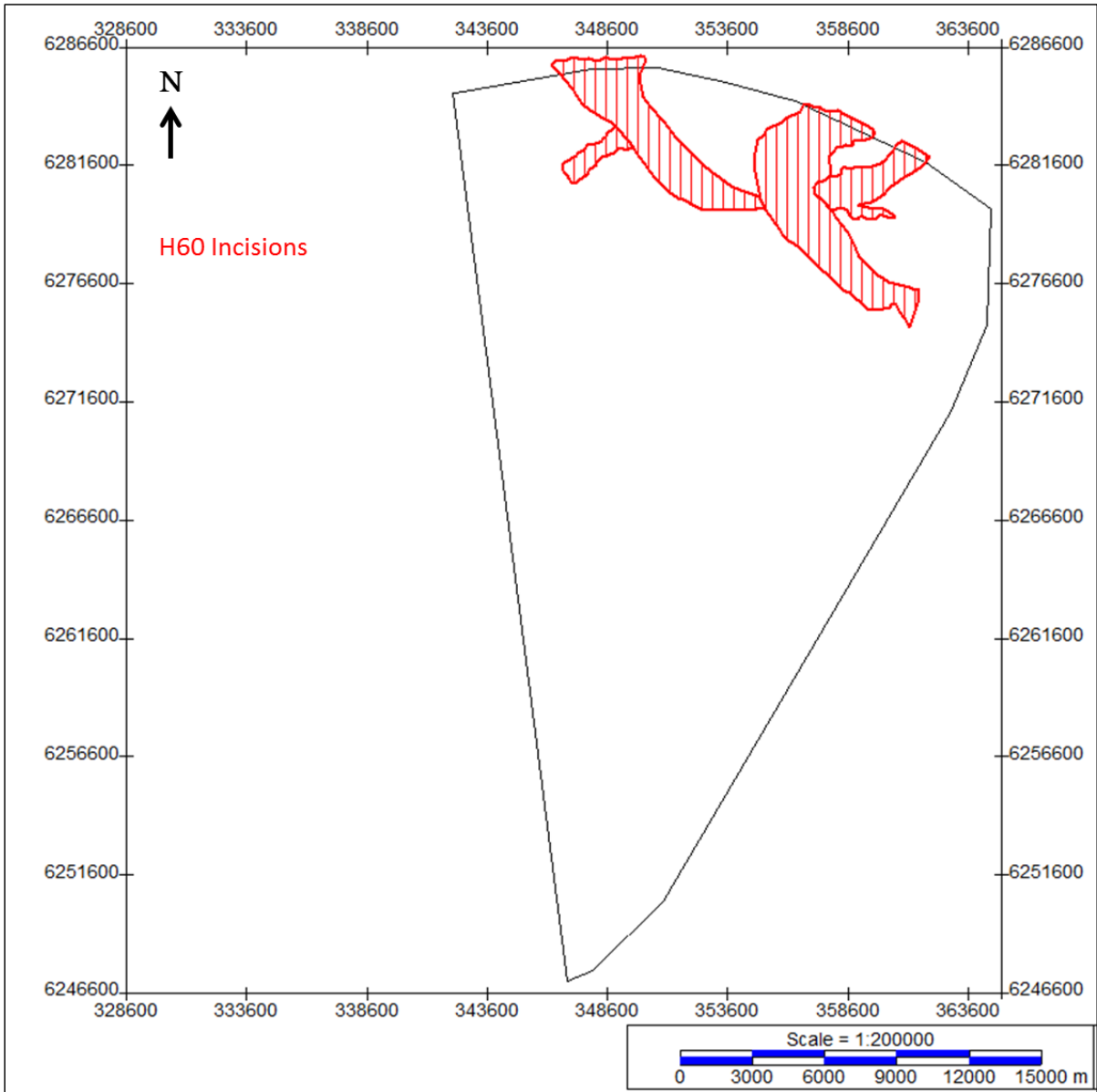


Figure 172 Spatial distribution of the major incisions identified for Seismic Unit U60.

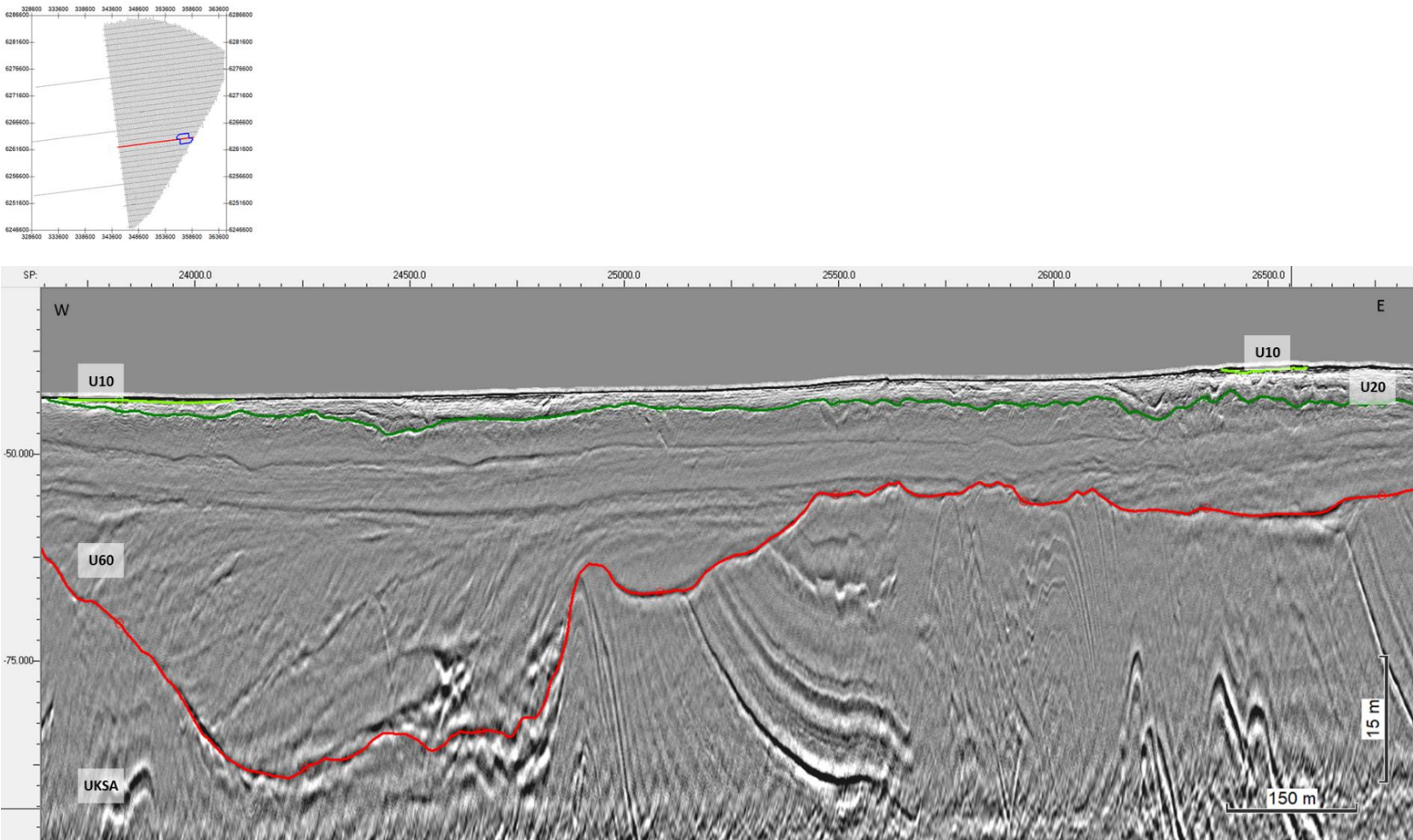


Figure 173 General facies of Seismic Unit U60, and the character of horizon H60. H60 is shown in red. Seismic profile BX3_OWF_E_XL_23000

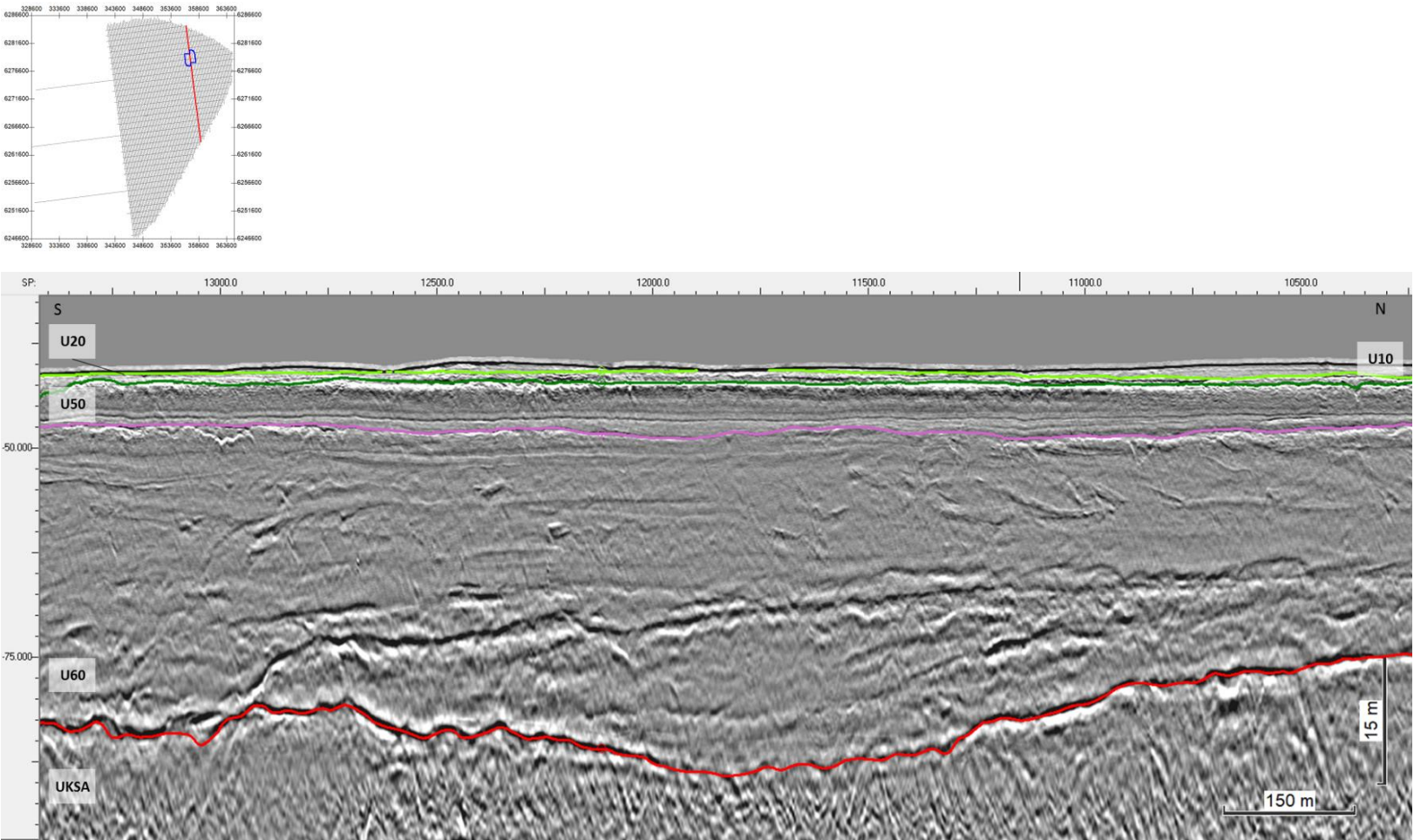


Figure 174 General facies of Seismic Unit U60, and the character of horizon H60. H60 is shown in red. Seismic profile BM5_OWF_E_2D_14070

8.6.10 | SEISMIC UNIT U70

Seismic unit U70 is a major element of the ground model, and extends spatially across the three sectors of the site. The base of Seismic Unit U70 is defined by horizon H70 and is present discontinuously within the survey area. The spatial distribution, vertical reference to MSL and the seabed, and thickness of the unit are presented in Figure 175, Figure 176, and Figure 177.

The main features of seismic unit U70 are large channel incisions delineated at the base by horizon H70. H70 is mapped either along medium-high amplitude reflector or tracing a vertical facies shift, truncating the units below it. H70 is locally undulating. Horizon H70 ranges in depth between 39.9 m and 193.7 m below MSL (Figure 175), and between <0.5 m and 152.8 m depth below the seabed (Figure 176).

The channel incisions of U70 exhibit a wide range of sizes, orientations, and internal facies. Nine major incisions were identified and delineated by polygons H70 CH_01 to CH_09 (Figure 178). Their general characteristics are summarised in Table 31.

Table 31 General characteristics of the large incisions within seismic unit U70. Polygons displayed in Figure 178.

Polygon ID	Shape	Orientation	Max Depth (m BSL)	Relief (m)	Width (m)	Length (m)
H70_CH_01	V asymmetric	E-W	130	<75	3500	5000
H70_CH_02	V asymmetric	NE-SW	170	<120	1500	2500
H70_CH_03	U open	NE-SW	190	<145	1500	2500
H70_CH_04	U open	E-W	120	<60	2000	12000
H70_CH_05	U open	E-W	175	<130	2000	11000
H70_CH_06	U open	NE-SW	140	<60	1200	23000
H70_CH_07	U open	NE-SW	170	<100	2500	33000
H70_CH_08	U open	N-S to NE-SW	160	<100	800	12000
H70_CH_09	U	WNW-ESE	170	<100	1200	6000

Incisions CH_01 and CH_02 have an asymmetric V-shaped profile (Figure 179); whereas CH_03 to CH_09 exhibit an open U-shaped base (Figure 180). All incisions exhibit a composite infill that may be partitioned into two facies associations: a lower corresponding to the base deposits; and an upper facies on top, often truncating the latter. Differences are observed between the V-shaped channels and the U-shaped incisions, described below.

The seismic character of the base deposits of CH_01 and CH_02 is characterised by medium to high amplitudes, chaotic-composite mound facies (Figure 179). On top, truncating the base, sits a facies association of composite channel-parallel-oblique of meso-micro scale, and medium to low amplitude.

The remaining seven major incisions (CH_03 to CH_09) exhibit basal facies of medium to high amplitude, with meso-scale mounds-channels-parallel, occasionally chaotic (Figure 181). The upper facies have a truncating base, generally lower amplitudes, and comprises meso-micro composite mounds-channels, parallel-obliques. Chaotic-homogeneous transparent facies are also common in these upper sections.

Most of these incisions rest above older deformed sediments which may be related to glaciotectionism and to the formation of the valley itself (evidenced by collapse structures directly below H70) (Figure 182). The deposits that infill these incisions have composite facies that is generally organised and

layered (albeit chaotic in places), which may be associated to glaci-fluvial deposition, in a proglacial, sub-aerial environment (e.g., reoccupation of tunnel valley depressions by fluvial systems).

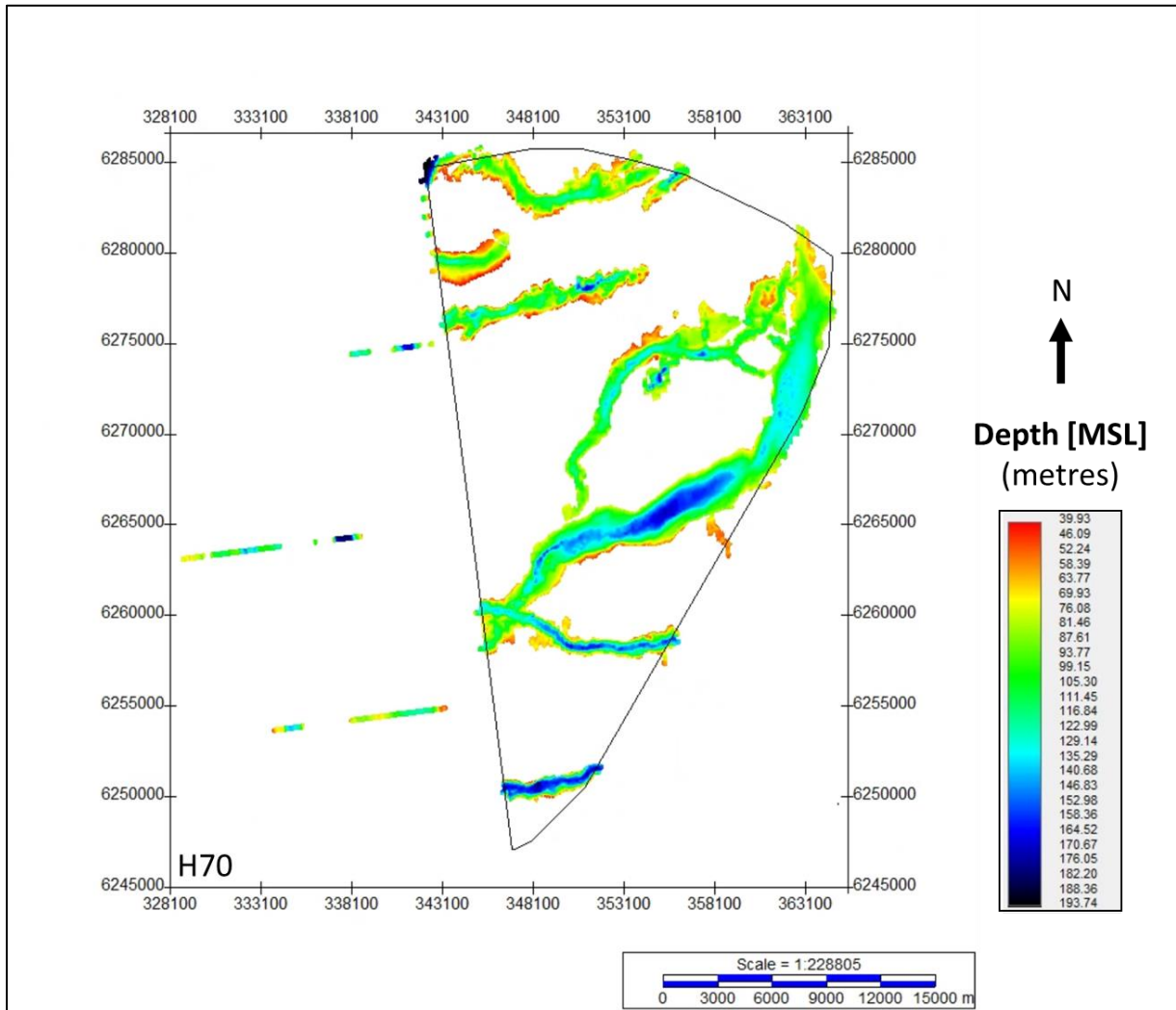


Figure 175 Map showing the lateral extent of U70.
Units in metres below MSL.

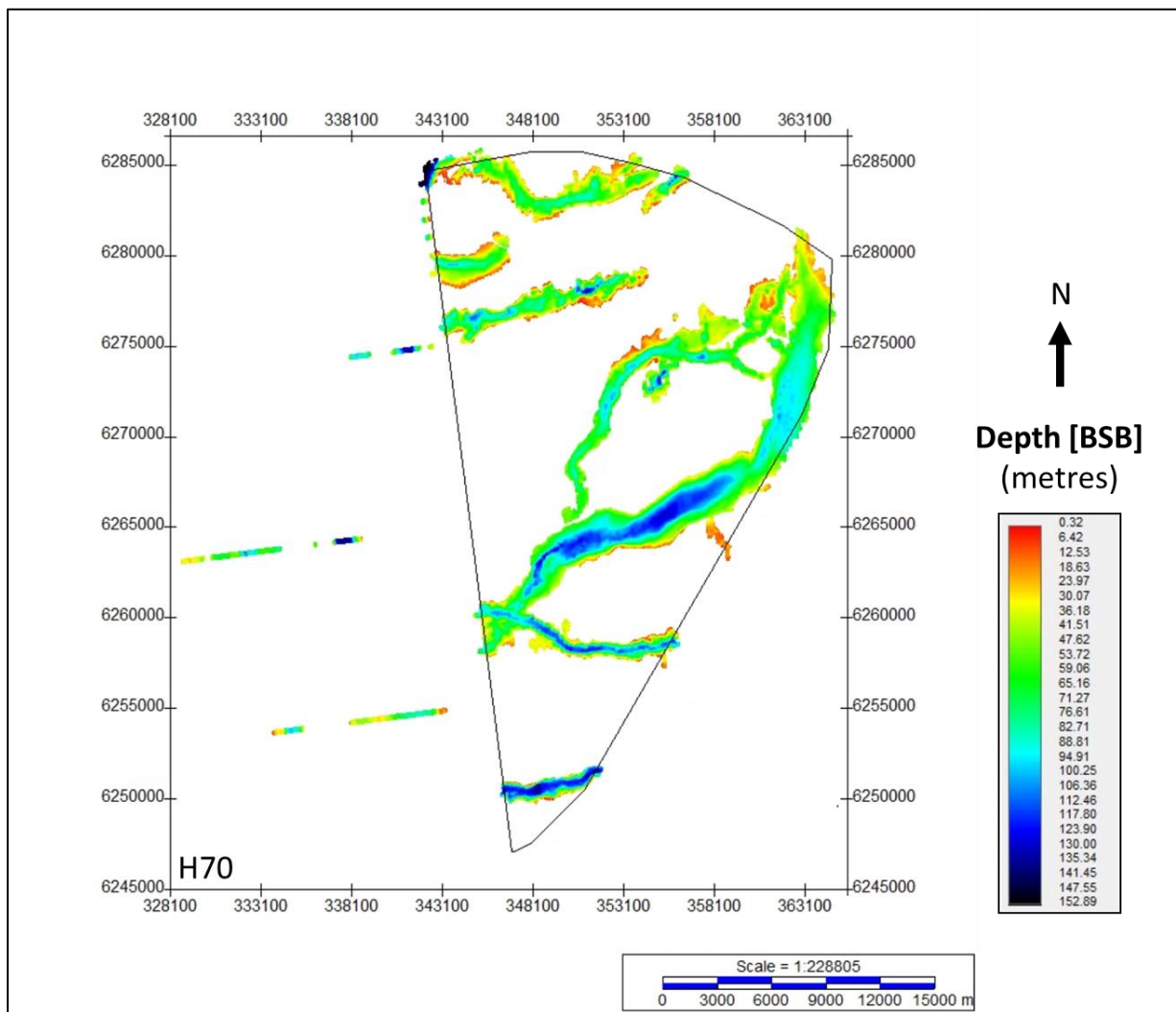


Figure 176 Depth below seabed of H70.
Units in metres below seabed.

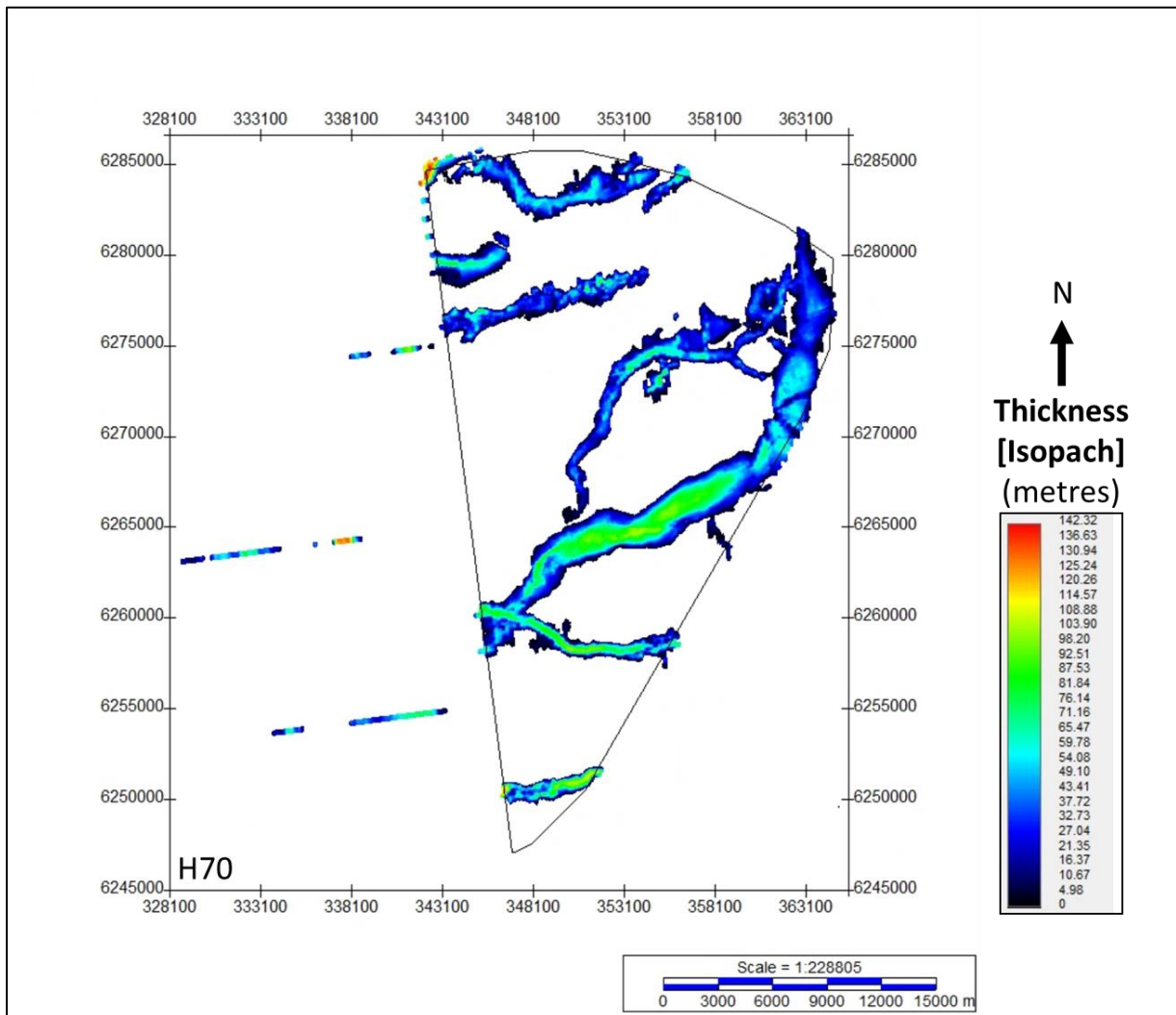


Figure 177 Thickness of unit U70.
 Units in metres.

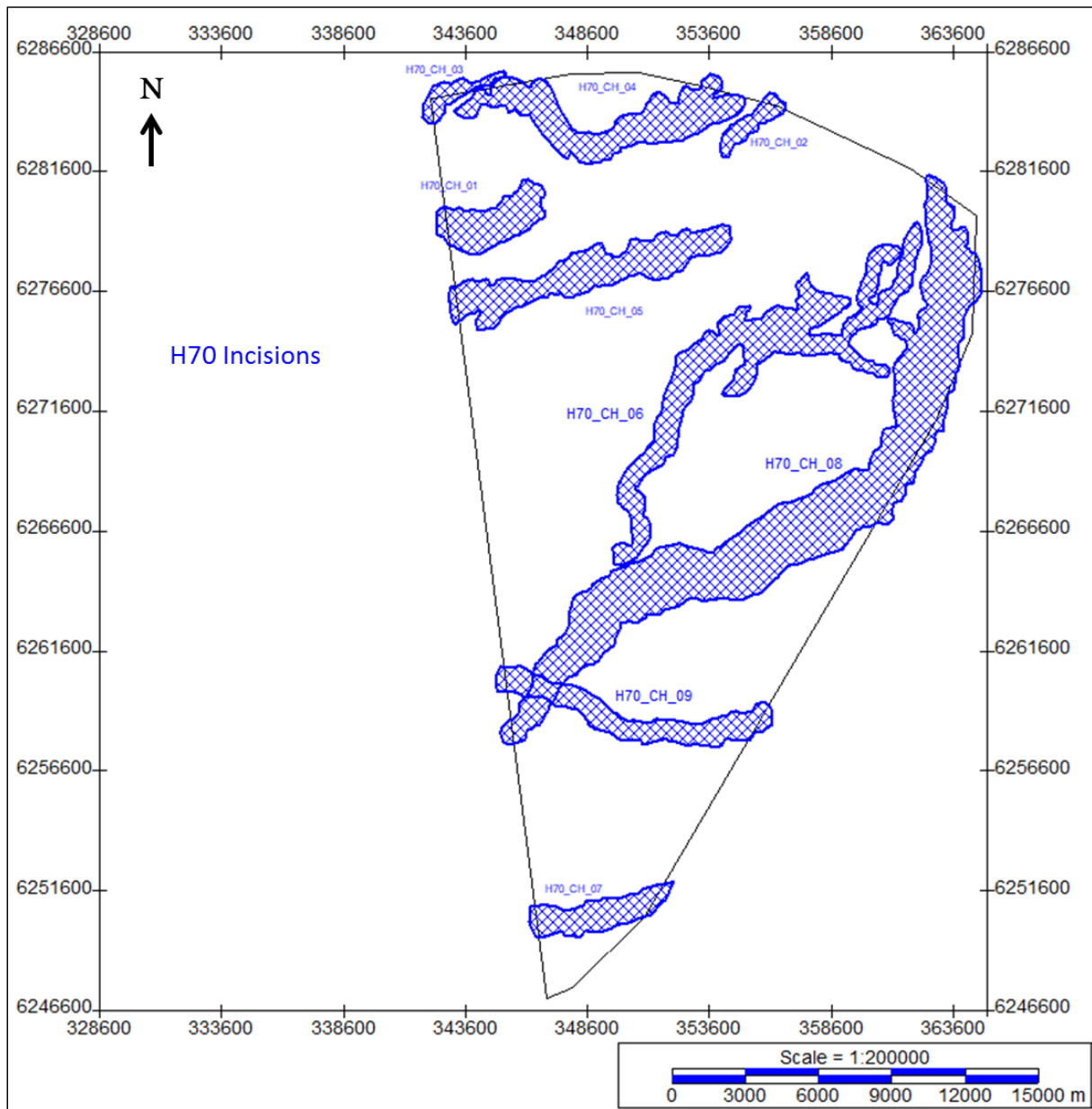


Figure 178 Spatial distribution of the major incisions identified for Seismic Unit U70.

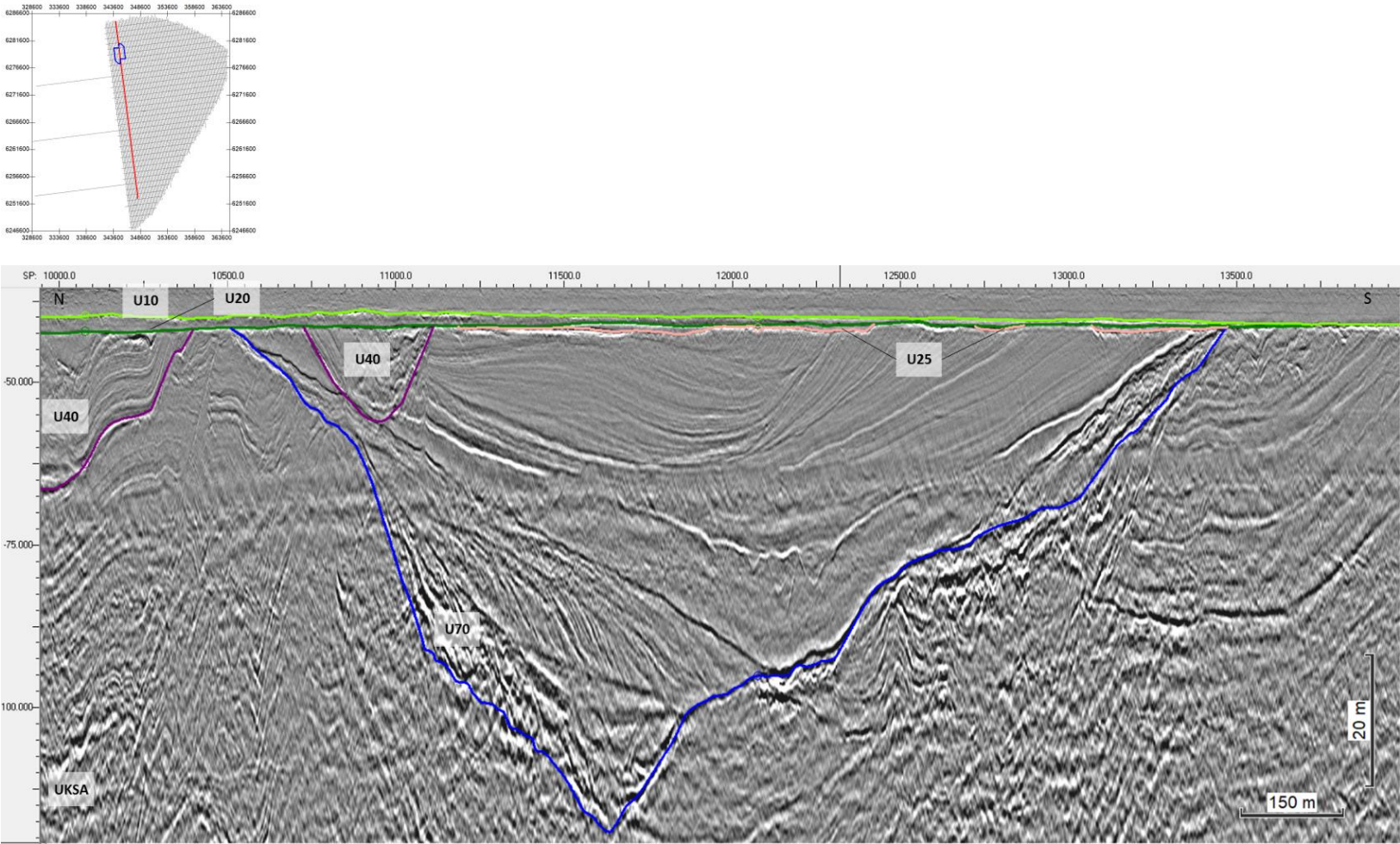


Figure 179 General facies of a V-shaped channel of Seismic Unit U70.
Seismic profile BM1_OWF_E_2D_01890_P2. Example shown: H70_CH_01.

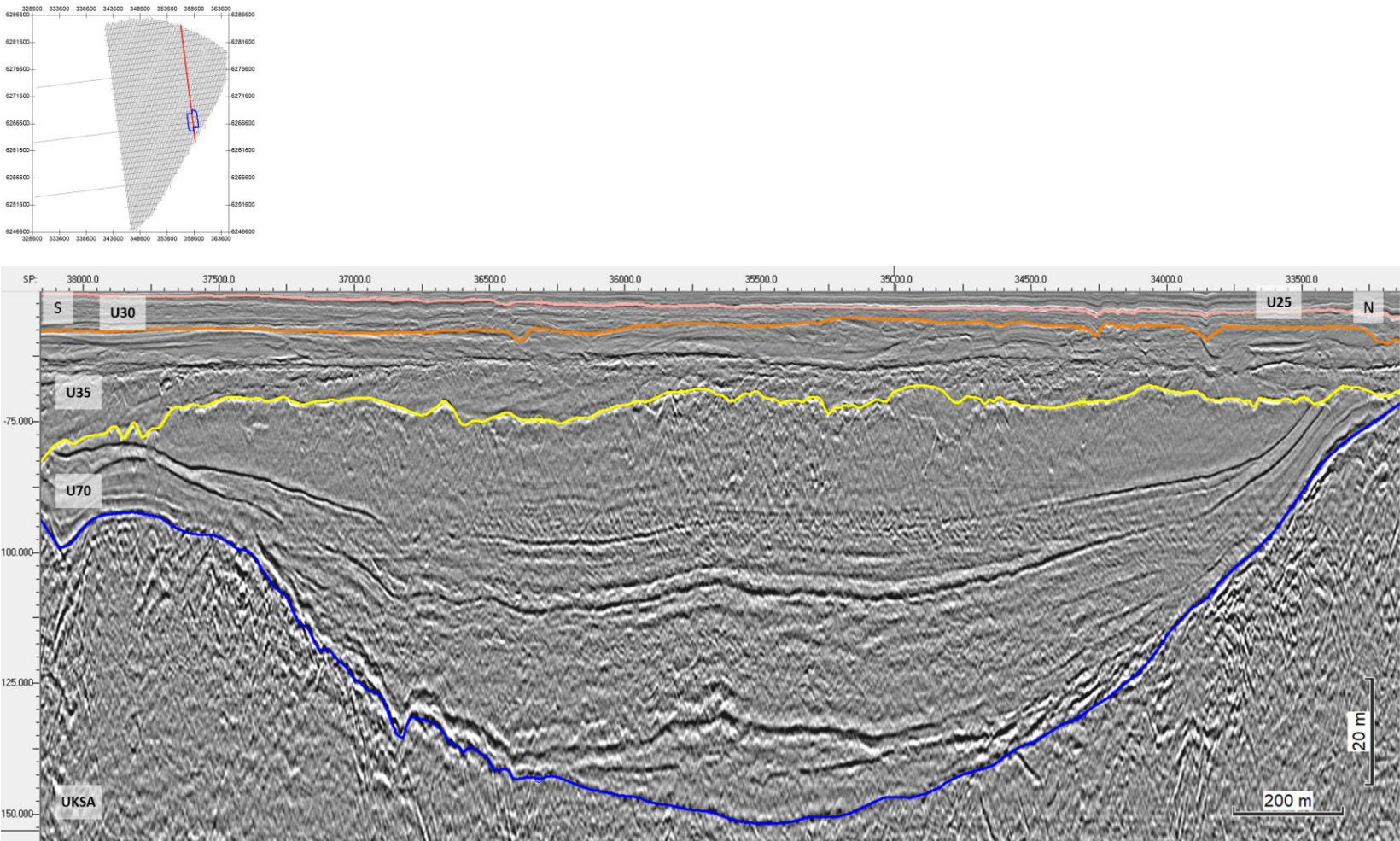


Figure 180 General facies of a U-shaped channel of Seismic Unit U70. Seismic profile BM3_OWF_E_2D_13860. Example shown: H70_CH_08.

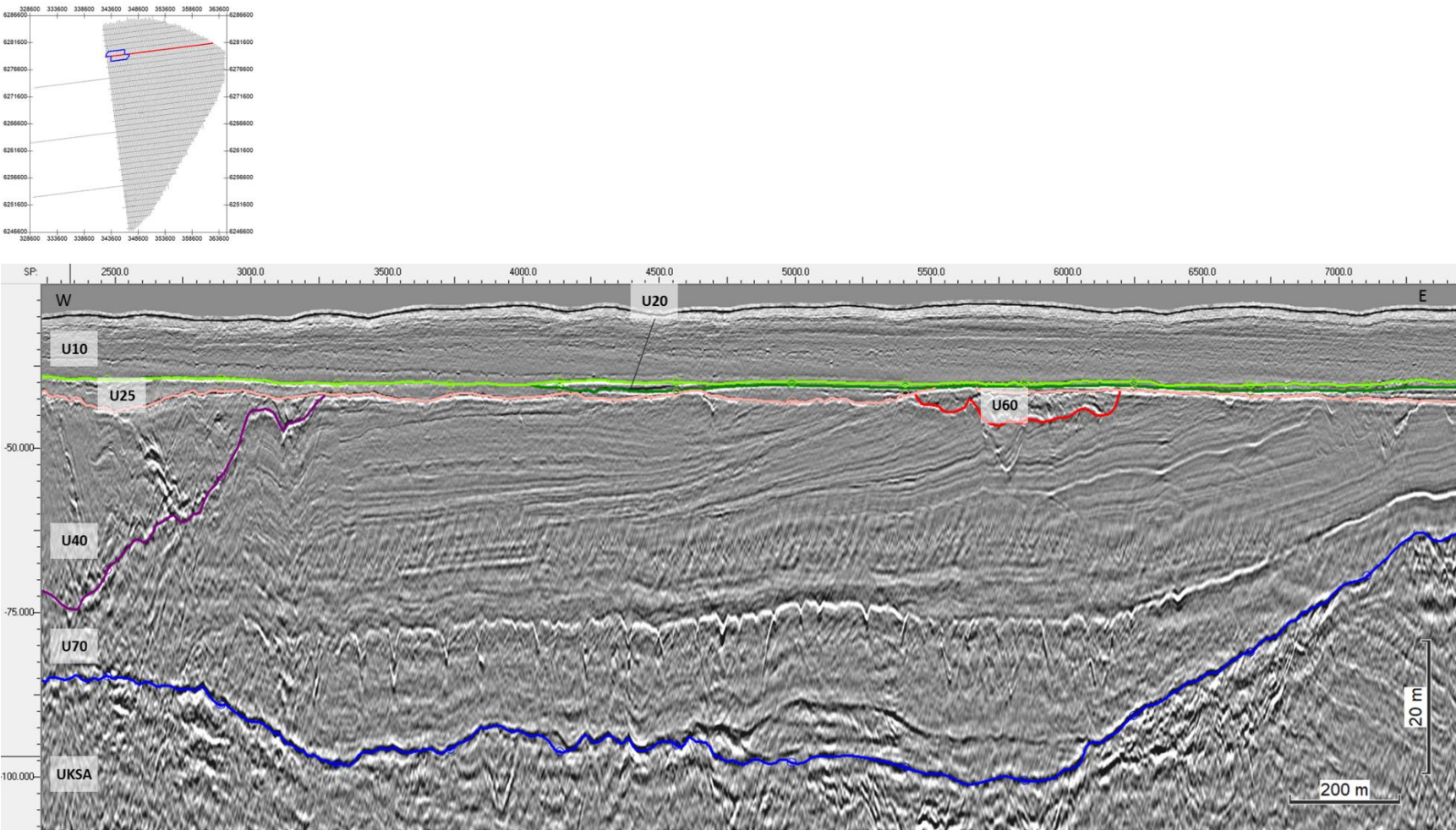


Figure 181 Composite facies in a U70 channel.
Seismic profile BX1_OWF_E_XL_06000

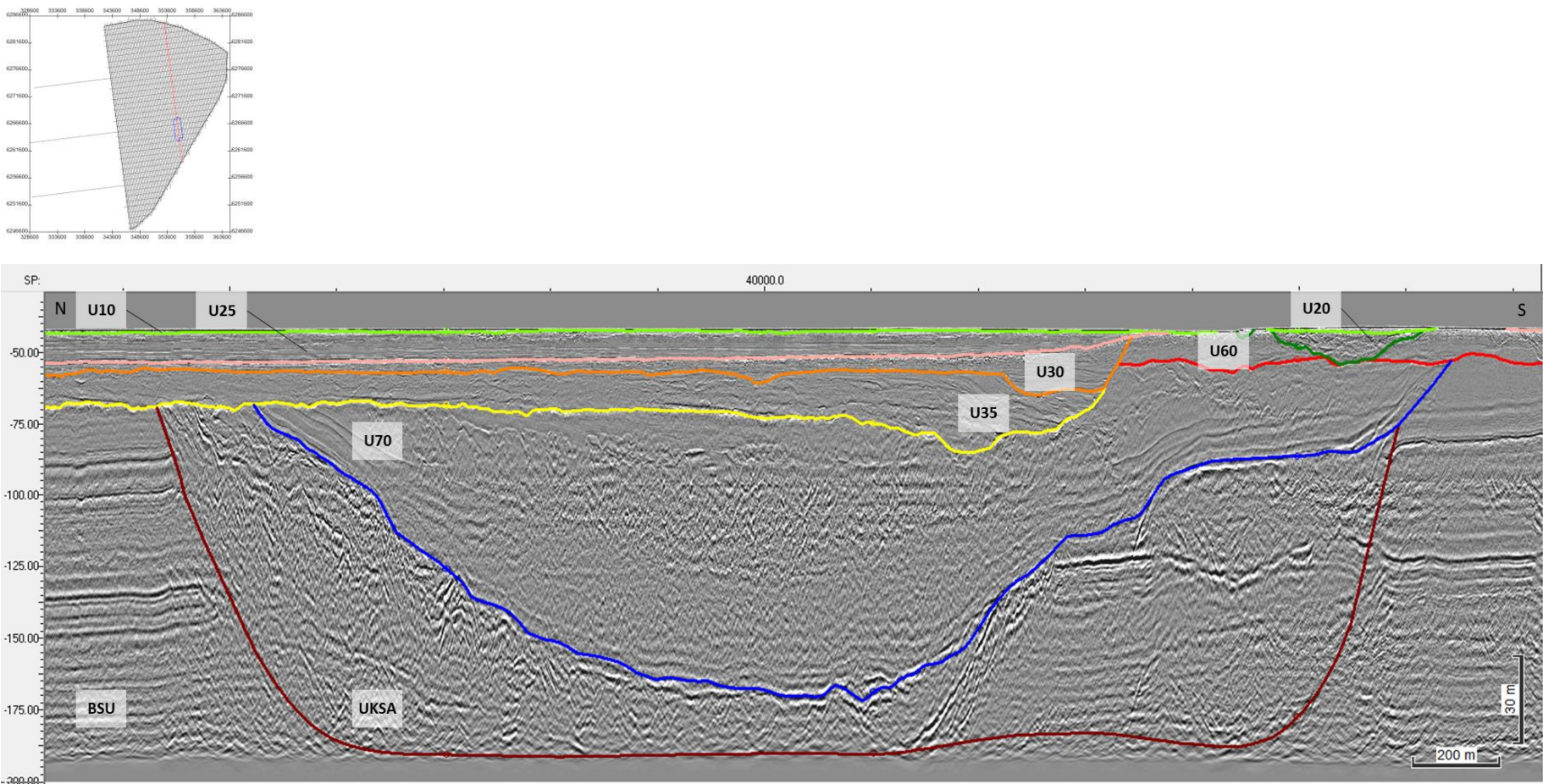


Figure 182 Composite facies in a U70 channel and the extensional features below H70. The features are interpreted to result from collapse of the valley flanks. Seismic profile BM4_OWF_E_2D_10920. Channel: H70_CH_08.

8.6.11 | SEISMIC UNIT U85

Seismic unit U85 occurs solely in the south sector of the area. The base of Seismic Unit U85 is defined by horizon H85 and is present discontinuously within the survey area. The spatial distribution, vertical reference to MSL and the seabed, and thickness of the unit are presented in Figure 183, Figure 184 and Figure 185.

Horizon H85 ranges in depth between 44.2 m and 100.2 m below MSL (Figure 183), and between 2.3 m and 55.6 m depth below the seabed (Figure 184). Horizon H85 traces an uneven, rugose, undulating surface, truncating the units below it (unconformity; Figure 186). Where present, H85 follows a positive reflector of high amplitude. However, H85 is mostly defined by a vertical facies shift.

Seismic unit U85 has generally sub-horizontal tabular morphology, with thicknesses ranging from <0.5 m to 51.4 m (Figure 185). Within the south sector, it is only present outside the limits of the two major basins.

Seismic unit U85 exhibits composite facies of low to high amplitude reflectors (Figure 186). Similar to U30 and U60, unit U85 comprises complex internal features of meso-scale proportions, such as mounds, channels, and lenses, with oblique reflectors. Internal surfaces separate these features, marked by medium-high amplitude. In a confined area towards the SW limit of the survey, a strong negative amplitude reflector (locally a pair of reflectors) located near or at the base of U85 (Figure 187). This reflector is discontinuous and is usually located in flattened areas of H85, adjacent to channel incisions. These strong negative amplitude reflectors are described as soft-kicks, and were mapped by horizon GHZ_SK_U85 (see section 8.8.3).

Seismic unit U85 sediments are interpreted to have been deposited in a high energy setting, likely of fluvial nature (possibly outwash plain?), as evidenced by the meso-scale seismic facies association, the numerous stacked subunits, internal surfaces, and channel incisions. Horizon H85 appears as an unconformity that shaped a pronounced paleo-relief. From the seismic character of U85 and its interpreted depositional system, it is estimated that the sediments are mainly sands with gravel and silt (?). Soft sediment deposits (such as muds, possibly organic-rich) are likely found near the base of U85, as indicated by the high amplitude negative reflectors.

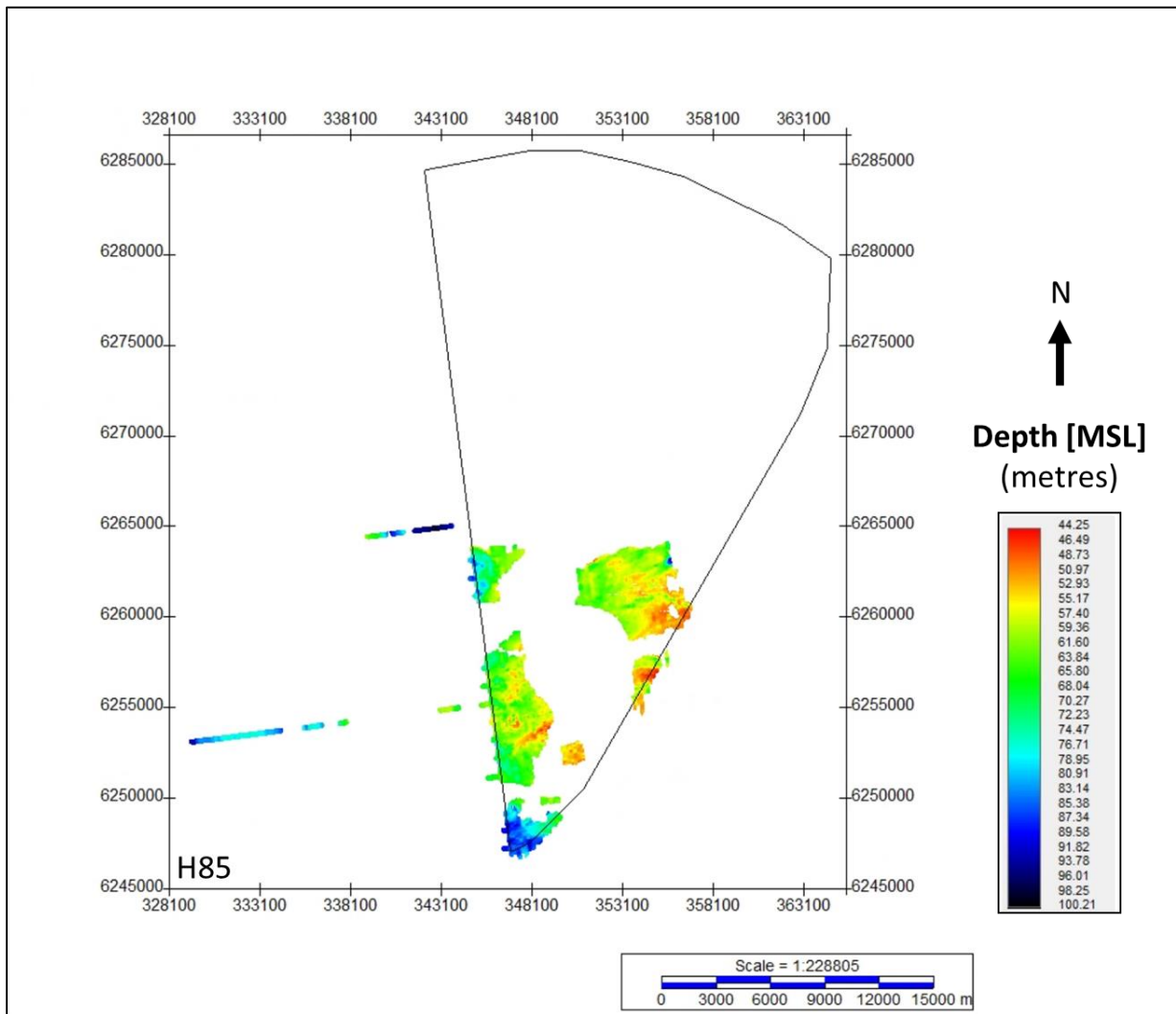


Figure 183 Map showing the lateral extent of U85.
Units in metres below MSL.

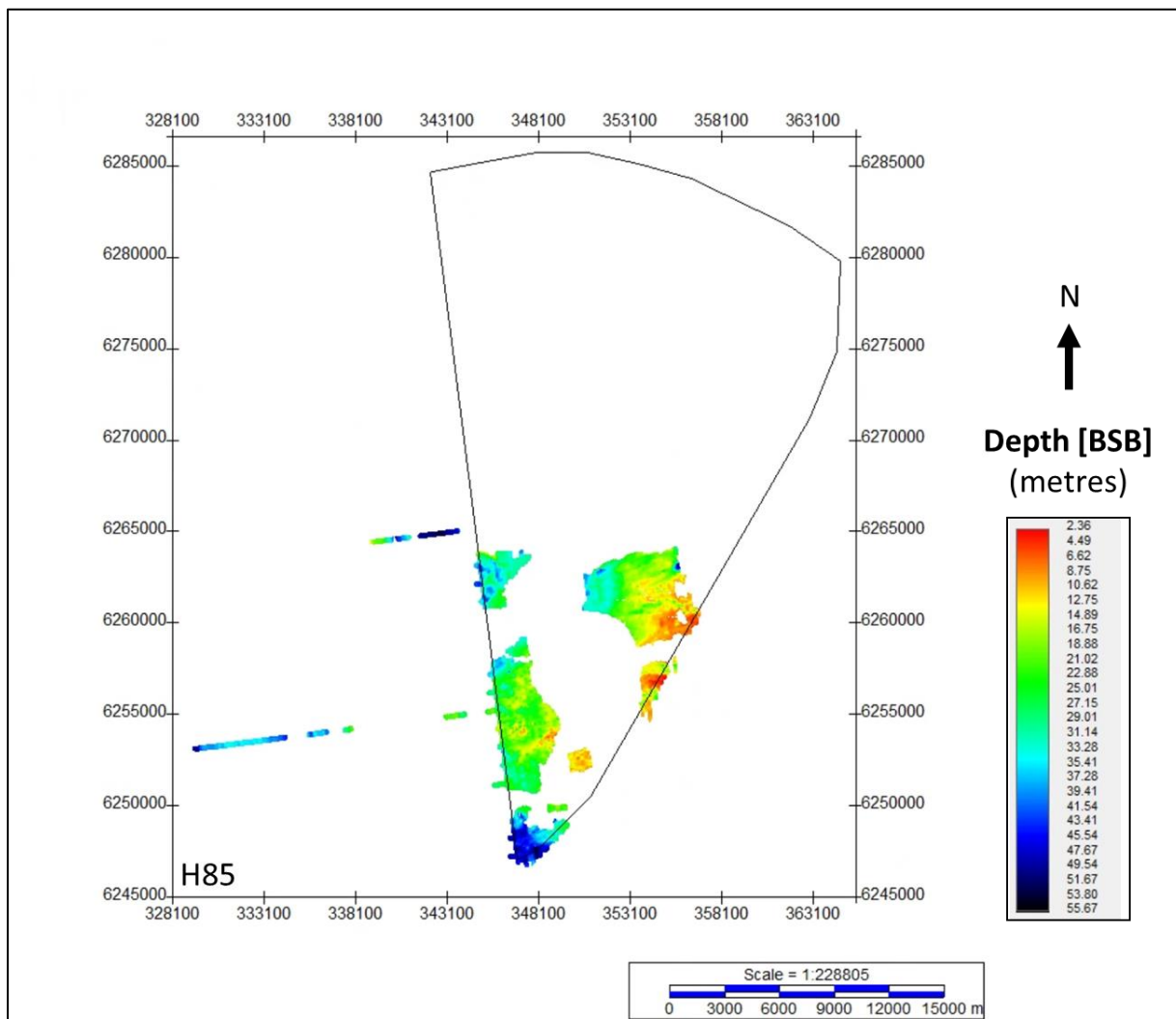


Figure 184 Depth below seabed of H85.
Units in metres below seabed.

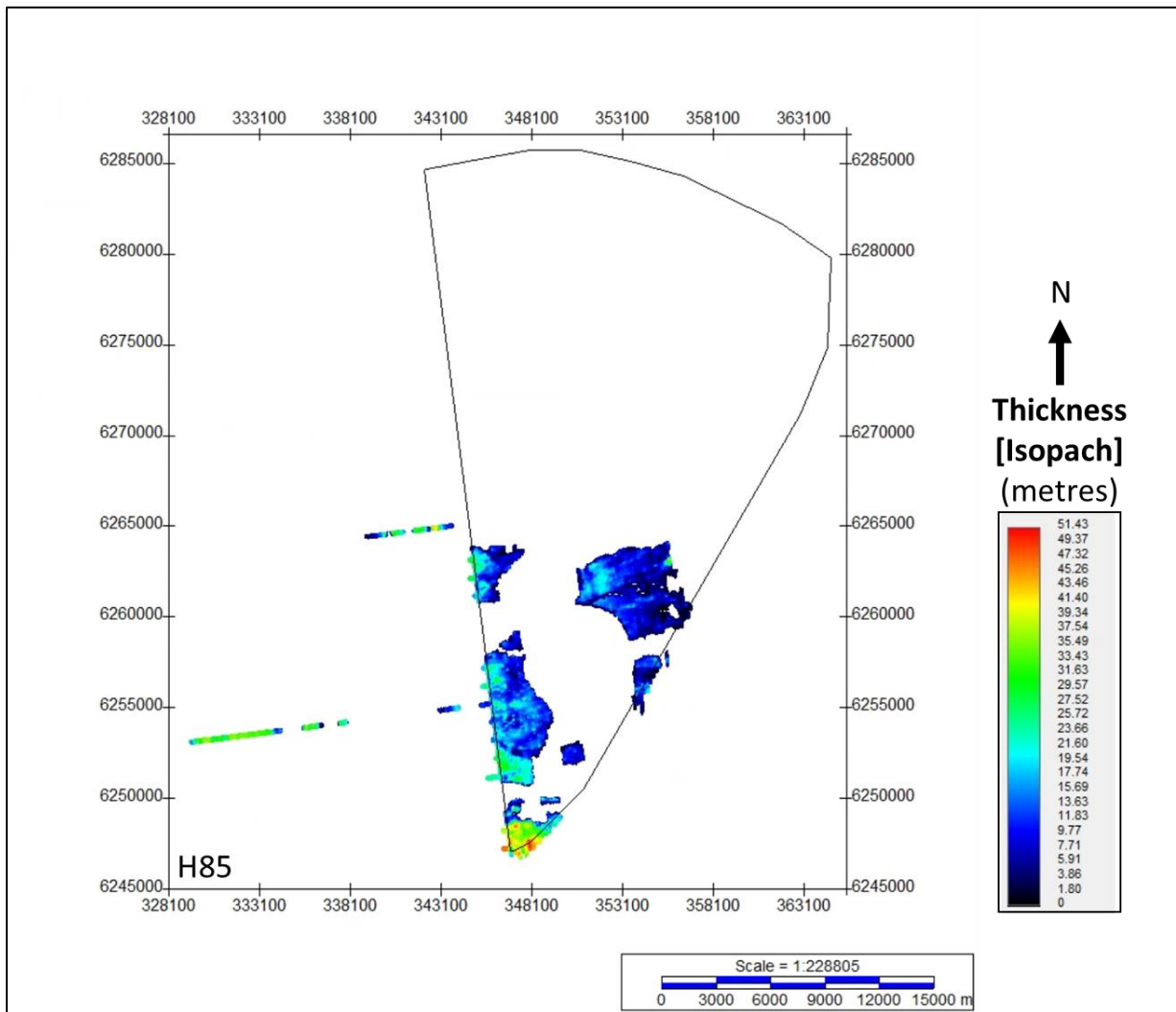


Figure 185 Thickness of unit U85.
Units in metres.

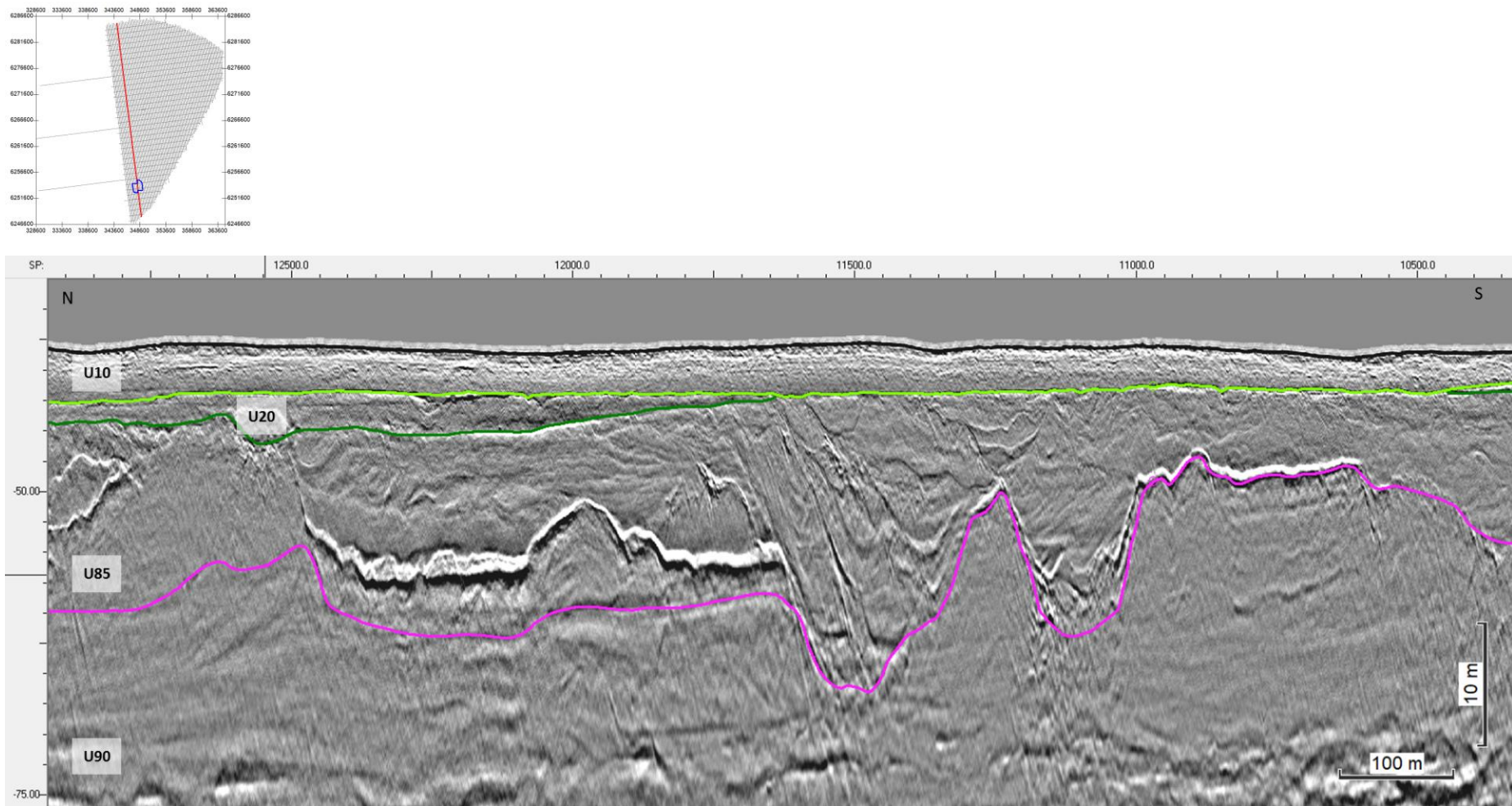


Figure 186 General facies of Seismic Unit U85, and the character of horizon H85
H85 is shown in hot pink. Note the negative high amplitude reflectors within and at the base of the unit. Seismic profile BM1_OWF_E_2D_02100

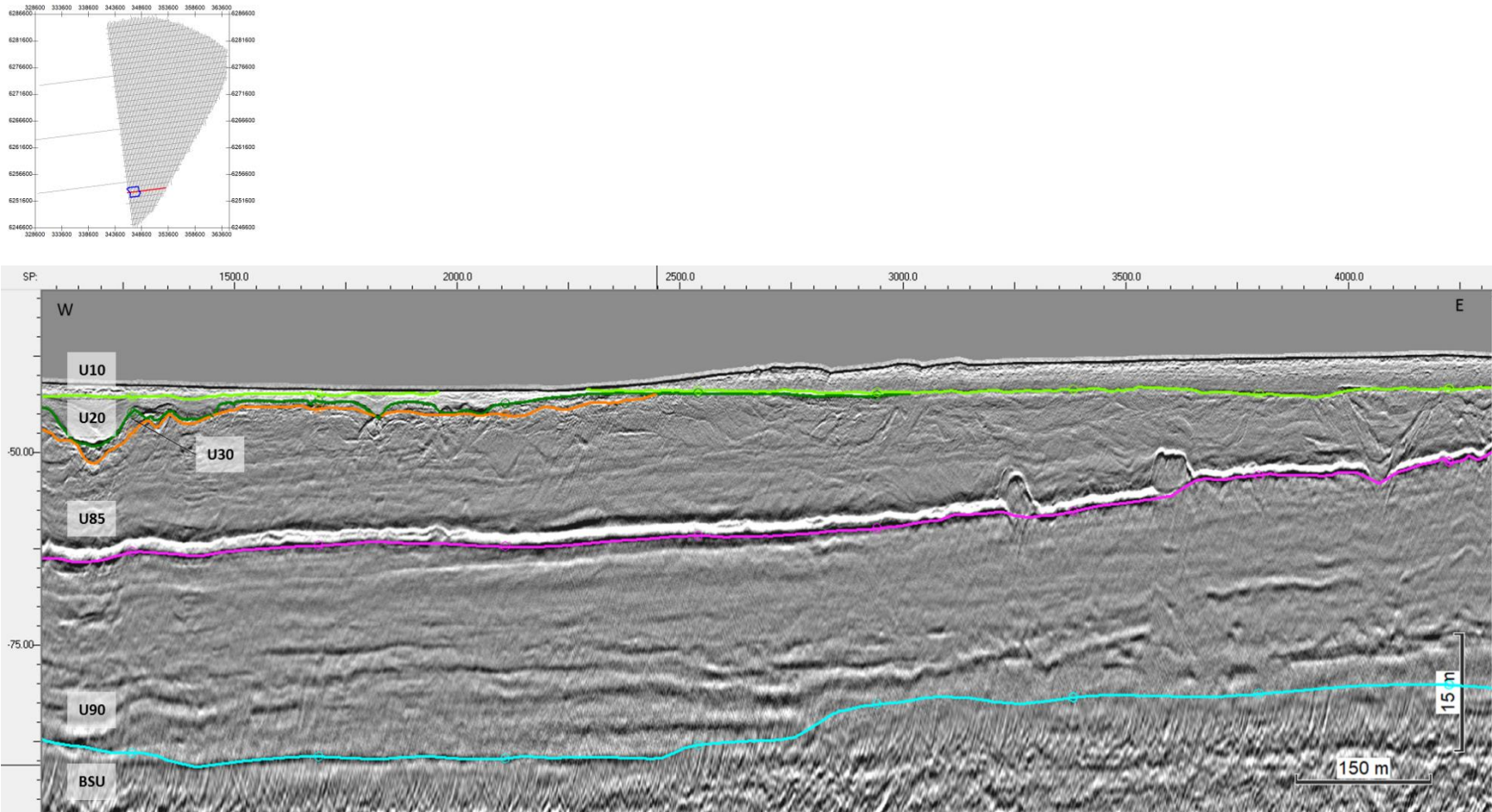


Figure 187 General facies of Seismic Unit U85, and the character of horizon H85
H85 is shown in hot pink. Note the negative high amplitude reflectors at the base of the unit. Seismic profile BX4_OWF_E_XL_32000

8.6.12 | SEISMIC UNIT U90

Seismic unit U90 occurs mostly in the south sector and within a restricted area of the north sector. The base of Seismic Unit U90 is defined by horizon H90 and is present discontinuously within the site. The spatial distribution, vertical reference to MSL and the seabed, and thickness of the unit are presented in Figure 188, Figure 189, and Figure 190.

Horizon H90 ranges in depth between 42.8 m and 117.1 m below MSL (Figure 188), and between 3.4 m and 74.1 m depth below the seabed (Figure 189). Horizon H90 is mostly defined by a vertical facies shift, corresponding to a planar, slightly undulating surface, generally gently dipping towards SW/SSW in the south sector and dipping NW/NNW in the north sector. Where present, H90 follows a positive reflector of medium amplitude, truncating the units below it (Figure 191).

Seismic unit U90 has generally tabular shape, with thicknesses ranging from <1.0 m to 64.0 m (Figure 190). Thickness variations are mostly the result of truncation of U90 by the units U85, U70, U40, U35, and U25 above it.

Seismic unit U90 is characterized by its parallel-homogeneous facies at the base and an association of parallel-mound-channel-shingled facies above, all prograding towards NW or W (Figure 191). Scattered along the internal surfaces are small-scale mounds-lenses, with a uniform positive amplitude character, and a negative reflector at the base. These features are most commonly seen at the base of the unit.

Seismic unit U90 sediments are interpreted to have been deposited in a delta setting, as evidenced by its internal progradational nature, dipping towards the deeper sections to the NW-W. From the seismic character of U90 and its interpreted depositional system, it is estimated that the sediments are mainly sands-fine sediments (?). The scattered internal mounds-lenses may correspond to sandbars (?).

In the north sector, U90 deposits show evidence of deformation, observed as thrusts and folds (Figure 192). This deformation and its probable origins are discussed in section (8.8.1|b).

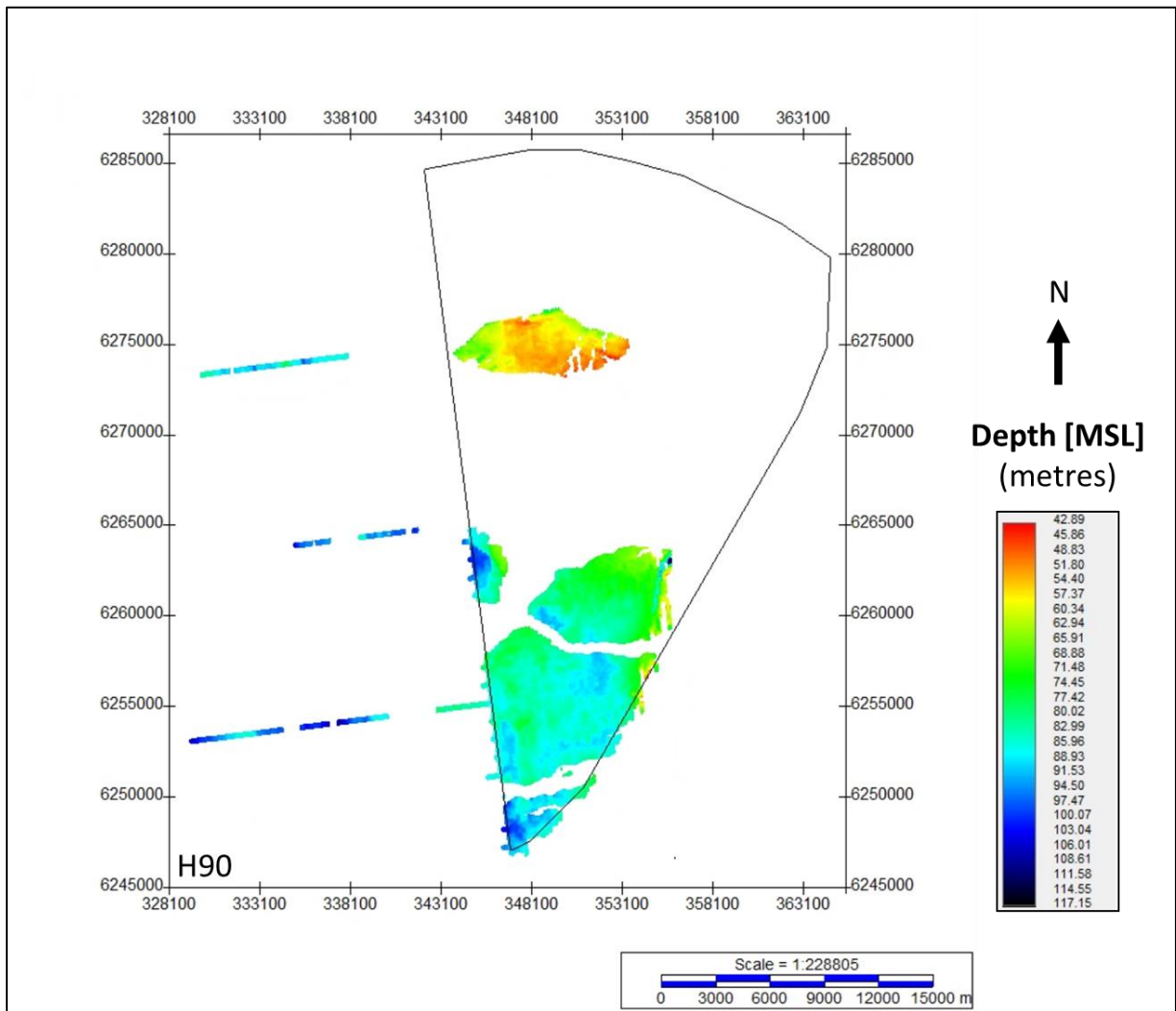


Figure 188 Map showing the lateral extent of U90.
Units in metres below MSL.

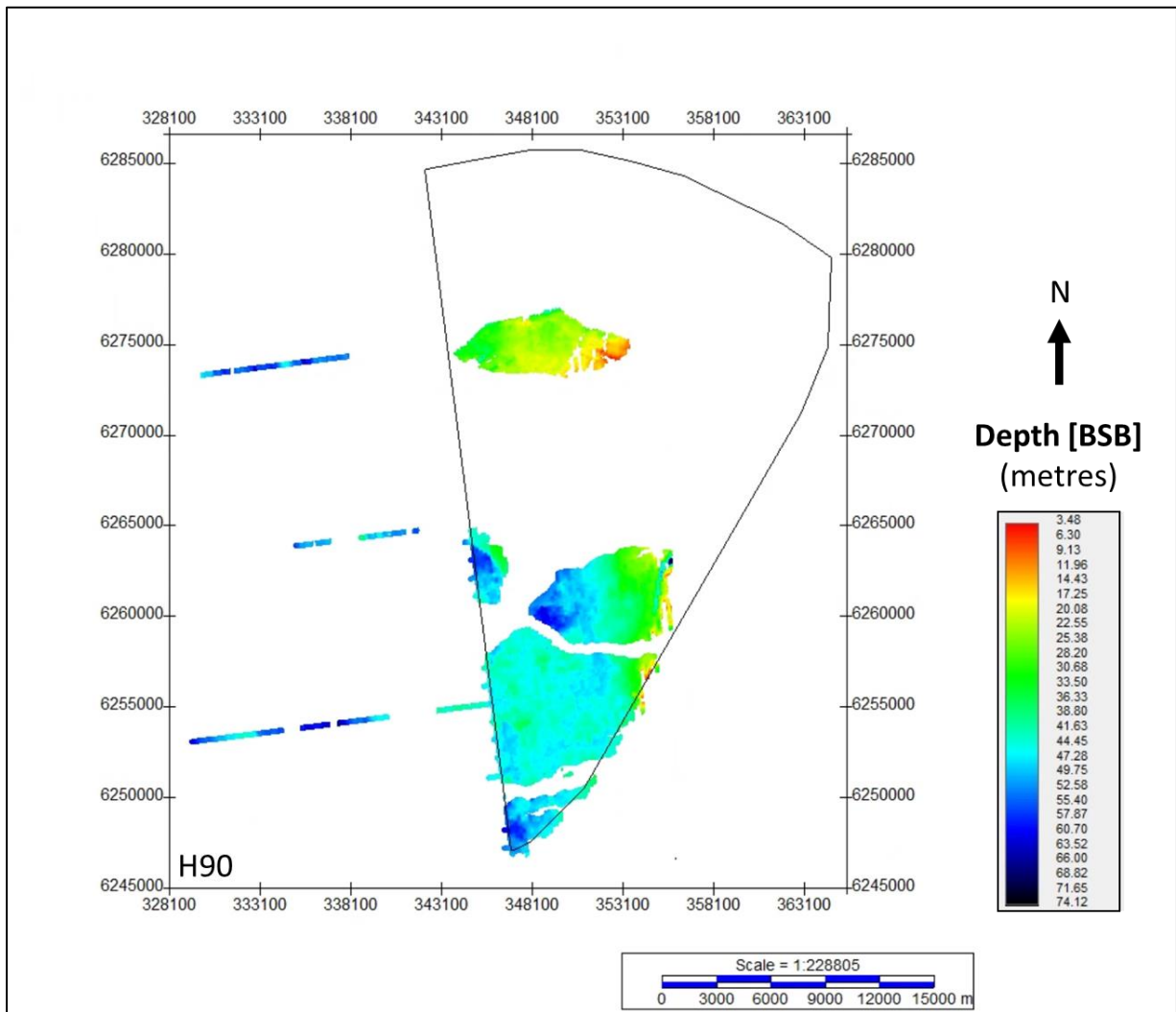


Figure 189 Depth below seabed of H90.
Units in metres below seabed.

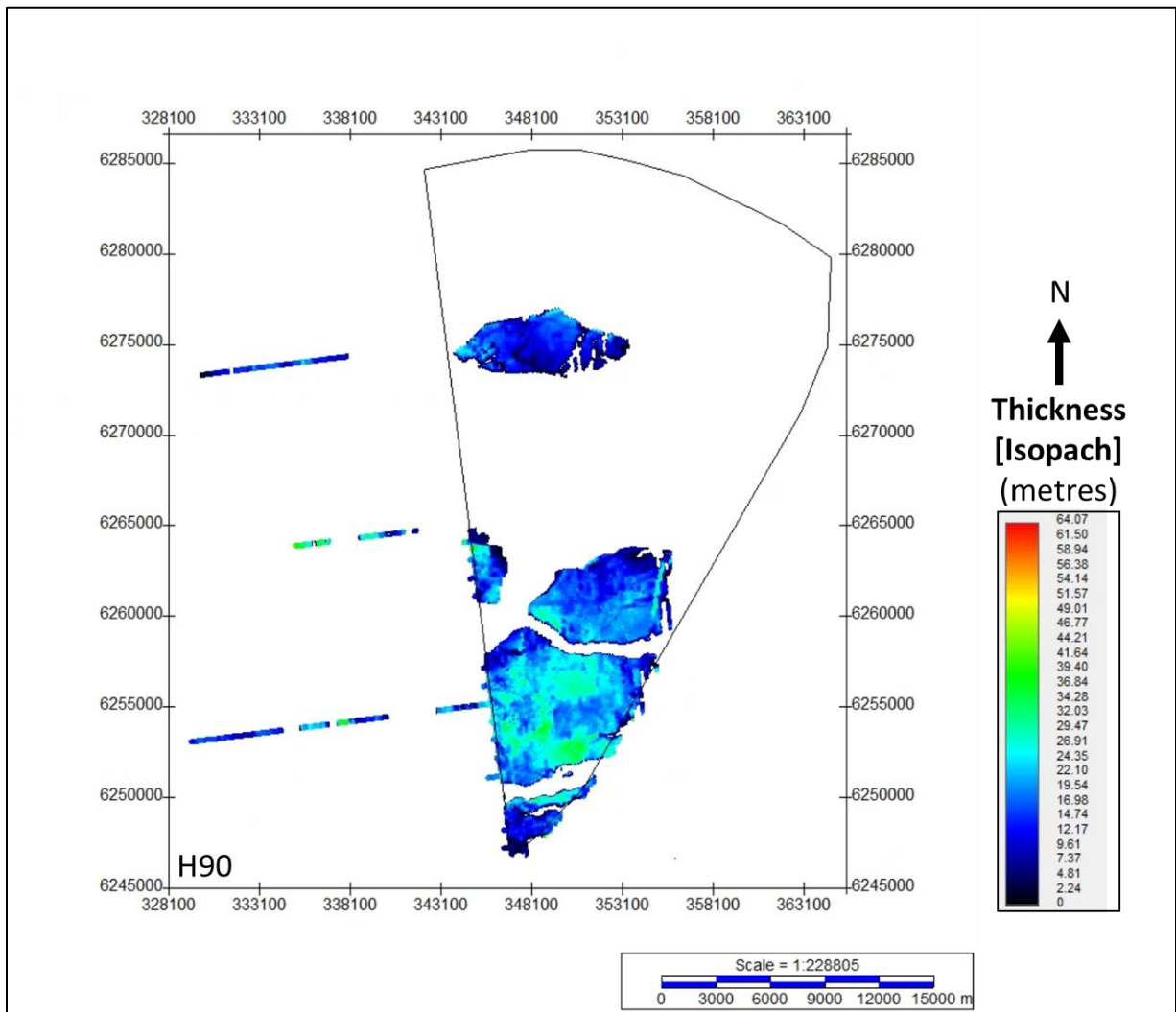


Figure 190 Thickness of unit U90.
Units in metres.

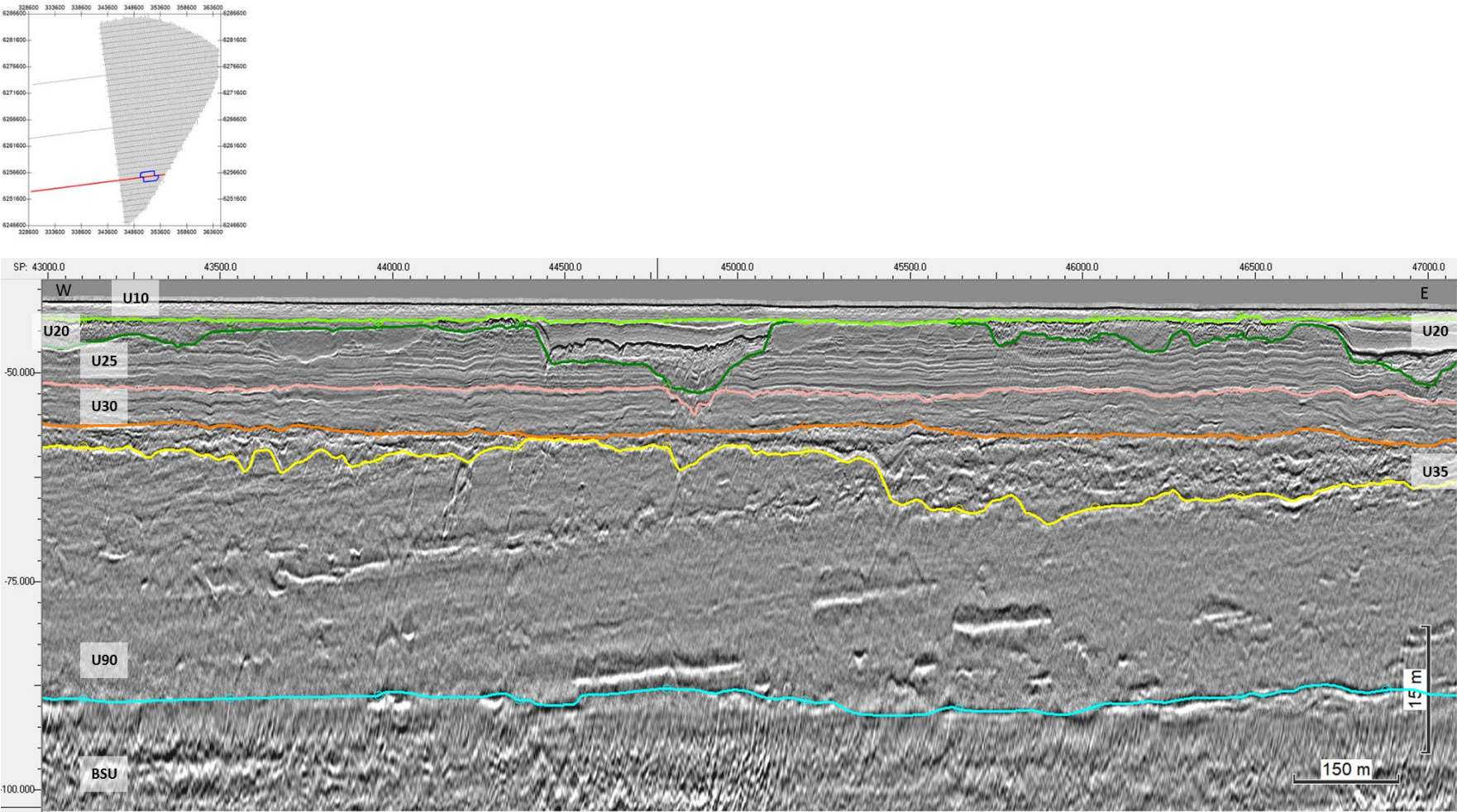


Figure 191 General facies of Seismic Unit U90, and the character of horizon H90. H90 is shown in cyan. Seismic profile BX4_OWF_2D_Baseline_3

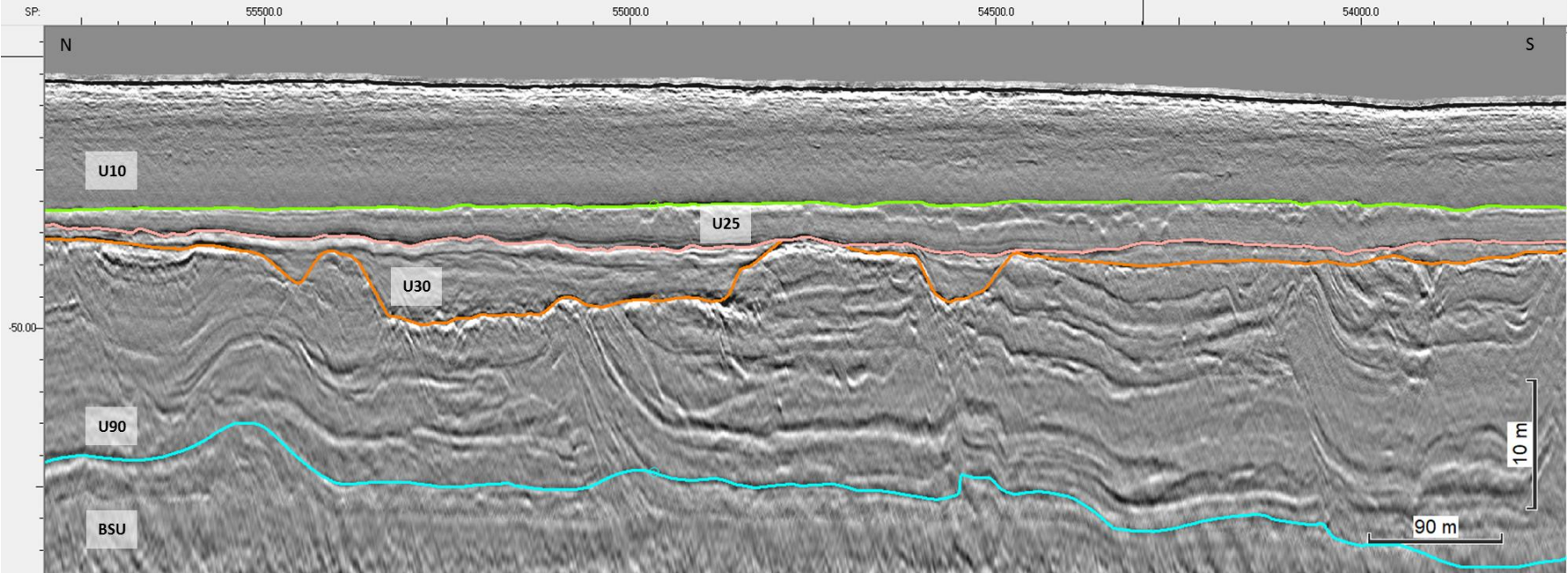
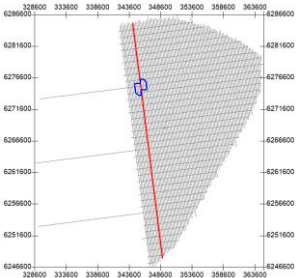


Figure 192 Thrust deformation affecting Seismic Unit U90.
Seismic profile BM1_OWF_E_2D_02100

8.6.13 | SEISMIC UNIT UKS

Seismic unit UKS is a major structural element of the ground model, and extends spatially across the three sectors of the site. The base of this unit is horizon KS. The spatial distribution, vertical reference to MSL and the seabed, and thickness of the unit are presented in Figure 193 to Figure 198.

Horizon KS defines a significant vertical and lateral facies shift, separating deformed sediments from preserved deposits older than H70. Horizon KS ranges in depth between 43.5 m and 216.1 m below MSL (Figure 193 and Figure 196), and between <5.0 m and 175.4 m depth below the seabed (Figure 194 and Figure 197).

Horizon KS represents a deformation front boundary and, although part of the geological model, should not be interpreted with a chronostratigraphic meaning. It is an amalgamation of surfaces of glacial erosion, decollements, fault planes, and shear/fracture zone boundaries (Figure 199).

Seismic unit UKS encompasses strongly deformed sediments of units U85, U90 (?), and the Base Seismic Unit (described below). The seismic facies of this unit is very complex, in a wide range of internal structures affected by variable degrees of deformation, from better-preserved faulted blocks to completely disturbed/chaotic regions (Figure 199). Where deformation has entirely erased primary depositional structure, seismic facies may be near transparent and incoherent.

Horizon KS was sub-divided into the two sub-horizons – KSA (Figure 193 to Figure 195) and KSB (Figure 196 to Figure 198) – each delineating distinct regions of deformation:

- Sub-horizon KSA extends across most of the north sector and parts of the central and south sector; it truncates all seismic units below H70 (Figure 199);
- Sub-horizon KSB is present in the south sector, and appears to be older than U85-U90, as these units truncate deformed deposits in this area (Figure 200).

Compressional thrusting and folding are the main types of deformation observed. It is interpreted that these structures are the result of glaciotectonics. However, extensional faults are also recognized in the UHRS. Details on the several types of deformation identified are discussed in section 8.8.1].

Due to the limitation in the contracted number of horizons but specially because of the difficulty in recognizing the complex old tunnel valleys that may be present within this unit, these features were not mapped.

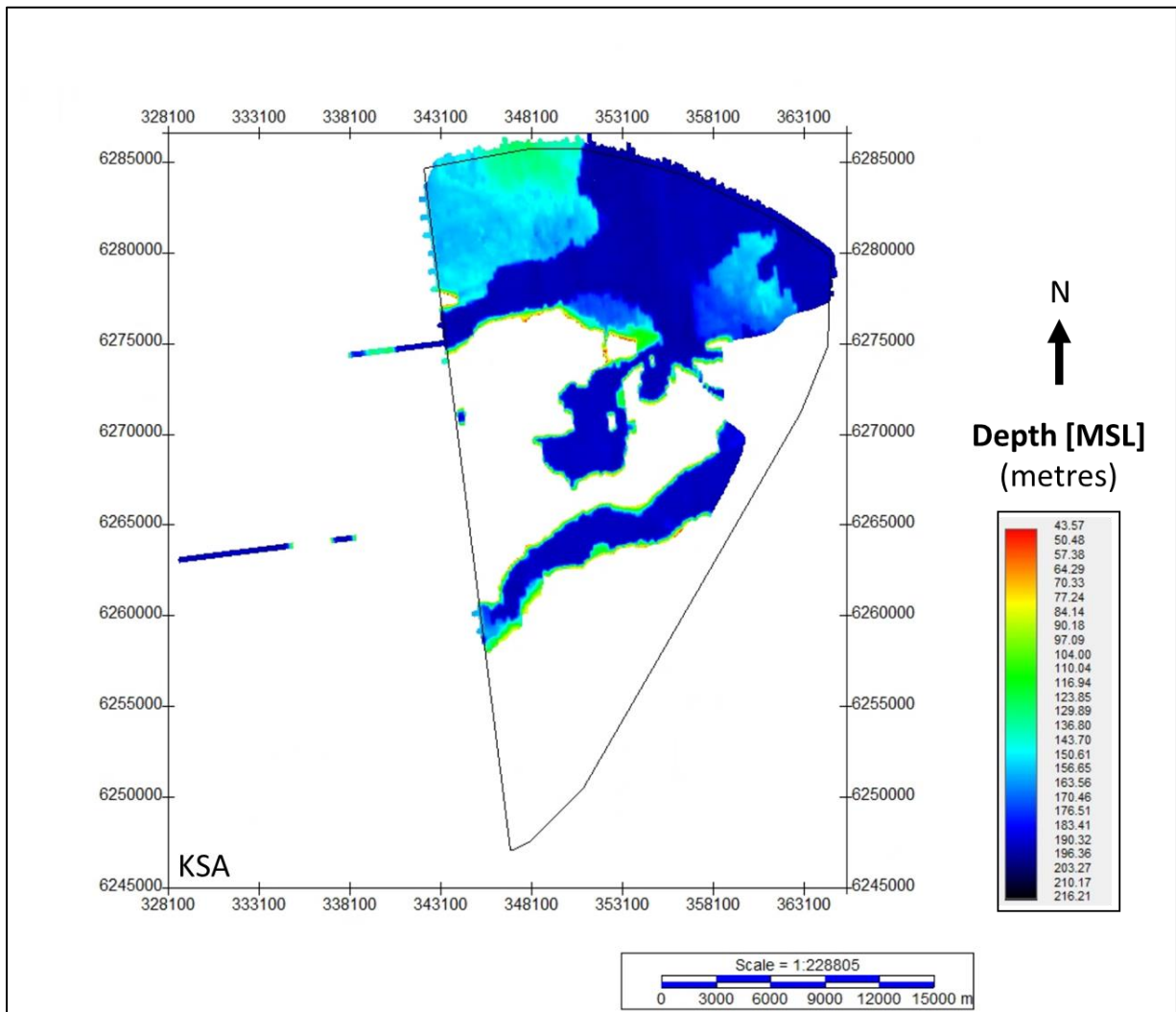


Figure 193 Map showing the lateral extent of horizon KSA.
Units in metres below MSL.

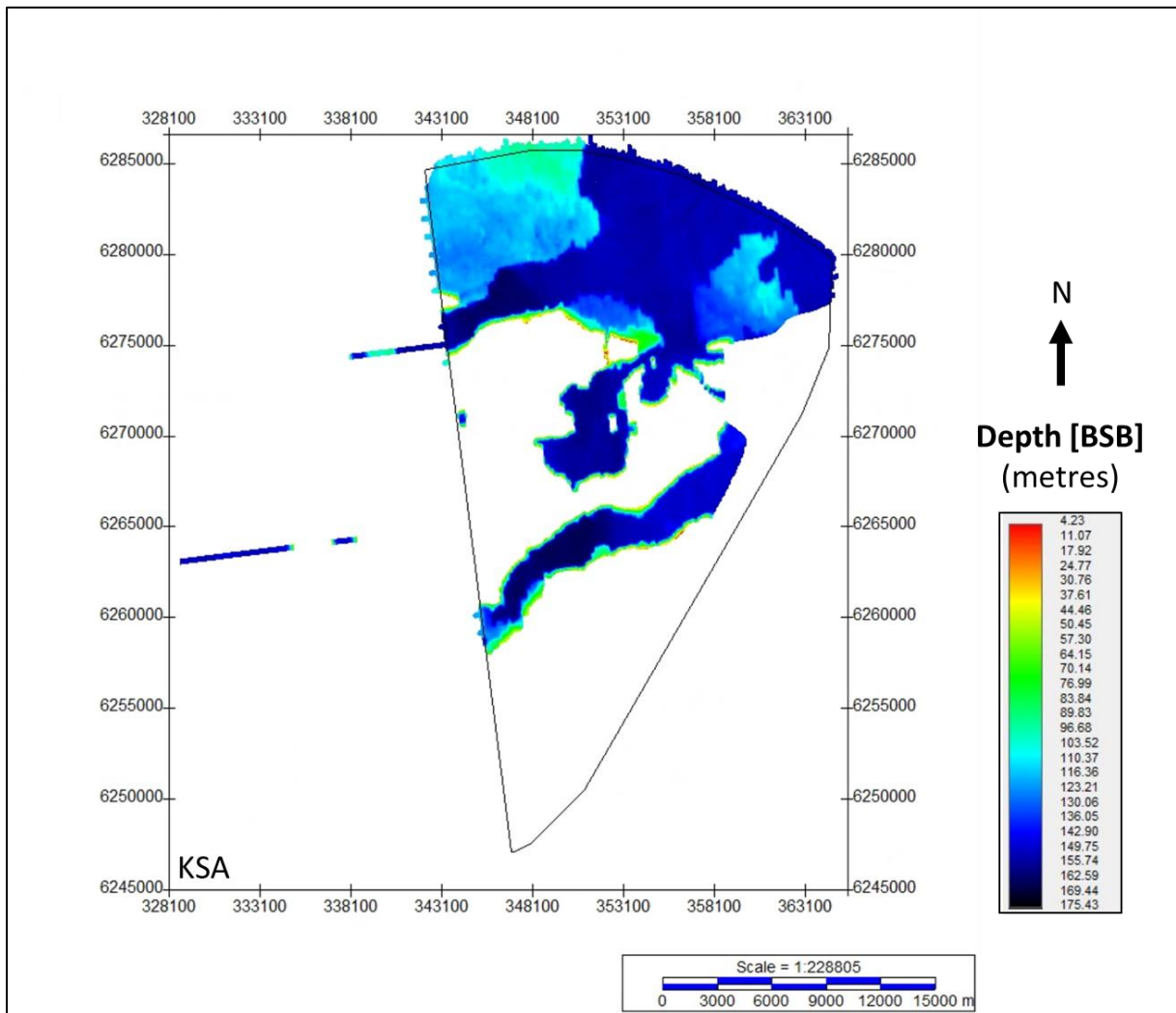


Figure 194 Depth below seabed of horizon KSA.
Units in metres below seabed.

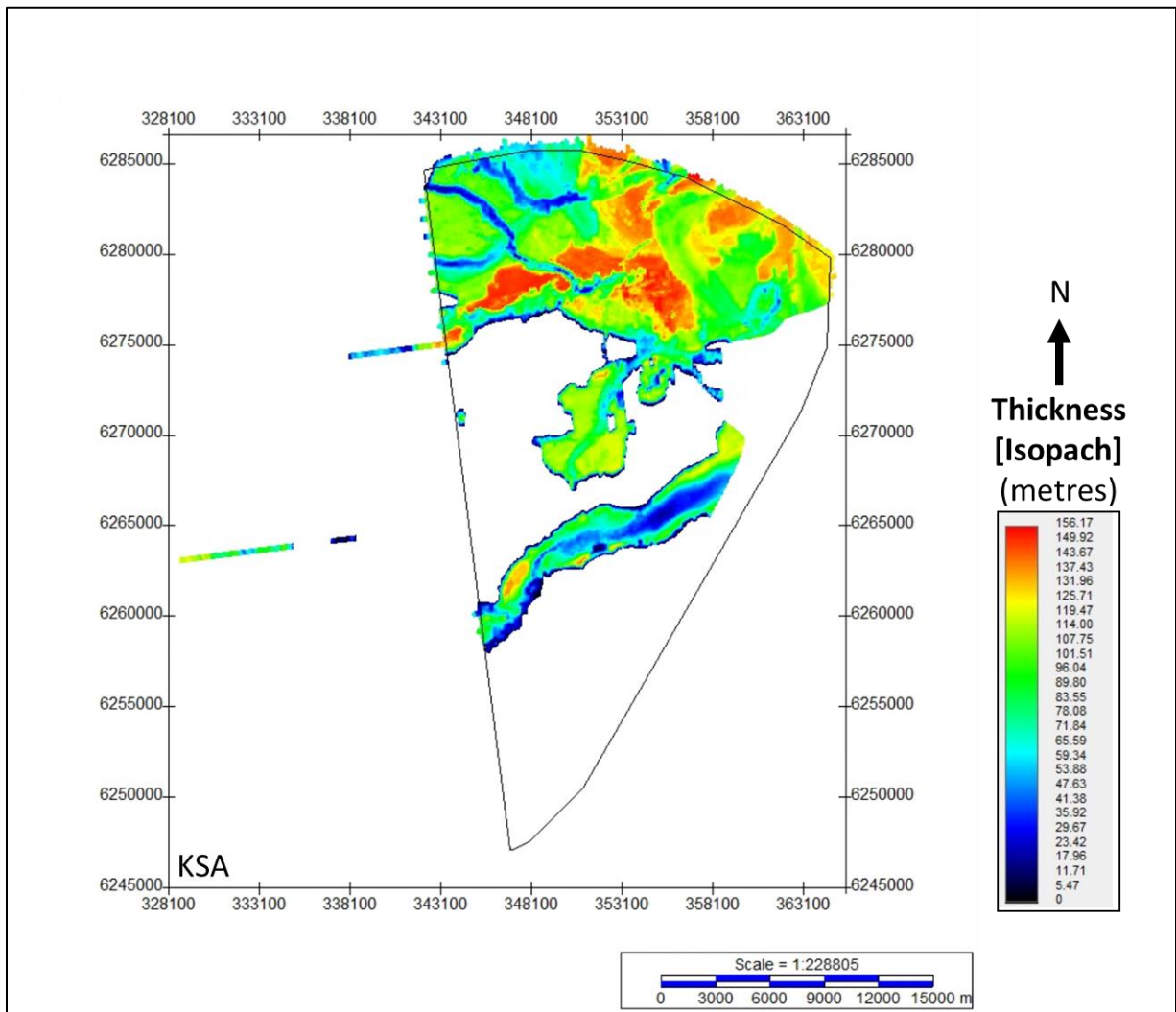


Figure 195 Thickness of unit UKSA.
Units in metres.

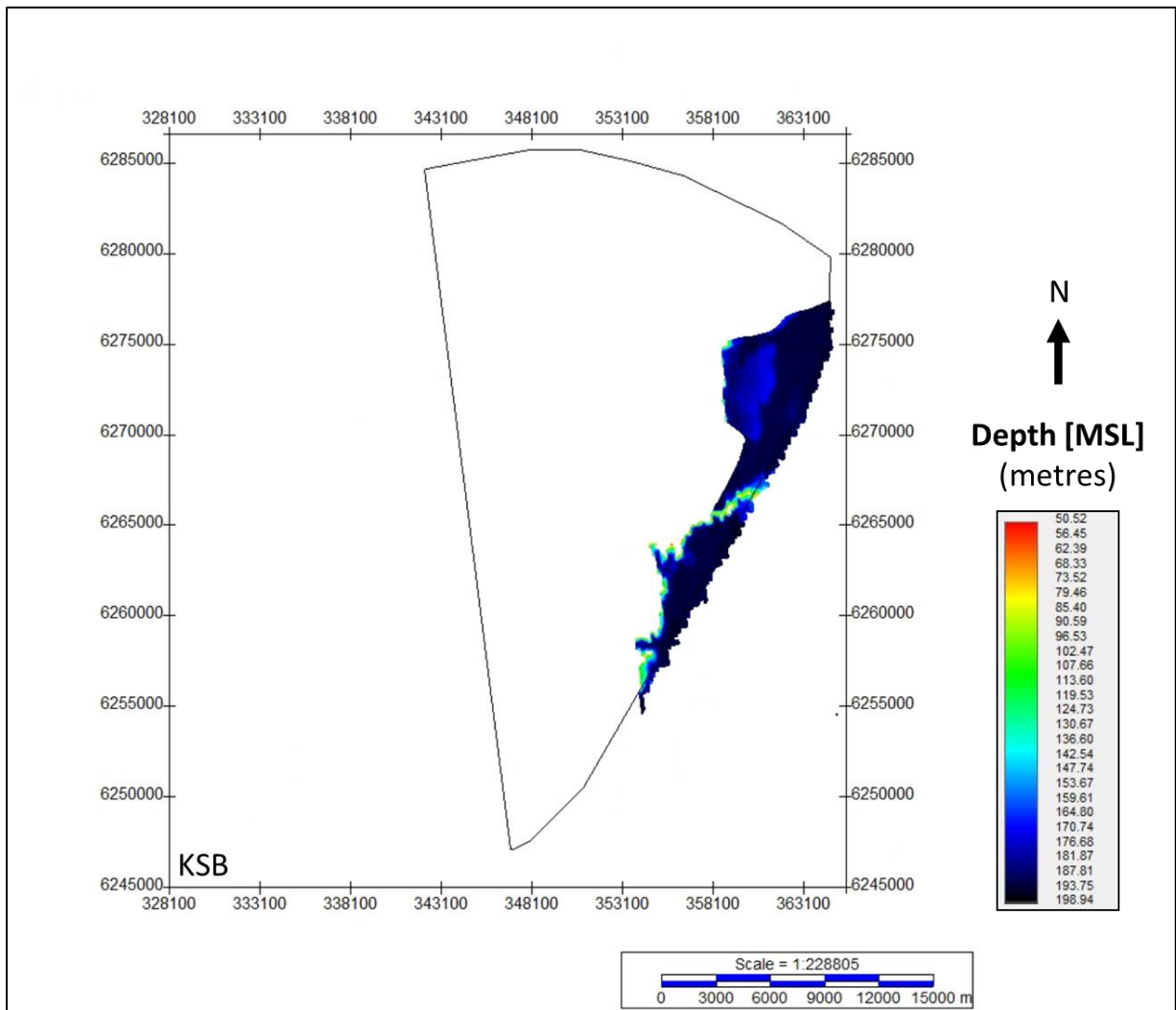


Figure 196 Map showing the lateral extent of horizon KSB.
Units in metres below MSL.

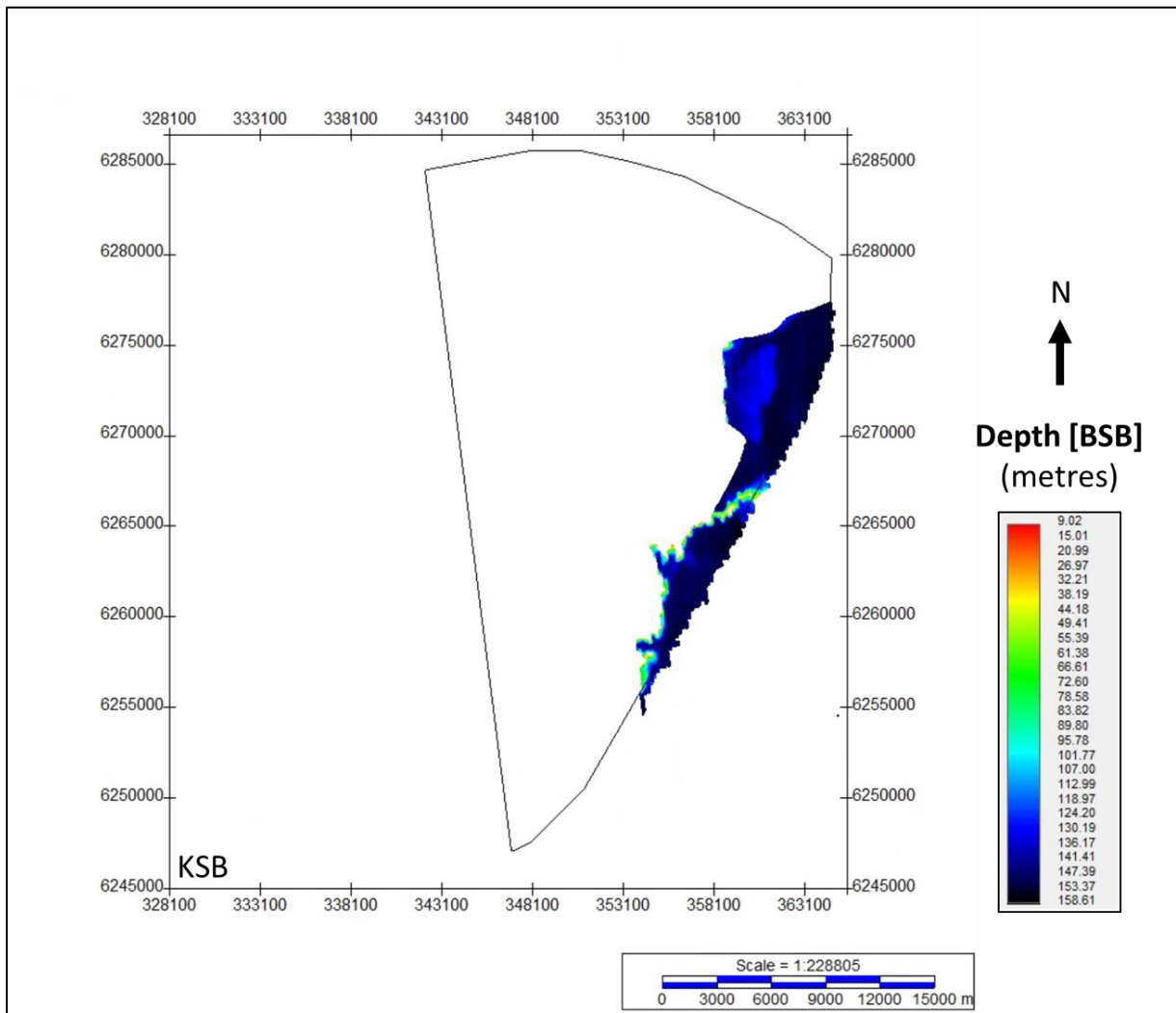


Figure 197 Depth below seabed of horizon KSB.
Units in metres below seabed.

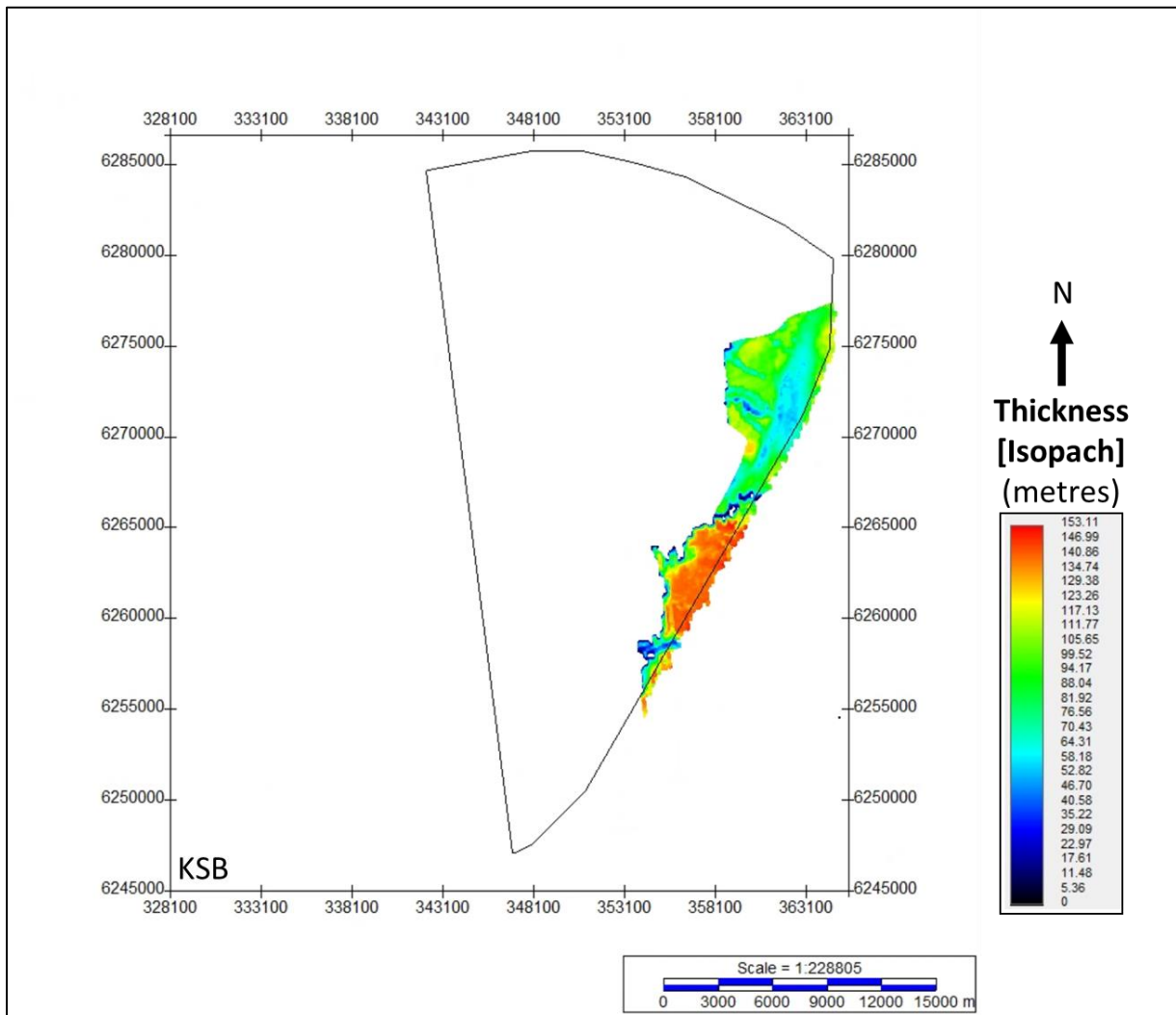


Figure 198 Thickness of unit UKSB.
Units in metres.

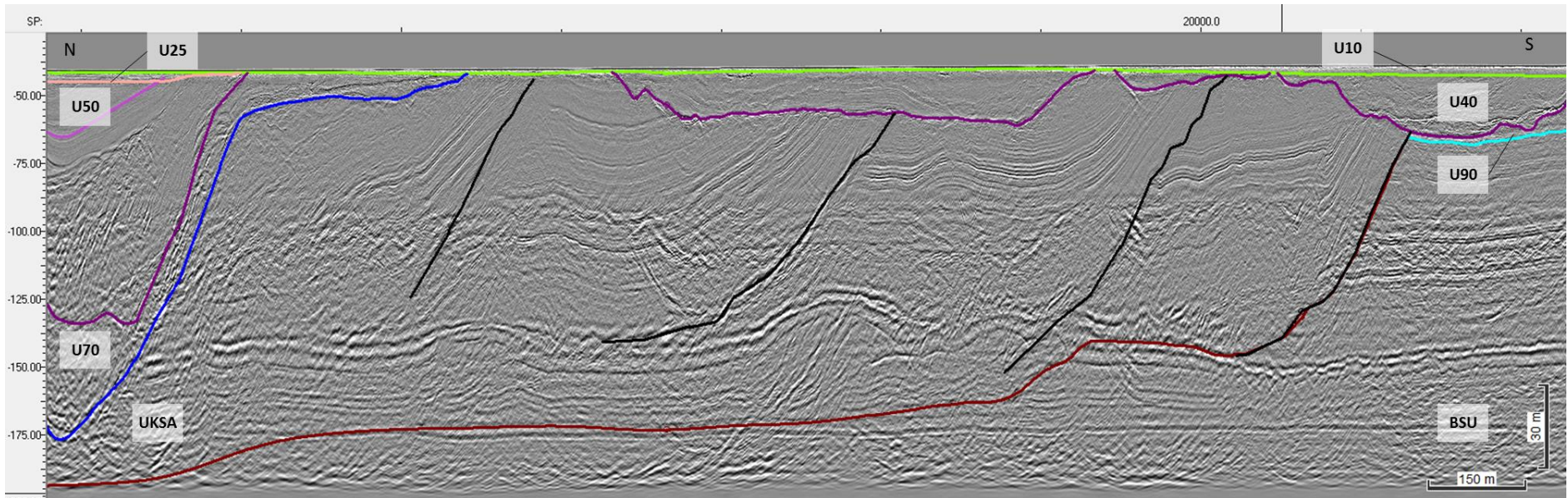
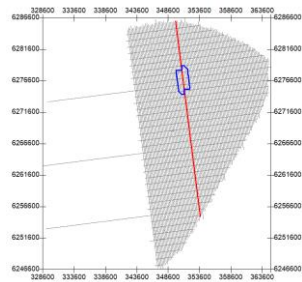


Figure 199 Thrust complex of Seismic Unit UKSA.
Horizon KSA delineating a decollement surface, flats and ramps, and the deformation front plane.
Thrust planes dip NE, indicating a compression advancing towards SW. Seismic profile BM3_OWF_E_2D_07770

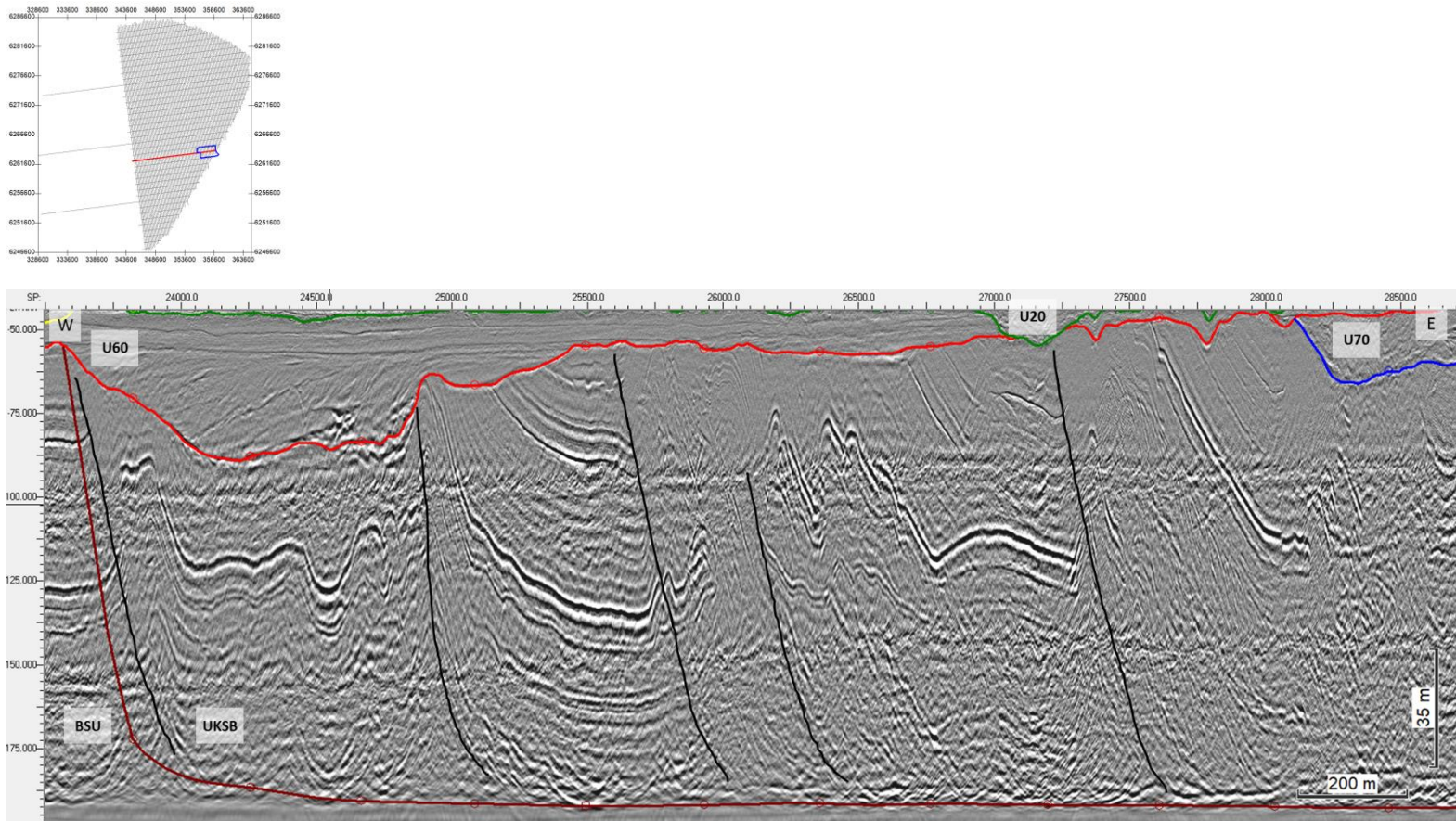


Figure 200 Thrust complex of Seismic Unit UKSB.
Horizon KSB delineating a decollement surface, and the deformation front plane.
Thrust planes dip SE, indicating a compression advancing towards NW. Seismic profile BX3_OWF_E_XL_23000.

8.6.14 | BASE SEISMIC UNIT BSU

The Base Seismic Unit BSU is a major element of the ground model, and extends spatially across the full site, except where UKS extends to the base of the seismic record. The base of the unit is at the processing "last knee", near the terminus of the record. The upper boundary is delineated by a contiguous union of all the deepest mapped horizons. The spatial distribution and (apparent) thickness of the unit are presented in Figure 201.

The seismic facies of BSU comprises a layered sequence of parallel facies of variable amplitude (Figure 202). Faults, fractures and gentle folding of the whole succession are locally observed, but the original configuration of the strata remain well-preserved (otherwise it would be included within the unit UKS). In the vicinity of the deformed deposits of UKS, the deformation of the Base Seismic unit intensifies (Figure 202).

From the characteristics of the Base Seismic Unit, it is interpreted that it corresponds to marine Pre-Quaternary strata.

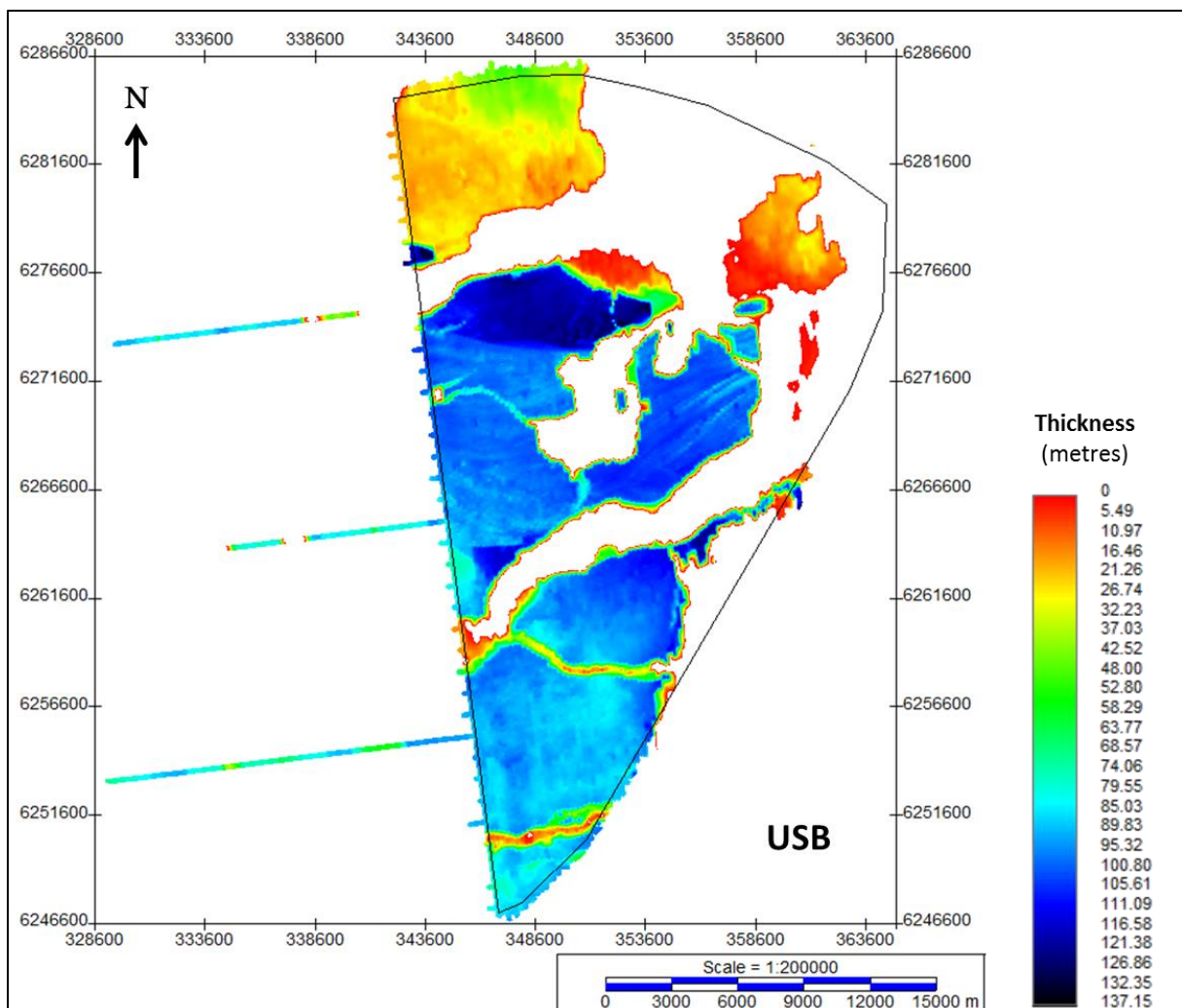


Figure 201 Thickness of Base Seismic Unit BSU.
 Units in metres.

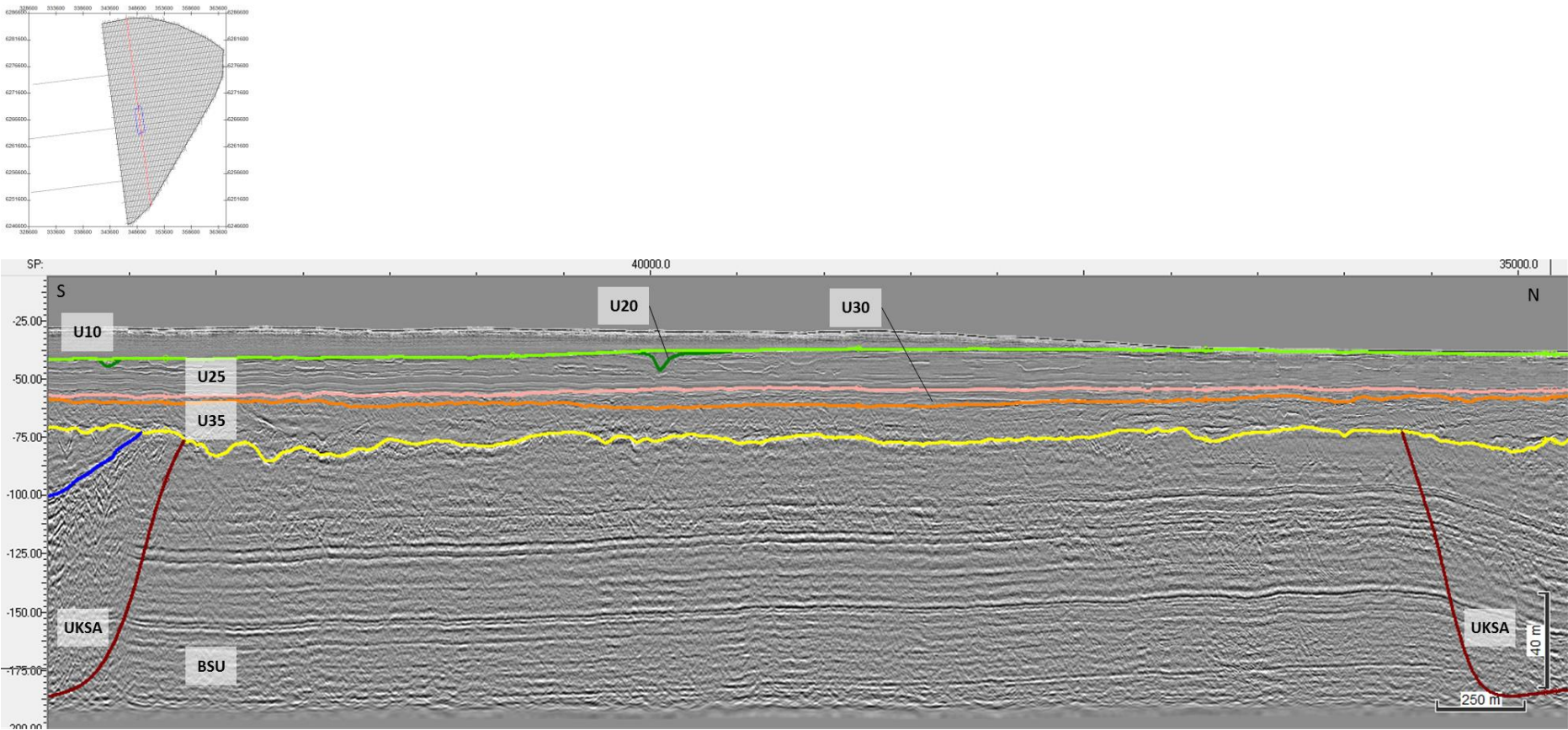


Figure 202 General facies of the Base Seismic Unit.
Seismic profile BM2_OWF_E_2D_04620

8.6.15 | SUMMARY AND DISCUSSION

The Ground Model presented in this report comprises 12 horizons, defining 13 seismic units that make up its geological framework. The geotechnical information available within the survey area was scarce and superficial. As such, the inferred depositional environments and sediment composition descriptions contained in this report are based largely on seismic interpretation techniques. Seismic facies analysis, reflector terminations, and stratigraphic architecture provided the foundation for the 2D UHR seismic interpretation. A review of the relevant scientific literature guided the interpretation process and placed the results within the known geologic context. However, it is important to understand that there are limitations associated to the interpretation provided, especially taking into account the lack of direct sampling of the deeper sub-surface (>5m BSB) deposits, that would provide ground-truthing information to complement our findings.

Also relevant is the complex geological architecture of the area. The degree of complexity, and by extension, heterogeneity and spatial and vertical variations, posed challenges to the interpretation of the UHRS data.

To facilitate the description of the model, the site was divided in three sectors (North, Central, and South), believed to represent distinct domains of sediment deposition and deformation. Furthermore, the large-scale depositional systems identified can be described as dominated by: 1) the direct and proximal influence of glacial processes; or 2) high frequency, variable amplitude, sea-level fluctuations and related depositional environments and shoreline migration. The separation of the two regimes is approximated by horizon H70 and H35. Most of the older seismic units beneath this boundary are characterized by glaciogenic deposition and deformation. The more recent units above this boundary exhibit characteristics of high frequency sequences. These are interpreted to represent cycles of deposition and erosion associated with sea-level fluctuations (transgressions and regressions).

Precise dating of seismic units to the Quaternary and its sea-level curve is not possible with the available data. One exception might be the last and most recent Holocene transgression. However, despite absolute chronological uncertainty, reasonable inferences can be made about the sea-level variations. Based on diagnostic characteristics of the seismic units' surfaces, stratal terminations and facies patterns, we have estimated sea-level behaviour for many of the seismic units. Alongside the model, the assessment of potential geohazards within the sub-surface provided important clues regarding the timing of the different deformation events that took place in the area, complementing our interpretations. These are described in section 8.8.1|Sediment Deformation.

The deposition of the deepest strata imaged in the UHRS data – Base Seismic Unit BSU – marks the beginning of the geological evolution of the survey area as defined by the Ground Model. These deposits correspond to the marine-deltaic Pre-Quaternary sequence. These sediments were likely affected by salt-tectonics (associated to the Zechstein salt diapirism; see section 8.8.1|c), as evidenced by the occurrence of extensional faulting and subsidence in the North and Central sectors. The Pre-Quaternary sequence exhibits evidence for deformation near the east limit of the site (deformed seismic unit UKS_B). There, fault pattern analysis suggest deformation towards the NW, possibly associated with Saalian glaciotectionism (maybe older) (see section 8.8.1|b). Following, a large sub-aerial exposure and associated erosion event took place. This is captured by H90, displaying truncation the locally deformed Pre-Quaternary deposits. Above this surface, a delta system is present in unit U90, followed by the fluvial deposits of U85.

A more recent and newer episode of glaciotectionism ensued, with thrust deformation advancing from NE (NE-SW oriented), forming the large thrust complexes. These are present in the North sector (unit UKS_A), evidenced by the intense deformation of units BSU, U90, and U85. This deformation is likely related to the Weichselian glaciation, synchronous to the generation of the large tunnel valleys (or re-use of older) in which the U70 glacio-fluvial system is present. High energy fluvial bedforms corresponding to unit U60 were deposited, possibly also associated to outwash plains, and flash flood events. Above U60 deposits, fine sediments of unit U50 accumulated in a lower energy setting. The origin of U50 is uncertain, as it may correspond to a glacial drift deposit (aqua till?), or comprised of glaciolacustrine sediments. Scattered point diffractors within U50 may be related to the presence of

boulders. Glacial meltdown and ice retreat may be associated with the establishment of the drainage network and subsequent sediment infilling of U40, alongside local glaciolacustrine deposition. This Weichselian (?) glaciogenic deposition and deformation is capped by the erosional event of H35, which carved the three major basins located in the Central and South sectors.

Sediment deposition above H35 appears to be dominated by high frequency sea-level fluctuations, related to eustatic-isostatic and autogenic processes, away from any glacial influence. An overall transgressive sequence infilled the basins, starting with the deposition of U35 fluvial bedforms at the base, followed by the finer deposits of U30. As the sea level rose, flooding of the basins led to the deposition of the lower section of unit U25, likely within a transgressive estuary setting, no longer constrained by the basins' margins. The increase of small channel-incisions within the upper deposits of U25 suggests the occurrence of a regressive event/fluctuation (at least in relative terms). The deposits of U20 consist of infills of small basins and/or channels, which could be related to a restricted marine-tidal deposition and partially to a subaerial fluvial infill. Above the ravinement surface of H10 (likely a wave cut) rests the last and most recent U10 deposits. This unit is made up of the recent transgressive deposits (possibly some high-stand) and includes the modern seabed marine sandy deposits

8.7 | SEABED HAZARDS

Below are summaries of various seabed hazards in the MMT OWF survey area.

8.7.1 | GRADIENTS

Slope angles across the site are typically very gentle ($<1^\circ$) and gentle (1° to 5°). Despite the fact that sand wave and sandbar areas constitute a large proportion of the seafloor topography, it is typically gently undulating. Areas of moderate to very steep slopes are largely restricted to the edges of sand bodies and the lee slopes of the most defined sand waves.

Very steep slope angles (15° to a maximum of 42°) are associated with boulders, the edges of depressions and steep banks on the western side of the Artificial Island area of investigation.

Slope angles up to 56° were observed on the sides of wrecks.

For complete details refer to section 8.2.5| Slope Analysis.

8.7.2 | MOBILE SEDIMENT AND BEDFORMS

Extensive areas of mobile sediments are present across the majority of the MMT OWF survey area. The mobile sediments range from smaller wavelength bedforms such as ripples, large ripples, megaripples to larger scale sediment bedforms such as sand waves and sandbars.

For complete details refer to section 8.3.2| Mobile Sediments.

8.7.3 | BOULDERS

Extensive boulder fields ranging from intermediate to high density are particularly common in the northeast of the survey area. They are found as more isolated features in the northwest, central eastern, central western and southern part of the area. Individual boulders more frequently occur in the vicinity of boulder fields, but scattered boulders are also present throughout the area.

For complete details refer to section 8.3.3| Boulders.

8.7.4 | EXISTING INFRASTRUCTURE AND WRECKS

The client supplied background data indicates the TAT-14 cable crosses the southern extent of the MMT OWF survey area, trending northwest to southeast. The cable is buried and only observed on MAG and SBP data.

Three charted wrecks (present in the background data provided by the client) were identified within the MMT OWF survey area; Wreck_94 (Contact ID: S_RE_B01_0324) was found at 347323.0 m E, 6253311.3 m N; Submarine HMS Tarpon Wreck_86 (Contact ID: S_FR_B03_0006) was found at 348875.5 m E, 6284051.0 m N; Wreck_85 (Contact ID: S_FR_B03_0069) was found at 349881.9 m E, 6284268.9 m N.

One possible unknown wreck (Contact ID: S_RE_B05_0547) was found at 358715.6 m E, 6272109.0 m N.

For complete details refer to sections 8.4.1| Wrecks and 8.5| Existing Infrastructure (Cables and Pipelines).

8.8 | SUB-SEABED HAZARDS

The 2D UHRS datasets were inspected in order to identify any potential constraints on future developments of the site; it does not directly correlate with a risk. This careful assessment revealed the presence of potential geohazards within the sub-surface of the survey area. The most relevant geohazards identified are:

- Sediment deformation:
 - Faulting;
 - Glaciotectonics;
 - Gravitational deformation;
 - Salt dome related tectonics;
- Buried channels and tunnel valleys;
- Soft sediments and organic-rich deposits;
- Coarse sediments, gravel beds, and boulders;
- Fluid flow and gas features;
- Lacustrine deposits.

The interpretation and mapping of all geohazards described in this section were performed using manual picking as seismic data resolution and human precision allowed.

A more detailed description of the aforementioned geological hazards is presented within the sections below.

8.8.1 | SEDIMENT DEFORMATION

Areas of tectonization/deformation were identified throughout the survey area, present in all three sectors. Distinct patterns and degrees of deformation are observed, depending on which deformation process took place. Deformation levels range within a large spectrum, from low (minor) to high (strong). In areas of low deformation, minor folding (wavy reflectors) and small-displacement faulting is observed within well-preserved strata, with the original stratigraphy of the unit mostly intact (Figure 203 A). With intensifying sediment deformation, large-scale/displacement faults, shear/fracture zones, decollements, and high amplitude folding occur (Figure 203 C). On the extreme end, strongly deformed sediments present themselves as seismically chaotic and incoherent, with no discernible internal seismic reflectors (Figure 203 D). The materials within these units are likely to have experienced variable and complex stress, i.e., compressional, tensional, and shear. These units should have geotechnical significance given their complex stress/load histories.

In the survey area, the process in which the sediments became deformed are interpreted to have different origins: glacio-tectonics; salt tectonics; and gravitational deformation. These processes may work independently or simultaneously, increasing even further the complexity of the units' seismic facies. Regardless of the process, fault surfaces/zones are always observed. Fault mapping in the survey area is described below, followed by the different modes of deformation identified.

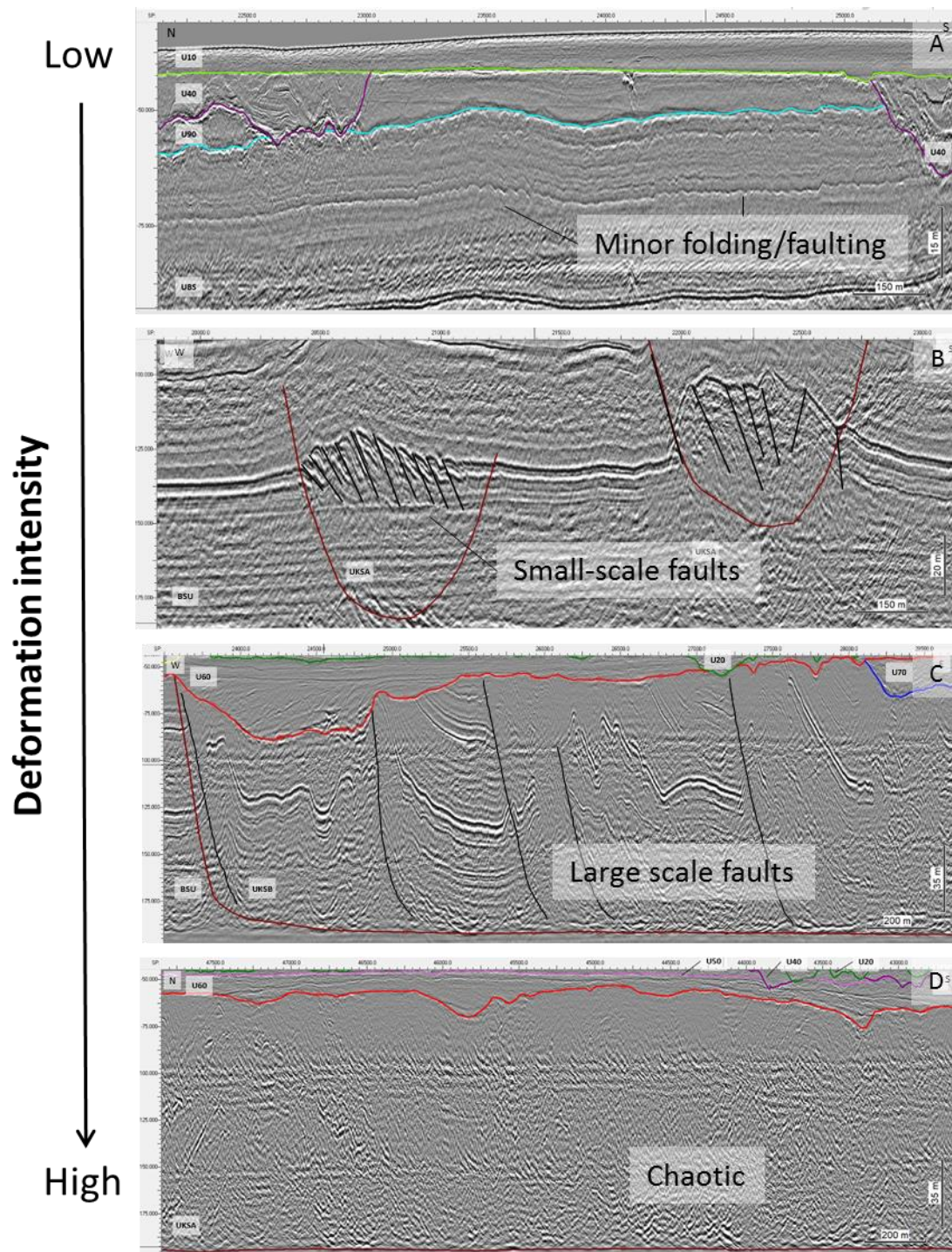


Figure 203 Different levels of deformation observed within the site. Deformation intensity ranges from (A) low (minor folding and small-displacement faulting) to (C) major (large-scale/displacement faults, shear/fracture zones, decollements, and high amplitude folding). Extreme deformation (D) is observed as seismically chaotic and incoherent. Detailed images of (A), (B), (C), and (D) are displayed in Figure 205, Figure 206, Figure 207 and Figure 208 respectively.

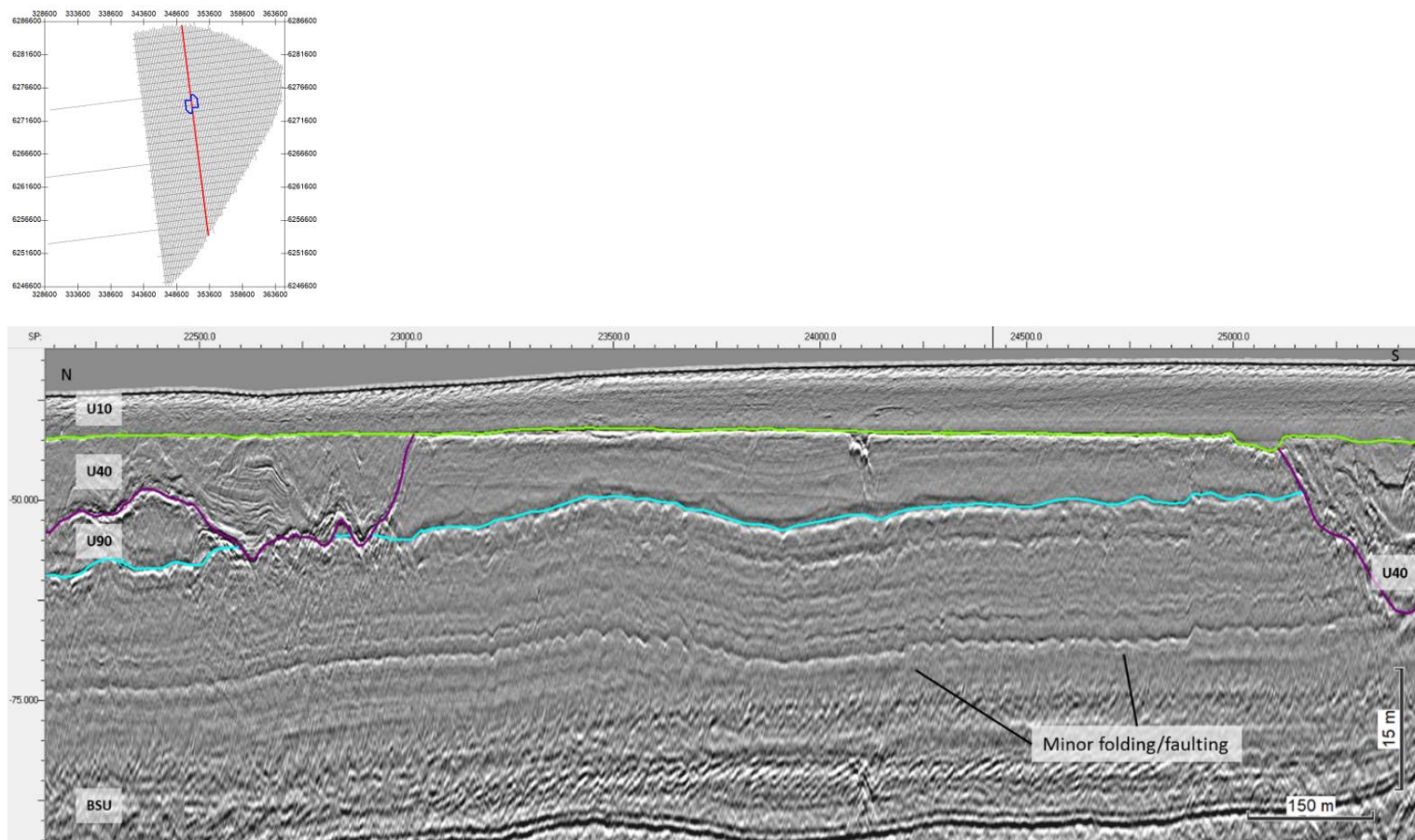


Figure 204 Minor folding and faulting affecting the BSU sequence.
Seismic profile BM3_OWF_E_2D_07350.

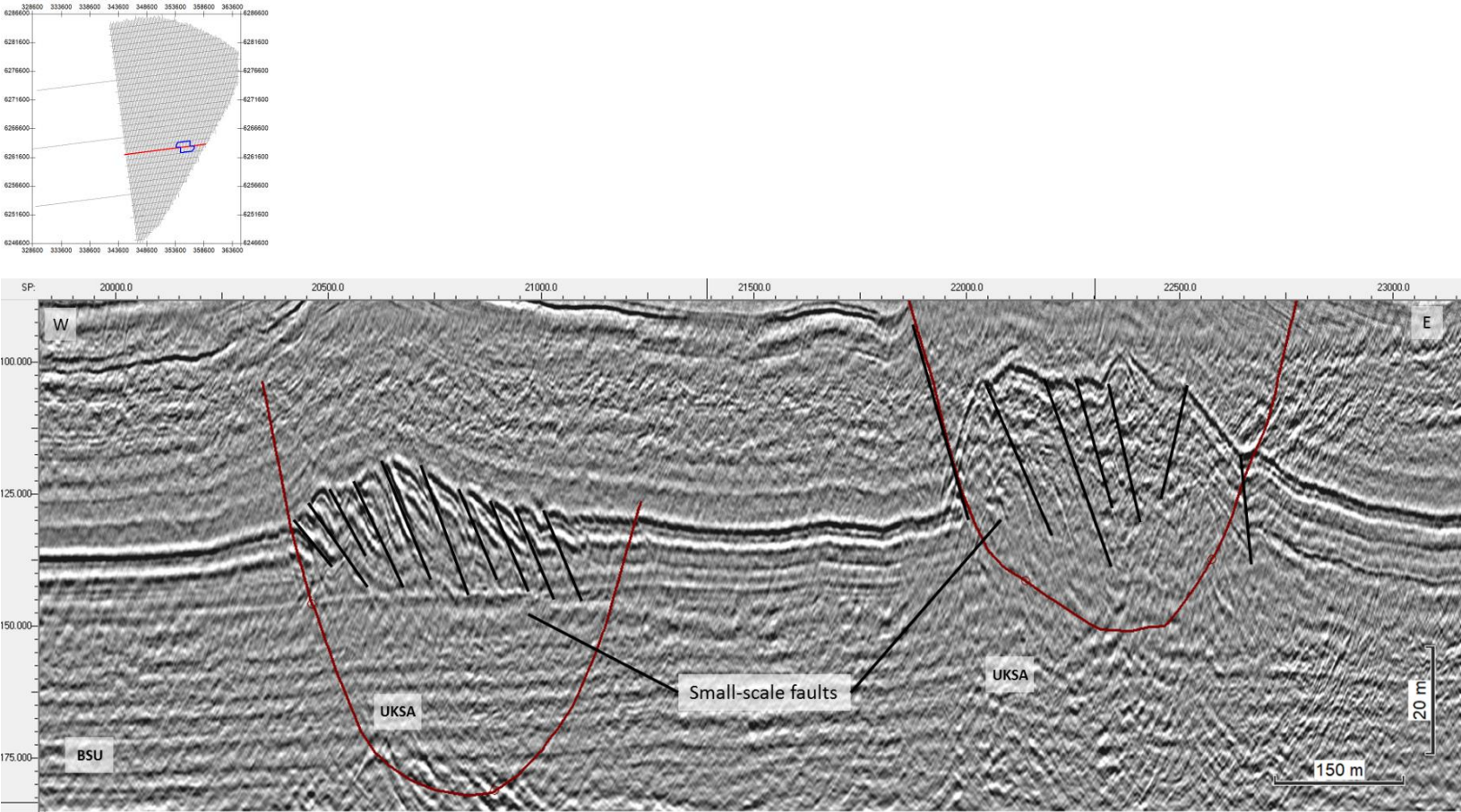


Figure 205 Small scale faults within a thrust complex.
Seismic profile BX4_OWF_E_XL_23000

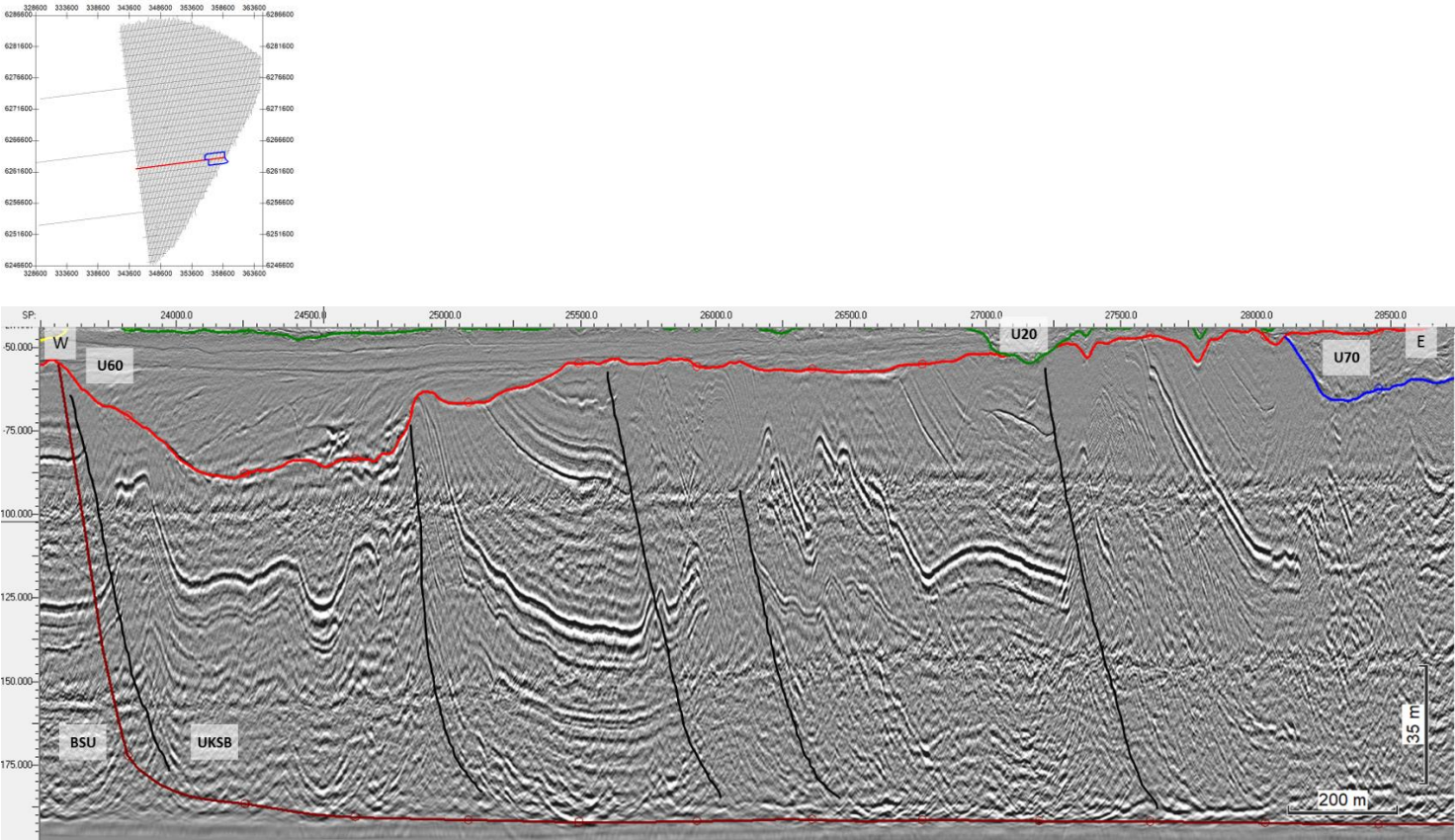


Figure 206 Large scale faults within a thrust complex.
Seismic profile BX4_OWF_E_XL_23000

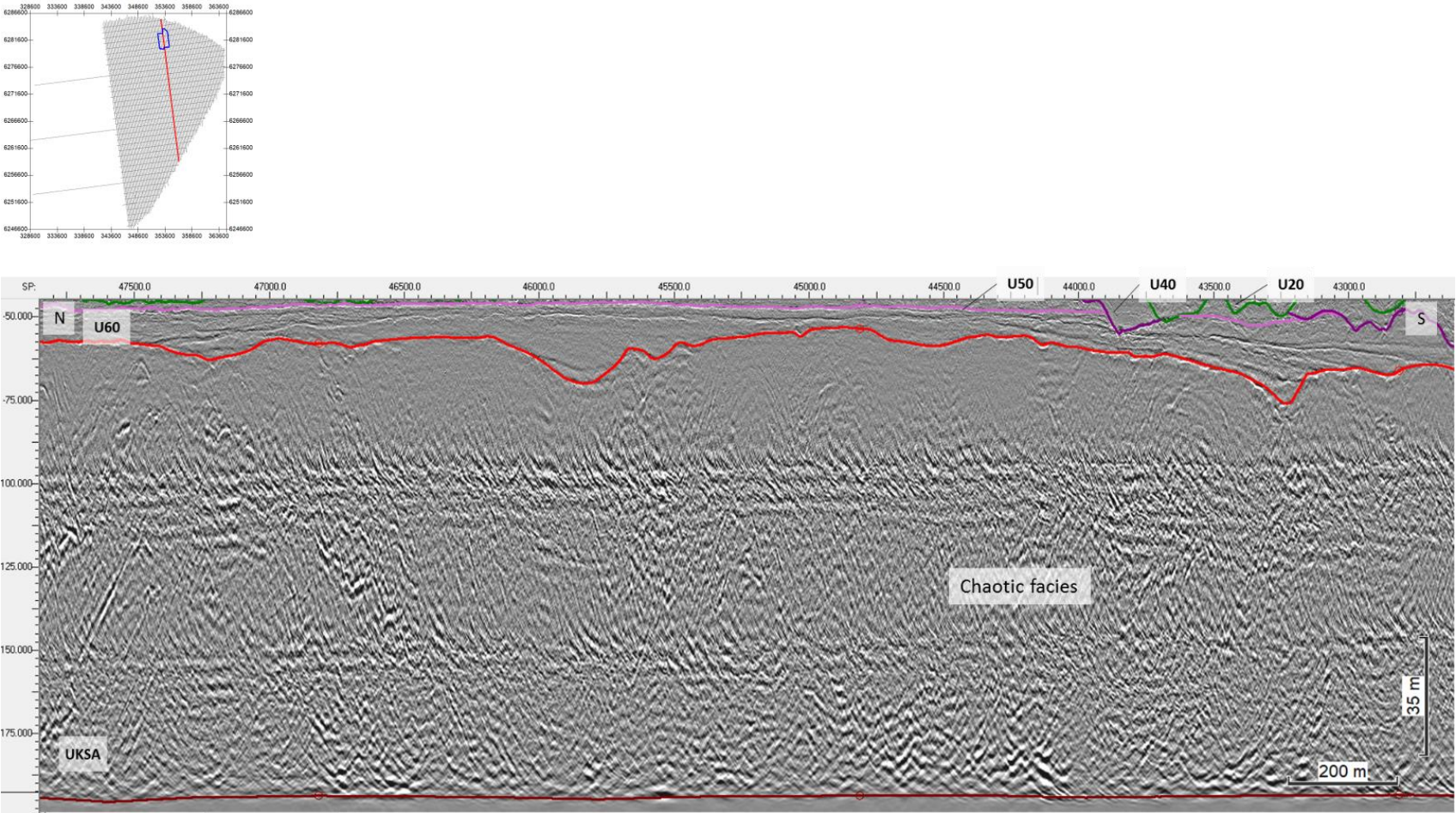


Figure 207 Intense deformation within a thrust complex.
The image shows obliterating reflector's continuity and organization – chaotic facies.
Seismic profile BM4_OWF_E_2D_10710

a) Faulting

Evidence of faulting has been identified across the site. Faults were picked manually where relevant planar discontinuities, displacement of seismic reflectors, and major reflector-fault drags were recognised on the seismic data. Depending on the angle between the faults and the seismic sections, some features may appear more noticeable than others. A way to mitigate this was by inspecting the fault basemap to ensure that features were digitized on a coherent and continuous manner; i.e., tracing was done from profiles where the faults were more evident to profiles with reduced expression. Figure 208 displays the final fault basemap produced. Minor, isolated, and dubious features may have been left out due to the complexity of the subsurface framework and difficulty in recognizing all features and faults, as line spacing dictates the resolution in which subsurface features can be traced laterally (ex., tectonic structures).

Faults are observed affecting all units, but do not greatly affect sediments of U20 and younger (Figure 209 to Figure 211). Their type and size are highly variable. The majority of faulting is captured within UKS, as this unit represents the extent of sediment deformation. Horizon KS, the surface that delineates the deformation front, may itself be a fault plane (Figure 209).

The majority of the faulting in the site is related to glaciotectonics (see section below). However, salt tectonics and gravitational deformation are also interpreted as fault-producing processes in the area (see sections below).

Lack of fault identification should not be taken as an assumption of total absence.

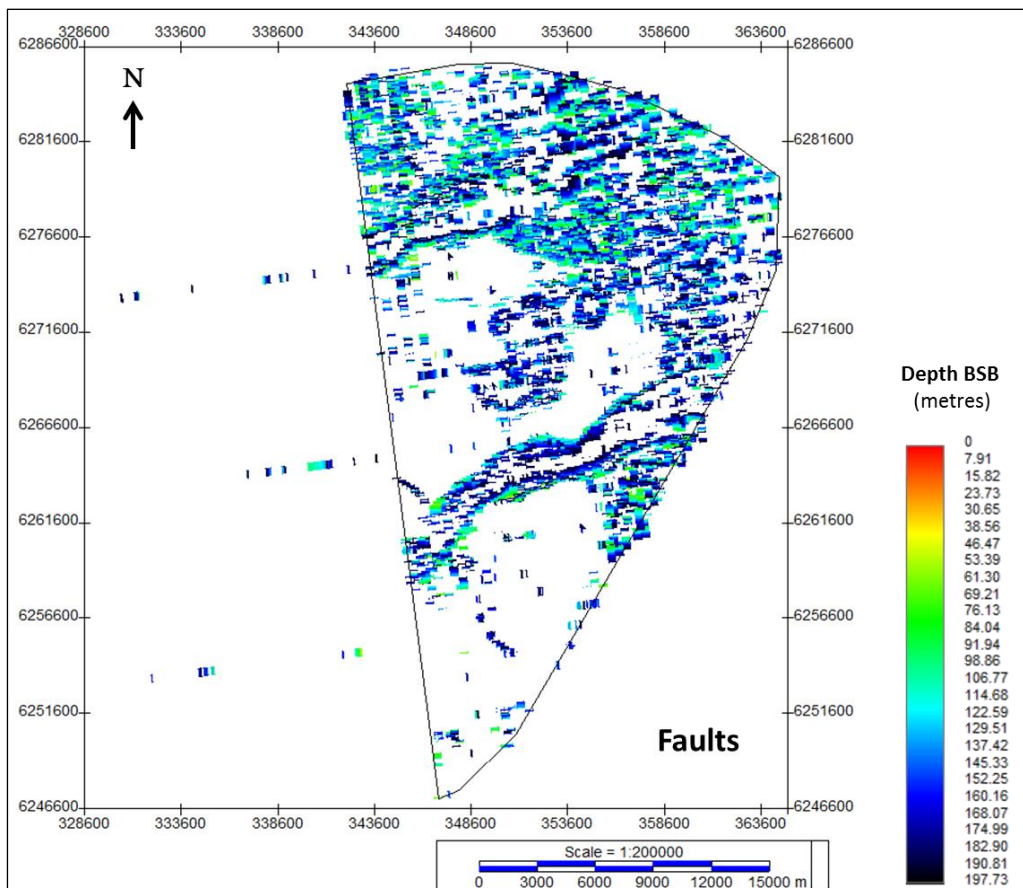


Figure 208 Map displaying all the interpreted faults in the site.
Units in metres below BSB.

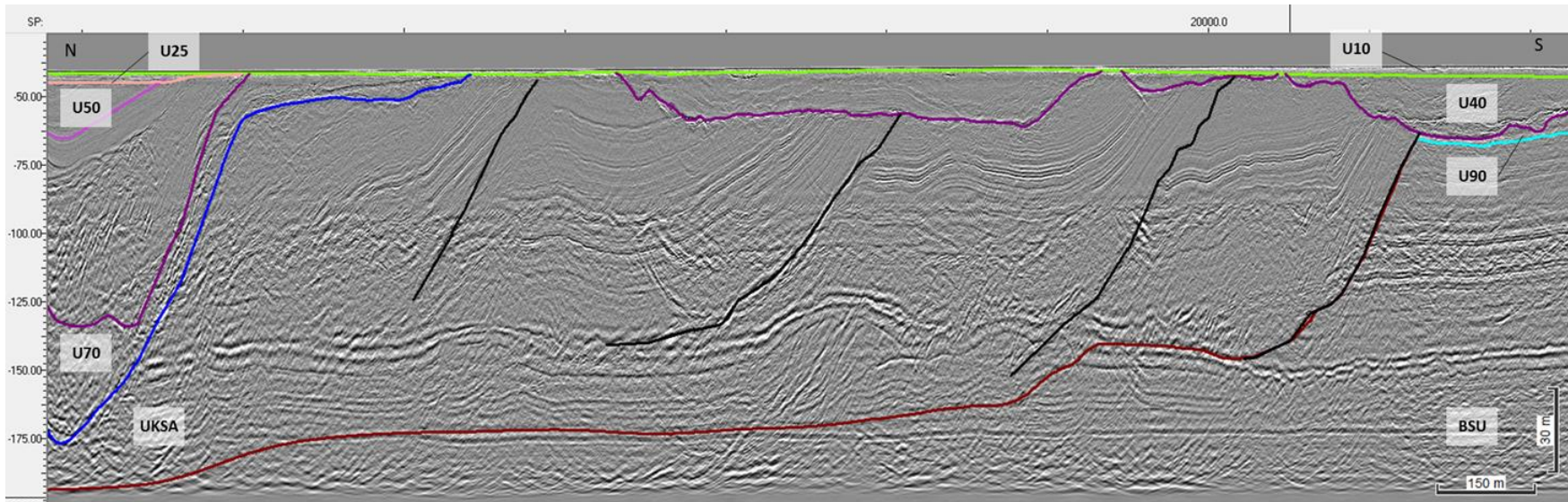
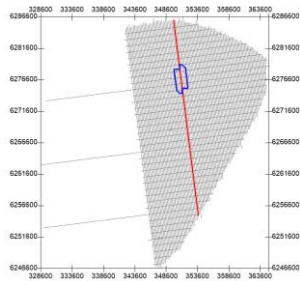


Figure 209 Thrust complex of Seismic Unit UKSA.
 The image shows horizon KSA delineating a decollement surface, flats and ramps, and the deformation front plane. Thrust planes dip NE, indicating a compression advancing towards SW. Seismic profile BM3_OWF_E_2D_07770

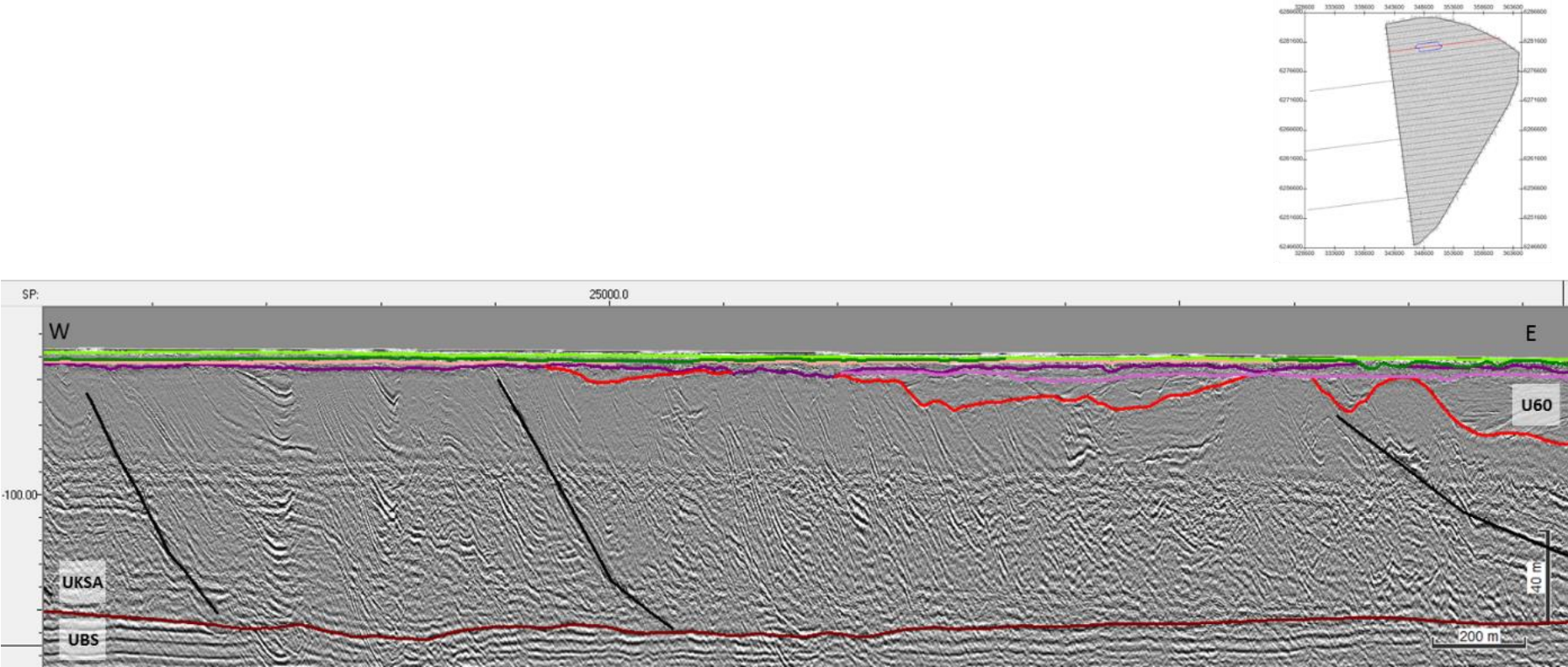


Figure 210 Thrust complex of Seismic Unit UKSA.
The image shows horizon KSA delineating a decollement surface.
Thrust planes dip NE, indicating a compression advancing towards SW. Seismic profile BX1_OWF_E_XL_05000.

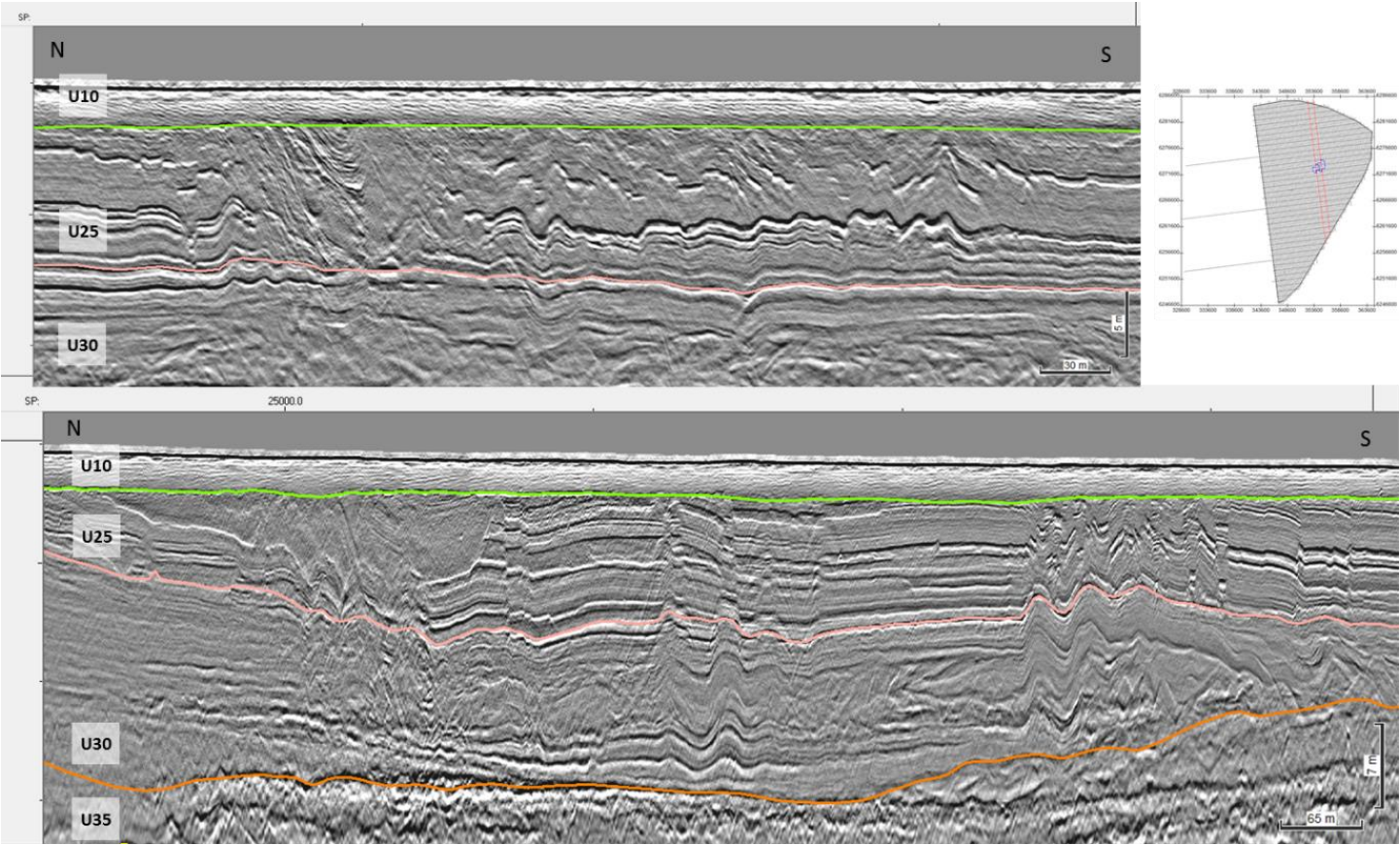


Figure 211 Internal deformation of Seismic Unit U25.
Seismic profiles BM4_OWF_E_2D_10290 and BM4_OWF_E_2D_11340

b) Glaciotectonics

Seismic unit UKS captures the vast majority of the tectonized deposits and the distribution of the different patterns of deformation identified (see section 8.6.13). The UHRS data clearly depicts the distribution and extent of glaciotectonism within unit UKS.

In the survey area, deformation is mostly interpreted as large-scale thrust structures (including imbricated faults, fault ramps, fault-drags, and folds; Figure 209), typical of glaciotectonic thrust complexes formed ahead of an ice sheet as it moves forward.

Two distinct areas of thrust deformation were identified within the survey area, delineated by the polygons KSA_Thrusting (Northern part of horizon KSA, within sector North) and KSB_Thrusting (Figure 212).

Horizon KSA truncates seismic units below H70, i.e., the glacial deformation within sector North (KSA_Thrusting) affects units U85, U90, and BSU (Figure 213). However, deformation within the SE edge of the site (KSB_Thrusting) appears to be older than U85-U90, as these units truncate deformed deposits in this area (Figure 214). As such, the glaciotectonic deformation of northern sector (KSA_Thrusting) is interpreted to be relatively younger than the deformation in the SE corner (KSB_Thrusting).

In order to better understand these two different stages of glaciotectonism in the area, a small sample of the largest thrust faults from each corresponding area were analysed according to their general orientation, to provide clues on the main directions of ice push acting on the site. The analysis was done in crossing survey lines (at the intersection point of Inlines and Crosslines) where a major thrust plane could be recognised in both.

Figure 215 displays all the measured thrust faults for area KSA_Thrusting (Total = 43 faults), and their general dip and strike. Thrust faults in this area generally dip towards NE (see rose diagram in Figure 215), towards an area of complex facies, mostly chaotic with disorganized fault displacements (shaded in grey). This area most likely corresponds to a moraine deposit, sitting behind the thrust complex, as exemplified by the diagram X-X'. The thrust fault dip analysis within this area indicates an overall thrust direction of NE-SW (orange arrows; mean = N32°).

Figure 216 displays all the measured thrust faults for area KSB_Thrusting (Total = 18 faults), and their general dip and strike. Thrust faults in this area generally dip towards SE (see rose diagram in Figure 216), indicating an overall thrust direction of SE-NW (orange arrows; mean = N117°).

The two distinct thrust directions given by the fault analysis further support the occurrence of at least two different stages of glaciotectonism.

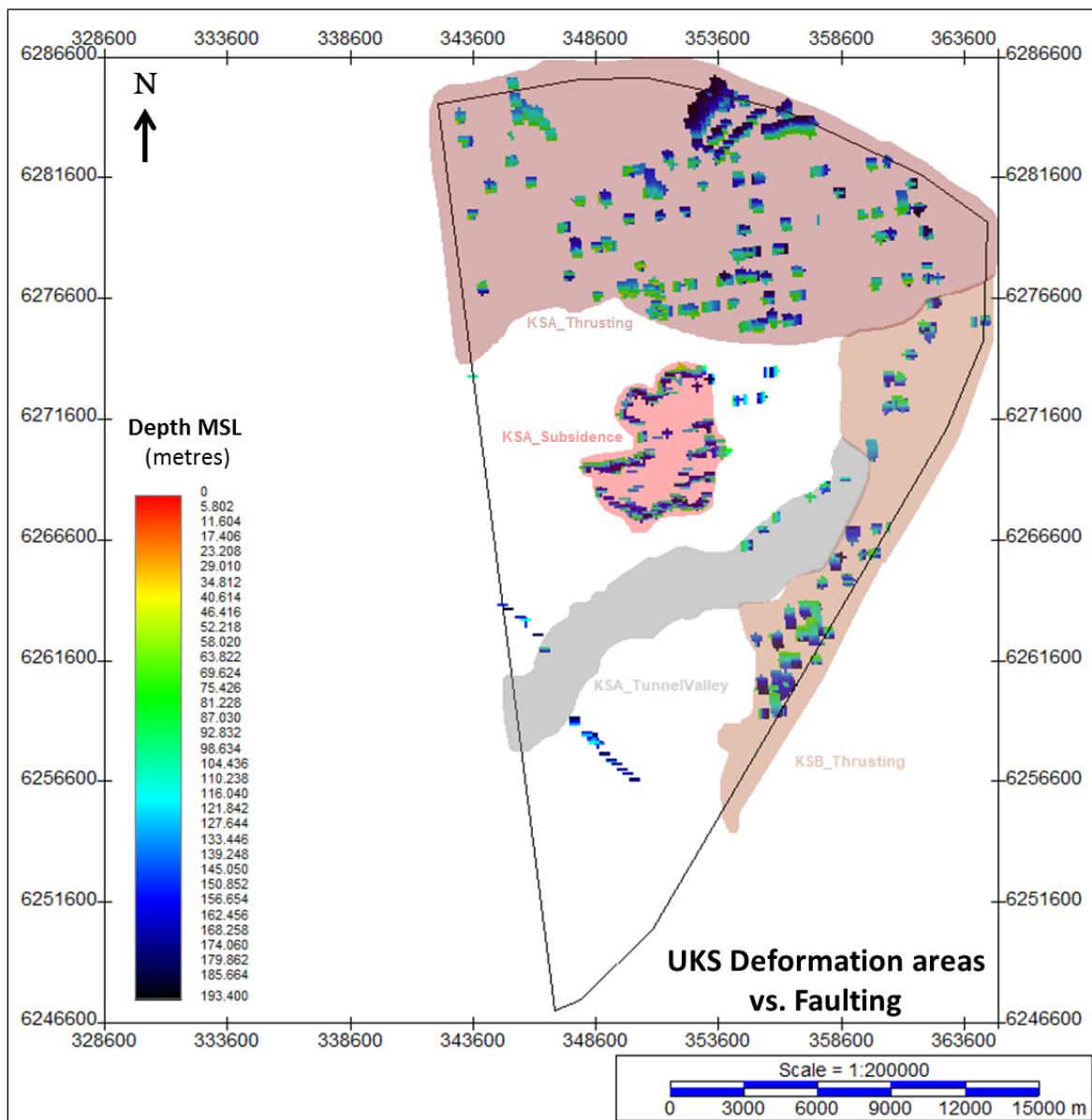


Figure 212 Deformation domains within the Seismic Unit UKS (composite of UKSA and UKSB)
 The image also shows sampled faults used for fault pattern analysis.

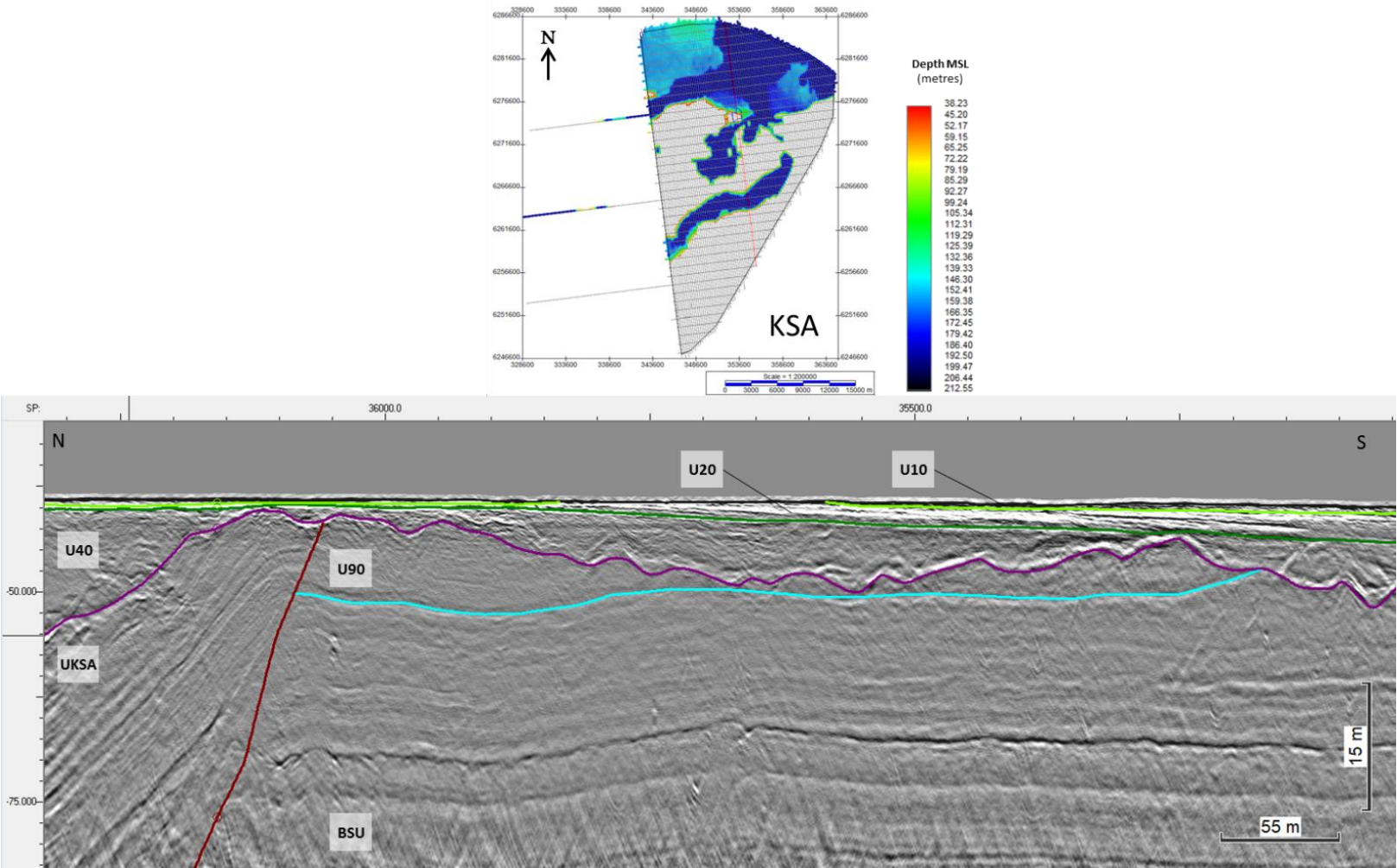


Figure 213 Seismic Unit UKSA truncating the deposits of the Base Seismic Unit BSU.
 Seismic profile BM4_OWF_E_2D_09870

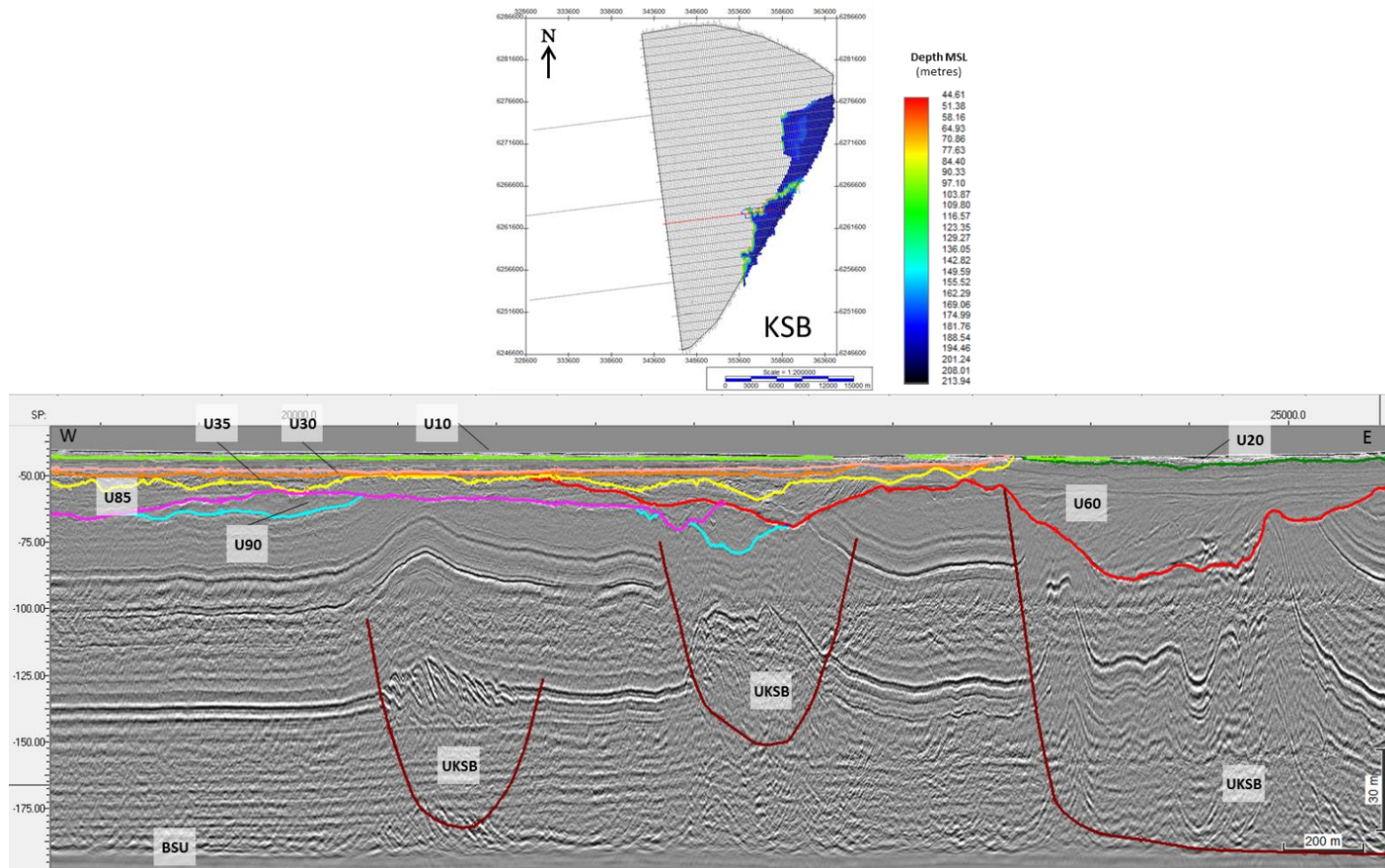


Figure 214 Seismic Units U85 and U90 not being affected by UKSB deformation, Truncating deformed the deposits of the Base Seismic Unit BSU. Seismic profile BX3_OWF_E_XL_23000

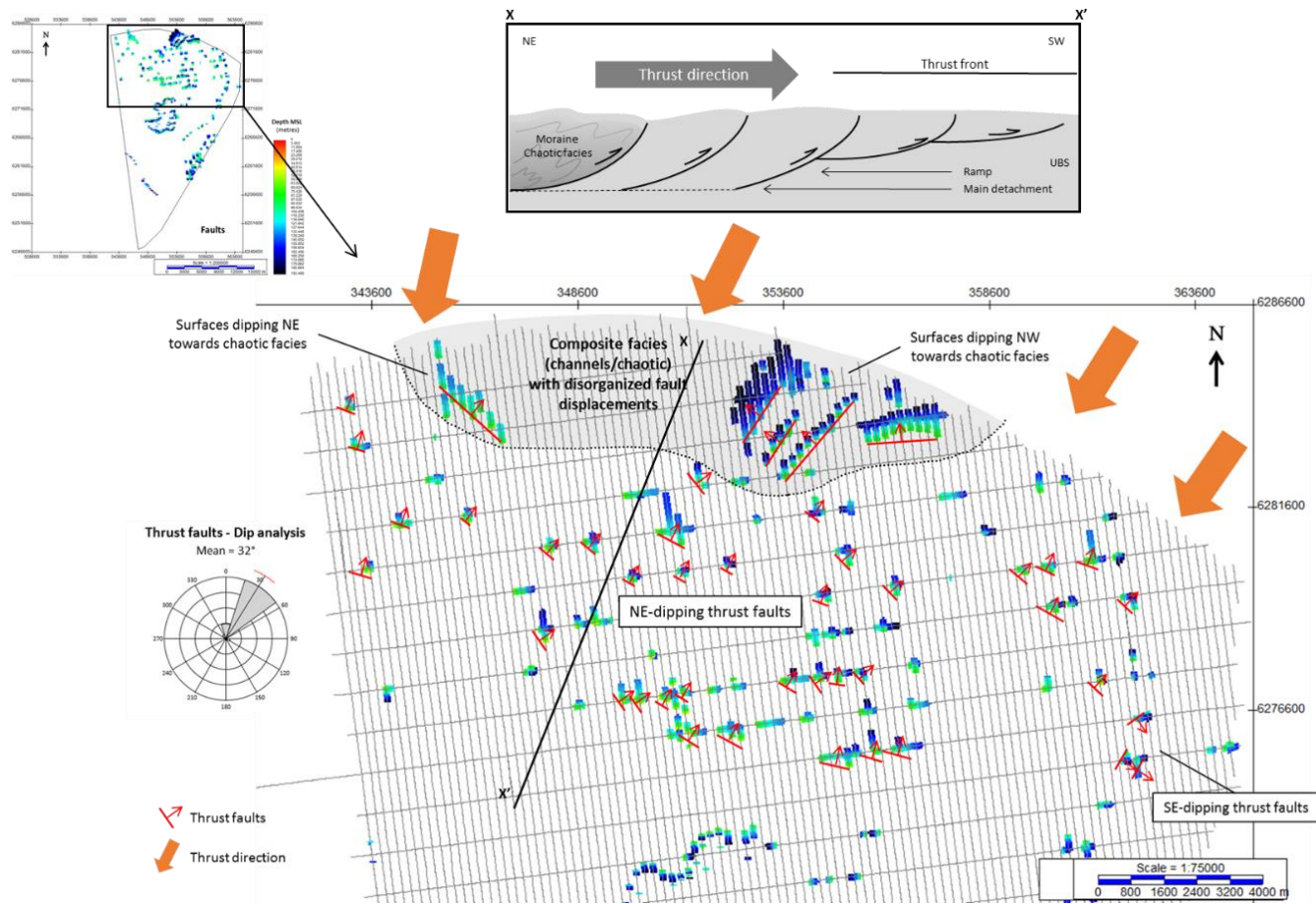


Figure 215 Fault pattern analysis of the faults present in the north sector. Sample analysed = dip of 43 major thrust faults mapped in crossing survey lines (at the intersection point of Inlines and Crosslines) where a major thrust plane could be recognised in both. Faults are assessed according to their general orientation, to provide clues on the main directions of ice push acting on the site. The rose diagram reveals that the majority of the thrusts in the north sector dip towards NE, indicating ice advance towards SW. The profile X-X' provides a visual schematic of the interpreted thrust complex.

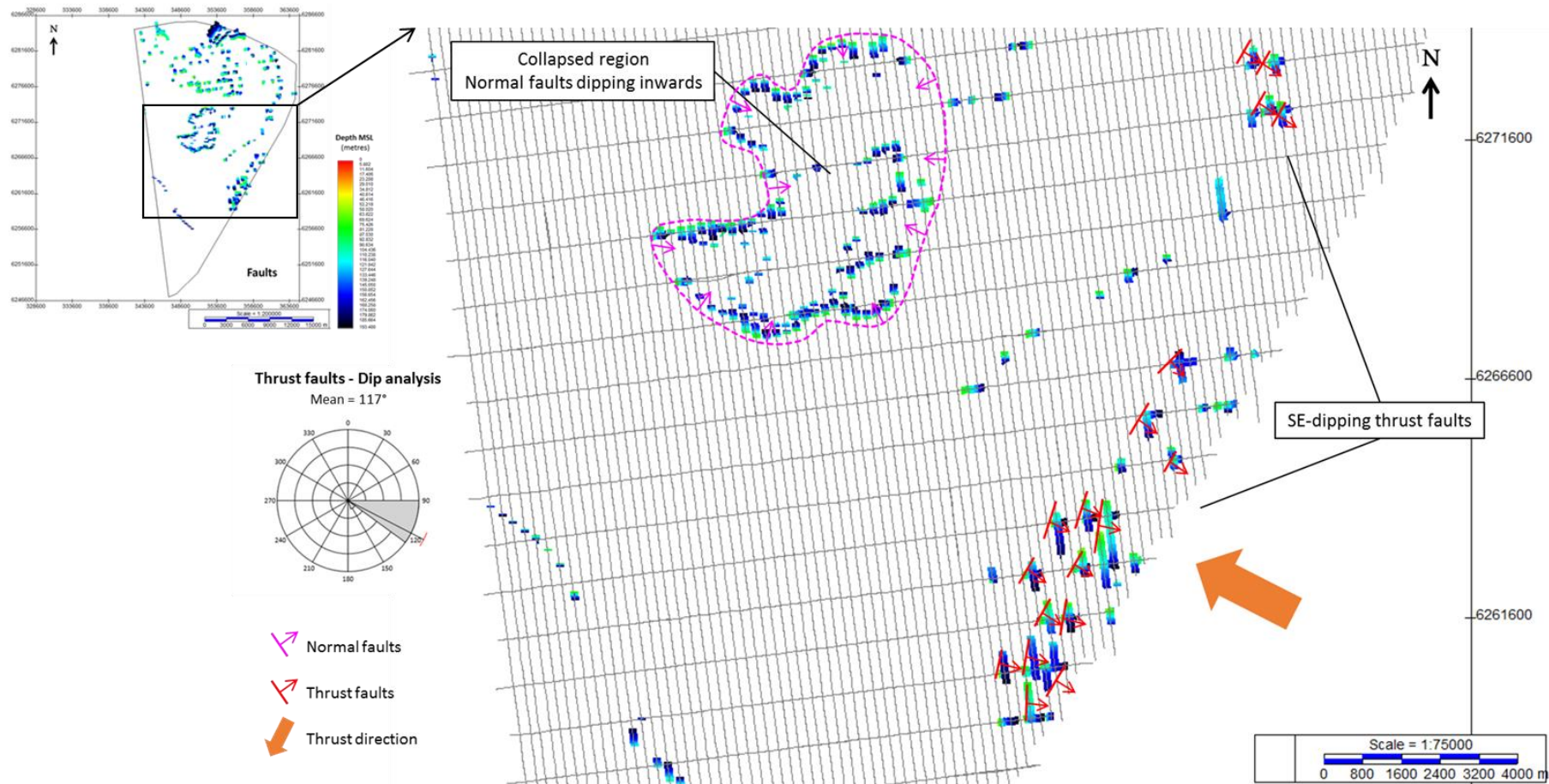


Figure 216 Fault pattern analysis of the faults present in the south sector. Sample analysed = dip of 18 major thrust faults mapped in crossing survey lines (at the intersection point of Inlines and Crosslines) where a major thrust plane could be recognised in both. Faults are assessed according to their general orientation, to provide clues on the main directions of ice push acting on the site. The rose diagram reveals that the majority of the thrusts in the south sector dip towards SE, indicating ice advance towards NW. As such, it is interpreted that the deformation associated with the southern thrust complex may be older than the Weishcelian glaciation (possibly Saalian?).

c) Salt tectonics

Large faults with extensional displacement are locally observed affecting the deeper Pre-Quaternary deposits, within unit UKS. The occurrence of these normal faults is limited to a region at the centre of the survey area. Large normal faults laterally bound this region, resulting in the subsidence of a Pre-Quaternary block delineated by the polygon KSA_Subsideance (Figure 217).

Towards the NE corner of the survey area, within the polygon KSA_Extension, Pre-Quaternary strata occur dipping in opposite directions, separated by a large fault zone (Figure 218). Internal deformation within these tilted blocks appears to be extensional in nature.

All the normal faults observed in the survey area extend deeper than the UHR seismic record. As such, and due to their extensional character, these areas were compared with the known basement structure of the region to assess the possibility of salt tectonics as their origin. Figure 219 displays the polygons KSA_Extension and KSA_Subsideance overlaid on the Base of Chalk Structure Map (GEUS). The highlighted areas of extension/subsidence occur vertically above previously identified major extensional faults associated to the Zechstein salt tectonism (Michelsen, 1993). Thus, it is interpreted that the deformation observed within these areas is most likely related to deep salt diapirism (ex., salt movement related to glacial load and melt back).

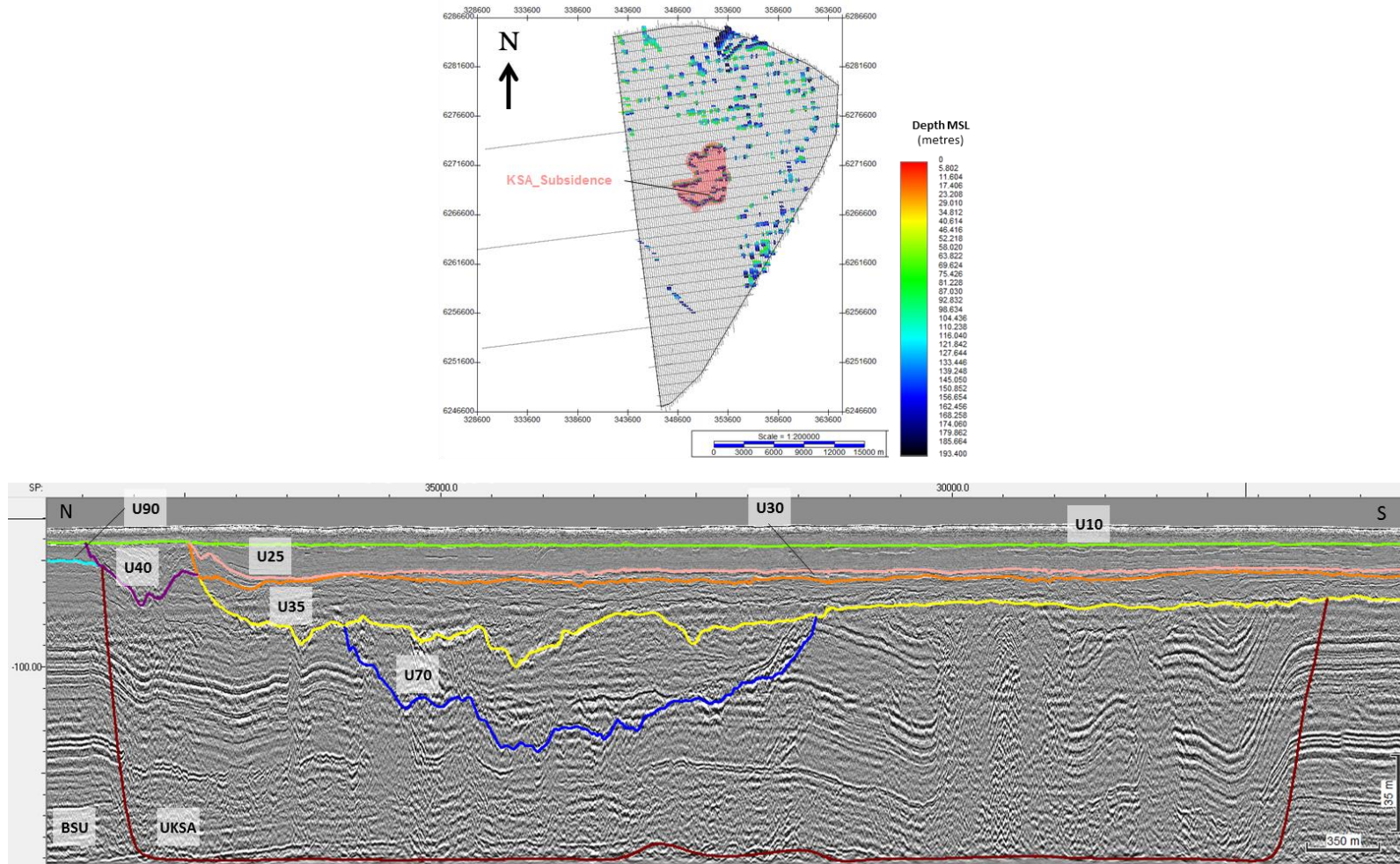


Figure 217 Subsidence area bounded by large normal faults at the centre of the survey area. The area is delimited by the polygon KSA_subsidence Seismic profile BM3_OWF_E_2D_08190 showing subsidence, bounded by two large normal faults.

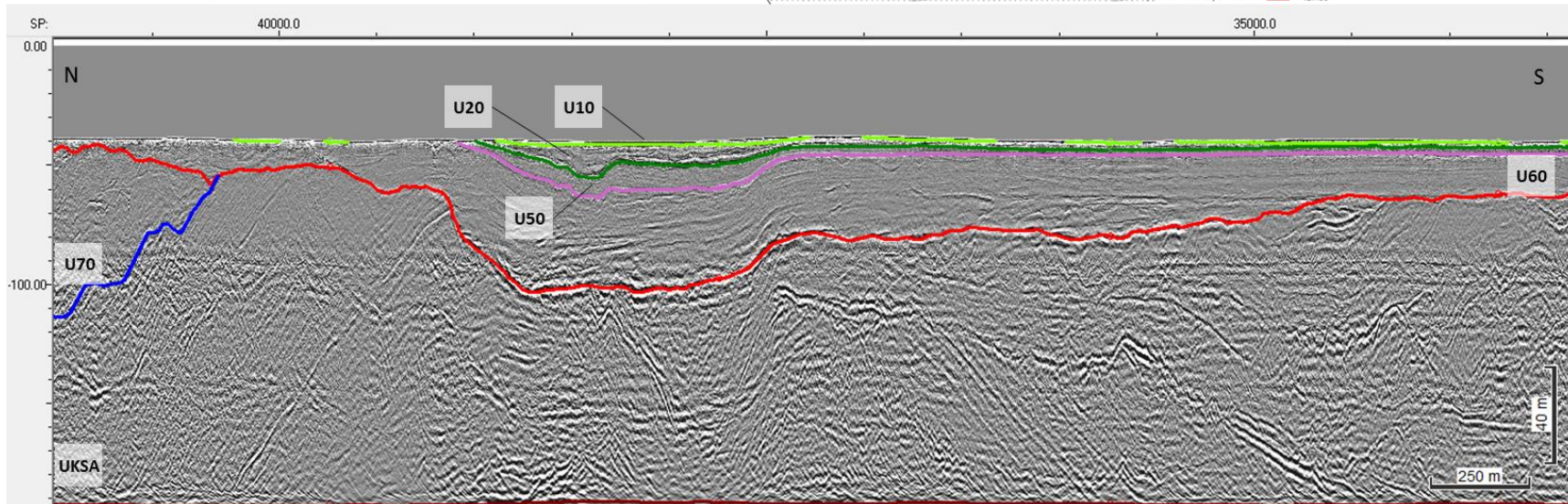
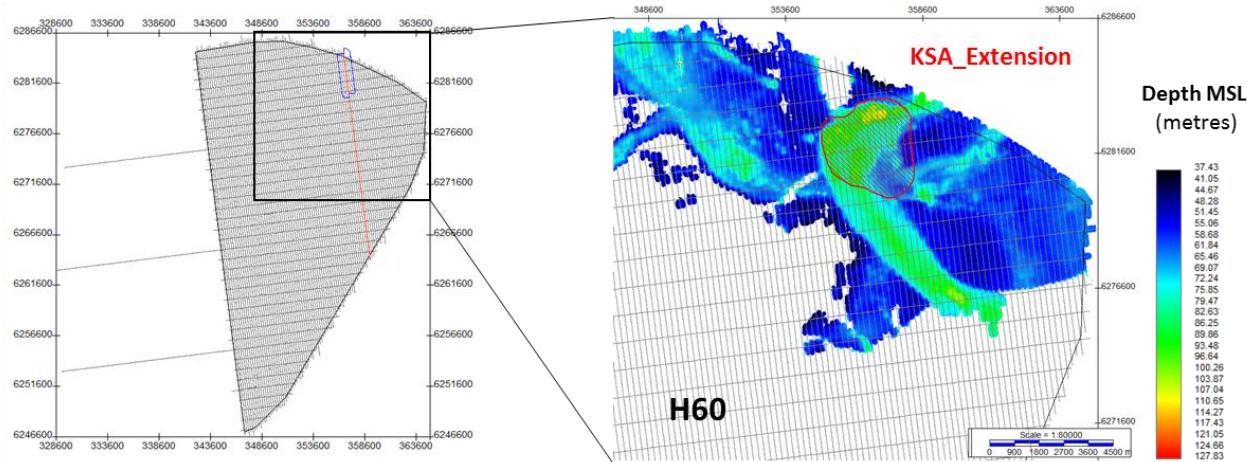


Figure 218 Older strata dipping opposite directions; likely related to salt tectonics deformation.
 Seismic profile BM5_OWF_E_2D_14280

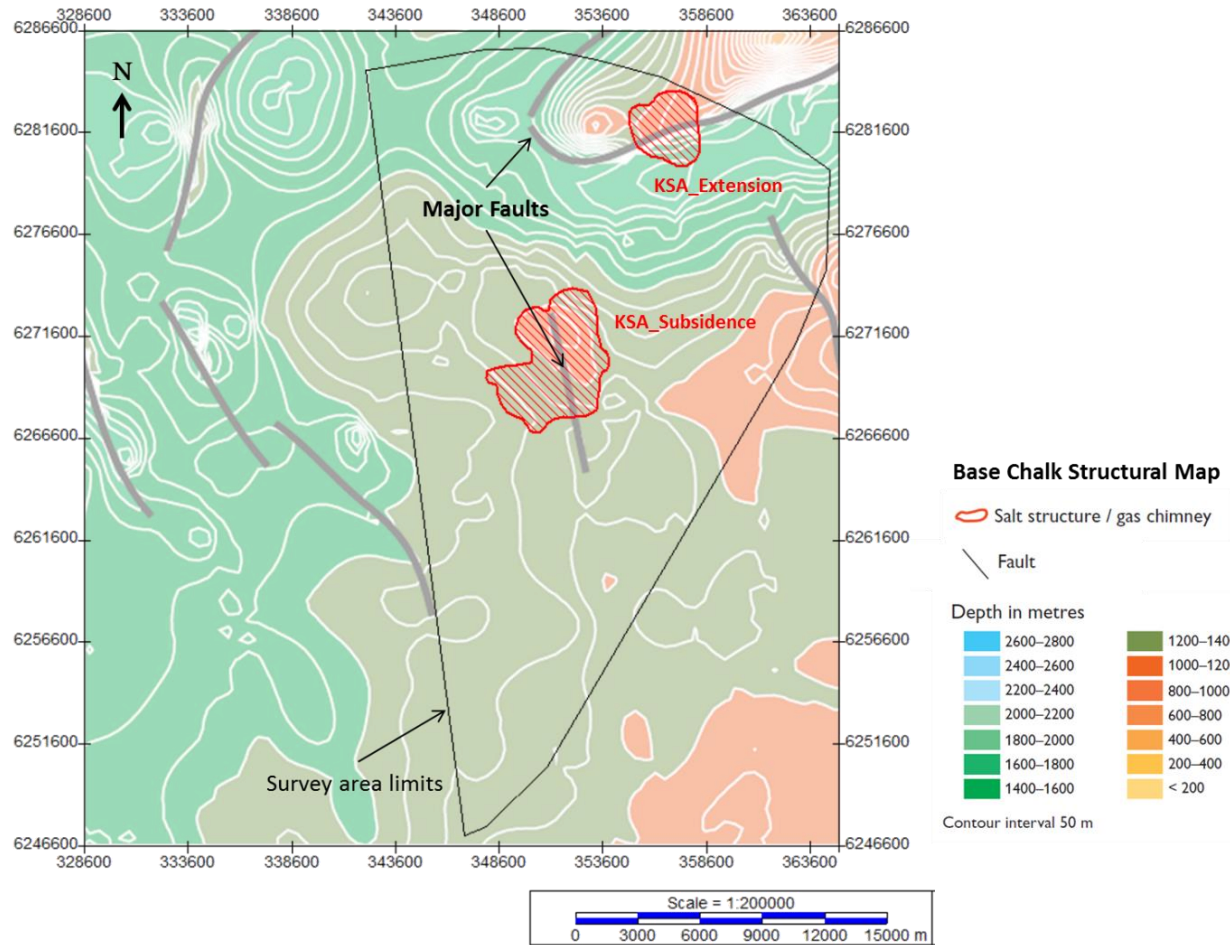


Figure 219 Structural map of the base of the Chalk deposits (GEUS).
 The image shows the main structural features related to salt tectonics in the area.
 Polygons KSA_Subsideance and KSA_Extension occurs vertically above major deep fault structures. As such, it is likely that extensional deformation observed in the area is related to salt movement.

d) Gravitational Deformation

Slope failure, collapse along the flanks of tunnel valleys and major incisions (upslope extensional faulting with chaotic facies at the base) are some of the structures observed in the survey area that may be related to gravitational deformation.

Polygon KSA_TunnelValley delineates deformation that occurs directly below the large NE-SW valley of U70 (delineated by the polygon H70_CH_08), along its full length (Figure 220). This deformation has mostly a disorganized character.

The base of the valley flanks is uneven (along H70), with numerous steps resembling small extensional displacements. In the upper sections of the deformed sediments, immediately below H70, better-preserved strata dip inwards towards the centre of the valley, showing disturbed/chaotic facies (stacked chaotic-mound facies association) towards the base. Such deposits could result from slope failure or collapse along the flanks, as a result of gravitational failure.

It is interpreted that the U70 valley was emplaced along the pre-existent deformation “corridor”, exploiting this weakened area.

These collapse features and small slump deposits are observed associated to the flanks of other large incisions in the survey area.

Local areas of seismic unit U25 exhibit variable degrees of internal deformation. Within the survey, this deformation is typically observed as minor folding in less-deformed areas and as intra-U25 faulting (with minor displacements, both extensional and compressional) in more intensely-deformed strata, typically occurring near the steep margins of the central basin (Figure 211). Extreme deformation is observed in profile Baseline_1 (towards W), where faulting and folding render U25 facies significantly disrupted and chaotic (Figure 221). These deformation patterns are intrinsic to U25, not affecting the units above and below. As such, it is interpreted that this deformation is most likely related to thin-skinned gravitational tectonics, possibly also associated to sediment dewatering.

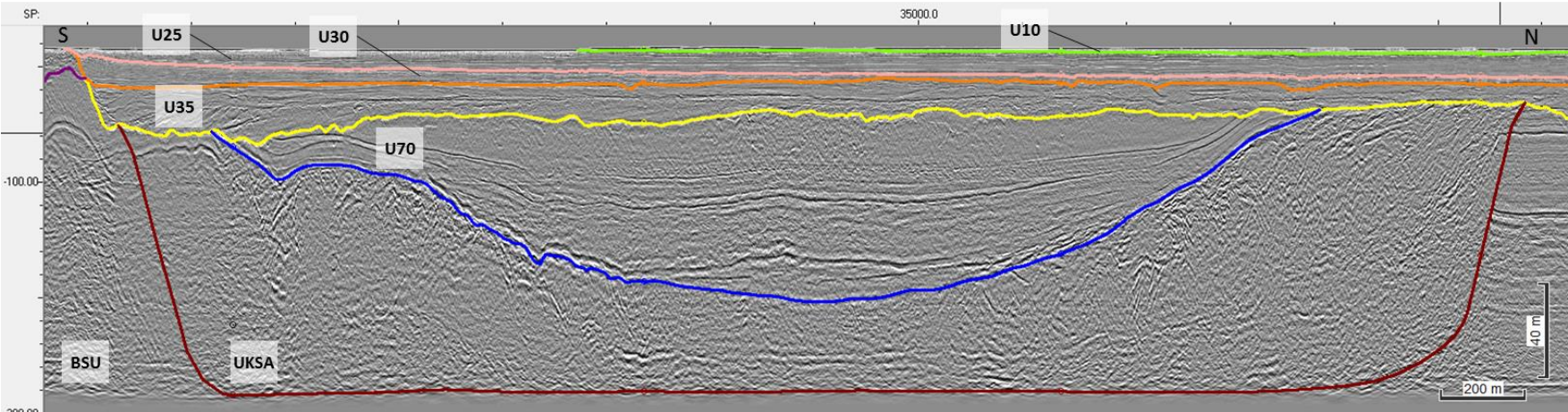
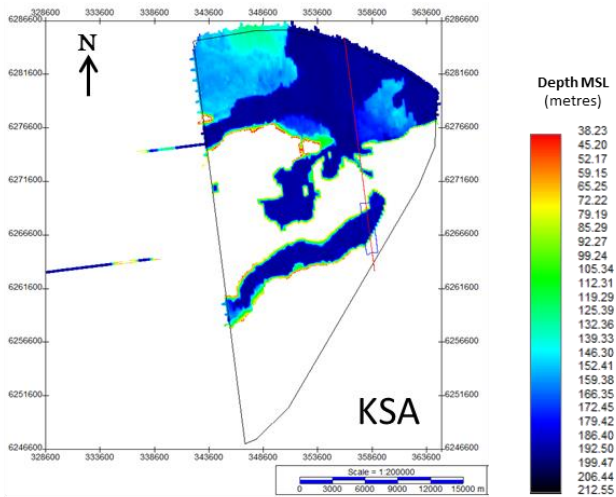


Figure 220 Extensional features below a U70 valley.
 The features are interpreted to result from collapse of the valley flanks.
 Seismic profile BM5_OWF_E_2D_13860 Channel H70_CH_08.

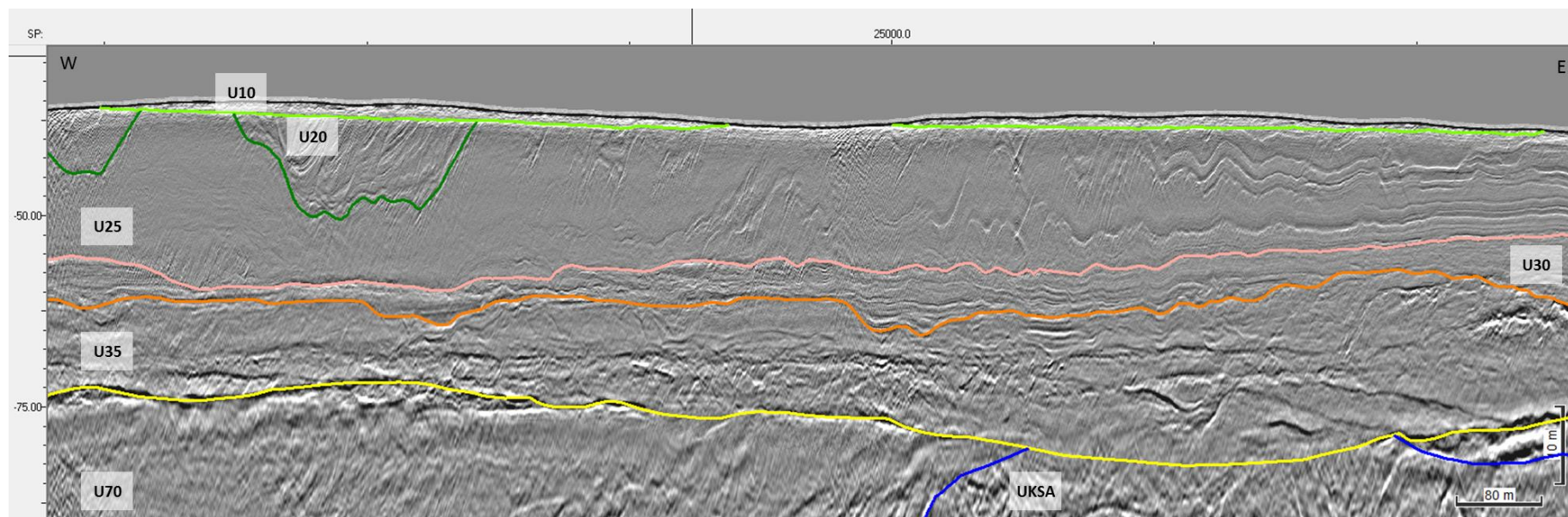
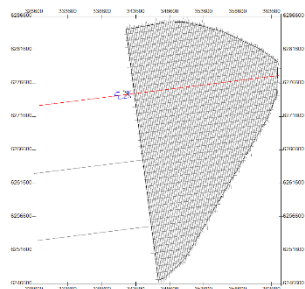


Figure 221 Internal deformation of U25, increasing in intensity from E to W.
The deformation is interpreted to be from folding to faulting and complete strata disruption.
Seismic profile BX2_OWF_2D_Baseline_1

8.8.2 | BURIED CHANNELS AND TUNNEL VALLEYS

Multiple paleo-valley, basins, and channel systems are widespread throughout the site, displaying a range of sizes and depositional characteristics. Often, the channels are interpreted as multi-generational, appearing as a vertical succession of channels/valleys nested one within another. The most significant erosional surfaces were identified and mapped; these major events correspond to the bases of the units described above. The channels can be easily identified in the various horizon basemaps presented in the previous chapter.

Figure 222 display a composite surface resulting from the addition of all base horizons of units U10 to U70. In this composite surface, all major channel and valley incisions are well observed, highlighting the diversity in size, drainage pathways, and vertical succession. Older and/or deeper incisions are displayed in greens, whereas younger channel generations are blue-dark blue. The major incisions are identified by the polygons marked in Figure 223, showing their associated seismic unit.

Due to the large number of paleo-incisions are numerous in this area, the mapping of these as geohazards was focused on the major features that are not already delineated by the unit's basal horizons (Figure 224 and Figure 225). Therefore, all minor paleo-valleys have not been included in this mapping. Details on the seismic character of major incisions marked by unit bases can be found in the respective unit's description (see section 8.6.1).

Channel morphology is diverse and ranges from V-shaped, U-shaped, to box-shaped (Figure 226 to Figure 228). Similarly, there exists a broad distribution of channel widths and depths observable in the UHRS data. The sediment infill of the channel features varies laterally and vertically. This degree of sediment heterogeneity may result in significant variability of geotechnical parameters within the channels.

From a hazard standpoint, the infill of tunnel valleys may be problematic for a variety of reasons. Tunnel valley infill is nearly always complex, with a heterogenous sediment composition, where lithological and mechanical properties may change rapidly over small spatial scales. Also, faulting and fracturing, from direct ice incision and pressurized hydraulic action, are common in tunnel valleys. Tills are commonly deposited near the base of tunnel valleys. Lastly, the complex load, and stress histories of tunnel valleys and their marginal deposits translates into abrupt differences in mechanical properties.

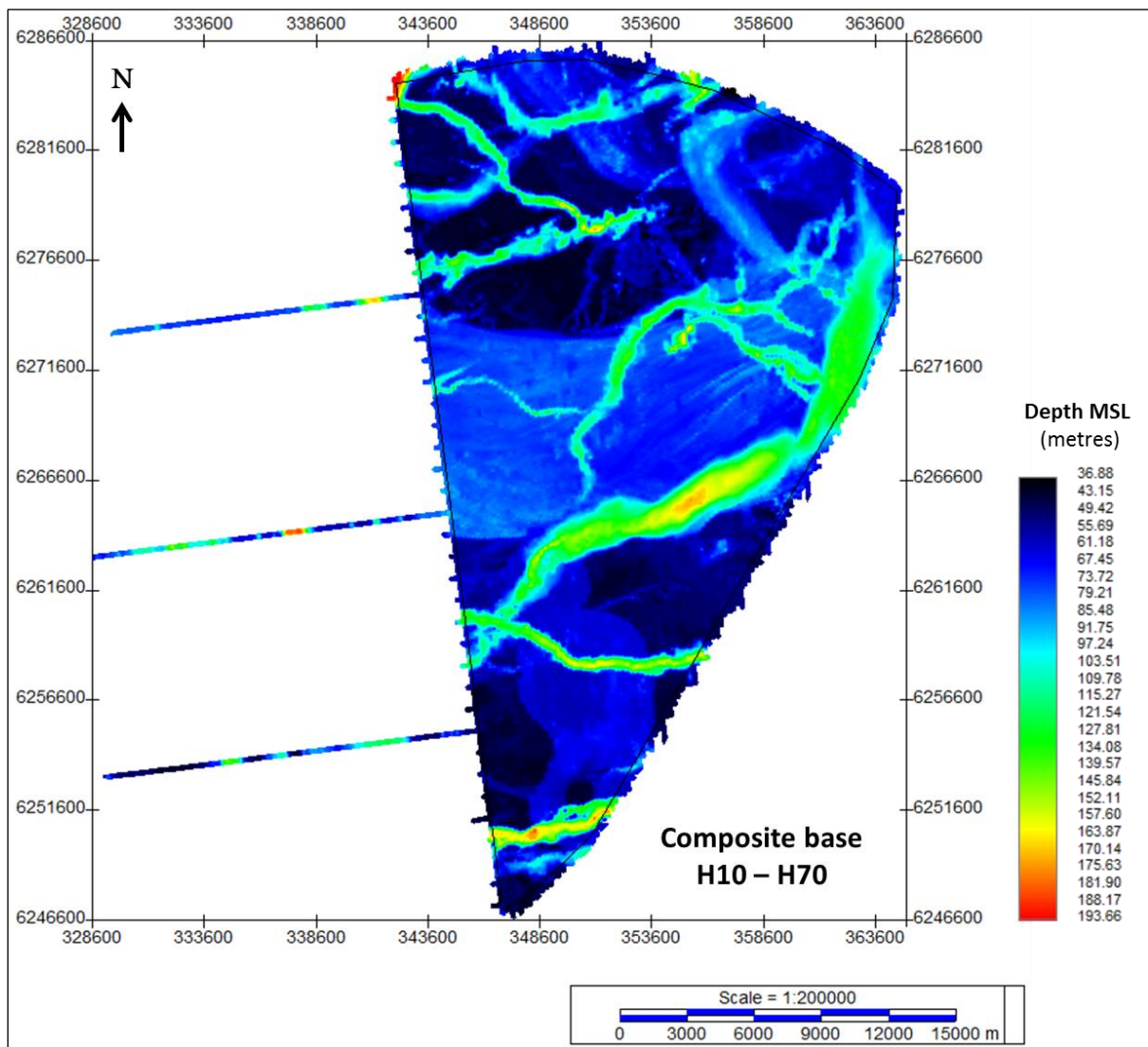


Figure 222 Composite surface from the addition of all base horizons of units U10 to U70. All major channel and valley incisions are well observed, highlighting the diversity in size, drainage pathways, and vertical succession. Older and/or deeper incisions are displayed in greens, whereas younger channel generations are blue-dark blue.

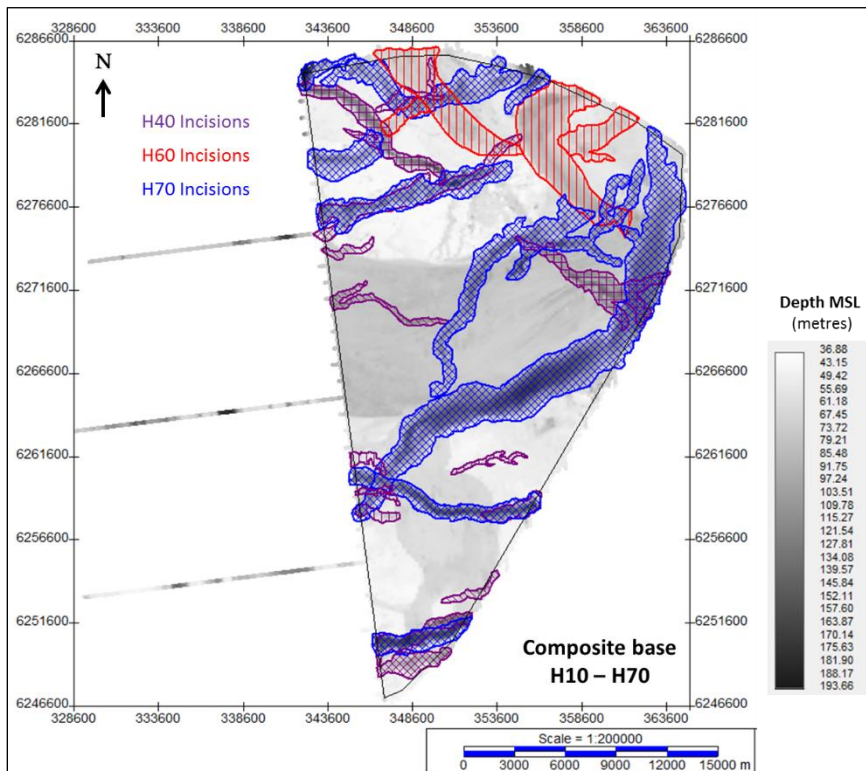
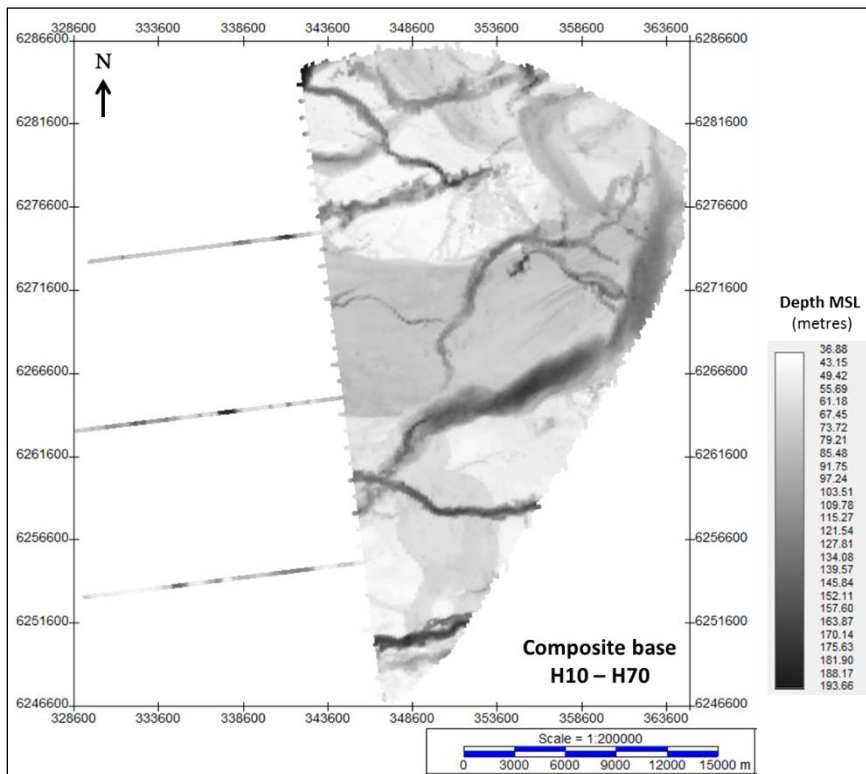


Figure 223 Composite surface.
 The surface is derived from the addition of all base horizons of units U10 to U70 (Black to white colour bar), against all the interpreted major incisions of U40, U60, and U70.

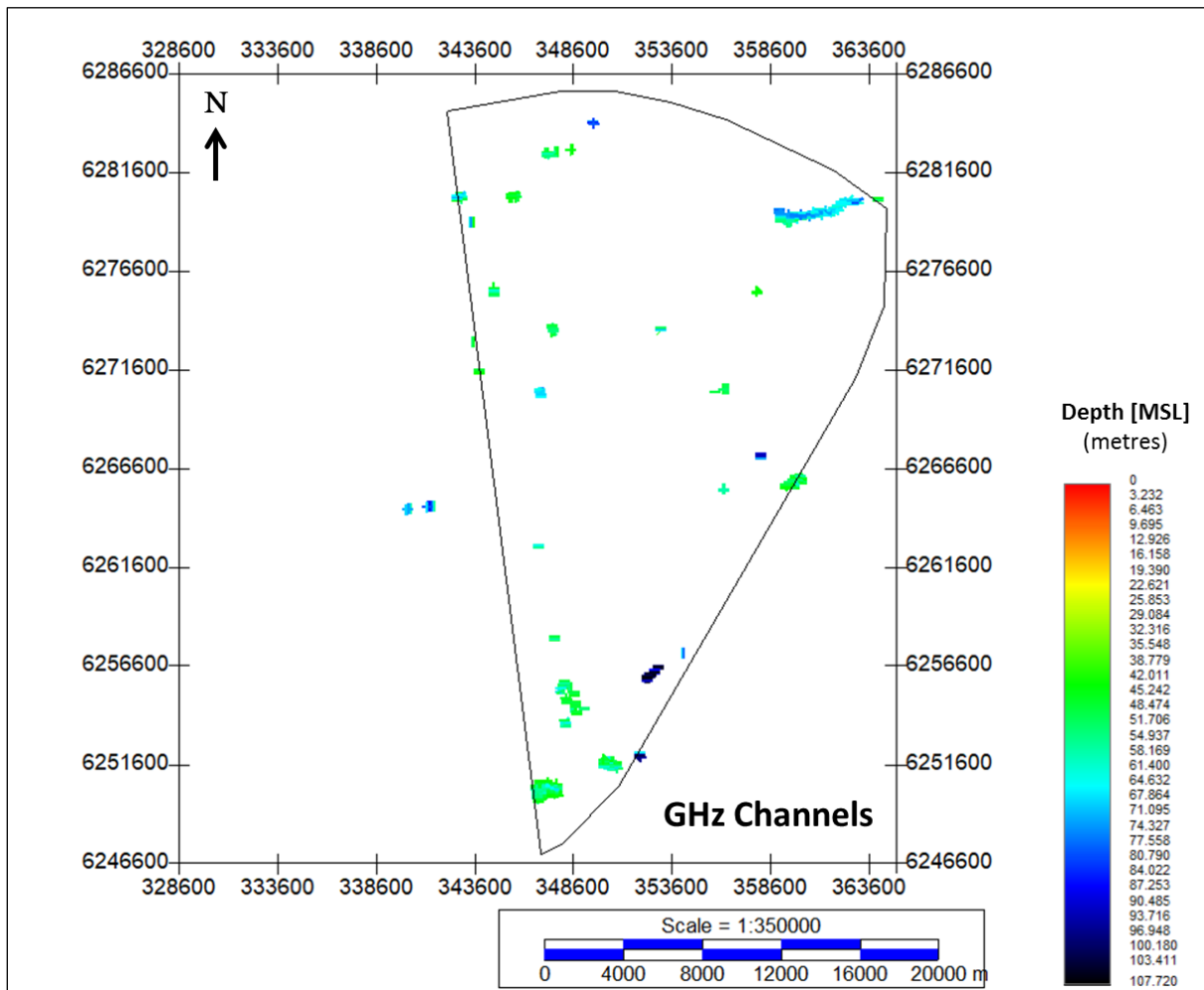


Figure 224 Interpreted major channels not delineated by any unit's basal horizon.
Units in metres below MSL.

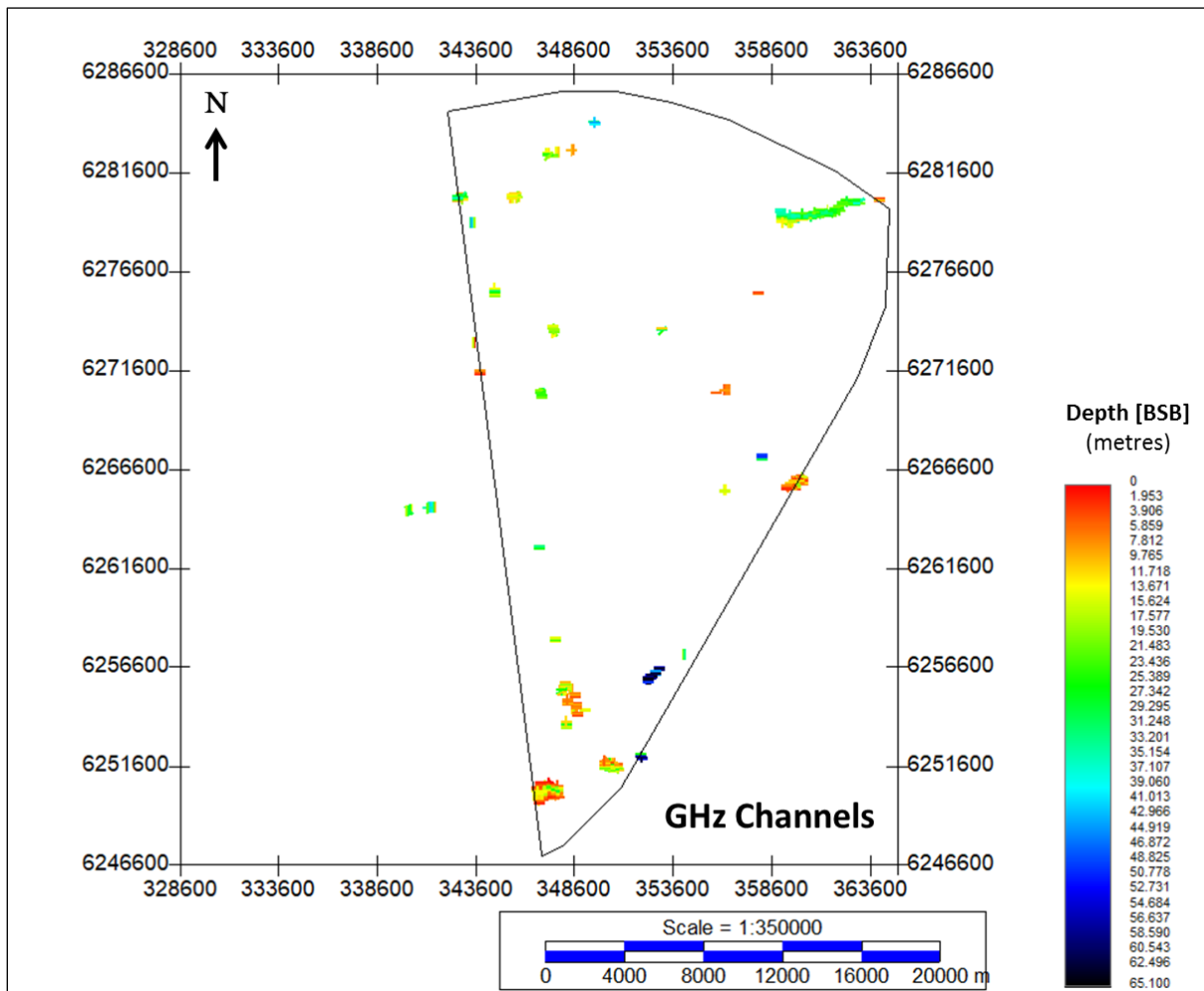


Figure 225 Interpreted major channels not delineated by any unit's basal horizon.
Units in metres below seabed.

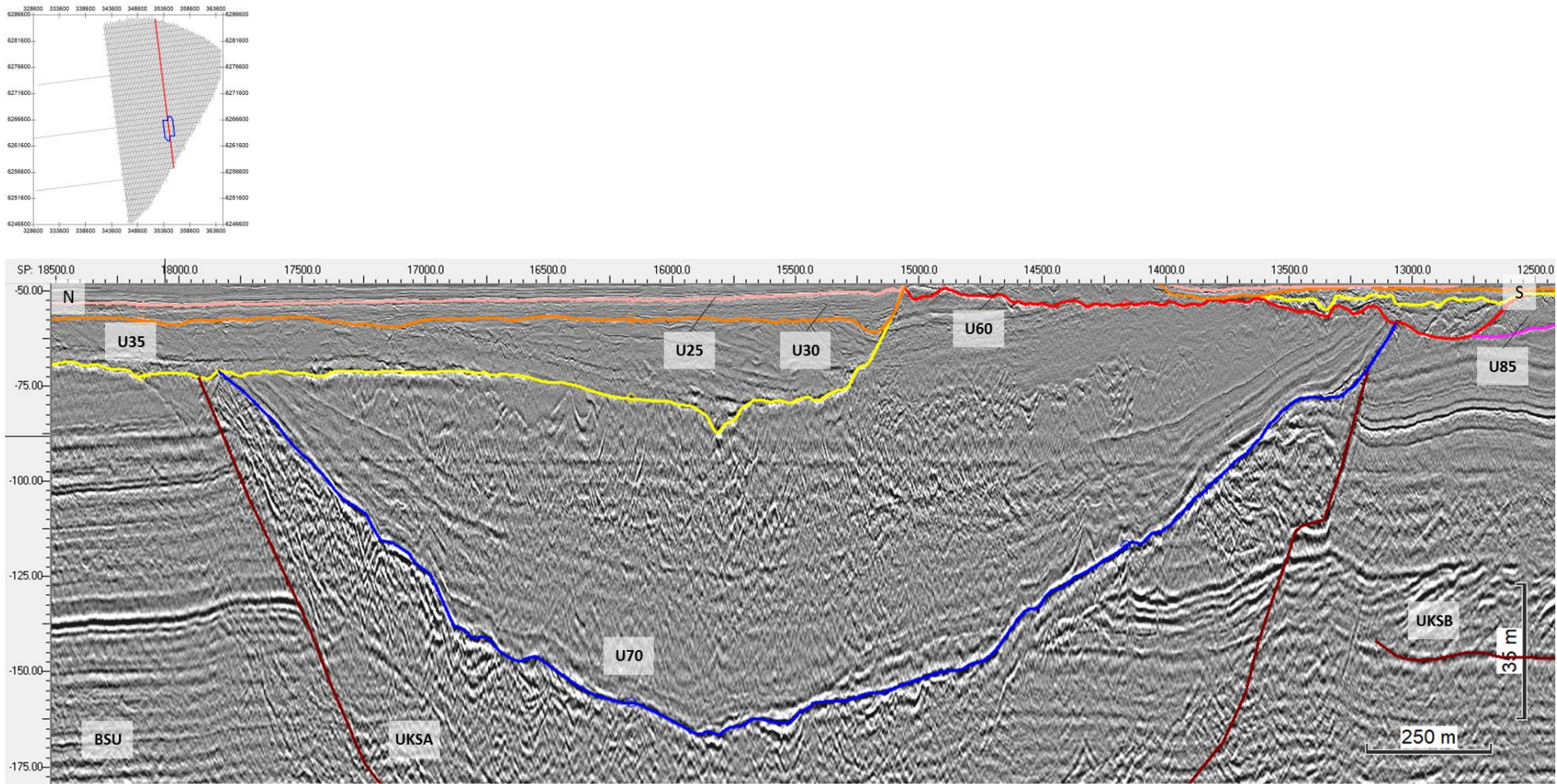


Figure 226 Major infilled valley H70_CH_08 and its internal facies associations.
Seismic profile BM4_OWF_E_2D_09870

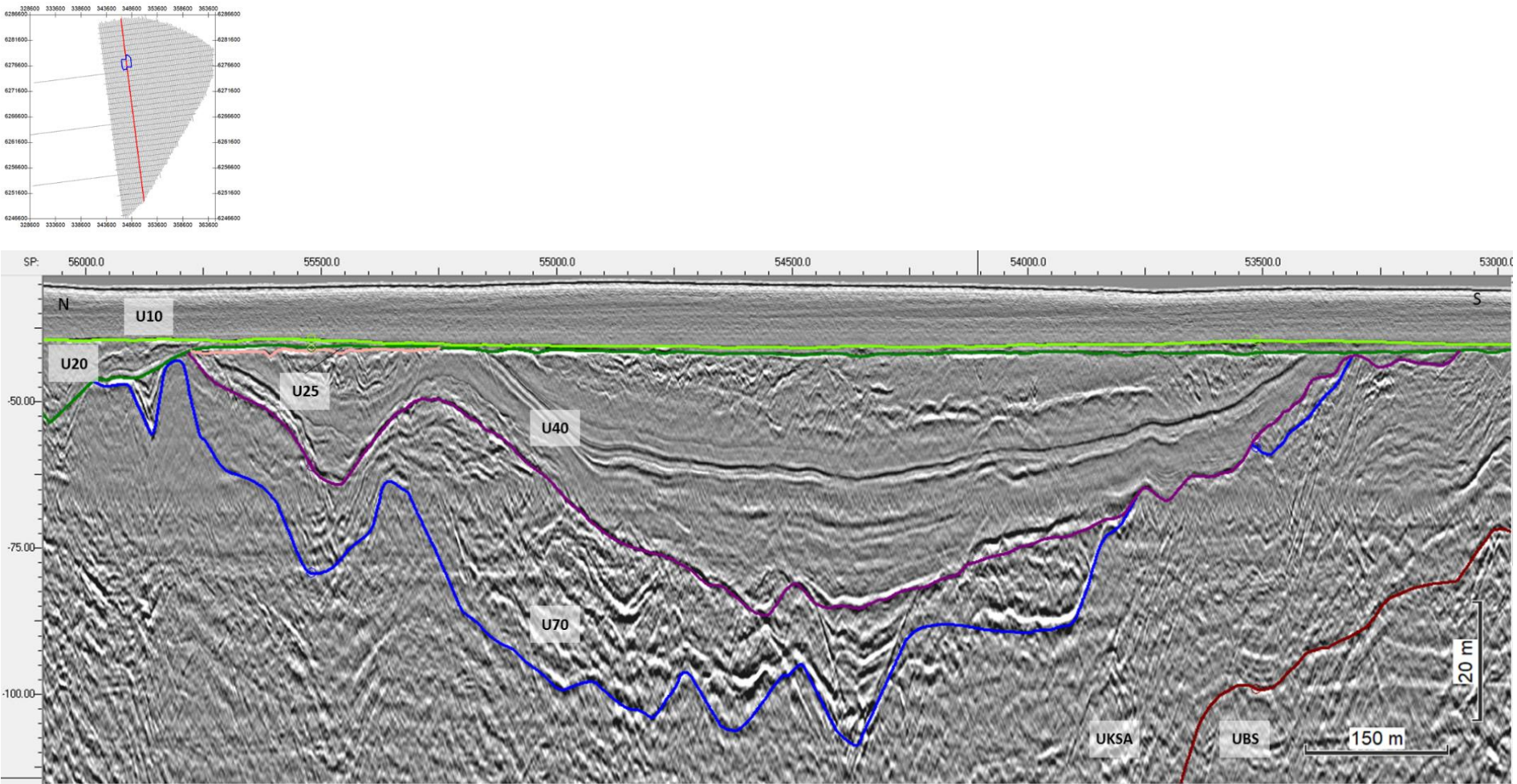


Figure 227 U40 channel exploiting an older U70 incision.
Seismic profile BM2_OWF_E_2D_04410

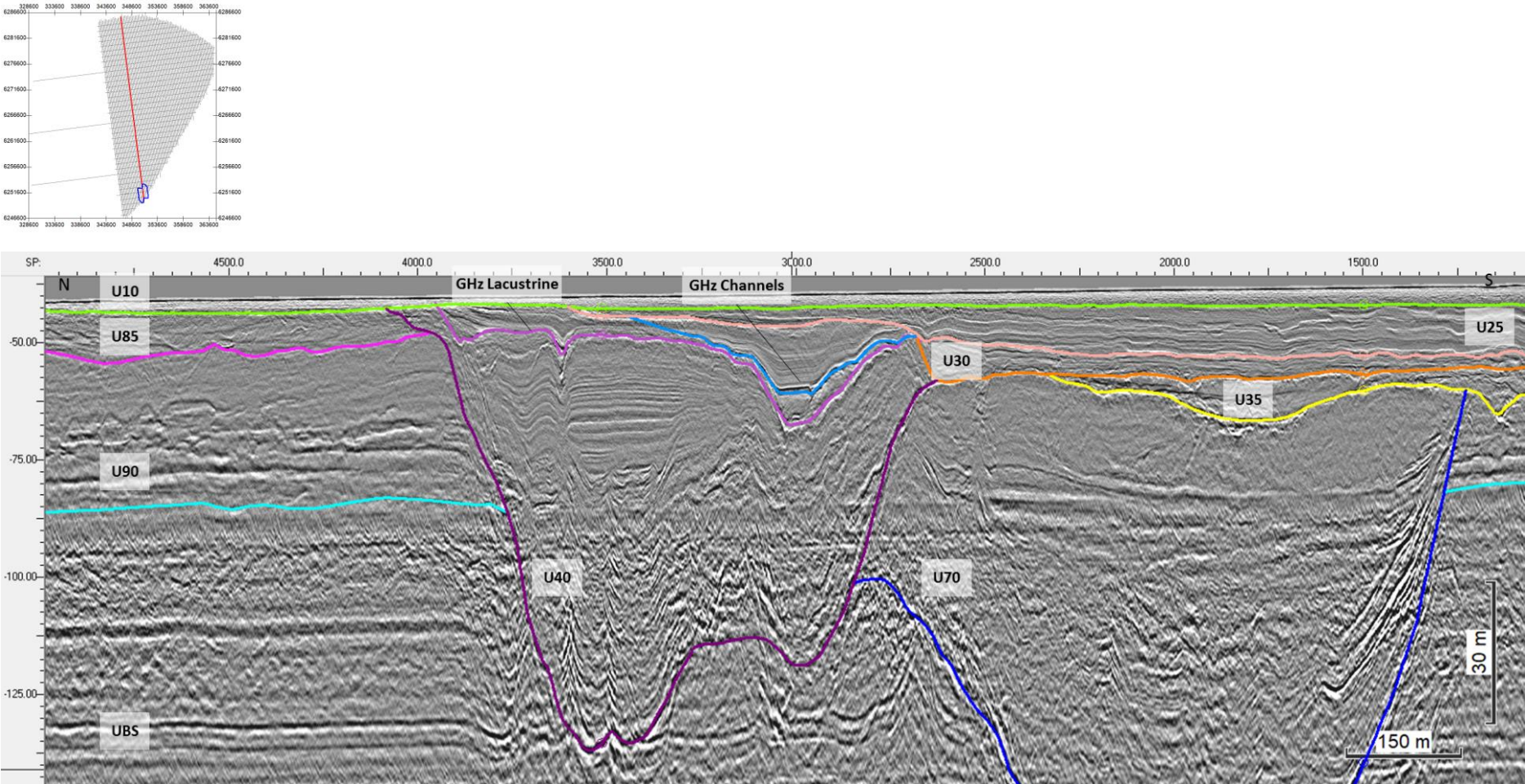


Figure 228 Different channel infills of U40 and U70.
 Seismic profile BM2_OWF_E_2D_04410

8.8.3 | SOFT SEDIMENTS AND ORGANIC-RICH DEPOSITS

Where a high-amplitude, negative impedance (soft kick) is present, a transition to less dense, lower velocity sediments may be inferred. The combination of the reflector's physical attributes and their geologic context, provides a means to delineate soft sediment deposits.

Soft kick features are common throughout the site and were mapped according to the unit where they are found. These are distributed as follows:

Table 32 Distribution of soft kick features within the survey area.

GHz_SK Horizon	Associated Seismic Unit	Depth MSL min	Depth MSL max	Depth BSB min	Depth BSB max	Figures
GHz SK 10	U10	28.25m	47.11m	<0.50m	9.37m	Figure 229 Figure 230
GHz SK 20	U20	32.67m	58.85m	<0.50m	26.14m	Figure 231 Figure 232
GHz SK 25	U25	33.85m	57.59m	<0.50m	27.73m	Figure 233 Figure 234
GHz SK 30	U30	54.09m	72.18m	15.15m	28.96m	Figure 235 Figure 236
GHz SK 35	U35	56.65m	79.88m	13.77m	39.11m	Figure 237 Figure 238
GHz SK 40	U40	48.00m	69.64m	13.43m	29.09m	Figure 239 Figure 240
GHz SK 50	U50	40.53m	41.85m	0.50m	4.04m	Figure 241 Figure 242
GHz SK 60	U60	43.72m	83.85m	0.84m	43.99m	Figure 243 Figure 244
GHz SK 85	U85	43.54m	68.23m	2.41m	28.09m	Figure 245 Figure 246

The highest concentrations of soft kicks are found within U10, U20, and U85 (Figure 247). These features are interpreted to be mud deposits, possibly organic-rich.

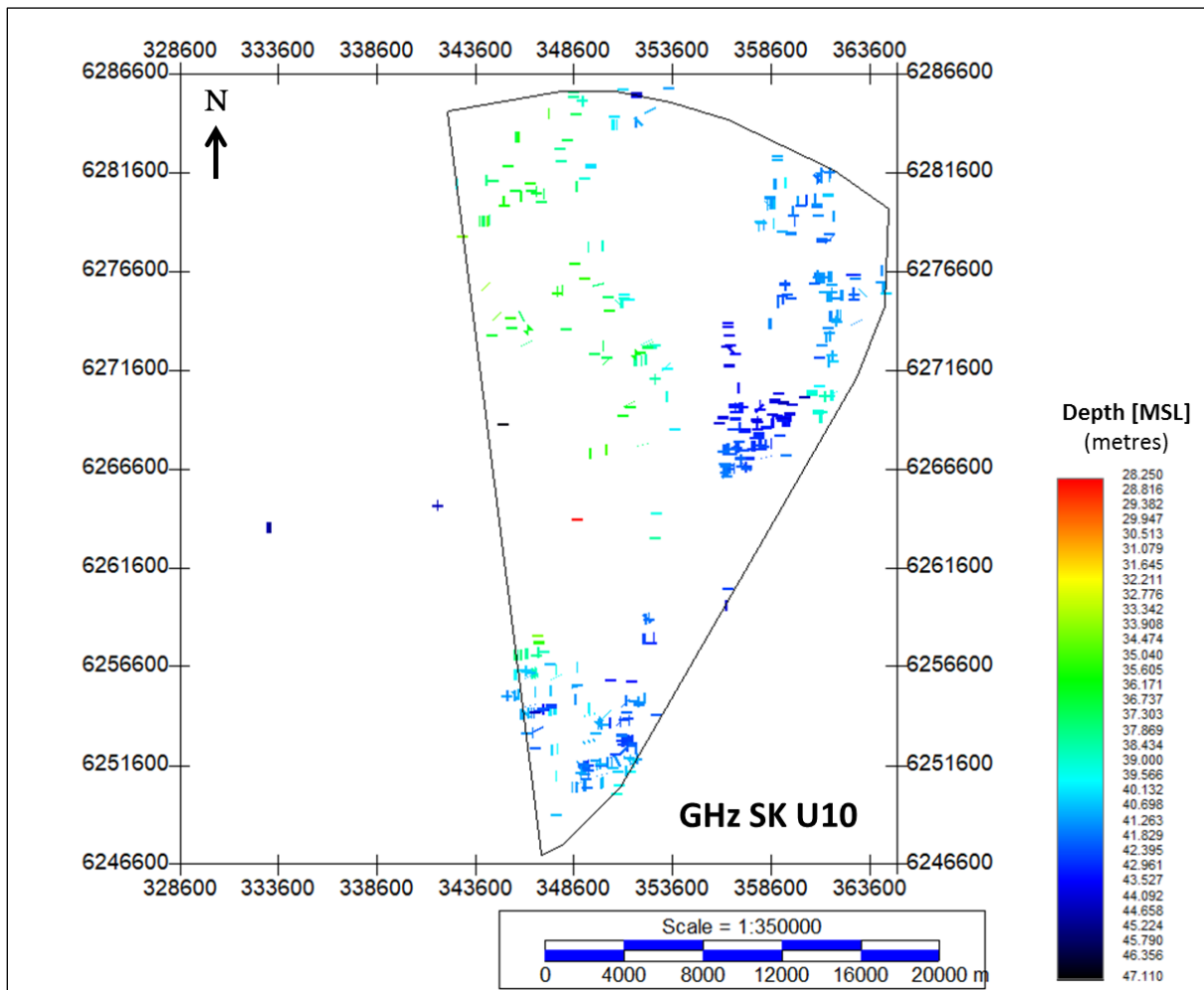


Figure 229 Lateral extent of the negative impedance contrast deposits within U10. Units in metres below MSL.

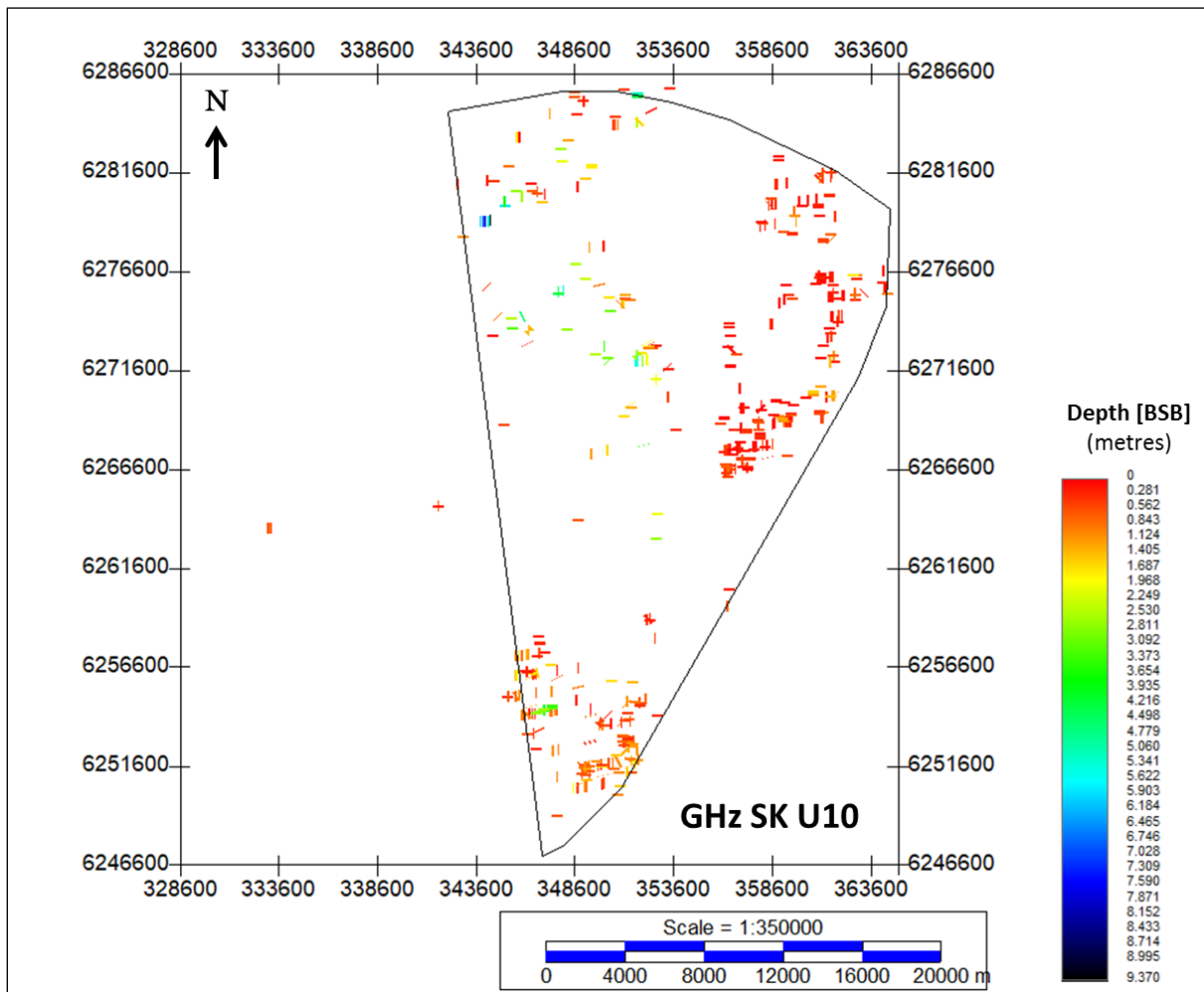


Figure 230 Depth below seabed of GHZ_SK_U10.
Units in metres below seabed.

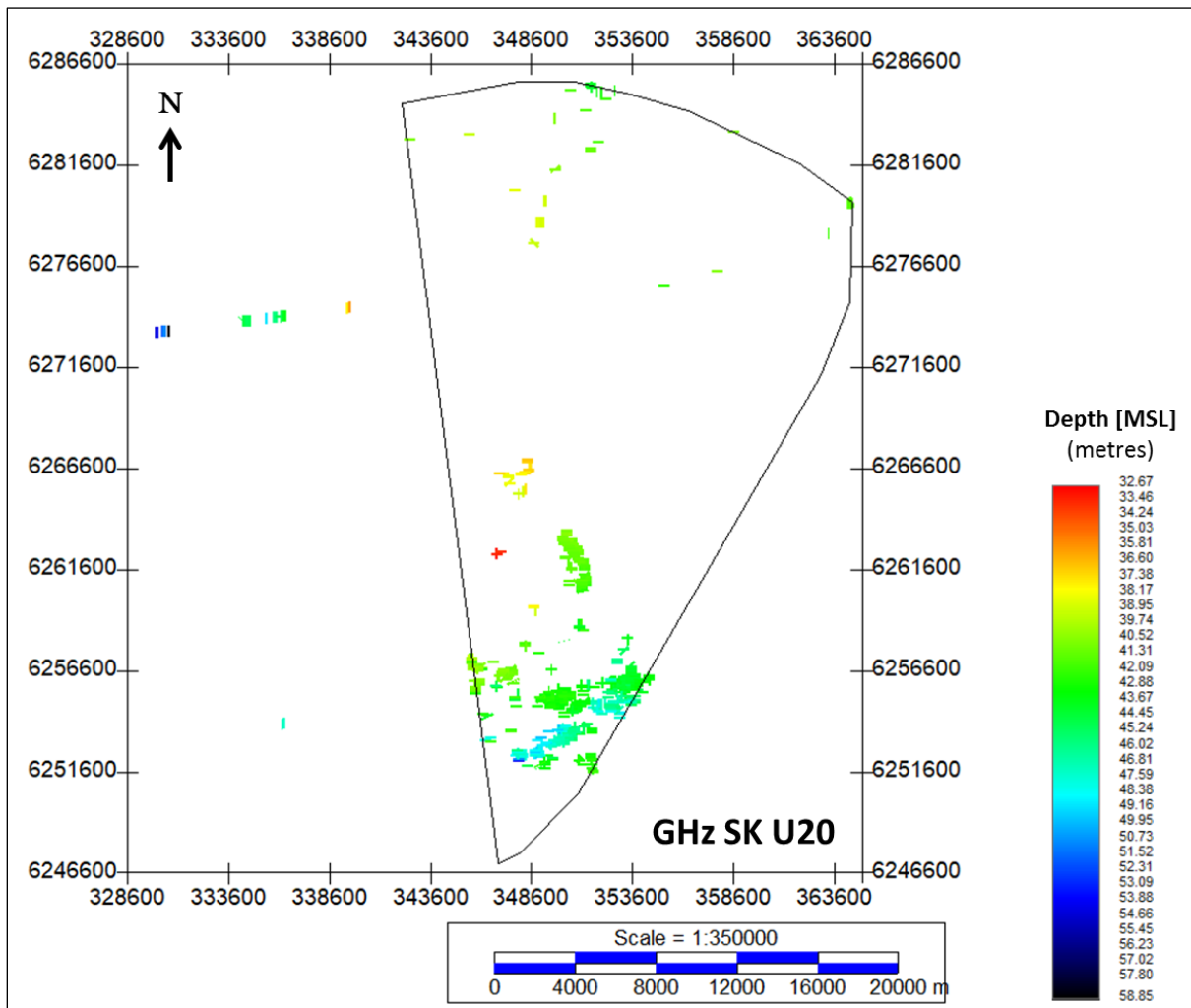


Figure 231 Lateral extent of the negative impedance contrast deposits within U20. Units in metres below MSL.

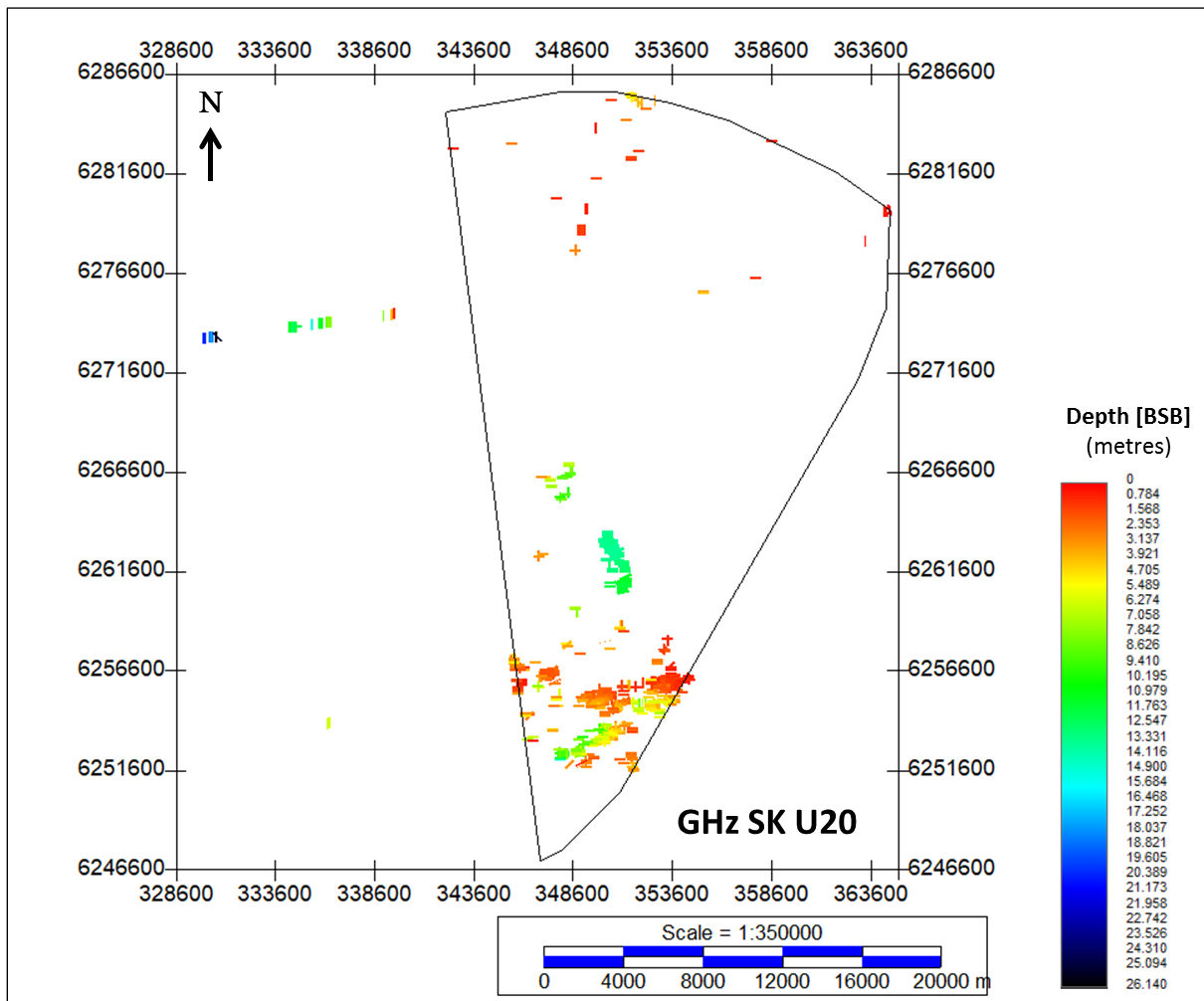


Figure 232 Depth below seabed of GHZ_SK_U20.
Units in metres below seabed.

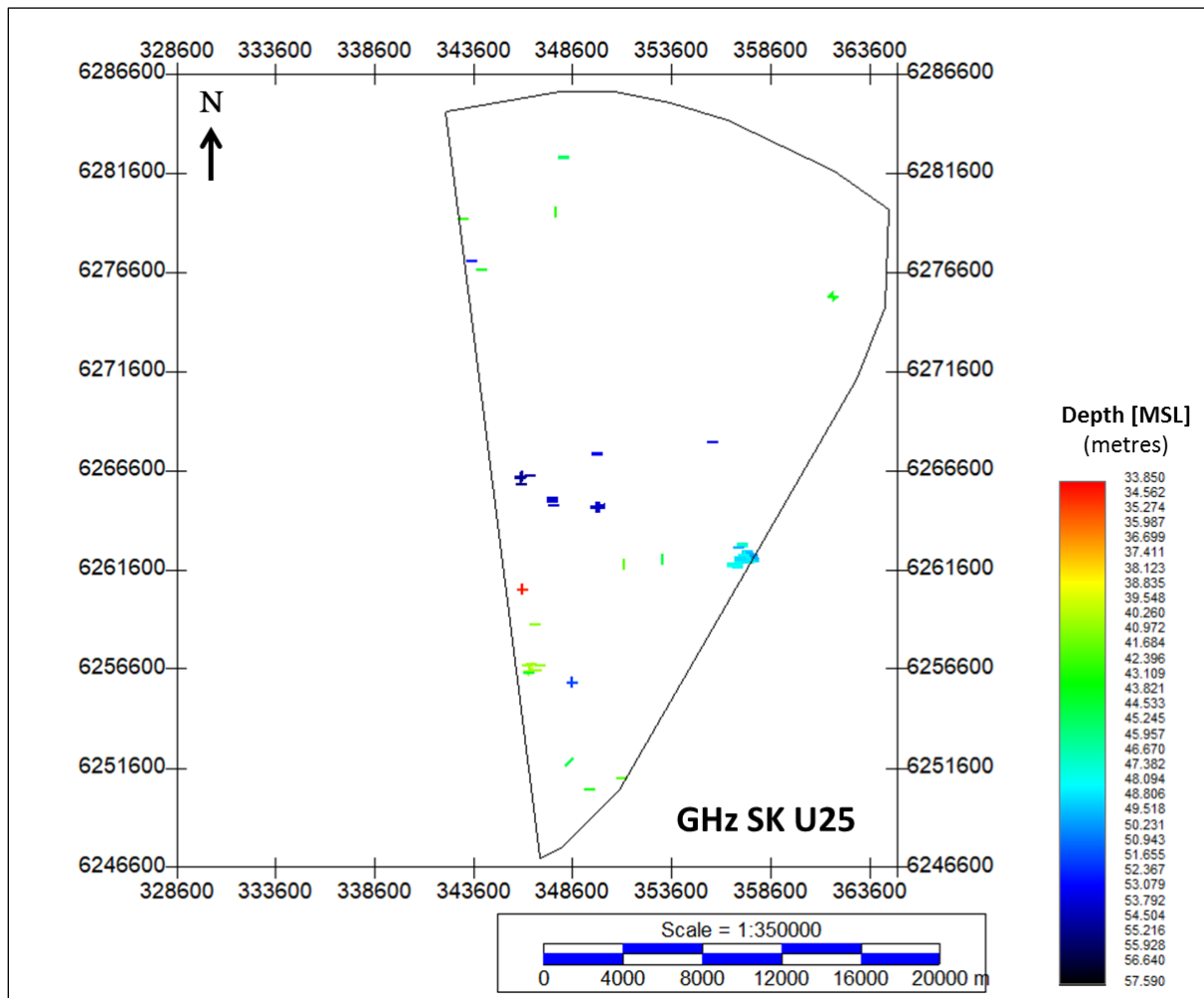


Figure 233 Lateral extent of the negative impedance contrast deposits within U25. Units in metres below MSL.

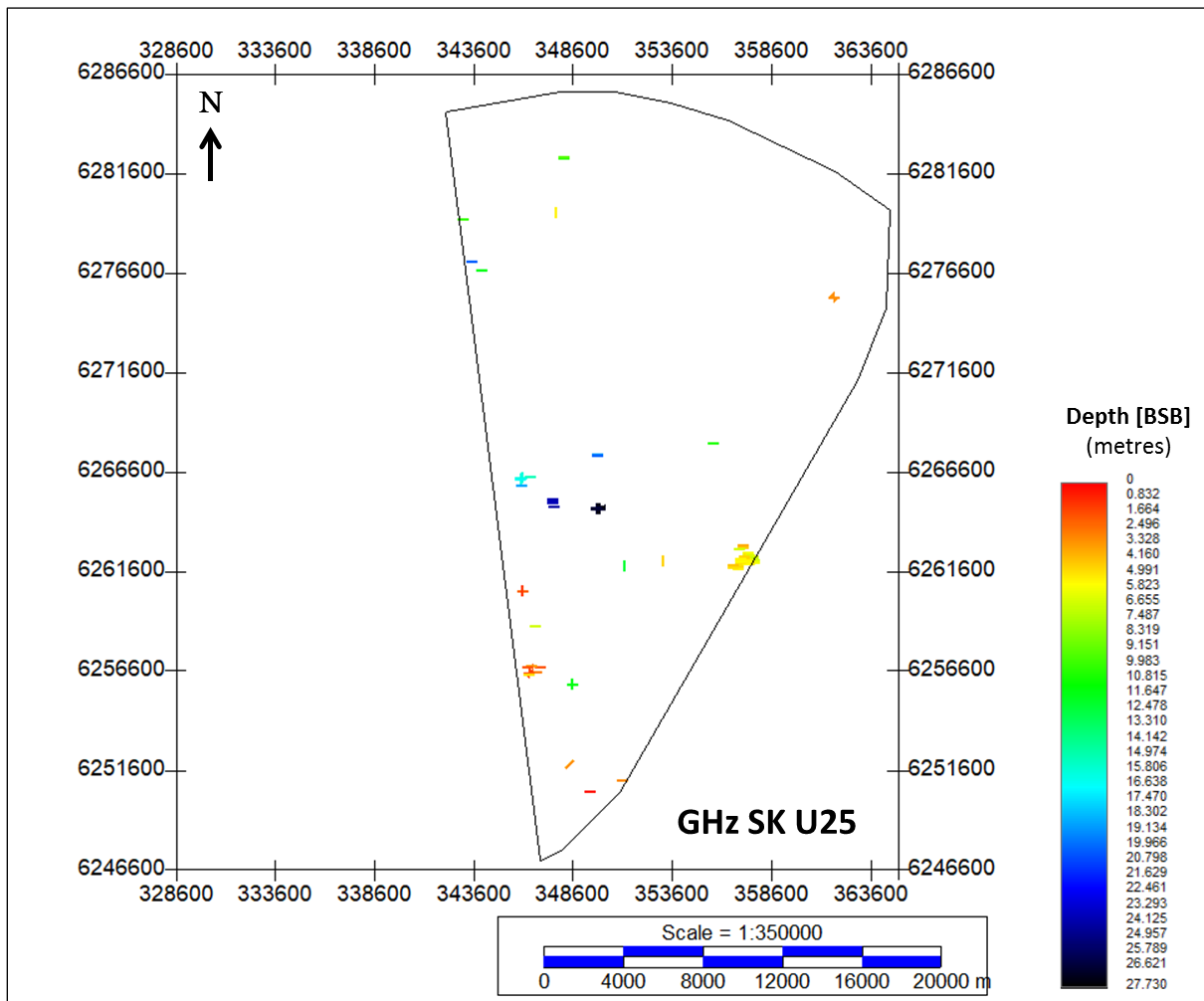


Figure 234 Depth below seabed of GHZ_SK_U25.
 Units in metres below seabed.

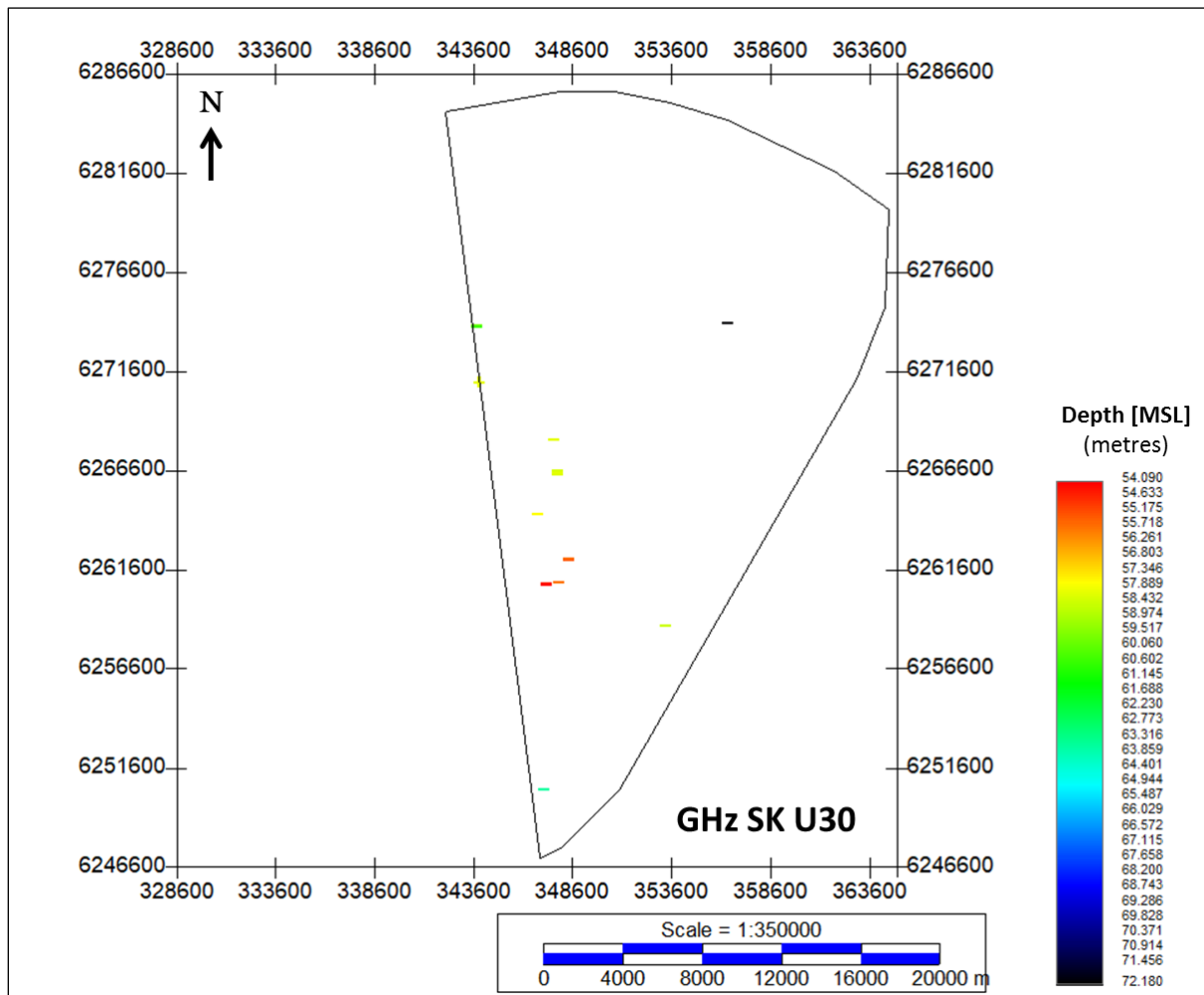


Figure 235 Lateral extent of the negative impedance contrast deposits within U30. Units in metres below MSL.

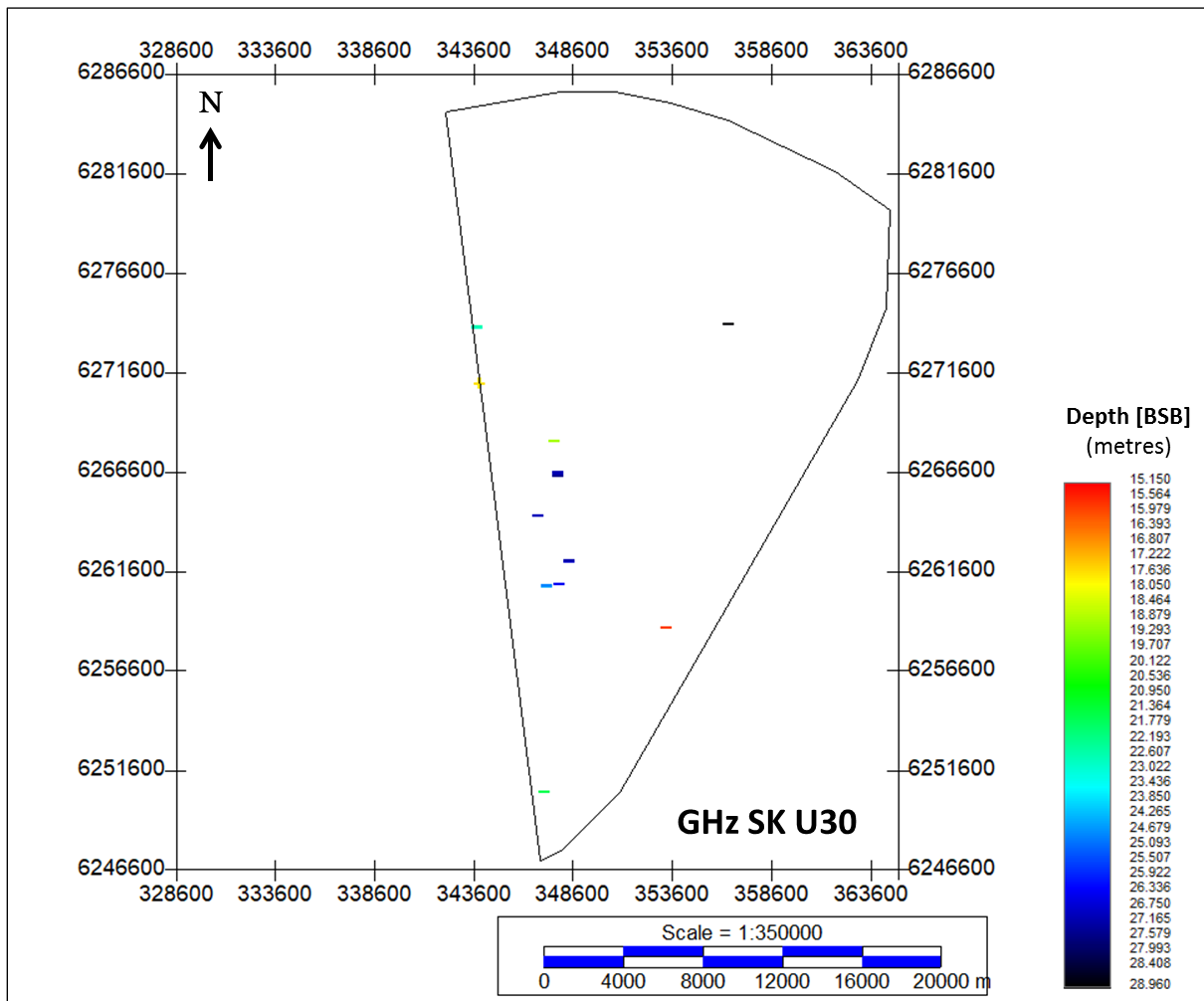


Figure 236 Depth below seabed of GHz_SK_U30.
 Units in metres below seabed.

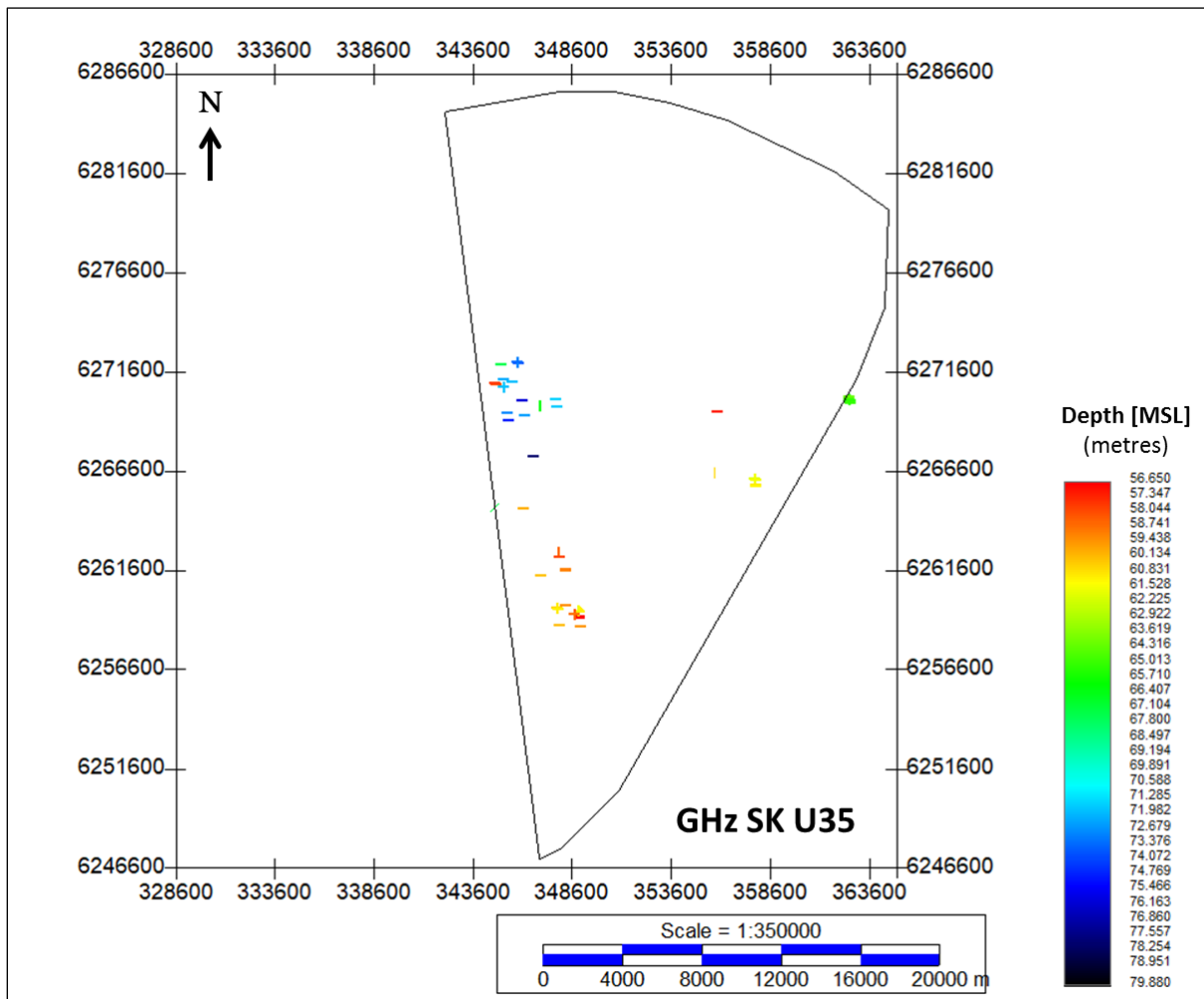


Figure 237 Lateral extent of the negative impedance contrast deposits within U35. Units in metres below MSL.

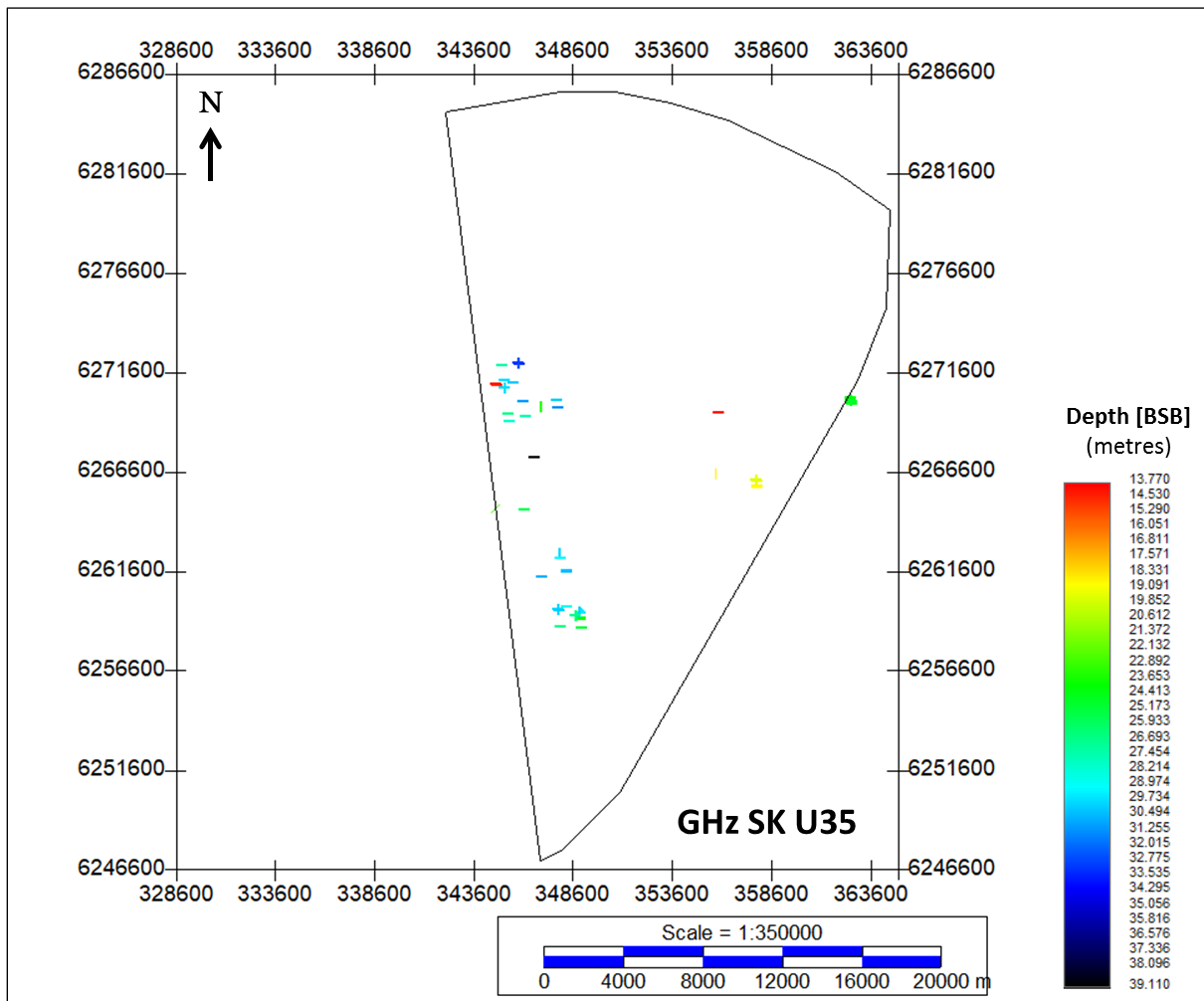


Figure 238 Depth below seabed of GHZ_SK_U35.
 Units in metres below seabed.

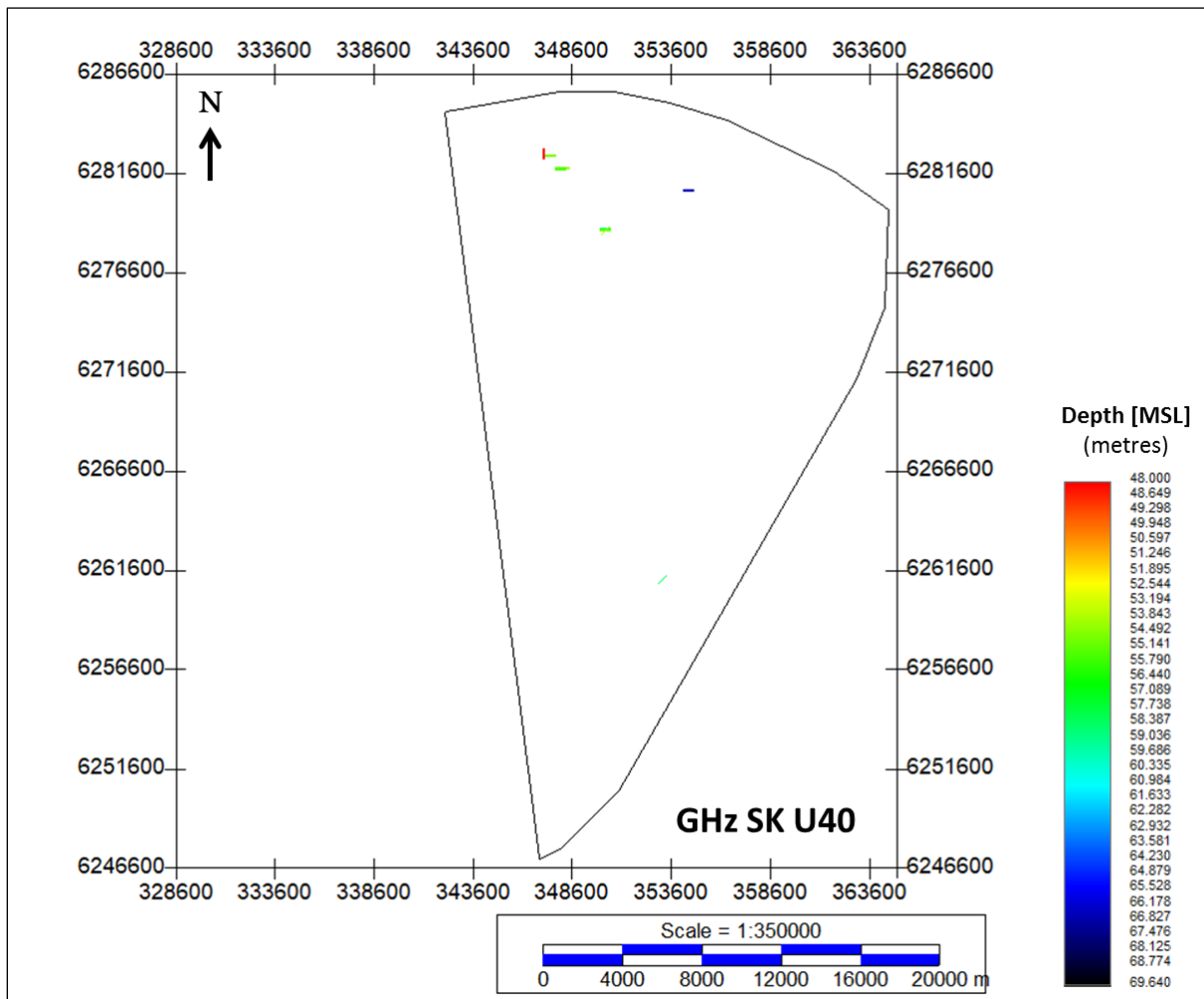


Figure 239 Lateral extent of the negative impedance contrast deposits within U40. Units in metres below MSL.

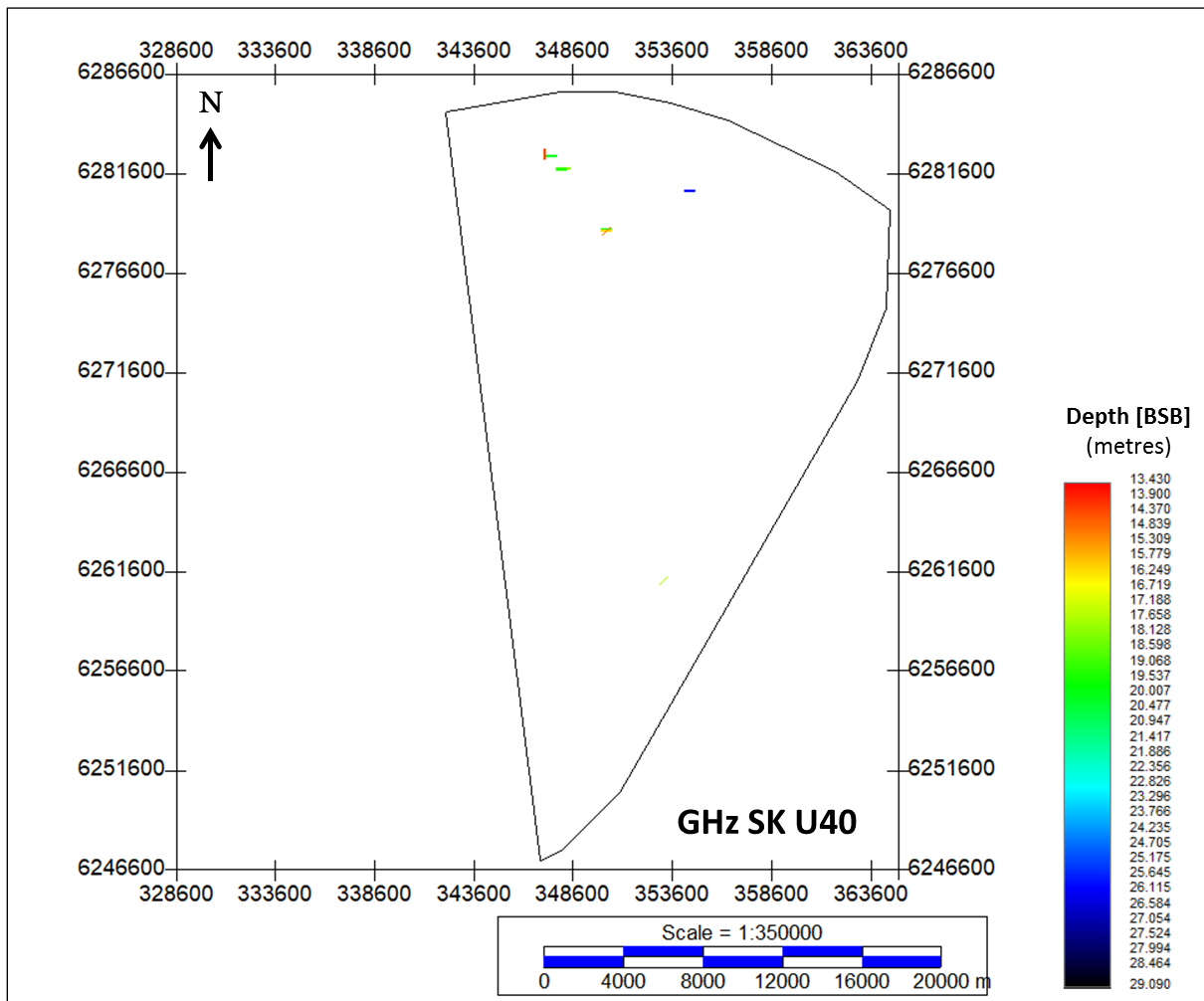


Figure 240 Depth below seabed of GHz_SK_U40.
 Units in metres below seabed.

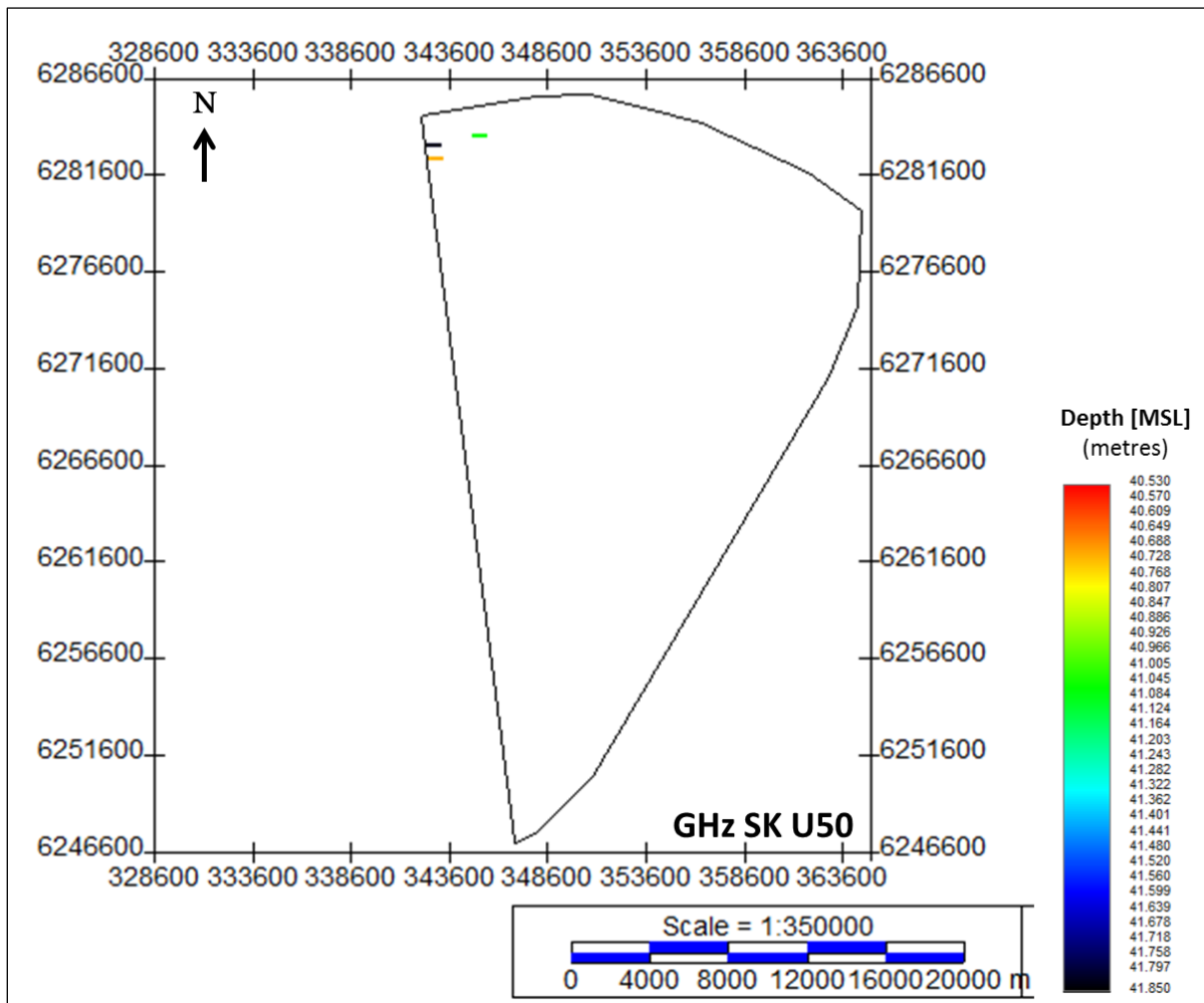


Figure 241 Lateral extent of the negative impedance contrast deposits within U40.
 Units in metres below MSL.

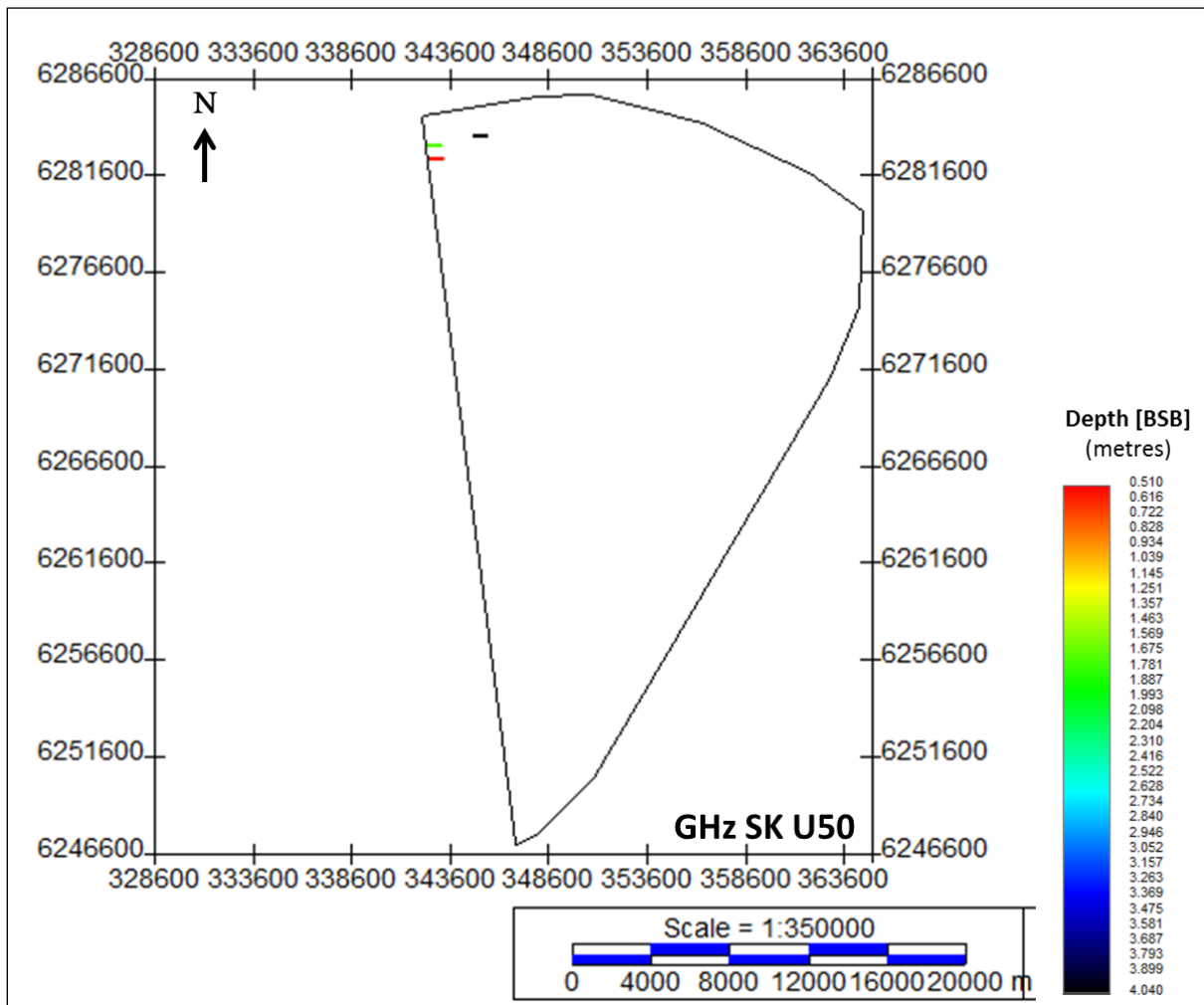


Figure 242 Depth below seabed of GHz_SK_U50.
 Units in metres below seabed.

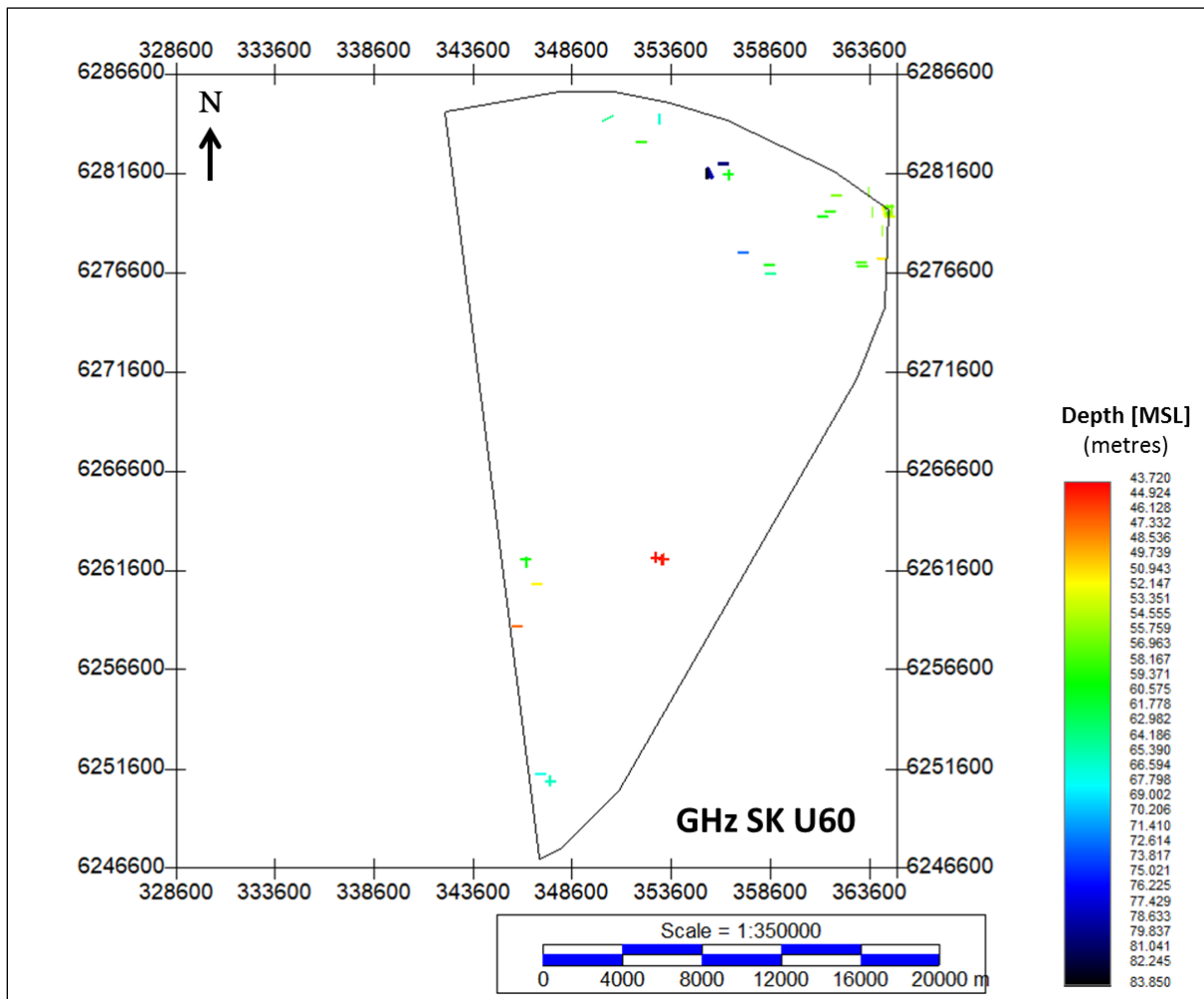


Figure 243 Lateral extent of the negative impedance contrast deposits within U60. Units in metres below MSL.

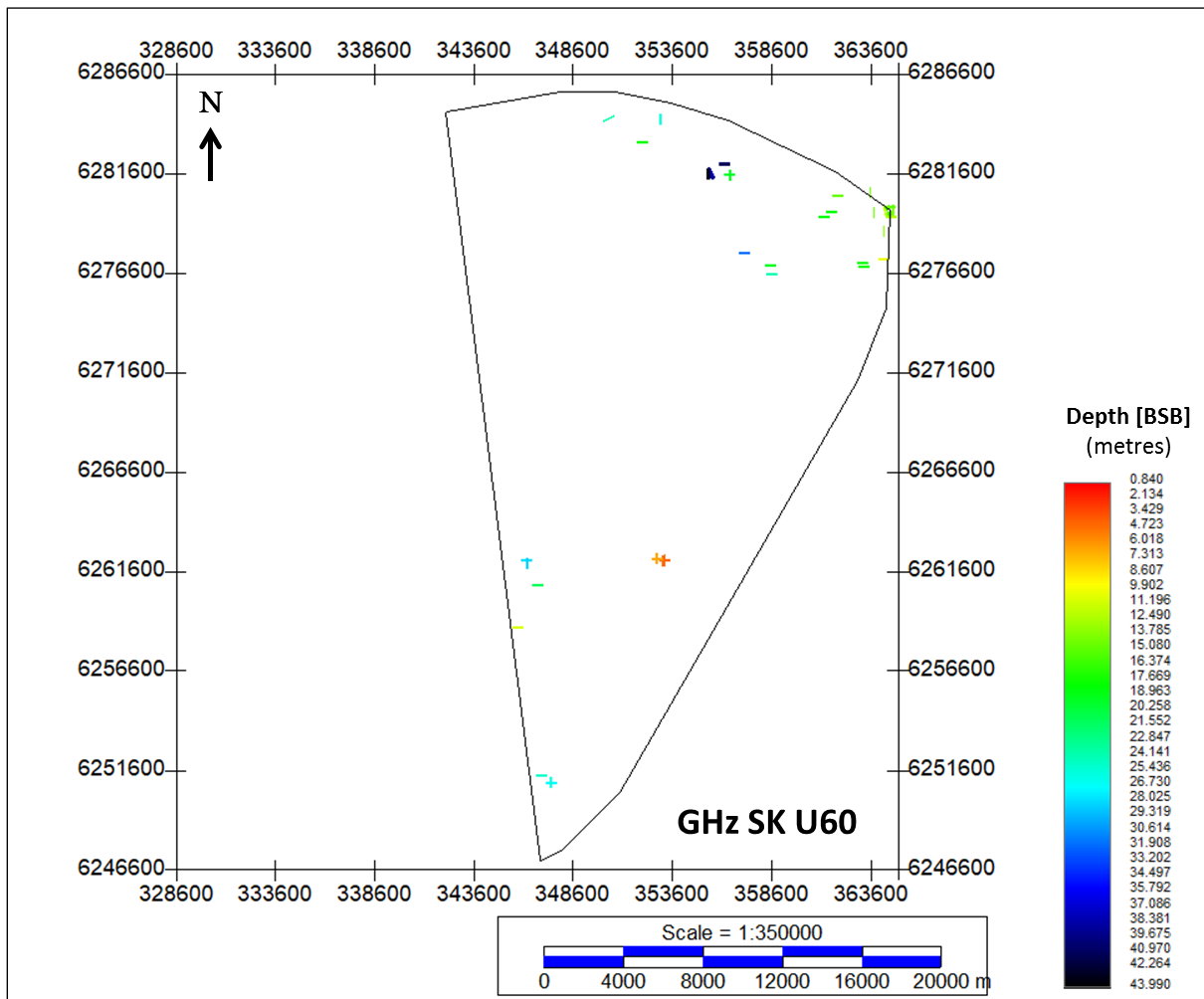


Figure 244 Depth below seabed of GHz_SK_U60.
 Units in metres below seabed.

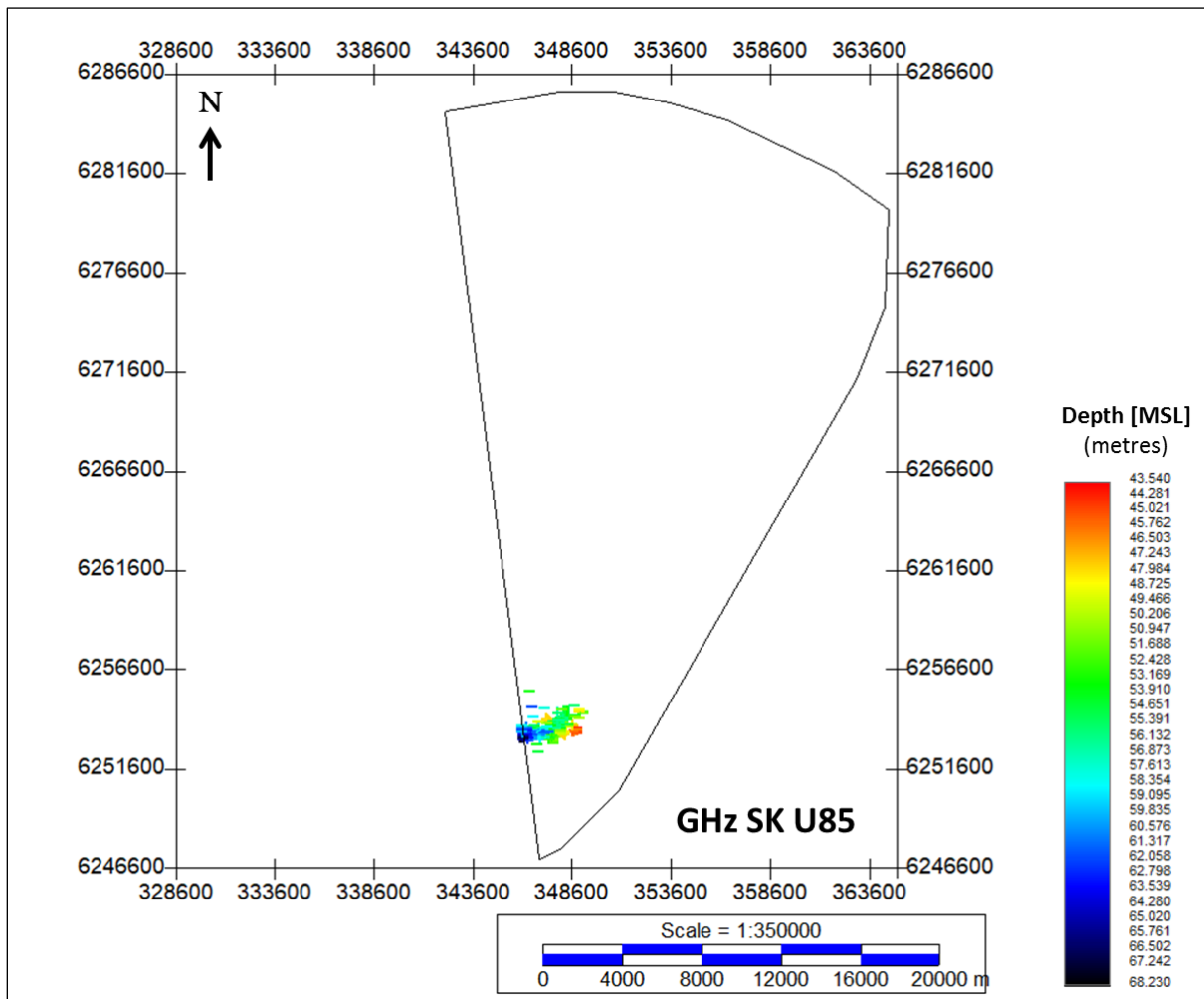


Figure 245 Lateral extent of the negative impedance contrast deposits within U85. Units in metres below MSL.

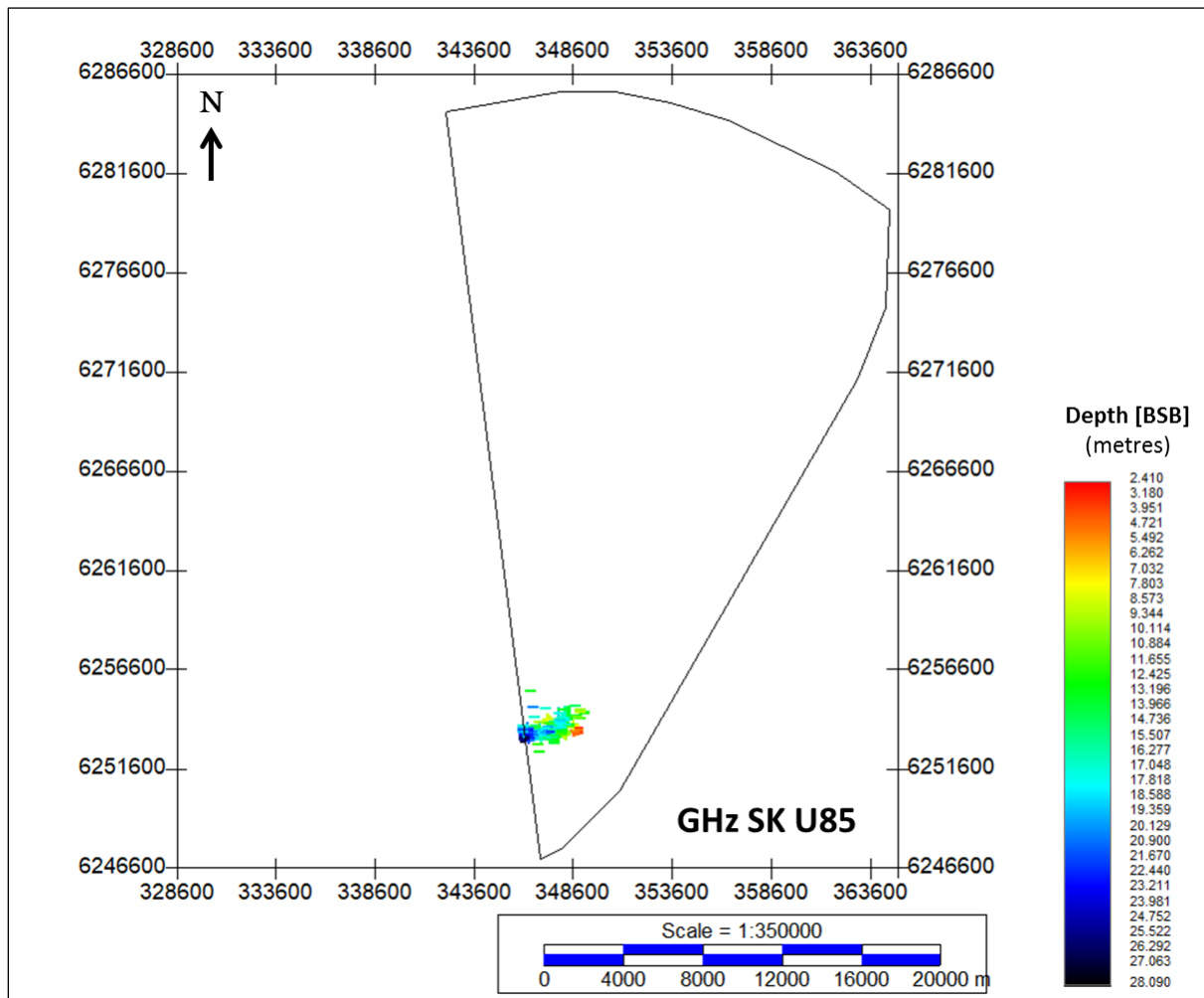


Figure 246 Depth below seabed of GHz_SK_U85.
 Units in metres below seabed.

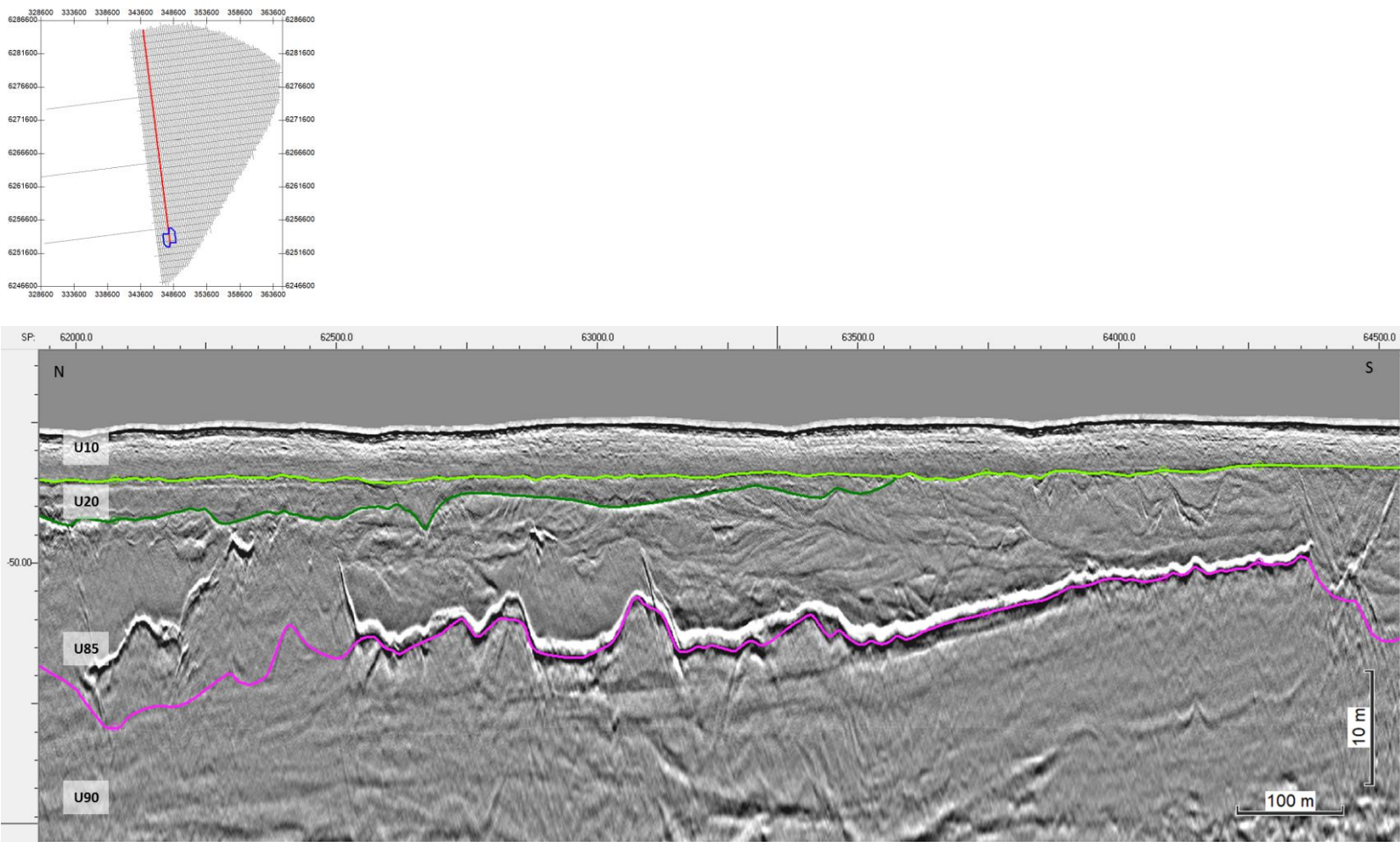


Figure 247 Negative impedance contrasts at the base of U85.
Seismic profile BM1_OWF_E_2D_01890_P2

8.8.4 | COARSE SEDIMENTS / GRAVEL BEDS / BOULDERS

Coarser material, such as boulder accumulations, cobbles, and gravel lags are present in glacial environments. These are potential hazards and may constitute a constraint on drilling and other operations.

Seismic diffractions, characterized by a parabolic or hyperbolic geometry in UHRS data, may be produced from the contact of the acoustic wave front and a boulder. However, in order to interpret such reflection patterns as boulders, the acoustic signature and geological/seismostratigraphic context have to be taken into consideration, since identical diffractions may originate from rugose surfaces, faulted layering, channelized acoustic interfaces, and out-of-plane echoes.

Interpreted areas of potential gravel/boulders were traced by horizon GHZ_Gravel. These areas were identified between 37.9 m and 87.7 m below MSL (Figure 248), and 1.1 m and 48.9 m BSB (Figure 249).

Mappable concentrations of interpreted gravel were delineated at the base of seismic units U35 and U40 (Figure 250). The gravel concentrations in U35 appear to be along the margins of the basin within the central sector (Figure 248 and Figure 249).

The highest probability for the occurrence of cobbles and boulders is estimated to be within seismic units related outwash products from tills. These units are U40, U70, UKS.

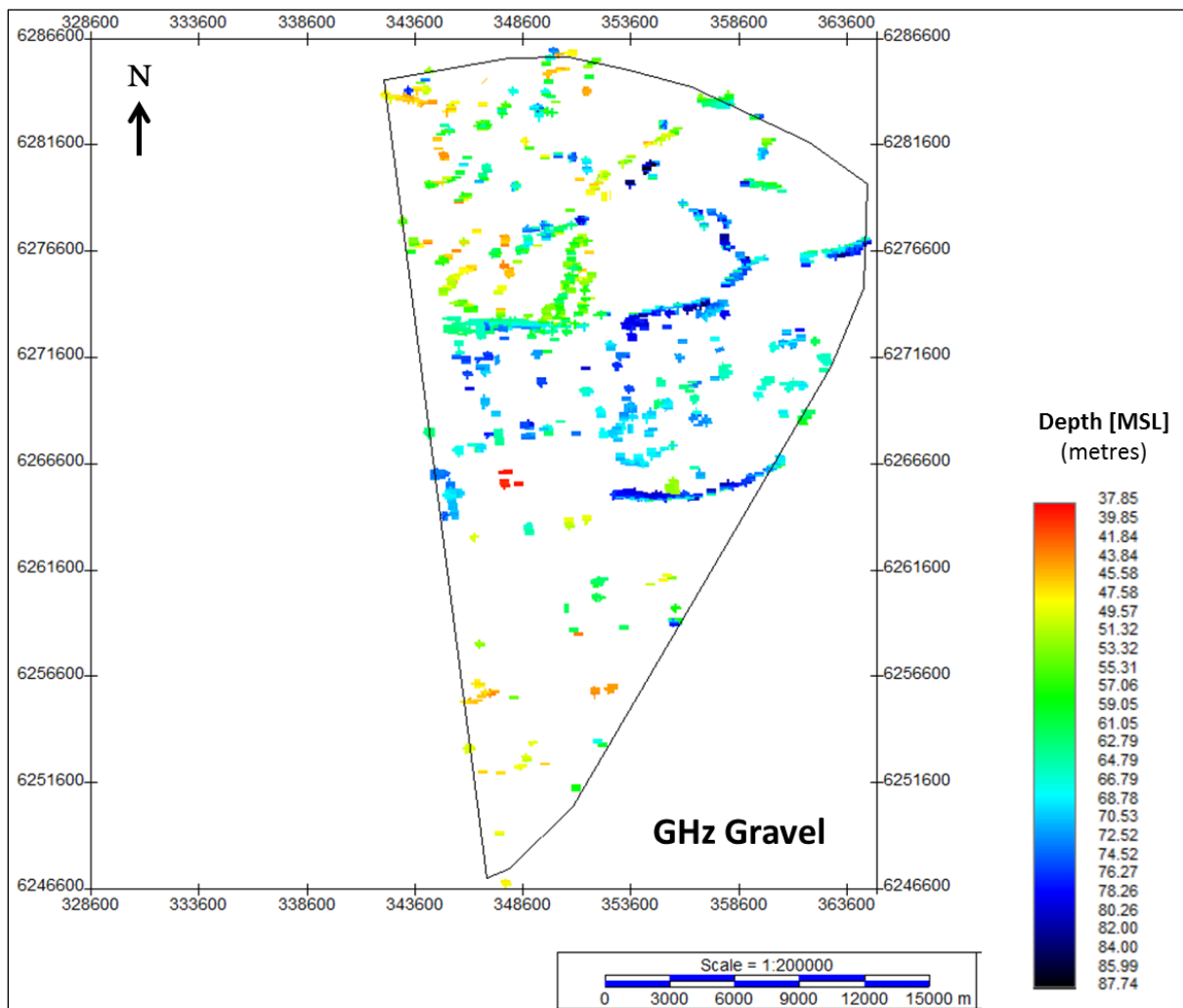


Figure 248 Lateral extent of GHz_Gravel.
 Units in metres below MSL.

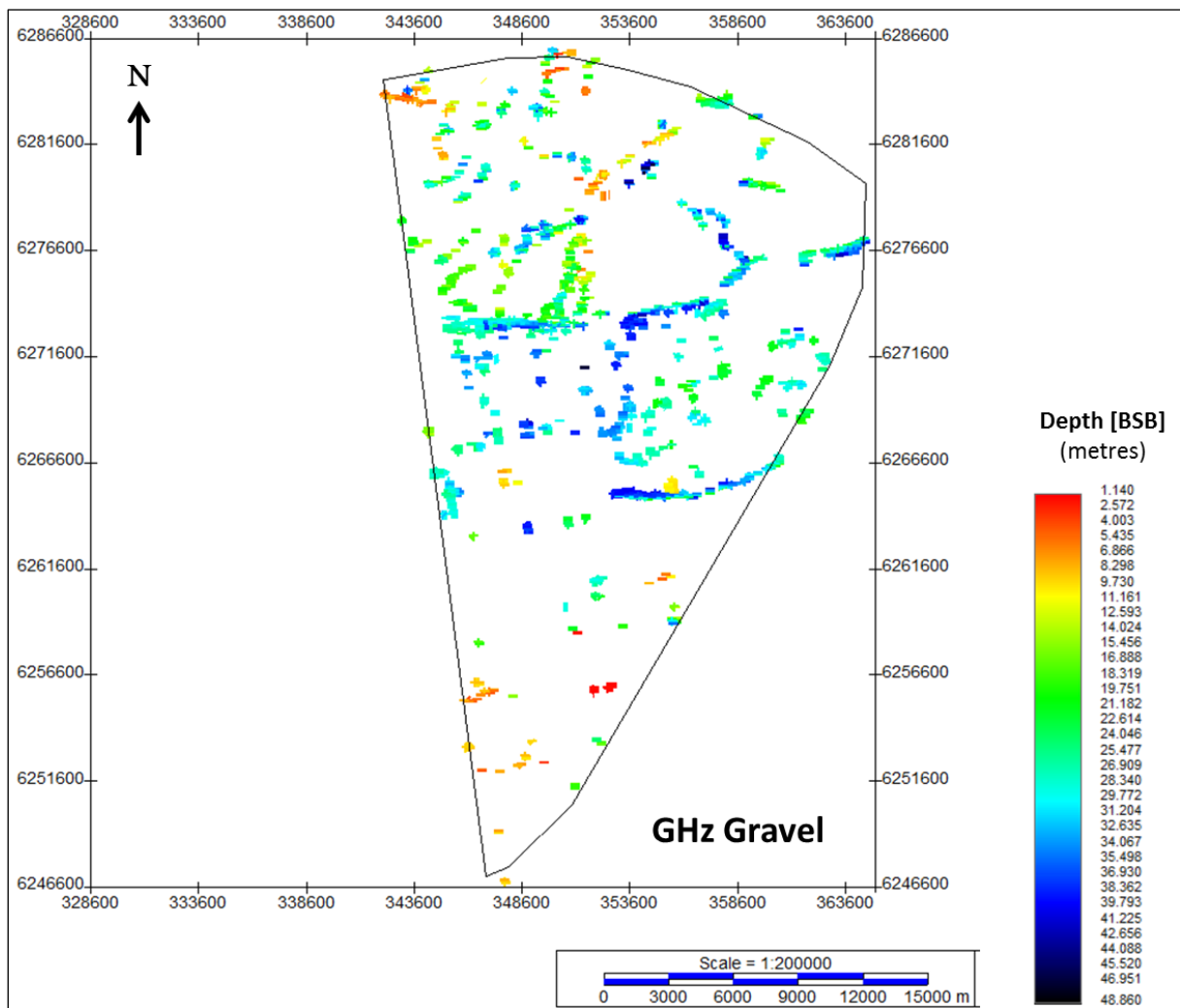


Figure 249 Depth below seabed of GHz_Gravel.
Units in metres below seabed.

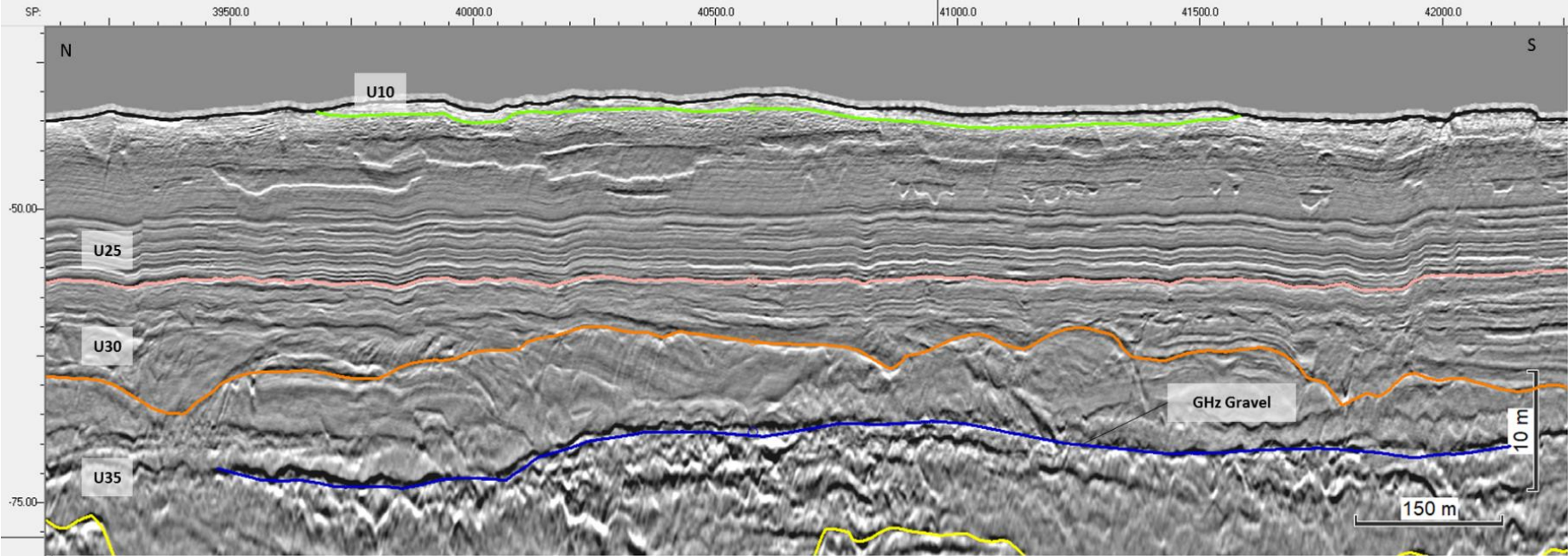
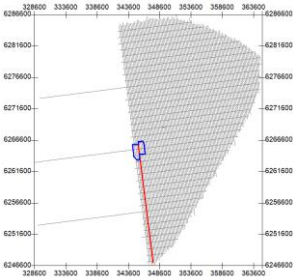


Figure 250 Possible coarse layer within U35.
Seismic profile BM1_OWF_E_2D_00630_01_P2

8.8.5 | TILL DEPOSITS

Interpreting till deposits in UHRS data with high confidence can be difficult. Given its broad classification, and that it may contain sediment of any grain size, predicting its seismic characteristics is uncertain. However, taking into account the geological setting of the area, there should be a reasonable expectation of till in the units directly associated with glaciation. Tills are commonly associated with and located in conjunction with glaciotectonism. Given this relationship, tills may be present within U40, U70, and UKS. Till may preferentially occur at the basal margins of the tectonized deposits, and associated to glacial surfaces of erosion or retreat (Figure 251).

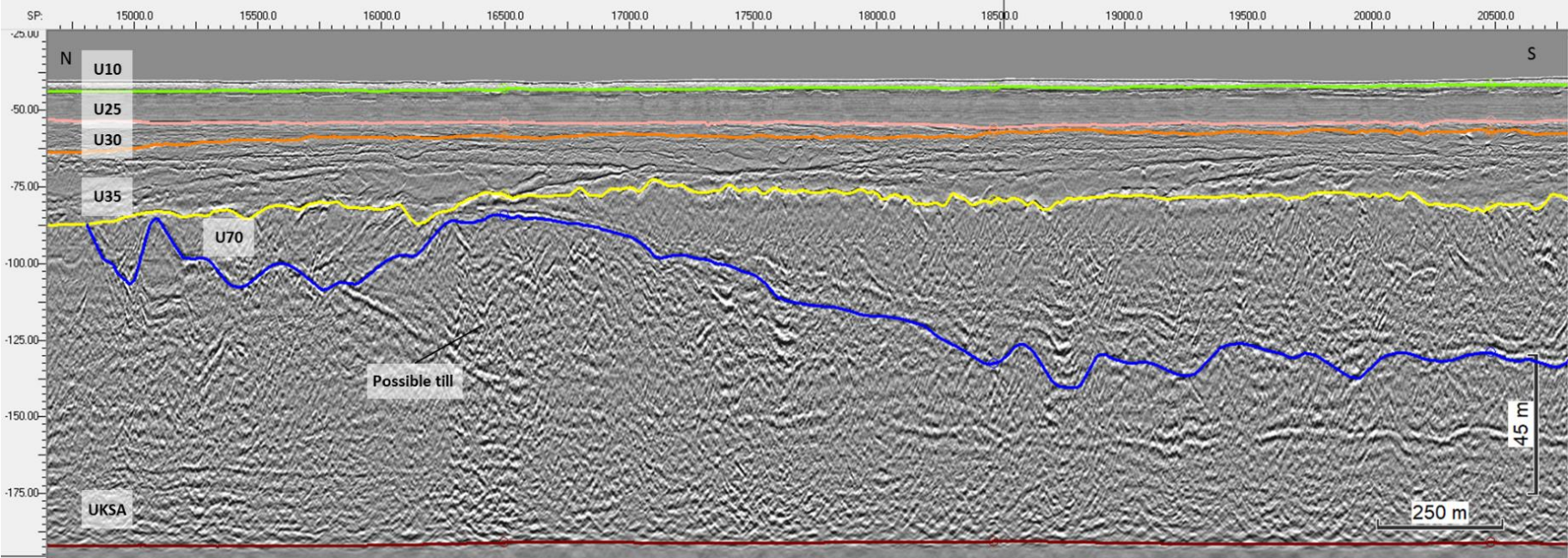
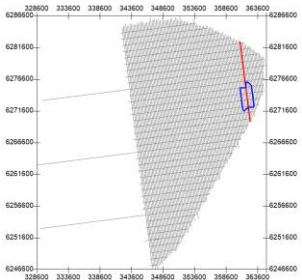


Figure 251 possible till deposits below H70.
 Seismic profile BM6_OWF_E_2D_18270

8.8.6 | FLUID FLOW AND GAS FEATURES

Acoustic blanking, amplitude anomalies, phase reversals, and hyperbolas in the MUL (non-migrated) datasets may indicate the presence of gas in UHRS data. These indicators typically appear quite prominently when concentrations of free gas are present in sediments. However, the presence of a single marker of the above-mentioned items was never taken as evidence for the presence of shallow gas as there are a number of geological features that can be responsible for each of them individually. Instead, it was the combined presence of the mentioned evidences that was taken as indicator of the likely presence of shallow gas. Furthermore, signal masking, or acoustic turbidity, or decreased amplitudes were inspected either directly on the migrated and un-migrated seismic sections or on other amplitude-derived attributes, like envelope and reflectance datasets.

No unambiguous seismic anomalies suggesting the presence of detectable gas in the subsurface were identified in the UHRS data. This statement is not an assertion that no gas exists within the survey area.

Rare localised features were identified that may be related to upward fluid migration within the sub-surface (Figure 254 and Figure 255). The top of these features was mapped as “GHz_Gas” (Figure 252 and Figure 253), as gas is not excluded as one of the components that may have originated them.

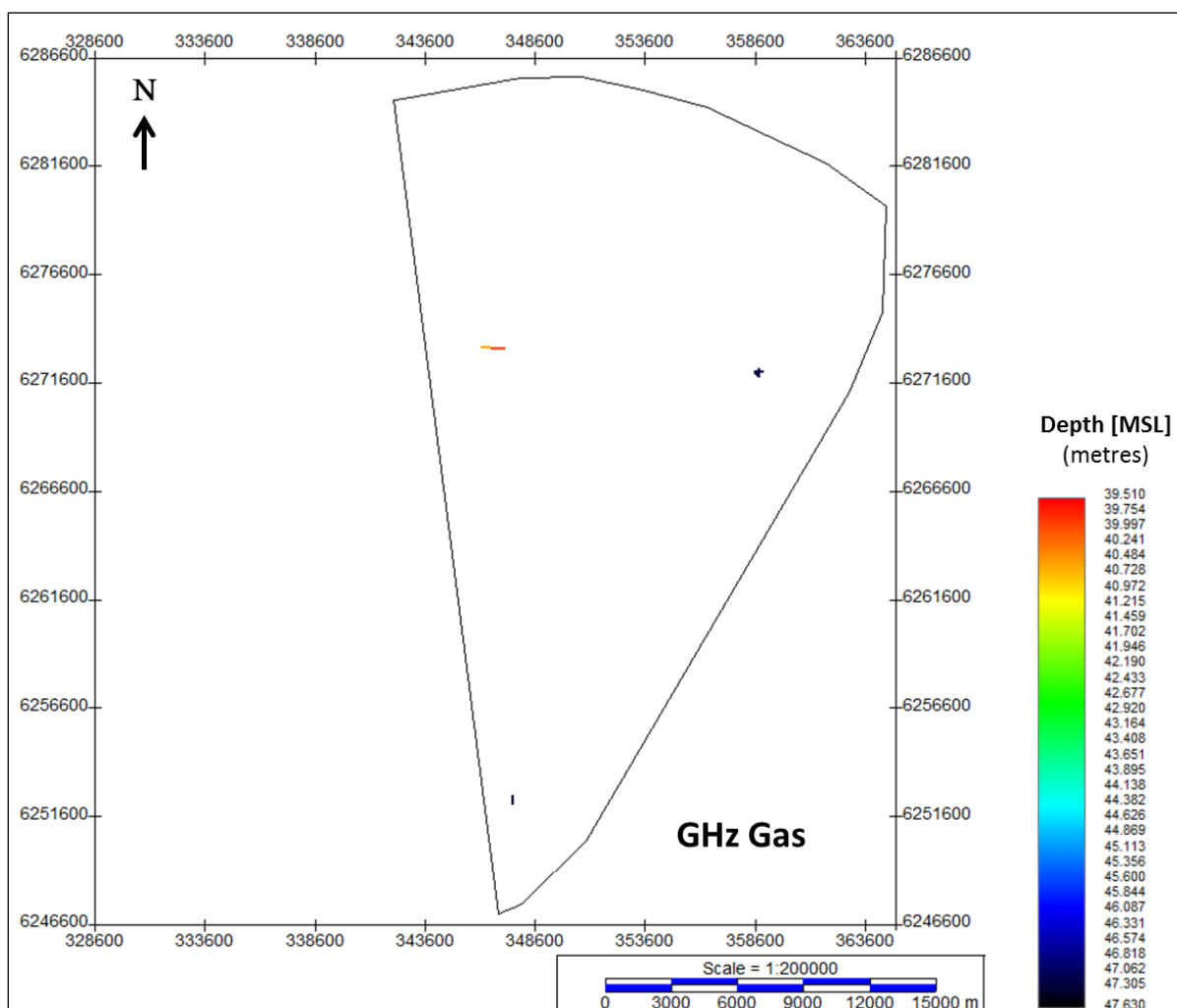


Figure 252 Lateral extent of horizon GHz_Gas.
 Units in metres below MSL.

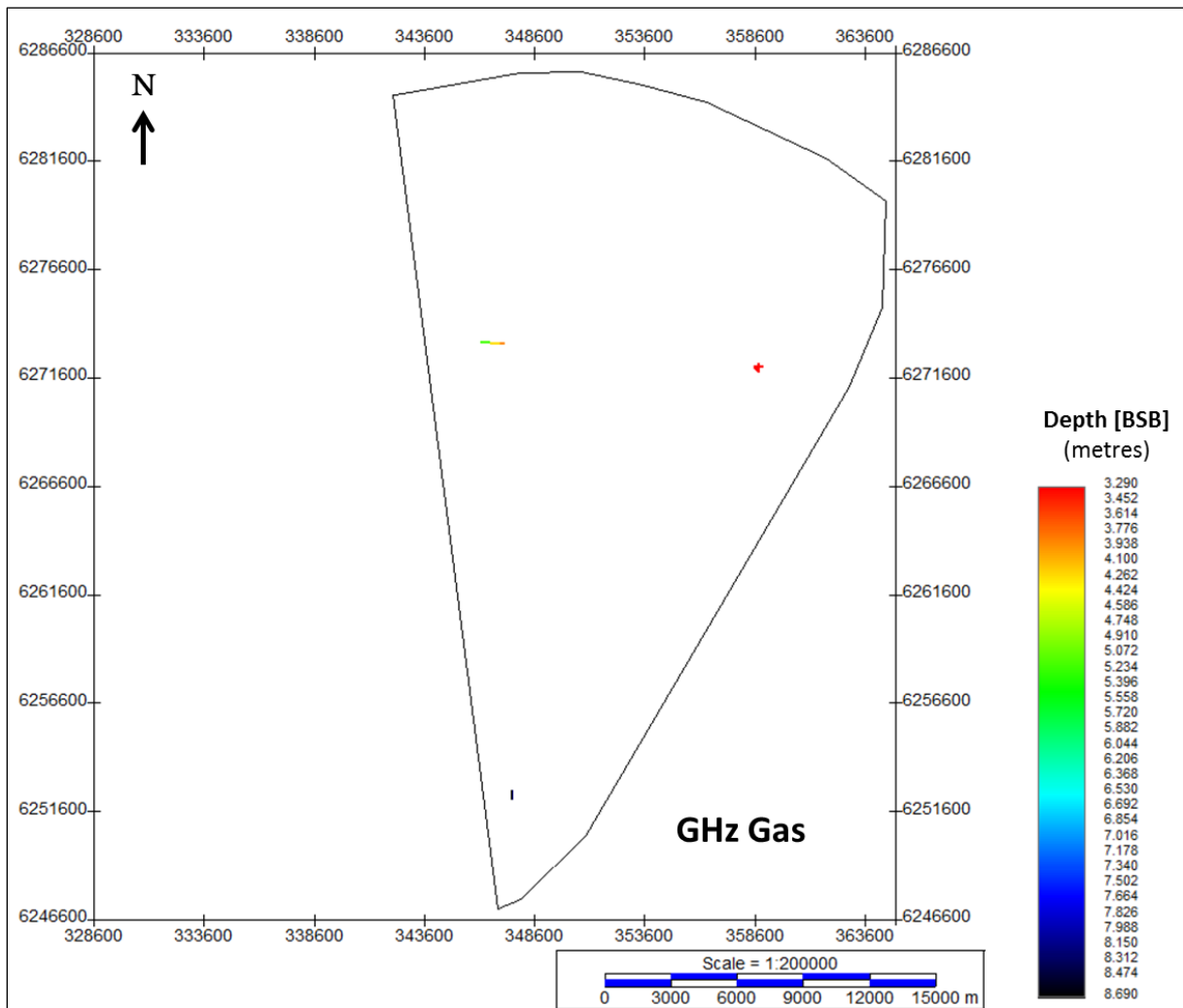


Figure 253 Depth below seabed of horizon GHz_Gas.
 Units in metres below seabed.

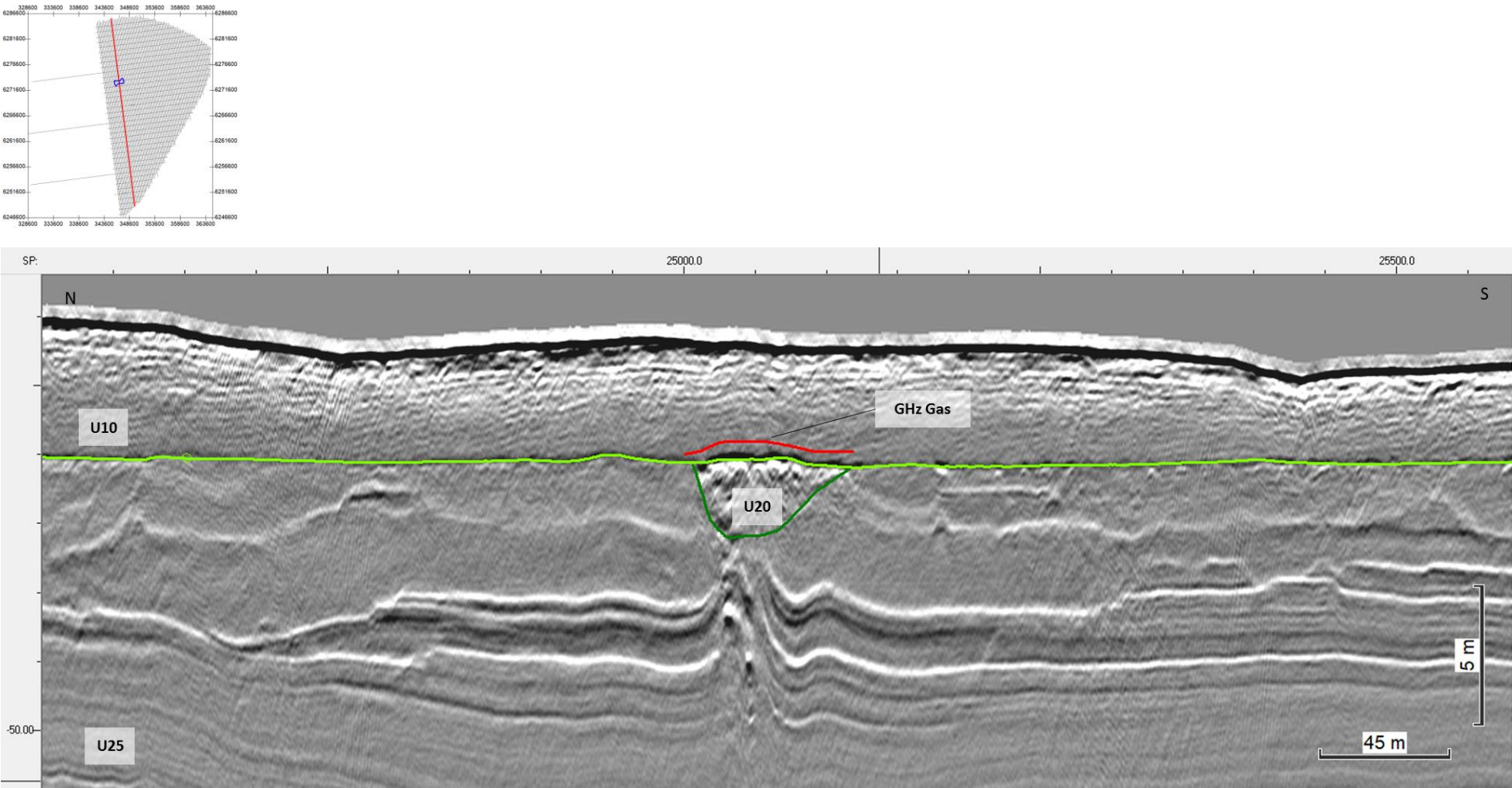


Figure 254 Structure within U25.
The structure may be related to the upward migration of fluids in the shallow subsurface. Seismic Profile BM2_OWF_E_2D_02940

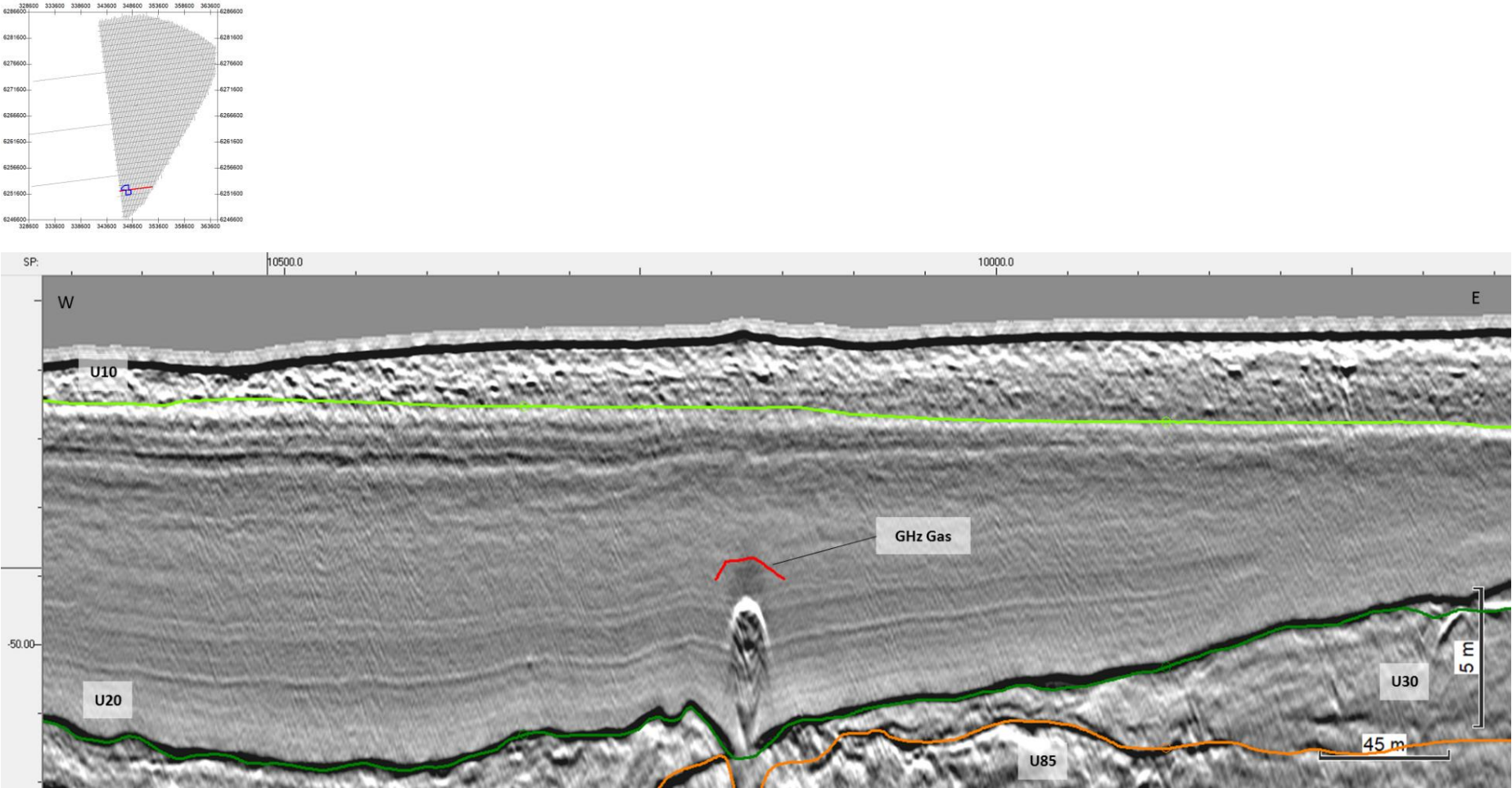


Figure 255 Structure within U20.
The structure may be related to the upward migration of fluids in the shallow subsurface. Seismic Profile BX4_OWF_E_XL_33000

8.8.7 | LACUSTRINE SEDIMENTS

Lake systems are typically low energy settings where fine sediment deposition prevails (silts, fine sands, and clays), and are commonly associated to glacial environments. On seismic data, lacustrine sediments are characterised by draping successions of micro-parallel, continuous reflectors. The materials within these deposits may differ significantly from adjacent units, constituting a hazard from a geotechnical point of view.

Such deposits were identified in the survey area. The base of these deposits was mapped as horizon GHz_Lacustrine (Figure 256 and Figure 257). Their occurrence is exclusively associated to U40 (Figure 258), and can be found between 40.1 m and 105.1 m depth MSL, or 0 m to 62 m depth BSB.

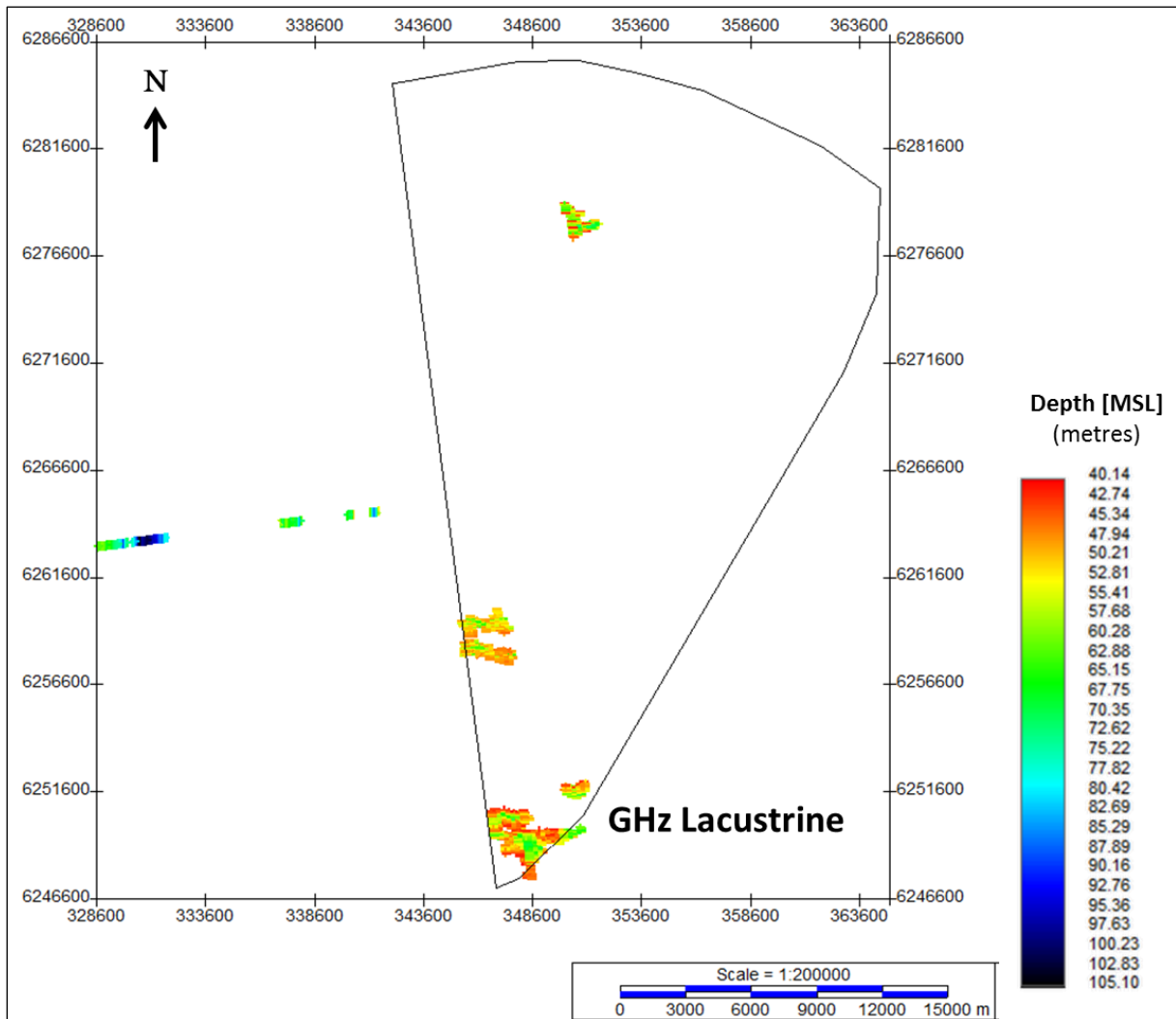


Figure 256 Lateral extent of the interpreted lacustrine deposits (Horizon: GHz_Lacustrine). Units in metres below MSL.

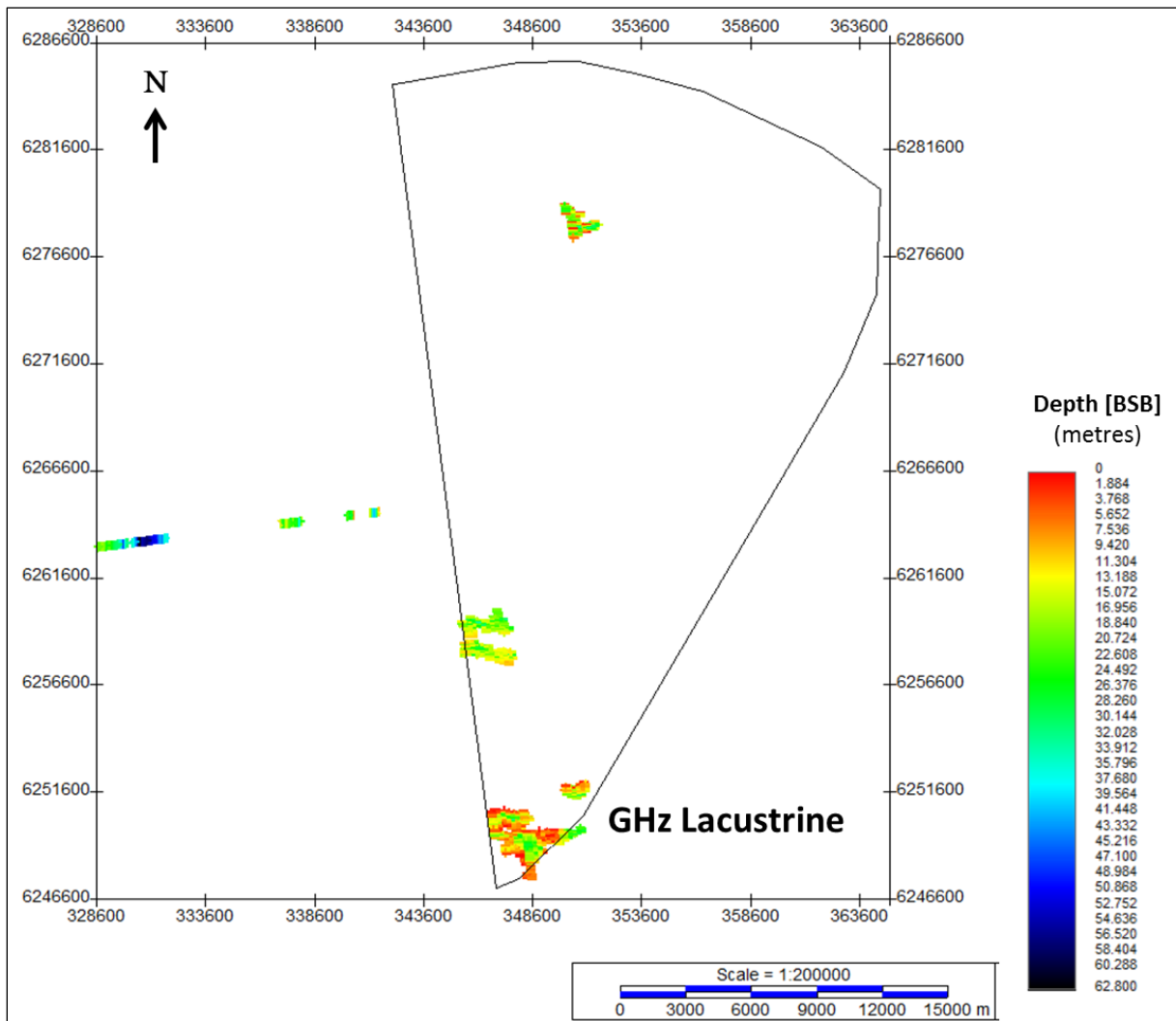


Figure 257 Depth below seabed of horizon GHz_Lacustrine.
Units in metres below seabed.

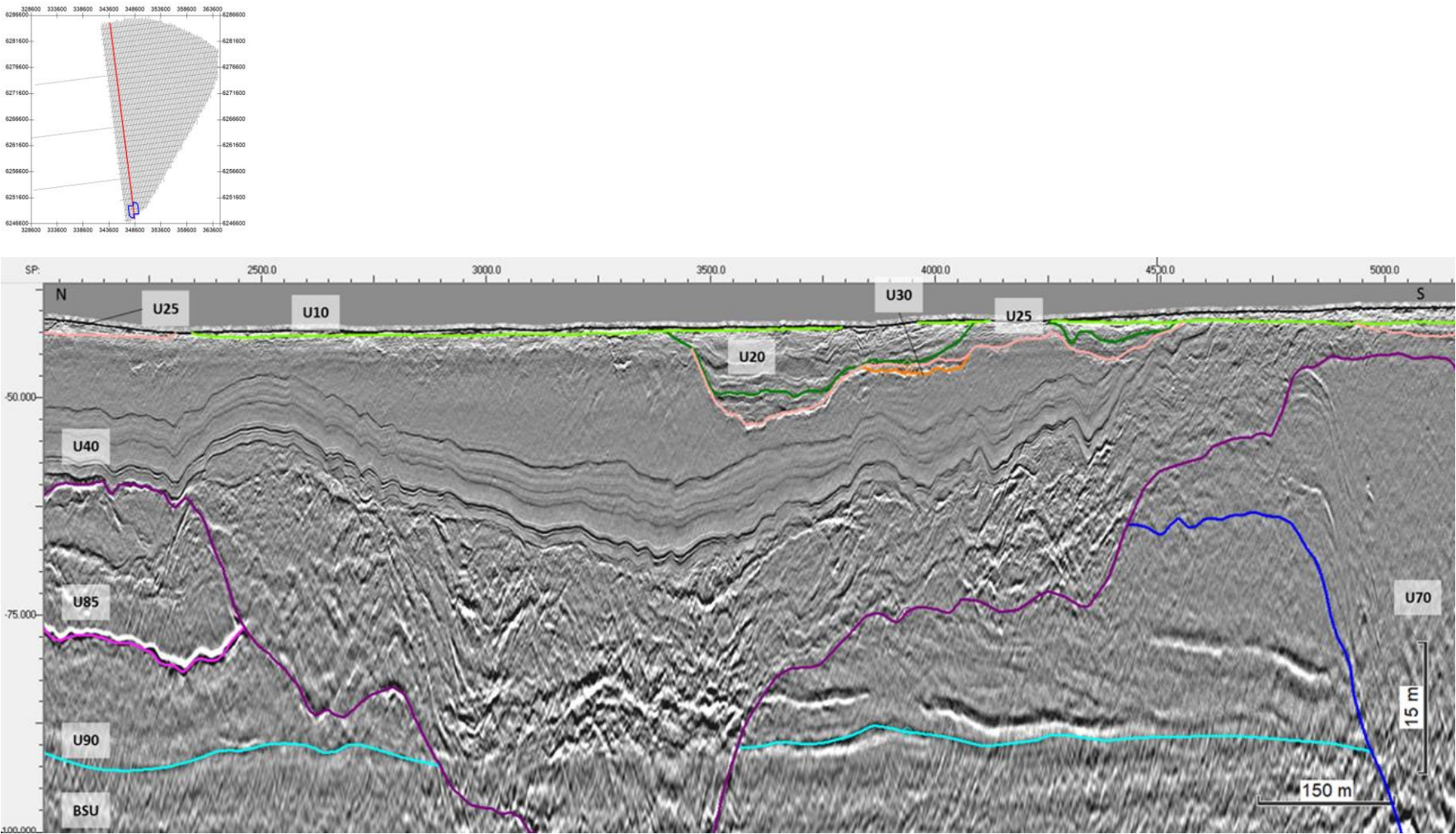


Figure 258 Interpreted glaciolacustrine deposits on the upper levels of Seismic Unit U40.
Seismic profile BM1_OWF_E_2D_01680

8.9 | ARCHAEOLOGY CONSIDERATIONS

During the survey no obvious archaeological findings were observed.

Three known wrecks and one possible unknown wreck have been described in Section 8.4.1|.

However, it is suggested that a full archaeology investigation be conducted on the data collected here by professionally qualified archaeologists in order to assess the possibility of paleo landscapes that could have been occupied by early man. This type of analysis is out with the scope for this report.

8.10 | GRAB SAMPLE SUMMARY

The MMT OWF survey area encompasses a variety of seabed conditions. Engineering within investigated depth profile below the seabed should consider the following general observations, which are neither exhaustive or prescriptive, and are related exclusively to the observed material presented in this report:

The results of the grab sampling provide good coverage of the surface seabed conditions, which are dominated by granular sediments, largely silty gravelly SAND with occasional patches of GRAVEL and sporadic areas of CLAY appearing towards the east of the area in BM05 and BM06 (Figure 259).

Table 33 Grab sample summary

Lithology	Number of Samples
SAND	97
GRAVEL	22
CLAY	5
SILT	1
Total	125

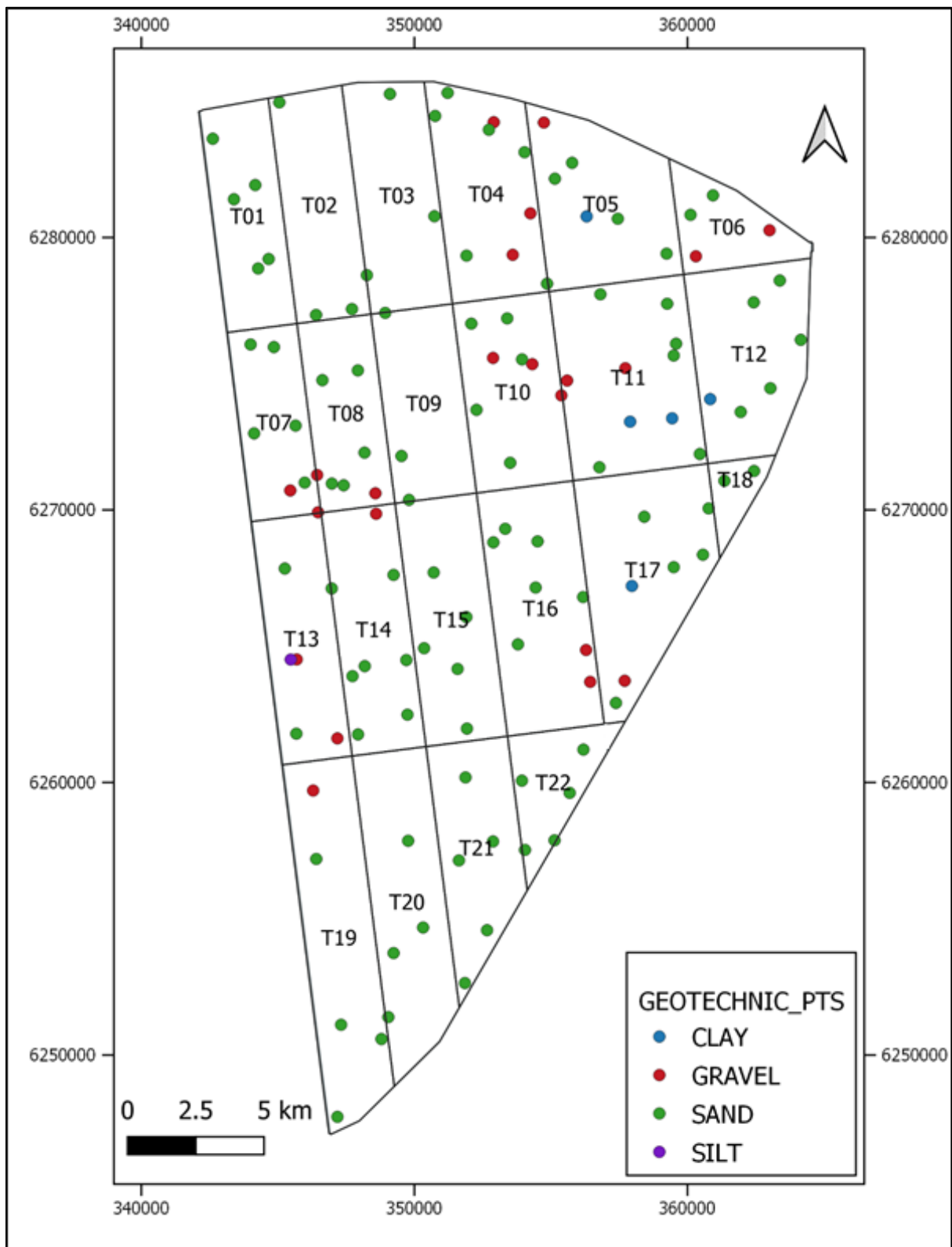


Figure 259 Location plot of grab sample with material types in MMT OWF survey area.

Particular 'exotic' features within a survey area may shallow seabed engineering, i.e., highly organic material, high gravel and/or cobble contents. Within the survey area, GRAVEL is common throughout

and COBBLES are encountered in 12 of the 125 locations, occupying between 14-71% of the sample in these cases. Due to the scattered nature of grab sampling, the geophysical data and interpretation should also be consulted as to whether there are significant deposits of coarse GRAVEL and/or COBBLES on the seabed. The presence of organic-rich CLAY and PEAT must also be taken into consideration, due to the undesirable thermal regime which such cohesive material can generate, together with their tendency for compressibility under load and typically low material strength. Whilst there was no presence of PEAT identified within the sampling sites, 5 samples were identified as CLAY, with smaller concentrations found in 34 other samples. As part of the laboratory analysis, 47 of the samples were tested for their total organic matter and total organic carbon which varied between 0.10-2.64 % for the total organic matter and 0.10-1.53 % for the total organic carbon. Whilst the thermal regime of the seabed has not been a subject of investigation in this report, the potential high thermal resistivities in organic-rich material and low strength cohesive CLAY should be borne in mind, especially with regards to any electrical cable installation activities.

The majority of the seabed sediments sampled were of Recent age, whilst occasional samples were Post Glacial and Late Glacial in age.

For a full description of the grab sample results please refer to the lab report and logs in Appendix C|.

9 | CONCLUSIONS

The results of the bathymetric survey found that the water depths across the site ranged between 25.75 m and 48.17 m with depth generally increasing from the western extent of the site to the eastern extent across the MMT OWF survey area.

The seabed has a range of natural topographic variability occurring throughout the site with extensive areas of mobile sediments present across much of the MMT OWF survey area. The mobile sediments range from smaller wavelength bedforms such as ripples, large ripples and megaripples to larger scale sediment migration bedforms such as sand waves and sandbars.

Slope angles across the site are typically very gentle ($<1^\circ$) and gentle (1° to 5°). Despite the fact that sand wave and sandbar areas constitute a large proportion of the area, the seafloor topography is typically gently undulating with areas of moderate to very steep gradients being largely restricted to the edges of sand bodies and the lee slopes of the most defined sand waves.

Very steep slope angles (15° to a maximum of 42°) were observed within the survey area but these were restricted to boulder features, the edges of depressions and steep banks on the western side of the Artificial Island area of investigation. Higher slope angles (up to 56°) were identified, however these were associated with known wrecks in the MMT OWF survey area.

The surficial geology in the area is dominated by muddy SAND, GRAVEL and coarse SAND, and SAND. The GRAVEL and coarse SAND, and the SAND are more prominent in the eastern and western extents of the area. The muddy SAND is concentrated more in a central north-south running band within the survey area. Infrequent and isolated patches of MUD and SANDY mud are occasionally present in the eastern and western extents of the area.

Extensive areas of mobile sediments, including ripples, large ripples and megaripples are observed across the survey area and are always associated with the GRAVEL and coarse SAND, or SAND. All ripple features have a northeast-southwest orientation indicating a dominating current regime from northwest to southeast. Sand waves areas are visible frequently, particularly in the northwest of the survey area, typically comprising of SAND or GRAVEL and coarse SAND. Across much of the survey area, larger scale sandbar bedforms are observed, upon which the smaller scale, more mobile and more recent bedforms are often superimposed. Areas of muddy SAND are usually featureless. One large (160 m x 120 m x 9.5 m), isolated sediment mound was also observed.

A total of 64595 individual seabed contacts (61309 MBES contacts and 3286 SSS contacts) were detected within the MMT OWF survey area. They were classified as boulders (64130) and man-made objects such as debris (437), fishing equipment (11) and wire (4). 9 contacts were classified as other which includes possible sediment mounds. Three known wrecks were identified, and one possible unknown wreck was observed. There are extensive boulder fields ranging from intermediate to high density throughout the survey area.

A total of 773 magnetic anomalies were detected within the MMT OWF survey area. 513 of these were individual discrete anomalies, whilst 260 anomalies were interpreted to form 33 linear anomalies. One of these linear anomalies corresponded to the database position of the buried TAT-14 cable.

Evidence of trawling is found across much of the survey area.

Occasional areas of interest have been identified and assessed as possible biogenic features. These areas have been evaluated by a senior biologist who determined these areas of interest are unlikely to be biogenic in nature. The areas have maintained their feature in case further investigation to these areas is deemed necessary. These areas are more likely to be erosional features.

Thirteen seismostratigraphic units were interpreted from the UHRS dataset from the MMT OWF survey area. Taken as a whole, these units represent the structural elements of the site's Geological Ground Model. The seismic units of the model were chosen primarily for their geotechnical significance, resulting

from distinct depositional and erosion events, marking relevant environmental changes, and shifts in sediment types.

The seismostratigraphy of the site is complex. The stratal architecture is interpreted as being controlled by the interplay of eustacy-isostasy, autogenic processes, and direct glaciation.

The lower deposits are interpreted to be related to glacial processes, where glaciotectionics have the strongest influence of the seismostratigraphy. Deposits from this mode are interpreted as glacitectorites, glaciofluvial, glaciolacustrine, glacial drift, and outwash accumulations. The sedimentological composition of these deposits is a mixture of unconsolidated, siliciclastic, sediments, i.e., sands, silts, clay, and gravel. The seismic units that represent the glacial processes are positioned above the Pre-Quaternary sequences that comprise the Base Seismic Unit.

The upper deposits comprise the high frequency sequences, where eustatic-isostatic movements have the strongest influence on the depositional environments. These deposits represent fluvial, tidal, estuarine, and coastal marine sediments. The sedimentological composition of these deposits is a mixture of unconsolidated, siliciclastic, sediments, i.e., sands, silts, clay, gravel, boulders, and organics.

The variety of sub-surface geohazards identified from the UHRS data is typical for depositional settings at high latitudes. The main interpreted geohazards were: paleo channels, tunnel valleys, glaciotectionized sediments, gravel, faults, soft sediments, organics, till, and unclassified amplitude anomalies. Boulders are likely, but a definitive declaration of their presence was not made.

10 | RESERVATIONS AND RECOMMENDATIONS

The results in this report, both geological descriptions and contact selection, are based on interpretations of geophysical data obtained during the survey. It should be taken into account that there is a natural limitation in the accuracy of interpretation. Results from grab sampling have been used for verification of the geological interpretations and is considered as ground truthing at those locations where collected. Where considered applicable, the sampling results have been extrapolated to constitute a base for verifications also in the surroundings.

Seismic interpretation presented in this report is based solely on seismic interpretation techniques. Unit definition is based on the identification and mapping of the most prominent reflectors and seismic facies shift that correspond to significant changes on depositional environments and sediment type. Seismic facies identification, internal reflector termination and geometry of the erosive surfaces are the basis for the unit's description, inferred depositional environments and sediment type. No type of subsurface ground truthing was incorporated into the present model. All units display a certain degree of vertical and horizontal variability and heterogeneity. This is due to intrinsic nature of the geological processes that took place, the rapidly changing environment and the great extent of the site. The interpretation derived from the geophysical data should be validated by means of ground sampling (bore hole, cone penetrometer test and any soil inspection technique). Key aspects to be investigated are (1) seismic units inferred soil composition, (2) geotechnical relevance of facies shift (laterally and vertically), (3) geotechnical relevance of internal erosive surfaces, (4) importance of linear features (channels) in terms of mechanical/lithological properties and its variability, (5) mechanical relevance of the identified deformation evidences (glaciotectonics, faults, folds), (6) importance of intra-formational negative impedance contrasts, (7) presence and potential hazard of the identified gas, (8) presence of constrains in engineering and site development (boulders, coarse sediments), (9) accuracy of used depth-conversion velocity model.

Not all existing contacts are detectable in the SSS data due to resolution, material, and orientation of the object.

MMT's recommendations for further planning within the MMT OWF survey area are:

- When the data is evaluated and more accurate positions of the planned MMT OWF sites are decided, a more detailed survey is recommended over the selected sites, including a full Unexploded Ordnance (UXO) survey, visual inspection of contacts and additional geotechnical sampling.

11 | REFERENCES

- Andersen, L. T. 2004. The Fanø Bugt glaciotectionic thrust fault complex, southeastern Danish North Sea. Ph.D.Thesis 2004. Danmarks og Grønlands Geologiske Undersøgelse Rapport 2004/30: 35-68.
- Anthony, D. and Leth, J. O. 2001. Large-scale bedforms, sediment distribution and sand mobility in the eastern North Sea off the Danish west coast. *Marine Geology* 182 (2002) 247-263
- Anthony, D., Møller, I. 2003. The geological architecture and development of the Holmsland Barrier and Ringkøbing Fjord area, Danish North Sea Coast. *Geografisk Tidsskrift, Danish Journal of Geography* 102 27
- Behre, K-E, 2007. A new Holocene sea-level curve for the southern North Sea. Behre, K.-E. 2007 (January): A new Holocene sea-level curve for the southern North Sea. *Boreas*, Vol. 36, pp. 82-102.
- Bennike, O., Jensen, J.B., Konradi, P., Lemke, W. and Heinemeier, J. 2000. Early Holocene drowned lagoonal deposits from the Kattegat, southern Scandinavia. *Boreas*, Vol. 29, pp. 272–286.
- Bennike, O., Jensen, J.B., 1998. Late- and postglacial shore level changes in the southwestern Baltic Sea. *Bulletin of the Geological Society of Denmark*, Vol. 45, pp. 27-38.
- Dalgas E. 1867–1868. *Geografiske billeder fra Heden* (H. 1 & 2).
- Ehlers, J. 1990. Reconstructing the dynamics of the north-west European Pleistocene ice sheets. *Quaternary Science Reviews* 3: 1-40.
- Fugro 2014. Fugro Seacore Limited, Energinet.dk, April 2014. Preliminary Geotechnical Investigations. Vesterhav Syd Nearshore Wind Farm. Factual Report on Ground Investigation.
- Geoviden 2005. De seneste 150.000 år i Danmark. *Istidslandskabets og Naturens udvikling* , Nr. 2.
- Gregersen, S., Hjelme, J. & Hjortenberg, E.: Earthquakes in Denmark. *Bulletin of the Geological Society of Denmark*, Vol. 44, pp. 115-127. Copenhagen 1998- 02-28.
- Houmark-Nielsen M. 2007. Extent and age of Middle and Late Pleistocene glaciations and periglacial episodes in southern Jutland, Denmark. *Bull. Geol. Soc. Denmark* 55: 9–35.
- Høyer A-S., Jørgensen F., Piotrowski A. J., Jakobsen P. R. 2013. Deeply routed glaciotectionism in the western Denmark. Geological composition, structural characteristics and origin Varde Hill Island. *Jour. of Quat. Science* 28 (7): 683-696.
- Huuse, M., and Lykke-Andersen, H. 2000. Overdeepened Quaternary Valleys in the eastern Danish North Sea: morphology and origin; *Quaternary Science Reviews*, vol 19 (12)
- Huuse, M. and Lykke-Andersen, H. 2000b. Large-Scale glaciotectionic thrust structures in the eastern Danish North Sea *Geological Society, London, Special Publications*, 1010.1144/GSL.SP,2000.176.01.22. p293-305
- Jakobsen P. R. 2003. GIS based map of glaciotectionic phenomena. *Denmark Geological Quarterly* 47 (4): 331–338
- Japsen, P. 2000. Fra Kidthav til Vesterhav. Nordsobasinets udvikling vurderet ud fra seismiske hastigheder. *Geologisk Tidsskrift, hæfte 2*. pp. 1-36 København
- Japsen, P., Rasmussen, E.S, Green P.F., Nielsen L.H. and Bidstrup T 2008. Cenozoic palaeogeography and isochores predating the Neogene exhumation of the eastern North Sea Basin. *Geological Survey of Denmark and Greenland Bulletin* 15, 25–28.

Johannessen, P. N., Nielsen, L. H., Nielsen, L., Møller, I., Pejrup, M., Andersen, T. J., Korshøj, J., Larsen, B. and Piasecki, S. 2008. Sedimentary facies and architecture of the Holocene to Recent Rømø barrier island in the Danish Wadden Sea. Geological Survey of Denmark and Greenland Bulletin 15, 49–52.

Jørgensen, F., Sandersen, P.B.E. 2006. Buried and open tunnel valleys in Denmark erosion beneath multiple ice sheets. Quaternary Science Reviews 25, 1339–1363

Larsen, B., and Andersen, L. T. Andersen. 2005. Late Quaternary stratigraphy and morphogenesis in the Danish eastern North Sea and its relation to onshore geology. Netherlands Journal of Geosciences 84-2, 113-128.

Leth, J.O. 1996. Late Quaternary geological development of the Jutland Bank and the initiation of the Jutland Current, NE North Sea. Nor. Geol. Unders. Bull. 430, 25-34.

Leth, J.O., Larsen, B., Anthony, D., 2004. Sediment distribution and transport in the shallow coastal waters along the west coast of Denmark Geological Survey of Denmark and Greenland Bulletin 4, 41–44.

Michelsen, O. 1993. Structural development of the Fennoscandian Border Zone, offshore Denmark. Marine and Petroleum Geology Volume 10, 24-134.

Nicolaisen, J. F. 2010. (Editor): Marin råstof- og naturtypekortlægning i Nordsøen, Naturstyrelsen.

Nielsen, L. H. Johannesen, P. 2004. Skagen Odde – et fuldskala, naturligt laboratorium. Nyt Fra GEUS, nr 1.

Nielsen, T., Mathiesen, A. and Bryde-Auken, M. 2008. Base Quaternary in the Danish part of the North Sea and Skagerrak; Geological Survey of Denmark and Greenland Bulletin 15, 37-40

Novak, B. Duarte, H. and Leth J.O. 2015. Glaciotectionic thrust complex offshore Holmsland, the Danish North Sea. Abstract in The Quaternary Geology of the North Sea, Annual discussion Meeting of the Quaternary Research association UK, Edinburgh, January, 71.

Novak B. and Duarte H. 2018. Glaciotectionic thrust complex offshore Holmsland, the Danish North Sea - New Results. Presentation: Nordic Geologic Winter Meeting. DTU, Lyngby, DK 2018.

Novak B., Pedersen G. K. 2000. Sedimentology, seismic facies and stratigraphy of a Holocene spit–platform complex interpreted from high-resolution shallow seismics, Lysegrund, southern Kattegat, Denmark. Marine Geology 162, 317–335.

Novak, B. and Bjørck S. 2002. Late Pleistocene–early Holocene fluvial facies and depositional processes in the Fehmarn Belt, between Germany and Denmark, revealed by high-resolution seismic and lithofacies analysis. Sedimentology, 49, 451–465

Pedersen, S. A. S. 2005. Structural analysis of the Rubjerg Knude glaciotectionic complex, Vendsyssel, Northern. Denmark. Geol. Surv. of Denmark, Bulletin 8.

Rasmussen, E. S., Dybkjær K., Piasecki S. 2010. Lithostratigraphy of the Upper Oligocene–Miocene succession of Denmark. Geological Survey of Denmark and Greenland Bulletin 22: 1–92.

Robertson, P., Campanella, R., Gillespie, D., & Greig, J. (1986). Use of Piezometer Cone. In-situ'86, Use of In-situ testing in Geotechnical Engineering, GSP 6, ASCE, Reston, 1263 - 1280.

Sandersen, P. B. E., Jørgensen F. 2003. Buried Quaternary valleys in western Denmark occurrence and inferred implications for groundwater resources and vulnerability. Journal of Applied Geophysics 53: 229– 248

Sjørring, S., Frederiksen, J. 1980. Glacialstratigrafiske observationer i de vestjyske bakkeøer. Dansk Geologisk Forenings Årsskrift 1979: 63–77.

Smed, P., 1979. Landskabskort over Danmark, Blad 1, Nordjylland. Geografforlaget, Brenderup, Denmark.

Smed, P., 1981. Landskabskort over Danmark, Blad 2, Midtjylland. Geografforlaget, Brenderup, Denmark.

Sorgenfrei, T. & Buch, A.; 1964; Deep Tests in Denmark 1935/1959. Geological Survey of Denmark, III. Series 36, Copenhagen

Vaughan-Hirsch, D.P., Phillips, E.R. 2017. Mid-Pleistocene thin-skinned glaciotectionic thrusting of the Aberdeen Ground Formation, Central Graben region, central North Sea. Journal Of Quaternary Science, 32(2) 196–212

Vejbæk, O. V. 1997. Dybe strukturer i danske sedimentære bassiner. Geologisk Tidsskrift, hæfte 4, pp. 1-31. København, 12-16.

Vejbæk, O.V., Bidstrup, T., Erlström, M, Rasmussen, E. S. and Sivhed, M. 2007. Chalk depth structure map Central to East North Sea, Denmark. GEUS. Geological Survey of Denmark and Greenland Bulletin 13, 9-12.

12 | DATA INDEX

The deliverables listed in Table 34 accompany this report.

Table 34 Deliverables.

Item	Group	Data Product
1	Bathy data	Bathymetry - Un-gridded soundings, (X,Y,Z) values in ASCII format.
2	Bathy data	Bathymetry - Gridded soundings, 0.25m resolution, (X,Y,Z) values in ASCII format (tiled following the UTM grid).
3	Bathy data	Bathymetry - Gridded soundings, 0.25m resolution, GeoTiff stored in esri file geodatabase (untiled).
4	Bathy data	Bathymetry - Gridded soundings, 1.00m resolution, (X,Y,Z) values in ASCII format (tiled following the UTM grid).
5	Bathy data	Bathymetry - Gridded soundings, 1.00m resolution, GeoTiff stored in esri file geodatabase (untiled).
6	Bathy data	Bathymetry - Gridded soundings, 5.00m resolution, (X,Y,Z) values in ASCII format (untiled).
7	Bathy data	Bathymetry - Gridded soundings, 5.00m resolution, GeoTiff stored in esri file geodatabase (untiled).
8	Bathy data	Bathymetry - Bathymetric contour curves with 50cm interval, as TSG object CONTOURS_LIN
9	Bathy data	Bathymetry - Vessel tracks, as TSG object TRACKS_LIN, indicate equipment carrier and equipment type in attributes.
10	Bathy data	Bathymetry - TVU 1.00 m resolution, (X,Y, TVU) values in ASCII format
11	Bathy data	Bathymetry - TVU 1.00 m resolution, GeoTiff stored in esri file geodatabase
12	Bathy data	Bathymetry - THU 1.00 m resolution (X,Y,THU) values in ASCII format
13	Bathy data	Bathymetry - THU 1.00 m resolution, GeoTiff stored in esri file geodatabase
14	Bathy data	Bathymetry - backscatter 32bit GeoTiff stored in esri file geodatabase (amplitude populated channels)
15	Bathy data	SVP - sound velocity profiles as SVP comparison spreadsheet
16	Bathy data	MBES - Anomaly target list, as TSG object MBES_ANOMALY_PTS, anomaly characteristics provided in attributes.
17	SSS data	Side scan sonar data as XTF-files with corrected navigation, High frequency
18	SSS data	Side scan sonar data as XTF-files with corrected navigation, Low frequency
19	SSS data	Navigation files, CSV-format
20	SSS data	SSS instrument tracks, as TSG object TRACKS_LIN, indicate equipment carrier and equipment type in attributes
21	SSS data	SSS Anomaly target list, as TSG object SSS_ANOMALY_PTS, anomaly characteristics provided in attributes.
22	SSS data	SonarWiz 7 project including the bottom-tracked and suitably processed .XTF files and SSS and Magnetometer targets
23	Mag data	MAG measurements, CSV-format
24	Mag data	MAG instrument tracks, as TSG object TRACKS_LIN, indicate equipment carrier and equipment type in attributes.
25	Mag data	MAG Anomaly target list, as TSG object MAG_ANOMALY_PTS, anomaly characteristics provided in attributes
26a	SBP & 2DUHRS data	Processed SBP recordings, SEG Y format
26b	SBP & 2DUHRS data	Processed UHRS recordings, SEG Y format
26c	SBP & 2DUHRS data	Traces are aligned with datum

Item	Group	Data Product
27a	SBP & 2DUHRS data	Processed SBP recordings, as image-files (Tiff or PNG)
27b	SBP & 2DUHRS data	Processed UHRS recordings, as image-files (Tiff or PNG)
28	SBP & 2DUHRS data	SBP and UHRS instrument tracks, as TSG object TRACKS_LIN, indicate equipment carrier and equipment type in attributes.
29	SBP & 2DUHRS data	SBP and UHRS Anomaly target list, as TSG object SBP_ANOMALY_PTS, anomaly characteristics provided in attributes.
30	SBP & 2DUHRS data	Interpretation of the processed seismic data. These data include interpretation points for digitized horizons identified in the seismic recordings (point list file in CSV-format).
31a	SBP & 2DUHRS data	Generated elevation grids relative to vertical datum for each interpreted horizon in 5 m resolution as GeoTiff grid
31b	SBP & 2DUHRS data	Generated elevation grids relative to vertical datum for each interpreted horizon in 5 m resolution as (X,Y,Z) values in ASCII format (Z as the horizon elevation in meter)
32a	SBP & 2DUHRS data	Generated depth below seabed (BSB) grids for each interpreted horizon in 5 m resolution as GeoTiff grid
32b	SBP & 2DUHRS data	Generated depth below seabed (BSB) grids for each interpreted horizon in 5 m resolution as (X,Y,Z) values in ASCII format (Z as the horizon depth BSB in meter)
33a	SBP & 2DUHRS data	Generated Isochore (layer thickness) grids for each interpreted soil unit in 5 m resolution as GeoTiff grid
33b	SBP & 2DUHRS data	Generated Isochore (layer thickness) grids for each interpreted soil unit in 5 m resolution as (X,Y,Z) values in ASCII format (Z as the layer thickness in meter)
34	SBP & 2DUHRS data	Kingdom project including SBP and UHRS data, both as TWT and as DEPTH conversion.
35	Grab sampling data	Grab sample positions, as TSG object GEOTECHNIC_PTS, indicate sampling characteristics in attributes.
36	Grab sampling data	Grab sample classification, MS-Excel spread sheet
37	Grab sampling data	Grab sample laboratory analysis, overview table and result tables, MS-Excel spread sheet.
38	Integrated seabed interpretation data	Seabed Surface Geology, as TSG object SEABED_GEOLOGY_POL, indicate surface geological unit in attributes
39	Integrated seabed interpretation data	Seabed Surface Features, as TSG object SEABED_SURFACE_PTS, indicate surface forms in attributes
40	Integrated seabed interpretation data	Seabed Surface Features, as TSG object SEABED_SURFACE_LIN, indicate surface forms in attributes
41	Integrated seabed interpretation data	Seabed Surface Features, as TSG object SEABED_SURFACE_POL, indicate surface forms in attributes
42	Integrated seabed interpretation data	Seabed Substrate type, as TSG object SEABED_SUBSTRATE_POL, indicate substrate type in attributes.
43	Integrated seabed interpretation data	Man-Made-Objects, as TSG object MMO_PTS, indicate MMO type in attributes.
45	Integrated seabed interpretation data	Man-Made-Objects, as TSG object MMO_LIN, indicate MMO type in attributes.
46	Report	Operations Report
47	Report	Geophysical site survey Report (charts as enclosures)

APPENDIX A 	LIST OF PRODUCED CHARTS
APPENDIX B 	CONTACT AND ANOMALY LIST
APPENDIX C 	GRAB SAMPLE LAB REPORT
APPENDIX D 	2D UHRS PROCESSING REPORT